1. Report No.	2. Government Accession No.	3. Recipient's Catalog No.
FHWA/TX-06/0-4361-1		

4. Title and Subtitle	5. Report Date
EVALUATION OF EFFECTS OF TIRE SIZE AND INFLATION PRESSURE ON TIRE CONTACT STRESSES AND PAVEMENT RESPONSE	June 2006 Resub: August 2006
	6. Performing Organization Code
7. Author(s)	8. Performing Organization Report No.
Emmanuel G. Fernando, Dilip Musani, Dae-Wook Park, and Wenting Liu	Report 0-4361-1
9. Performing Organization Name and Address	10. Work Unit No. (TRAIS)
Texas Transportation Institute The Texas A&M University System College Station, Texas 77843-3135	11. Contract or Grant No. Project 0-4361
12. Sponsoring Agency Name and Address	13. Type of Report and Period Covered
Texas Department of Transportation Research and Technology Implementation Office P. O. Box 5080 Austin, Texas 78763-5080	Technical Report: September 2001 – August 2004
	14. Sponsoring Agency Code

15. Supplementary Notes

Project performed in cooperation with the Texas Department of Transportation and the Federal Highway Administration.

Project Title: Determine Effects of Tire Size and Inflation Pressure on Tire Contact Pressure and Primary Pavement Responses to Loading

URL: http://tti.tamu.edu/documents/0-4361-1.pdf

16. Abstract

Recent years have seen an increase in the number of permitted oversized and overweight loads on Texas highways. The motor carrier industry uses a number of tire sizes in transporting oversized and overweight loads. Tire inflation pressures for these transports are often higher than those used for regular line hauling to match the higher wheel loads of the overweight truck or trailer. In evaluating the structural adequacy of pavements to applied wheel loads, existing practice typically assumes the tire pressure to be uniform over the contact area with magnitude equal to the inflation pressure. This analysis ignores the differences in tire footprints among various tire types. To determine the effects of these differences, researchers investigated existing procedures for predicting pavement response to applied surface tractions at the tire-pavement interface. A specific objective was to establish how tire contact stresses may be modeled in existing layered elastic programs to better approximate the effects of non-uniform tire contact pressure distributions, and account for differences in tire construction, tire load, and tire inflation pressure on predicted pavement response. To this end, researchers assembled a data base of measured tire contact stresses and performed a comparative evaluation of methods for representing tire contact pressure distributions in existing models to predict performance-related pavement response variables. A computer program called *TireView* was developed that provides estimates of tire contact area as a function of tire type, tire load, and tire inflation pressure and predicts the stress distribution at the tire-pavement interface based on polynomial interpolations of measured tire contact stresses in the data base. A method for predicting pavement response using layered elastic analysis is proposed that is based on the predicted tire contact area. Alternatively, the predicted tire contact pressure distribution from *TireView* may be used in a finite element program for applications where a more rigorous analysis is desired.

17. Key Words	18. Distribution Statement
Tire Contact Pressures, Tire Contact Stress Measurement, Pavement Response Modeling, Polynomial Interpolation	No restrictions. This document is available to the public through NTIS: National Technical Information Service Springfield, VA 22161 http://www.ntis.gov

19. Security Classif.(of this report)	20. Security Classif.(of this page)	21. No. of Pages	22. Price
Unclassified	Unclassified	288	

EVALUATION OF EFFECTS OF TIRE SIZE AND INFLATION PRESSURE ON TIRE CONTACT STRESSES AND PAVEMENT RESPONSE

by

Emmanuel G. Fernando
Research Engineer
Texas Transportation Institute

Dilip Musani
Former Graduate Research Assistant
Texas Transportation Institute

Dae-Wook Park
Former Assistant Transportation Researcher
Texas Transportation Institute

Wenting Liu
Assistant Research Engineer
Texas Transportation Institute

Report 0-4361-1
Project 0-4361
Project Title: Determine Effects of Tire Size and Inflation Pressure on Tire Contact Pressure and Primary Pavement Responses to Loading

Performed in cooperation with the
Texas Department of Transportation
and the
Federal Highway Administration

June 2006

Resubmittal: August 2006

TEXAS TRANSPORTATION INSTITUTE
The Texas A&M University System
College Station, Texas 77843-3135

DISCLAIMER

The contents of this report reflect the views of the authors, who are responsible for the facts and the accuracy of the data presented. The contents do not necessarily reflect the official views or policies of the Texas Department of Transportation (TxDOT) or the Federal Highway Administration. This report does not constitute a standard, specification, or regulation, nor is it intended for construction, bidding, or permit purposes. The United States Government and the State of Texas do not endorse products or manufacturers. Trade or manufacturers' names appear herein solely because they are considered essential to the object of this report. The engineer in charge of the project was Dr. Emmanuel G. Fernando, P.E. # 69614.

ACKNOWLEDGMENTS

The work reported herein was conducted as part of a research project sponsored by the Texas Department of Transportation and the Federal Highway Administration. The authors gratefully acknowledge the steadfast support and technical guidance of the project director, Mr. Joe Leidy, of the Materials and Pavements Section of TxDOT. In addition, the authors give thanks to Dr. Duchwan Ryu for providing his statistical expertise in the analysis of the test data collected in this project, and to Ms. Geetha Kakarlapudi for her work in determining tire footprint areas from imprints taken on various tires. The contributions of all three individuals are noted and sincerely appreciated.

TABLE OF CONTENTS

Page

Page

LIST OF FIGURES

Figure Page

Figure Page

Figure Page

Figure Page

Figure Page

Figure Page

Figure Page

Figure Page

Figure Page

Figure Page

Figure Page

Figure Page

Figure Page

Figure Page

Figure Page

Figure Page

Figure Page

Figure Page

LIST OF TABLES

Table Page

CHAPTER I. INTRODUCTION

The last five years have seen an increase in the number of permitted oversized and overweight loads on Texas highways. Already, two state routes near the Texas-Mexico border in Brownsville are routinely used to carry products to and from Mexico on trucks having gross vehicle weights (GVWs) of up to 125,000 lb. The payloads carried by permitted trucks (Figure 1.1) are mostly coiled metal sheets, oil and powder mineral (fluorite), which are transported from the Port of Brownsville to Mexico and vice versa. Superheavy load moves are also increasingly routed on weaker Farm-to-Market roads to avoid bridge structures and clearance restrictions. Gross vehicle weights associated with these moves range from 250,000 to 2,000,000 lb and include loads like oil pressure vessels, off-shore oil drilling components and electric transformers used by the petrochemical and power generation industries (Figure 1.2). Loads are typically transported on specialized trailers with multiple axles and tires.

A number of tire sizes are used by the motor carrier industry in transporting oversized and overweight loads. These tires range from super singles having cross-sectional widths of 14 inches or more, to narrow 7.5-inch wide tires used on specialized hydraulic trailers. Tire inflation pressures are often higher than those used for regular line hauling to match the higher wheel loads of the overweight truck or trailer. On superheavy load moves, tire inflation pressures can range up to 130 – 140 psi.

Under existing practice, the effects of tire loads on pavements are typically evaluated assuming that the tire pressure over the contact area is uniform, with magnitude equal to the inflation pressure. The shape of the contact patch is assumed to be a circle with an area equal to the ratio of the wheel load over the inflation pressure. In reality, the pressure distribution is non-uniform and the tire contact area is not circular. The present method for predicting pavement response to wheel loads using layered elastic analysis neglects the bending stiffness of the tire and cannot differentiate between the effects of different tire types that have the same load and inflation pressure. In this regard, the motor carrier industry has argued that the same wheel load placed on different tires cannot induce the same pavement response. However, the magnitudes of the differences need to be established.

Figure 1.1. Types of Payloads Carried by Permitted Trucks.

Figure 1.2. Examples of Superheavy Loads.

As the demand for point-to-point delivery of materials, manufactured commodities and agricultural products grows, motor carriers will increasingly find ways to increase their efficiency by decreasing tare weight to allow for more cargo room, leading perhaps to increased use of low-profile and wide-base truck tires, also referred to as super singles. Likewise, the number of requests for overweight permits will continue to grow as truckers try to improve efficiency by maximizing the use of their equipment on any given haul.

Clearly, if highway agencies are to respond effectively to the increased truck use of state highways and provide pavements that will sustain higher wheel loads, existing procedures for analyzing pavement response to loads need to be reviewed and revised as necessary to permit a more realistic modeling of tire contact stresses, which are significantly influenced by the tire construction, tire load and inflation pressure. To realistically evaluate the effects of overweight vehicles, the Texas Department of Transportation (TxDOT) funded a research project with the Texas Transportation Institute (TTI) to:

- characterize tire contact stresses for various tire types, tire loads and tire inflation pressures;
- evaluate the effects of tire construction, tire load and tire inflation pressure on pavement response;
- develop a methodology for estimating tire contact stresses; and
- establish how such stresses may be represented in existing layered elastic analysis programs to achieve a better approximation of the effects of non-uniform tire contact stresses on performance-related pavement response variables.

The effects of tire-related factors on tire contact pressures and predicted pavement response have been investigated in previous research projects including those that were conducted in Texas in the mid-1980s. Researchers initially conducted a literature review to establish the present state of knowledge in this area, identify what can be used from previous research and establish where additional work/data are necessary to accomplish the objectives of the present project. This literature review identified existing sources of measured tire contact stresses and established current trends in truck tire usage. Researchers used the findings from this review to assemble available data on tire contact stresses and to set up a test plan for additional measurements of tire contact stresses that were made in this project. The present report documents the research performed and is organized into the following chapters:

- Chapter I provides the rationale for this project and states its objectives;
- Chapter II describes the data base of tire contact stresses that researchers established to conduct a comparative evaluation of predicted pavement response under various loading assumptions, i.e., uniform versus non-uniform. The data base includes measurements collected from tests conducted at the University of California at Berkeley (UCB) in 1997 and in this project in 2002. Tests were conducted using an instrumented pad developed by the Council for Scientific and Industrial Research (CSIR) in South Africa. Chapter II describes the equipment used to measure tire contact stresses, identifies the tires tested, and presents the test matrices of tire loads and tire inflation pressures at which measurements were made.

- Chapter III discusses the repeatability of the tire contact measurements, which was evaluated as part of establishing a data base of tire contact stresses for analyzing pavement response and developing an approximate procedure to predict tire contact stress distributions through interpolation of measured data.
- Chapter IV presents relationships to predict tire contact area as a function of tire type, tire load and tire inflation pressure. The equations presented are based on imprints taken of tire contact patches tested at various tire loads and inflation pressures in the UCB and TTI studies. These equations are used in the approximate procedure established in this project to model tire contact stresses using layered elastic computer programs implemented by TxDOT.
- Chapter V compares pavement response predictions obtained from three-dimensional (3D) finite element analyses of measured tire contact stresses with corresponding predictions based on layered elastic theory. To provide a benchmark for assessing the accuracy of layered elastic predictions, researchers evaluated pavement response under measured tire contact stresses using a 3D finite element program. This investigation covered a representative range of pavement structures and compared pavement response parameters presently used in load-zoning analysis and evaluation of proposed superheavy load or overweight truck routes.
- Chapter VI presents the computer program developed in this project for estimating tire contact stresses. This program, called *TireView*, incorporates a data base of tire contact stresses established from test data collected in the UCB and TTI studies. *TireView* uses an interpolation routine with this data base to estimate tire contact stresses for a given tire at a specified load and inflation pressure.
- Chapter VII summarizes the findings from this project and suggests a two-stage approach for modeling tire contact stresses for predicting pavement response to wheel loads. This approach permits the use of TxDOT's existing layered elastic programs and accommodates applications where a detailed level of analysis using a 3D finite element program may be warranted.

The appendices provide supporting material referred to in the different chapters, beginning with the literature review presented in Appendix A. Appendix B presents charts of the tire contact stress measurements on the 11R24.5 radial tire, while Appendix C shows the same charts for the 215/75R17.5 radial. Both tires were tested in this project. Finally, Appendix D presents the tire imprints taken from tests conducted on these tires. Researchers used these imprints to develop relationships for estimating tire contact areas as functions of the tire type, tire load and tire inflation pressure.

CHAPTER II. MEASUREMENTS OF TIRE CONTACT STRESSES

Measurements of tire contact stresses were conducted by CSIR staff at the University of California at Berkeley in 1997. These measurements were made using a pad instrumented with triaxial load pins, referred to by CSIR at that time as the vehicle-road surface pressure transducer array (VRSPTA). In the UCB tests, CSIR staff used the VRSPTA in conjunction with the heavy vehicle simulator (HVS) owned by the California Department of Transportation (CALTRANS) to measure tire contact stresses at various tire loads and tire inflation pressures (de Beer and Fisher, 1997). Tests were conducted on the tires identified in Table 2.1. The UCB tests included two of the most popular truck tires used today (the 295/75R22.5 and 11R22.5 radial tires) based on a literature review conducted by researchers in the UCB study. In this project, tire contact measurements were collected on 11R24.5 and 215/75R17.5 radial truck tires. The selection of tires for testing in this project was based on the findings from the literature review given in Appendix A. The 11R24.5 tire is among the popular tires identified in a survey conducted by the Center for Transportation Research (CTR) in a previous TxDOT project (Wang et al., 2000). This tire is commonly used on steering axles. The 215/75R17.5 tire is the smallest of the tires listed in Table 2.1. It is often found on trunion axles of multi-axle trailers used for superheavy load moves in Texas.

TIRE TESTING

In this project, CSIR staff conducted tire tests at their research facility in South Africa, using the HVS shown in Figure 2.1. Underneath the HVS is a pit where the pressure transducer array was positioned (see Figure 2.2). This pressure transducer array is referred to by CSIR as the stress-in-motion (SIM) pad, similar in concept to a weigh-in-motion (WIM) pad except that tire contact forces (in the lateral, longitudinal and vertical directions) are measured under a moving wheel load. The transducer array used by CSIR in this project is the SIM Mk IV system, which is a later version of the VRSPTA system used in the UCB study (a SIM Mk II). The SIM Mk IV has newer electronics that are designed to eliminate noise much better than the previous VRSPTA system and permits higher sampling rates with variable measurement times. For the measurements conducted in this project, CSIR set the sampling rate at 1001 Hz, about seven times higher than the fixed sampling rate of 150 Hz

Table 2.1. Tires Tested in CALTRANS and TxDOT Projects[1].

Research Project	Tire Type	Tire Size/Load Range	Tread Pattern
UCB	Bias-ply	10.00 × 20 (G)	
	Radial	11R22.5 (G)	G159A
	Radial	295/75R22.5 (G)	G159A
	Radial (wide-base)	425/65R22.5 (J)	G286
	Radial (wide-base)	385/65R22.5 (J)[2]	G178
TxDOT Project 0-4361	Radial	11R24.5 (G)	G159A
	Radial	215/75R17.5 (H)	G114

[1] All tires made by Goodyear
[2] Lug tire for off-road hauling

Figure 2.1. Heavy Vehicle Simulator Used for Tire Testing (de Beer and Fisher, 2002).

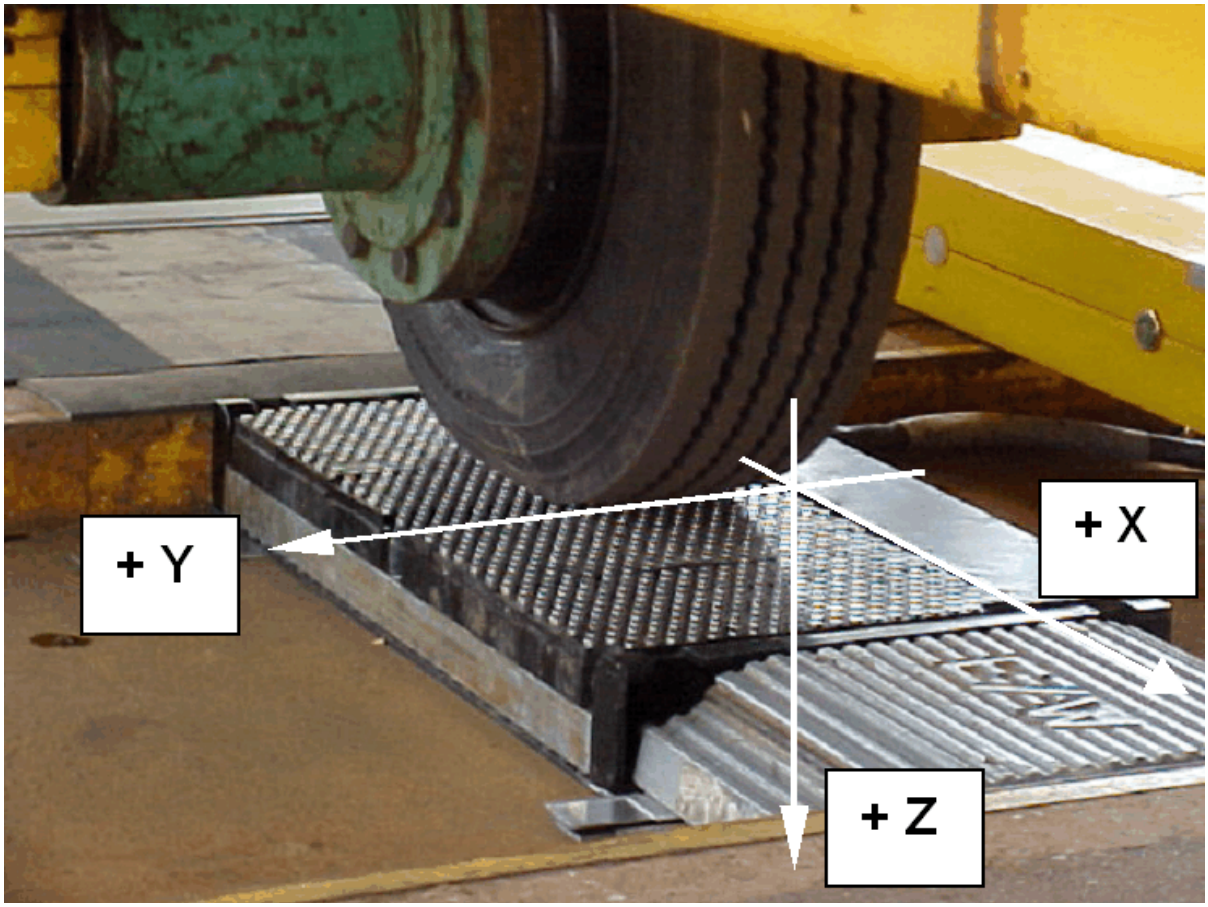

Figure 2.2. Picture of Tire Test with SIM Pad under Heavy Vehicle Simulator (de Beer and Fisher, 2002).

used in the UCB tests, resulting in data with higher resolution and better repeatability. In addition, the SIM Mk IV has one more load pin in the test pad, for a total of 21, compared to the 20 load pins in the earlier model. Table 2.2 provides information on the test parameters for the SIM pads used in the UCB and TxDOT projects.

Figure 2.2 is a snapshot taken of the 215/75R17.5 radial tire as it rolled along the SIM pad during a measurement. For testing, the SIM pad is placed inside a pit underneath the HVS. The pad is about 33 inches long by 18.5 inches wide. Triaxial load pins located transversely across the pad (along the y-axis shown in Figure 2.2) measure simultaneously the *x*, *y* and *z* forces across the tire patch as the tire rolls along the pins. Figure 2.2 shows the sign convention used for the measurements conducted in this project. The origin of the *x*, *y* and *z* coordinate system shown in this figure corresponds to pin 1 of the SIM pad. Twenty-one pins, spaced at 0.67-inch intervals are located along the pad's mid-section. Each pin

Table 2.2 Test Parameters for the TTI and UCB Studies.

Test Variable	TTI Study	UCB Study
Measuring instrument used	Stress-in-Motion (SIM) Mk IV system	Vehicle-Road Surface Pressure Transducer Array (SIM Mk II)
Test vehicle	Heavy Vehicle Simulator (HVS Mk III)	Heavy Vehicle Simulator (Cal-HVS 1)
Number of load pins	21	20
Approximate test speed (fps)	1.148	1.066
Sampling frequency (Hz)	1001	150
Distance between consecutive rows of data (inches)	0.0138	0.0853
Center-to-center distance between pins (inches)	0.6693	0.6693
Diameter of pin (inches)	0.3819	0.3819
Effective diamond shaped area covered by each pin (in^2)	0.3879	0.3879

covers an effective diamond-shaped area of about 0.39 in^2. This geometry is used to convert the measured *x*, *y* and *z* load components into corresponding average contact stresses over the effective area (de Beer and Fisher, 1997). Surrounding the load pins are about 1041 non-instrumented pins used to support the tire on the pad. According to de Beer et al. (1999), the friction characteristics of the pad surface made up of these pins approximate that of a typical dry asphalt concrete pavement surface.

During a test, the operator sets the HVS to apply the specified load on the tire for a given run and to move the tire across the SIM pad at the prescribed test speed and direction. For this project, CSIR staff took measurements with the test tire rolling in the same direction at a speed of about 1.1 ft/sec for all runs. A static scale positioned in line with the SIM pad within the test pit (Figure 2.2) provided for load control of the HVS during testing. Specifically, CSIR personnel adjusted the pressure in the hydraulic system of the HVS such that the total load determined from the SIM measurements was within ±5 percent of the

target load as measured from the static scale (de Beer and Fisher, 2002). Data satisfying this criterion were accepted. Otherwise, CSIR repeated the given test sequence.

The SIM Mk IV system also incorporates acoustic and laser sensors housed within two yellow beams (Figure 2.3) positioned alongside the test pit parallel to the direction of the test tire. The acoustic sensor initializes the system as the tire enters the active zone while the two lasers measure the speed of the tire as it crosses the SIM pad. For the tests made in this project, the coefficient of variation of the speed measurements is within ±1 percent.

Tables 2.3 and 2.4 show, respectively, the test matrices for the 11R24.5 and 215/75R17.5 radial tires. To establish the combinations of tire load and tire inflation pressure at which to collect tire contact stress measurements, researchers reviewed the manufacturer's recommendations on tire loads for various levels of cold inflation pressures. Figures 2.4 and 2.5 show the manufacturer's recommended tire loads at various cold inflation pressures for the tires tested in this project. The figures show the recommended tire loads for both single and dual tire configurations. Also shown in these figures are the combinations of tire load and tire inflation pressure selected for testing. As shown, the test matrices cover the recommended tire load/tire inflation curves for each tire.

In addition to the measurement of contact stresses, a tire imprint was taken for each combination of tire load and tire inflation pressure included in the test plan. Figure 2.6 illustrates the methodology used for taking these imprints. In this procedure, blackboard paint was applied on the surface of the test tire. It was then lowered to a white paper placed on top of a steel plate and loaded through the HVS. Researchers used the tire imprints to determine relationships between tire contact area, tire load and tire inflation pressure for the different tires considered in this project.

DATA BASE OF TIRE CONTACT PRESSURES

To support the comparative evaluation of predicted pavement response under assumptions of uniform versus non-uniform loading, and the development of a methodology for estimating tire contact pressures, researchers assembled a data base of tire contact stresses using test data collected from the UCB study and this project. This data base covers measurements of longitudinal, lateral and vertical contact stresses for the following tire sizes listed in Table 2.1:

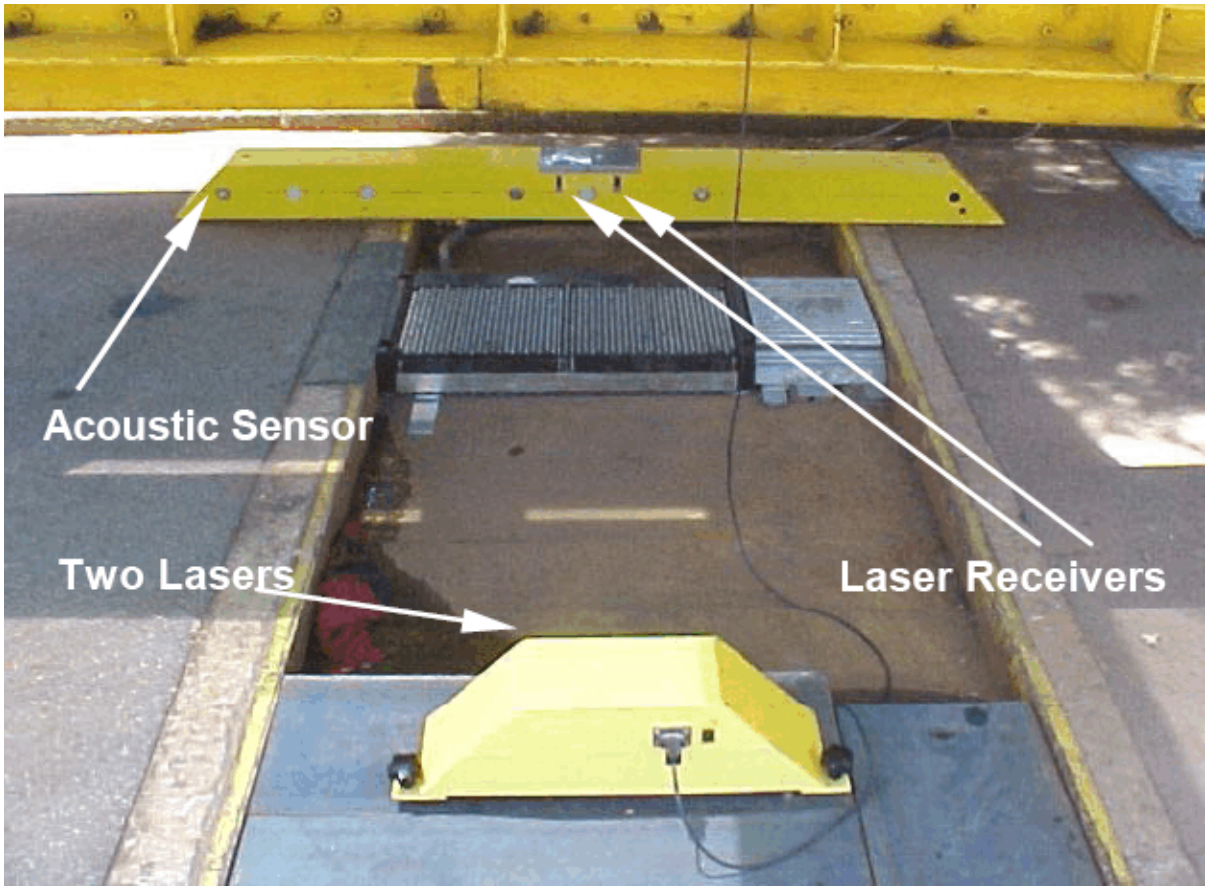

Figure 2.3. Acoustic and Laser Sensor Boxes Used with SIM Mk IV System (de Beer and Fisher, 2002).

Table 2.3. Tire Load and Inflation Pressure Combinations for Testing 11R24.5 Tire.

Tire load (lb)	Tire inflation pressure (psi)				
	70	85	100	115	130
4600	✓	✓	✓	✓	✓
5400	✓	✓	✓	✓	✓
6200	✓	✓	✓	✓	✓
7000	✓	✓	✓	✓	✓
7800	✓	✓	✓	✓	✓

Table 2.4. Tire Load and Inflation Pressure Combinations for Testing 215/75R17.5 Tire.

Tire load (lb)	Tire inflation pressure (psi)				
	85	100	115	130	145
3000	✓	✓	✓	✓	✓
4000	✓	✓	✓	✓	✓
5000	✓	✓	✓	✓	✓
6000	✓	✓	✓	✓	✓
7000	✓	✓	✓	✓	✓

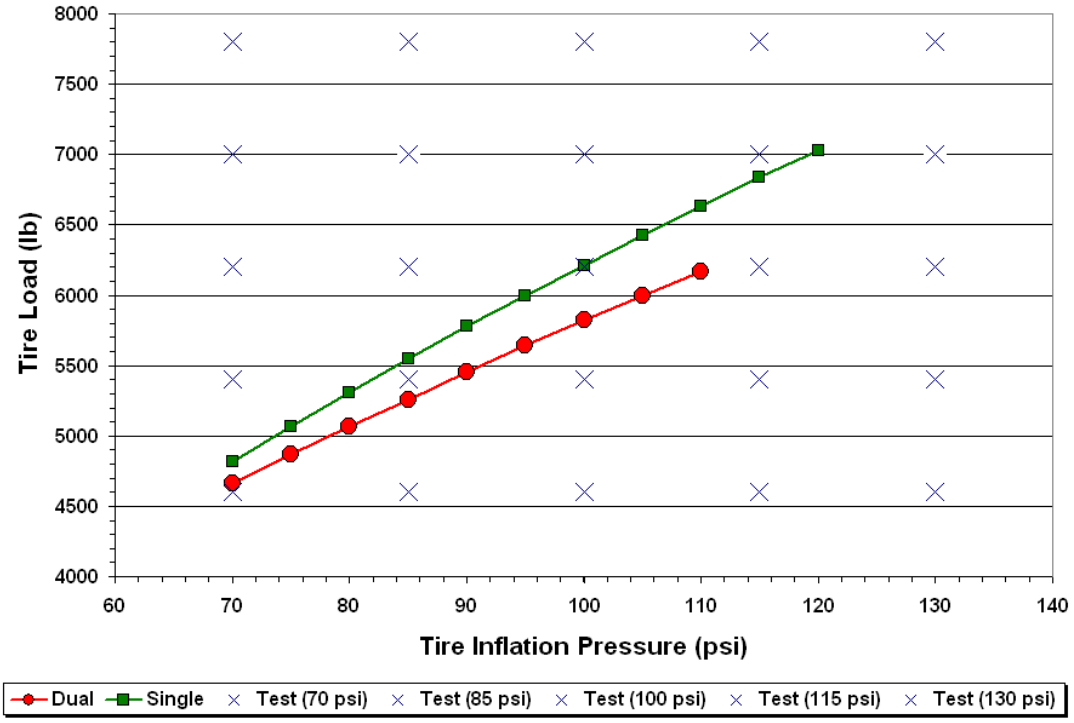

Figure 2.4. Recommended Tire Loads at Various Tire Inflation Pressures for 11R24.5 Radial Truck Tire.

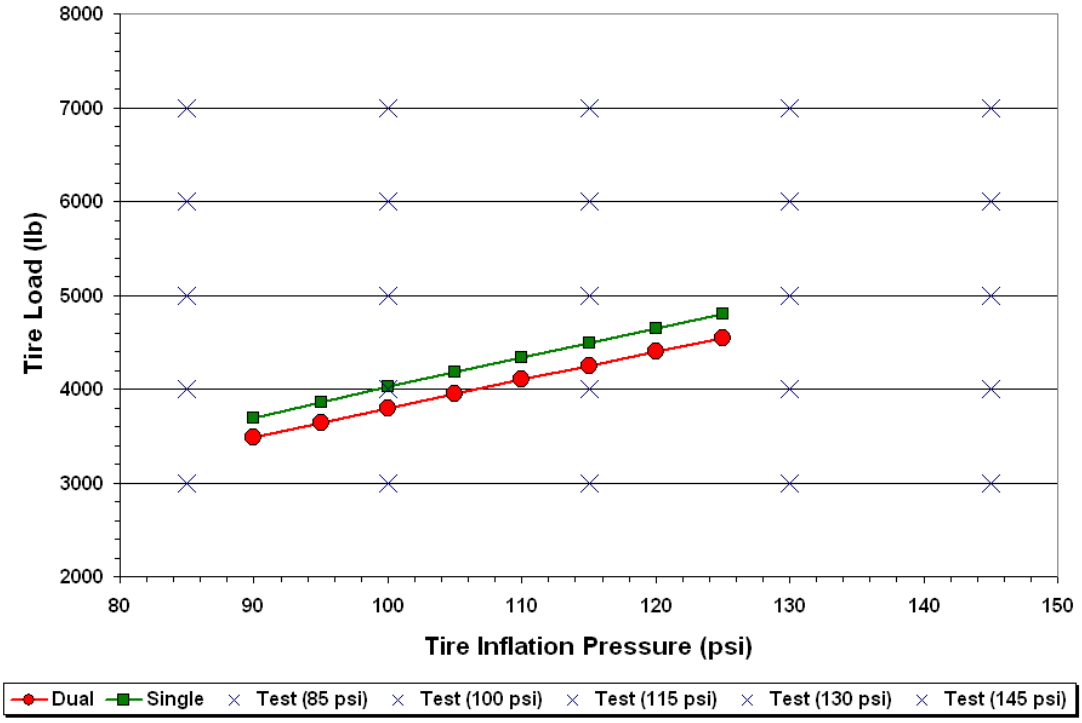

Figure 2.5. Recommended Tire Loads at Various Tire Inflation Pressures for the 215/75R17.5 Radial Truck Tire.

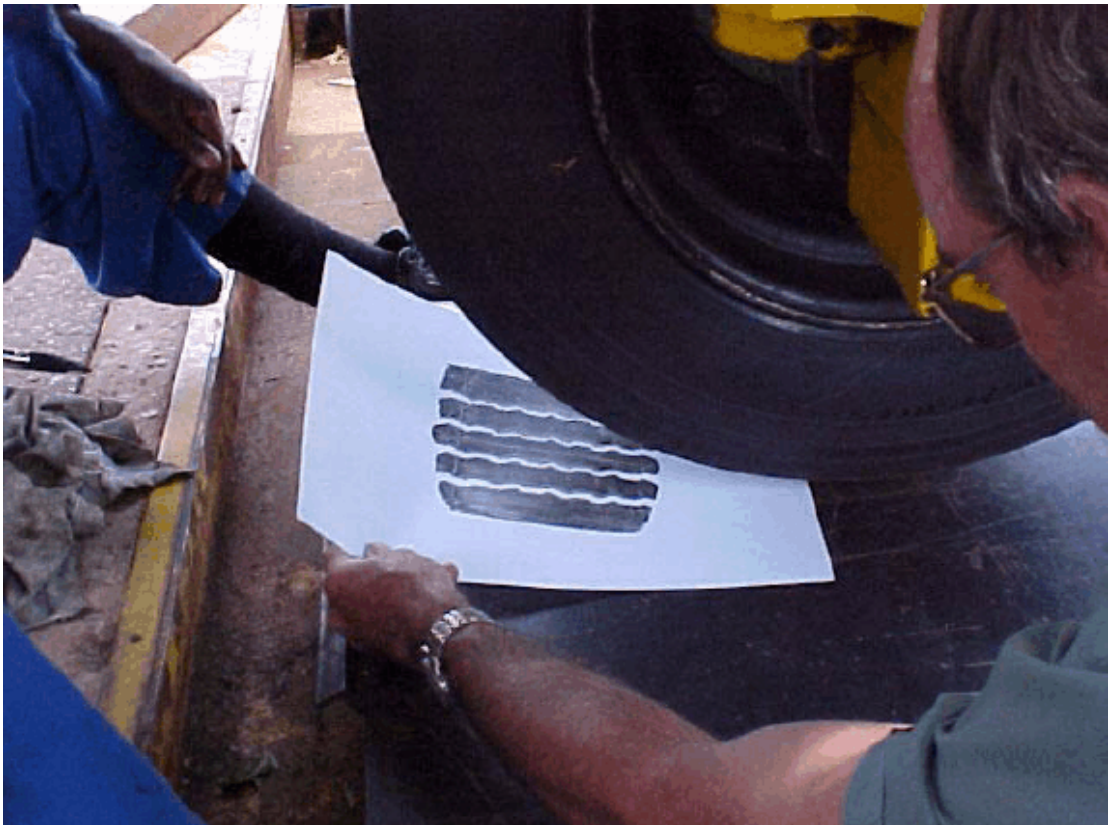

Figure 2.6. Illustration of Tire Imprint from Tire Testing.

- 11R24.5 radial,
- 215/75R17.5 radial,
- 295/75R22.5 radial,
- 11R22.5 radial,
- 425/65R22.5 wide-base radial, and
- 10.00 × 20 bias-ply.

With the concurrence of the project director, researchers omitted the 385/65R22.5 wide-base radial tire from the data base since it is primarily used for off-road hauling. Tables 2.3 to 2.7 show the combinations of tire load and tire inflation pressure at which contact stress measurements were compiled into the data base. This data base is used in an interpolation procedure researchers developed to predict tire contact stresses for other combinations of tire load and tire inflation pressure not included in the UCB and TTI tests. As part of developing this data base, researchers examined the repeatability of tire contact measurements from the tests conducted. The results from this evaluation are presented in the next chapter.

Table 2.5. Tire Load and Inflation Pressure Combinations at which Measured Contact Stresses for the 295/75R22.5 Tire are Available in the Data Base.

Tire load (lb)	Tire inflation pressure (psi)			
	61	75	100	119
5860	✓	✓	✓	✓
6980	✓	✓	✓	✓
8110	✓	✓	✓	✓
9240	✓	✓	✓	✓

Table 2.6. Tire Load and Inflation Pressure Combinations at which Measured Contact Stresses for the 11R22.5 Radial and 10 × 20 Bias-Ply Tires are Available in the Data Base.

Tire load (lb)	Tire inflation pressure (psi)							
	32	61	75	90	100	104	119	133
5860	✓	✓	✓	✓	✓	✓	✓	✓
6980	✓	✓	✓	✓	✓	✓	✓	✓
8110	✓	✓	✓	✓	✓	✓	✓	✓
9240		✓	✓	✓	✓	✓	✓	✓
10,360		✓	✓	✓	✓	✓	✓	✓
11,490			✓	✓	✓	✓	✓	✓
12,620			✓	✓	✓	✓	✓	✓

Table 2.7. Tire Load and Inflation Pressure Combinations at which Measured Contact Stresses for the 425/65R22.5 Wide-Base Radial Tire are Available in the Data Base.

Tire load (lb)	Tire inflation pressure (psi)			
	73	102	131	145
5860	✓	✓	✓	✓
10,360	✓	✓	✓	✓
12,610	✓	✓	✓	✓
14,870	✓	✓	✓	✓
19,370		✓	✓	✓
23,880		✓	✓	✓

CHAPTER III. REPEATABILITY OF MEASURED TIRE CONTACT FORCES

INTRODUCTION

During the tests conducted in this project, a static scale was used to control the HVS load on the SIM pad. As a check, CSIR staff integrated the measured vertical tire contact forces from the triaxial load pins and compared the calculated load to the corresponding value from the static scale for a given test. Data that gave a difference within ±5 percent of the target load were deemed acceptable and data that fell outside this range led to a retest. This verification provided an indication that the magnitudes of the measured tire contact forces are good and valid.

To provide additional verification of the data, researchers examined the repeatability of the measurements from the tests conducted in this project and the CALTRANS study reported by de Beer and Fisher (1997). Figures 3.1 to 3.6 illustrate the repeatability of data from tests conducted on the 11R24.5 and 215/75R17.5 radial tires for the combinations of tire load and inflation pressure noted in the figures. The longitudinal axis in each figure refers to the record number for a given set of measurements collected from the row of 21 triaxial load pins positioned laterally across the SIM pad. The distance between records is 0.0138 inches as given in Table 2.2.

It is observed that the patterns in the data show good repeatability. A factor contributing to this repeatability is the consistency in the positioning of the tires for the tests conducted in this project. As shown in Figure 3.7, marks were placed on the tire and on the ground to ensure that the tire rolled over the SIM pad the same way from run to run (in terms of having measurements taken as close as possible over the same contact area). To quantify the repeatability of the measurements, researchers conducted pairwise comparisons of the tire contact stress distributions and evaluated the correlations and the point-to-point differences between measurements from repeat runs. The following statistics were computed to assess the repeatability of the data:

- the correlation coefficient between tire contact stress distributions for each pair of repeat runs, and
- the average of the point-to-point absolute differences of measured tire contact forces for the given pair.

The findings from this evaluation are presented in the following.

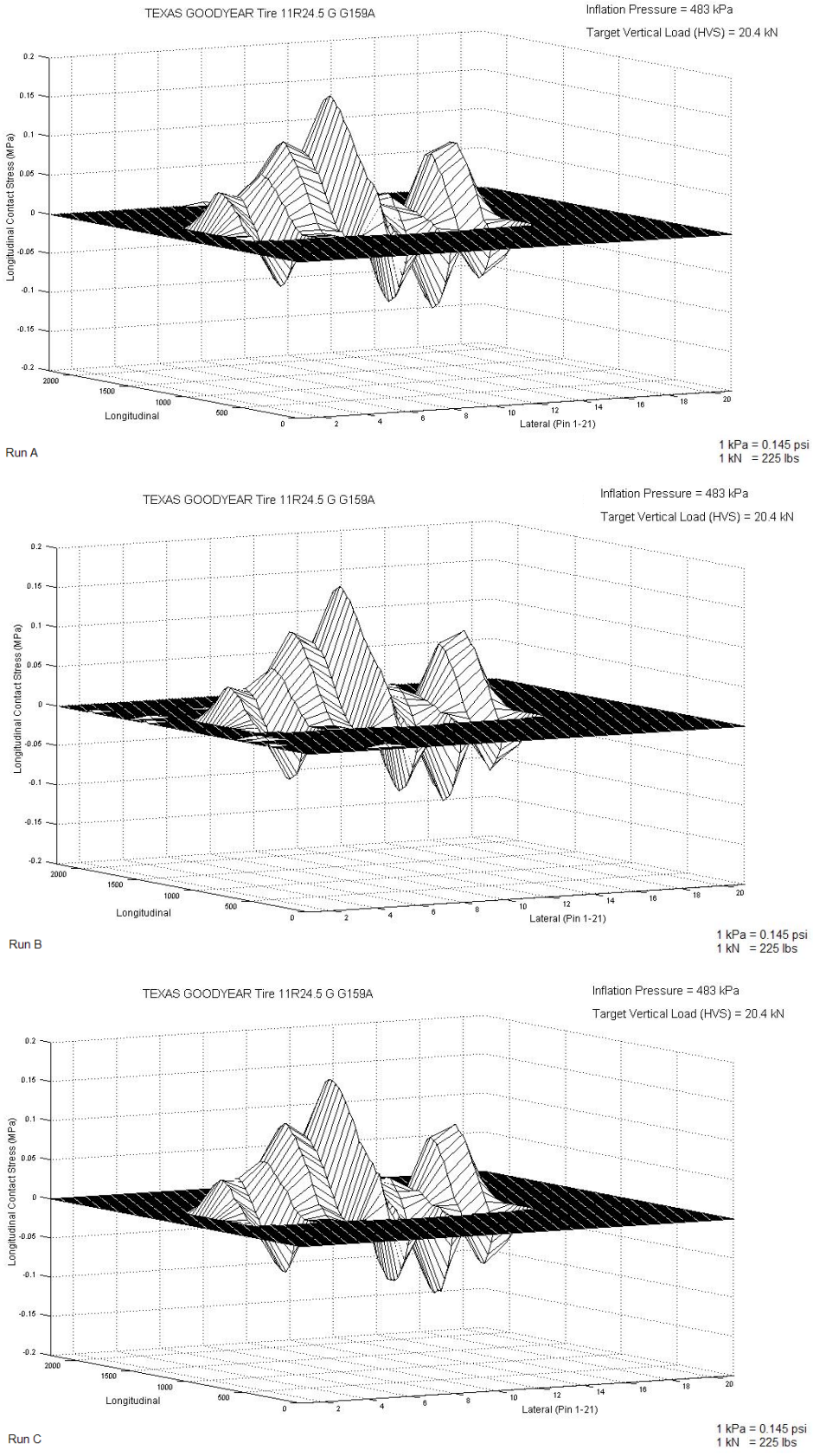

Figure 3.1. Repeat Measurements of Longitudinal Tire Contact Stresses for 11R24.5 Radial Tire (4600 lb Tire Load and 70 psi Tire Inflation Pressure).

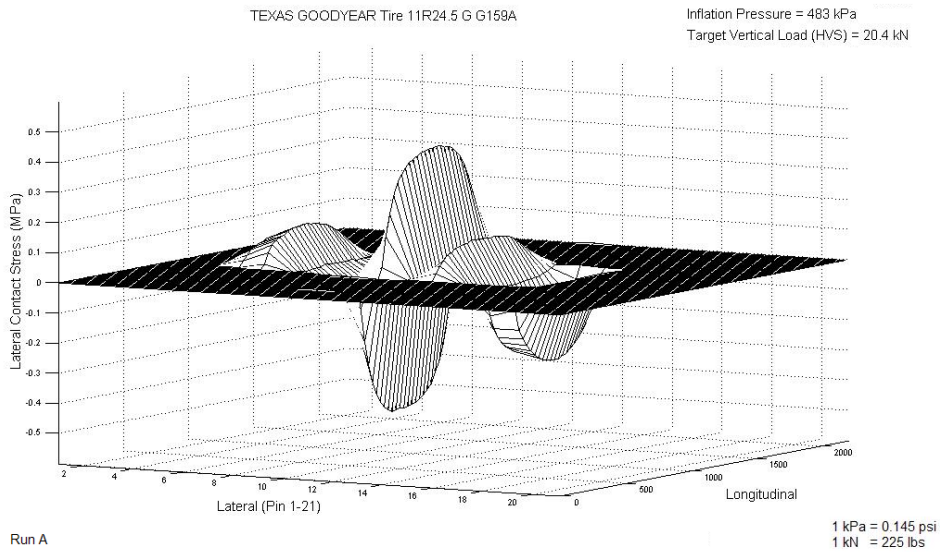

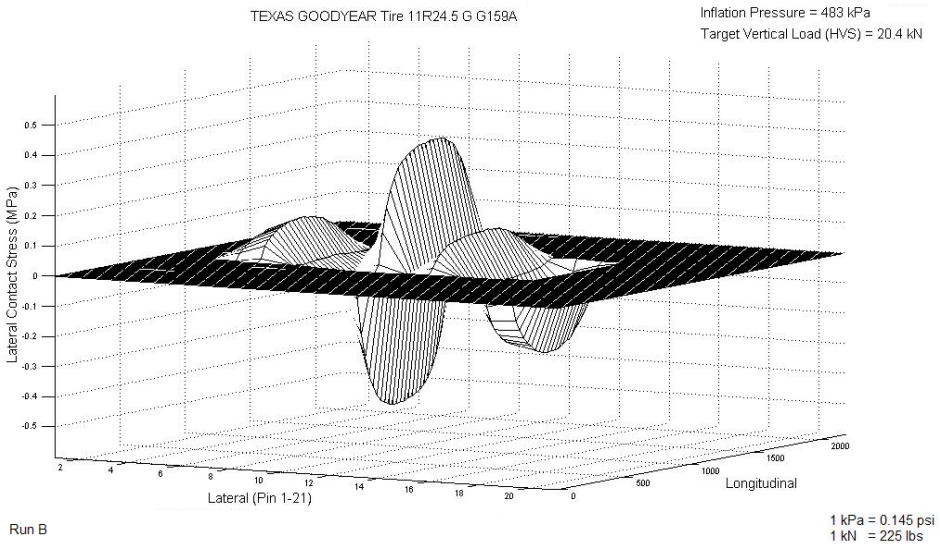

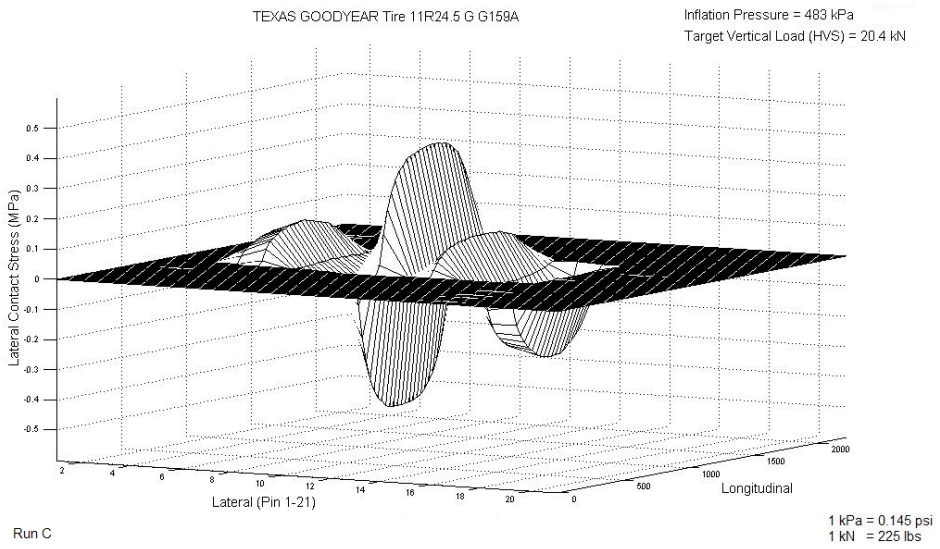

Figure 3.2. Repeat Measurements of Lateral Tire Contact Stresses for 11R24.5 Radial Tire (4600 lb Tire Load and 70 psi Tire Inflation Pressure).

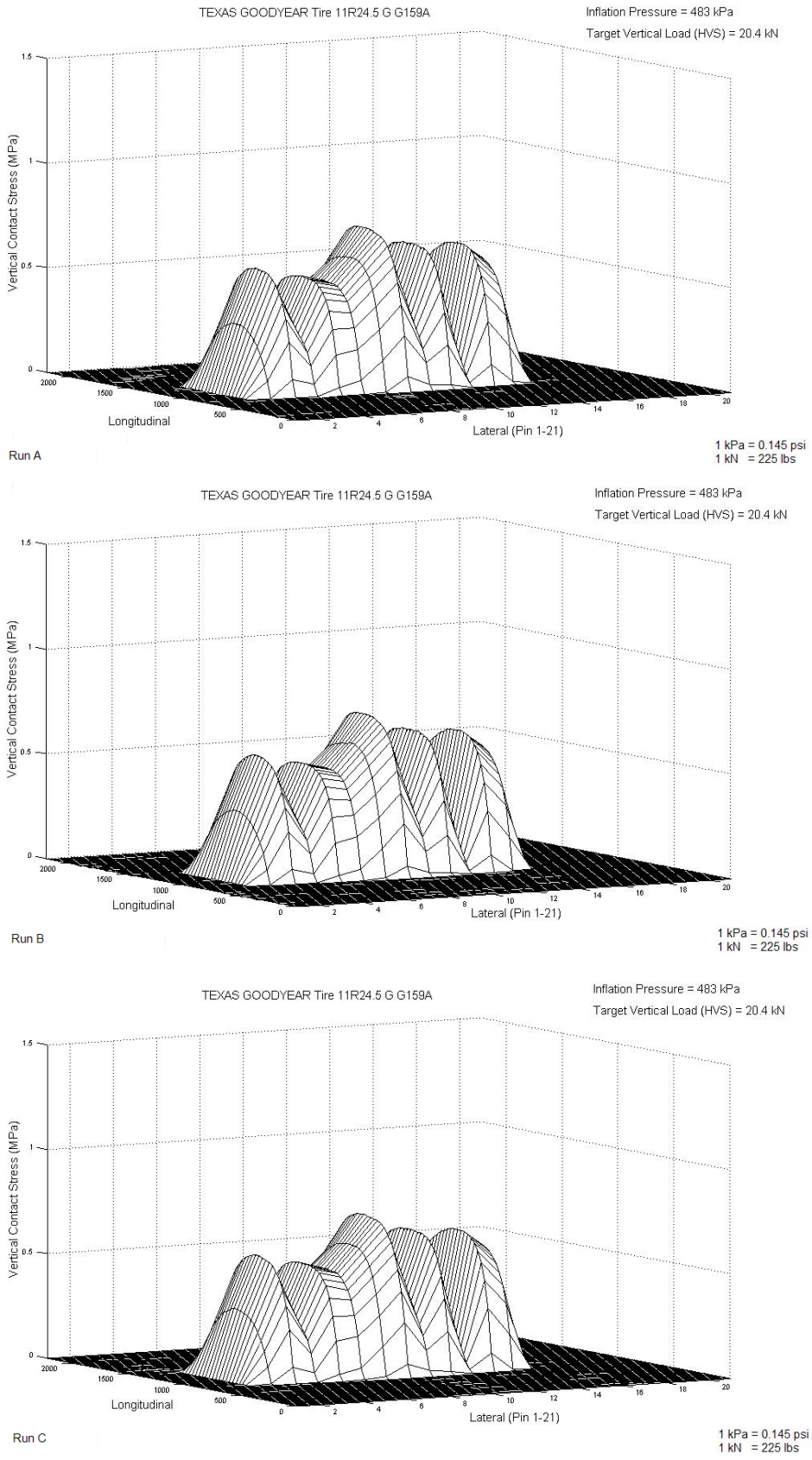

Figure 3.3. Repeat Measurements of Vertical Tire Contact Stresses for 11R24.5 Radial Tire (4600 lb Tire Load and 70 psi Tire Inflation Pressure).

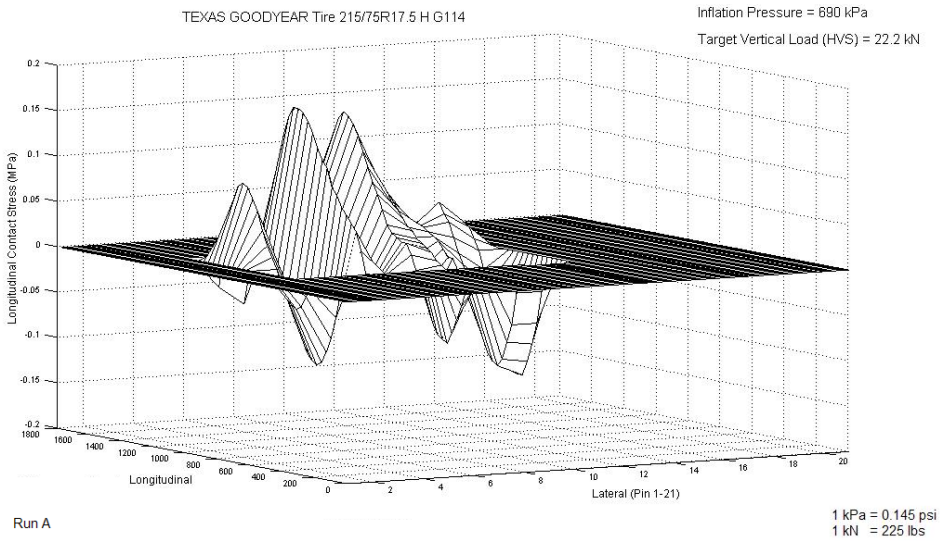

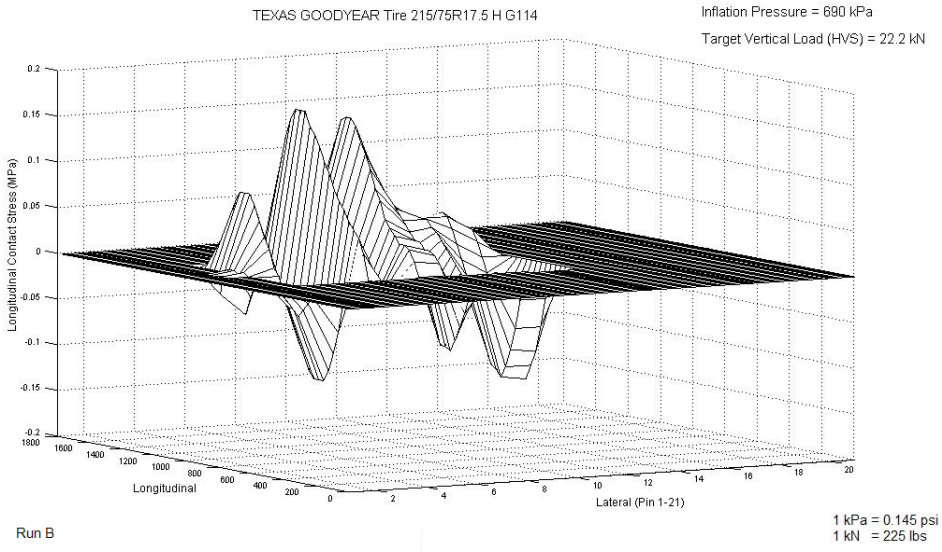

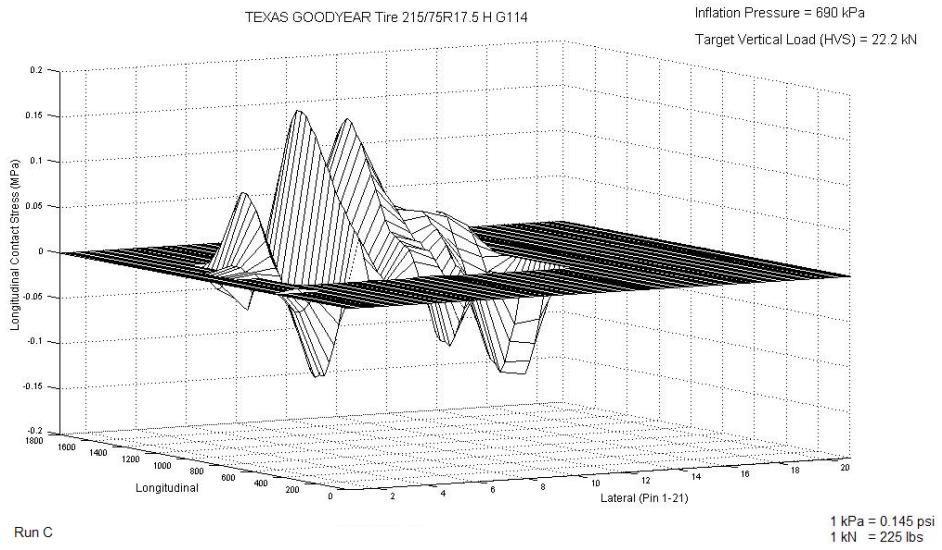

Figure 3.4. Repeat Measurements of Longitudinal Tire Contact Stresses for 215/75R17.5 Radial Tire (5000 lb Tire Load and 100 psi Tire Inflation Pressure).

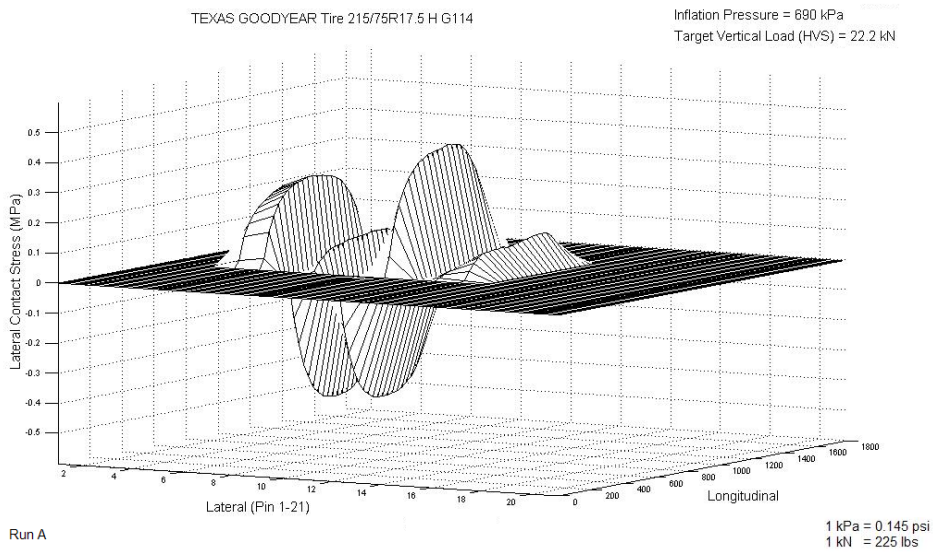

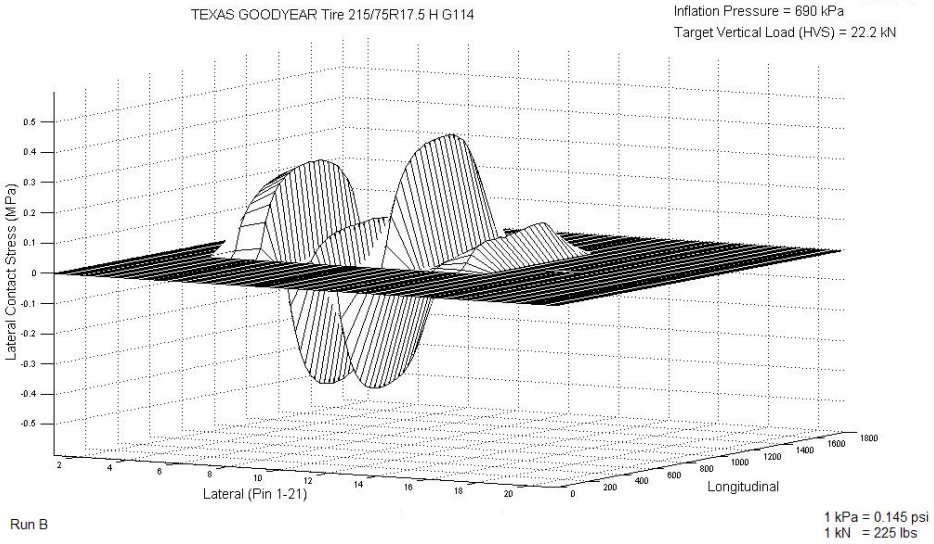

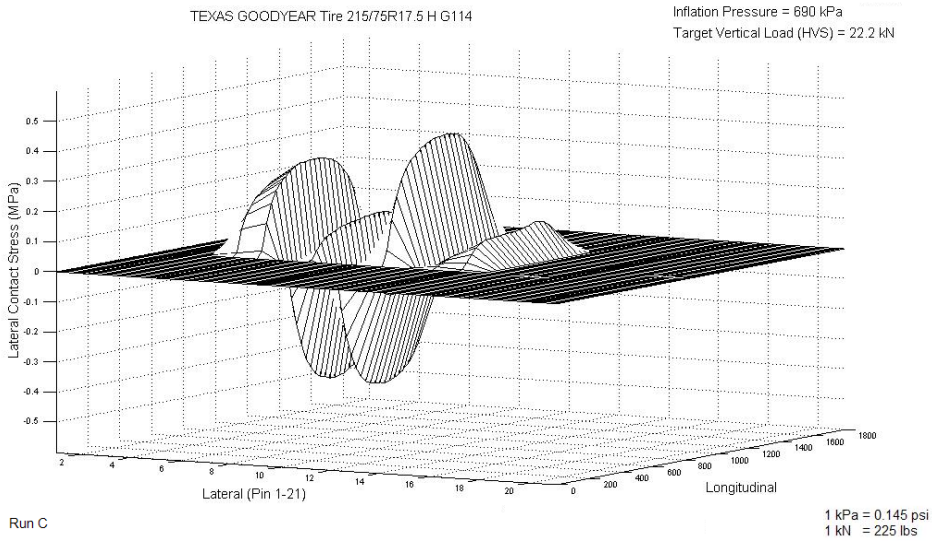

Figure 3.5. Repeat Measurements of Lateral Tire Contact Stresses for 215/75R17.5 Radial Tire (5000 lb Tire Load and 100 psi Tire Inflation Pressure).

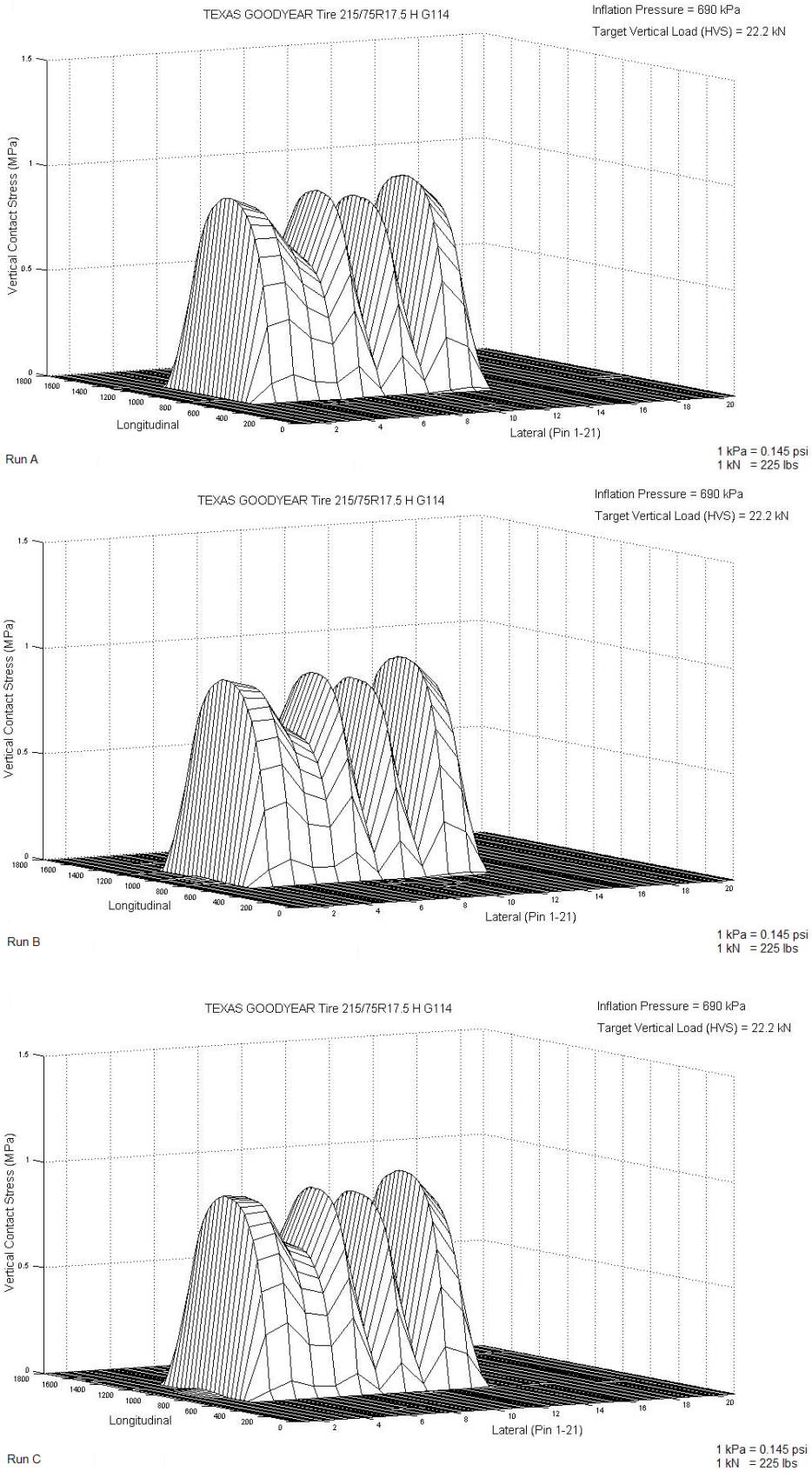

Figure 3.6. Repeat Measurements of Vertical Tire Contact Stresses for 215/75R17.5 Radial Tire (5000 lb Tire Load and 100 psi Tire Inflation Pressure).

Figure 3.7. Marks Used to Position Tire for a Test Run.

ASSESSMENT OF DATA REPEATABILITY

Researchers performed a few operations on the data files prior to evaluating the repeatability of tire contact stress measurements from repeat runs. The sequence of operations to prepare data files for processing involves the following steps:

- Following de Beer and Fisher (1997), researchers applied a 3 N cutoff filter to remove any noise from the data. Thus, measurements from load pins with magnitudes of 3 N (0.675 lb) or less were zeroed out.
- Columns and rows of zeros in the data files were then removed. Columns of zeros result when the tire does not touch one or more of the triaxial load pins on the SIM pad, indicating that the data are outside of the tire contact area.

Likewise, rows of zeros occur as data recording is triggered some distance away from the SIM pad and terminated when the tire is completely off the pad.

- Researchers subsequently lined up the data from repeat runs using the first non-zero row of each file. In view of the consistency (noted earlier) by which tires were positioned prior to a given run, the automatic initialization of the instrumented pins on the SIM pad, and the fixed path of the test tire (i.e., no wheel wander), researchers observed that the data from repeat runs generally lined up on the first non-zero row of each file. This last step defined a common data block to evaluate the repeatability of a given set of replicate runs.

Following the above procedure, researchers generated three data files representing three repeat runs, A, B and C, for each tire tested at a given tire load and tire inflation pressure. Pairwise comparisons of the data files (AB, BC and AC) were conducted to evaluate repeatability based on the correlation between corresponding pairs of measurements and the average of the point-to-point absolute differences of measured tire contact forces for the given pair. Figures 3.8 to 3.13 show the distributions of the correlation coefficients from all pairwise comparisons made for each tire. These comparisons were done on data collected for each of the three stress directions, *x*, *y* and *z*.

For any given chart, the height of each bar shows the number of correlation coefficients falling within the range defined by the previous and current limits. In Figure 3.8 for example, the distribution of correlation coefficients based on repeat measurements in the z-direction shows six correlation coefficients falling within the 0.94 and 0.95 range. A vertical bar plotted at the lower limit of each chart shows the number of correlation coefficients that are less than or equal to that limit. Thus, in Figure 3.10, the distribution of correlation coefficients based on repeat measurements in the z-direction show five correlation coefficients that are less than or equal to 0.91.

The correlation coefficient ranges from -1 to +1 with -1 indicating a perfect inverse relationship between the given data pair and +1 indicating a perfect positive relationship. From the results shown in Figures 3.8 to 3.13, the following observations are noted:

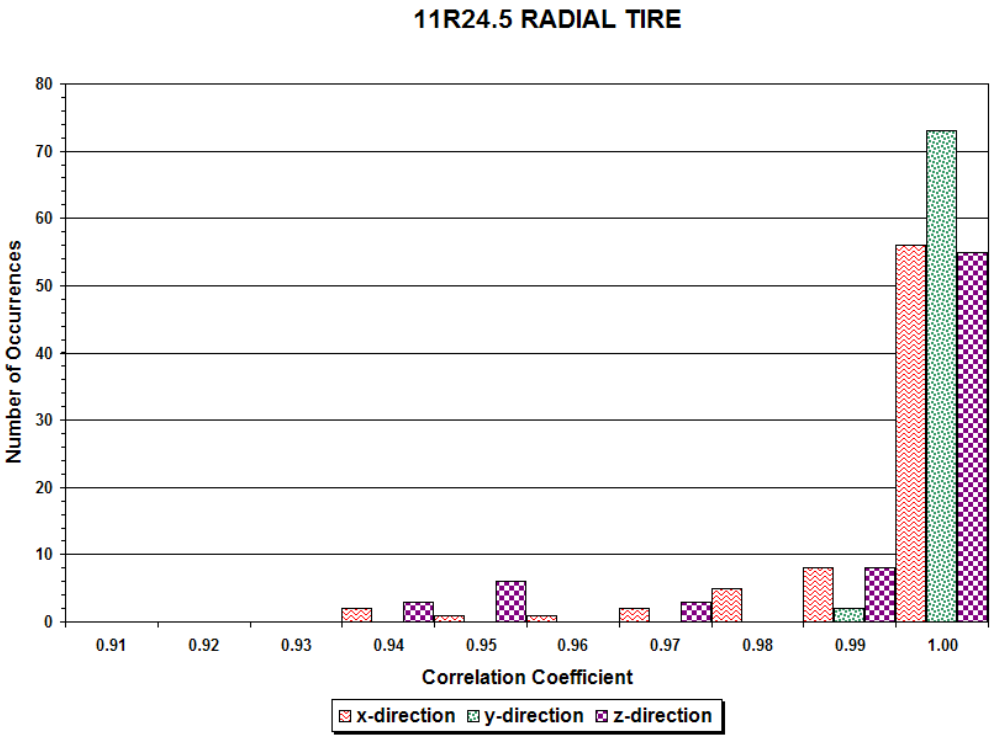

Figure 3.8. Distributions of Correlation Coefficients Determined from Pairwise Comparisons of Test Data on 11R24.5 Radial Tire.

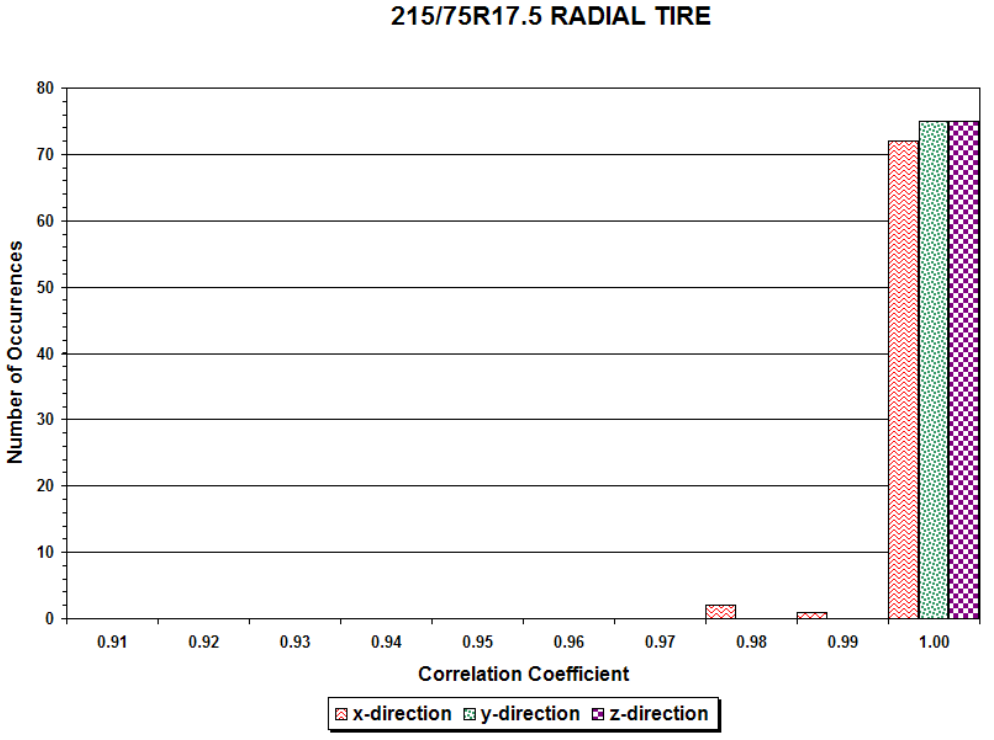

Figure 3.9. Distributions of Correlation Coefficients Determined from Pairwise Comparisons of Test Data on 215/75R17.5 Radial Tire.

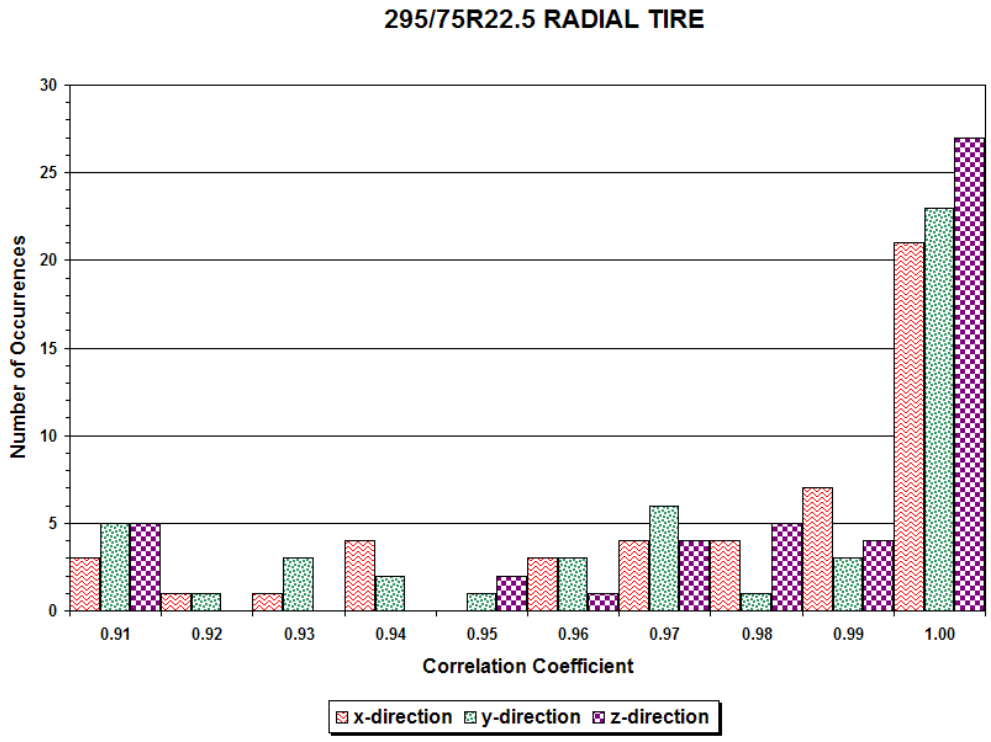

Figure 3.10. Distributions of Correlation Coefficients Determined from Pairwise Comparisons of Test Data on 295/75R22.5 Radial Tire.

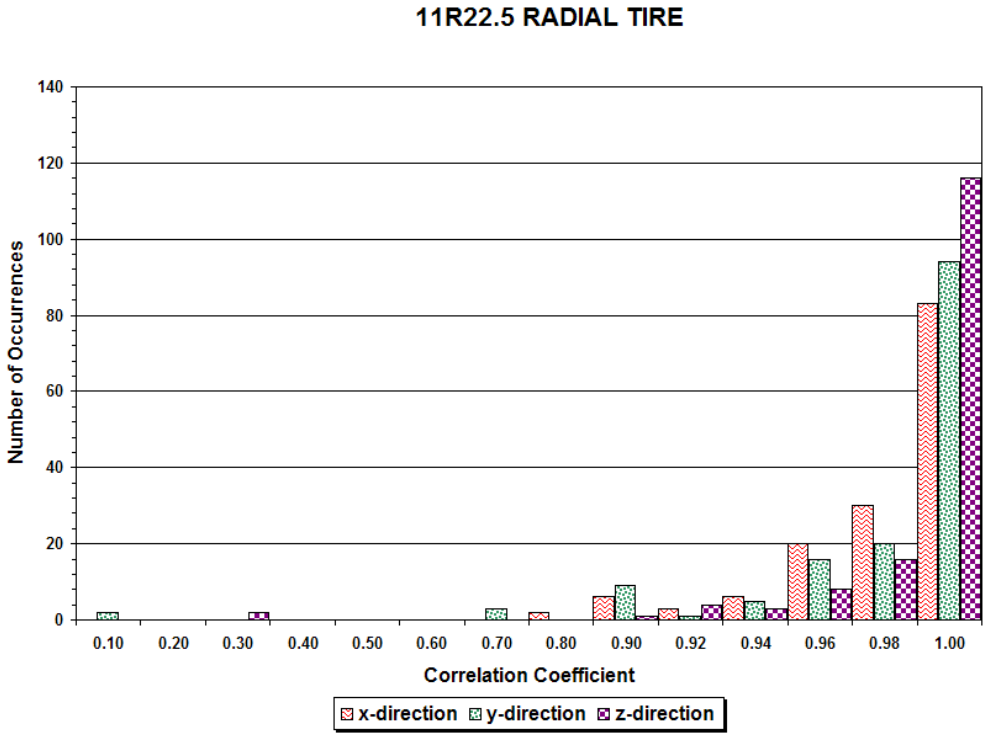

Figure 3.11. Distributions of Correlation Coefficients Determined from Pairwise Comparisons of Test Data on 11R22.5 Radial Tire.

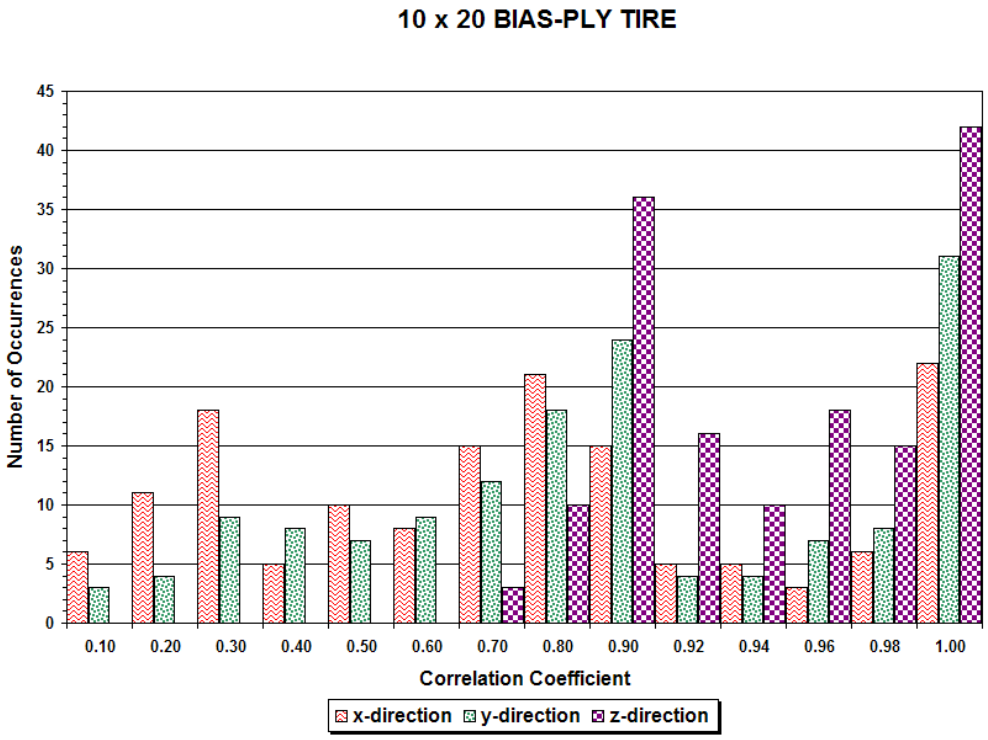

Figure 3.12. Distributions of Correlation Coefficients Determined from Pairwise Comparisons of Test Data on 10 × 20 Bias-Ply Tire.

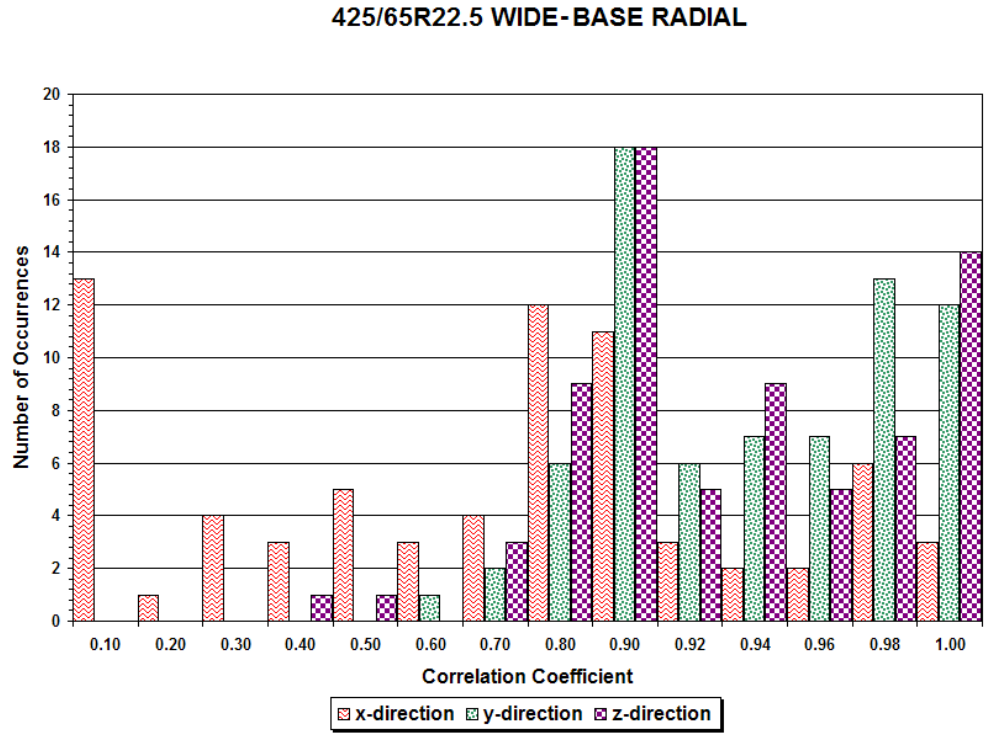

Figure 3.13. Distributions of Correlation Coefficients Determined from Pairwise Comparisons of Test Data on 425/65R22.5 Wide-Base Radial Tire.

- The correlation coefficients determined from pairwise comparisons of the data collected in this project are all higher than 93 percent. In fact, many of the observations fall within 99 and 100 percent, particularly for the 215/75R17.5 radial tire. The high correlation coefficients indicate a high degree of similarity in the replicate measurements made on the 11R24.5 and the 215/75R17.5 radial tires tested in this project.
- In general, the correlation coefficients from pairwise comparisons of repeat measurements on the 295/75R22.5 tire are higher than 90 percent. There is only one combination of tire load and tire inflation pressure at which lower correlation coefficients were obtained, i.e., at the 100 psi tire inflation pressure and 6980 lb tire load. At this combination of the test variables, correlation coefficients higher than 93 percent were obtained only from pairwise comparisons of data from runs A and B. Comparisons of data from run C with corresponding data from run A or run B showed lower correlation coefficients, ranging from 52 to 91 percent, indicating that run C is somewhat different from runs A and B for this combination of the test variables.
- For the 11R22.5 radial tire, most replicate runs give correlation coefficients higher than 90 percent. However, coefficients below this value were obtained for the following combinations of tire load and tire inflation pressure:
  - 5860 lb and 104 psi,
  - 6980 lb and 119 psi, and
  - 9240 lb and 119 psi.

  Pairwise comparisons of replicate measurements made in the *x*, *y* and *z* directions for the above combinations of the test variables show runs B and C to be the most correlated, with correlation coefficients ranging from 92 to almost 100 percent. Thus, while not all replicate measurements showed a level of correlation above 90 percent, for the few cases where lower correlation coefficients were obtained, researchers found a pair of replicates that are highly correlated, similar to the finding presented previously for the 295/75R22.5 radial tire.
- Of the tires tested in the CALTRANS project, the bias-ply and wide-base radial tires have relatively more replicates that exhibited correlation coefficients below

90 percent, particularly for stress measurements in the *x* (longitudinal) and *y* (lateral) directions. For these tires, there are a few cases (representing various combinations of tire load and tire inflation pressure) at which no correlation coefficients above 70 percent were determined from among the possible pairwise comparisons of replicate measurements made in the *x* and *y* directions. These cases are identified later in this chapter.

While a pair of replicate runs may be highly correlated, this characteristic, by itself, is not necessarily a good indicator of the repeatability of the measurements. Consider, for example, the hypothetical data shown in Figures 3.14a and 3.14b. The trends of the data are alike, but the magnitudes are different. For the data shown, the correlation coefficient between each corresponding pair of data sets is 100 percent. Thus, while data might be perfectly correlated, as given in this example, the high level of correlation simply indicates the agreement in the trends or patterns exhibited by the corresponding data series. To check the agreement in the magnitudes of measured contact stresses between replicate runs, researchers computed the point-to-point absolute differences of corresponding replicate measurements, and used the average of the absolute differences (μ) as an indicator of the agreement in the magnitudes of the measured contact stresses. In the extreme, if a pair of replicate runs showed an average absolute difference of zero, the contact stress distributions from the two runs would be identical and the repeatability perfect.

Figures 3.15 to 3.20 show the distributions of the averages of absolute differences determined from pairwise comparisons of repeat runs made on the tires tested in the TxDOT and CALTRANS projects. In the analysis, the absolute difference in the triaxial load pin readings at a given position within the tire contact area was determined point-by-point. Researchers then computed the average of the absolute differences over all points within the tire contact area for a given pair of repeat runs. The distributions of these averages for the three stress directions are plotted in Figures 3.15 to 3.20. From these figures, the following observations are noted:

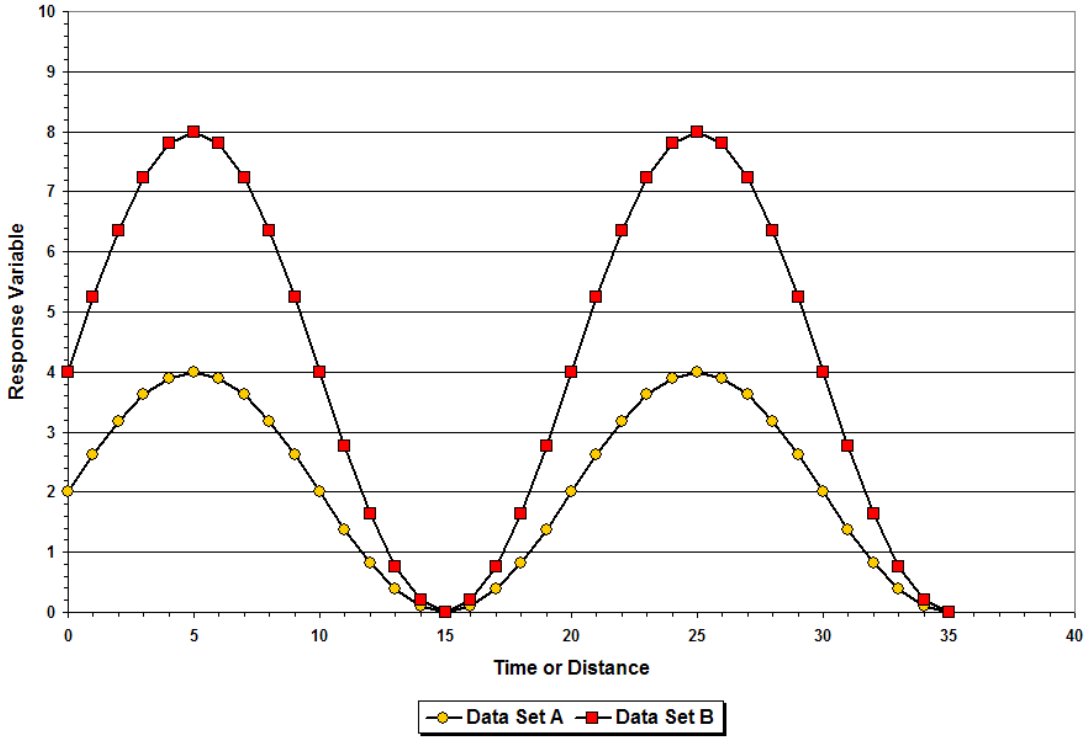

(a)

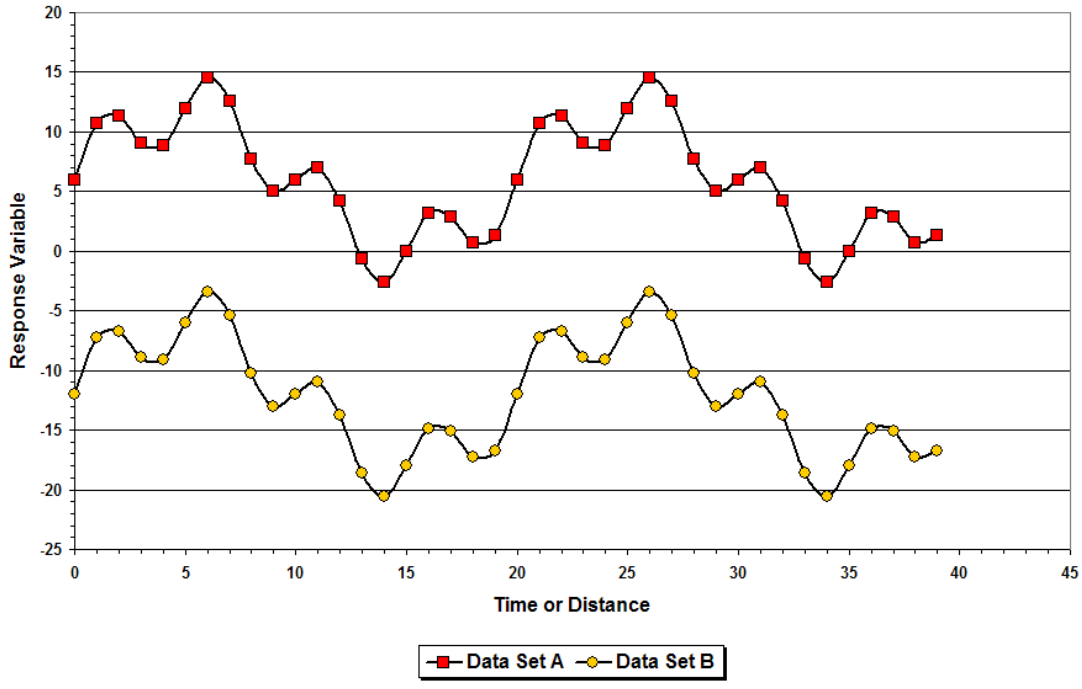

(b)

Figure 3.14. Examples of Data with 100 Percent Correlation but Differ in Magnitudes.

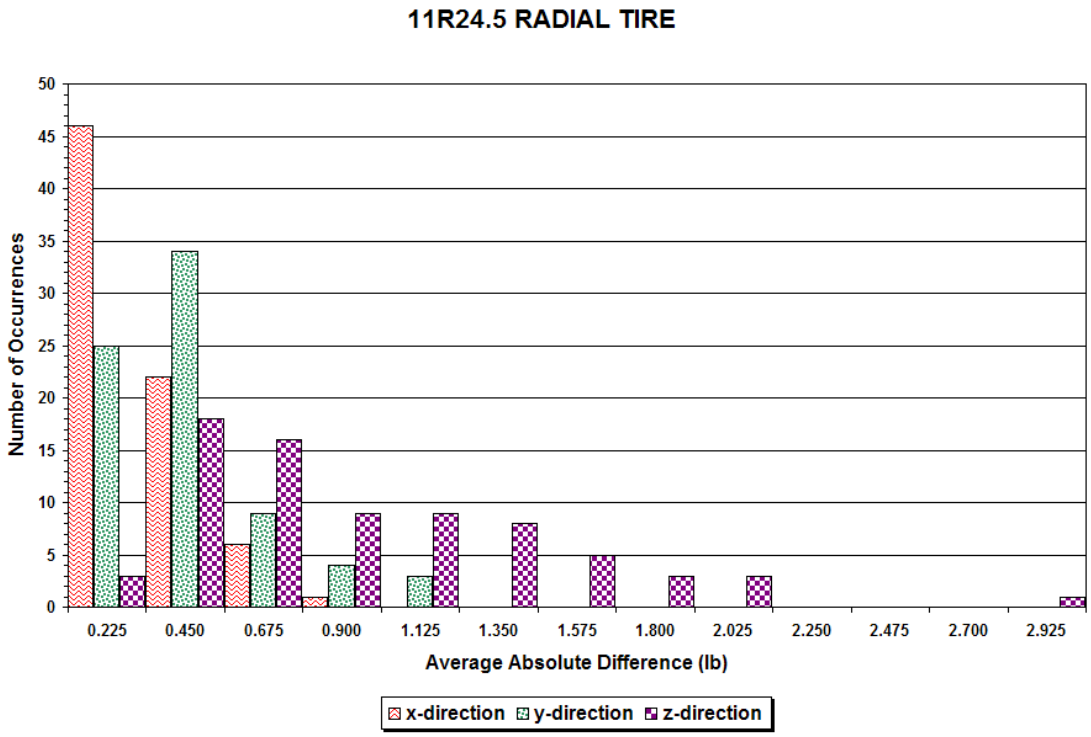

Figure 3.15. Distributions of Averages of Absolute Differences Determined from Pairwise Comparisons of Test Data on 11R24.5 Radial Tire.

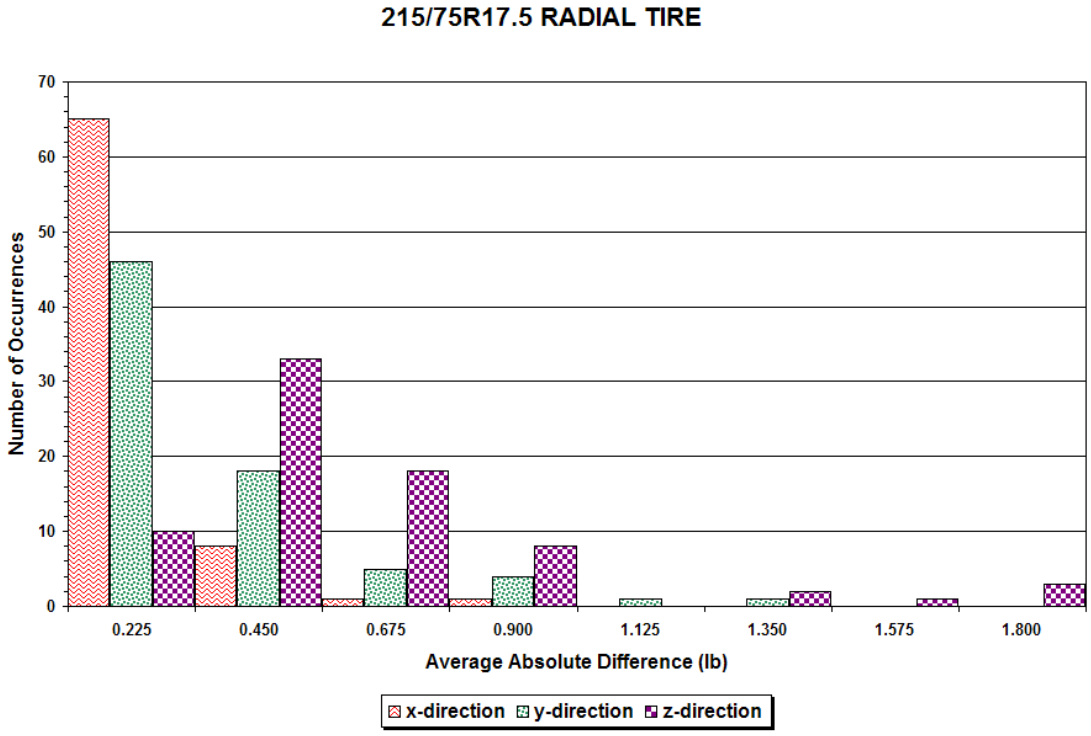

Figure 3.16. Distributions of Averages of Absolute Differences Determined from Pairwise Comparisons of Test Data on 215/75R17.5 Radial Tire.

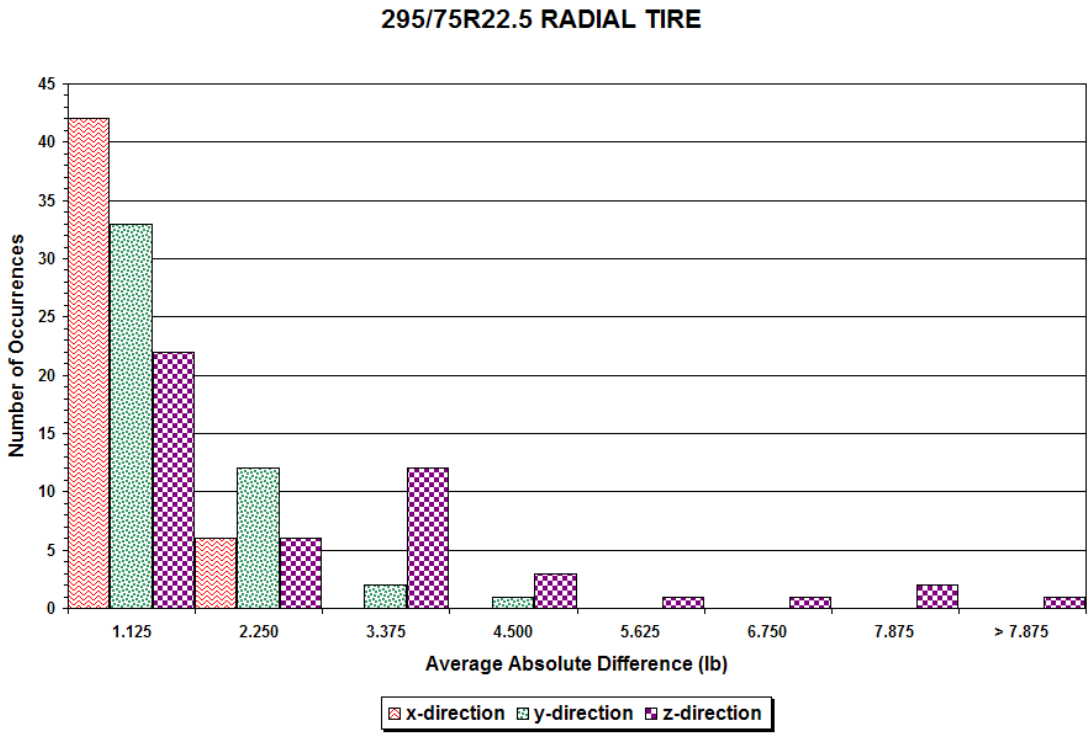

Figure 3.17. Distributions of Averages of Absolute Differences Determined from Pairwise Comparisons of Test Data on 295/75R22.5 Radial Tire.

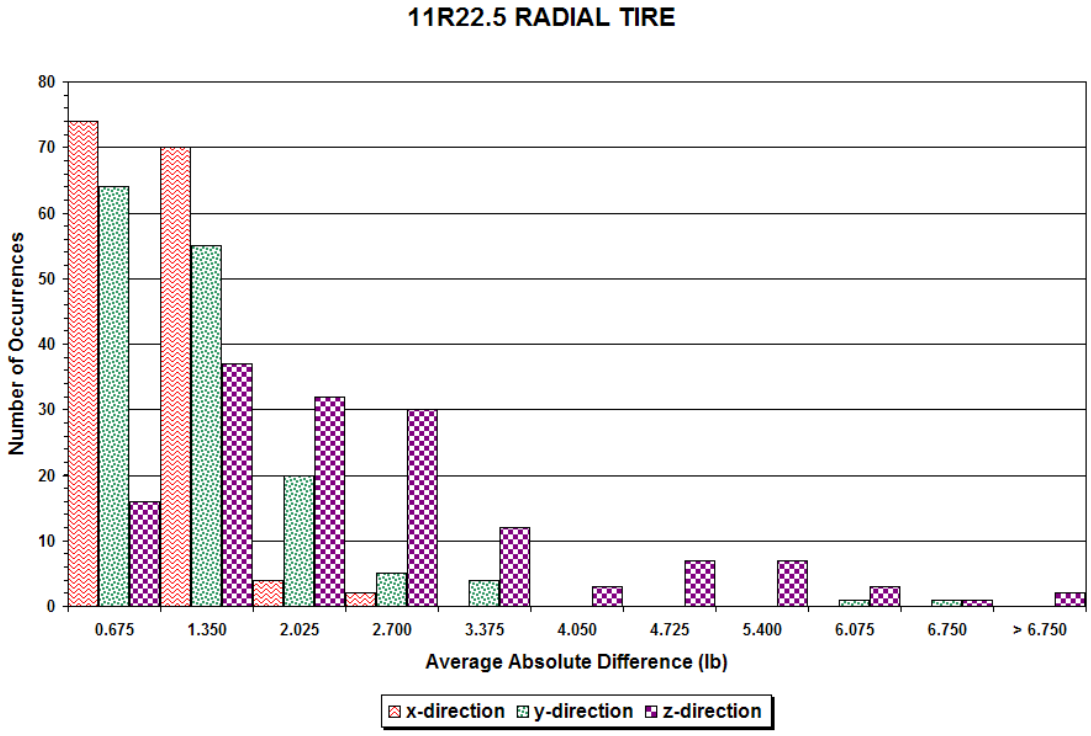

Figure 3.18. Distributions of Averages of Absolute Differences Determined from Pairwise Comparisons of Test Data on 11R22.5 Radial Tire.

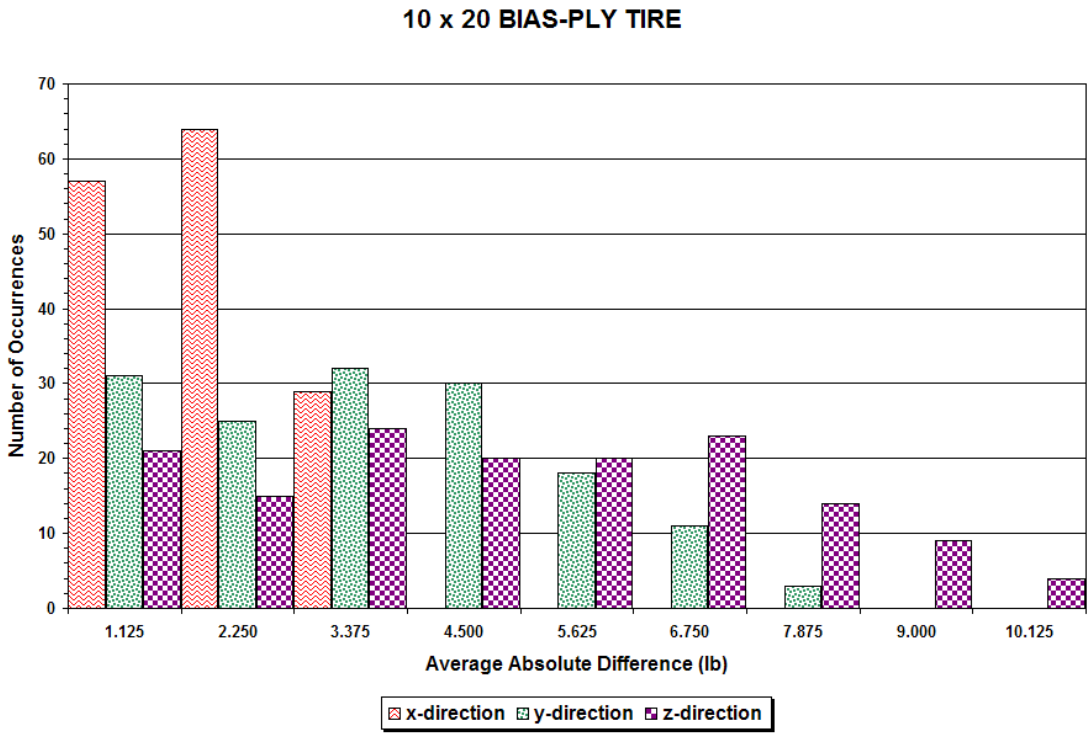

Figure 3.19. Distributions of Averages of Absolute Differences Determined from Pairwise Comparisons of Test Data on 10 × 20 Bias-Ply Tire.

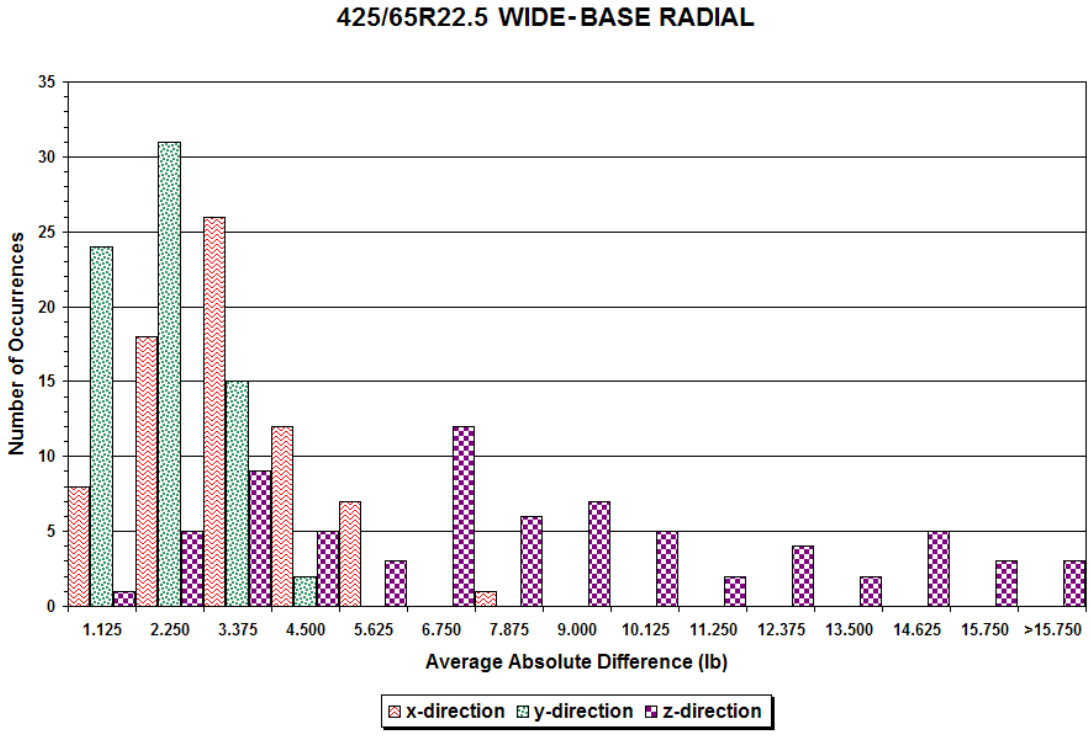

Figure 3.20. Distributions of Averages of Absolute Differences Determined from Pairwise Comparisons of Test Data on 425/65R22.5 Wide-Base Radial Tire.

- The best agreement (in terms of average absolute difference) between repeat runs is observed from test data collected on the 11R24.5 and 215/75R17.5 radial tires. The averages of the absolute differences are lower for these tires compared to the other tires on which researchers compiled contact stress data in this project. For the 11R24.5 tire, the largest values of μ are 0.8, 1.1 and 2.8 lb, from pairwise comparisons of contact forces in the *x*, *y* and *z* directions, respectively. These statistics correspond, respectively, to 4.8, 2.1 and 4.4 percent of the maximum load amplitudes in the *x*, *y* and *z* directions, for the corresponding combinations of tire load and tire inflation pressure at which the maximum differences were observed. The overall means of the averages of absolute differences are 0.2, 0.4 and 0.8 lb for the *x*, *y* and *z* directions, respectively. Similarly, the largest values of μ for the 215/75R17.5 tire are 0.7, 1.2 and 1.7 lb corresponding, respectively, to 4.2, 2.0 and 2.6 percent of the corresponding maximum load amplitudes in the *x*, *y* and *z* directions. The overall means of the μ statistics are 0.2, 0.3 and 0.5 lb for the *x*, *y* and *z* directions, respectively. Based on these results and the higher correlations observed from pairwise comparisons of replicate measurements, researchers conclude that test data on the 11R24.5 and 215/75R17.5 radial tires exhibit the best repeatability among the tires investigated.
- In terms of the average absolute difference, repeat measurements on the 295/75R22.5 and 11R22.5 radial tires exhibit a level of agreement in between that observed on the two tires discussed previously, and the 10 × 20 bias-ply and 425/65R22.5 wide-base radial tires. For the 11R22.5 tire, the largest values of μ are 2.1, 6.1 and 21.9 lb, from pairwise comparisons of contact forces in the *x*, *y* and *z* directions, respectively. These statistics correspond, respectively, to 12.0, 24.1 and 33.9 percent of the maximum load amplitudes in the *x*, *y* and *z* directions, for the corresponding combinations of tire load and tire inflation pressure at which the maximum differences were observed. However, as Figure 3.18 indicates, the agreement between replicate measurements is generally good, with the overall means of the μ statistics being 0.7, 1.0 and 2.3 lb, for the *x*, *y* and *z* directions, respectively.

- Replicate measurements on the 10 × 20 bias-ply and 425/65R22.5 wide-base radial tires show the largest averages of absolute differences as may be observed from the distributions shown in Figures 3.15 to 3.20. For the 10 × 20 bias-ply tire, the largest values of μ are 3.0, 7.6 and 10.1 lb, from pairwise comparisons of contact forces in the *x*, *y* and *z* directions, respectively. These statistics correspond, respectively, to 18.0, 19.5 and 14.0 percent of the maximum load amplitudes in the *x*, *y* and *z* directions, for the corresponding combinations of tire load and tire inflation pressure at which the maximum differences were observed. The overall means of the averages of absolute differences are 1.4, 2.9 and 4.3 lb, for the *x*, *y* and *z* directions, respectively. Similarly, the largest values of μ for the wide-base radial tire are 7.7, 3.8 and 24.3 lb corresponding, respectively, to 27.3, 16.4 and 26.4 percent of the corresponding maximum load amplitudes in the *x*, *y* and *z* directions. The overall means of the μ statistics for this tire are 2.8, 1.6 and 7.9 lb for the *x*, *y* and *z* directions, respectively.

In summary, the statistics determined from the test data indicate that the repeatability of the measurements may be ranked from best to worst according to the following order: (215/75R17.5, 11R24.5) → (295/75R22.5, 11R22.5) → (10 × 20, 425/65R22.5). Researchers used the findings from this evaluation to develop the data base of tire contact stresses that is presented in the next section of this chapter.

ESTABLISHING THE DATA BASE OF TIRE CONTACT STRESSES

To compile the data base of tire contact stresses, researchers identified the measurements that exhibit excellent to fair repeatability. For these measurements, researchers computed the average of the data from repeat runs point-by-point, to come up with the representative contact stress distribution for the given tire, tested at the specified level of tire load and inflation pressure. In the majority of cases, all three replicates from a given test were used in computing the average contact stress distribution for each of the three stress directions (*x*, *y* and *z*). This statement is particularly applicable for test data collected on the 215/75R17.5, 11R24.5, 295/75R22.5 and 11R22.5 radial tires. For the first two tires, all replicates show excellent repeatability while for the last two, all replicates generally showed excellent to good repeatability, except for the four cases identified previously where, in each case, only two out of three replicates were found to be repeatable.

Replicate runs from the bias-ply and wide-base radial tires show less repeatability compared to the other four tires. However, except for a few cases, researchers found at least a pair of replicates for the range of tests conducted on these tires that exhibit fair (between 70 and 80 percent) to excellent (90 percent or higher) correlation. The average contact stress distributions were computed using corresponding replicates that exhibit acceptable repeatability. For cases where the repeatability of all three replicates is less than desired, researchers examined charts of the test data, as well as data that bound the measurements in question to make decisions on which data to use for determining representative contact stress distributions.

Table 3.1 identifies the cases where corresponding replicates correlate by less than 70 percent. To resolve these cases, researchers first examined charts and the repeatability statistics computed from the data. Figure 3.21, for example, shows charts of the stress measurements collected from replicate runs of the bias-ply tire loaded to 8110 lb at an inflation pressure of 104 psi. Table 3.2 shows the corresponding repeatability statistics determined from pairwise comparisons of runs A, B and C. It is observed that runs A and C show the highest correlation and the lowest average absolute difference among the pairwise comparisons. In the absence of other measurements, and considering that the correlation of runs A and C is close to 70 percent, researchers determined the average contact stress distribution from these runs and entered this distribution into the data base of tire contact stresses for the given combination of test variables.

A similar procedure was followed to resolve the other cases shown in Table 3.1. Researchers found that, for the bias-ply tire, five of the remaining six cases shown in Table 3.1 have corresponding pairs of replicate runs with correlation coefficients ranging between 61 and 70 percent. Researchers used these replicate pairs to determine the average contact stress distributions for entry into the data base.

The last case involving the bias-ply tire tested at a tire load of 5860 lb and an inflation pressure of 104 psi was resolved in a different way. For this case, researchers had force measurements in the *y* direction from just two repeat runs (A and C). Figure 3.22 illustrates the data from these runs. The correlation of the force measurements shown is just 46 percent. To establish which run (A or C) would be more reasonable and appropriate to use for the data base, researchers examined corresponding data from other runs to establish

Table 3.1. Cases with No Two Replicates Showing Acceptable Repeatability.

Tire	Stress-Direction	Tire Load (lb)	Inflation Pressure (psi)
10 × 20 bias-ply	X	5860	90
		8110	104
		8110	119
		9240	100
		10,360	133
	Y	5860	100
		5860	104
425/65R22.5	X	5860	131
		5860	145
		10,360	102
		12,610	145

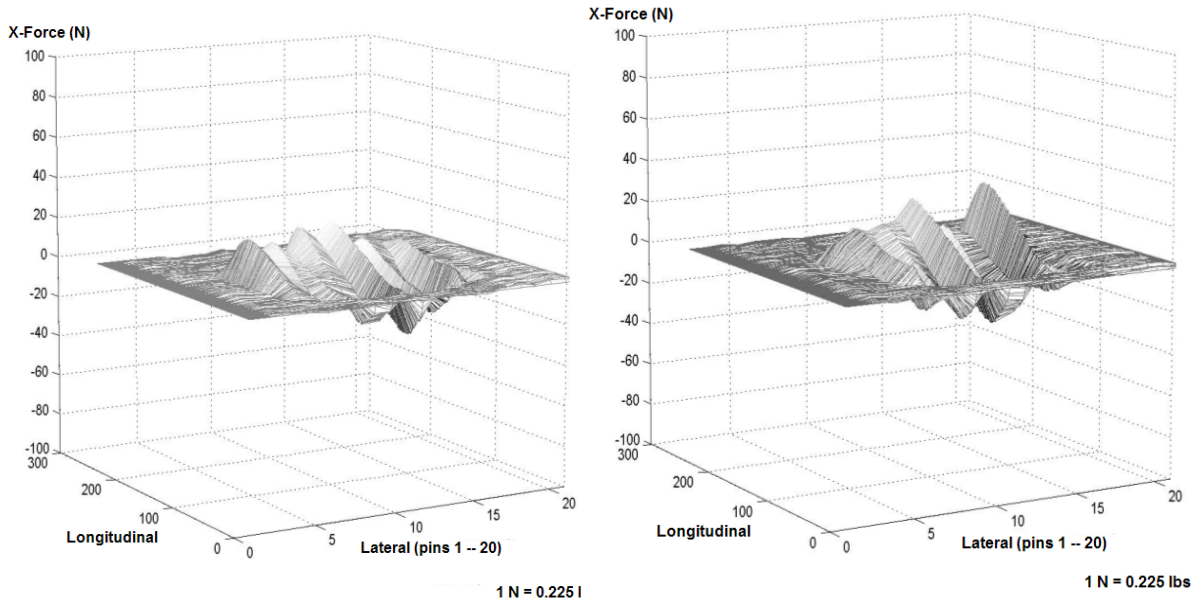

Run A ***Run B***

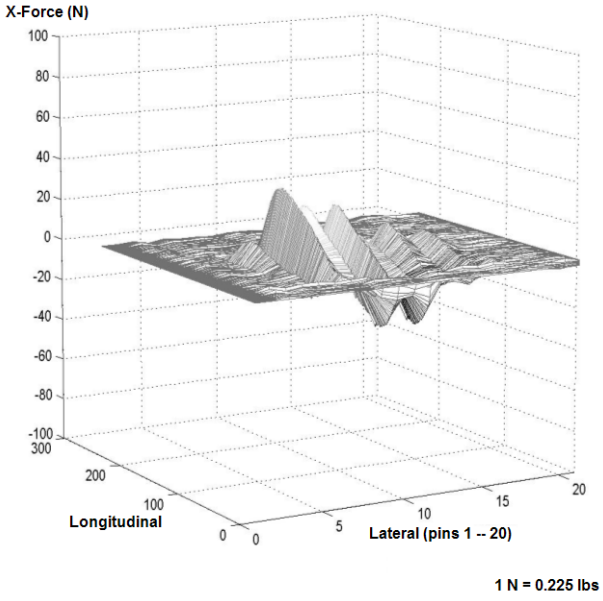

Run C

Figure 3.21. Distributions of Contact Forces in the *X* Direction from Repeat Runs (A, B and C) of the Bias-Ply Tire Tested at a Tire Load of 8110 lb and Inflated to 104 psi.

Table 3.2. Repeatability Statistics from Pairwise Comparisons of Data on Bias-Ply Tire Tested at a Tire Load of 8110 lb and Inflated to 104 psi.

Statistic	Data Pair		
	AB	BC	AC
Correlation Coefficient	0.42	0.34	0.68
Average Absolute Difference (lb)	1.7	1.9	1.3

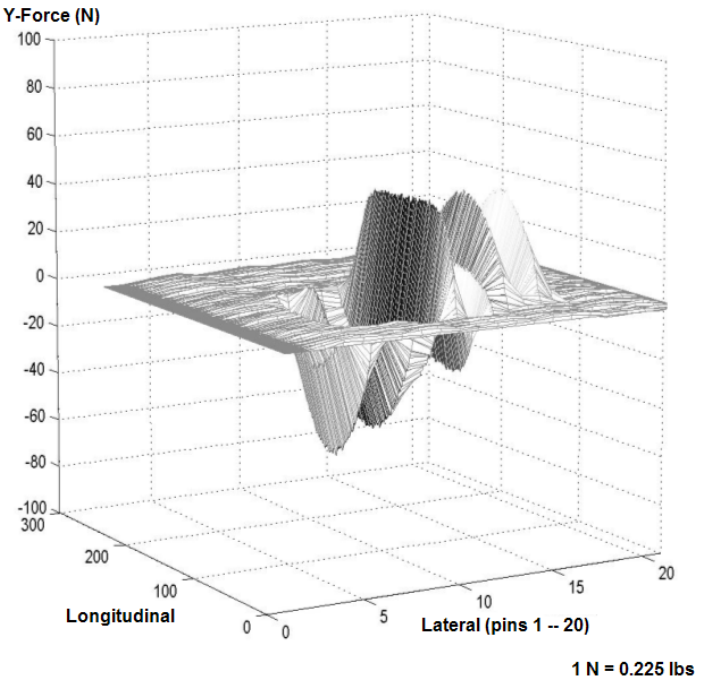

Run A

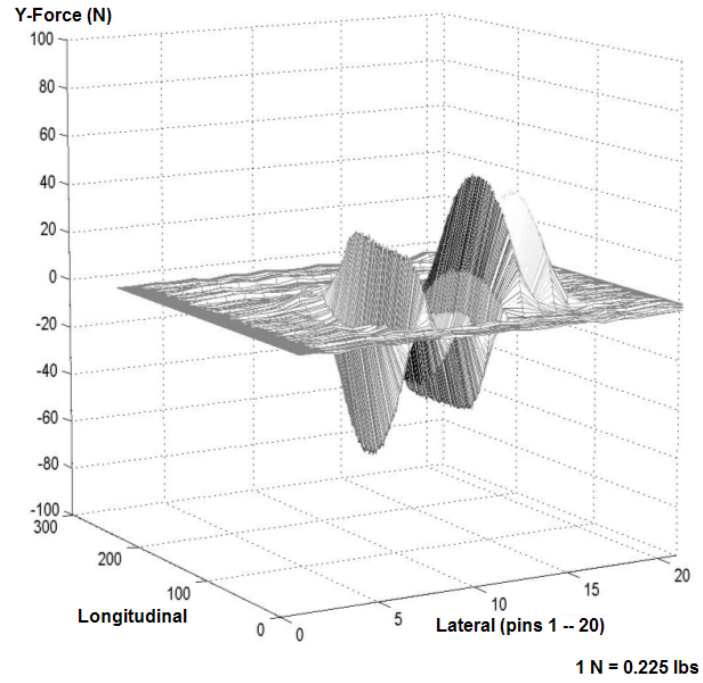

Run C

Figure 3.22. Distributions of Contact Forces in the *Y* Direction from Repeat Runs of the Bias-Ply Tire Tested at a Tire Load of 5860 lb and Inflated to 104 psi.

how the trends or patterns in the *y* force measurements for the bias-ply tire change as the inflation pressure is varied for the given tire load of 5860 lb. Specifically, researchers examined the data taken at the lower inflation pressures of 75 and 90 psi, and at the higher inflation pressures of 119 and 133 psi for the same tire load of 5860 lb. Note that the data from these tests bracket the data from those conducted at the tire inflation pressure of 104 psi. In addition, the data from these other tests had replicates with correlations ranging from fair to excellent. To develop a sketch of how data at 104 psi would plot, researchers used a method known as polynomial interpolation to predict the contact forces based on data taken at the other inflation pressures that show acceptable repeatability. In this analysis, researchers tried a number of techniques for predicting tire contact forces that included curve-fitting methods, bilinear interpolation, cubic splines and polynomial interpolation. This work showed polynomial interpolation as the most effective among the methods evaluated to predict tire contact forces. A description of this method is presented later in this report.

Figure 3.23 shows the predicted contact forces in the *y* direction using polynomial interpolation. The authors compared these predictions with data from runs A and C of the bias-ply tire for the given combination of tire load and tire inflation pressure. In essence, the authors treated the predictions as data from a pseudo-run. Pairwise comparisons involving data from runs A and C, the average of these two runs, and the interpolated data were conducted. These comparisons showed that run C correlates best with the predictions of the *y* contact forces based on polynomial interpolation. The correlation coefficient between these two data sets was found to be 95 percent with an average absolute difference of 3.8 lb. Given this finding, researchers incorporated the data from run C into the data base.

The cases for the wide-base radial tire listed in Table 3.1 were resolved in a similar manner. Figure 3.24 compares, for example, the data from runs A, B and C of the wide-base radial tire, with the predicted contact forces, for a tire load of 10,360 lb and an inflation pressure of 102 psi. For this case, pairwise comparisons of the data sets identified run C as having the best agreement with the predicted contact forces, with a correlation of 92 percent and an average absolute difference of 1.1 lb. Thus, the measured contact forces for this run were entered into the data base. The remaining cases for this tire were resolved in a similar manner.

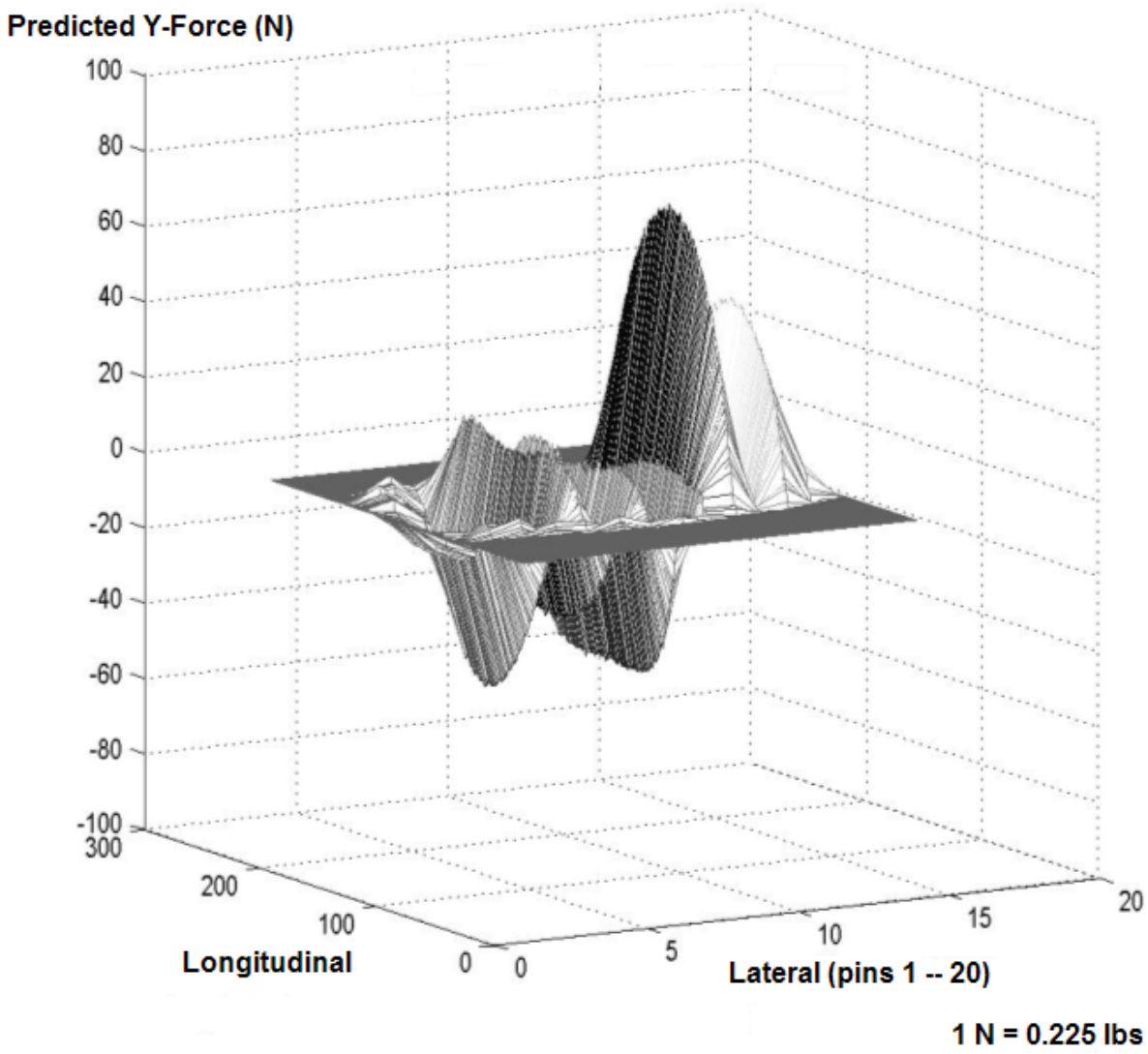

Figure 3.23. Predicted Distribution of Contact Forces in the *Y* Direction for a Bias-Ply Tire Tested at a Tire Load of 5860 lb and Inflated to 104 psi.

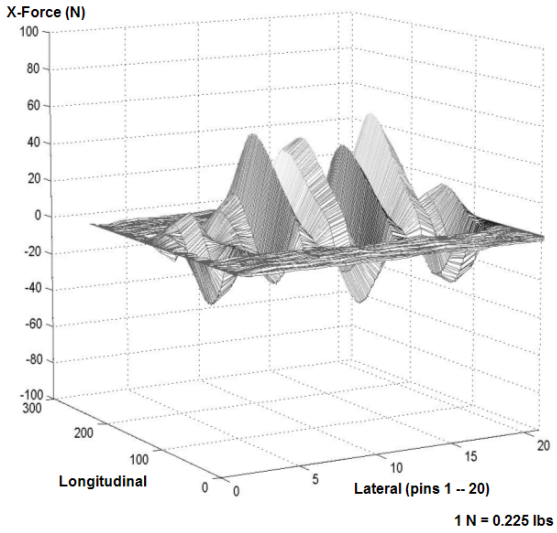

Run A

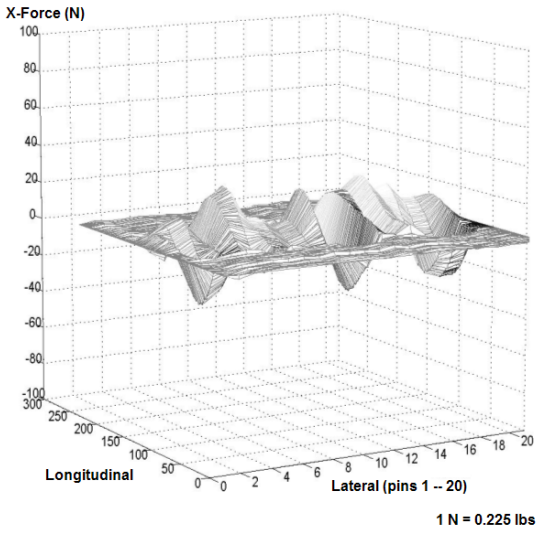

Run B

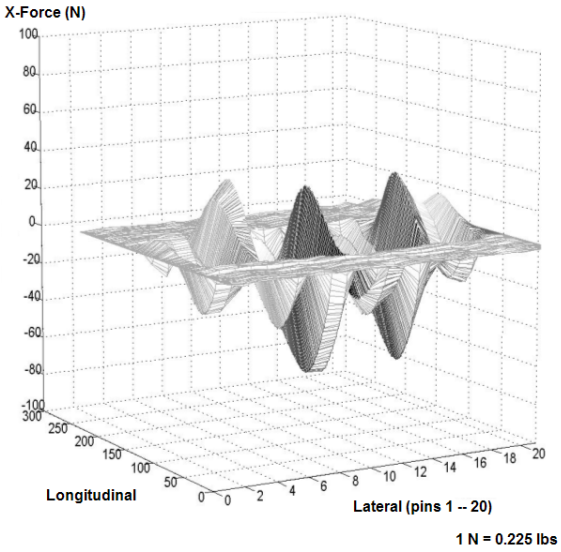

Run C

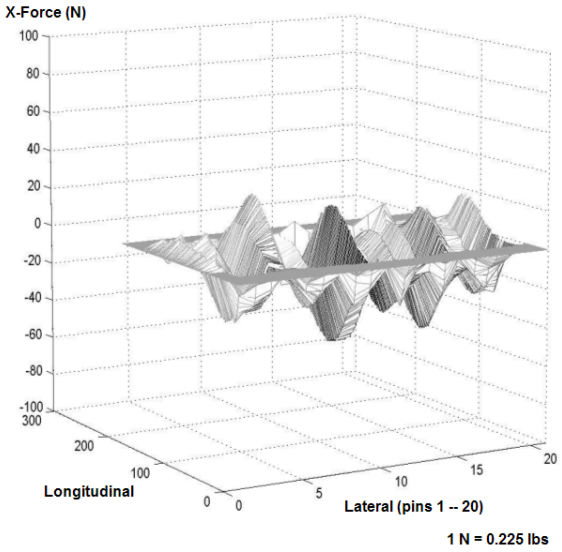

Predicted Distribution

Figure 3.24. Distributions of Contact Forces in the X Direction for a Wide-Base Radial Tire Tested at a Tire Load of 10,360 lb and Inflated to 102 psi.

Thus, a data base of tire contact stresses was compiled from this research effort. Appendix B shows charts of the measured tire contact stresses for the 11R24.5 radial, while Appendix C shows the same charts for the 215/75R17.5 tire. In view of the excellent repeatability exhibited by the data from these tests, Appendices B and C only present the tire contact stress distributions from run A for each combination of tire load and tire inflation pressure included in the test matrices for these tires. The data base established by researchers is a component of the computer program *TireView* (Fernando, 2005) that was developed in this project for estimating tire contact stresses. *TireView* is described in Chapter VI of this report.

CHAPTER IV. EVALUATION OF TIRE CONTACT AREAS

INTRODUCTION

A major objective of this project is to evaluate how tire contact stresses may be used in existing layered elastic programs to predict performance-related pavement response parameters. Since the tire contact stress distribution is influenced by the size of the tire footprint, researchers investigated relationships between tire contact area, tire load and tire inflation pressure for the six tires included in the data base described in Chapter II. For this evaluation, researchers used the tire imprints taken during testing (Figure 2.6) to determine tire contact areas for the range of tire loads and tire inflation pressures at which the six tires were tested. Tire imprints for the 11R24.5 and 215/75R17.5 tires are given in Appendix D of this report.

Figure 4.1 shows an example of a tire imprint taken on the 11R24.5 tire loaded to 4600 lb and inflated to 70 psi. The contact area and tire grooves are clearly evident in this figure. For the imprint shown, researchers estimated the tire area in contact with the ground to be 63.8 in^2 based on the scale given in the figure. This determination was made using a computer program that processed the electronic scan of the imprint and calculated the contact area based on the shading intensities of the pixels read. Contact areas for other test conditions were determined in a similar fashion. Researchers then used the resulting data to investigate how tire contact area varies with tire load and tire inflation pressure for each of the six tires represented in the data base. The findings from this investigation are presented in the next section.

RELATIONSHIPS FOR PREDICTING TIRE CONTACT AREA

Figure 4.2 illustrates the variation of tire contact area with tire load and tire inflation pressure for the 11R24.5 tire. It is observed that the contact area decreases with increasing inflation pressure and increases with increasing tire load based on the trend lines fitted to the data. Note also that the data points plot almost parallel for the different levels of tire load, indicating a negligible interaction effect between tire load and inflation pressure. Similar observations were made on the data for the other tires, suggesting that a simple additive model is appropriate to evaluate the relationships between tire contact area, tire load and tire

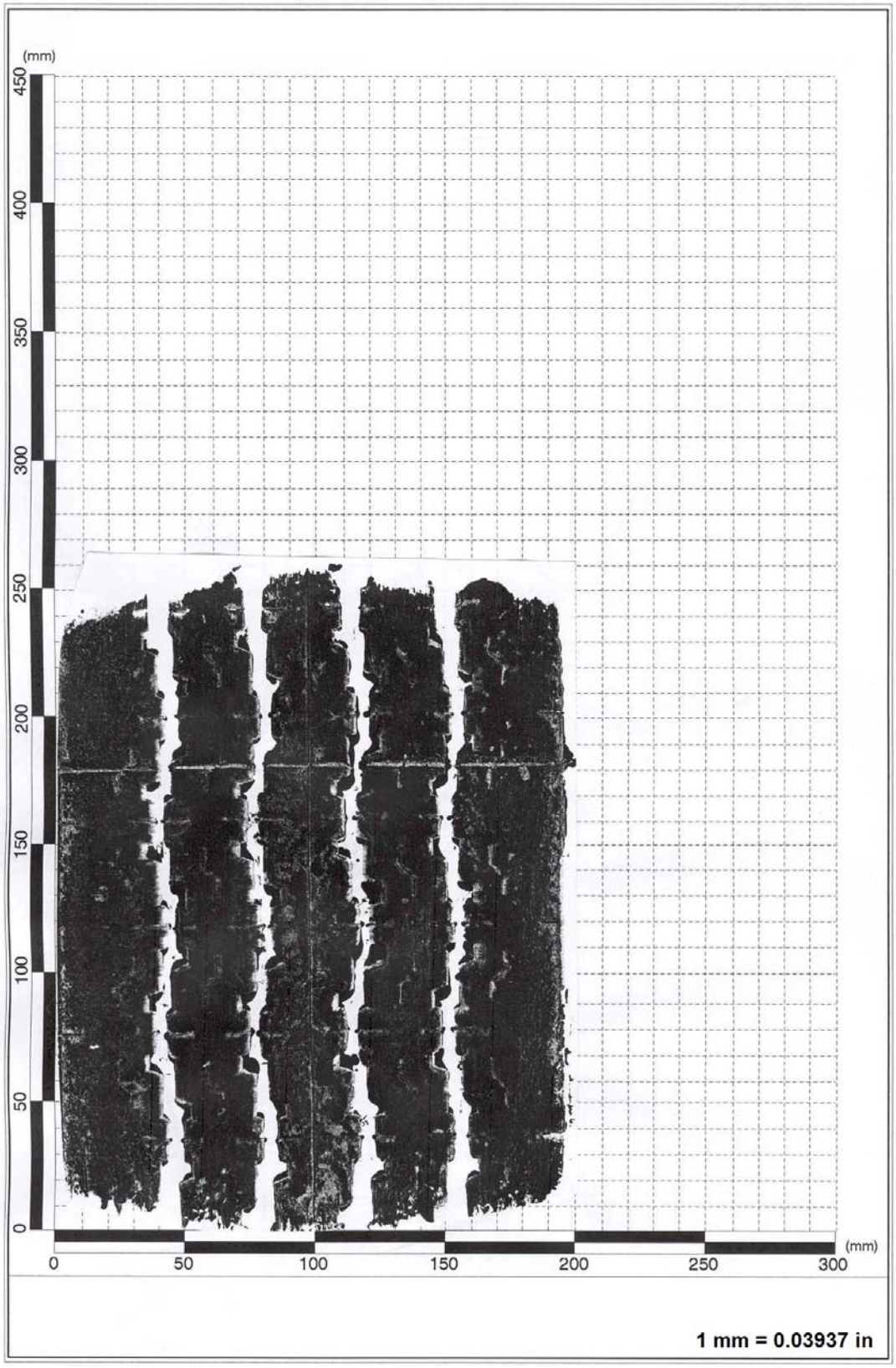

Figure 4.1. Tire Imprint for 11R24.5 Tire Taken at a Tire Load of 4600 lb and an Inflation Pressure of 70 psi.

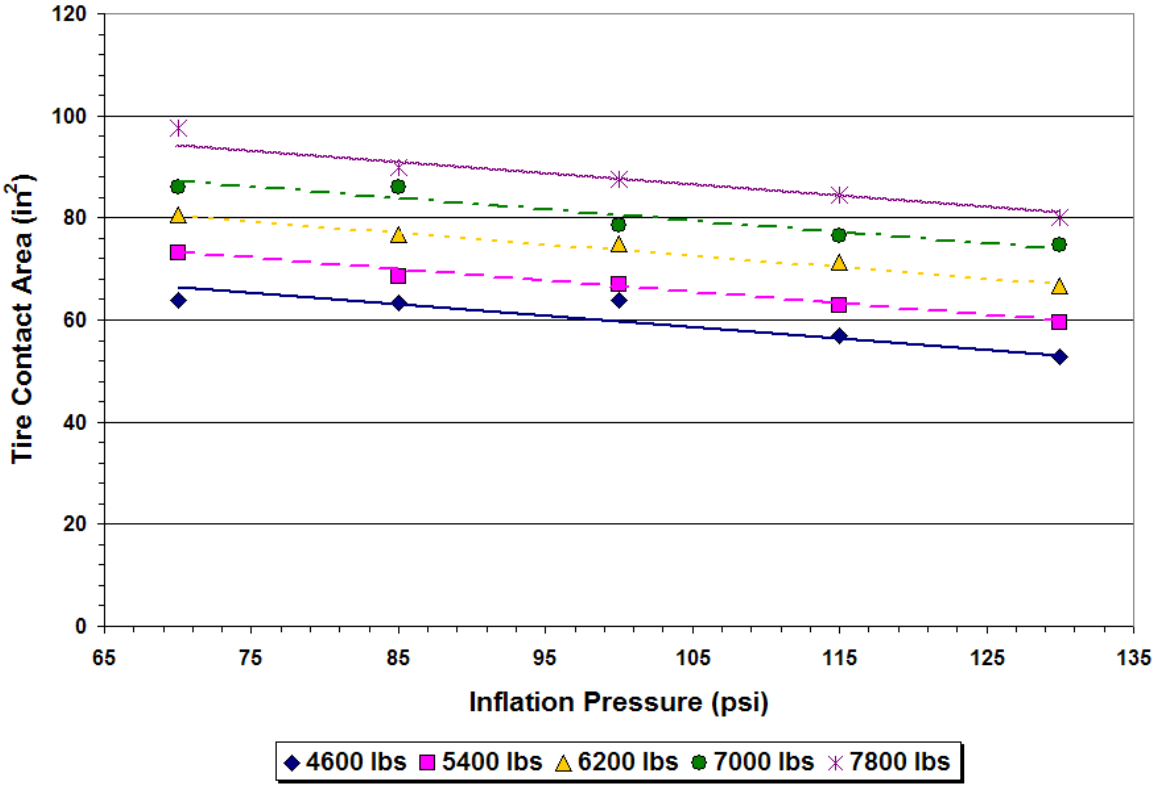

Figure 4.2. Variation of Tire Contact Area with Tire Load and Inflation Pressure for the 11R24.5 Radial Tire.

inflation pressure. Using multiple linear regression, researchers determined the following equations for predicting tire contact area:

11R24.5: $A = 41.9417 + 0.0087\,T_L - 0.2228\,T_P$ (4.1)

$R^2 = 0.98$ $SEE = 1.57$ in^2 $N = 25$

215/75R17.5: $A = 36.9172 + 0.0059\,T_L - 0.1965\,T_P$ (4.2)

$R^2 = 0.97$ $SEE = 1.54$ in^2 $N = 25$

11R22.5: $A = 54.474 + 0.0066\,T_L - 0.4258\,T_P$ (4.3)

$R^2 = 0.91$ $SEE = 5.44$ in^2 $N = 49$

295/75R22.5: $A = 173.2141 + 0.0061\,T_L - 3.1981\,T_P + 0.0164\,T_P^2$ (4.4)

$R^2 = 0.90$ $SEE = 3.81$ in^2 $N = 16$

425/65R22.5: $A = 53.64 + 0.0055\,T_L - 0.2915\,T_P$ (4.5)

$R^2 = 0.93$ $SEE = 6.57\ \text{in}^2$ $N = 20$

10×20: $A = 66.6831 + 0.0059\,T_L - 0.4218\,T_P$ (4.6)

$R^2 = 0.86$ $SEE = 6.39\ \text{in}^2$ $N = 50$

where,

A = predicted tire contact area (in^2),

T_L = tire load (lb),

T_P = tire inflation pressure (psi),

R^2 = coefficient of determination,

SEE = standard error of estimate, and

N = number of observations.

Table 4.1 summarizes the results from statistical tests of significance on the coefficients of the above equations. It is observed that the coefficients are highly significant as reflected in the low p values for all parameter estimates given in Table 4.1. These results indicate the significance of the relationships determined between tire contact area, tire load and tire inflation pressure. These relationships are illustrated in Figures 4.2 to 4.7. Researchers used these relationships to evaluate how wheel loads may be modeled in layered elastic pavement analysis programs currently implemented by TxDOT to provide a better approximation of pavement response parameters for pavement design and evaluation purposes. The next chapter presents this evaluation.

Table 4.1. Results from Significance Testing of Model Coefficients.

Tire	Variable	Parameter Estimate	Standard Error	*t*-statistic*
11R24.5	Intercept	41.9417	2.2864	18.34
	T_L	0.0087	0.0003	31.49
	T_P	-0.2228	0.0148	-15.08
215/75R17.5	Intercept	36.9172	2.0134	18.34
	T_L	0.0059	0.0002	27.02
	T_P	-0.1965	0.0145	-13.56
11R22.5	Intercept	54.4740	3.9797	13.69
	T_L	0.0066	0.0004	18.23
	T_P	-0.4258	0.03	-14.27
295/75R22.5	Intercept	173.2141	22.1153	7.83
	T_L	0.0061	0.0008	8.12
	T_P	-3.1981	0.5	-6.40
	T_P^2	0.0164	0.0028	5.92
425/65R22.5	Intercept	53.64	7.4097	7.24
	T_L	0.0055	0.0004	15.74
	T_P	-0.2915	0.0563	-5.18
10 × 20	Intercept	66.6831	4.5255	14.74
	T_L	0.0059	0.0004	14.25
	T_P	-0.4218	0.0346	-12.19

*Pr > |*t*| (*p* value) < 0.0001 for all parameter estimates.

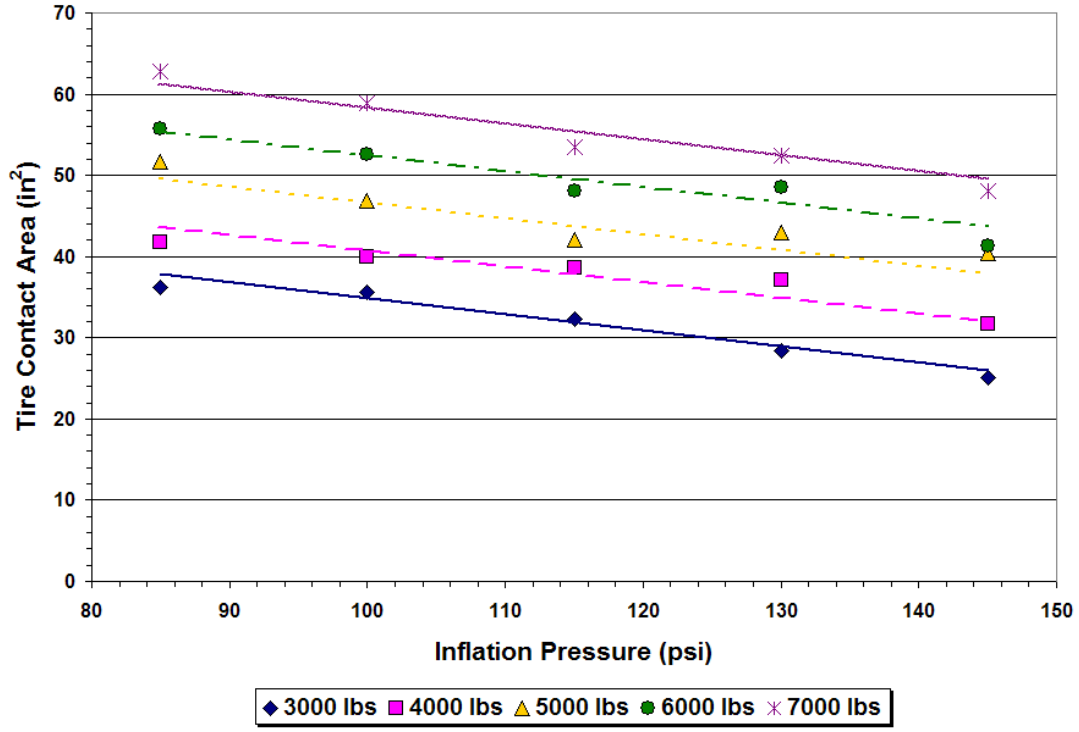

Figure 4.3. Variation of Tire Contact Area with Tire Load and Inflation Pressure for the 215/75R17.5 Radial Tire.

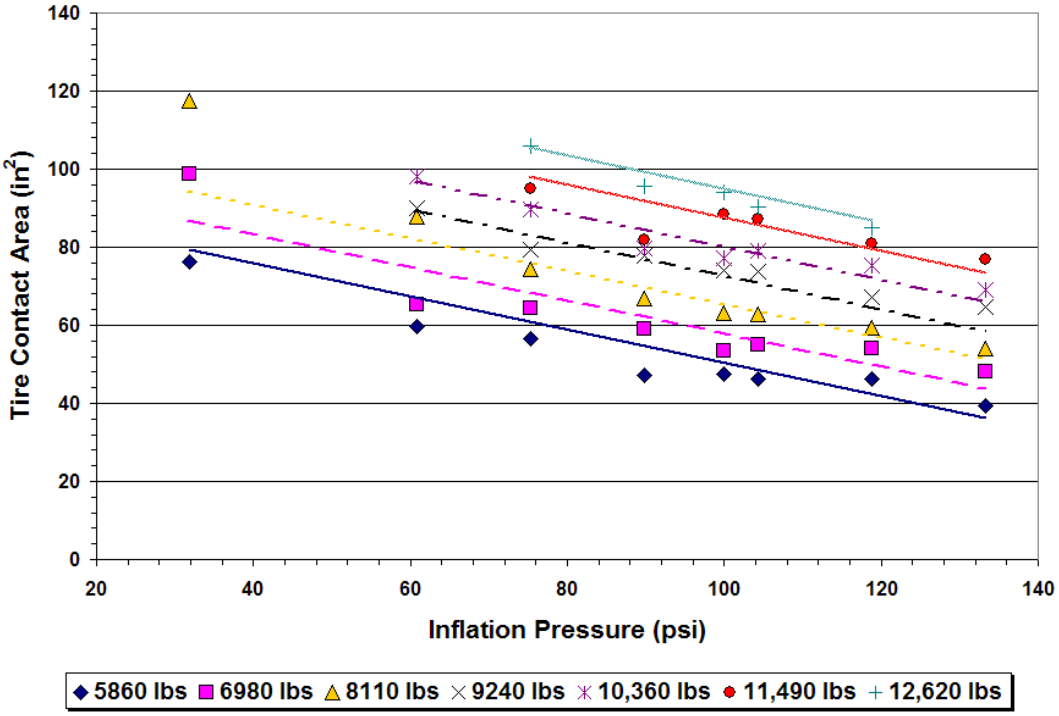

Figure 4.4. Variation of Tire Contact Area with Tire Load and Inflation Pressure for the 11R22.5 Radial Tire.

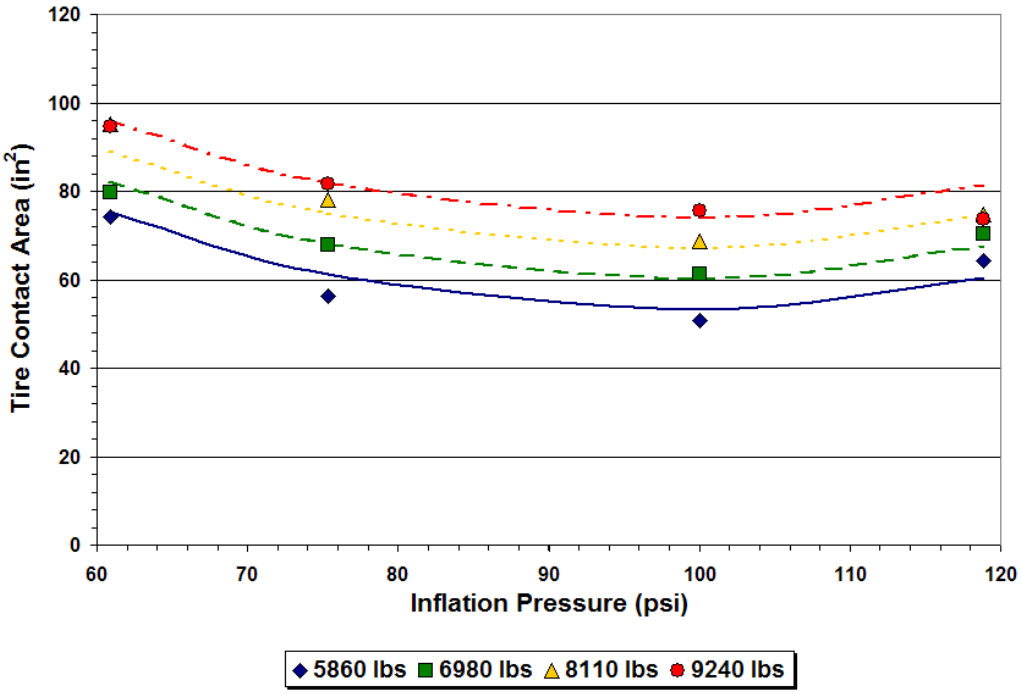

Figure 4.5. Variation of Tire Contact Area with Tire Load and Inflation Pressure for the 295/75R22.5 Radial Tire.

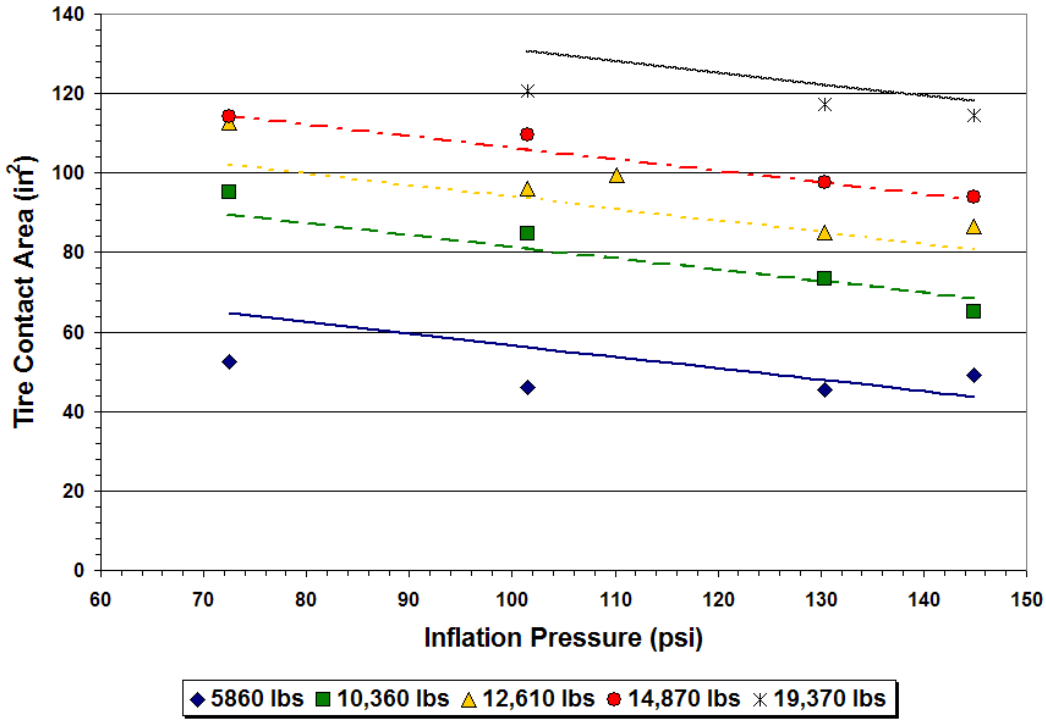

Figure 4.6. Variation of Tire Contact Area with Tire Load and Inflation Pressure for the 425/65R22.5 Wide Base Radial Tire.

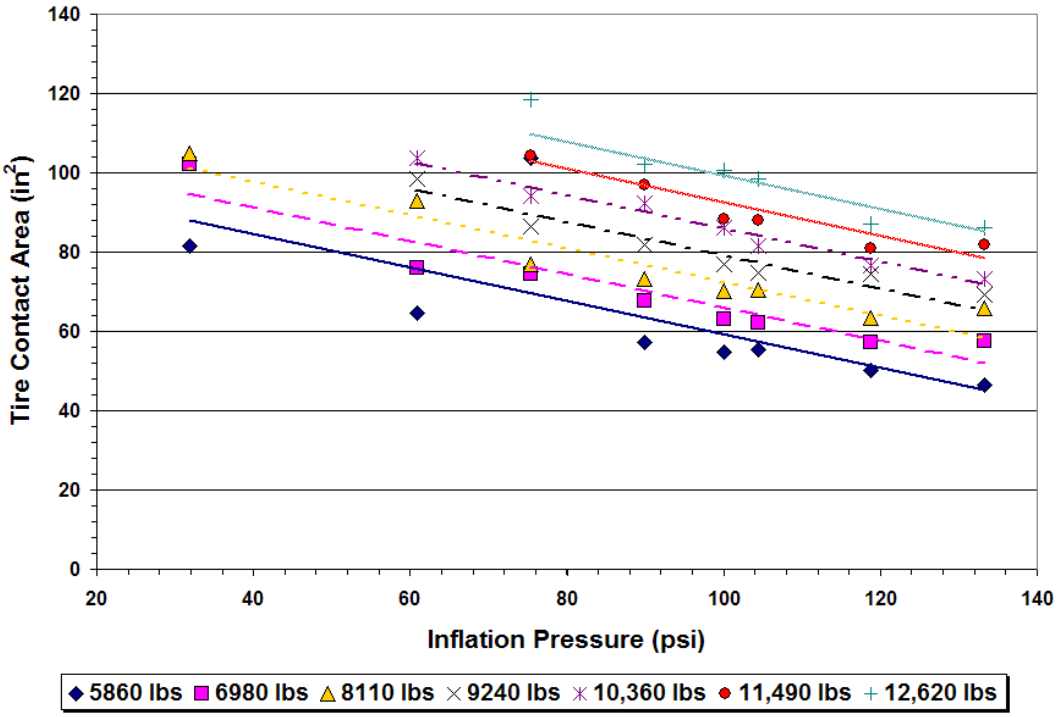

Figure 4.7. Variation of Tire Contact Area with Tire Load and Inflation Pressure for the 10 × 20 Bias-Ply Tire.

CHAPTER V. EVALUATION OF PREDICTED PAVEMENT RESPONSE USING MEASURED TIRE CONTACT STRESSES

INTRODUCTION

Advances in computing power and experimental characterization techniques have led to increased use of the finite element method (FEM) to predict the response of asphalt and concrete pavements under actual complex loading conditions. Pavement response under measured tire contact stresses have been evaluated using FEM. Novak et al. (2003) conducted an analysis of pavement response under measured radial tire contact stresses using the finite element code, ADINA. In their analysis, the measured tire contact stresses were applied as nodal forces in a three-dimensional finite element (FE) model. The predictions showed that radial tire contact stresses result in larger magnitudes and more concentrated stress distributions within the asphalt layer compared to the results obtained from uniform vertical stresses. Novak et al. (2003) linked the non-uniform stress distribution to rutting in the near surface of an asphalt concrete (AC) layer.

Long (2001) conducted finite element simulations of rutting under the heavy vehicle simulator using viscoelastic material properties for the asphalt concrete mix. In his study, Long applied tire contact forces measured using the VRSPTA as nodal forces. Although localized effects were computed, the results did not match well with the observed localized rutting patterns because of the coarseness of the VRSPTA data. However, the simulation of the average rut profile was more reasonable away from the immediate location where the load was applied.

Hua and White (2002) conducted FE simulations of an accelerated pavement tester (APT) developed for the Indiana Department of Transportation and of PURWheel, a laboratory APT, to investigate the effect of fine aggregate angularity on rutting resistance of hot mix asphalt mixtures using a creep model implemented in ABAQUS. They used non-uniform tire contact pressures measured with the VRSPTA. The predicted shape of the deformed surface and the magnitude of the rut depth showed good agreement with measured values.

Blab and Harvey (2002) conducted a finite element simulation of HVS test data using a linear viscoelastic model. They used the nodal forces in the longitudinal, transverse and vertical directions measured by the VRSPTA to provide a more realistic representation of the

surface pressure distribution for their simulations rather than the uniform circular stress distribution typically assumed in pavement design practice. Blab and Harvey (2002) concluded that their approach could be useful for evaluating strains and stresses under different loading conditions, and to rank different mixtures based on expected performance.

In this project, researchers constructed and used a 3D finite element model of asphalt concrete pavements to investigate the influence of 3D tire contact stresses on predicted pavement response and service life. The results of the 3D FE model were compared with corresponding results obtained using the layered linear elastic program, BISAR (De Jong et al., 1973). Three different analysis methods were used:

- 3D FE with measured tire contact stresses in the *x*, *y* and *z* directions;
- BISAR using measured tire contact areas to determine equivalent uniform circular pressure distributions (BM analysis); and
- BISAR using the conventional procedure of calculating the equivalent circular loaded area by dividing the tire load with the tire inflation pressure (BC analysis).

For the 3D finite element modeling, researchers used measured contact stresses from tests conducted on the 11R22.5, 295/75R22.5, 11R24.5 and 215/75R17.5 radial tires to predict performance-related pavement response parameters using the ABAQUS computer program. These tire sizes were selected because of their wide use among truck carriers. In the finite element and layered elastic analyses, the horizontal strain at the bottom of the asphalt layer, compressive strain at the top of the subgrade, and the principal stresses at different depths were predicted. These pavement response variables are used in a number of pavement design and evaluation programs implemented by TxDOT. From the predicted strains, researchers estimated service life for a range of pavements, tire loads, and tire inflation pressures based on limiting strain criteria. In addition, Mohr-Coulomb (MC) yield function values were calculated from the predicted principal stresses at different depths. The MC yield function values and pavement life estimates from the 3D finite element and layered elastic analyses were compared to establish guidelines with respect to modeling wheel loads using existing layered elastic analysis procedures.

3D FINITE ELEMENT MODEL

Researchers established a 3D finite element model based on the ABAQUS multi-purpose finite element package. Initially, a suitable mesh configuration had to be determined

for predicting pavement response under measured tire contact stresses. For this purpose, researchers evaluated a number of mesh configurations (of varying numbers of elements and element types) by comparing finite element predictions with corresponding predictions from the BISAR program. To be consistent with the assumptions of horizontally infinite pavement layers and a semi-infinite subgrade, the lateral and longitudinal dimensions of the finite element mesh were varied until predictions of pavement response compared reasonably well with the layered elastic analysis results. From this analysis, a finite element mesh with lateral and longitudinal dimensions of 150 inches × 150 inches was found to be appropriate. In addition, the subgrade was modeled using infinite elements. The asphalt concrete and base layers were varied in the analyses as shown in Table 5.1. In this table, the shaded cells identify the eight pavement structures on which pavement response predictions were made using 3D finite element and layered elastic analyses. The selected pavements represent a ¼ fraction of a 2^5 factorial design where all main effects can be estimated.

In the authors' opinions, the range of thicknesses used is representative of pavements found in practice. While AC layers thicker than 6 inches exist, previous research shows that the effects of tire contact pressures are mainly seen near the surface. Thus, AC layers thicker than 6 inches were not considered in this investigation.

Figures 5.1 and 5.2 illustrate the 3D finite element mesh used in this evaluation. Elements in the region of the tire contact stresses are approximately 0.7 inch (column) × 0.2 inch (row) in size, with the tire contact area consisting of 20 columns and 68 rows. A coarser mesh was used outside of the wheel load area, with the element size progressively increasing with distance from the load. With this biased mesh configuration, computation times were kept within reasonable limits. The interface between layers was assumed to be fully bonded in the finite element runs made by researchers. Since the measured tire contact stresses were not symmetrical, a full 3D finite element model was used. In the analyses, each layer was assumed to be linear elastic to compare with the BISAR predictions. The elastic modulus of each layer was varied according to Table 5.1. In addition, a Poisson's ratio of 0.4 was assumed for all pavement layers.

To check the 3D finite element model, researchers conducted an analysis where the same uniform pressure loading condition and pavement structure were input into ABAQUS and BISAR. Figures 5.3 and 5.4 compare, respectively, the predicted horizontal and vertical strains from both methods of analysis. It is observed that the predicted strains from

Table 5.1. Pavements Considered in Comparative Evaluation of Pavement Response.

Subgrade Modulus (ksi)	Base Modulus (ksi)	Asphalt Modulus (ksi)	Asphalt Thickness (inches)			
			2		6	
			Base Thickness (inches)		Base Thickness (inches)	
			6	12	6	12
7.5	50	400				7
		650	1			
	100	400			5	
		650		3		
15	50	400		4		
		650			6	
	100	400	2			
		650				8

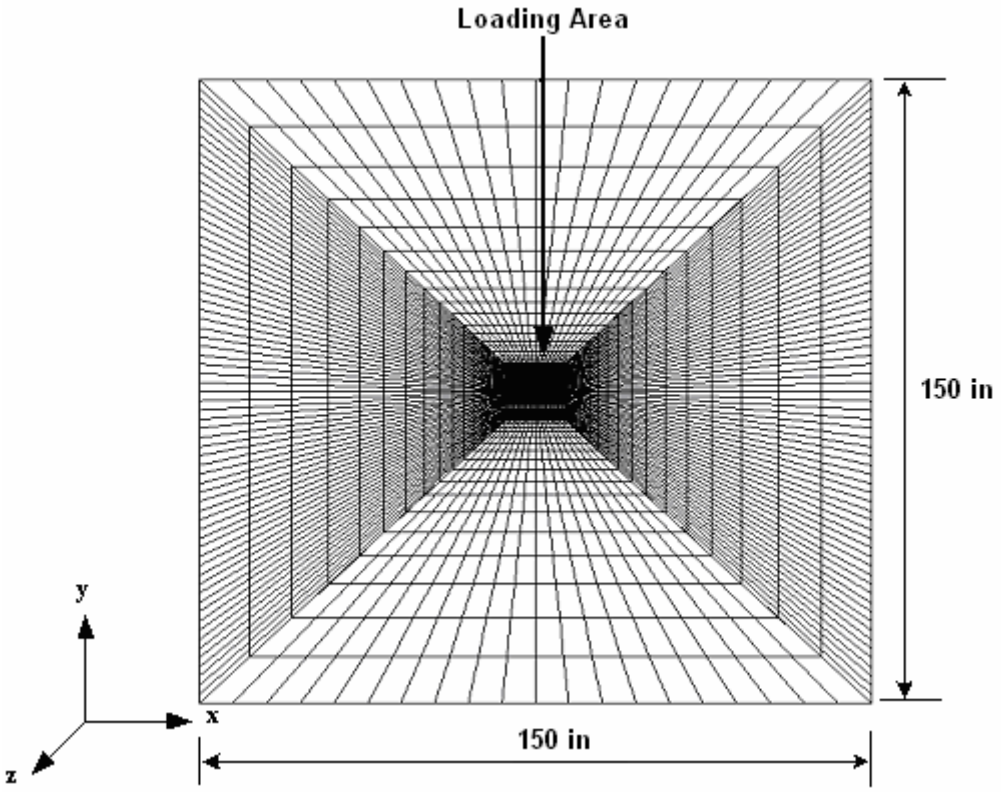

Figure 5.1. Top View of Finite Element Mesh for Predicting Pavement Response under Measured Contact Stresses (Direction of Wheel Travel is along *y*-axis).

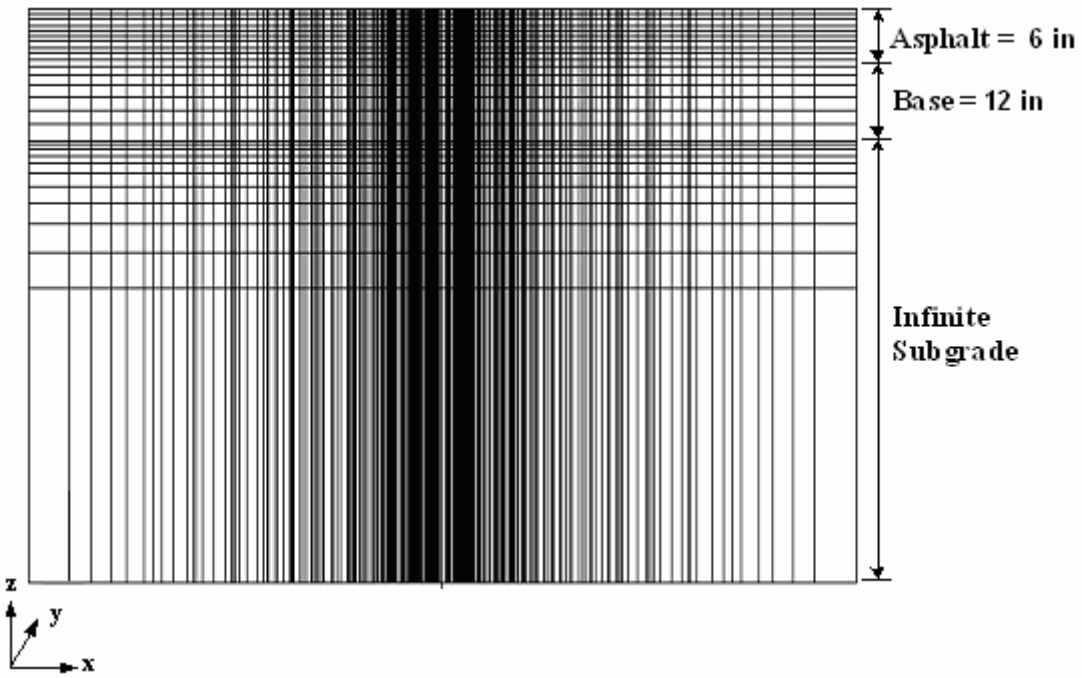

Figure 5.2. Vertical View of Finite Element Mesh for Thick Pavement Considered in the Analysis.

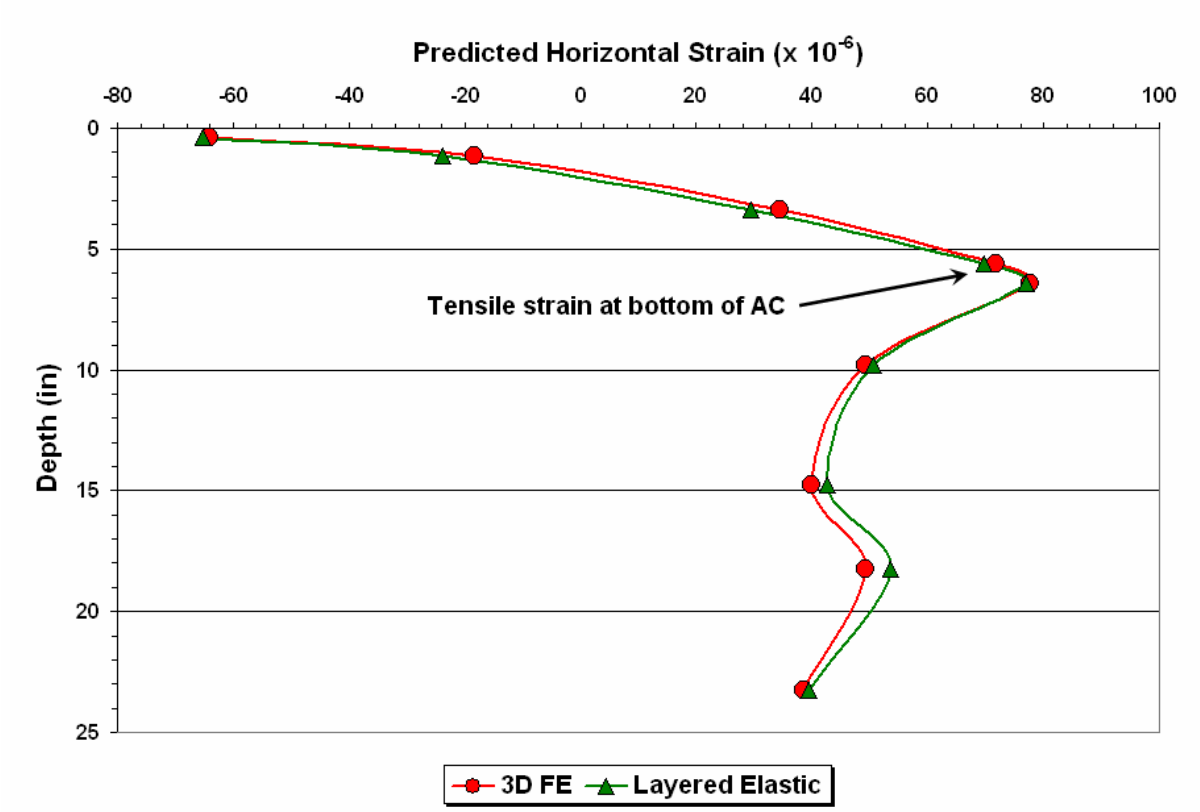

Figure 5.3. Comparison of Predicted Horizontal Strains from ABAQUS and BISAR.

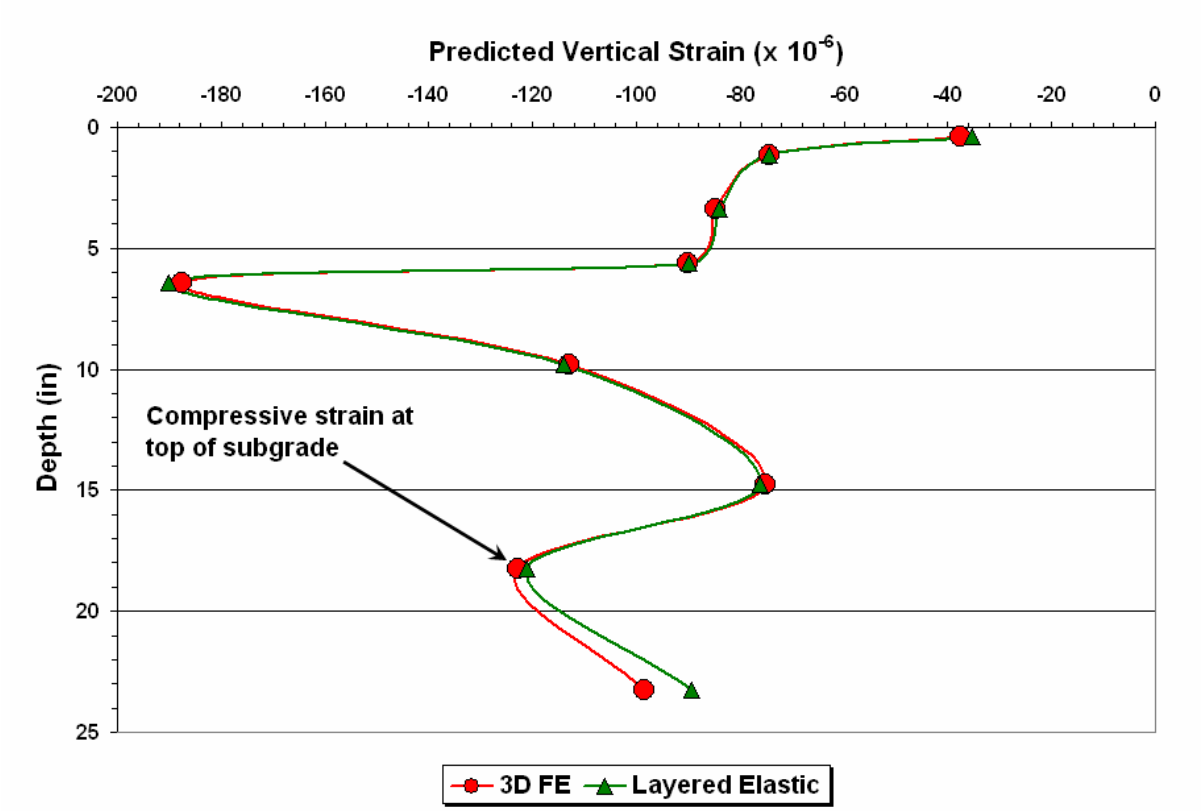

Figure 5.4. Comparison of Predicted Vertical Strains from ABAQUS and BISAR.

ABAQUS using the generated finite element mesh compare reasonably with the BISAR results. This finding verifies the suitability of using the finite element mesh for the comparative evaluation of pavement response predictions based on measured contact stresses and corresponding predictions based on uniform circular pressure distributions.

PROCESSING OF TIRE CONTACT STRESS DISTRIBUTIONS FOR INPUT INTO 3D FINITE ELEMENT RUNS

Tire contact stresses were measured along the longitudinal direction at approximately 0.01-inch intervals for the TxDOT tests and at approximately 0.09-inch intervals for the CALTRANS tests. These measurements are too fine to use directly in a 3D finite element analysis. To reduce computation time to a feasible level, researchers used a simple routine to reduce the sampling rate without significant accuracy loss. This process is called decimation because the original data set is decimated or reduced in number (Stearns and David, 1993). The decimation was accomplished using a procedure that preserves the frequency content of the original data, and resulted in a mesh configuration where the finest mesh size is approximately 0.2 inch in the direction of wheel travel. Figures 5.5 and 5.6 show,

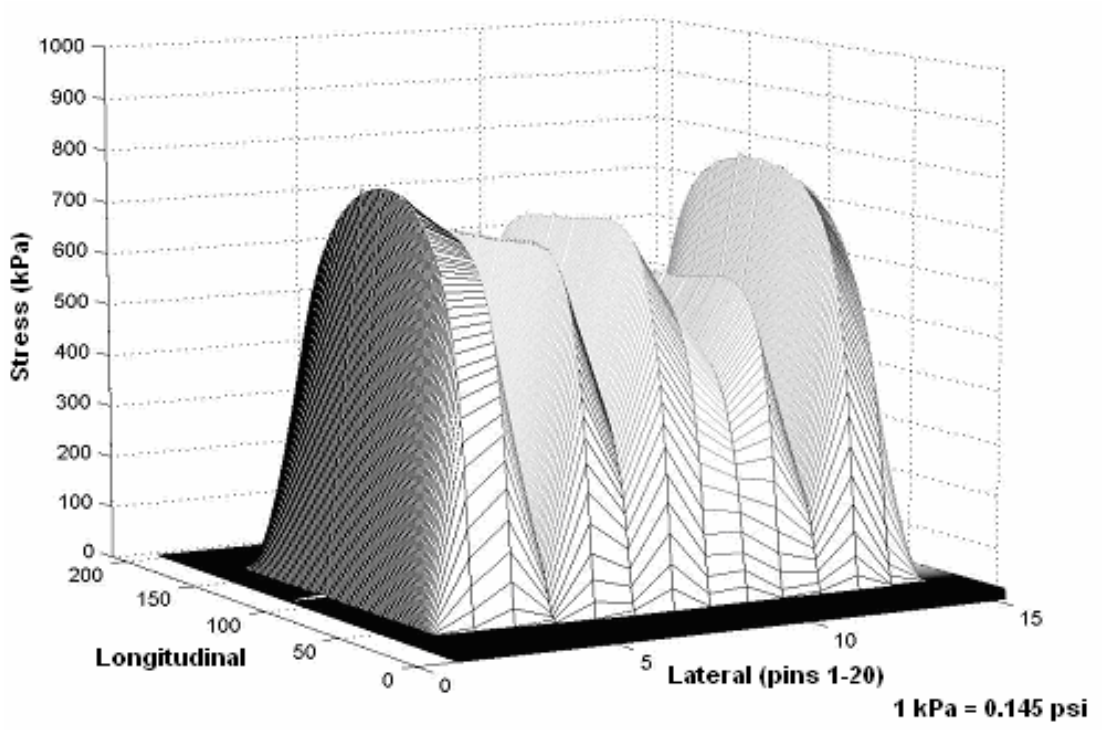

Figure 5.5. Measured Vertical Contact Stress Distribution for 11R22.5 Radial Tire Inflated to 75 psi and Loaded to 5860 lb.

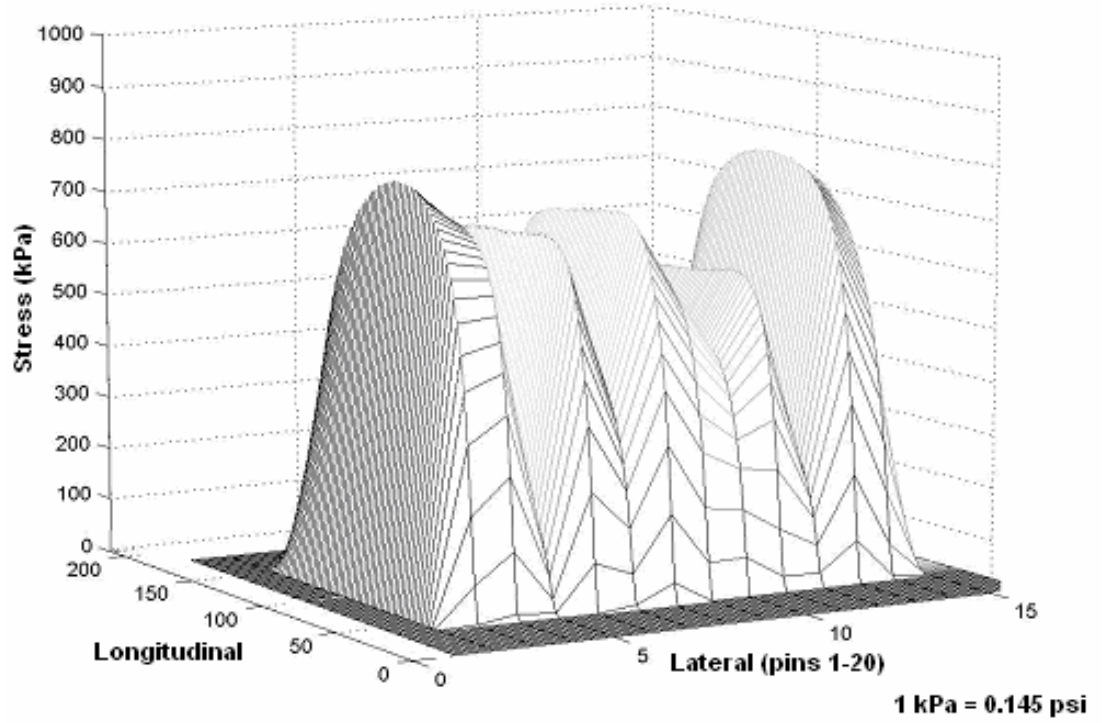

Figure 5.6. Vertical Contact Stress Distribution for 11R22.5 Tire after Decimation.

respectively, the original and decimated vertical contact stress distributions for the 11R22.5 radial tire tested at an inflation pressure of 75 psi and a tire load 5860 lb.

To check the applicability of the decimated data, researchers verified the total load by integrating the individual measurements at each active pin. Following the procedure by de Beer and Fisher (1997), the total loads for the original and decimated data were computed as follows:

$$Total\ Load = \sum P_i \times \frac{S}{F} \times \frac{1}{L_e} \quad (5.1)$$

where,

P_i = measured load on active pin I;

S = tire test speed;

F = sampling frequency, Hz; and

L_e = effective length of diamond shaped area (≈ 0.6 inch).

Figure 5.7 compares the total loads determined for the original and decimated data. It is observed that the total loads agree well between the two data sets. Thus, researchers used the decimated tire contact pressures in the 3D finite element analyses.

Three different loading conditions were selected to analyze pavement response. These represent the low, middle and high combinations of tire load and tire inflation pressure used for a given tire during the tests. The low load-high inflation pressure and the high load-low inflation pressure combinations were not considered in this investigation as these conditions represent extreme deviations from manufacturer recommended tire load/tire inflation pressure guidelines. Table 5.2 identifies the load and tire inflation pressures used in the analyses.

LAYERED ELASTIC ANALYSIS

Layered elastic analysis is commonly used in pavement design and evaluation programs implemented within transportation agencies. On the other hand, 3D finite element programs, while more powerful and versatile, are more difficult to implement and are thus, not used on a routine basis, except for in-house research or specialized investigations. Consequently, a comparison of 3D FE and layered elastic analysis results was conducted in an attempt to establish guidelines on how existing layered elastic programs may be used to

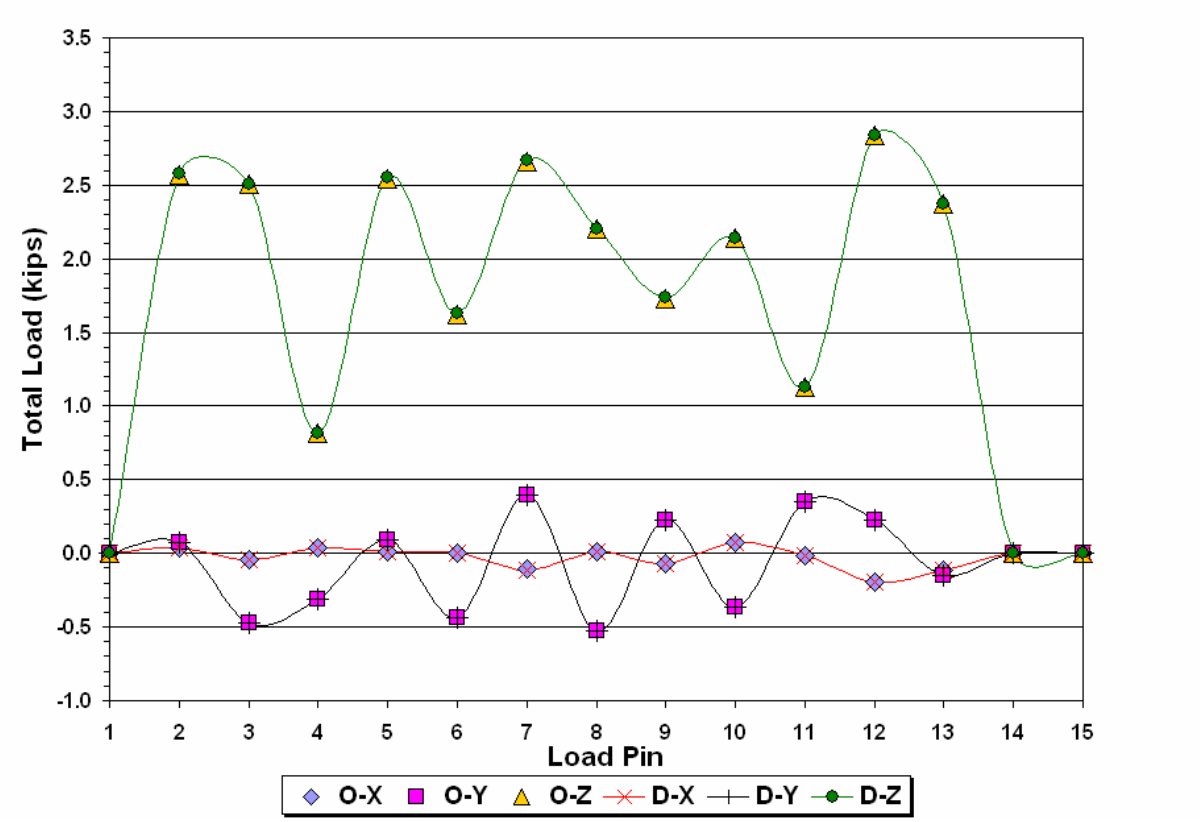

Figure 5.7. Comparison of Total Loads Based on Original (O) and Decimated (D) Vertical Contact Pressures.

Table 5.2. Load and Tire Inflation Pressure Combinations Used in Analyses.

Tire Load-Inflation Pressure Combination	Tire Size							
	11R22.5		295/75R22.5		11R24.5		215/75R17.5	
	Load (lb)	Inflation Pressure (psi)	Load (lb)	Inflation Pressure (psi)	Load (lb)	Inflation Pressure (psi)	Load (lb)	Inflation Pressure (psi)
Low	5860	75	5860	75	4600	70	3000	85
Middle	6980	100	6980	100	6200	100	5000	115
High	9240	119	9240	119	7800	130	7000	145

provide a better approximation of pavement response parameters for pavement design and evaluation purposes. Two types of layered elastic analysis were used as noted earlier. In the BM analysis, the measured tire contact area for a given tire type, tire load and tire inflation pressure was used to determine an equivalent uniform circular pressure distribution according to the following relations:

$$p_e = \frac{P}{A_m} \quad (5.2)$$

$$r_e = \sqrt{\frac{A_m}{\pi}} \quad (5.3)$$

where,

P = applied tire load,

A_m = measured tire contact area,

p_e = equivalent uniform circular contact pressure, and

r_e = radius of equivalent circular contact area.

In the case of the conventional (BC) analysis, the tire contact area and its radius were determined from the following relations (Huang, 1993):

$$A_c = \frac{P}{p_i} \quad (5.4)$$

$$r_c = \sqrt{\frac{A_c}{\pi}} \quad (5.5)$$

where,

A_c = tire contact area for conventional analysis,

p_i = tire inflation pressure, and

r_c = radius of circular contact area for conventional analysis.

Table 5.3 gives the tire contact areas used in the BM and BC analyses. In the conventional analysis, the tire inflation pressure is assumed as the tire contact stress on the pavement surface. This approach provides no differentiation between tire types, even though tire footprints vary with tire type.

COMPARISON OF 3D FINITE ELEMENT AND LAYERED ELASTIC ANALYSIS RESULTS

Researchers compared the predicted AC tensile strains and subgrade vertical strains from the finite element and layered elastic analyses. To find the critical point for a given condition, the tensile strain at the bottom of the AC layer, and the compressive strain at the top of subgrade were evaluated at the center and along the four edges of the tire contact area.

Table 5.3. Tire Contact Areas and Equivalent Tire Contact Pressures Used in Analyses.

Tire Size	Tire Load (lb)	Tire Inflation Pressure[1] (psi)	Calculated Tire Contact Area[2] (in^2)	Measured Tire Contact Area[3] (in^2)	Equivalent Tire Contact Pressure[4] (psi)
11R22.5	5860	75	78.13	56.71	103
	6980	100	69.75	53.55	130
	9240	119	77.52	67.25	137
295/75R22.5	5860	75	78.13	56.30	104
	6980	100	69.75	61.18	114
	9240	119	77.52	73.55	125
11R24.5	4600	70	65.71	63.79	72
	6200	100	62.00	74.87	83
	7800	130	58.46	80.19	96
215/75R17.5	3000	85	35.29	36.14	83
	5000	115	43.48	42.08	119
	7000	145	48.28	48.13	146

[1] Used in the BC analysis
[2] Used in the BC analysis and calculated by dividing the tire load by the tire inflation pressure
[3] Used in the BM analysis
[4] Used in the BM analysis and calculated as tire load over the measured tire contact area

Researchers found the predicted response at the center of the loaded area to be critical. In lieu of comparing the strain predictions from the 3D FE and layered elastic analyses, pavement service lives were predicted using the Asphalt Institute (1982) performance equations for fatigue cracking and rutting. In this way, the relative differences in predicted strains between uniform and non-uniform loading conditions were assessed in terms of predicted service life. The Asphalt Institute performance equations are given by:

$$(N_f)^c = 0.0796(\varepsilon_{ac})^{-3.291}(E_{ac})^{-0.854} \quad (5.6)$$

$$(N_f)^r = 1.365\times10^{-9}(\varepsilon_{sg})^{-4.477} \quad (5.7)$$

where,

$(N_f)^c$ = allowable number of load repetitions based on fatigue cracking,

$(N_f)^r$ = allowable number of load repetitions based on rutting,

ε_{ac} = predicted tensile strain at the bottom of the AC layer,

E_{ac} = asphalt concrete modulus (psi), and

ε_{sg} = predicted vertical compressive strain at the top of the subgrade.

In terms of the predicted service life based on subgrade compressive strain, the results show no significant differences between the 3D finite element and layered elastic (BM and BC) analyses, as may be observed from Figure 5.8. This finding indicates that the effects of differences in tire contact pressure distributions are mainly seen near the surface and diminish with depth. This result, however, does not imply that tire contact pressure distributions have no effect on rutting. In particular, results from the Mohr-Coulomb analysis show that the contact pressure distributions influence the predicted stresses in the surface layer, especially within the top two inches. This finding indicates that tire contact stresses will influence the development of rutting in the surface layer as well as top down cracking.

Figures 5.9 to 5.12 compare the predicted fatigue lives based on the computed AC tensile strains from the 3D FE and layered elastic analyses. For the 11R22.5 and 295/75R22.5 radial tires, the equivalent uniform circular contact stresses based on the measured tire contact areas are larger than the tire inflation pressures (see Table 5.3), which are used as contact stresses in the conventional layered elastic (BC) analysis. Thus, the predicted fatigue lives from the modified layered elastic (BM) analysis are less than the corresponding predictions from the BC analysis. For the 11R24.5 tire, the equivalent uniform circular contact stresses based on the measured tire contact areas are smaller than the corresponding tire inflation pressures used in the BC analysis. Thus, the BC fatigue predictions are lower than the corresponding BM predictions for this tire. For the 215/75R17.5 radial tire, the equivalent uniform circular contact stresses based on the measured tire contact areas are similar to the corresponding tire inflation pressures used in the BC analysis. Thus, the predicted fatigue lives from the BM and BC analyses are similar.

Researchers conducted a statistical test of the differences in the predicted logarithms of the fatigue lives from the 3D FE, BM, and BC analyses. At a 95 percent confidence level, it was found that the differences between the predicted fatigue lives from the 3D FE and modified layered elastic (BM) analyses are not statistically significant. However, the differences in the fatigue predictions between the 3D FE and BC analyses are significant.

Researchers also compared the analysis methods on the basis of the predicted Mohr-Coulomb yield function values. The Mohr-Coulomb yield function f is given by (Chen and Baladi, 1985):

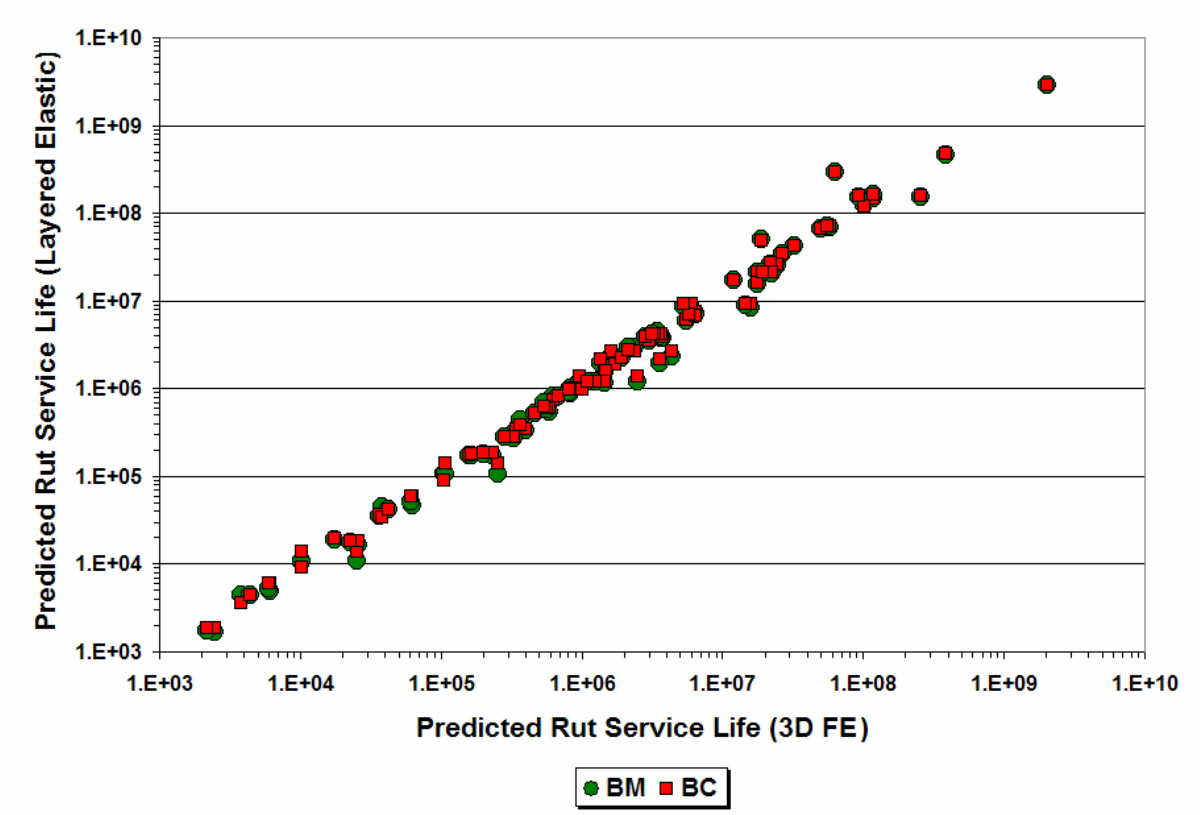

Figure 5.8. Comparisons of Predicted Service Lives Based on Subgrade Compressive Strain.

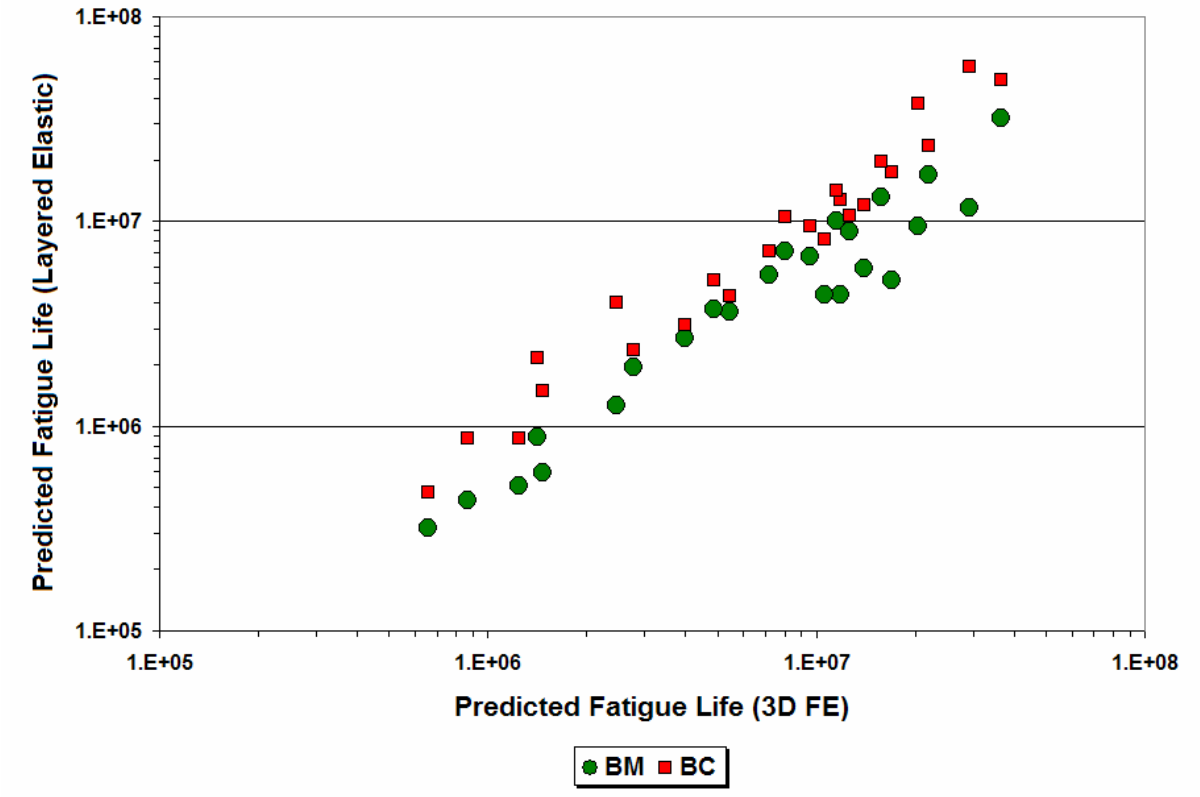

Figure 5.9. Comparisons of Predicted Fatigue Lives for 11R22.5 Radial Tire.

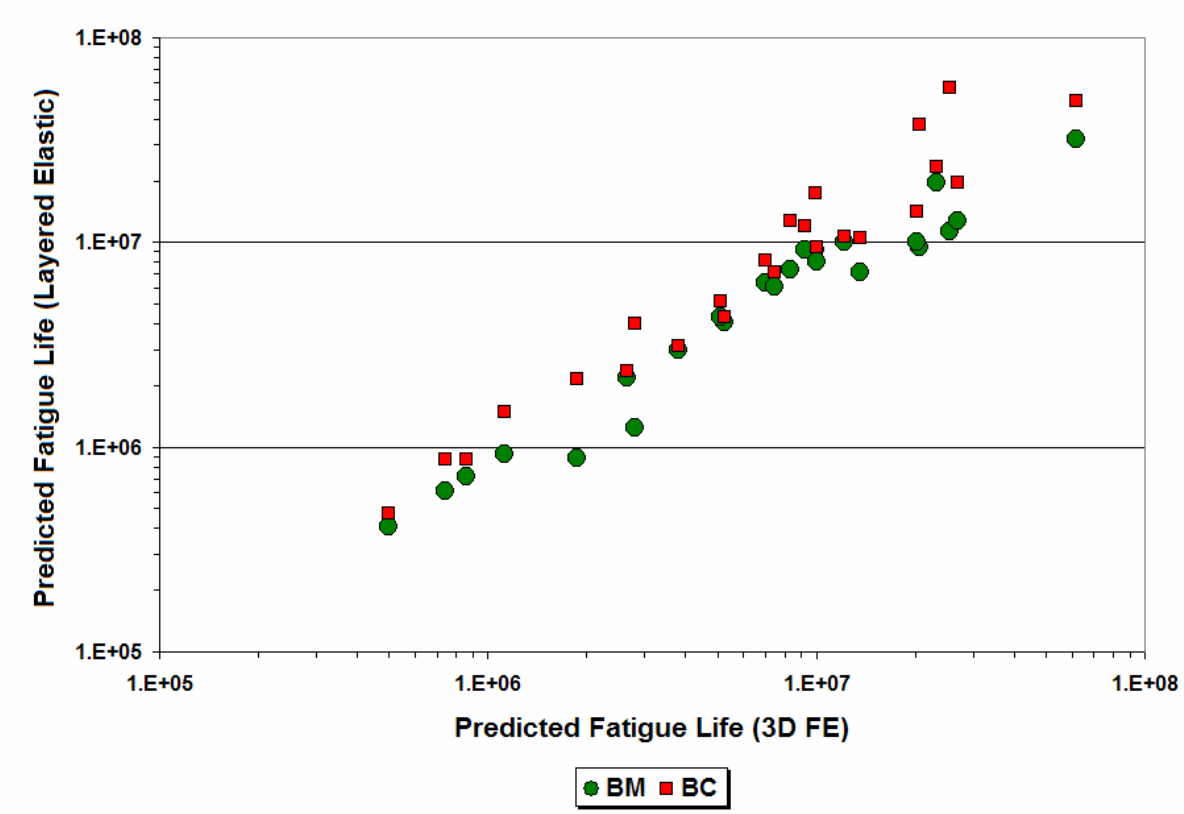

Figure 5.10. Comparisons of Predicted Fatigue Lives for 295/75R22.5 Radial Tire.

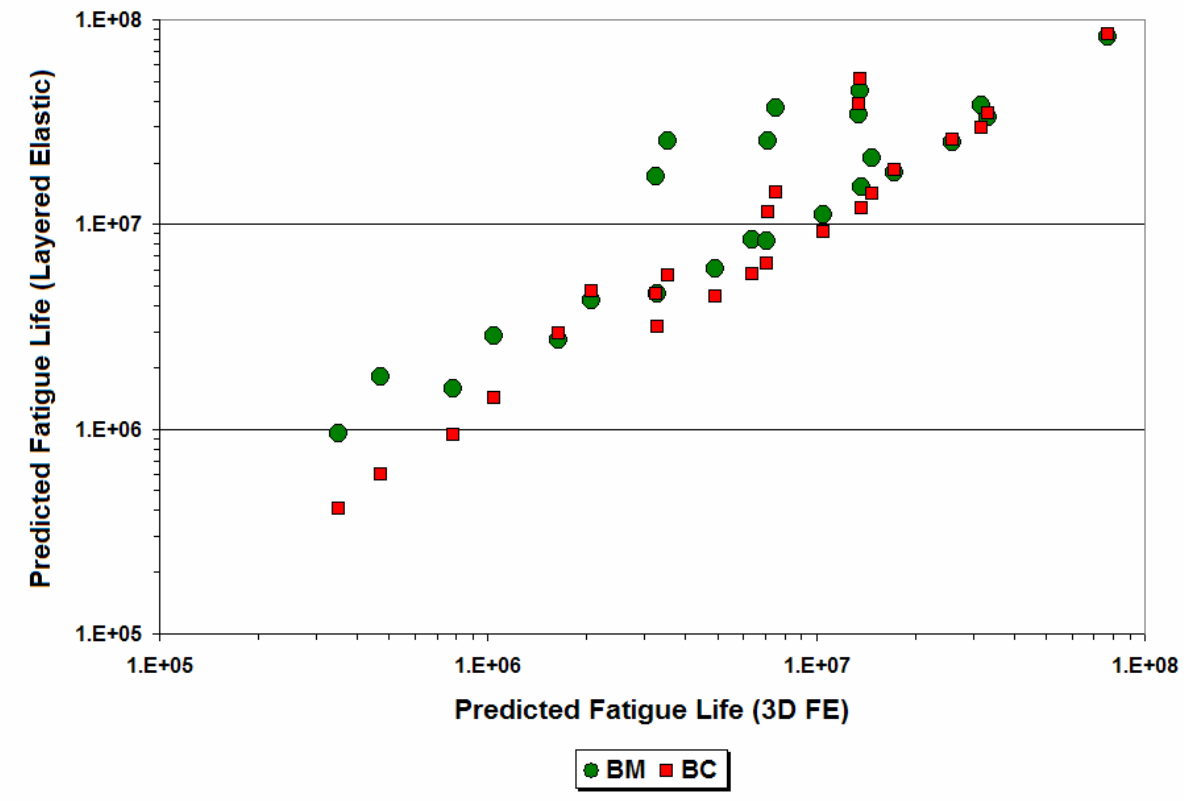

Figure 5.11. Comparisons of Predicted Fatigue Lives for 11R24.5 Radial Tire.

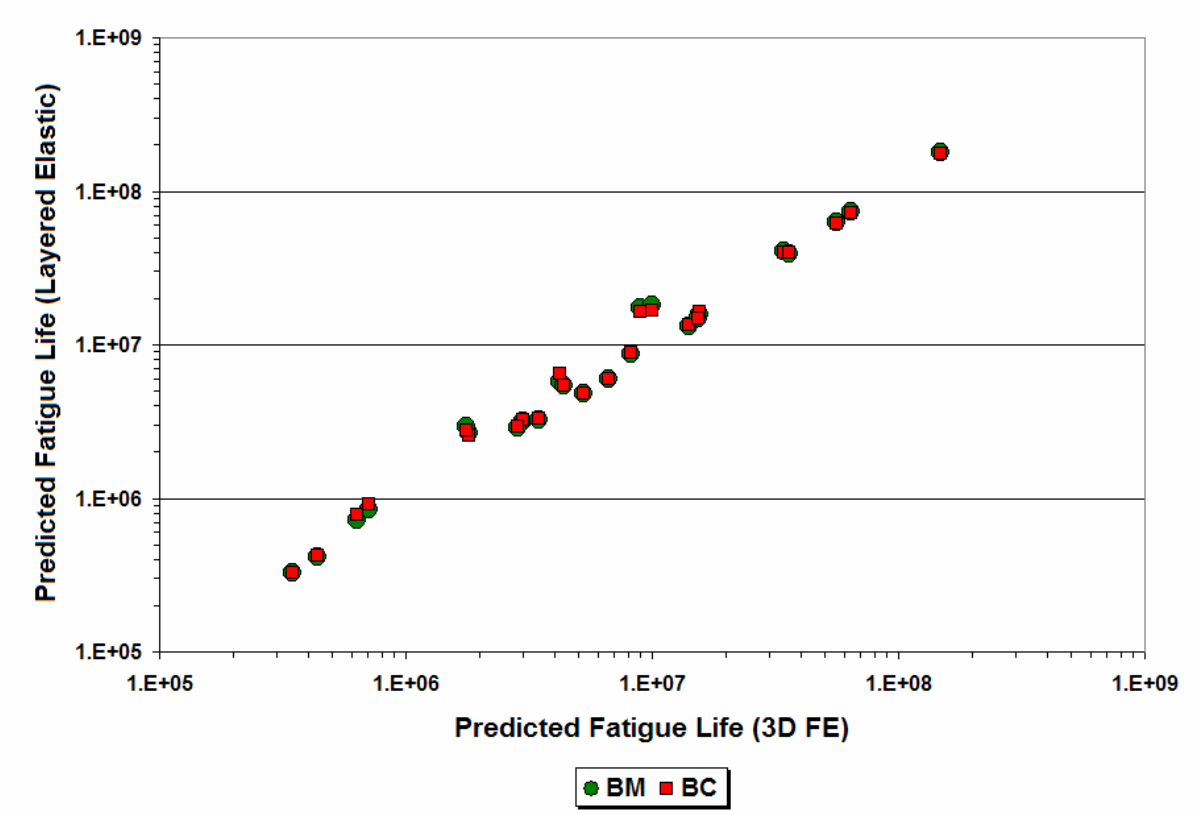

Figure 5.12. Comparisons of Predicted Fatigue Lives for 215/75R17.5 Radial Tire.

$$f = \frac{I_1}{3}\sin(\phi) + \sqrt{J_2}\,\sin(\theta + \frac{\pi}{3}) + \frac{\sqrt{J_2}}{\sqrt{3}}\cos(\theta + \frac{\pi}{3})\sin(\phi) - c\cos(\phi) \qquad (5.8)$$

where,

I_1 = first stress invariant,

J_2 = second deviatoric stress invariant,

c = cohesion,

ϕ = friction angle, and

θ = Lode angle.

The Lode angle is calculated as follows:

$$\theta = \frac{1}{3}\cos^{-1}\left[\frac{3\sqrt{3}}{2}\frac{J_3}{J_2^{3/2}}\right] \qquad (5.9)$$

where, J_3 is the third deviatoric stress invariant.

The first stress invariant is associated with volume change in a material under loading, while the second deviatoric stress invariant is associated with distortion of the

material. The onset of yield or inelastic deformation is predicted when the value of the yield function is zero in Eq. (5.8).

In this study, the MC yield function values were calculated at the center and edge of the loaded area at different depths using the 3D FE, BM and BC methods. The MC strength properties assumed in this evaluation are given in Table 5.4. Figures 5.13 to 5.16 show, respectively, the predicted MC yield function values at different depths along the center of the loaded area for pavements 1, 3, 5 and 7 identified in Table 5.1. Results are given for the 11R22.5 radial tire tested at a tire load of 5860 lb and a tire inflation pressure of 75 psi.

It is observed that the differences in the MC values between the 3D FE and layered elastic analyses are greatest near the surface and diminish quite rapidly with depth. In general, researchers observed that for the cases investigated, the differences were largest within the top 2 inches of the surface layer. Within the base and subgrade, the differences are not considered significant.

The critical MC yield function values occurred near the top and bottom of the AC layer for the cases considered. At these depths, researchers examined the differences between the 3D FE and layered elastic procedures. At a confidence level of 95 percent, it was found that the differences between the predicted MC values from the 3D FE and BM analyses are not statistically significant. However, the differences in the predicted MC values between the 3D FE and BC analyses are significant.

SUMMARY OF RESULTS

Based on the results from the comparative evaluation of predicted pavement response, researchers note the following findings:

- The decimated 3D tire contact stresses gave computed tire loads that are close to the original data. To reduce computation time, the decimated *x*, *y* and *z* contact stresses were used in the 3D finite element analyses.
- The suitability of the 3D FE model used in the analyses was verified by comparing the predicted pavement response with corresponding predictions from the BISAR program. For a uniform circular pressure distribution, researchers found that the predicted strains with depth from a 3D FE analysis using ABAQUS are quite comparable with the corresponding predictions from BISAR.

Table 5.4. Mohr-Coulomb Strength Parameters Assumed in Comparative Evaluation of Predicted Pavement Response.

Pavement Layer	Strength Parameter	
	Cohesion (psi)	Friction angle (degrees)
Asphalt Concrete	130	0
Base	15	40
Subgrade	13	20

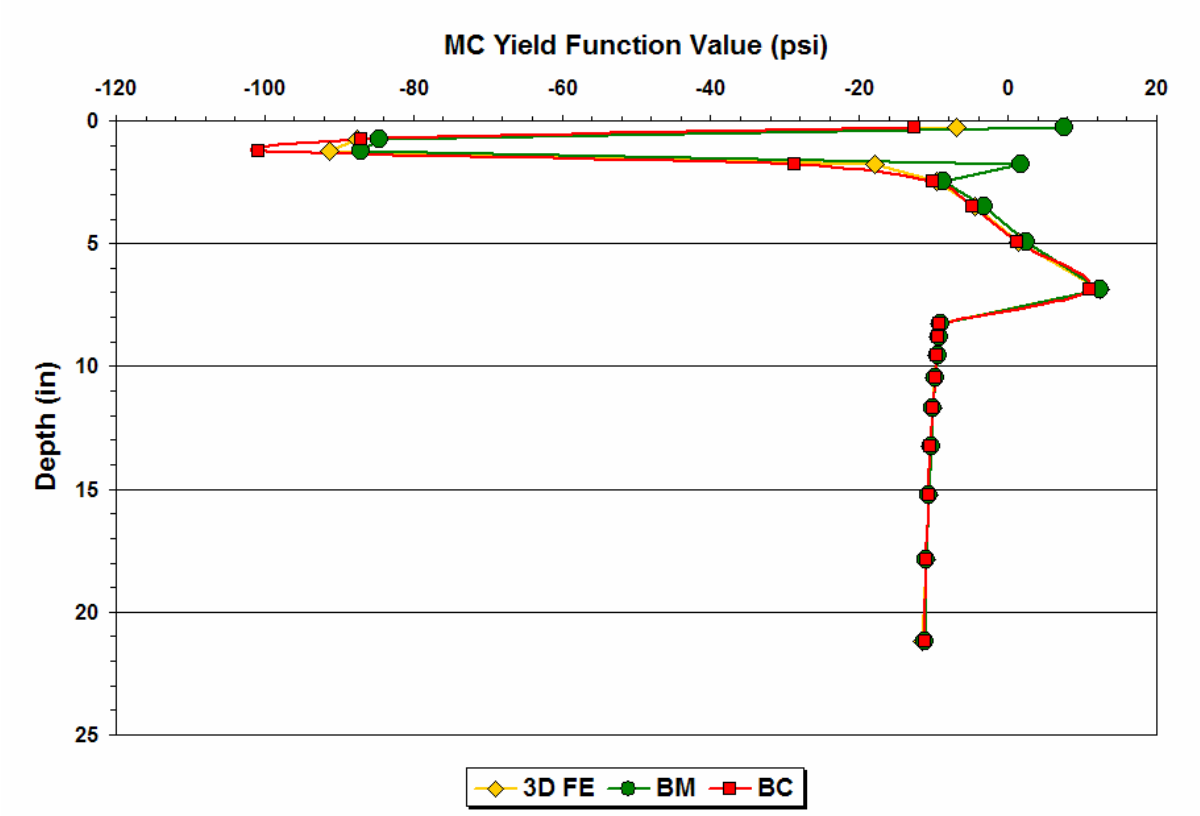

Figure 5.13. Predicted MC Values at Center of Loaded Area (Pavement #1, 11R22.5 Radial Tire at 75 psi Inflation Pressure and 5860 lb Tire Load).

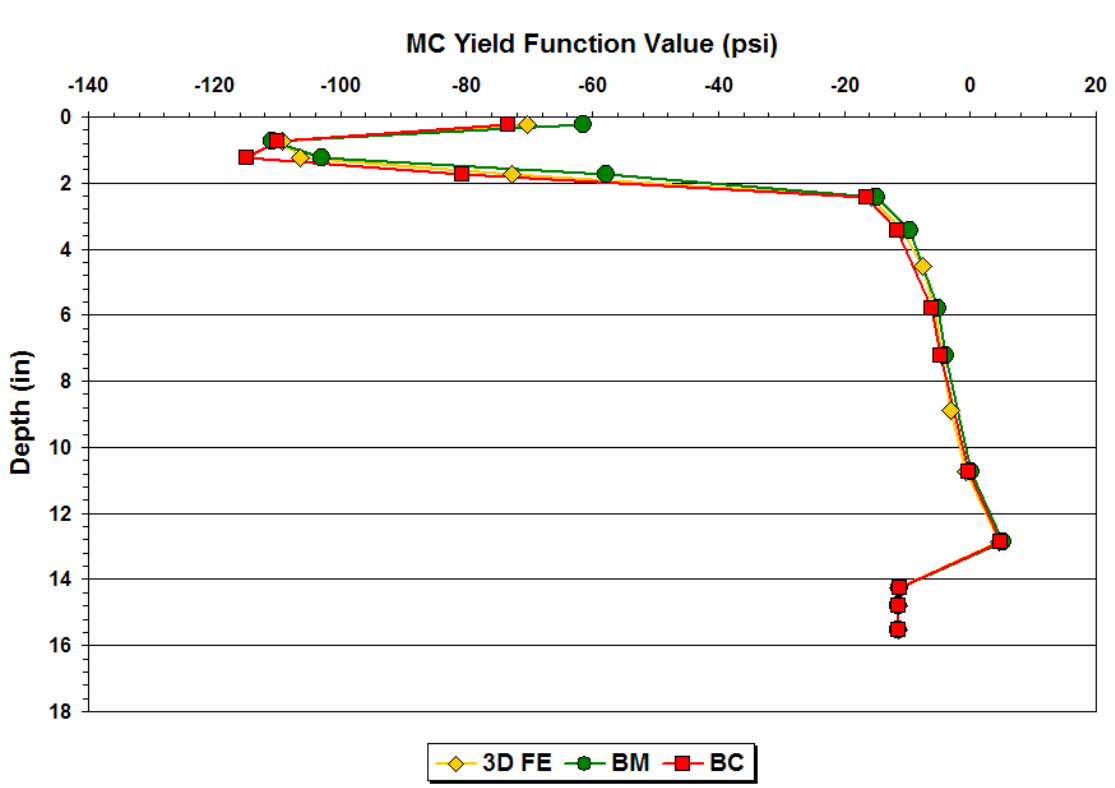

Figure 5.14. Predicted MC Values at Center of Loaded Area (Pavement #3, 11R22.5 Radial Tire at 75 psi Inflation Pressure and 5860 lb Tire Load).

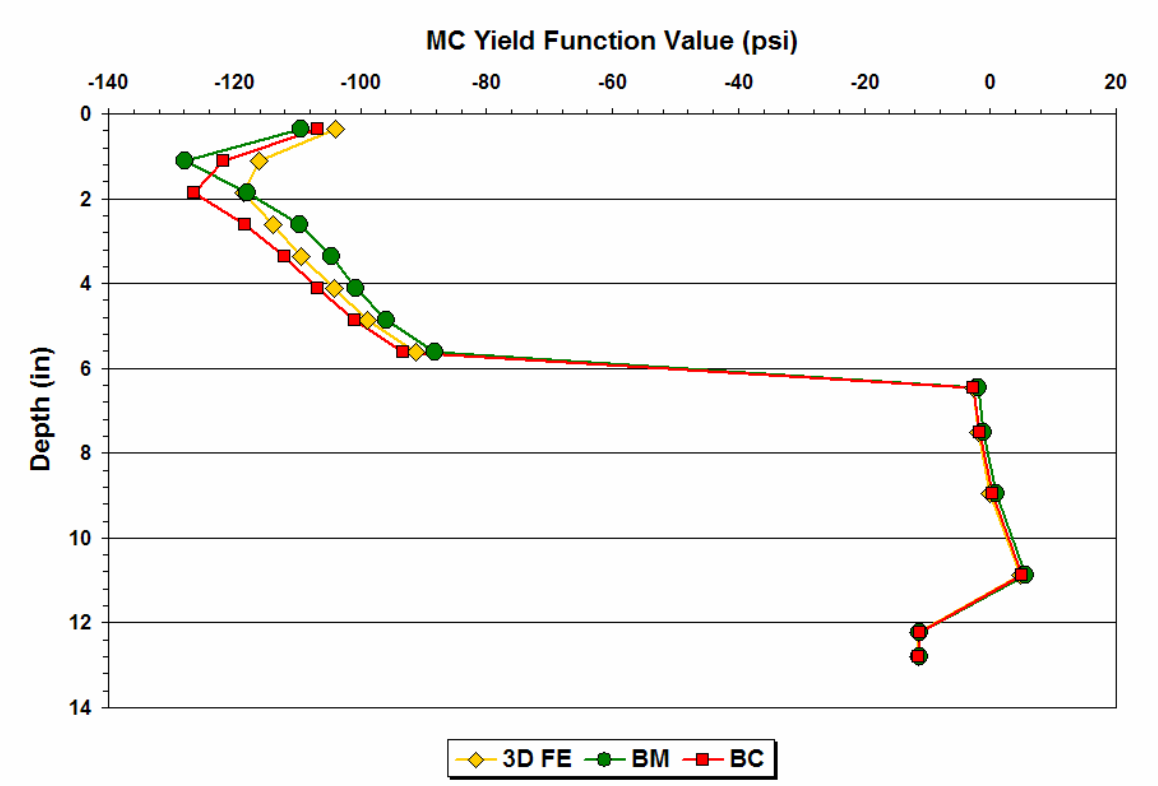

Figure 5.15. Predicted MC Values at Center of Loaded Area (Pavement #5, 11R22.5 Radial Tire at 75 psi Inflation Pressure and 5860 lb Tire Load).

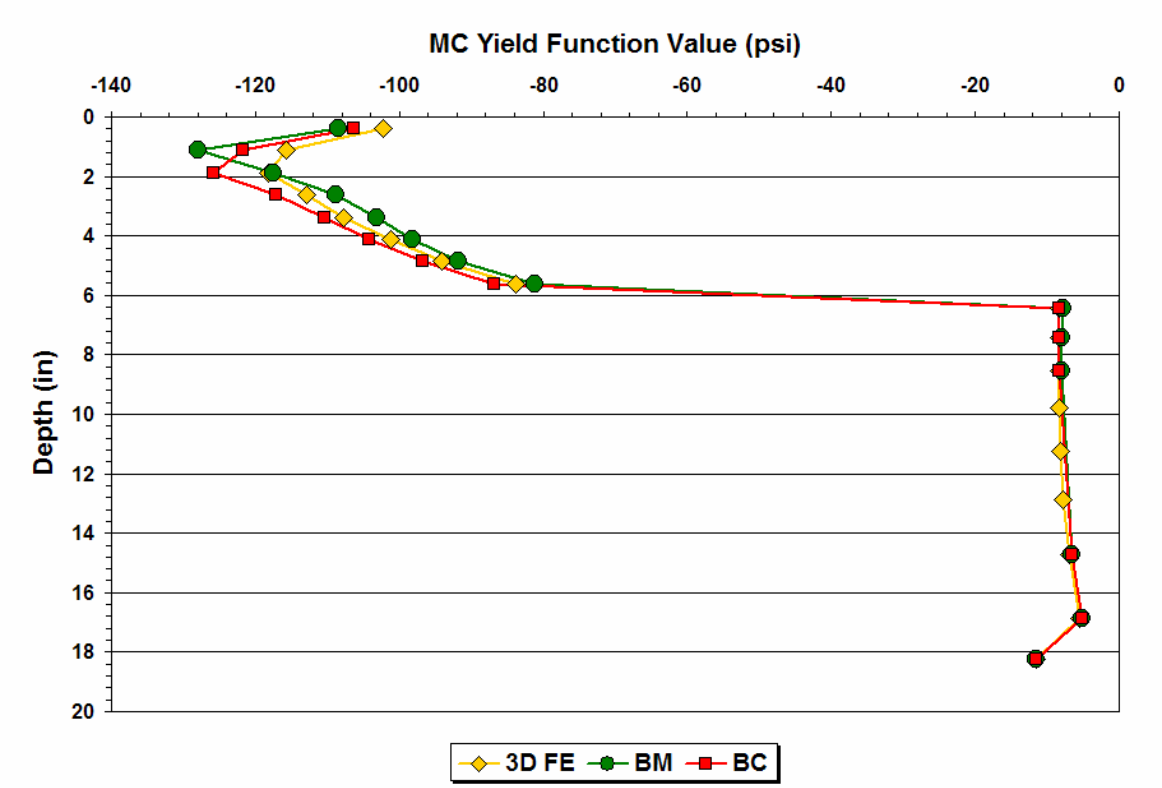

Figure 5.16. Predicted MC Values at Center of Loaded Area (Pavement #7, 11R22.5 Radial Tire at 75 psi Inflation Pressure and 5860 lb Tire Load).

- Comparison of the results from the 3D FE, BM and BC analyses showed that the differences in the fatigue predictions between the 3D FE and BM methods are not statistically significant. However, the differences in fatigue predictions between the 3D FE and BC methods are significant. Similar findings were obtained with respect to the critical Mohr-Coulomb yield function values from the three analysis methods.
- All three analysis methods gave similar predictions of pavement life based on the subgrade strain criterion. Thus, in terms of the effect of tire contact stresses on pavement rutting, the permanent deformation properties of the surface material would be critical.
- Differences in the fatigue predictions between the BM and BC methods showed the effect of tire contact area in the predicted AC tensile strains. For a given tire load and tire inflation pressure, the conventional method of analysis ignores the differences in the tire footprints between various tire types.

- The predicted pavement response from the three analysis methods differed primarily in the surface layer. In particular, the differences in MC values computed from the principal stresses were observed to be greatest within the top 2 inches of the surface.

Based on the results from comparisons of the 3D FE, BM and BC methods, the authors recommend the application of the BM method in layered elastic analyses of pavement response. For this purpose, Eqs. (4.1) to (4.6) may be used in practice to estimate the tire contact area for a given tire type, tire load and tire inflation pressure in order to determine an equivalent uniform circular contact pressure for layered elastic analyses.

Using the data base of measured tire contact stresses compiled in this project, researchers developed a computer program to predict tire contact stresses for a given tire type, tire load and tire inflation pressure based on a polynomial interpolation of the measured values stored in the data base. The outputs from the computer program include the predicted longitudinal, lateral and vertical contact stresses; the estimated tire contact area; and the equivalent uniform circular contact pressure. In this way, a layered elastic analysis may be conducted using the BM method following Eqs. (5.2) and (5.3). Alternatively, the predicted tire contact stresses can be input into a 3D finite element program, if a more rigorous analysis of predicted pavement response is warranted. The next chapter presents the computer program *TireView* for estimating tire contact stresses and tire contact areas.

CHAPTER VI. TIREVIEW PROGRAM

INTRODUCTION

TireView is a computer program to estimate tire contact pressure distributions in the longitudinal, lateral and vertical directions. The program uses an interpolation routine on the data base of measured tire contact pressures established in this project to estimate contact pressure distributions for a given tire load and tire inflation pressure. Researchers note that the data are specific to the tires tested. The data base included with the *TireView* program covers measurements made on new tires (not retreads) that are typically used for highway hauling as opposed to off-road hauling. All six tires were from one manufacturer (Goodyear). Since differences in tire construction will affect tire contact pressures, the estimates from *TireView* are tied to the data base of tire contact pressures on which the interpolations are made. Nevertheless, the program authors are of the opinion that *TireView* will provide useful data for pavement design applications, particularly for establishing or verifying design requirements for pavements subjected to heavy truck traffic, through comparative analyses of the effects of different tires and differences in wheel load assumptions on predicted pavement response and performance.

INTERPOLATION METHODOLOGY

Since the measurement of tire-pavement contact stress for different tires was done at specific intervals of tire load and tire inflation pressure, researchers initially established a procedure to predict tire contact pressure distributions for any given tire load and tire inflation pressure within the range of the compiled test data. Based on evaluating a number of curve fitting methods, researchers selected polynomial interpolation as the basis for predicting tire contact pressure distributions in the *TireView* program. Polynomial interpolation can be defined as the act of fitting a given function with defined values in certain discrete data points. This "function" may actually be any discrete data set (such as obtained by sampling), but it is generally assumed that such data may be described by a function. Thus, given n points (x_1, y_1), (x_2, y_2), (x_3, y_3),....., (x_n, y_n), where $\{x_1, x_2, x_3,....,x_n\}$ are all different, the interpolating polynomial for these n points is a function of the form

$p(x) = a_0 + a_1x + a_2x^2 + a_3x^3 + ... + a_nx^n$ such that $p(x_j) = y_j$ for all x_j, j = 1 to n. The Lagrange form of the interpolating polynomial satisfying this condition is given by:

$$p(x) = \sum_{j=1}^{n} y_j \, l_j(x) \tag{6.1}$$

where,

$$l_j(x) = \prod_{\substack{k=1 \\ k \neq j}}^{n} \frac{x - x_k}{x_j - x_k} \tag{6.2}$$

To illustrate, given three points (x_1, y_1), (x_2, y_2) and (x_3, y_3), application of Eqs. (6.1) and (6.2) gives the forms of $l_j(x)$, and the values of $l_j(x)$ and $p(x)$ shown in Table 6.1.

Numerically, *TireView* uses Neville's algorithm (Press et al., 2002) to construct the Lagrange interpolating polynomial. The program does a series of one-dimensional interpolations in stages to estimate the tire contact pressure distribution for a given tire type, tire load and tire inflation pressure using the data base of measured tire contact pressures for the given tire type. To check the algorithm, researchers used *TireView* to determine the tire contact force distributions for the 11R24.5 radial tire loaded to 6200 lb and inflated to 130 psi. Figures 6.1 to 6.3 compare the measured and predicted tire contact forces in the lateral, longitudinal and vertical directions, respectively. Researchers note that the predictions from the interpolations match the measured values. These results indicate that the program is working as it should since the measurements at 6200 lb and 130 psi inflation pressure are points that the interpolating polynomials must go through as discussed previously.

To gauge the predictive accuracy of the algorithm used in *TireView*, researchers re-did the predictions for the 11R24.5 radial tire without the measured contact forces at the tire load of 6200 lb and 130 psi inflation pressure. Figures 6.4 to 6.6 show the results from these recalculations. Considering that the measured contact forces for the cases considered were not used in the prediction, the interpolated force distributions still reasonably approximate the measured distributions, in the authors' opinion.

Table 6.1. Example of Lagrange Interpolating Polynomial for Three Data Points.

j	$l_j(x)$	Value of $l_j(x)$ given x			$p(x_j)$
		$x = x_1$	$x = x_2$	$x = x_3$	
1	$\frac{(x-x_2)(x-x_3)}{(x_1-x_2)(x_1-x_3)}$	1	0	0	y_1
2	$\frac{(x-x_1)(x-x_3)}{(x_2-x_1)(x_2-x_3)}$	0	1	0	y_2
3	$\frac{(x-x_1)(x-x_2)}{(x_3-x_1)(x_3-x_2)}$	0	0	1	y_3

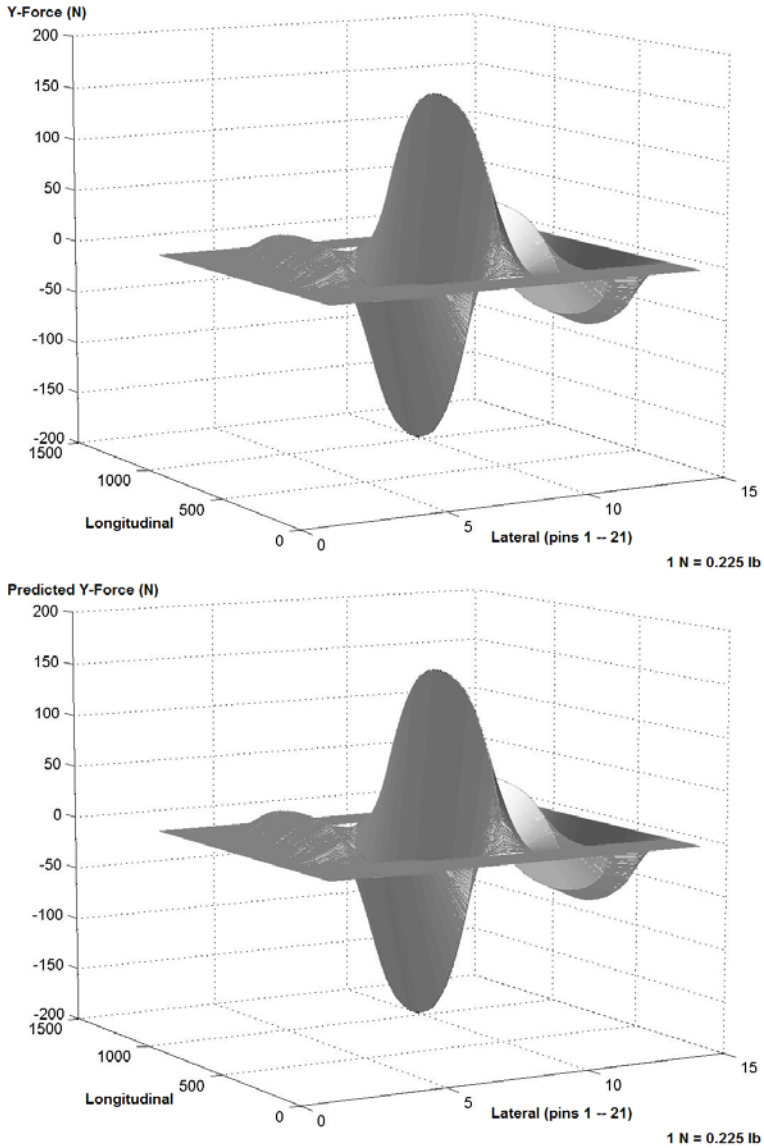

Figure 6.1. Comparison of Measured and Predicted Lateral Tire Contact Forces for 11R24.5 Radial Tire (6200 lb Tire Load and 130 psi Tire Inflation Pressure).

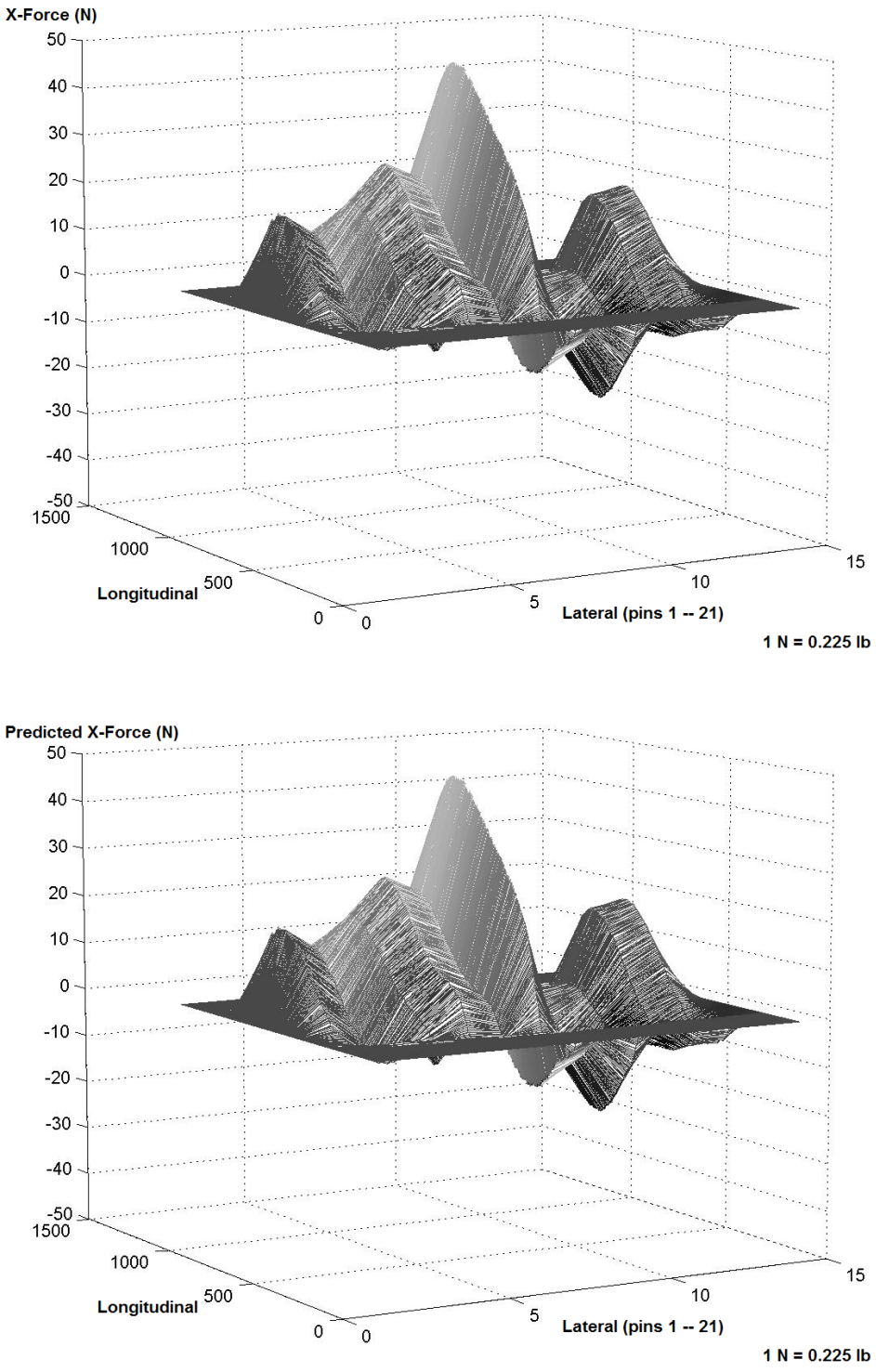

Figure 6.2. Comparison of Measured and Predicted Longitudinal Tire Contact Forces for 11R24.5 Radial Tire (6200 lb Tire Load and 130 psi Tire Inflation Pressure).

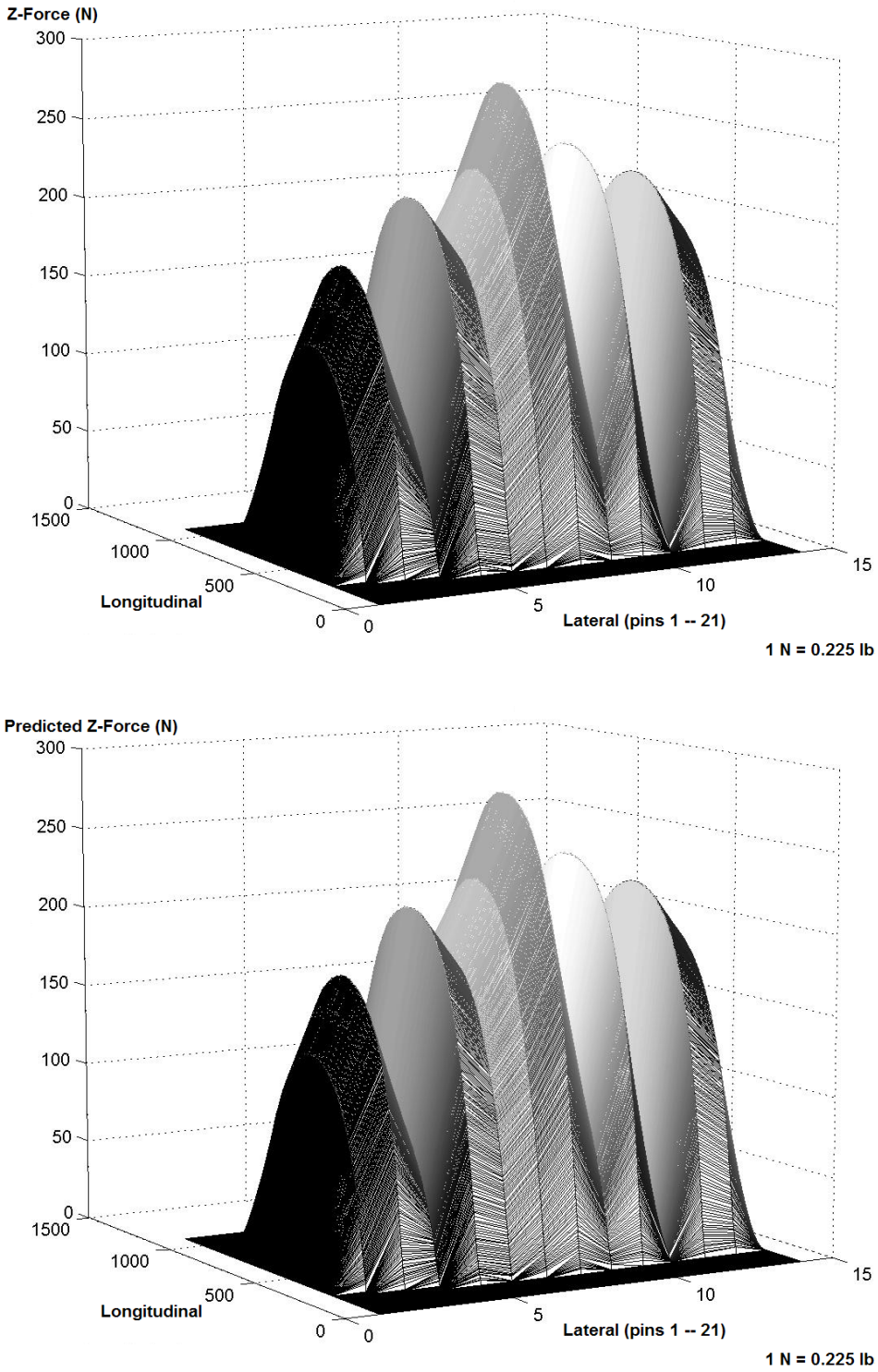

Figure 6.3. Comparison of Measured and Predicted Vertical Tire Contact Forces for 11R24.5 Radial Tire (6200 lb Tire Load and 130 psi Tire Inflation Pressure).

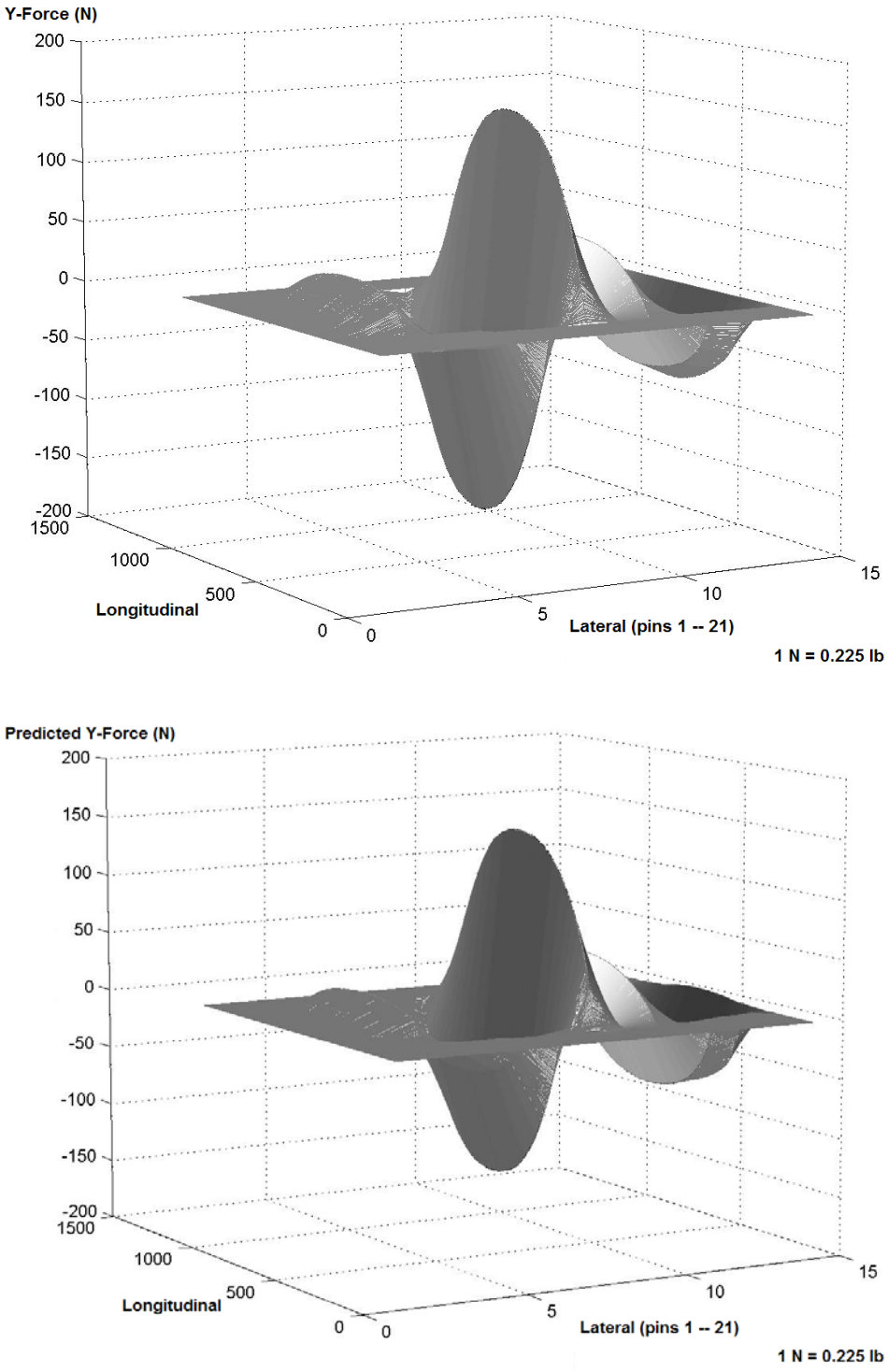

Figure 6.4. Comparison of Measured and Predicted Lateral Tire Contact Forces for 11R24.5 Radial Tire when Data at 6200 lb Tire Load and 130 psi Tire Inflation Pressure Are Not Used in Interpolation.

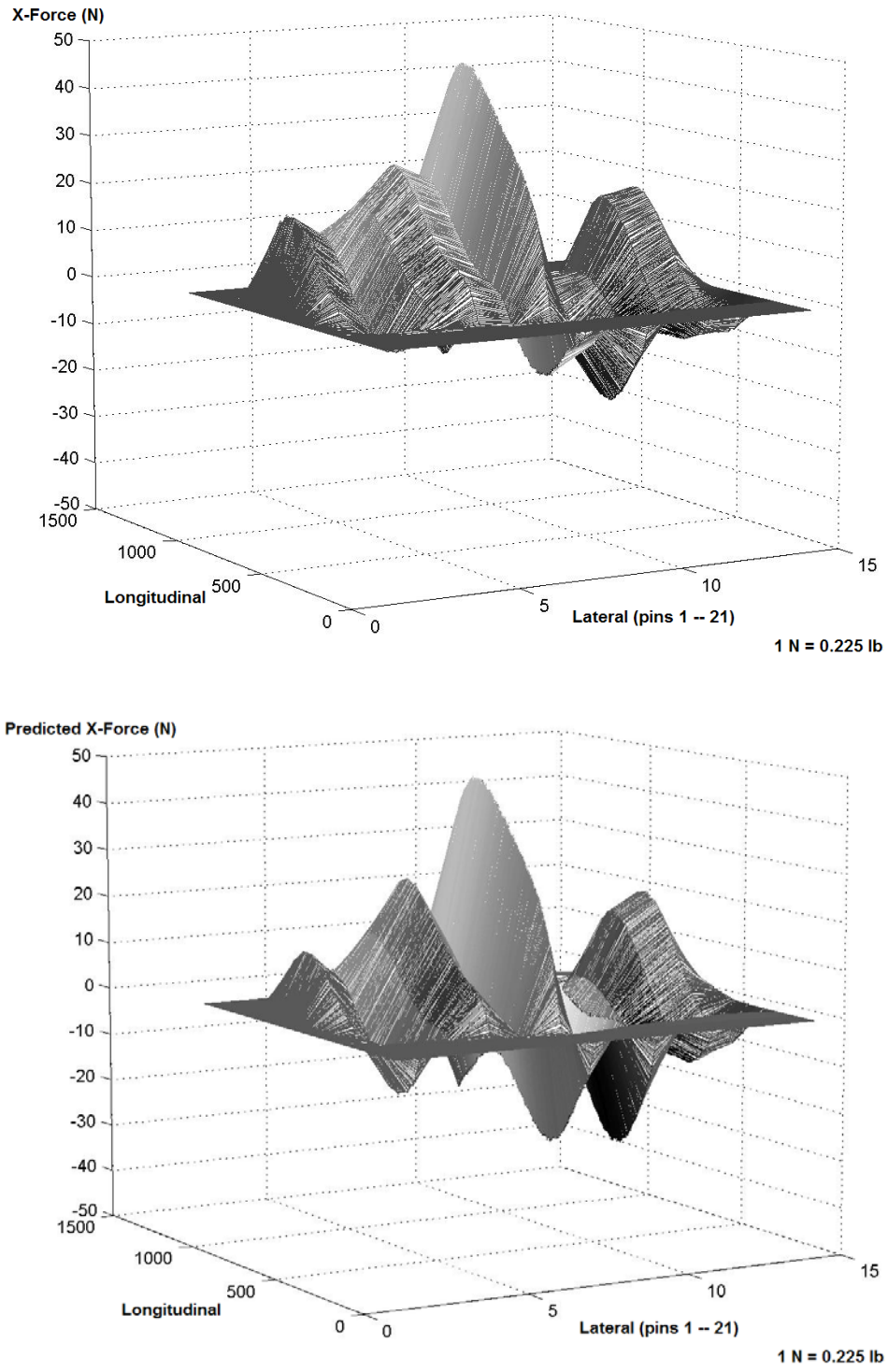

Figure 6.5. Comparison of Measured and Predicted Longitudinal Tire Contact Forces for 11R24.5 Radial Tire when Data at 6200 lb Tire Load and 130 psi Tire Inflation Pressure Are Not Used in Interpolation.

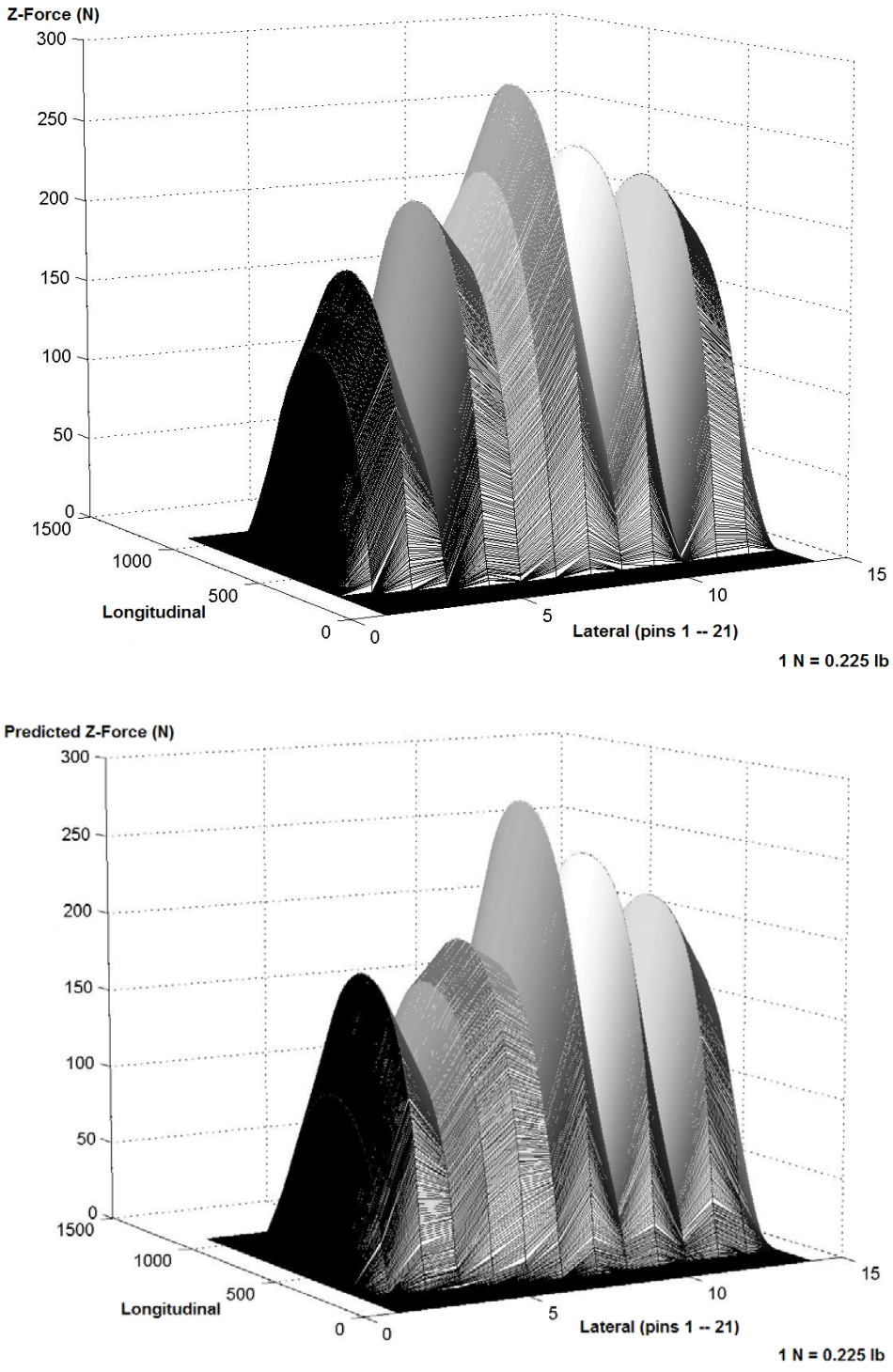

Figure 6.6. Comparison of Measured and Predicted Vertical Tire Contact Forces for 11R24.5 Radial Tire when Data at 6200 lb Tire Load and 130 psi Tire Inflation Pressure Are Not Used in Interpolation.

SYSTEM REQUIREMENTS AND PROGRAM INSTALLATION

The *TireView* computer program is installed from the set-up disk submitted as the product from this research project (Fernando, 2005). *TireView* requires a microcomputer operating under Windows 98SE or higher. Program use requires a working knowledge of the Windows operating system. To install *TireView*, load the installation disk into the computer's CD-ROM drive. Click on the ***Start*** button in Windows and select ***Run***. At the dialog box, type ***drive letter:\Tire_view_setup***, where ***drive letter*** specifies the CD-ROM drive (e.g., ***E:***\). Click on the ***OK*** button of the dialog box to run the installation program. Simply follow the instructions that appear on screen. The setup program will prompt for a subdirectory or folder in which to store the *TireView* files on the computer's hard drive. By default, the files are copied to ***C:\TireView***; however, you have the option to specify a different subdirectory, such as ***C:\Program Files\TireView***.

After installation, users can execute *TireView* using the shortcut placed on the desktop during setup, or through the ***Programs*** list. To access this list, simply click on the ***Start*** button, move the pointer to ***All Programs***, then to ***TireView.*** The program icon will appear. Click on the icon to load the program. The next section provides instructions in the use of *TireView* and describes the program output.

USING TIREVIEW

Figure 6.7 shows the main menu of the *TireView* program. Through this menu, users specify the tire type, tire load and tire inflation pressure on which estimates of tire contact pressures are to be generated. The tires that users may select are limited to the six tires shown in Figure 6.7. For the selected tire, specify the tire load (in lb) and the inflation pressure (in psi). The values specified for the interpolation should be within the range of values at which the selected tire was tested. Otherwise, *TireView* displays a message prompting users to specify an input value within the permissible range of the given variable.

The permissible ranges are displayed to the right of the input fields for tire load and tire inflation pressure. For example, Figure 6.7 shows that the tire loads used in testing the 215/75R17.5 radial tire range from 3000 to 7000 lb. Additionally, the tire inflation pressures varied from 85 to 145 psi. Tables 2.3 to 2.7 show the specific combinations of tire load and tire inflation pressure at which tire contact pressure measurements were made for the six tires tested. The data from these tests are used in *TireView* to interpolate tire

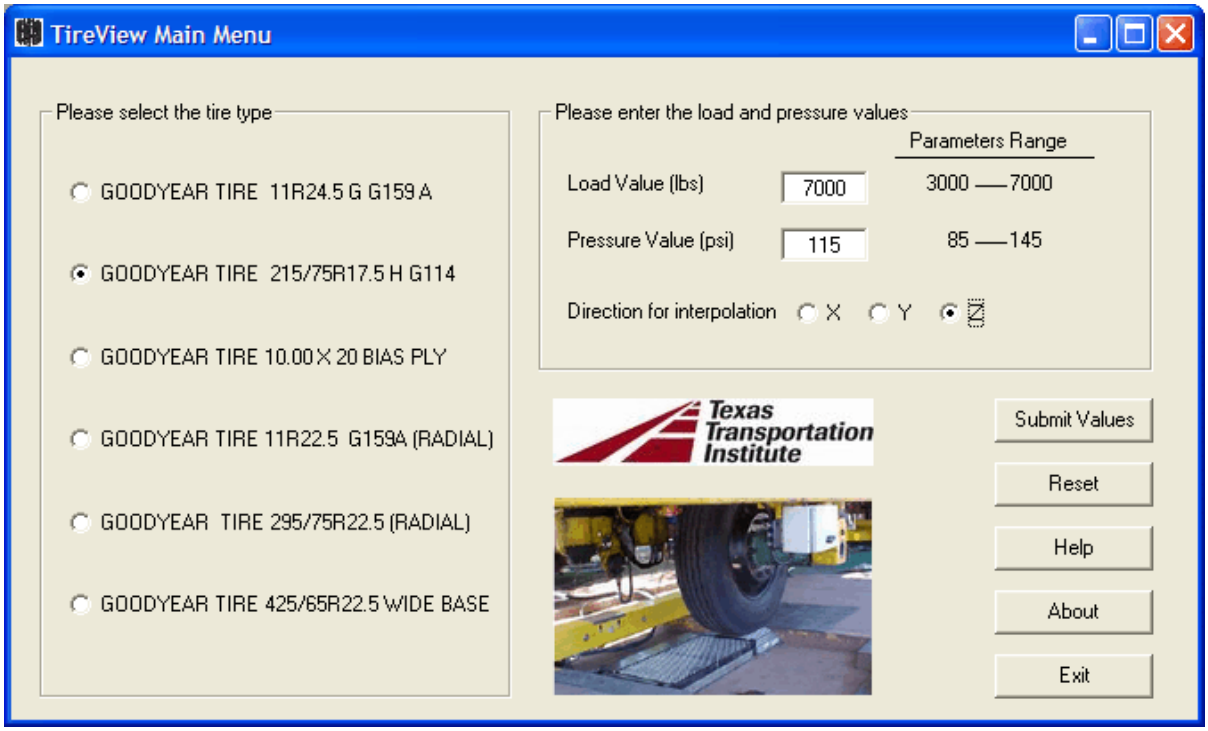

Figure 6.7. *TireView* Main Menu.

contact stresses at the specified values of load and inflation pressure for the selected tire. Thus, specify inputs within the range of the test conditions for the different tires.

Users also need to specify the component of the stress (or force) to be estimated by clicking the X, Y or Z buttons corresponding, respectively, to the longitudinal (in the direction of wheel travel), lateral and vertical contact stresses. After specifying all input data, click on ***Submit Values*** in the main menu to proceed with the interpolation. *TireView* then displays the dialog box shown in Figure 6.8 where users specify the name of the file where the results from the interpolation will be saved. By default, the output file is named ***TireView***. After specifying the output file name, click on the ***Save*** button of the dialog box to proceed with the interpolation.

TireView lets users know when the calculations are done by displaying a message box (Figure 6.9) that informs them where the output has been saved. Click on the ***OK*** button of this dialog box. The results from the interpolation are then displayed in the output screen illustrated in Figure 6.10, which graphically gives the estimates of vertical contact stresses within the tire patch. The following information are provided in this figure:

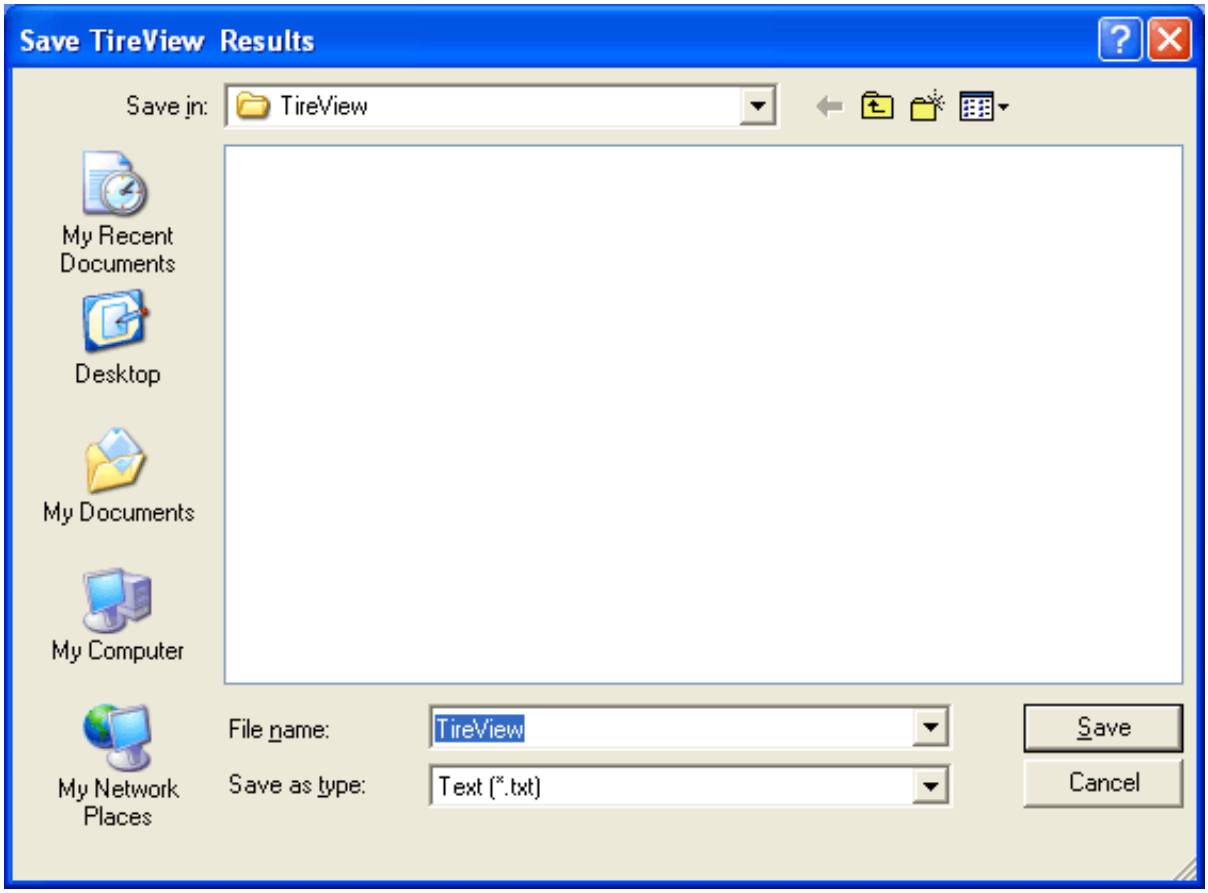

Figure 6.8. Dialog Box for Specifying Name of *TireView* Output File.

Figure 6.9. Message Displayed after Calculations are Completed.

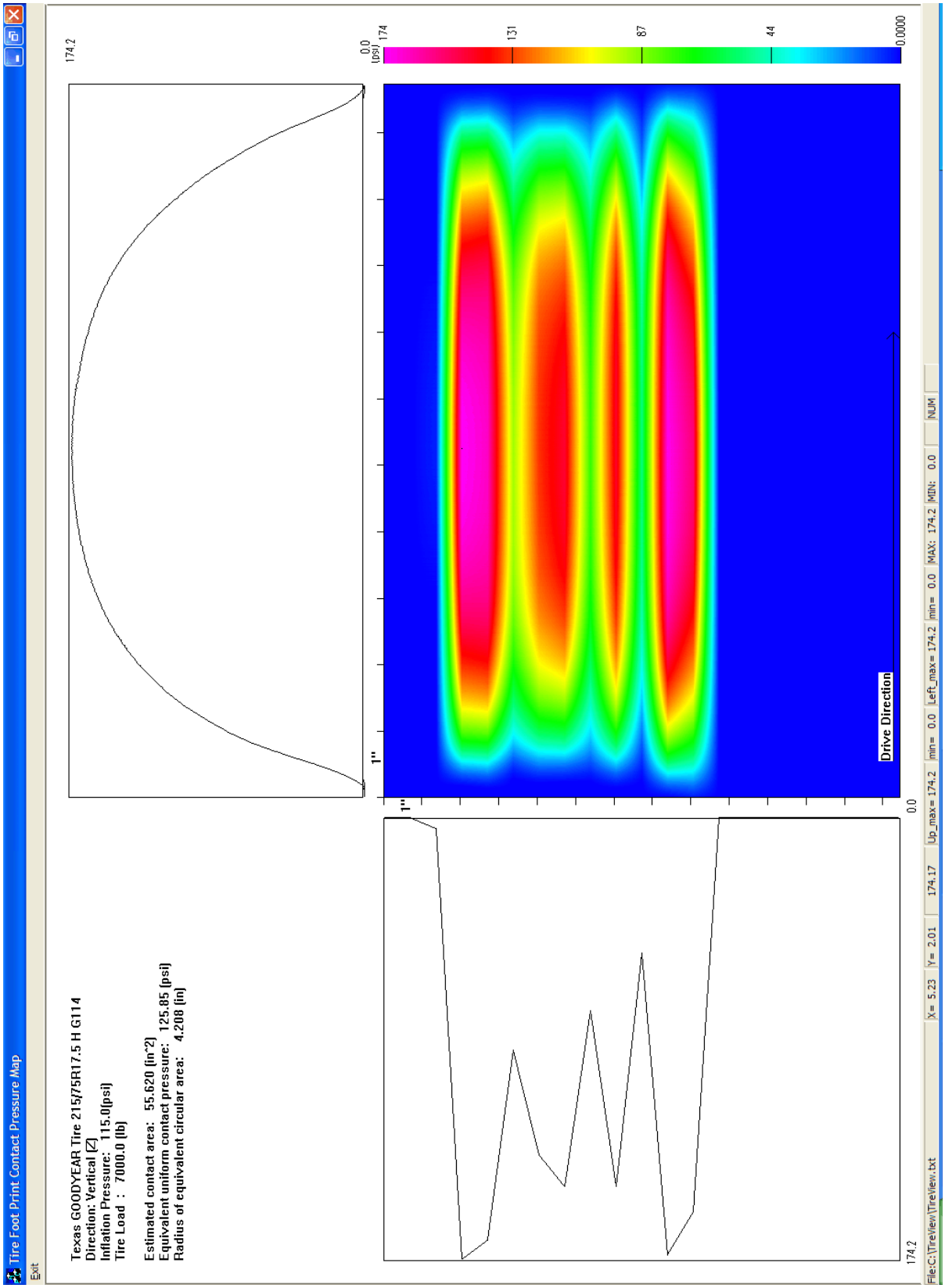

Figure 6.10. *TireView* Output Screen.

- Tire type selected and the stress component,
- Tire inflation pressure and tire load specified,
- An estimate of the tire contact area for the specified tire load and tire inflation pressure determined using Eqs. (4.1) to (4.6),
- The equivalent uniform contact pressure determined by dividing the tire load by the estimated contact area,
- The radius of the equivalent circular patch having the same tire contact area, and
- A color-coded chart of the estimated contact stresses with a color bar to the right of the chart that maps the predicted contact stresses to the different color ranges.

The estimate of the tire contact area, equivalent uniform contact pressure and radius of the equivalent circular area can be used, as discussed in Chapter V, to characterize the wheel load in a layered elastic analysis to predict pavement response for a given tire type, tire load and tire inflation pressure. In this way, the effect of tire type on the tire footprint can be considered using existing layered elastic programs implemented within TxDOT.

Clicking the mouse within the color-coded chart displays the variation of the estimated contact stresses along the longitudinal and lateral directions. The longitudinal variation of the predicted stresses is displayed at the top of the color-coded chart, which shows a plot of the variation of the predicted contact stresses along a line parallel to the direction of wheel travel and passing through the point where the user clicked the mouse. A similar logic applies for the lateral variation of the predicted stresses shown to the left of the color-coded chart.

The coordinates of the point within the chart where the user clicked the mouse are given on the left-hand side of the information bar located at the bottom of the *TireView* output screen. For example, Figure 6.10 shows that the X and Y coordinates are 5.23 and 2.01 inches, respectively, based on using the top left corner of the color-coded chart as the origin. Also shown to the right of these coordinates in the information bar are:

- The estimated contact stress at the current cursor location (174.17 psi in the example output screen shown in Figure 6.10). This output variable is continually updated as the cursor is moved within the color-coded chart of estimated contact pressures;

- The maximum and minimum values in the plot of the longitudinal variation of estimated contact stresses shown above the color-coded chart (174.2 and 0.0 psi, respectively, in the example given in Figure 6.10);
- The maximum and minimum values in the plot of the lateral variation of estimated contact stresses given to the left of the color-coded chart (174.2 and 0.0 psi, respectively); and
- The maximum and minimum of the predicted contact stresses within the entire contact area (174.2 and 0.0 psi, respectively, in Figure 6.10).

TIREVIEW OUTPUT FILE

Figure 6.11 illustrates the output file from the *TireView* program. There will generally be many records in this file. Thus, the example given in Figure 6.11 only shows snapshots of a typical output file, enough to describe the output, which follows the format of the data files from the tests conducted. The first four lines of the file are header records that show:

- The tire type analyzed (first line) and the project from which test data were collected (Texas or UCB).
- The force component (X, Y or Z) on which interpolations were made (second line) and the unit in which the forces are reported (lb).
- The first 12 characters of the output file name, inflation pressure (psi) and tire load (lb) specified for the interpolation (third line). Also given in the third line are the test speed (fps) and the sampling rate (Hz) at which tests were conducted for the selected tire (the test speed and the sampling rate varied between the UCB and TTI tire tests as shown in Table 2.2).
- The load pin numbers (fourth line). There are 21 load pins in the SIM pad used for the TTI tests, and 20 for the UCB tests.

Each record following the fourth line consists of $N+1$ entries where N is the number of load pins used for testing the given tire. The first entry is simply a counter for the record. The next N entries are the interpolated contact forces corresponding to the different load pins. From these measurements, the contact stress is calculated by dividing the contact force by the effective area of each load pin (0.3879 in^2 as given in Table 2.2). This table also gives the distances between consecutive rows of data and between load pins. The data

FILENAME (.txt)	Pressure (psi)	HVS (lbs)	SPEED (fps)	Hz (sam/sec)	SIM LOAD (lbs)	Texas GOODYEAR Tire 215/75R17.5 H G114 Z Direction Data in Pounds											
TireView.txt	115	7000	1.148	1001	7000												
COUNTS/PINS	1	2	3	4	5	6	7	8	9	10	11	12	13	14	15 • • • •		21
1	0.0000	0.0000	0.0000	0.0000	0.0000	0.0000	0.0000	0.0000	0.0000	0.0000	0.0000	0.0000	0.0000	0.0000	0.0000 • • • •		0.0000
2	0.0000	0.0000	0.0000	0.0000	0.0000	0.0000	0.0000	0.0000	0.0000	0.0000	0.0000	0.0000	0.0000	0.0000	0.0000 • • • •		0.0000
3	0.0000	0.0000	0.0000	0.0000	0.0000	0.0000	0.0000	0.0000	0.0000	0.0000	0.0000	0.0000	0.0000	0.0000	0.0000 • • • •		0.0000
4	0.0000	0.0000	0.0000	0.0000	0.0000	0.0000	0.0000	0.0000	0.0000	0.0000	0.0000	0.0000	0.0000	0.0000	0.0000 • • • •		0.0000
5	0.0000	0.0000	0.0000	0.0000	0.0000	0.0000	0.0000	0.0000	0.0000	0.0000	0.0000	0.0000	0.0000	0.0000	0.0000 • • • •		0.0000
6	0.0000	0.0000	0.0000	0.0000	0.0000	0.0000	0.0000	0.0000	0.0000	0.0000	0.0000	0.0000	0.0000	0.0000	0.0000 • • • •		0.0000
7	0.0000	0.0000	0.0000	0.0000	0.0000	0.0000	0.0000	0.0000	0.0000	0.0000	0.0000	0.0000	0.0000	0.0000	0.0000 • • • •		0.0000
8	0.0000	0.0000	0.0000	0.0000	0.0000	0.0000	0.0000	0.0000	0.0000	0.0000	0.0000	0.0000	0.0000	0.0000	0.0000 • • • •		0.0000
9	0.0000	0.0000	0.0000	0.0000	0.0000	0.0000	0.0000	0.0000	0.0000	0.0000	0.0000	0.0000	0.0000	0.0000	0.0000 • • • •		0.0000
10	0.0000	0.0000	0.0000	0.0000	0.0000	0.0000	0.0000	0.0000	0.0000	0.0000	0.0000	0.0000	0.0000	0.0000	0.0000 • • • •		0.0000
•	•	•	•	•	•	•	•	•	•	•	•	•	•	•	•	•	•
•	•	•	•	•	•	•	•	•	•	•	•	•	•	•	•	•	•
•	•	•	•	•	•	•	•	•	•	•	•	•	•	•	•	•	•
•	•	•	•	•	•	•	•	•	•	•	•	•	•	•	•	•	•
•	•	•	•	•	•	•	•	•	•	•	•	•	•	•	•	•	•
•	•	•	•	•	•	•	•	•	•	•	•	•	•	•	•	•	•
409	0.0000	0.0000	1.4987	67.2179	64.2954	35.5947	51.4812	56.7268	29.5249	56.2772	20.5326	66.6933	60.2488	0.0000	0.0000 • • • •		0.0000
410	0.0000	0.0000	1.5737	67.1429	64.2954	35.5198	51.4812	56.5769	29.5998	56.3521	20.3827	66.6184	60.0989	0.0000	0.0000 • • • •		0.0000
411	0.0000	0.0000	1.5737	67.2928	64.4452	35.5947	51.4063	56.5020	29.4500	56.4270	20.5326	66.6933	60.2488	0.0000	0.0000 • • • •		0.0000
412	0.0000	0.0000	1.4238	67.2928	64.4452	35.5198	51.3314	56.5020	29.5998	56.3521	20.3827	66.6184	60.2488	0.0000	0.0000 • • • •		0.0000
413	0.0000	0.0000	1.5737	67.2928	64.4452	35.5198	51.4063	56.5769	29.4500	56.4270	20.4576	66.6933	60.2488	0.0000	0.0000 • • • •		0.0000
414	0.0000	0.0000	1.6486	67.2928	64.3703	35.5947	51.3314	56.5769	29.5249	56.3521	20.6075	66.6933	60.3237	0.0000	0.0000 • • • •		0.0000
415	0.0000	0.0000	1.6486	67.2928	64.4452	35.5947	51.4812	56.7268	29.5249	56.5020	20.6075	66.6184	60.3237	0.0000	0.0000 • • • •		0.0000
416	0.0000	0.0000	1.4987	67.2179	64.4452	35.6697	51.3314	56.5769	29.5249	56.4270	20.6075	66.7683	60.3237	0.0000	0.0000 • • • •		0.0000
417	0.0000	0.0000	1.4987	67.3677	64.4452	35.5198	51.3314	56.6519	29.5249	56.5769	20.4576	66.6933	60.2488	0.0000	0.0000 • • • •		0.0000
418	0.0000	0.0000	1.5737	67.2928	64.4452	35.5198	51.3314	56.7268	29.5249	56.5020	20.4576	66.6933	60.2488	0.0000	0.0000 • • • •		0.0000
419	0.0000	0.0000	1.5737	67.4427	64.3703	35.5198	51.4812	56.5769	29.5998	56.3521	20.6075	66.6933	60.2488	0.0000	0.0000 • • • •		0.0000
420	0.0000	0.0000	1.5737	67.2928	64.4452	35.4449	51.4812	56.5769	29.5998	56.4270	20.5326	66.6184	60.2488	0.0000	0.0000 • • • •		0.0000
421	0.0000	0.0000	1.6486	67.3677	64.3703	35.5947	51.4812	56.5769	29.6748	56.5020	20.5326	66.6933	60.3237	0.0000	0.0000 • • • •		0.0000
422	0.0000	0.0000	1.4987	67.2928	64.4452	35.5198	51.5562	56.5769	29.5998	56.4270	20.5326	66.6933	60.2488	0.0000	0.0000 • • • •		0.0000
423	0.0000	0.0000	1.5737	67.3677	64.3703	35.5198	51.4812	56.5020	29.5998	56.4270	20.4576	66.6184	60.3237	0.0000	0.0000 • • • •		0.0000
424	0.0000	0.0000	1.6486	67.3677	64.3703	35.5198	51.4063	56.5769	29.5998	56.4270	20.6075	66.6184	60.1739	0.0000	0.0000 • • • •		0.0000
425	0.0000	0.0000	1.5737	67.4427	64.5202	35.5198	51.4812	56.6519	29.5249	56.3521	20.6075	66.6184	60.3237	0.0000	0.0000 • • • •		0.0000
426	0.0000	0.0000	1.5737	67.4427	64.4452	35.5198	51.4812	56.5769	29.5998	56.4270	20.5326	66.6184	60.3237	0.0000	0.0000 • • • •		0.0000
427	0.0000	0.0000	1.6486	67.4427	64.3703	35.5198	51.4063	56.5020	29.5998	56.5020	20.6075	66.7683	60.3237	0.0000	0.0000 • • • •		0.0000
428	0.0000	0.0000	1.5737	67.2928	64.3703	35.5198	51.4063	56.5020	29.5249	56.4270	20.5326	66.6184	60.3237	0.0000	0.0000 • • • •		0.0000
429	0.0000	0.0000	1.6486	67.4427	64.4452	35.4449	51.4063	56.5020	29.6748	56.5020	20.6075	66.7683	60.3237	0.0000	0.0000 • • • •		0.0000
430	0.0000	0.0000	1.4987	67.2928	64.4452	35.4449	51.4812	56.5020	29.5249	56.4270	20.5326	66.6933	60.3987	0.0000	0.0000 • • • •		0.0000
431	0.0000	0.0000	1.4987	67.2928	64.4452	35.5198	51.4812	56.6519	29.5249	56.5020	20.4576	66.5434	60.2488	0.0000	0.0000 • • • •		0.0000
•	•	•	•	•	•	•	•	•	•	•	•	•	•	•	•	•	•
•	•	•	•	•	•	•	•	•	•	•	•	•	•	•	•	•	•
•	•	•	•	•	•	•	•	•	•	•	•	•	•	•	•	•	•
•	•	•	•	•	•	•	•	•	•	•	•	•	•	•	•	•	•
•	•	•	•	•	•	•	•	•	•	•	•	•	•	•	•	•	•
•	•	•	•	•	•	•	•	•	•	•	•	•	•	•	•	•	•
875	0.0000	0.0000	0.0000	0.0000	0.0000	0.0000	0.0000	0.0000	0.0000	0.0000	0.0000	0.0000	0.0000	0.0000	0.0000 • • • •		0.0000
876	0.0000	0.0000	0.0000	0.0000	0.0000	0.0000	0.0000	0.0000	0.0000	0.0000	0.0000	0.0000	0.0000	0.0000	0.0000 • • • •		0.0000
877	0.0000	0.0000	0.0000	0.0000	0.0000	0.0000	0.0000	0.0000	0.0000	0.0000	0.0000	0.0000	0.0000	0.0000	0.0000 • • • •		0.0000
878	0.0000	0.0000	0.0000	0.0000	0.0000	0.0000	0.0000	0.0000	0.0000	0.0000	0.0000	0.0000	0.0000	0.0000	0.0000 • • • •		0.0000
879	0.0000	0.0000	0.0000	0.0000	0.0000	0.0000	0.0000	0.0000	0.0000	0.0000	0.0000	0.0000	0.0000	0.0000	0.0000 • • • •		0.0000
880	0.0000	0.0000	0.0000	0.0000	0.0000	0.0000	0.0000	0.0000	0.0000	0.0000	0.0000	0.0000	0.0000	0.0000	0.0000 • • • •		0.0000
881	0.0000	0.0000	0.0000	0.0000	0.0000	0.0000	0.0000	0.0000	0.0000	0.0000	0.0000	0.0000	0.0000	0.0000	0.0000 • • • •		0.0000
882	0.0000	0.0000	0.0000	0.0000	0.0000	0.0000	0.0000	0.0000	0.0000	0.0000	0.0000	0.0000	0.0000	0.0000	0.0000 • • • •		0.0000
883	0.0000	0.0000	0.0000	0.0000	0.0000	0.0000	0.0000	0.0000	0.0000	0.0000	0.0000	0.0000	0.0000	0.0000	0.0000 • • • •		0.0000

Figure 6.11. Illustration of *TireView* Output File.

provided in the output file can be used in a three-dimensional finite element analysis to predict pavement response, should a more rigorous analysis of the effects of tire contact pressure distributions be warranted.

CHAPTER VII. SUMMARY OF FINDINGS AND RECOMMENDATIONS

This research investigated existing procedures for predicting pavement response to applied surface tractions at the tire-pavement interface. The objective was to establish how tire contact stresses may be modeled in existing layered elastic programs to better approximate the effects of non-uniform tire contact stresses and account for differences in tire construction, tire load and tire inflation pressure on predicted pavement response. To carry out this investigation, researchers executed a work plan, which covered the following tasks:

- a literature review that identified findings from previous studies, sources of available data on tire contact stresses, and additional tests conducted in this project to carry out its objectives,
- measurements of tire contact stresses on two radial truck tires (the 11R24.5 and 215/75R17.5 tire sizes) identified from the literature review as having significant use among truck carriers in Texas,
- development of a data base of measured tire contact pressure distributions,
- comparative evaluation of methods for representing tire contact stresses in existing models to predict pavement response variables used in existing TxDOT programs for pavement design and evaluation, and
- development of a computer program for estimating tire contact stresses.

Based on the research conducted, the following findings are noted:

- To establish the data base of tire contact pressure distributions, researchers initially examined the repeatability of measurements conducted in this project and the earlier study sponsored by CALTRANS. To quantify repeatability, researchers conducted pairwise comparisons of measured tire contact stress distributions and evaluated the correlations and the point-to-point differences between measurements from repeat runs. The statistics determined from the test data indicate that the repeatability of the measurements may be ranked from best to worst according to the following order: (215/75R17.5, 11R24.5) → (295/75R22.5, 11R22.5) → (10 × 20, 425/65R22.5). For the tires tested in this project, researchers found the data from all replicate runs to be highly repeatable for each combination of tire load and tire inflation pressure included in the test matrices for both tires. The data from tests conducted on the 295/75R22.5

and 11R22.5 radials generally show excellent to good repeatability except for a few cases where only two out of the three replicates were found to be repeatable. Replicate runs from the bias-ply and wide-base radial tires showed the least repeatability among the tires tested. Based on the literature review, truck carriers in Texas do not used these tires much. Nevertheless, measured tire contact stresses for these tires were included in the data base. For these tires, researchers identified a few cases where the repeatability of all three replicates is less than desired. For these cases, researchers examined charts of the test data, as well as data that bound the measurements in question to make decisions on which data to use for determining representative contact stress distributions to enter into the data base.

- Since the tire contact stress distribution is influenced by the size of the tire footprint, researchers investigated relationships between tire contact area, tire load and tire inflation pressure from the test data. For this evaluation, researchers used the tire imprints taken during testing to determine tire contact areas for the range of tire loads and tire inflation pressures at which the different tires were tested. Researchers observed that the contact area decreases with increasing inflation pressure and increases with increasing tire load based on trend lines fitted to the data. In addition, the measured contact areas for various inflation pressures plot almost parallel for different levels of tire load, indicating a negligible interaction effect between tire load and inflation pressure. Thus, researchers used a simple additive model to evaluate the relationships between tire contact area, tire load and tire inflation pressure. From this analysis, the effects of tire load and tire inflation pressure were found to be statistically significant.
- Researchers constructed and used a 3D finite element model of asphalt concrete pavements to compare predictions of pavement response based on measured tire contact stresses with corresponding results obtained using layered linear elastic analyses. The suitability of the 3D FE model used in the analyses was verified by comparing the predicted pavement response with corresponding predictions from the layered linear elastic program, BISAR. For a uniform circular pressure distribution, researchers found that the predicted strains with depth from the 3D FE analysis using ABAQUS are quite comparable with the corresponding predictions from BISAR.

- In terms of the predicted service life based on subgrade compressive strain, the results show no significant differences between the 3D finite element and layered elastic (BM and BC) analyses. This finding indicates that the effects of differences in tire contact pressure distributions are mainly seen near the surface and diminish with depth. Thus, in terms of the effect of tire contact stresses on pavement rutting, the permanent deformation properties of the surface material would be critical.
- Researchers conducted a statistical test of the differences in the predicted logarithms of the fatigue lives from the 3D FE, BM, and BC analyses. At a 95 percent confidence level, it was found that the differences between the predicted fatigue lives from the 3D FE and modified layered elastic (BM) analyses are not statistically significant. However, the differences in the fatigue predictions between the 3D FE and BC analyses were found to be significant.
- Differences in the fatigue predictions between the BM and BC methods showed the effect of tire contact area in the predicted AC tensile strains. For a given tire load and tire inflation pressure, the conventional method of analysis ignores the differences in the tire footprints between various tire types.
- Researchers calculated the Mohr-Coulomb yield function values at the center and edge of the loaded area at different depths using the 3D FE, BM and BC methods. It was observed that differences in the MC values between the 3D FE and layered elastic analyses are greatest near the surface and diminish quite rapidly with depth. In general, researchers observed that for the cases investigated, the differences were largest within the top 2 inches of the surface layer. Within the base and subgrade, the differences are not considered significant.
- The critical MC yield function values occurred near the top and bottom of the AC layer for the cases considered. At these depths, researchers examined the differences between the 3D FE and layered elastic procedures. At a confidence level of 95 percent, it was found that the differences between the predicted MC values from the 3D FE and BM analyses are not statistically significant. However, the differences in the predicted MC values between the 3D FE and BC analyses are significant.

Based on the findings from the comparative evaluation of 3D finite element and layered elastic analysis methods, the authors recommend the application of the BM method in the layered elastic analysis of pavement response. For this purpose, Eqs. (4.1) to (4.6) may be

used in practice to estimate the tire contact area for a given tire type, tire load and tire inflation pressure, in order to determine an equivalent uniform circular contact pressure and footprint for layered elastic analyses using Eqs. (5.2) and (5.3). These calculations may be done using the *TireView* program developed during this project. In this way, differences in tire footprints can be considered in the layered elastic analysis.

In addition, *TireView* provides estimates of tire contact stress distributions for a given tire type, tire load and tire inflation pressure based on polynomial interpolations of the measured values stored in the data base. Pavement engineers may use these estimates in a 3D finite element program to predict pavement response for applications where a rigorous analysis is warranted or desired. Researchers note that the predictions are specific to the tires tested. Since differences in tire construction will affect tire contact pressures, the predicted tire contact stress distributions are tied to the data base on which the interpolations were made. In addition, the predictions are limited to the range of the available data. For cases outside this range, researchers recommend that tests be conducted to measure tire contact stresses for the variables of interest. Future program updates should then be made as additional data become available.

Notwithstanding these constraints, researchers consider the establishment of the data base and the development of *TireView* to be significant outcomes of this project. The authors are of the opinion that *TireView* will provide useful data for pavement design applications, particularly for establishing or verifying design requirements for pavements subjected to heavy truck traffic, through comparative analyses of the effects of different tires and differences in wheel load assumptions on predicted pavement response and performance.

REFERENCES

AASHO Road Test – Report 5: Pavement Research. Highway Research Board Special Report 61E, Washington, D.C., 1962.

Asphalt Institute. *Research and Development of the Asphalt Institute's Thickness Design Manual (MS-1), 9th edition*, Research Report 82-2, Asphalt Institute, Ky., 1982.

Blab, R. and T. J. Harvey. *Modeling Measured 3D Tire Contact Stresses in a Viscoelastic FE Pavement Model*. The International Journal of Geomechanics, Vol. 2, 2002, pp. 271–290.

Chen, W. F. and G. Y. Baladi. *Soil Plasticity*, Elsevier Science Publishing Company Inc., New York, N.Y., 1985.

Cho, Y., B. F. McCullough and J. Weissmann. *Considerations on Finite-Element Method Application in Pavement Structural Analysis*. Transportation Research Record 1539, Transportation Research Board, Washington, D.C., 1996, pp. 96–101.

CIRCLY 4: User Manual. MINCAD Systems Pty. Ltd., Australia, 1999.

de Beer, M. and C. Fisher. *Tire Contact Stress Measurements with the Stress-In-Motion (SIM) Mk IV System for the Texas Transportation Institute (TTI), USA: [Part of TxDOT Project 0-4361]*. Restricted Contract Report CR-2002/82, CSIR Transportek, South Africa, 2002.

de Beer, M., L. Kannemeyer and C. Fisher. *Towards Improved Mechanistic Design of Thin Asphalt Layer Surfacings Based on Actual Tire/Pavement Contact Stress-in-Motion (SIM) Data in South Africa.* 7th Conference on Asphalt Pavements in Southern Africa, 1999.

de Beer, M. and C. Fisher. *Contact Stresses of Pneumatic Tires Measured with the Vehicle-Road Surface Pressure Transducer Array (VRSPTA) System for the University of California at Berkeley (UCB) and the Nevada Automotive Test Center (NATC).* Confidential Contract Research Report CR-97/053, Vol. 1, Transportek, CSIR, Pretoria, South Africa, 1997.

de Beer, M. and C. Fisher. *Contact Stresses of Pneumatic Tires Measured with the Vehicle-Road Surface Pressure Transducer Array (VRSPTA) System for the University of California at Berkeley (UCB) and the Nevada Automotive Test Center (NATC).* Confidential Contract Research Report CR-97/053, Vol. 2, Transportek, CSIR, Pretoria, South Africa, 1997.

De Jong, D. L., M. G. F. Peutz and A. R. Korswagen. *Computer Program BISAR*. External Report, Koninklijke/Shell-Laboratorium, The Netherlands, 1973.

El-Gindy, M. and H. Lewis. *Development of a Tire/Pavement Contact-Stress Model Based on Artificial Neural Networks*. PTI Report 9904, Pennsylvania Transportation Institute, The Pennsylvania State University, University Park, Pa., 2001.

Fernando, E. *TireView: Set-up File for Program*. Research Product 0-4361-P1, Texas Transportation Institute, The Texas A&M University System, College Station, Tex., 2005.

Flugrad, D. R. and B. A. Miller. *Experimental and Finite Element Study of a Standing Torus under Normal and Tangential Loads*. Iowa State University, Ames, Iowa, 1981.

Groenendijk, J. *Accelerated Testing and Surface Cracking of Asphaltic Concrete Pavements*. PhD Thesis, Delft University of Technology, The Netherlands, 1998.

Hua, J. and T. White. *A Study of Nonlinear Tire Contact Pressure Effects on HMA Rutting*. The International Journal of Geomechanics, Vol. 2, 2002, pp. 353–376.

Huang, Y. H. *Pavement Analysis and Design*. Prentice Hall, Englewood Cliffs, N.J., 1993.

Hugo, F. and T. Kennedy. *Surface Cracking of Asphalt Mixtures in Southern Africa*. Journal of the Association of Asphalt Paving Technologists, Vol. 54, 1985, pp. 454–496.

Jacobs, M. M. J., A. H. de Bondt, A. A. A. Molenaar and P. C. Hopman. *Cracking in Asphalt Concrete Pavements*. Proceedings, Seventh International Conference on Asphalt Pavements, Nottingham, England, Vol. 1, Design, 1992, pp. 89–105.

Jacobs, M. M. J. *Mechanical Characteristics of Tires and their Effects on the Stress Distribution in the Contact Area between Tire and Roadway*. Road and Railroad Research Laboratory, Delft University of Technology, Delft, Netherlands, 1989.

Jayawickrama, P. W., R. E. Smith, R. L. Lytton and M. R. Tirado. *Development of Asphalt Concrete Overlay Design Equations: Vol. I - Development of Design Procedures.* Final Report No. DTFH61-84-C-00053, Federal Highway Administration, Va., 1987.

Johansen, J. M. and P. Senstad. *Effects of Tire Pressures on Flexible Pavement Structures*. Publication No. 62, Directorate of Public Roads, Norwegian Road Research Laboratory, Oslo, Norway, 1992.

Long, F. M. *Permanent Deformation of Asphalt Concrete Pavement: A Nonlinear Viscoelastic Approach to Mix Analysis and Design*. PhD Dissertation, University of California at Berkeley, Calif., 2001.

Lytton, R. L., J. Uzan, E. G. Fernando, R. Roque, D. Hiltunen and S. M. Stoffels. *Development and Validation of Performance Prediction Models and Specifications for Asphalt Binders and Paving Mixes*. SHRP-A-357, Strategic Highway Research Program, National Research Council, Washington, D.C., 1993.

Mack, M. J., D. E. Hill Jr. and J. R. Baumgarten. *Analytical and Experimental Study of a Standing Torus with Normal Loads*. Tire Modeling, NASA Conference Publication 2264, 1982.

Marshek, K. M., W. R. Hudson, R. B. Connell, H. H. Chen and C. L. Saraf. *Experimental Investigation of Truck Tire Inflation Pressure on Pavement-Tire Contact Area and Pressure Distribution*. Research Report 386-1, Center for Transportation Research, The University of Texas at Austin, Austin, Tex., 1985.

Marshek, K. M., W. R. Hudson, R. B. Connell, H. H. Chen, C. L. Saraf and R. B. Connell. *Effect of Truck Tire Inflation Pressure and Axle Load on Pavement Performance*. Research Report 386-2F, Center for Transportation Research, The University of Texas at Austin, Austin, Tex., 1985.

Modern Tire Dealer. *2002 Fact Book*. Akron, Ohio, 2002.

Myers, L., R. Roque, B. Ruth and C. Drakos. *Measurement of Contact Stresses for Different Truck Tire Types to Evaluate their Influence on Near-Surface Cracking and Rutting*. Transportation Research Record 1655, Transportation Research Board, Washington, D.C., 1999, pp. 175–184.

Myers, L., R. Roque and B. Ruth. *Mechanisms of Surface-Initiated Longitudinal Wheel Path Cracks in High-Type Bituminous Pavements*. Proceedings, Technical Sessions of the Association of Asphalt Paving Technologists, Massachusetts, Vol. 67, 1998, pp. 401–432.

Novak, M., B. Birgisson and R. Roque. *Near-Surfaced Stress States in Flexible Pavements using Measured Radial Tire Contact Stresses and ADINA*. Computers and Structures, Vol. 81, 2003, pp. 859–870.

Perdomo, D. and B. Nokes. *Theoretical Analysis of the Effects of Wide-Base Tires on Flexible Pavements using CIRCLY*. Transportation Research Record 1388, Transportation Research Board, Washington, D.C., 1994, pp. 108–119.

Press, W. H., S. A. Teukolsky, W. T. Vetterling and B. P. Flannery. *Numerical Recipes in C^{++}: The Art of Scientific Computing*. Cambridge University Press, 2nd edition, Cambridge, United Kingdom, 2002.

Roberts, F. L., J. T. Tielking, D. Middleton, R. L. Lytton and K. Tseng. *Effects of Tire Pressures on Flexible Pavements*. Research Report 372-1F, Texas Transportation Institute, The Texas A&M University System, College Station, Tex., 1986.

Roque, R., L. Myers and B. Ruth. *Loading Characteristics of Modern Truck Tires and their Effects on Surface Cracking of Asphalt Pavements.* Proceedings, Fifth International Conference on the Bearing Capacity of Roads and Airfields, Trondheim, Norway, Vol. 1, 1998, pp. 93–102.

Rubber Manufacturers Association. *Factbook 2001: US Tire Shipment Activity Report for Statistical Year 2000*. Washington, D.C., 2001.

Stearns, S. D and R. David. *Signal Processing Algorithms in Fortran and C*. Prentice Hall, Englewood Cliffs, N.J., 1993.

Tielking, J. T. and M. A. Abraham. *Measurement of Truck Tire Footprint Pressures*. Transportation Research Record 1435, Transportation Research Board, Washington, D.C., 1994, pp. 92–99.

Tielking, J. T. *The Tire-Pavement Interface*. Tire Technology, 1986.

Tielking, J. T. *A Finite Element Tire Model*. Tire Science and Technology, Vol. 11, Nos. 1–4, 1983, pp. 50–63.

Wang, F., R. F. Inman, R. B. Machemehl, Z. Zhang and C. M. Walton. *Study of Current Truck Configurations*. Research Report 1862-1, Center for Transportation Research, The University of Texas at Austin, Austin, Tex., 2000.

Yap, P. *A Comparative Study of the Effect of Truck Tire Types on Road Contact Pressures*. SAE Transactions, 881846, 1988.

APPENDIX A. LITERATURE REVIEW

INTRODUCTION

Project 0-4361 is concerned with the effects of tire size, inflation pressure, and tire load on the contact pressures at the tire-pavement interface, and how tire contact pressures may be modeled with existing layered elastic analysis programs to achieve a more realistic assessment of the induced pavement response. As part of evaluating current design assumptions used to represent wheel loads in existing pavement design and evaluation procedures, researchers established a data base of measured tire contact pressures and conducted a comparative evaluation of predicted pavement response based on the measurements collected, with the corresponding predictions based on current design assumptions. In establishing this data base, tests to measure tire contact pressures were conducted in this project. To establish a test plan for these measurements, researchers undertook a literature review of previous investigations to determine the state of knowledge in this area, identify what can be used from previous research, and establish where additional work is necessary to accomplish the objectives of this project. This literature review covered the following areas:

- methods for measuring tire contact pressures,
- findings from previous studies,
- models for predicting tire contact pressures, and
- models for predicting pavement response.

It is obvious that tires must be considered in any discussion of the truck/pavement damage relationship. Tires transmit the truck loads to the pavement, are dynamically active, very complex, available in a wide range of configurations, and differ in design among various tire manufacturers. Depending on design, recommended tire inflation pressures vary to optimize tire performance (e.g., minimize rolling resistance, and maximize life) for the properties of a given tire at a given load. The newer low-profile tires, which have smaller diameters than regular tires, are getting a larger share of the tire market for long-haul highway trucks due to the reduction in vehicle height, and the associated increase in trailer cubic capacity that these tires permit. Tire inflation pressures maintain the tire's design profile, and thus, proper road contact under vehicle loading. Vehicle operations with improper tire pressures lead to excessive tire wear, particularly with radial tires, and

influence vehicle-handling characteristics. Too low a pressure at a particular load causes the tire to flatten out, leading to added flexure and heat buildup during operation. Too high a pressure reduces contact area and stiffens the tire, increasing greater stress at the surface of the pavement. Truck operators are more aware of the adverse effects of under inflation than the effects of over inflation so they tend to err on the side of over inflation. Clearly, evaluation of the effects of tire contact pressures is a complex problem. In the opinion of the researchers, the present project was an important step toward verifying and improving current practice with respect to modeling wheel loads for pavement design and evaluation purposes.

MEASUREMENT OF TIRE CONTACT PRESSURES

Pressure Sensitive Film

Marshek et al. (1985) measured tire contact pressures using pressure sensitive film in a research project sponsored by the Texas Department of Transportation (TxDOT) in the mid-1980s. Figure A1 shows a schematic of the pressure sensitive film used by the researchers. As shown, the film consists of two sheets, labeled A and C. The A-sheet contains capsules of a developer that is deposited on the C-sheet when the capsules break under the applied load. The capsules vary in breaking strength, allowing for a range of pressures to be captured. When a capsule breaks, the developer is released onto the C-sheet (a developing layer) producing a red spot on the sheet. The intensity of the color produced is proportional to the applied pressure.

To obtain a pressure print, the film is placed and secured on a flat surface. The test tire is then lowered onto the film. Figure A2 illustrates the test configuration. As shown, Marshek et al. (1985) also placed a piece of shimstock between the tire and the pressure film to minimize frictional effects and ensure that only the normal load is transmitted to the film. Researchers interpreted the data obtained using an optical device called a densitometer, which projects beams of light to the developed print. Depending on the color intensity, light is reflected back to a photocell, which then outputs a voltage proportional to the pressure applied at the particular spot read on the pressure film. The output voltage is then measured with a voltmeter, and the pressure corresponding to this voltage is estimated from the calibration curve established for the given film. A complete pressure distribution is obtained by scanning the developed print on the C-sheet. To summarize, the following are the main features of this method of measuring tire contact pressures:

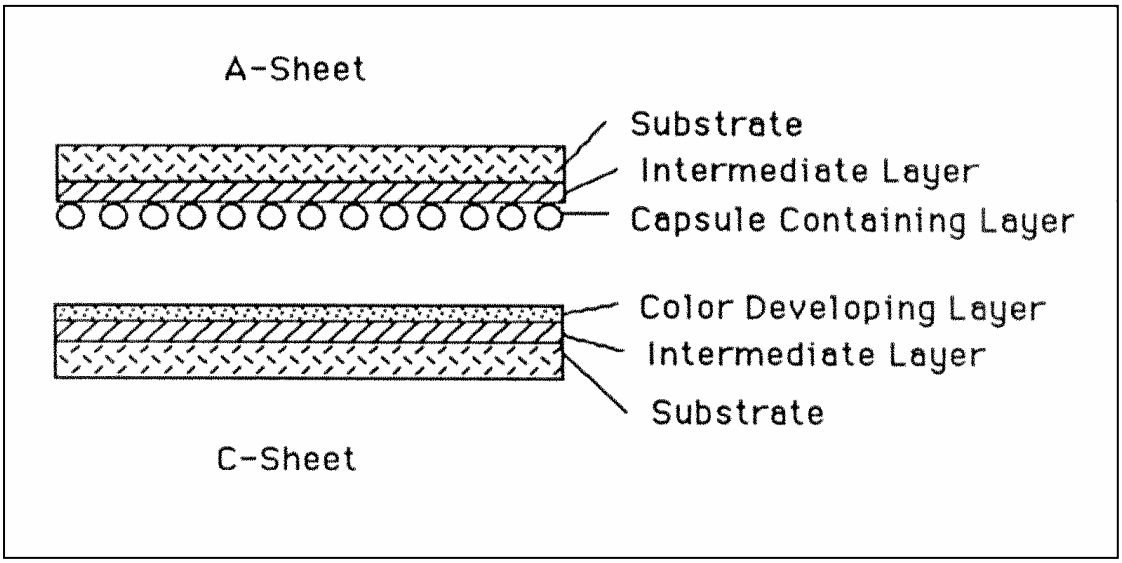

Figure A1. Schematic of Pressure Sensitive Film (Marshek et al., 1985).

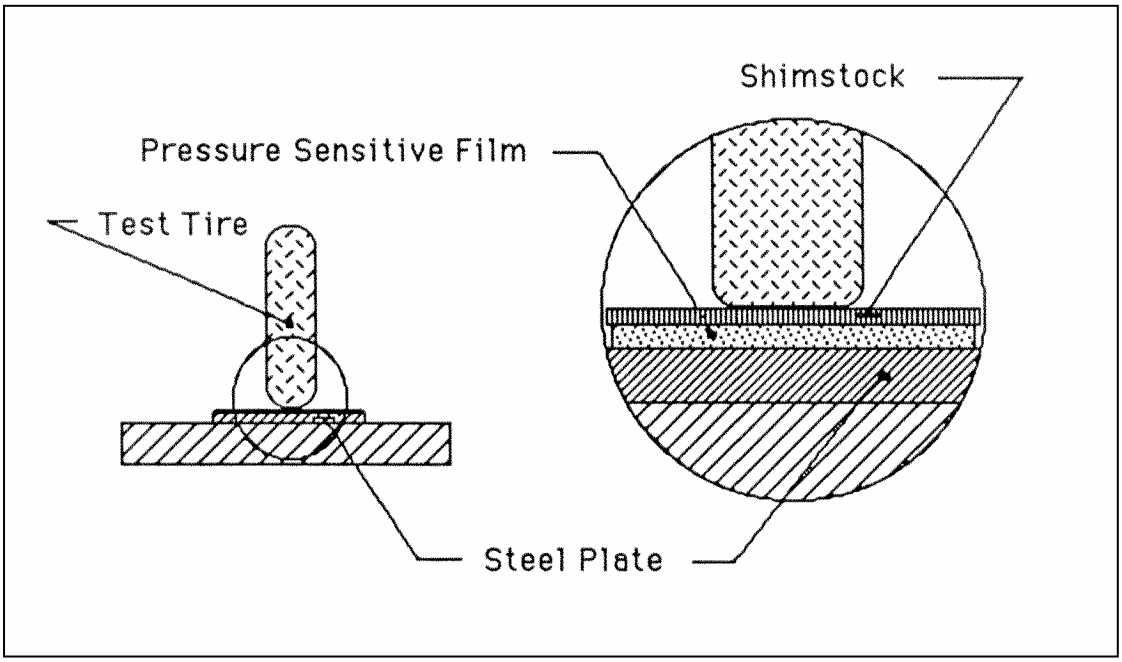

Figure A2. Configuration of Pressure Film Test (Marshek et al., 1985).

- Measurements are done in the laboratory using pressure sensitive film that produces a print with a color intensity pattern proportional to the applied pressures.
- The developed print is interpreted using a densitometer and the calibration curve established for the film used in the test.
- The tire load is applied statically onto the pressure film.
- Only vertical contact pressures are measured.

Laboratory Measurements with Triaxial Load Pins

The tire industry uses triaxial load pins to measure tire contact pressures. This particular sensor has two important advantages over pressure-sensing film (Tielking and Abraham, 1994):

- Tire-pavement shear pressures may be measured.
- The load pin signal will respond to dynamic tire contact pressure.

Tielking and Abraham (1994) used a triaxial load pin array to conduct laboratory measurements of footprint pressures under conventional and wide-base radial truck tires. Tests were conducted using the setup shown in Figure A3. In this setup, a U-shaped load frame held the tire above the contact plate that housed the movable shoe containing the load pin array. The array itself consisted of 10 pins. By moving the shoe laterally, Tielking and Abraham (1994) measured tire contact pressures at different transverse positions along the tire. In their tests, the tire was held in a stationary position. The load was applied through an actuator that moved the contact plate up against the tire until the specified load was reached. A load cell attached to the U-shaped load frame measured the resultant force within the tire footprint.

Laboratory Measurements under a Rolling Tire

Other systems used by the tire industry permit measurement of contact pressures under a rolling tire. Smithers Scientific Services developed the system illustrated in Figure A4. In this setup, the tire is held fixed on a steel bed instrumented with a row of transducers that measure vertical, longitudinal and transverse forces, as well as transverse and longitudinal displacements. The bed is moved in the longitudinal direction, causing the tire to roll over the transducers. By taking measurements with the tire placed at different transverse positions, a detailed pattern of the tire contact pressures in all three directions may be obtained.

Field Measurements under a Rolling Tire

The California Department of Transportation sponsored a research project with the University of California at Berkeley to measure tire-pavement contact pressures under bias-ply, conventional radial, low-profile radial and wide-base radial truck tires. The measurements were made at the heavy vehicle simulator facility operated by UCB using the vehicle road surface pressure transducer array developed in South Africa. Figure A5 shows

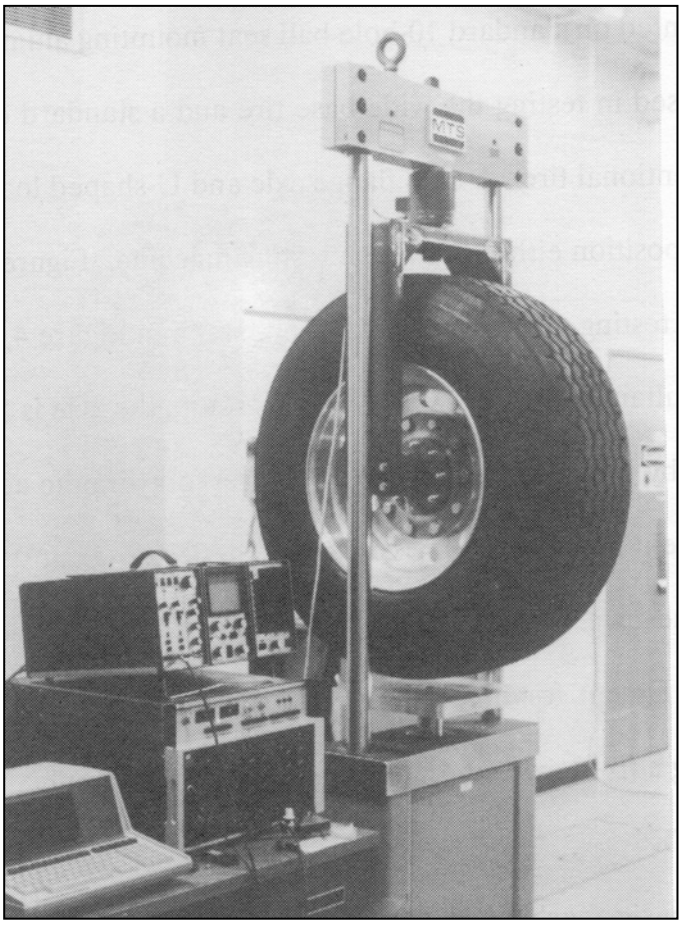

Figure A3. Test Setup of Tielking and Abraham (1994).

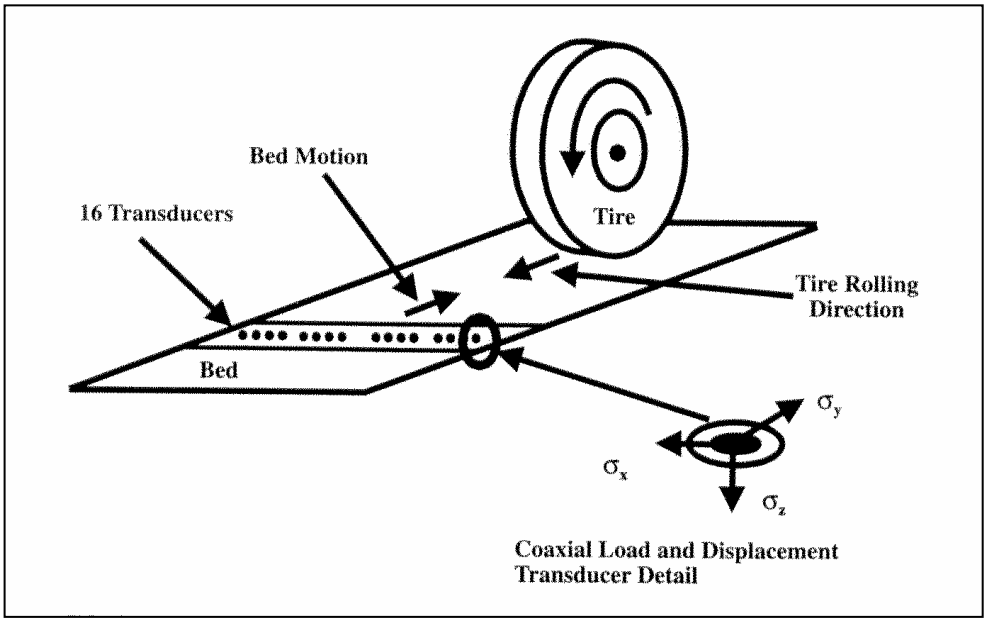

Figure A4. Schematic of System Developed by Smithers Scientific Services (Myers et al., 1999).

a schematic of the VRSPTA. The device consists of an array of calibrated strain-gauged pins fixed to a steel base-plate that is buried flush with the pavement surface. The load cell pins are installed at right angles to the direction of travel. The strain outputs from these pins are scanned at a high rate while the wheel traverses the pins, giving an indication of the vertical, transverse and longitudinal loads acting on each pin. The system is approximately 29.5 inches long, 14 inches wide and 4.3 inches high. The vertical, lateral and longitudinal loads are measured in one line across the tire footprint by a row of 20 instrumented pins. As the tire is moved across the instrumented pins at a constant speed, the loads are measured at a fixed sampling frequency until the tire footprint has traversed the surface of the VRSPTA (El-Gindy and Lewis, 2001).

Figure A6 illustrates the setup used in the UCB tests. The equipment, experimental plan and data from the tests are documented in a two-volume report by de Beer and Fisher (1997). Figure A6 shows the version of the VRSPTA, referred to as Mk II, which was developed for use under the HVS. There is another version, referred to as VRSPTA Mk III, which provides for simultaneous measurement of tire contact pressures under four tires of a standard truck axle. Figure A7 shows this system.

FINDINGS FROM PREVIOUS STUDIES

Common Themes

The importance of this research project was suggested in the following themes, which are common concerns expressed by researchers in previous investigations:

- Tire inflation pressures have increased over the years. The findings from the road test conducted by the American Association of State Highway Officials (AASHO, 1962) have provided the basis for many pavement design procedures implemented worldwide. At the time of the AASHO road test, truck tires were typically inflated to pressures of 75 to 80 psi. Today, recommended cold inflation pressures are typically in the range of 85 to 115 psi, with inflation pressures reaching as high as 130 to 145 psi in certain applications. de Beer et al. (1999) noted that tire inflation pressures in South Africa increased from an average of 90 psi in 1974 to 106 psi in 1995. Johansen and Senstad (1992) gave a number of reasons for the increase in tire inflation pressures, as follows:

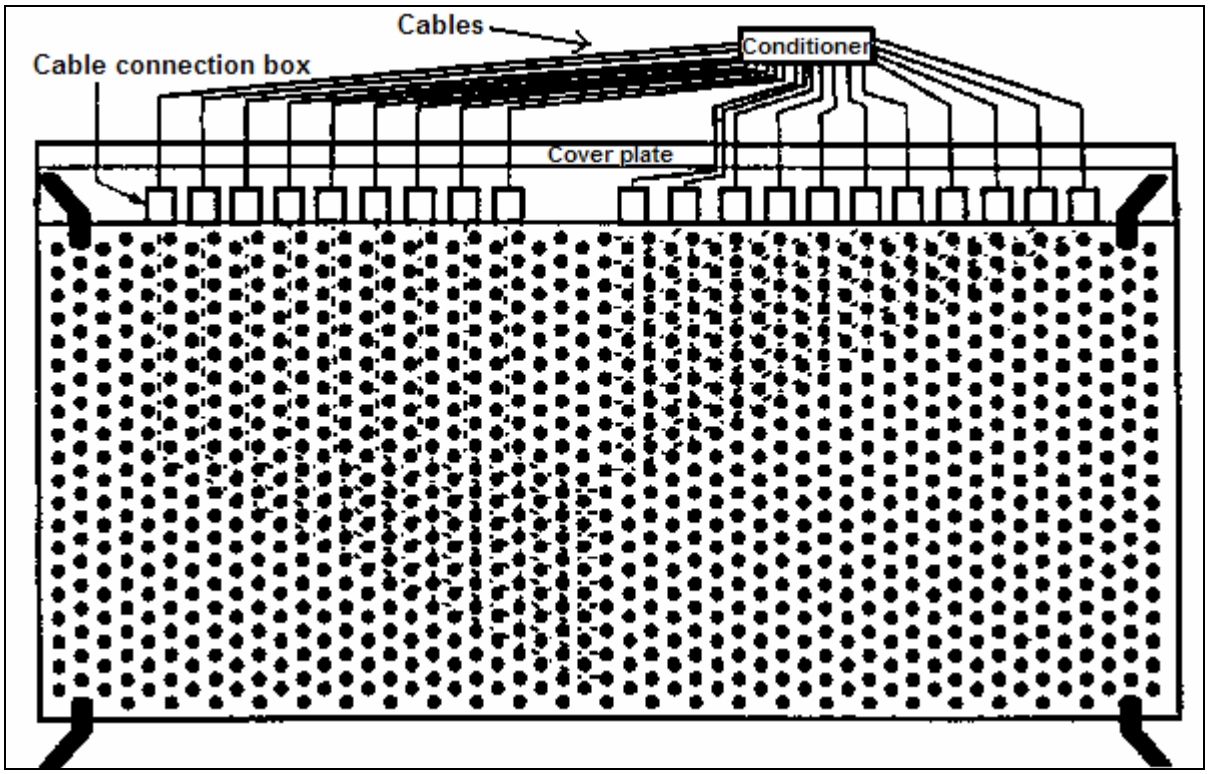

Figure A5. Schematic Illustration of VRSPTA (de Beer and Fisher, 1997).

Figure A6. VRSPTA Mk II (Single-Unit System Used with HVS).

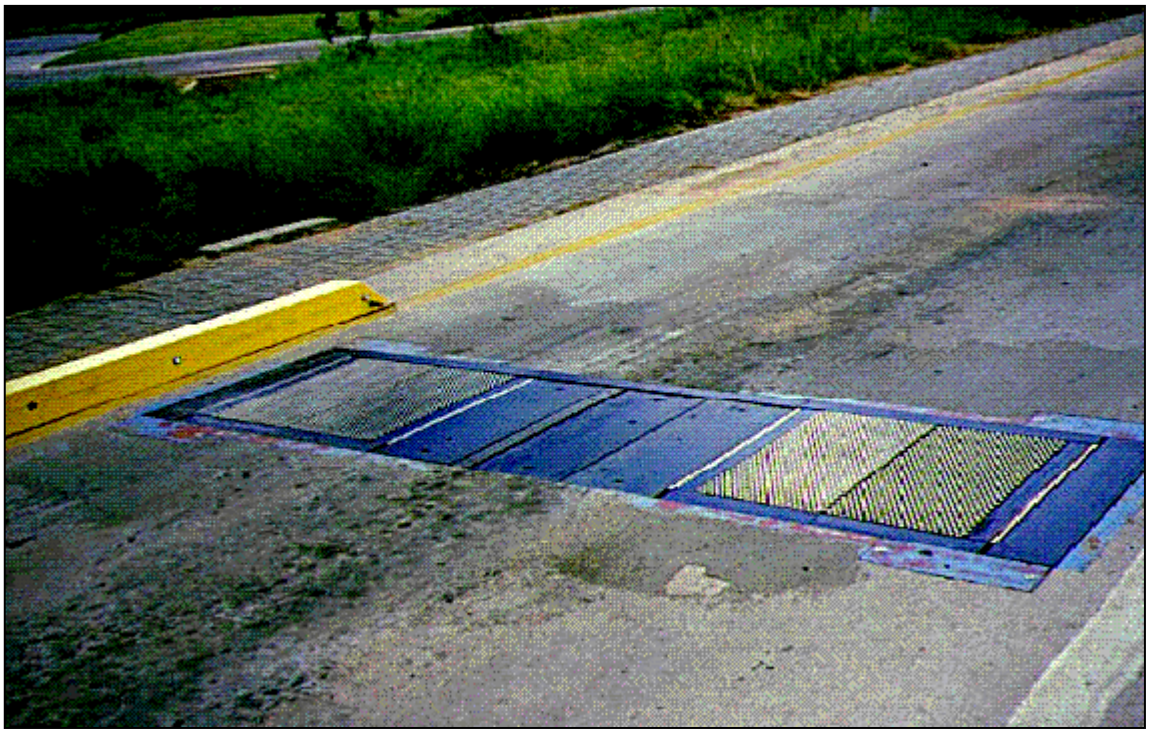

Figure A7. VRSPTA Mk III (Four-Unit System for Truck Axle Measurements).

- the shift from bias-ply to radial tires, which are typically inflated at higher air pressures than bias-ply tires;
- increase in legal load limits; and
- manufacture and use of tires with higher load ratings.

In Texas, the number of permitted over-sized and overweight loads has increased over the last decade. TxDOT can expect this trend to continue as long as the economy remains strong and the demand for point-to-point delivery of partially constructed heavy industry components continues. Texas is particularly impacted by the North American Free Trade Agreement, which has fueled increased trade with neighboring Mexico, and increased pressure to promote greater efficiency and higher trucking productivity. This situation has already resulted in a dedicated overweight truck route along SH 4/48 in Brownsville, where trucks with gross vehicle weights up to 125 kips are routinely permitted. Higher tire loads generally require higher inflation pressures to maintain optimal tire performance.

- Tire inflation pressures are significantly higher than values used in pavement design. Many highway agencies use the standard 18-kip single axle load to

convert mixed traffic to an equivalent number of standard axle load repetitions for pavement design. In most cases, the equivalency factors used to carry out this conversion are based on the performance model developed from the AASHO road test, where test vehicles were equipped with bias-ply tires operated at inflation pressures ranging from 75 to 80 psi. Since the AASHO model was developed using the observed performance data from the sections tested, the equivalency factors determined from the model are tied to the load parameters used during the test. Today's truck traffic operates at inflation pressures significantly higher than those at the time of the AASHO Road Test (AASHO, 1962). In addition, most trucks now run on radial tires, in lieu of bias-ply tires.

- Tire contact pressures are not used in pavement design. In most pavement design procedures presently implemented, the tire load is represented as a uniform vertical pressure distribution, acting on a circular area with a footprint radius determined by the tire inflation pressure. In reality, measurements of tire contact pressures show that the pressure distribution is non-uniform, with high gradients existing at the tread gaps. The maximum vertical pressure at the tire footprint may vary from 1 to 2 times the tire inflation pressure (Johansen and Senstad, 1992), and even by a factor of 2 to 3 (de Beer et al., 1999). Figure A8 shows the cumulative frequency distributions of vertical tire contact pressures measured under the tires of a deflectograph with the VRSPTA. It is interesting to note that, for the tests conducted, the measured tire contact stresses exceed the design value of 75 psi (520 kPa) over 50 percent of the time. These observations indicate that current design assumptions may lead to pavements that are inadequate to carry the expected wheel load applications over the design life. On top of this, most design procedures do not account for the shear stresses that exist at the tire-pavement interface. A number of studies indicate the potential of surface initiated cracking under these shear stresses in asphalt concrete pavements (Hugo and Kennedy, 1985; Jacobs et al., 1992; and Roque et al., 1998).
- There are many reported observations of pavement failures originating from the top layer. The predicted tensile strain at the bottom of the asphalt layer, and the compressive strain at the top of the subgrade are generally used as criteria for pavement design in many of the procedures presently implemented. Under this

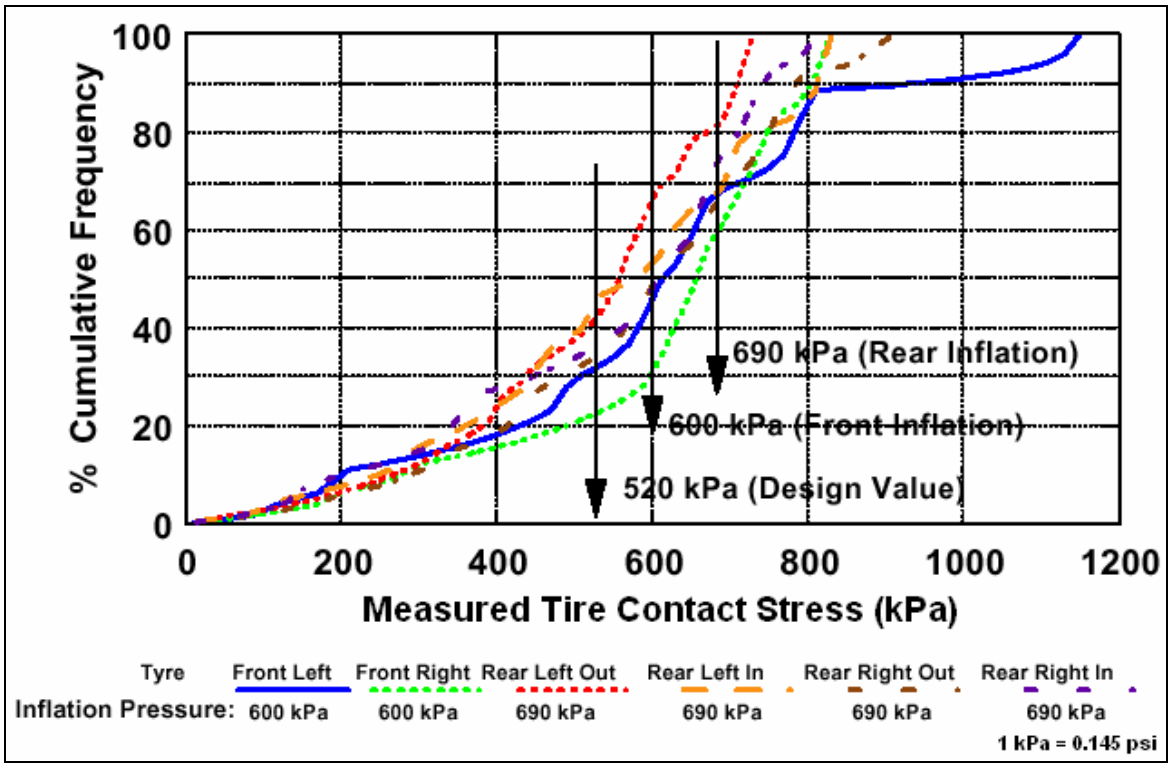

Figure A8. Cumulative Frequency Distributions of Measured Tire Contact Stresses under the Deflectograph Tires (de Beer et al., 1999).

approach, fatigue cracking is assumed to initiate from the bottom of the surface layer due to tensile stresses that are generated from repeated flexure of the layer under traffic loading. After initiation, the crack then propagates to the surface under the action of bending and shear stresses with the shear mode becoming more dominant as the crack length increases (Jayawickrama et al., 1987 and Lytton et al., 1993). In addition, rutting is assumed to originate from the subgrade. By controlling the compressive strain at the top of the subgrade, a pavement design is determined that meets the desired service life prior to the development of a critical rut depth. While conditions are found on which these traditional criteria are applicable for pavement design, there are numerous reported observations in the literature of pavement failures originating from the surface. Jacobs (1989) noted that cracks initiating at the surface started to be observed in the Netherlands in 1975. He further stated that this type of cracking could not be predicted with layered elastic theory assuming a uniform tire contact pressure distribution. It is interesting to note that the initial observations of surface-initiated cracking occurred during the time radial tires were becoming

more popular than bias-ply tires. Using measurements of tire contact pressures, Roque et al. (1998) analyzed the near-surface pavement stresses that may be induced under bias-ply and radial tires. The authors noted that significant transverse tensile stresses were predicted under the treads of radial tires, which can potentially initiate surface cracks along the wheel path. However, transverse tensile stresses were not predicted under bias-ply tires. Based on these results, the authors pointed to the need for better defining tire-pavement contact stresses and their consideration in modern pavement and mixture design procedures. Other observations of pavement failures originating from the surface have been reported in the following studies:

- Myers et al. (1998) noted that surface-initiated longitudinal wheel path cracking has become the predominant mode of failure in Florida's asphalt concrete pavements.
- Research results from HVS tests in South Africa show that most pavement failures in that country originate from the top downward and not from a lack of subgrade support (de Beer et al., 1997).
- A study from the Netherlands (Groenendijk, 1998) indicates that non-structural cracking and surface disintegration are the predominant types of distress affecting the Dutch highway system, consuming about 65 percent of the total maintenance expenditure.

In summary, the change in tire use from bias-ply to radial tires, and the reported observations of top-down cracking suggest the need to re-examine the applicability of current wheel load assumptions used in pavement design. Measured tire contact pressure distributions are non-uniform, and are influenced by numerous variables such as tire load, tire inflation pressure, tread pattern, tire construction, and tire wear. Due to the many variables that influence tire contact pressures, it is not feasible to characterize tire contact pressures for the many loading conditions that could arise in practice. However, the implications of the simplifying assumptions used in pavement design need to be established.

Truck Tire Usage

To establish the experimental plan for measurement of tire contact pressures in this project, researchers reviewed available data on truck tire usage to identify which tires are popular among truck operators. For this purpose, researchers reviewed the findings from a study conducted by the Center for Transportation Research (CTR) at the University of Texas at Austin that aimed to characterize, among other things, the inflation pressure and size distributions of tires found on trucks using Texas highways. The data from the surveys are presented by Wang et al. (2000). Figure A9 shows the distribution of tire sizes based on data obtained from the trucks sampled by CTR researchers. The following findings are noted:

- The four most popular tire sizes found in the trucks sampled during the surveys are 295/75R22.5, 11R24.5, 11R22.5 and 285/75R24.5. These four sizes account for about 80 percent of the tires sampled.
- The above tire sizes were found to be the most popular in both border, and non-border areas of Texas.
- Size 11R24.5 was most frequently found on the steering axles of the trucks sampled, accounting for about 24 percent of the steering tires. On the other hand, the 295/75R22.5 tire was most frequently found on the non-steering axles, accounting for about 26 percent of the non-steering tires sampled.
- The top four popular sizes are radial tires. Bias-ply tires accounted for about 2 percent of the tires sampled. In addition, very few wide-base tires were observed (about 0.1 percent). This latter finding indicates that wide-base tires have not quite gained the popularity initially projected for these tires in the U.S. One possible reason stems from concerns by truckers of safely maneuvering a truck with a failed wide-base tire to a complete stop. In comparison, if a tire of a dual set fails, one good tire remains to carry the load until the driver can safely pull over to a complete stop.
- Comparison of the CTR data collected in 2000 with data from a similar survey conducted by TTI researchers in the mid-1980s (Roberts et al., 1986) show a significant decrease in bias-ply tire usage, from about 32 percent in the mid-

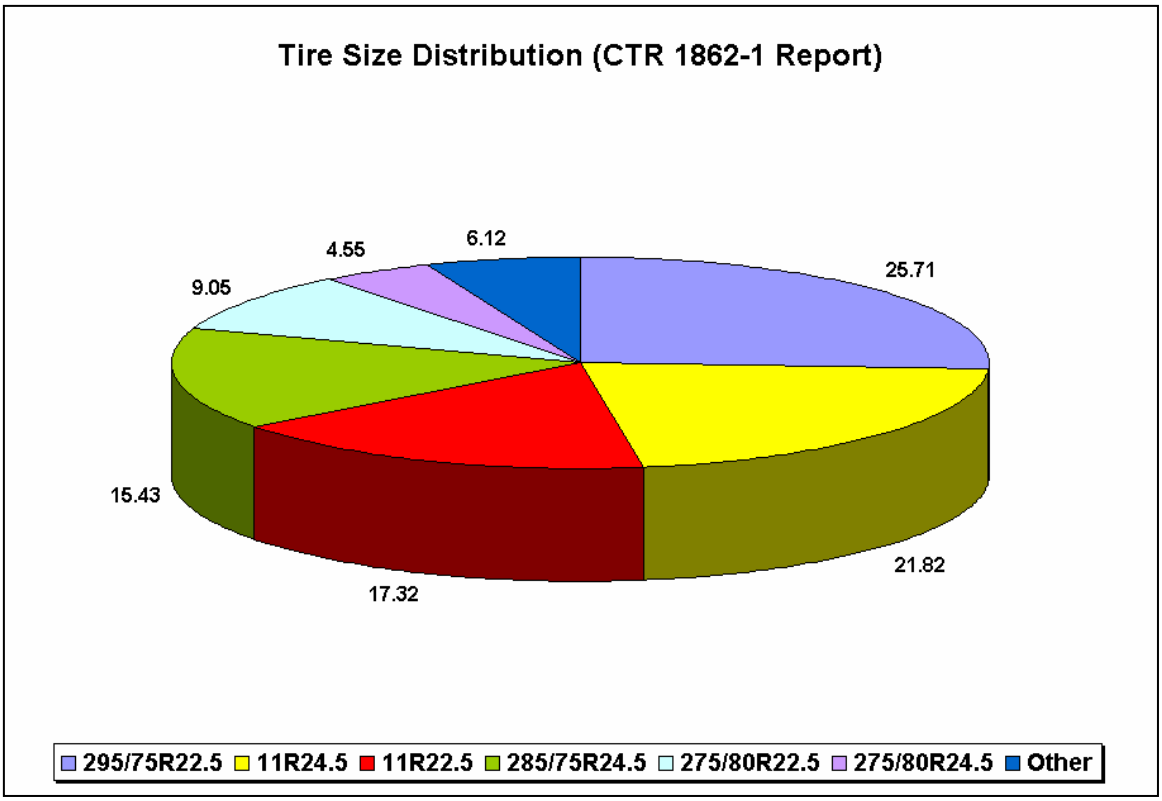

Figure A9. Tire Size Distribution Based on CTR Survey Data.

1980s to about 2 percent in the CTR survey. This finding indicates that radial tires are almost always used in today's trucks. The market share of bias-ply tires has shrunk considerably.

TTI researchers also reviewed data published by the tire industry to identify nationwide trends in truck tire usage. Figures A10 and A11 show tire size popularity data taken from the annual tire industry factbook published by the Rubber Manufacturers Association (RMA). Figure A10 identifies the top five tire sizes based on shipments made to original equipment manufacturers (OEMs), while Figure A11 shows similar data based on shipments to tire distributors, dealers and stores. It is observed from these figures that four of the top five tire sizes in RMA's factbook are the same as those identified in the CTR survey, i.e., 295/75R22.5, 11R24.5, 11R22.5 and 285/75R24.5. Over the five-year period (1996 to 2000), the top five tire sizes accounted for 79 to 83 percent of OEM tire shipments, and 72 to 76 percent of replacement tire shipments.

TTI researchers obtained additional statistics from the *Modern Tire Dealer* (MTD), an industry magazine. Figures compiled by MTD show that in 2001, radial truck tire

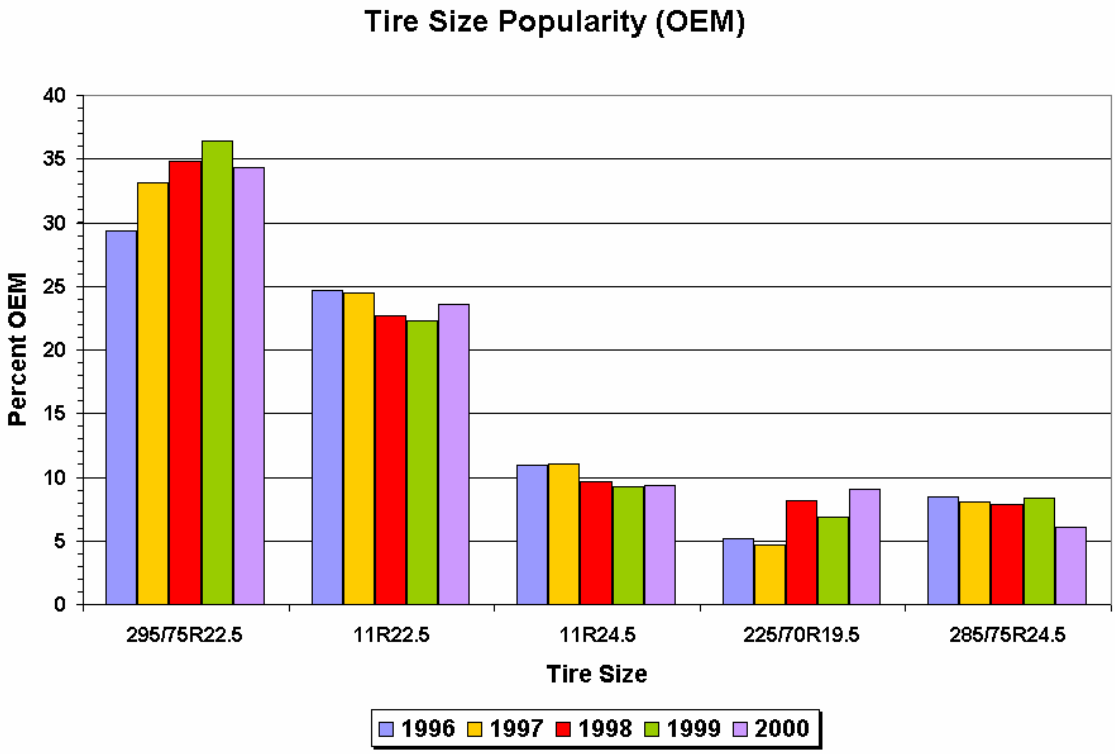

Figure A10. Tire Size Popularity Based on OEM Shipments (RMA, 2001).

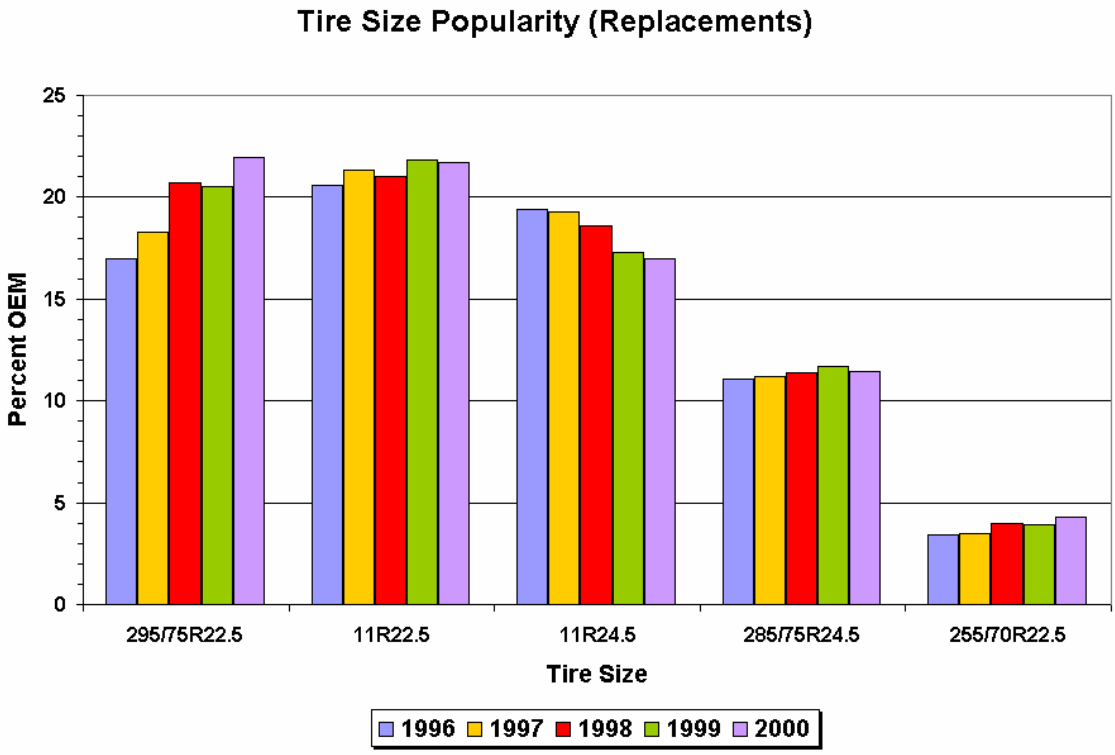

Figure A11. Tire Size Popularity Based on Replacement Shipments (RMA, 2001).

shipments made up 94 percent of the replacement medium truck tire market, and 99.7 percent of the original equipment market. Table A1 shows the top radial medium truck tire replacement sizes as determined by MTD. Note that the top four sizes are the same as those identified in the CTR survey. However, the MTD estimates include among the 295/75R22.5 tires, the European alternative size, 275/80R22.5. Also, the figures for the 285/75R24.5 tire include the European alternative size, 275/80R24.5. These European alternative tire sizes were grouped separately in the CTR survey (see Figure A9).

In terms of truck tire retreads, MTD figures show that 94 percent of the 15.7 million retreads produced in 2001 were radial, and 6 percent were bias-ply. Among the retreads, 65 percent were produced with a rib tread design. The remaining 35 percent were lug design. Table A2 shows the market share of different manufacturers of medium and heavy truck tires, while Figure A12 shows the 2001 market share of retreaded truck tires. In terms of market share, Table A2 shows that Goodyear, Michelin and Bridgestone were the top three manufacturers of replacement truck tires in 1997, 1999 and 2001. Researchers note that the CTR survey (Wang et al., 2000) also identified these tire manufacturers as the three most popular tire providers among the trucks sampled. In the non-border areas of Texas, CTR researchers found that Bridgestone, Michelin and Goodyear ranked as the top three, having shares of about 29, 24 and 16 percent, respectively, of the truck tires sampled. In the border areas, the top three manufacturers were Goodyear, Bridgestone and Michelin, representing about 22, 19, and 17 percent of the tires sampled. Among retreaded truck tires, Figure A12 shows that Bandag and Goodyear occupied the top two positions in 2001, garnering 44 and 32 percent, respectively, of the retread market.

Available Tire Contact Pressure Measurements

In 1997, Transportek of the Council for Scientific and Industrial Research of South Africa conducted tire contact pressure measurements at the heavy vehicle simulator facility of the University of California at Berkeley (de Beer and Fisher, 1997). Vertical, lateral and longitudinal tire contact pressures were measured under a slow, moving tire using the VRSPTA. A total of six tires were tested, at several tire loads and inflation pressures. Table A3 identifies the tires tested at the UCB HVS facility.

The California Department of Transportation and the University of California at Berkeley have made available to this project the data from the UCB tests. Figures A13 to A15 illustrate measured tire contact stresses for the 295/75R22.5 radial tire tested at an

Table A1. Distribution of Radial Replacement Truck Tire Sizes in 2001 (MTD, 2002).

Tire Size	Percent of Total Shipped
295/75R22.5[a]	23.0
11R22.5	21.2
11R24.5	15.9
285/75R24.5[b]	10.8
255/70R22.5[c]	4.2
225/70R19.5	3.7
315/80R22.5	3.0
10R22.5	2.3
245/70R19.5	2.0
215/75R17.5	1.5
12R22.5	1.4
425/65R22.5	1.1

[a] Includes European alternative size 275/80R22.5
[b] Includes European alternative size 275/80R24.5
[c] Tubeless equivalent of 10.00R15 tire

Table A2. 2001 U.S. Replacement Medium/Heavy Truck Tire Brand Shares (MTD, 2002).

Brand	Percentage based on 13.7 million units*		
	2001	1999	1997
Goodyear	22.0	22.0	22.5
Michelin	17.5	18.5	19.0
Bridgestone	16.5	16.0	15.5
Firestone	6.5	6.5	6.0
General	6.0	6.0	6.0
Yokohama	4.5	5.0	4.5
Dunlop	4.0	3.5	3.5
Kelly	4.0	3.5	4.0
Toyo	3.5	3.5	3.5
Cooper	3.0	3.5	3.5
BFGoodrich	2.5	3.0	1.5
Sumitomo	2.5	1.5	1.0
Continental	2.0	1.5	1.0
Hankook	2.0	2.0	2.0
Power King	2.0	2.0	2.0
Hercules	1.5	1.5	1.0
Kumho	1.5	2.0	2.0
Others	2.5	2.0	4.0

* Because numbers are rounded to the nearest 0.5 percent, the total may not equal 100 percent. Brands must have at least 1 percent of the market in shipment numbers to be listed at 1 percent.

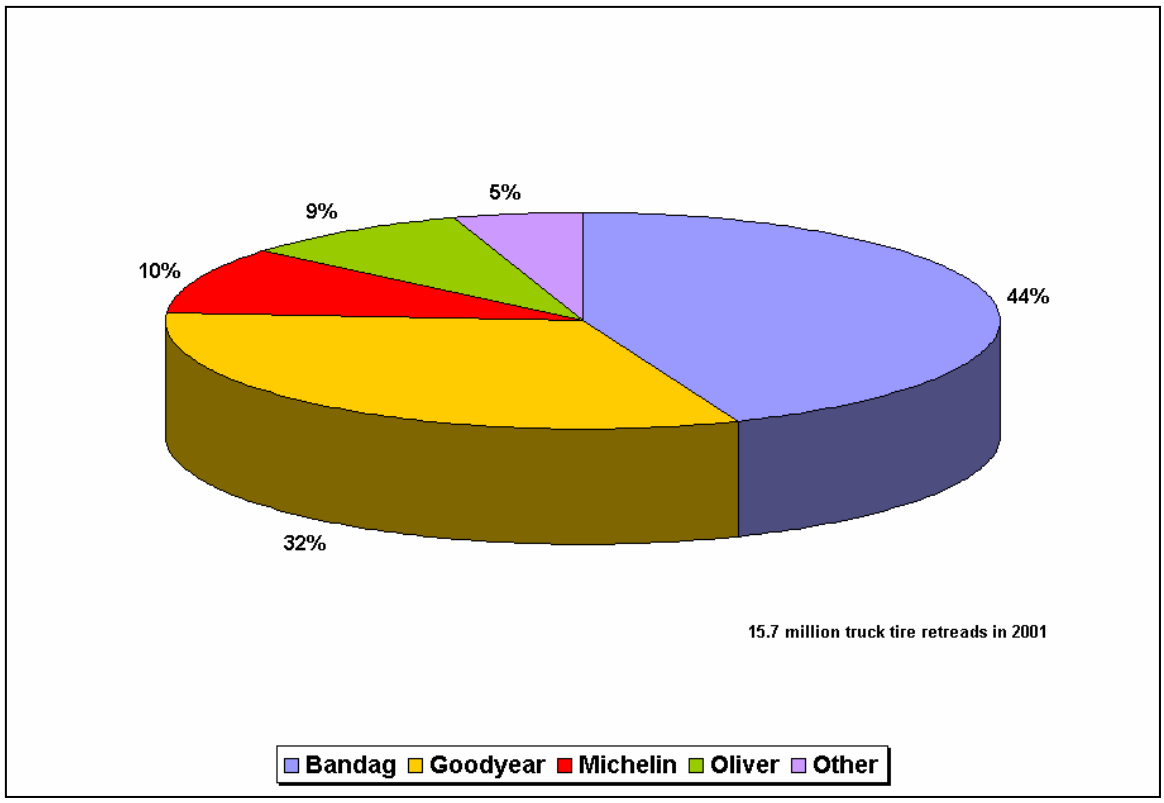

Figure A12. 2001 U.S. Market Share of Retreaded Truck Tires by Manufacturer (MTD, 2002).

Table A3. Tires Tested at UCB HVS Facility Using VRSPTA.

Brand	Tire Type	Tire Size[a]	Tread Pattern
Goodyear	Bias-ply	10.00 × 20 (G)	
Goodyear	Radial	11R22.5 (G)	G159A
Goodyear	Radial	295/75R22.5 (G)	G159A
Goodyear	Radial	425/65R22.5 (J)[b]	G286
Goodyear	Radial	385/65R22.5 (J)[b]	G178
BF Goodrich	Aircraft tire		

[a] Letter inside parentheses following the tire size indicates the load range
[b] Wide base tire

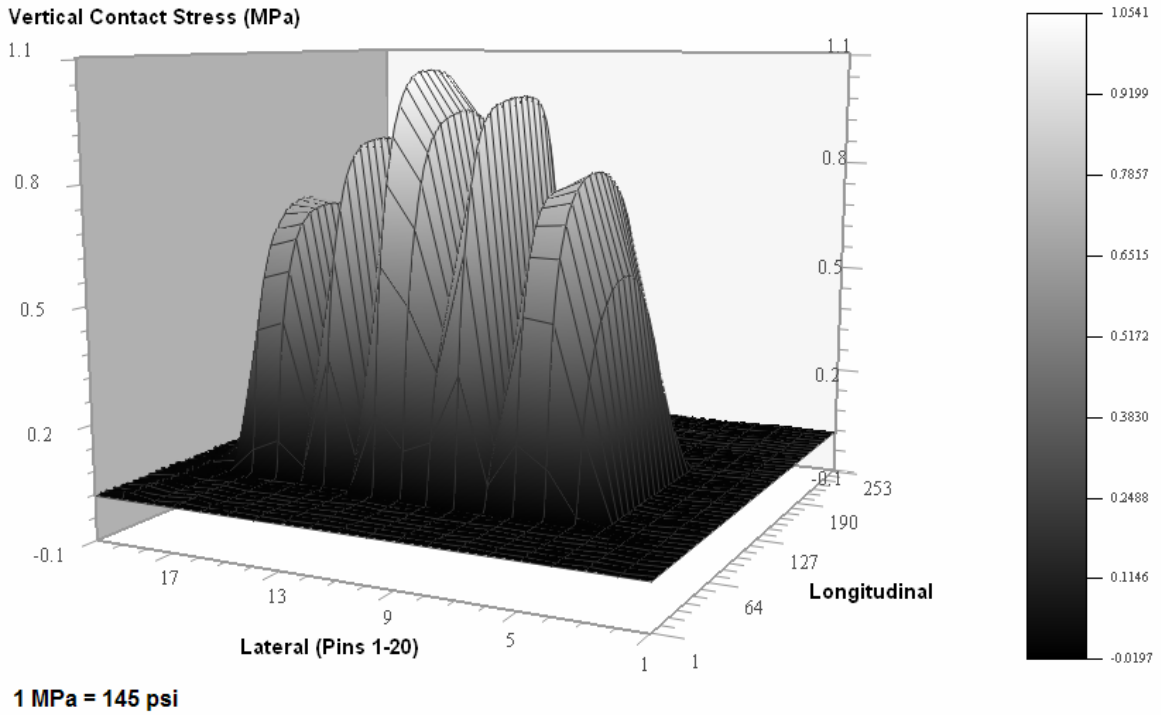

Figure A13. Measured Vertical Contact Stresses under the 295/75R22.5 Radial Tire Inflated to 100 psi and Loaded to 5850 lb.

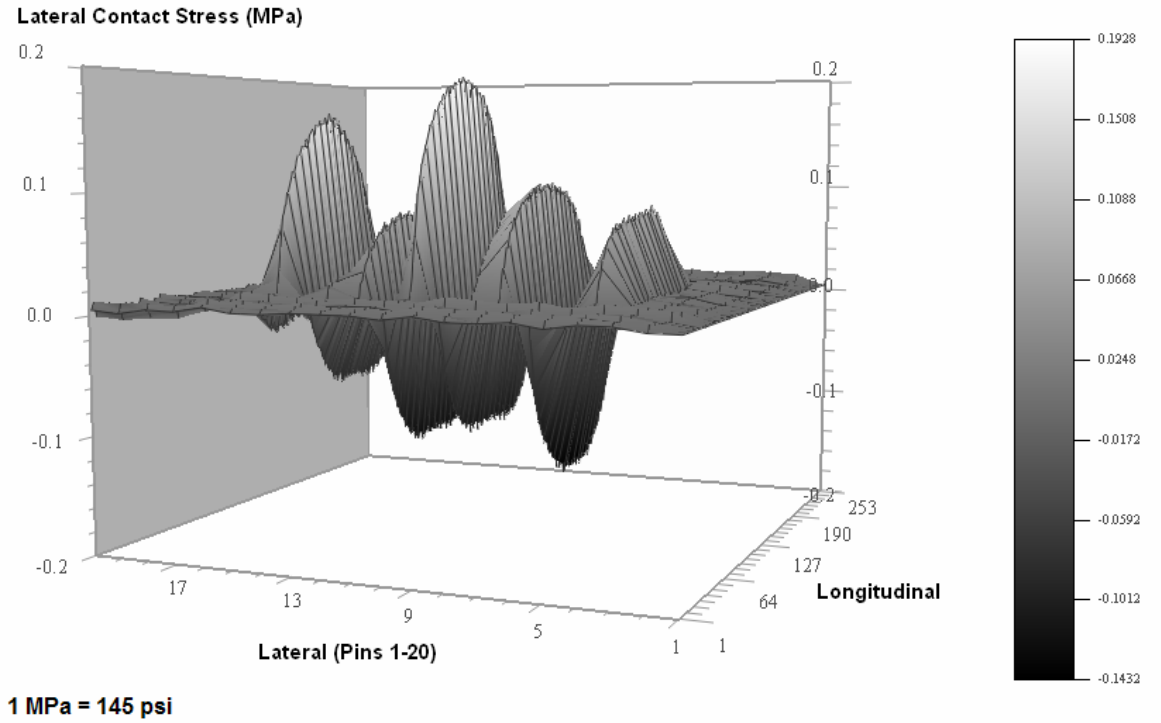

Figure A14. Measured Lateral Contact Stresses under a 295/75R22.5 Radial Tire Inflated to 100 psi and Loaded to 5850 lb.

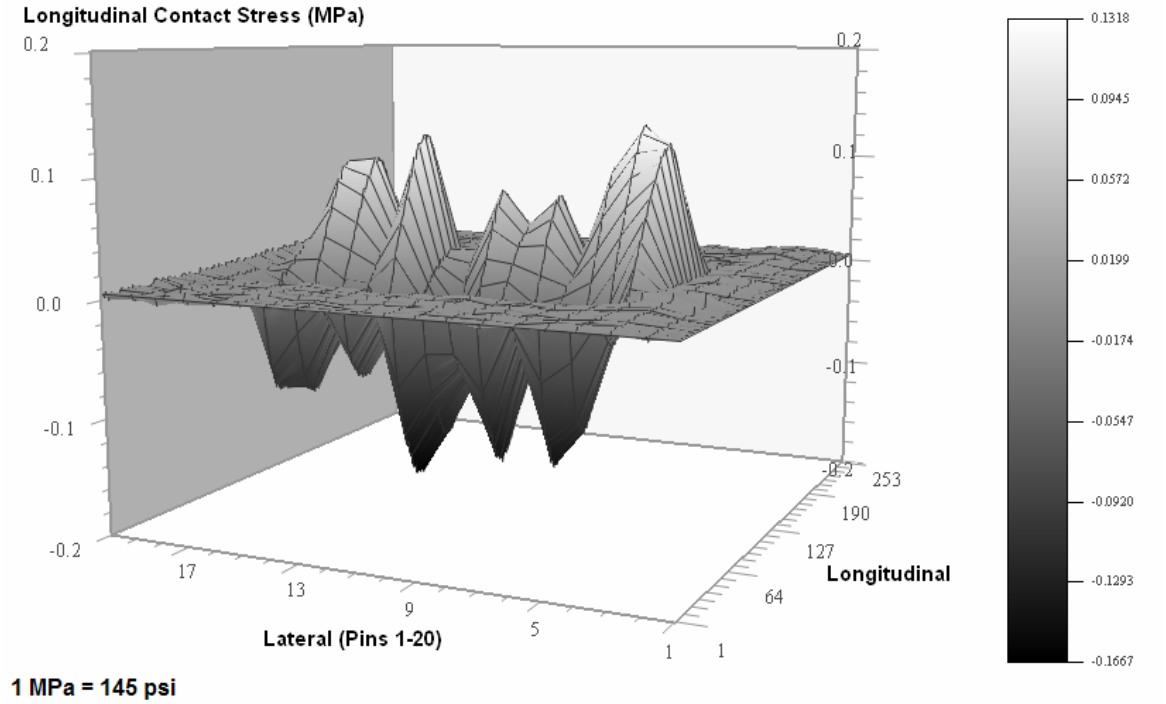

Figure A15. Measured Longitudinal Contact Stresses under a 295/75R22.5 Radial Tire Inflated to 100 psi and Loaded to 5850 lb.

inflation pressure of 100 psi and a tire load of 5850 lb. These figures clearly show the non-uniformity of contact stresses at the tire footprint. Note from Figure A13 that the measured contact stresses are about 1.5 times the inflation pressure around the middle of the tire.

MODELS FOR PREDICTING TIRE CONTACT PRESSURES

The pneumatic tire is a complicated structure that is designed to meet a wide variety of performance criteria. Virtually all tire performance attributes are associated with the tire-pavement contact region, known as the tire footprint. Within the tire footprint are found non-uniform distributions of vertical and shear contact pressures acting against the pavement. A comprehensive mathematical model of the pneumatic tire that is capable of predicting a variety of tire performance features can easily be more complex (and more unwieldy) than a model of the pavement system or the vehicle on which the tire is mounted.

During the 1970s, major tire manufacturers began to develop tire models for tire design analysis. All of these models are based on the finite element method, which enables a comprehensive and realistic tire model to be developed. These development efforts, however, focused on internal behavior and the prediction of stresses and strains in the tire carcass, instead of tire-pavement interaction. Industry-developed tire models are also proprietary, are generally not available to the public for external applications, and utilize a

very large number of finite elements to model details of the carcass design, therefore requiring extraordinary amounts of computing time.

Outside of the tire industry, researchers have used simpler finite element models to analyze the tire footprint. Flugrad and Miller (1981), and Mack et al. (1982) modeled the tire as a standing torus using the finite element method and predicted an elliptical tire footprint. At Texas A&M University, Tielking (1983) developed a finite element model for studying tire-pavement interaction. In this model, the tire is represented as an assembly of axisymmetric shell elements positioned along the carcass mid-ply surface. Figure A16 illustrates an assembly of 17 elements representing the midsurface of a 10-ply truck tire. Each finite element is considered to be homogeneous orthotropic, with the ply structure specified separately to define the laminated carcass.

The tire model is first loaded by specifying the inflation pressure. A solution for the axisymmetric inflated shape is obtained. The structural stiffness of the inflated tire is then calculated prior to bringing the model into contact with the pavement. A tire-pavement contact load is applied by specifying the axle height R_l (see Figure A17), which is equivalent to specifying the tire deflection against the pavement. The tire pressure distribution, which is predicted during the contact solution procedure, is integrated over the contact area to calculate the load necessary to maintain the specified axle height R_l.

Finite element tire models offer the capability to evaluate the effects of tire operating characteristics on footprint pressures and shape of the contact area. Depending on the features built into the computer program, a finite element tire model can provide flexibility in modeling different tire types, operated at various inflation pressures and tire loads. However, in practice, these models have seen very limited use for pavement design. There are a number of possible reasons for this:

- The more sophisticated tire models developed by the industry are generally geared toward tire design. In addition, these models are not generally available to the public.
- The computer programs require geometric and engineering data on tire construction that are difficult to get in practice. Perhaps due to the competitive nature of the industry, published data on tires do not include geometric and material properties that are required for modeling purposes.

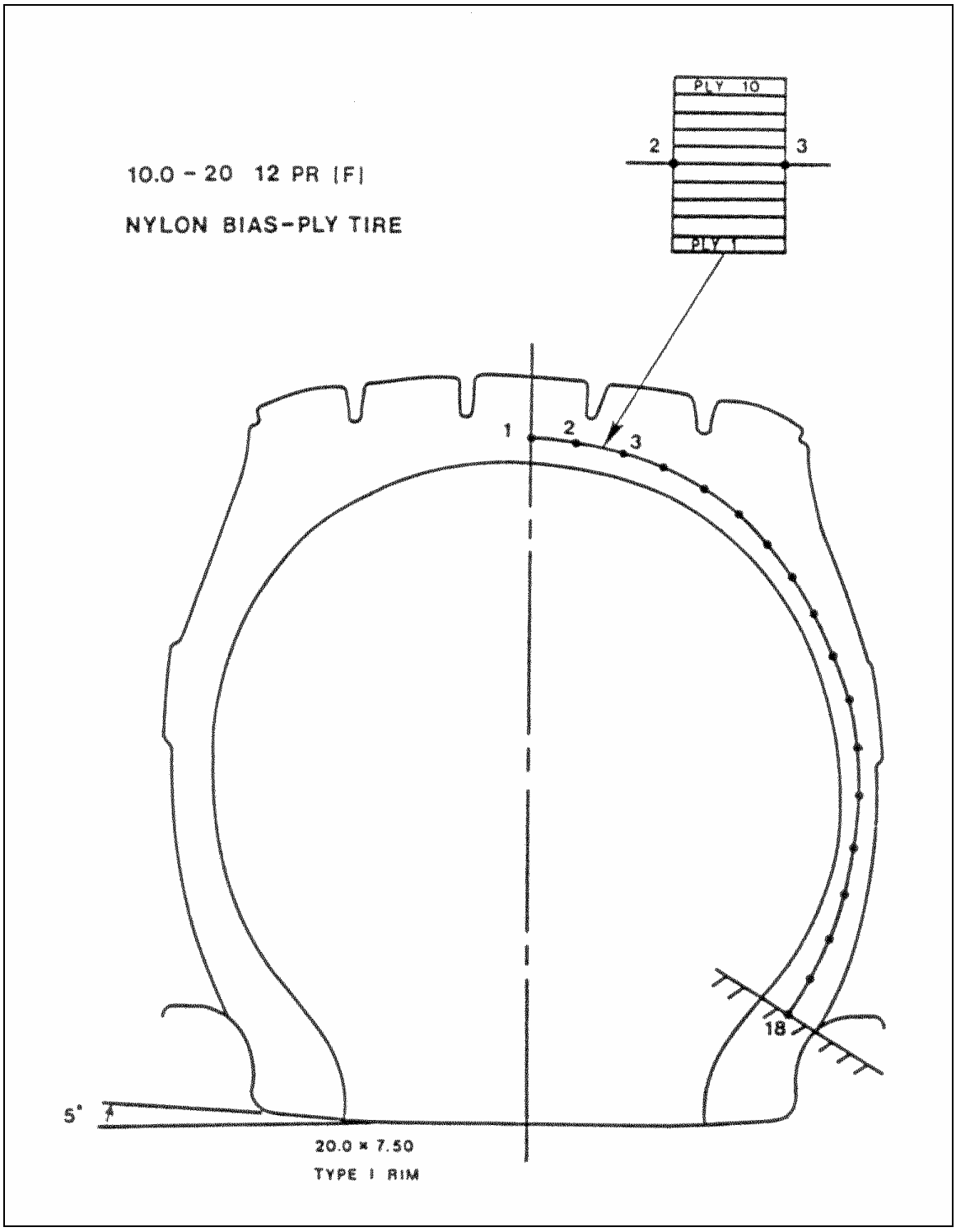

Figure A16. Assembly of Finite Elements for a 10.00–20 Bias-Ply Truck Tire (Tielking, 1986).

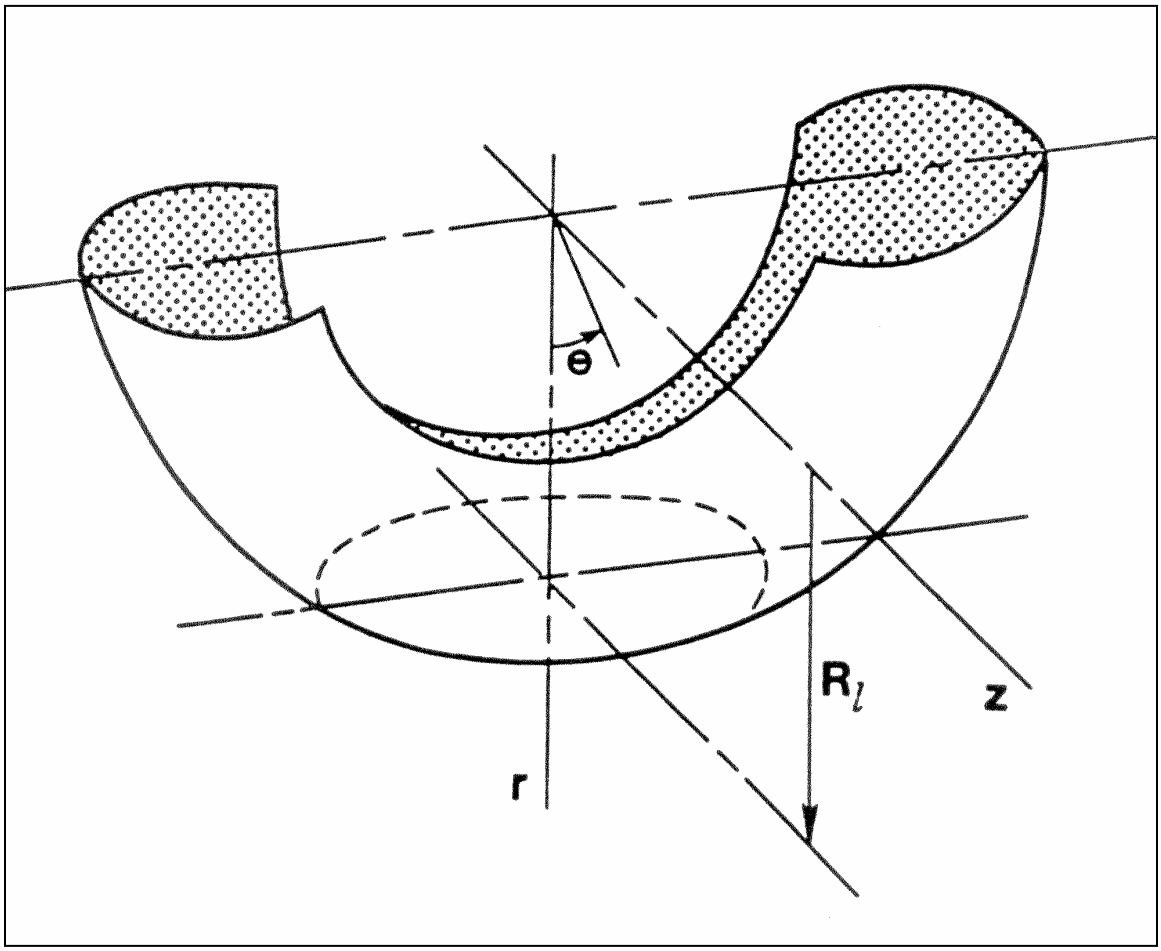

Figure A17. Illustration of the Tire Contact Surface for the Specified Loaded Radius R_l.

- Finite element tire models are difficult to implement for pavement design. In addition to the lack of published data on geometric and material properties of tires, data on tire types, sizes, and inflation pressures are not collected in existing design practice. Predictions of tire contact stresses are significantly influenced by these variables, in addition to the tire load.

Researchers note that finite element tire modeling is outside the scope of this project. Rather, the research aimed to use measured tire-pavement contact stresses for common truck tires to assess the pavement design implications of assuming uniform versus actual tire-pavement contact stresses. For this purpose, researchers acquired available tire contact pressure measurements and conducted a review of truck tire usage to identify additional tires for testing (to the extent feasible within available project funds), and expand the available data base to cover other tire sizes and operating conditions encountered in practice. A procedure was developed to estimate tire-pavement contact pressures using an interpolation

technique for the range of tires, tire loads and tire inflation pressures represented in the data base. In a previous study, El-Gindy and Lewis (2001) developed artificial neural network models to predict vertical tire contact pressures. This work used the VRSPTA data collected at the UCB HVS facility from tests ran on the 10 × 20 bias-ply and the 11R22.5 radial tires.

MODELS FOR PREDICTING PAVEMENT RESPONSE

Layered elastic and finite element computer programs have been used in previous investigations of the effects of tire contact pressures. Marshek et al. (1985) used the multi-layered linear elastic program, BISAR (De Jong et al., 1973), to predict pavement response based on vertical contact stresses measured using pressure sensitive film. BISAR is a general purpose computer program for computing stresses, strains and displacements in layered elastic systems subjected to one or more uniform loads, acting over circular areas. In their analyses, Marshek et al. (1985) characterized the measured vertical pressure distribution from a given test as a series of concentric annular rings, as illustrated in Figure A18. In this way, the researchers considered the non-uniformity of measured vertical contact pressures, and modeled regions of high-pressure gradients, such as those that exist at the tread gaps and tire shoulders. The radial distances defining the areas on which the pressures act were adjusted such that the total tire load equaled that used for a given test.

Jacobs (1989) also used the BISAR computer program to predict stresses and strains induced under non-uniform pressure distributions representative of the tire footprint. In his work, Jacobs (1989) used published tire contact pressure data for a free-rolling truck tire, and mapped the pressure distributions as illustrated in Figures A19 and A20. Subsequently, in the BISAR runs, he replaced the loaded squares in the figures with loaded circles having the same areas. A similar approach was used by Myers et al. (1998) to investigate the potential of surface-initiated cracks due to non-uniform vertical and shear stress distributions at the tire-pavement interface. This more recent study used tire contact stresses measured under bias-ply and conventional radial truck tires using the test setup illustrated in Figure A4.

Perdomo and Nokes (1994) used the CIRCLY program to investigate the effects of wide-base tires on flexible pavement response. CIRCLY (1999) provides additional options for modeling surface loads not found in other existing layered elastic programs. Specifically, horizontal and vertical pressure distributions may be defined using general polynomial expressions. In addition, moments about horizontal and vertical axes may be specified.

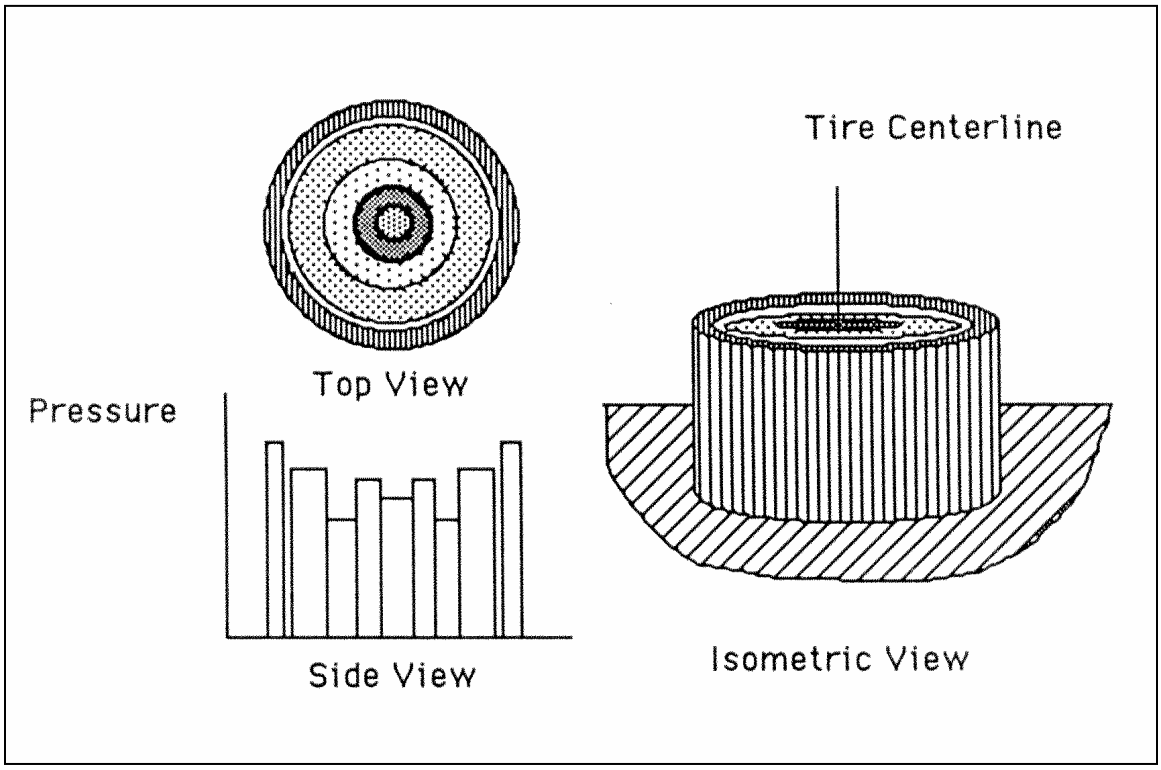

Figure A18. Representation of Vertical Contact Pressure Distribution Using Concentric Annular Rings (Marshek et al., 1985).

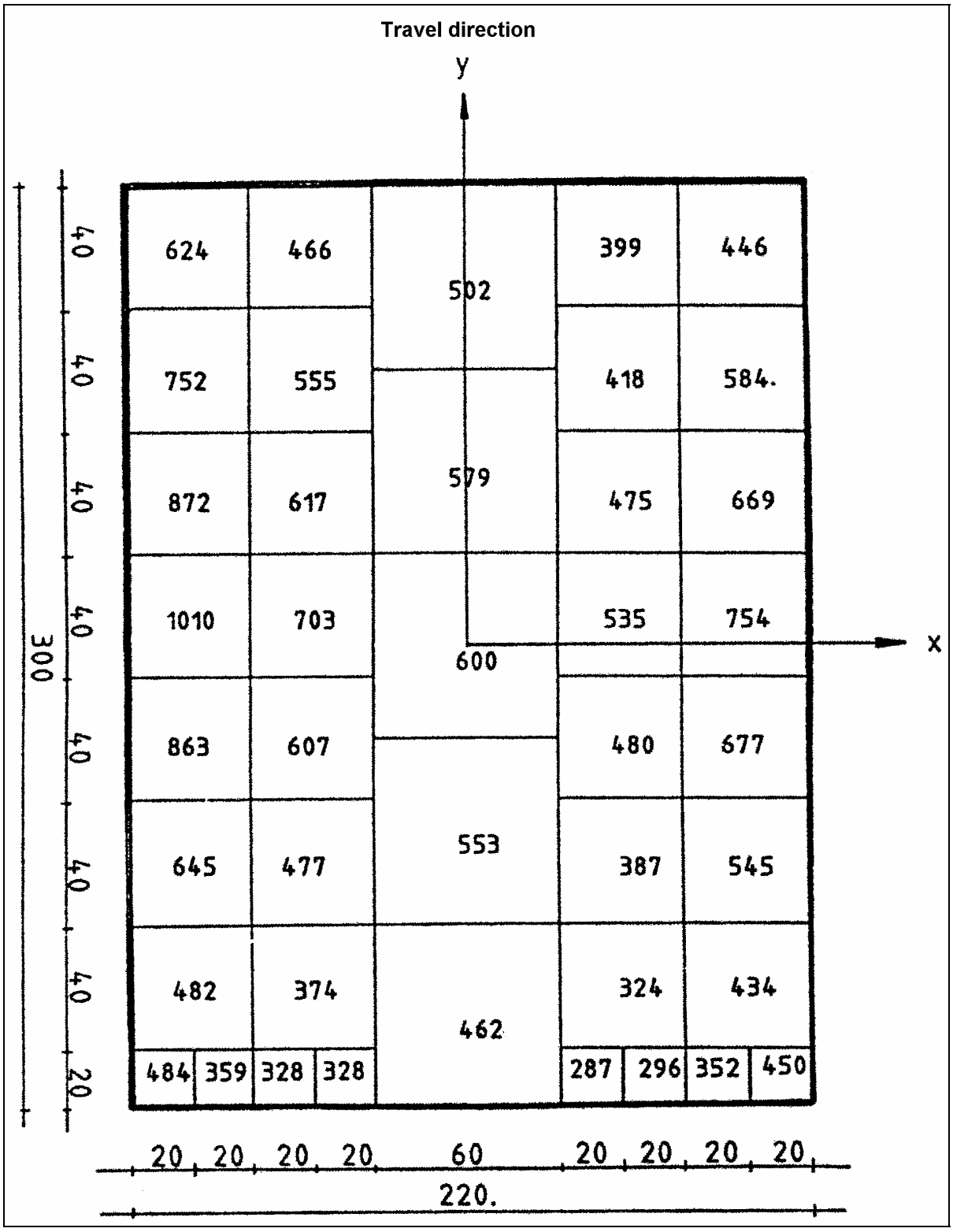

Figure A19. Mapping of Vertical Contact Pressures for Analyzing Pavement Response (Jacobs, 1989).

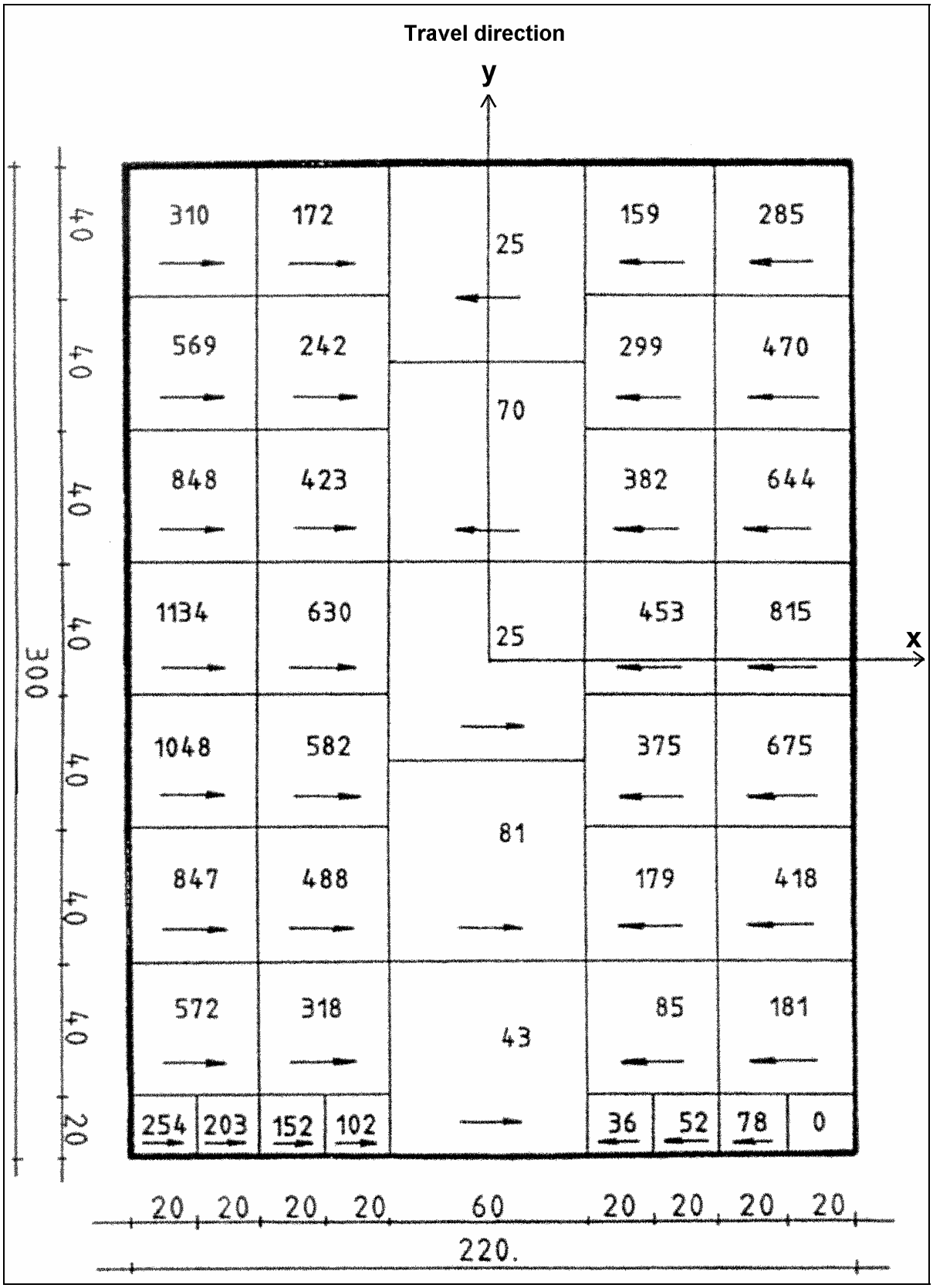

Figure A20. Mapping of Transverse Contact Shear Stresses for Analyzing Pavement Response (Jacobs, 1989).

Using CIRCLY, Perdomo and Nokes (1994) characterized the vertical and inward shear stress distributions under dual and wide-base tires using polynomial expressions determined based on measured tire contact pressures reported by Yap (1988).

Researchers note that most pavement analysis programs used by TxDOT are based on multi-layered elastic theory. This approach is much easier to use and implement in practice than the finite element method. However, for analyzing the effects of measured tire contact stresses on predicted pavement response, the finite element method provides greater versatility in specifying surface loading conditions. In this project, researchers used the finite element method to predict performance-related pavement response variables as part of evaluating how tire contact stresses may be represented in existing layered elastic programs implemented by TxDOT.

Application of the finite element method will involve discretizing the pavement into a set of finite elements connected at the nodal points. The continuous variation of stresses and strains in the pavement is represented by an assumed linear or quadratic displacement function over each element. In FEM, careful attention must be given to constructing the finite element mesh as the mesh construction significantly affects the results. Cho et al. (1996) evaluated the effects of using different element types, element sizes, aspect ratios and finite element formulations on FEM results. Their findings show that stress calculations using 3D finite element analyses gave comparable predictions with multi-layered elastic theory when quadratic elements coupled with infinite elements were used. Thus, in using FEM to analyze tire contact stresses, careful attention should be given to constructing the finite element mesh, particularly within the near surface regions that are influenced by tire pressure effects.

APPENDIX B

CHARTS OF TIRE CONTACT STRESS DISTRIBUTIONS FROM TESTS CONDUCTED ON THE 11R24.5 RADIAL TIRE

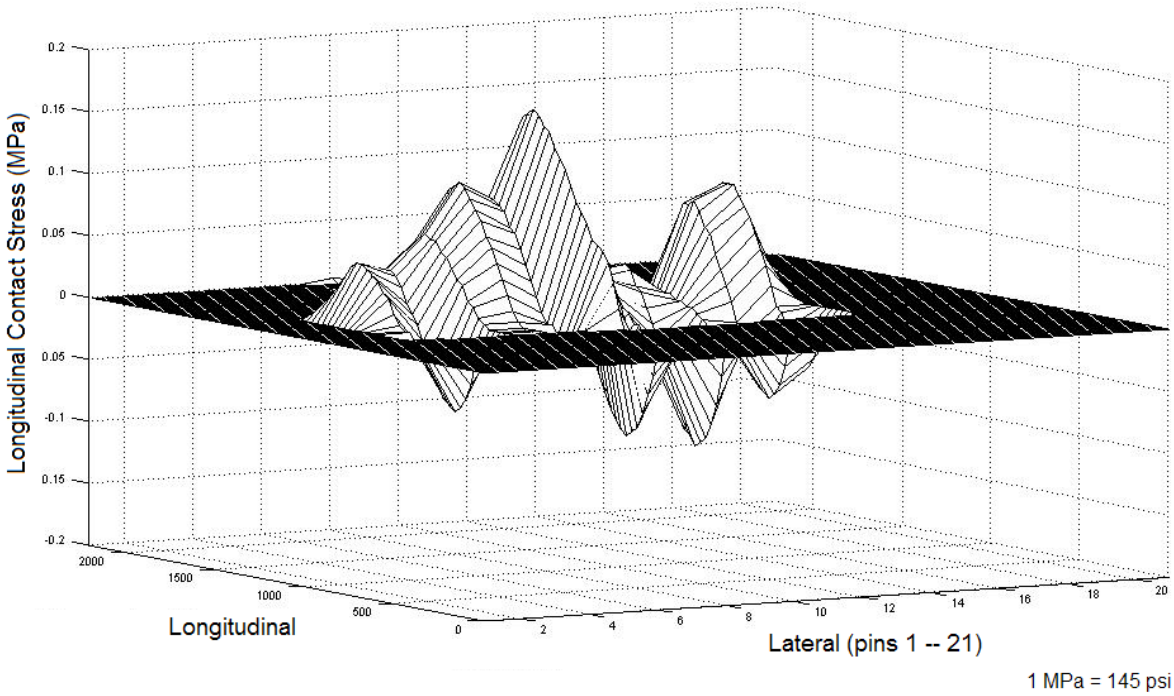

Figure B1. Measured Longitudinal Contact Stress Distribution for 11R24.5 Radial Tested at a Tire Load of 4600 lb and an Inflation Pressure of 70 psi.

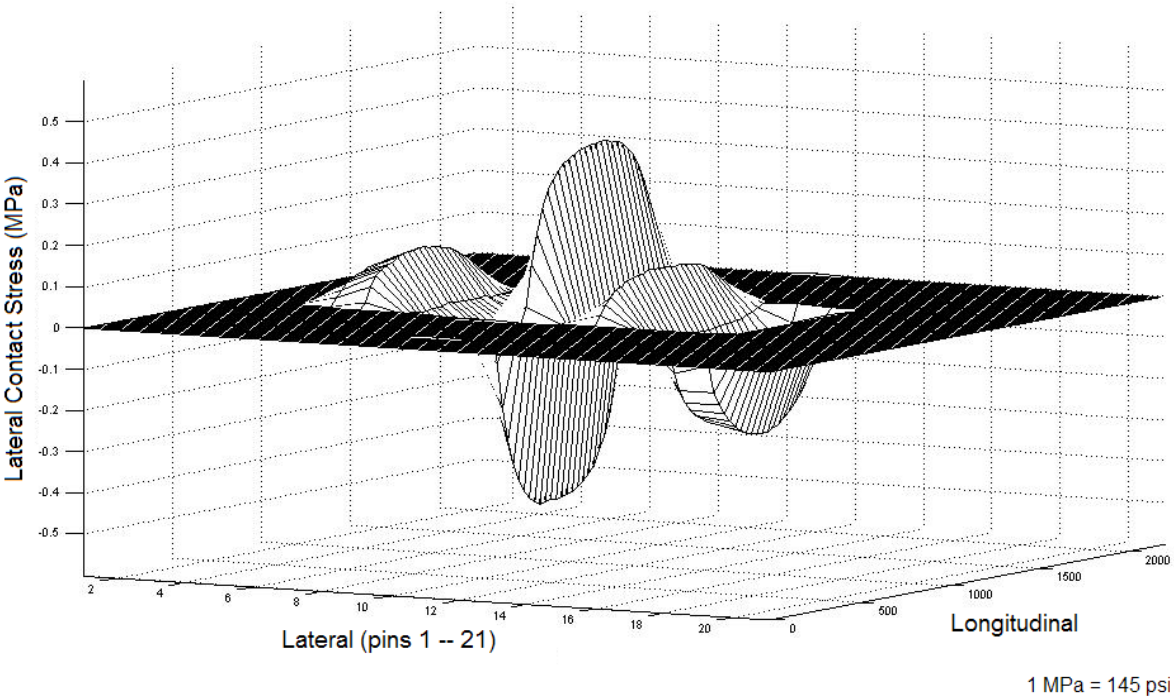

Figure B2. Measured Lateral Contact Stress Distribution for 11R24.5 Radial Tested at a Tire Load of 4600 lb and an Inflation Pressure of 70 psi.

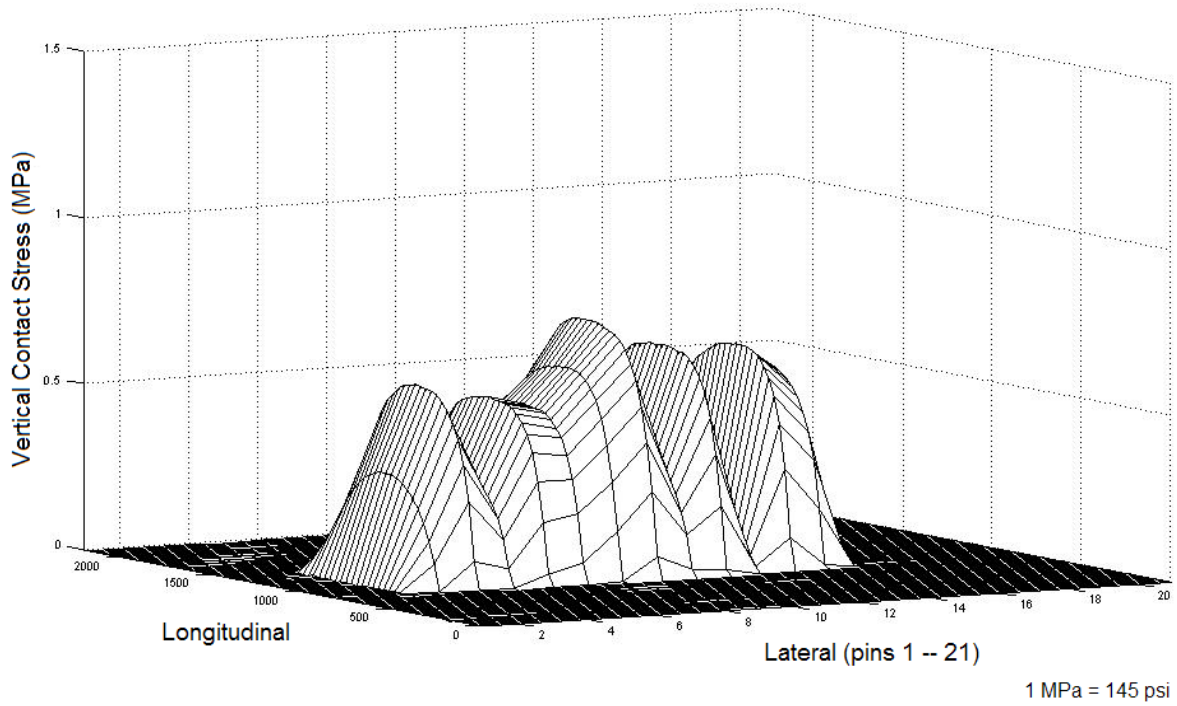

Figure B3. Measured Vertical Contact Stress Distribution for 11R24.5 Radial Tested at a Tire Load of 4600 lb and an Inflation Pressure of 70 psi.

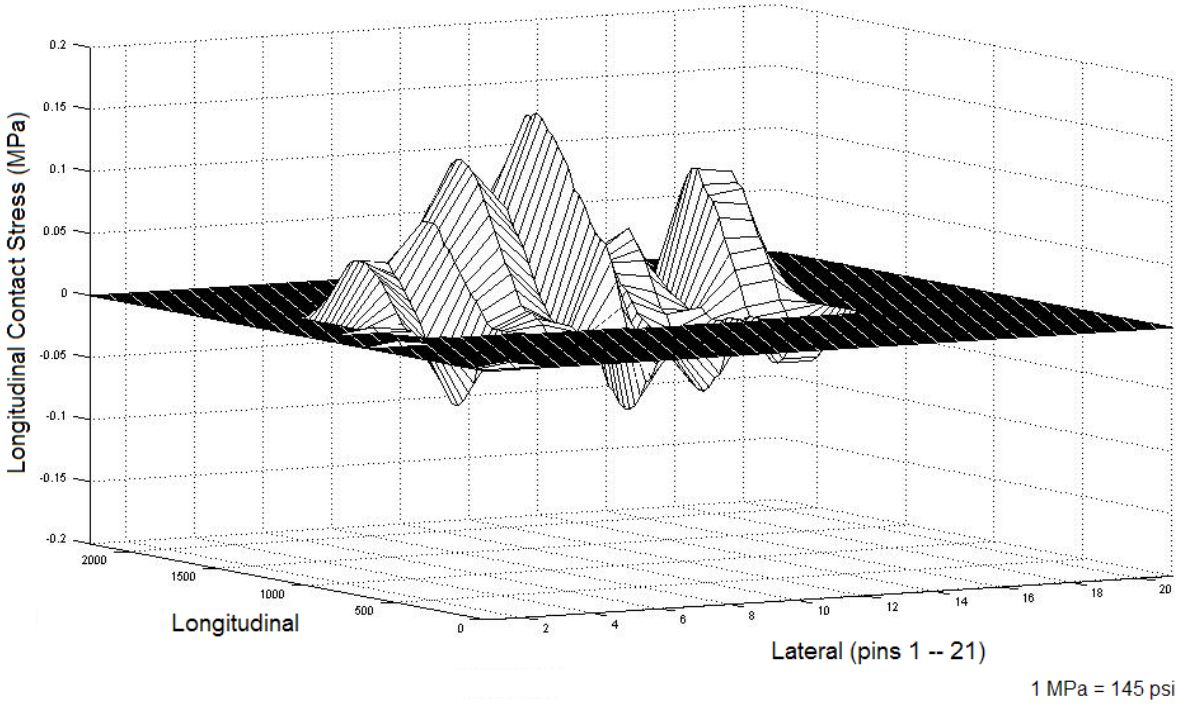

Figure B4. Measured Longitudinal Contact Stress Distribution for 11R24.5 Radial Tested at a Tire Load of 4600 lb and an Inflation Pressure of 85 psi.

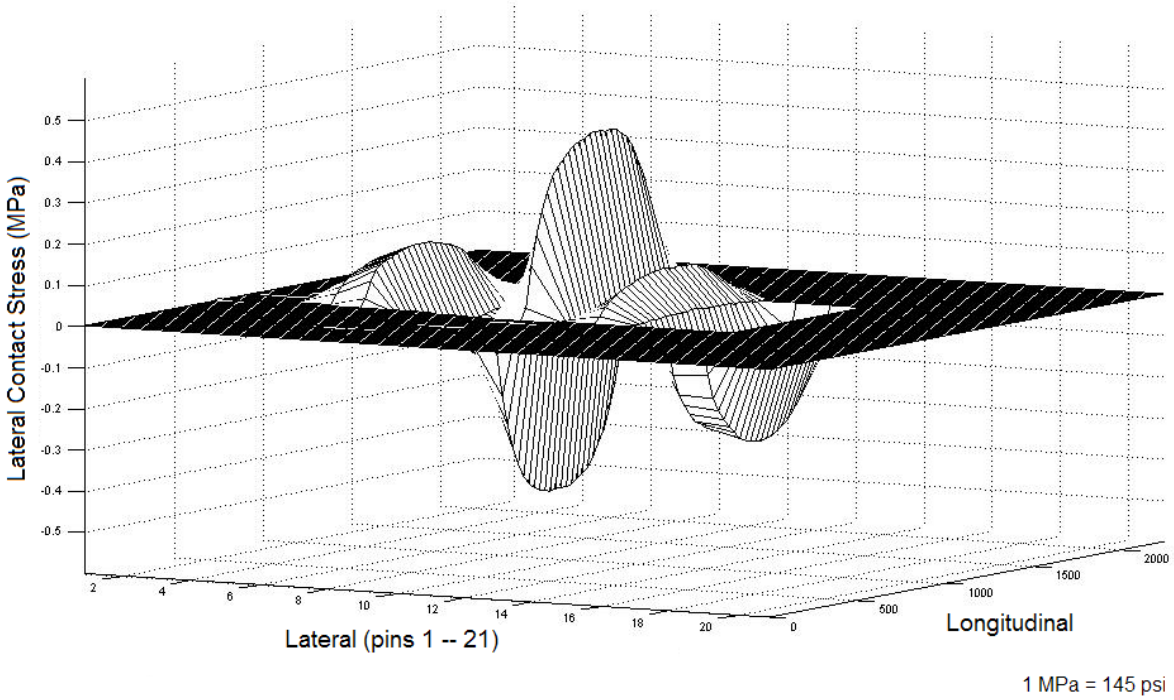

Figure B5. Measured Lateral Contact Stress Distribution for 11R24.5 Radial Tested at a Tire Load of 4600 lb and an Inflation Pressure of 85 psi.

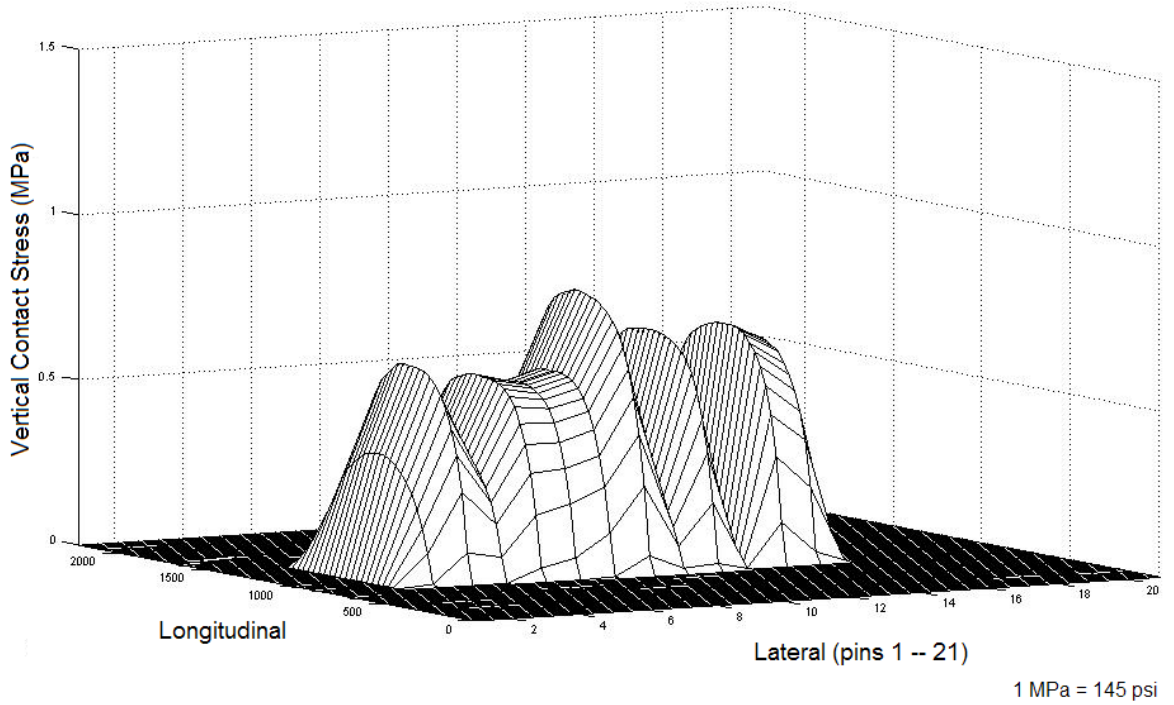

Figure B6. Measured Vertical Contact Stress Distribution for 11R24.5 Radial Tested at a Tire Load of 4600 lb and an Inflation Pressure of 85 psi.

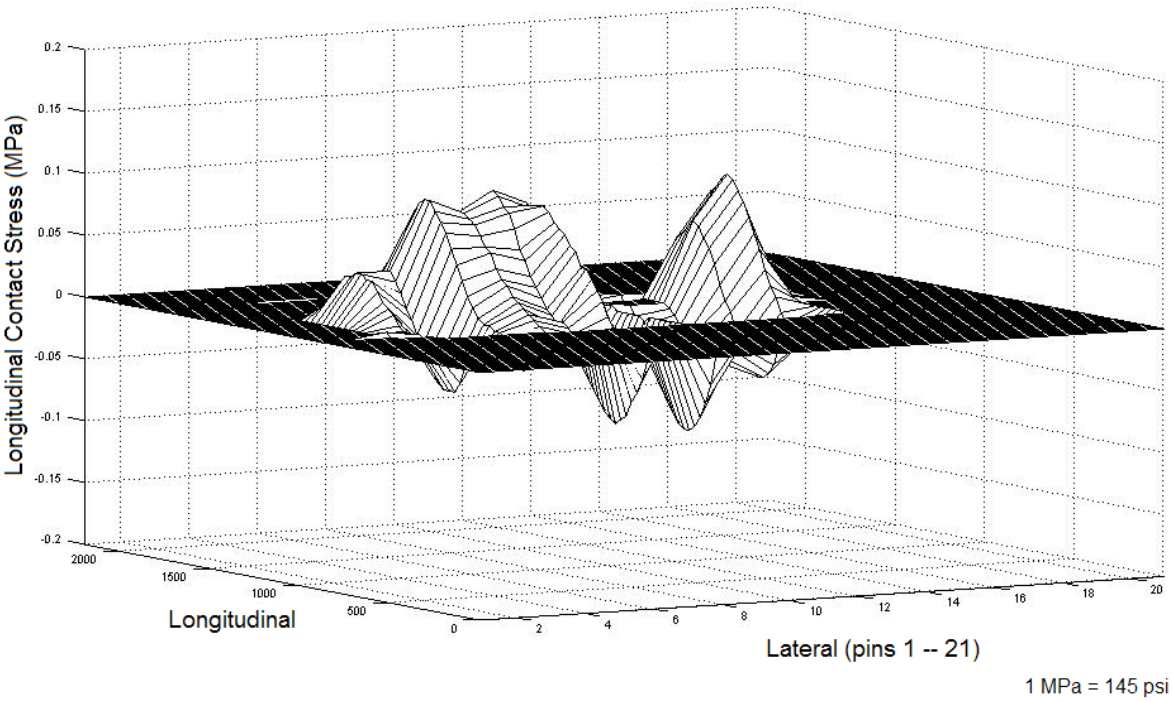

Figure B7. Measured Longitudinal Contact Stress Distribution for 11R24.5 Radial Tested at a Tire Load of 4600 lb and an Inflation Pressure of 100 psi.

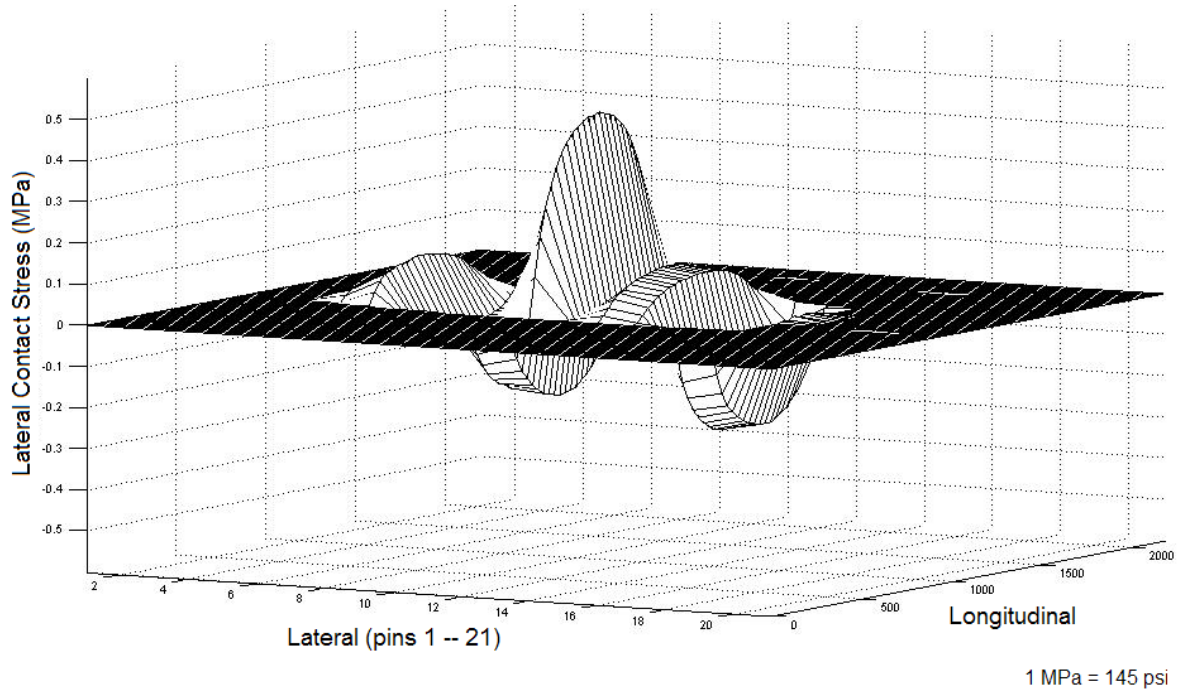

Figure B8. Measured Lateral Contact Stress Distribution for 11R24.5 Radial Tested at a Tire Load of 4600 lb and an Inflation Pressure of 100 psi.

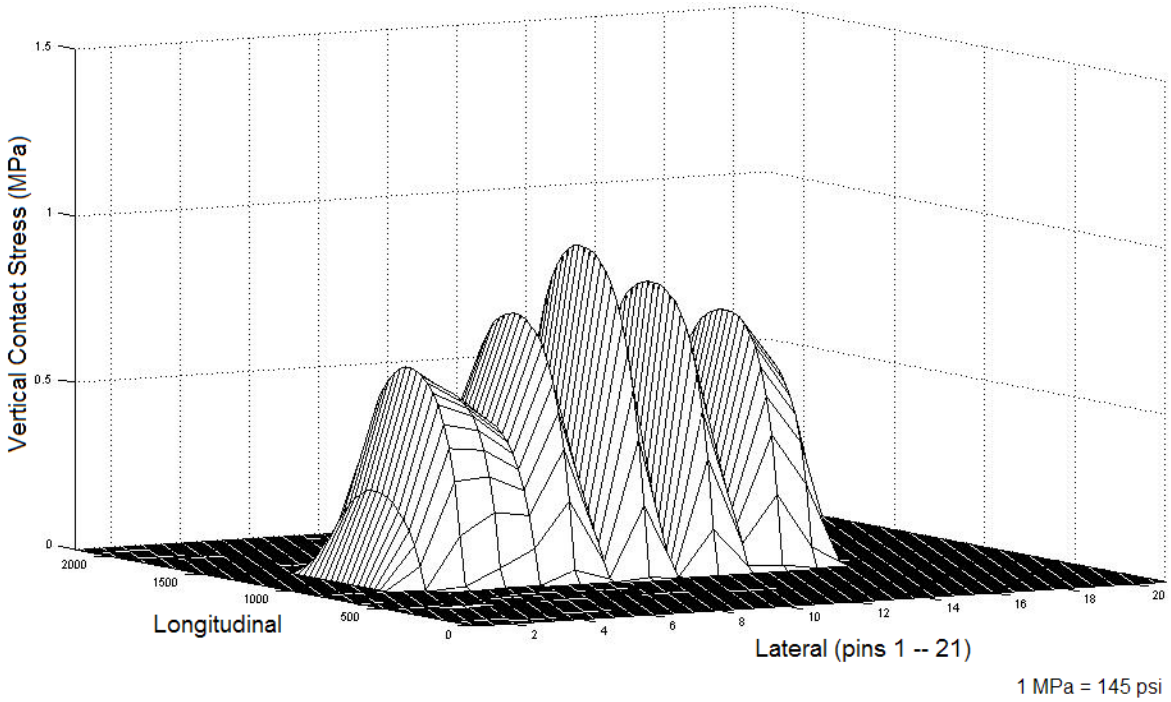

Figure B9. Measured Vertical Contact Stress Distribution for 11R24.5 Radial Tested at a Tire Load of 4600 lb and an Inflation Pressure of 100 psi.

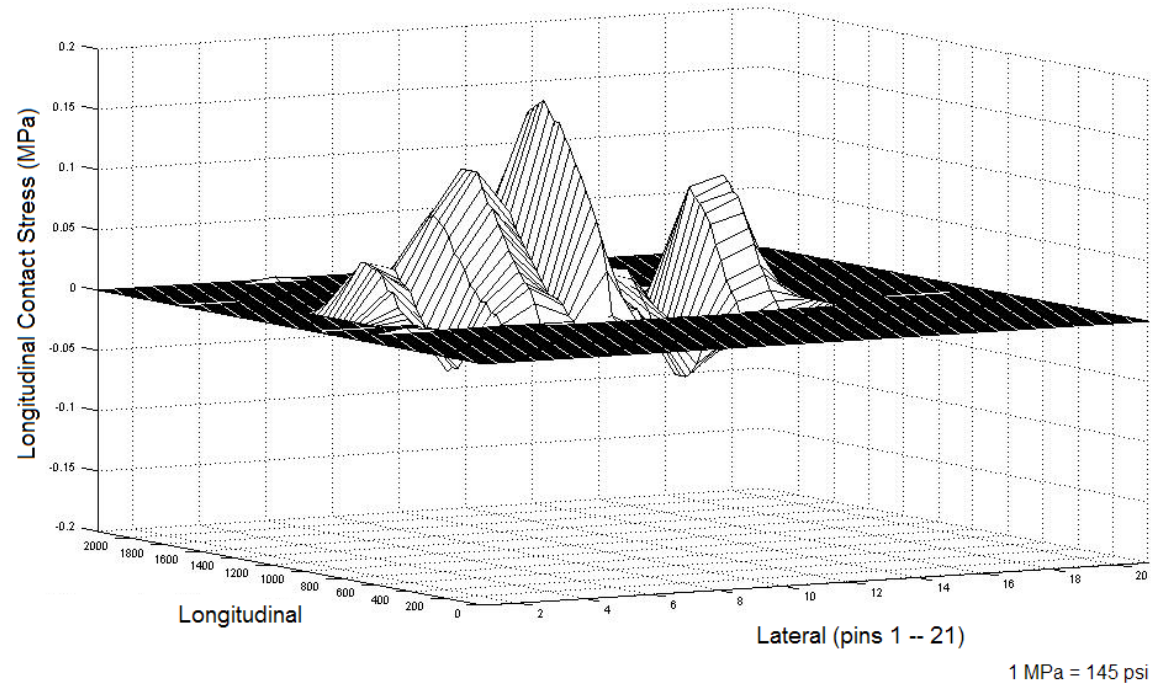

Figure B10. Measured Longitudinal Contact Stress Distribution for 11R24.5 Radial Tested at a Tire Load of 4600 lb and an Inflation Pressure of 115 psi.

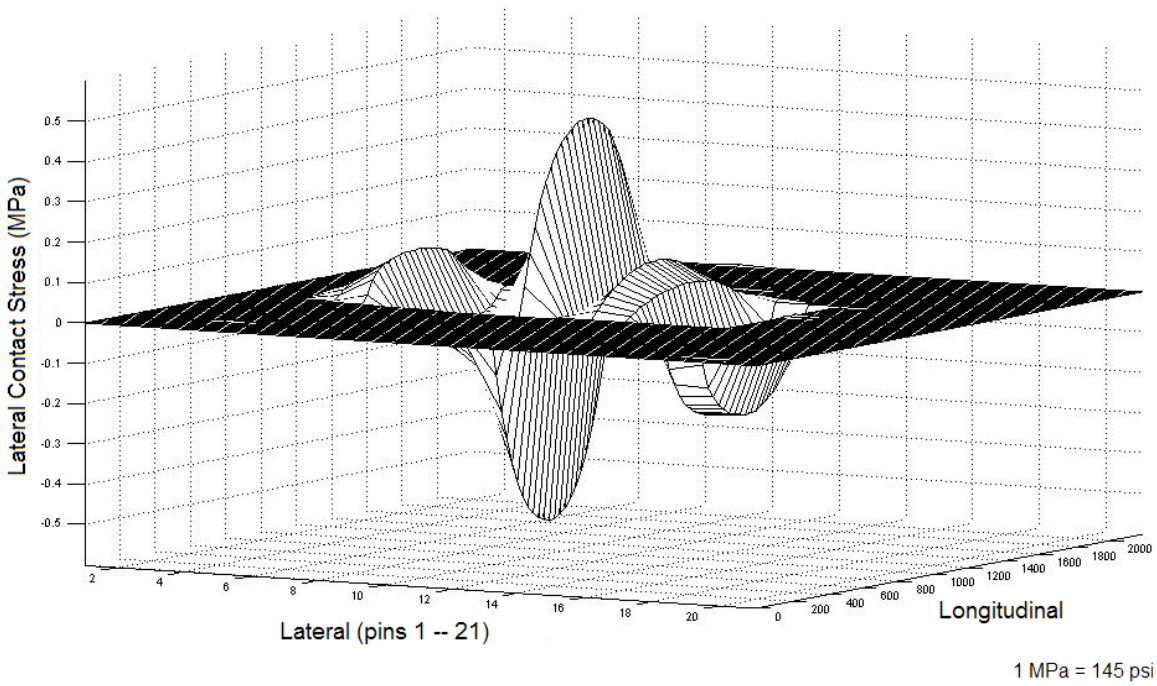

Figure B11. Measured Lateral Contact Stress Distribution for 11R24.5 Radial Tested at a Tire Load of 4600 lb and an Inflation Pressure of 115 psi.

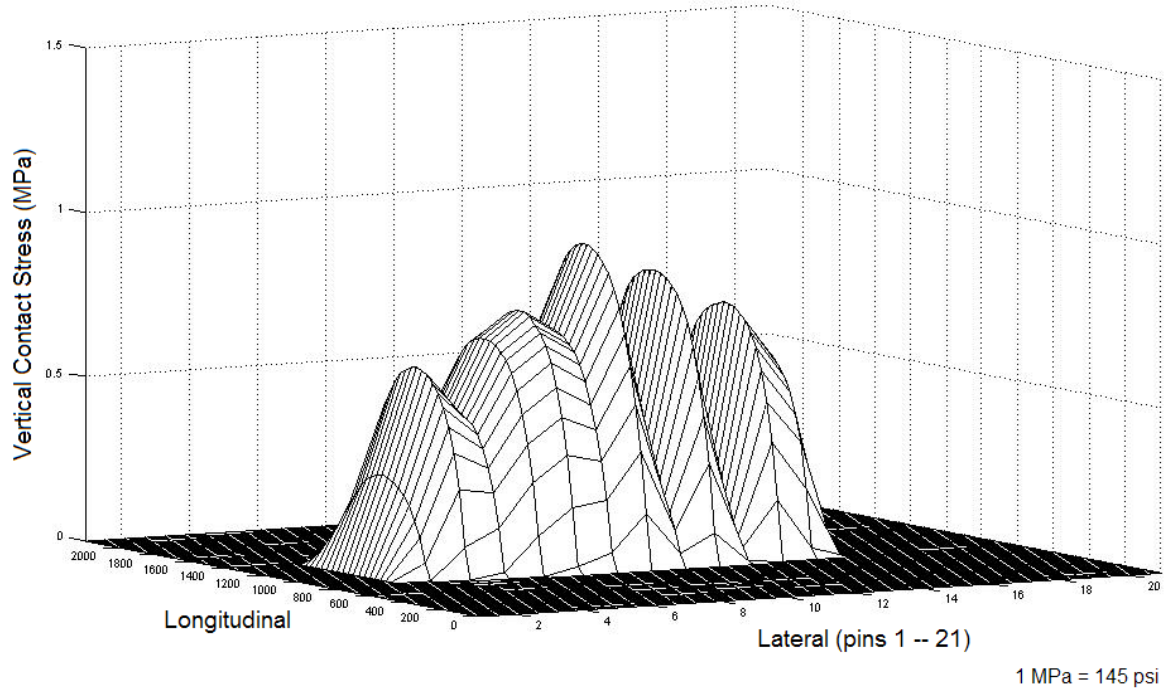

Figure B12. Measured Vertical Contact Stress Distribution for 11R24.5 Radial Tested at a Tire Load of 4600 lb and an Inflation Pressure of 115 psi.

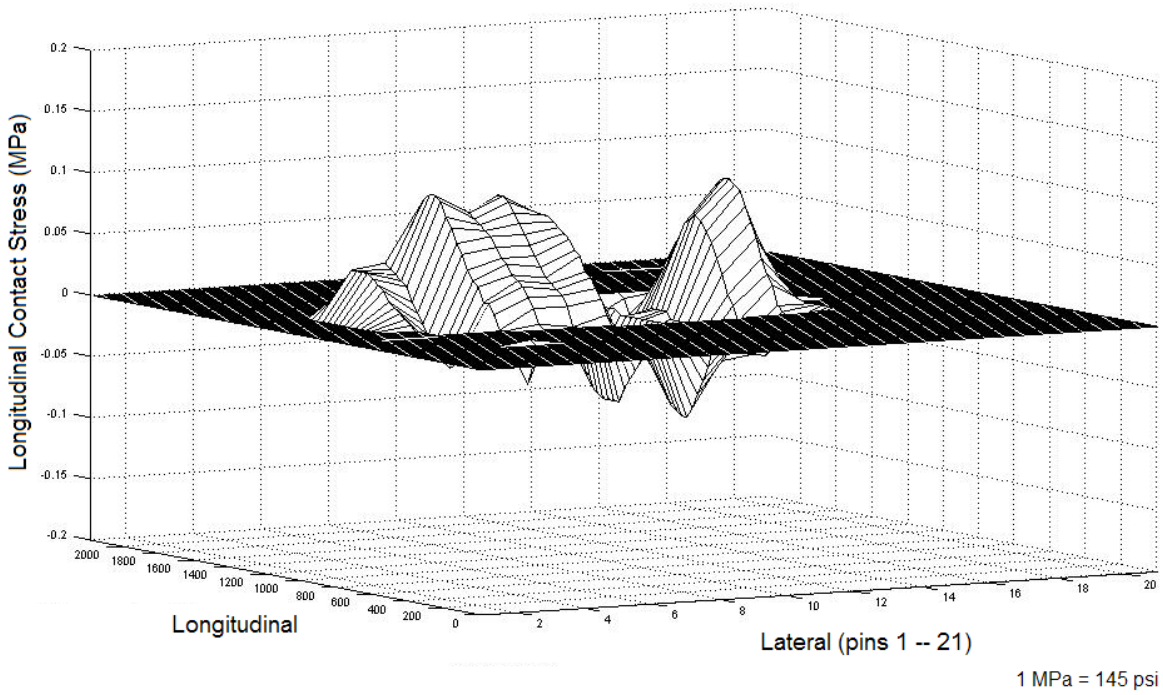

Figure B13. Measured Longitudinal Contact Stress Distribution for 11R24.5 Radial Tested at a Tire Load of 4600 lb and an Inflation Pressure of 130 psi.

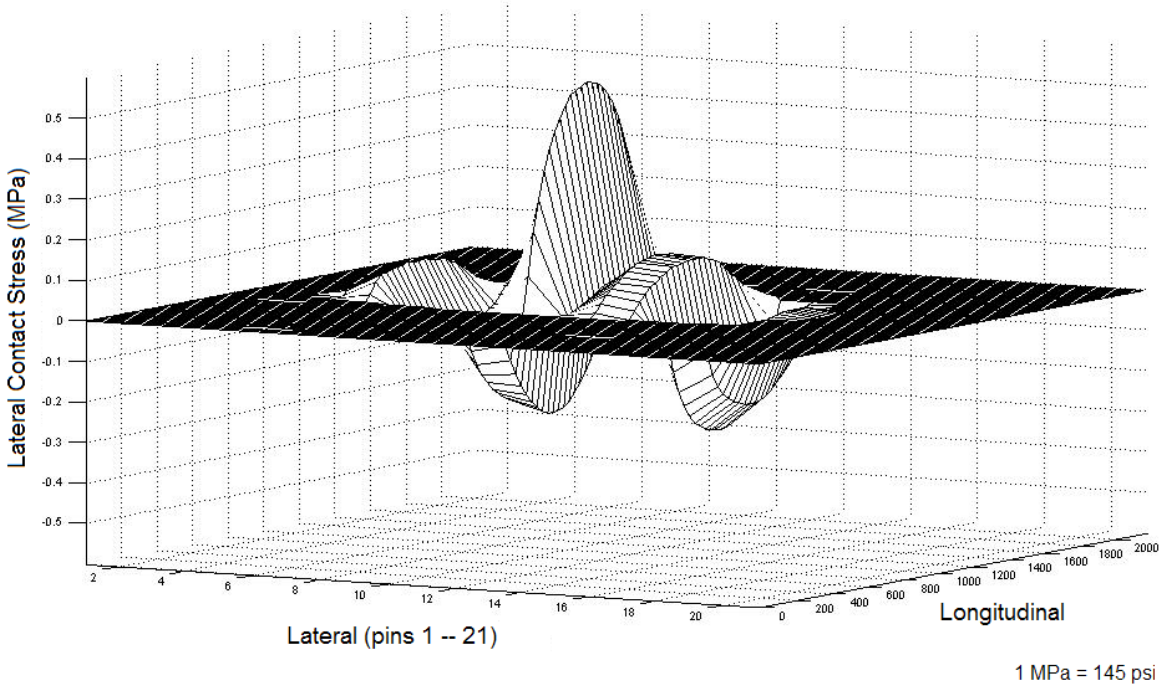

Figure B14. Measured Lateral Contact Stress Distribution for 11R24.5 Radial Tested at a Tire Load of 4600 lb and an Inflation Pressure of 130 psi.

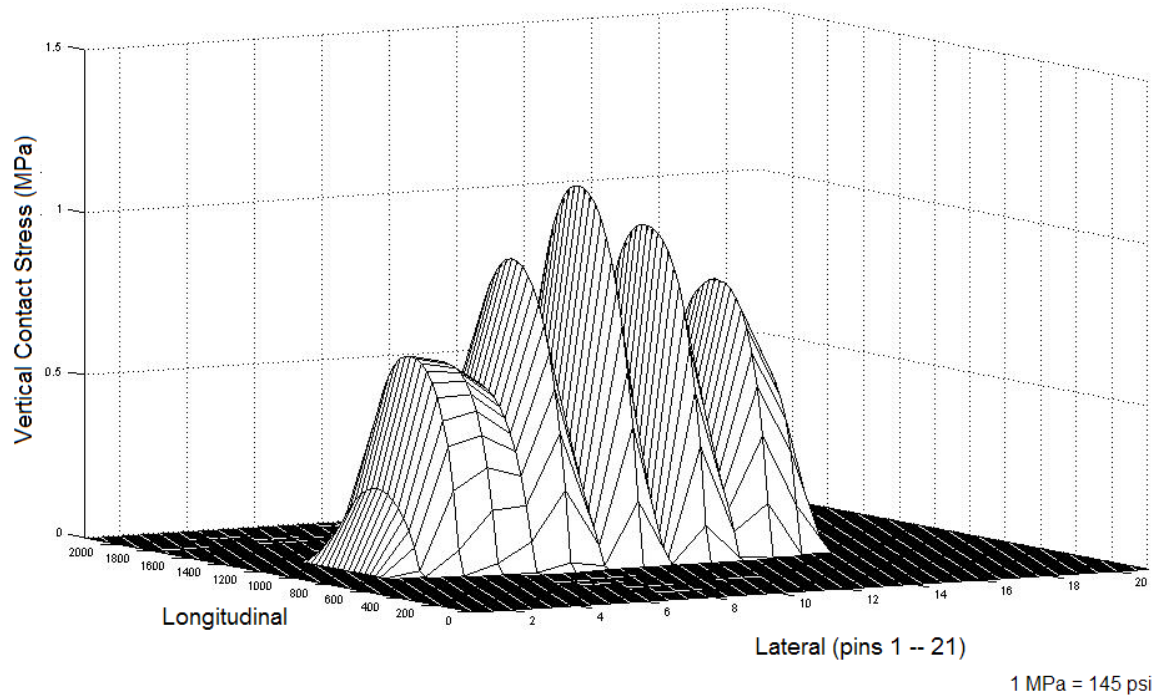

Figure B15. Measured Vertical Contact Stress Distribution for 11R24.5 Radial Tested at a Tire Load of 4600 lb and an Inflation Pressure of 130 psi.

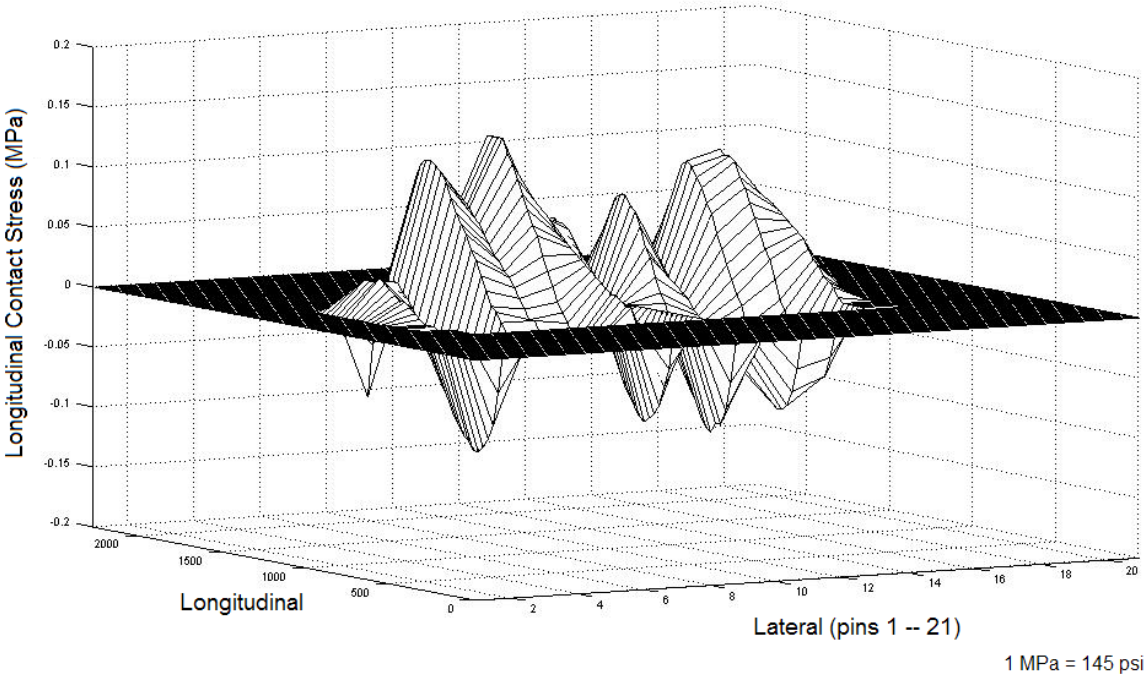

Figure B16. Measured Longitudinal Contact Stress Distribution for 11R24.5 Radial Tested at a Tire Load of 5400 lb and an Inflation Pressure of 70 psi.

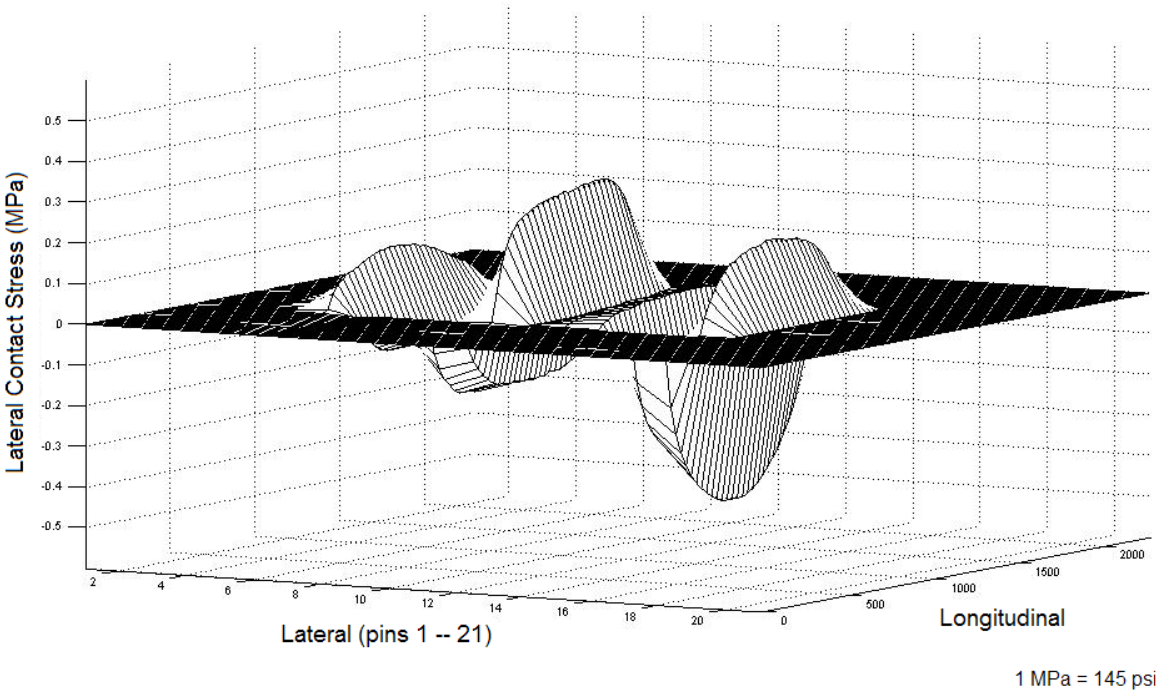

Figure B17. Measured Lateral Contact Stress Distribution for 11R24.5 Radial Tested at a Tire Load of 5400 lb and an Inflation Pressure of 70 psi.

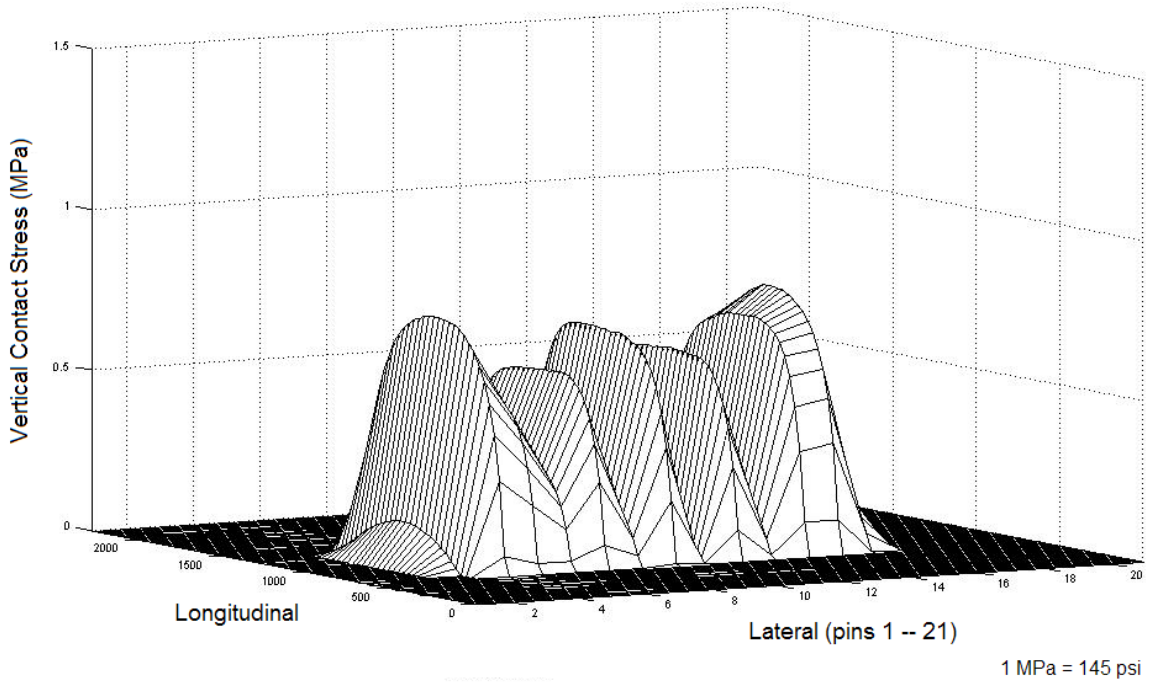

Figure B18. Measured Vertical Contact Stress Distribution for 11R24.5 Radial Tested at a Tire Load of 5400 lb and an Inflation Pressure of 70 psi.

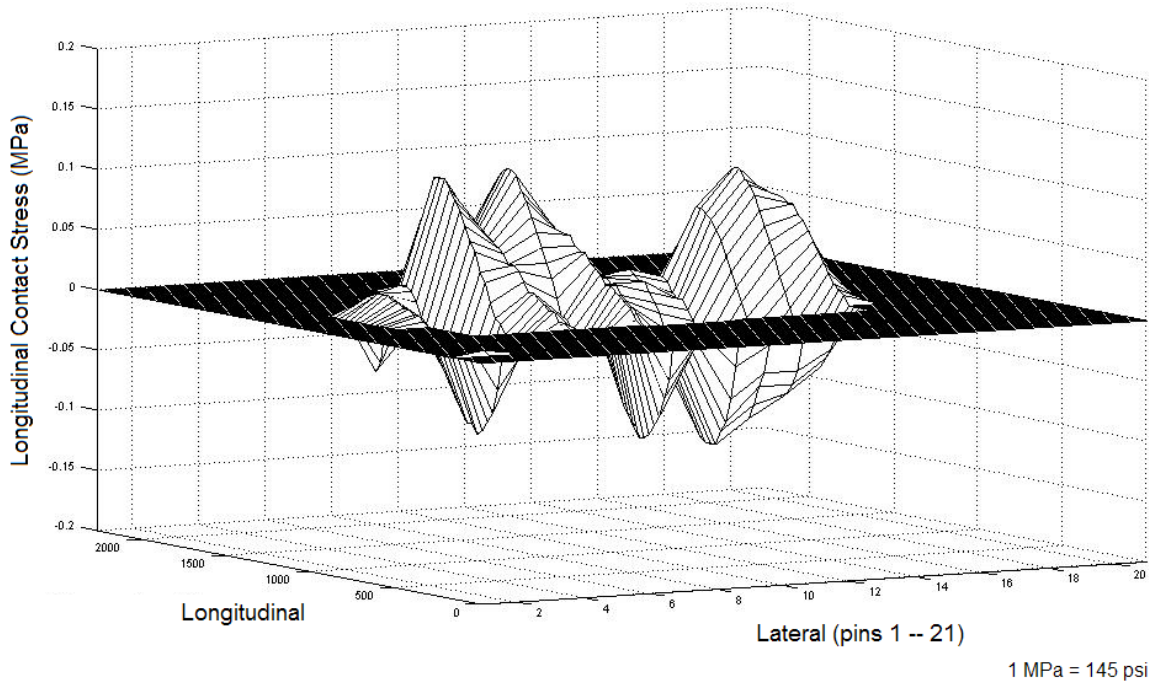

Figure B19. Measured Longitudinal Contact Stress Distribution for 11R24.5 Radial Tested at a Tire Load of 5400 lb and an Inflation Pressure of 85 psi.

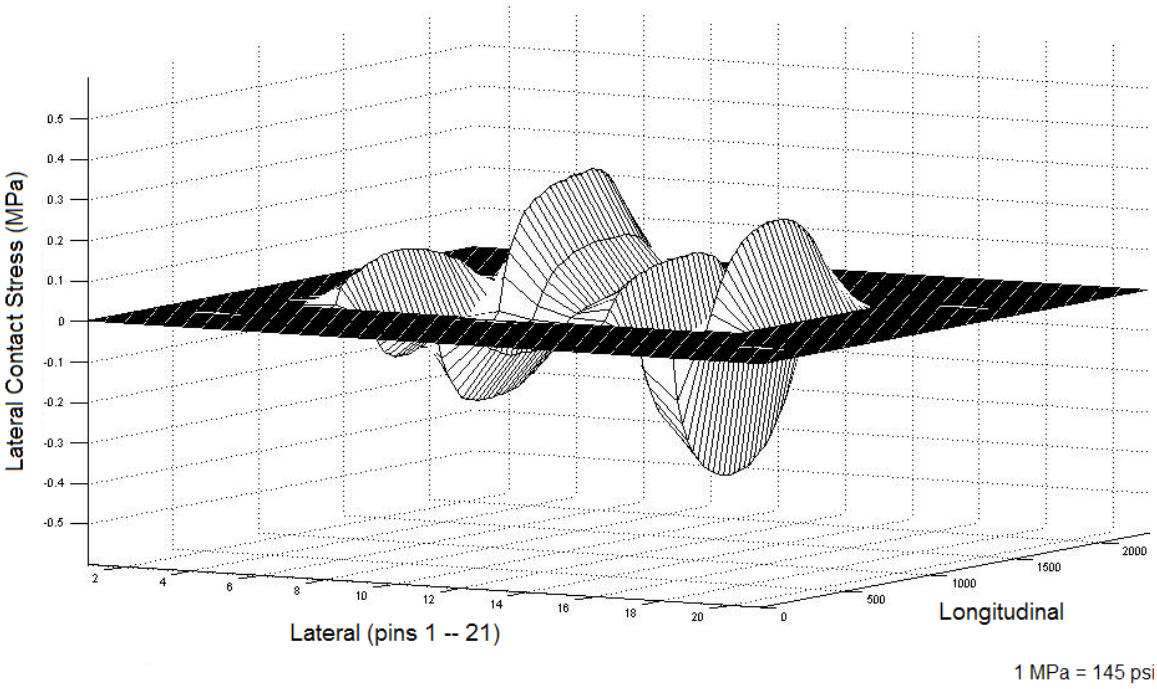

Figure B20. Measured Lateral Contact Stress Distribution for 11R24.5 Radial Tested at a Tire Load of 5400 lb and an Inflation Pressure of 85 psi.

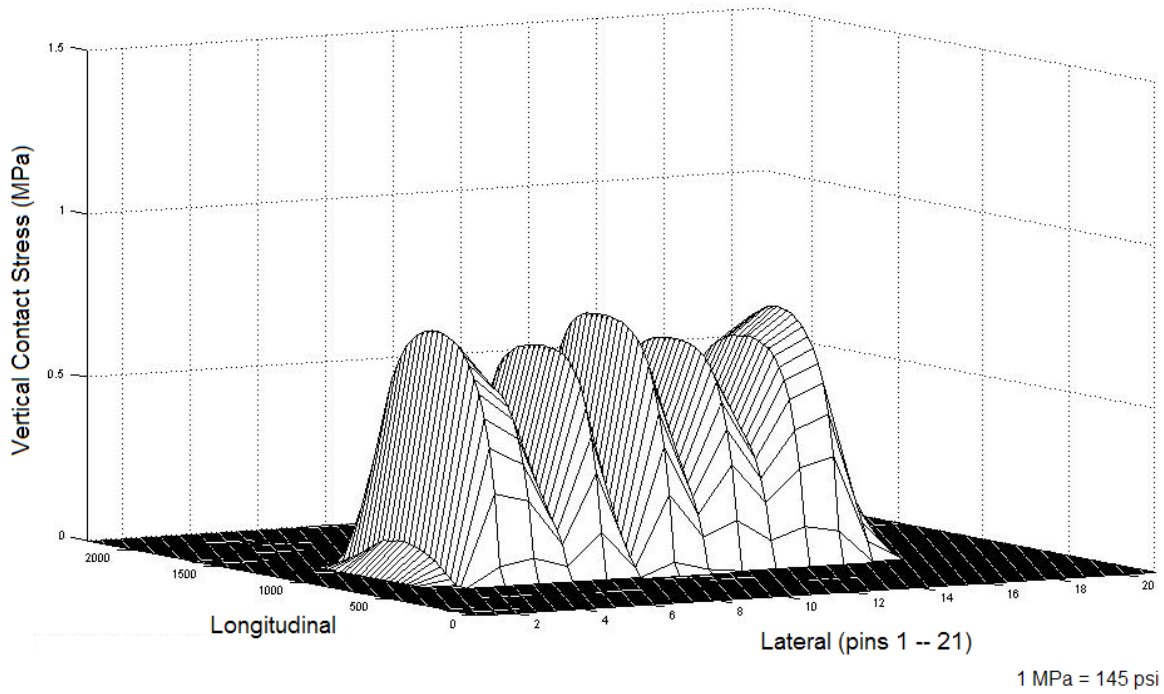

Figure B21. Measured Vertical Contact Stress Distribution for 11R24.5 Radial Tested at a Tire Load of 5400 lb and an Inflation Pressure of 85 psi.

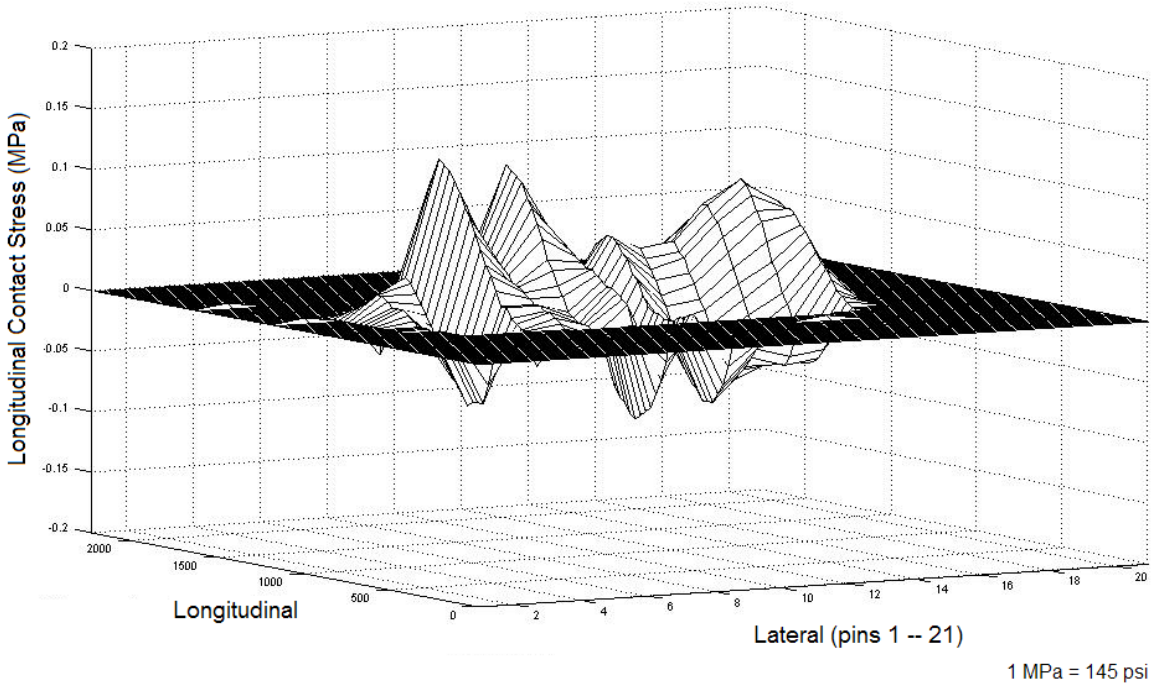

Figure B22. Measured Longitudinal Contact Stress Distribution for 11R24.5 Radial Tested at a Tire Load of 5400 lb and an Inflation Pressure of 100 psi.

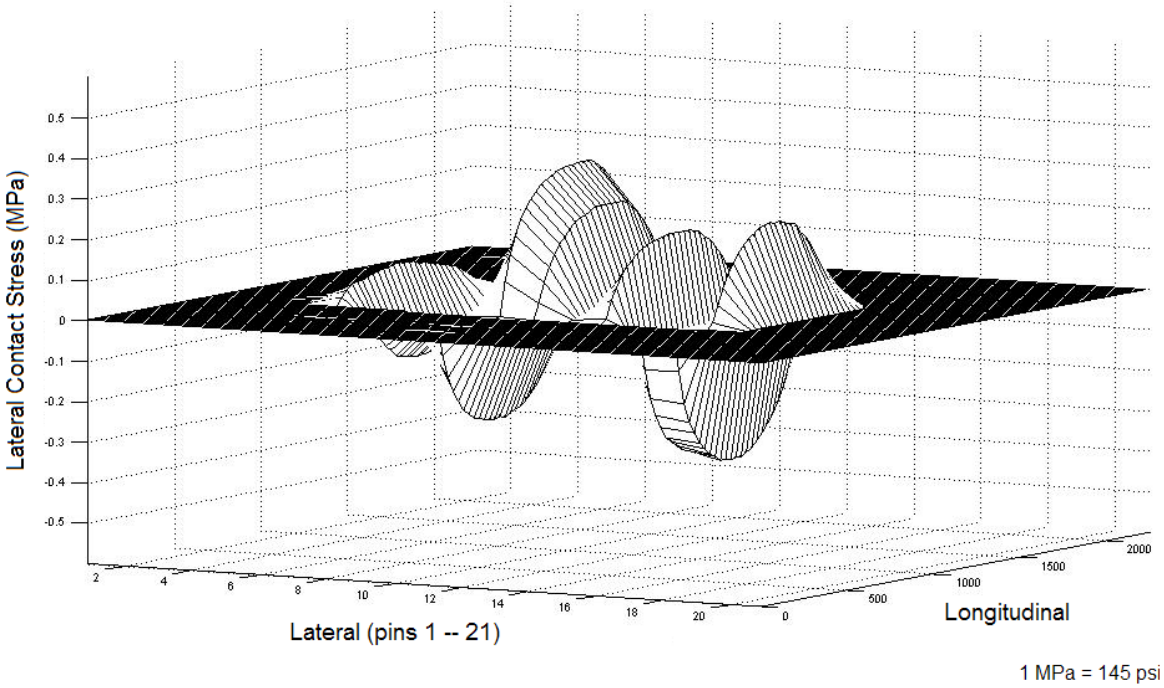

Figure B23. Measured Lateral Contact Stress Distribution for 11R24.5 Radial Tested at a Tire Load of 5400 lb and an Inflation Pressure of 100 psi.

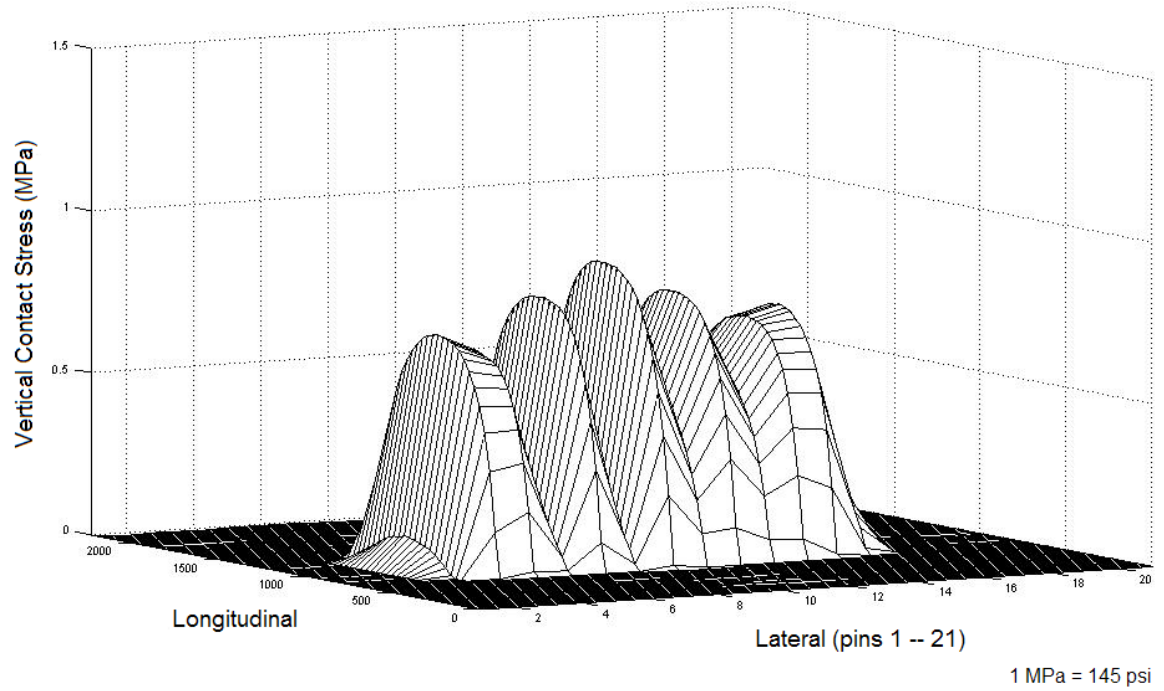

Figure B24. Measured Vertical Contact Stress Distribution for 11R24.5 Radial Tested at a Tire Load of 5400 lb and an Inflation Pressure of 100 psi.

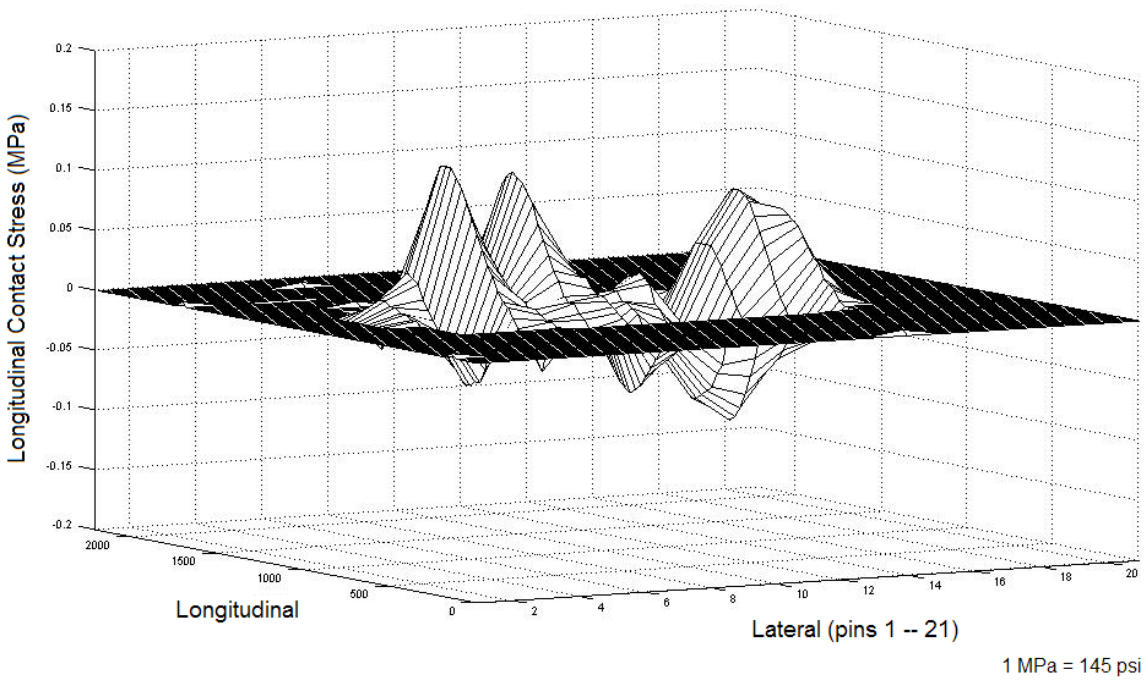

Figure B25. Measured Longitudinal Contact Stress Distribution for 11R24.5 Radial Tested at a Tire Load of 5400 lb and an Inflation Pressure of 115 psi.

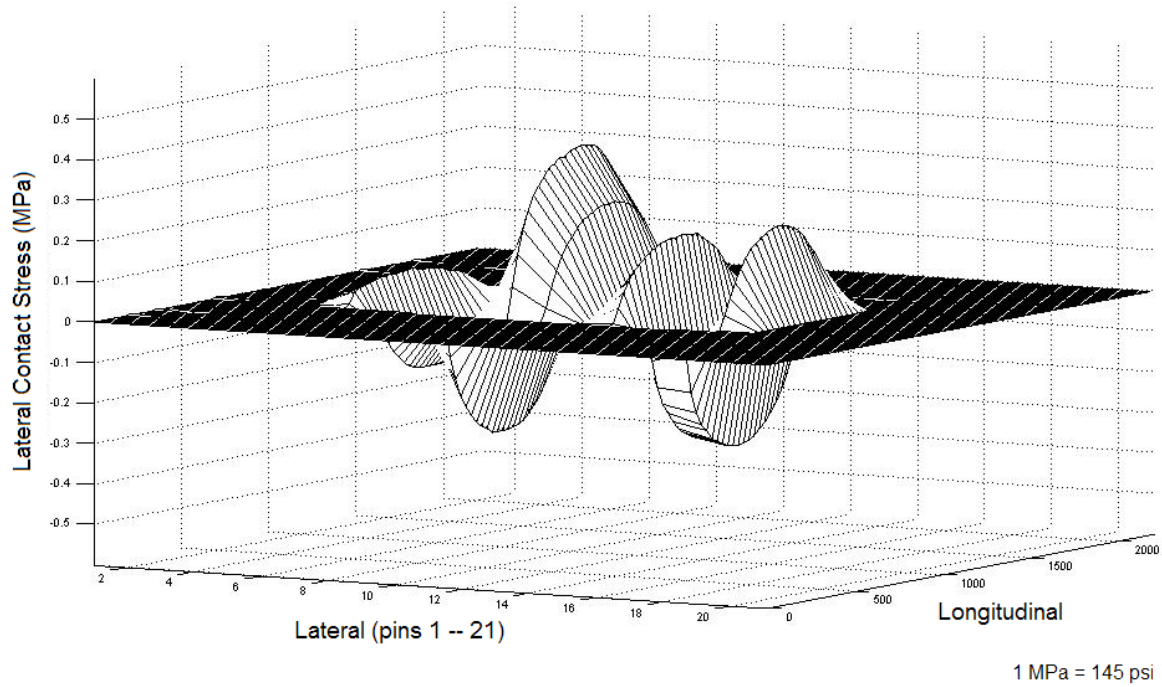

Figure B26. Measured Lateral Contact Stress Distribution for 11R24.5 Radial Tested at a Tire Load of 5400 lb and an Inflation Pressure of 115 psi.

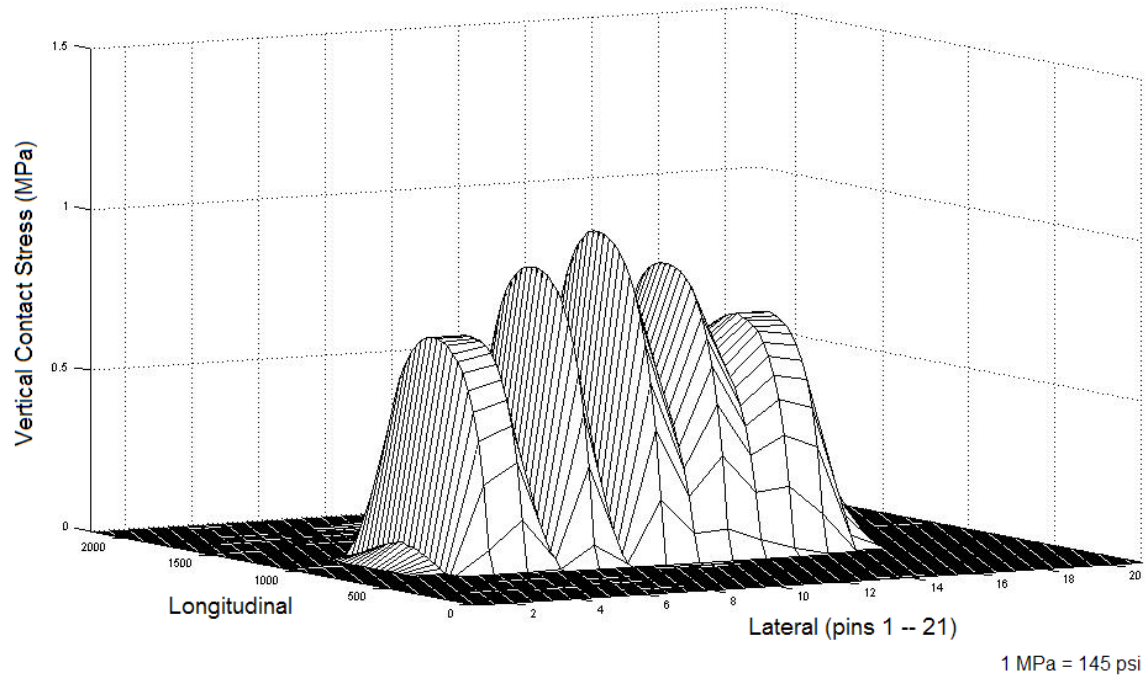

Figure B27. Measured Vertical Contact Stress Distribution for 11R24.5 Radial Tested at a Tire Load of 5400 lb and an Inflation Pressure of 115 psi.

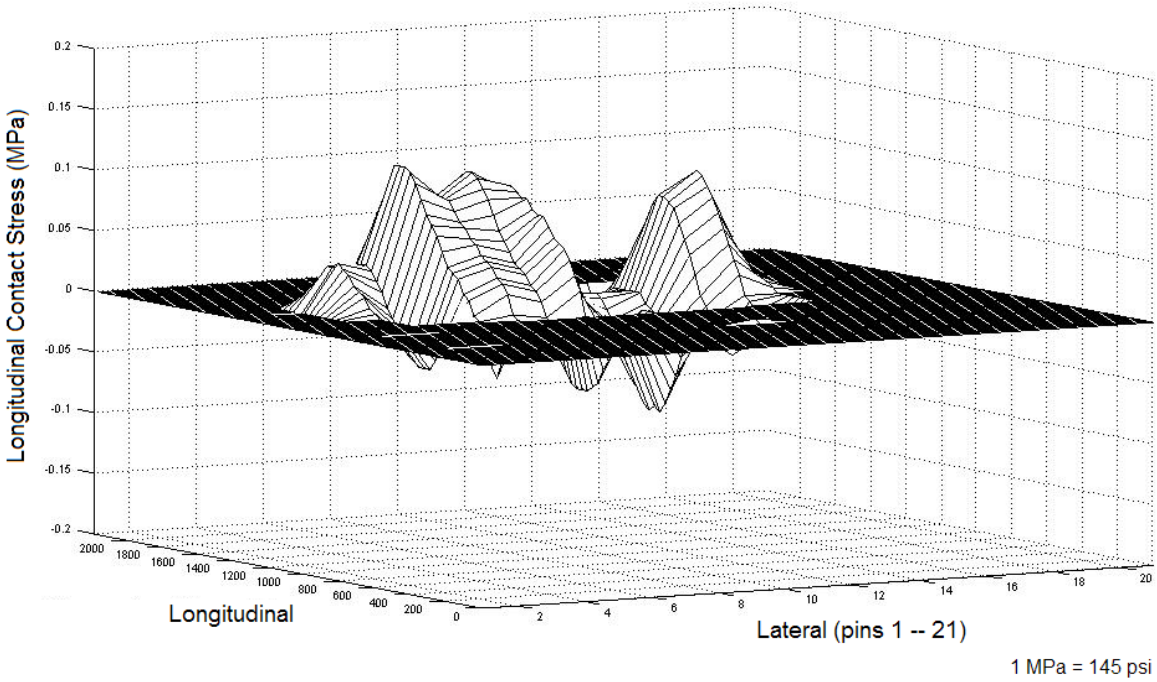

Figure B28. Measured Longitudinal Contact Stress Distribution for 11R24.5 Radial Tested at a Tire Load of 5400 lb and an Inflation Pressure of 130 psi.

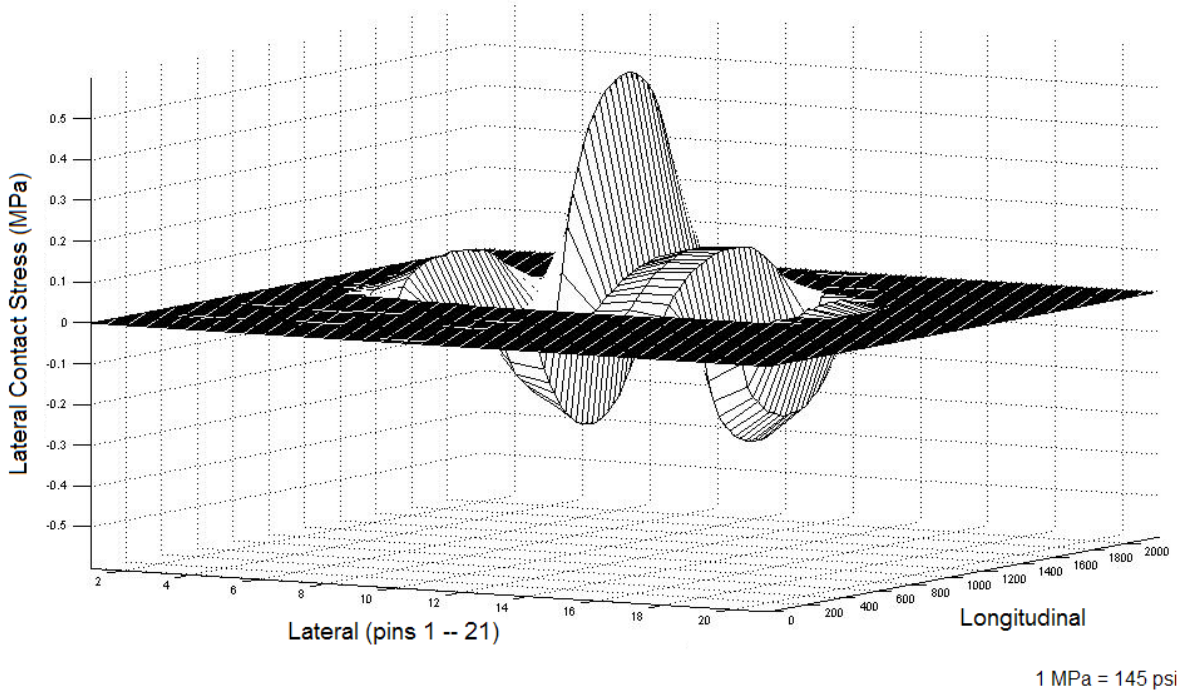

Figure B29. Measured Lateral Contact Stress Distribution for 11R24.5 Radial Tested at a Tire Load of 5400 lb and an Inflation Pressure of 130 psi.

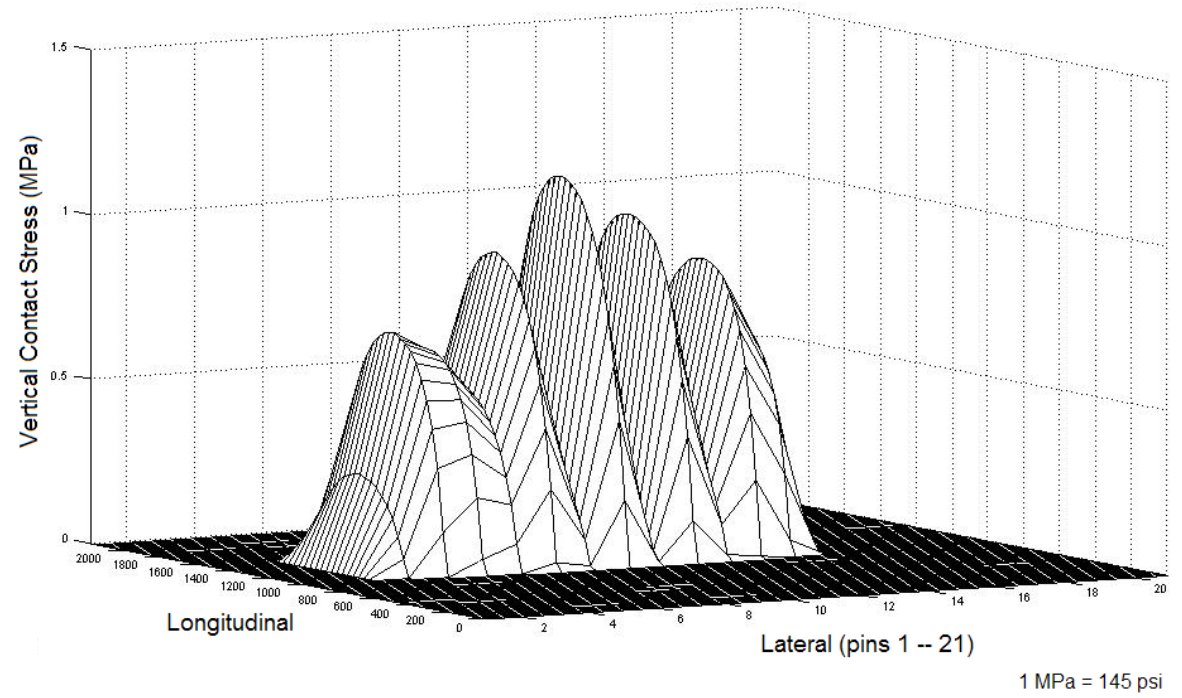

Figure B30. Measured Vertical Contact Stress Distribution for 11R24.5 Radial Tested at a Tire Load of 5400 lb and an Inflation Pressure of 130 psi.

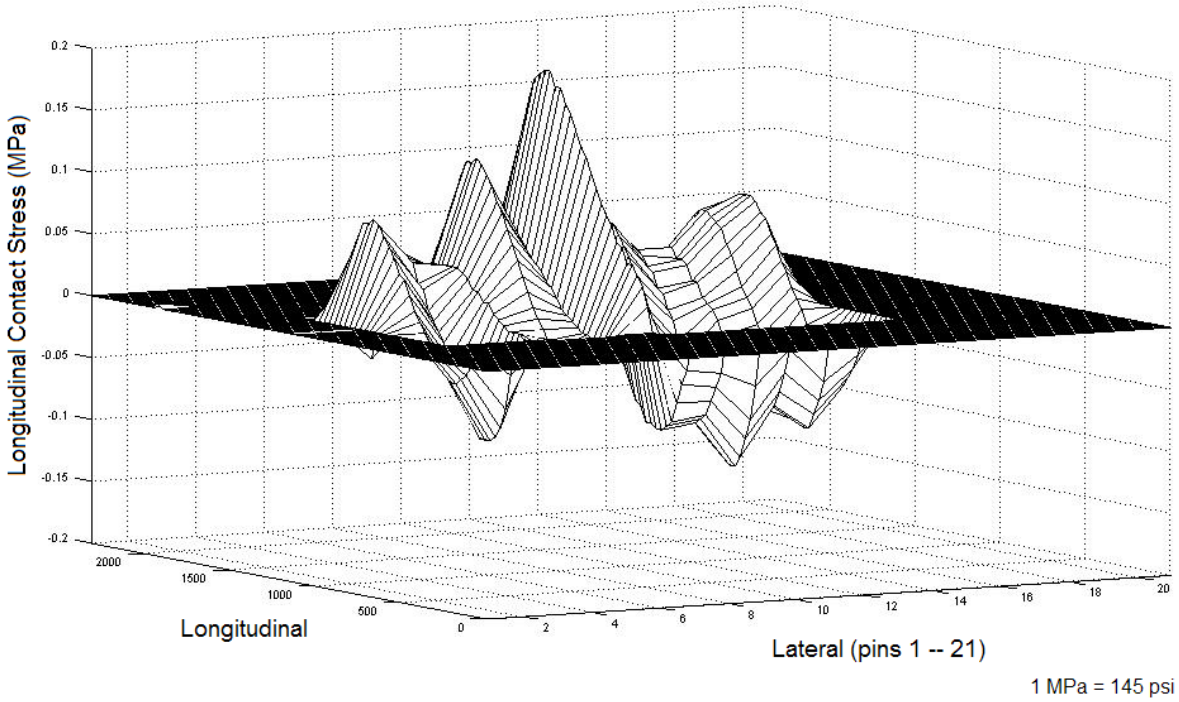

Figure B31. Measured Longitudinal Contact Stress Distribution for 11R24.5 Radial Tested at a Tire Load of 6200 lb and an Inflation Pressure of 70 psi.

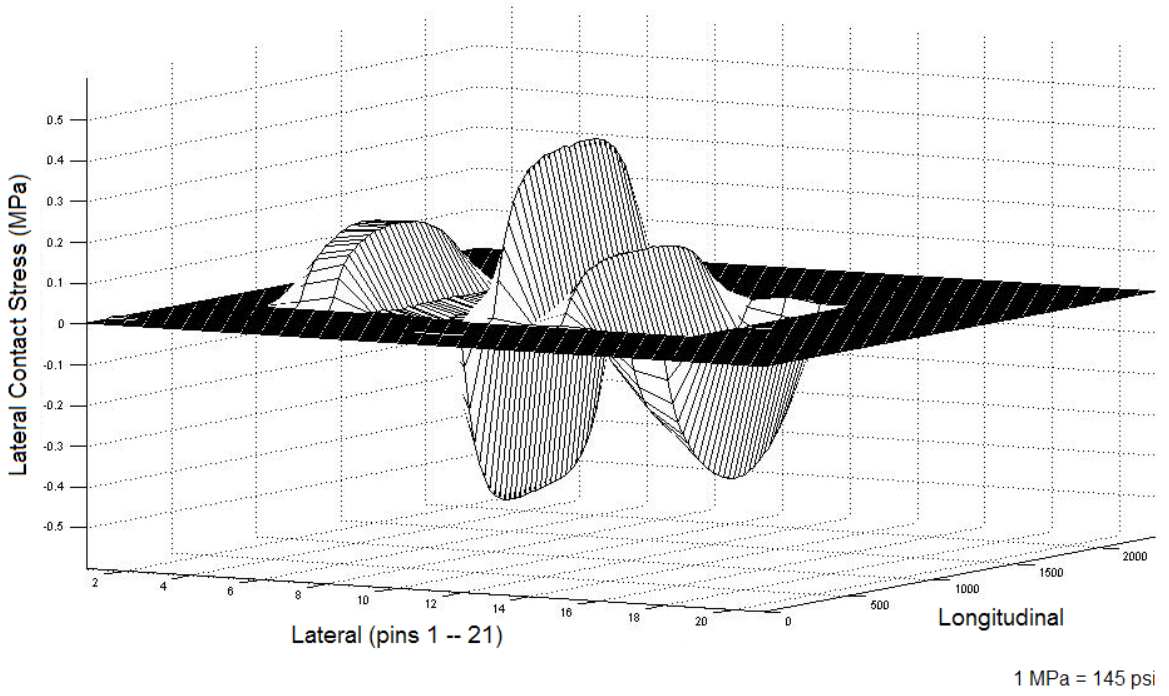

Figure B32. Measured Lateral Contact Stress Distribution for 11R24.5 Radial Tested at a Tire Load of 6200 lb and an Inflation Pressure of 70 psi.

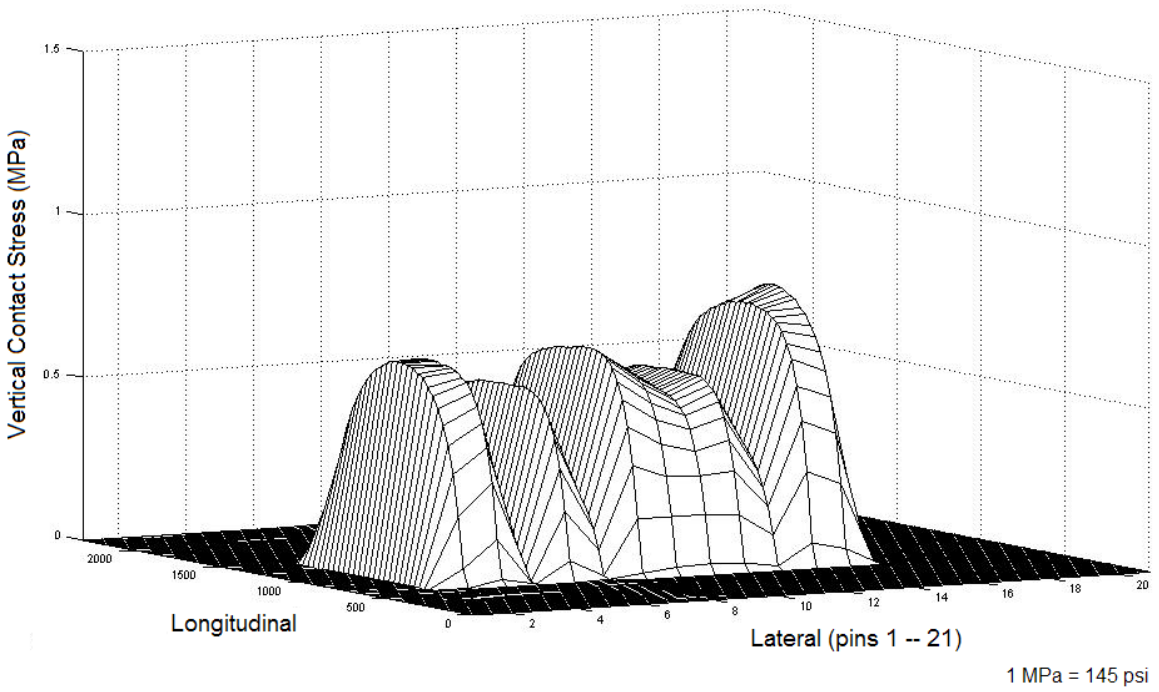

Figure B33. Measured Vertical Contact Stress Distribution for 11R24.5 Radial Tested at a Tire Load of 6200 lb and an Inflation Pressure of 70 psi.

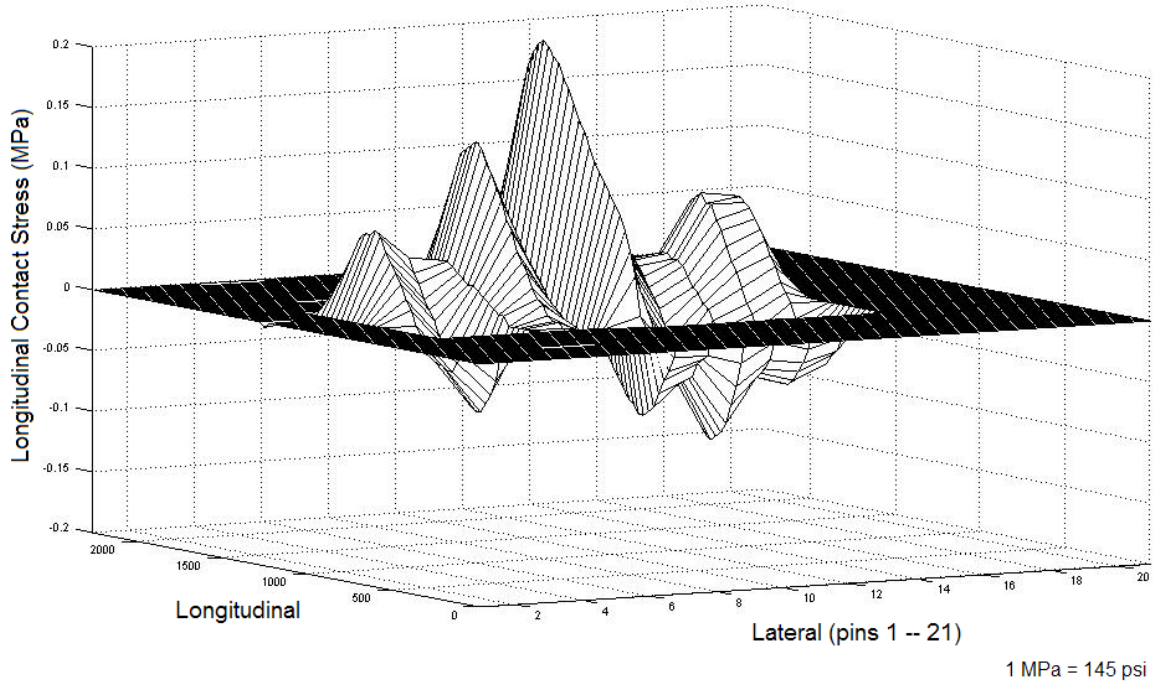

Figure B34. Measured Longitudinal Contact Stress Distribution for 11R24.5 Radial Tested at a Tire Load of 6200 lb and an Inflation Pressure of 85 psi.

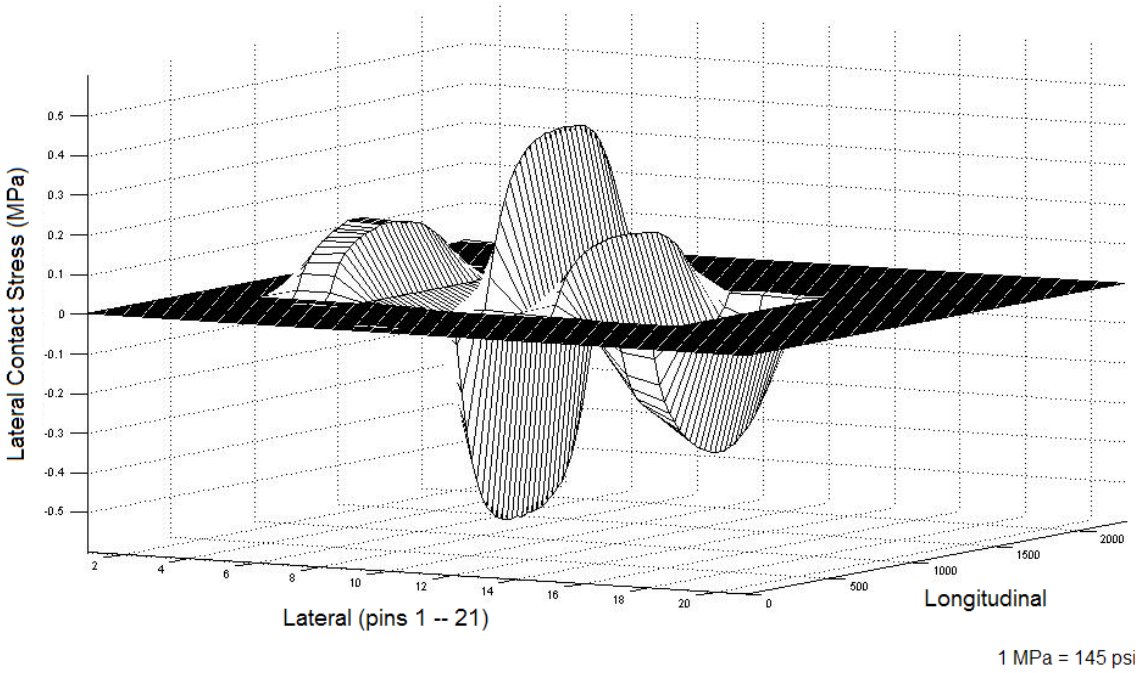

Figure B35. Measured Lateral Contact Stress Distribution for 11R24.5 Radial Tested at a Tire Load of 6200 lb and an Inflation Pressure of 85 psi.

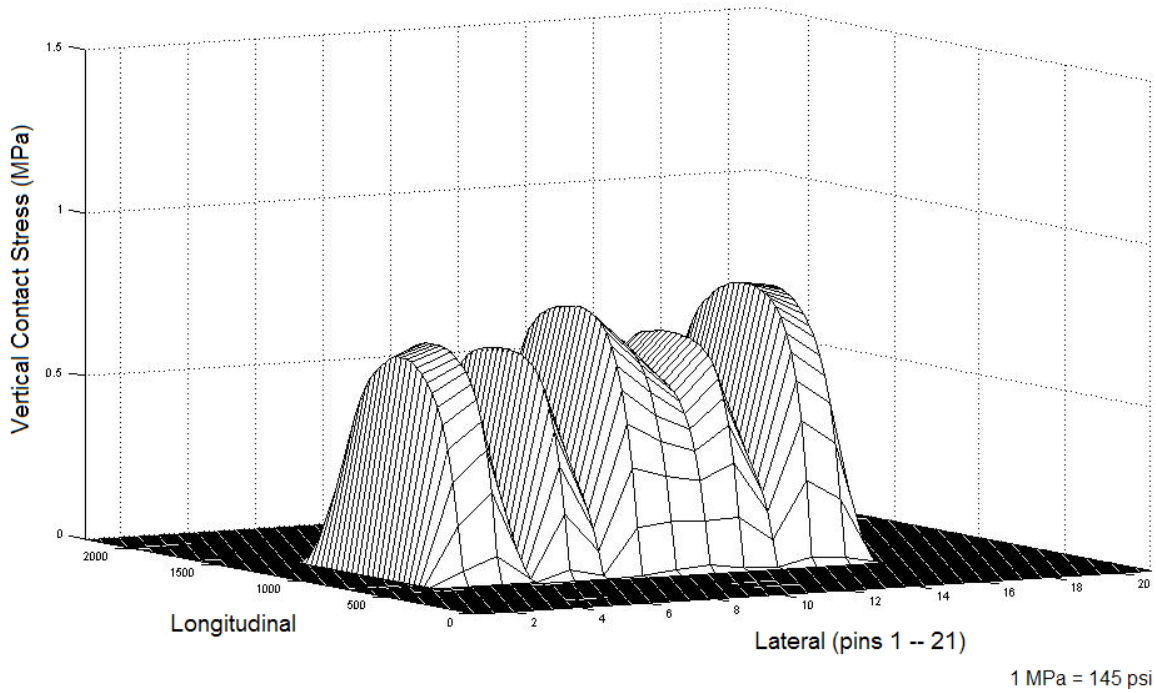

Figure B36. Measured Vertical Contact Stress Distribution for 11R24.5 Radial Tested at a Tire Load of 6200 lb and an Inflation Pressure of 85 psi.

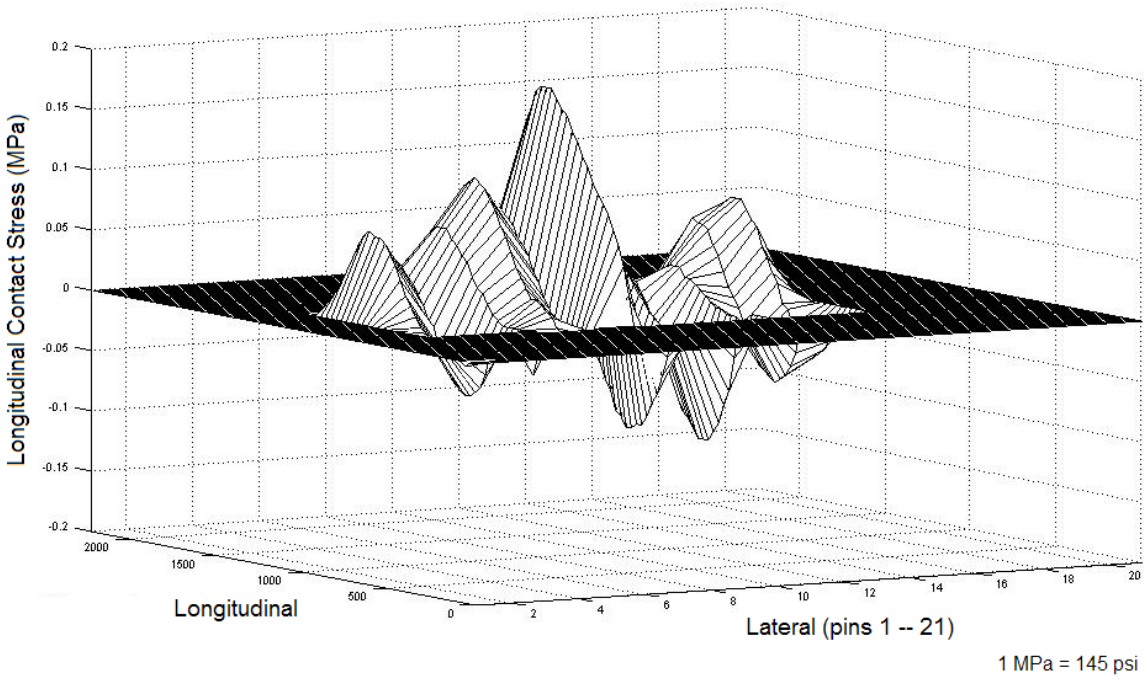

Figure B37. Measured Longitudinal Contact Stress Distribution for 11R24.5 Radial Tested at a Tire Load of 6200 lb and an Inflation Pressure of 100 psi.

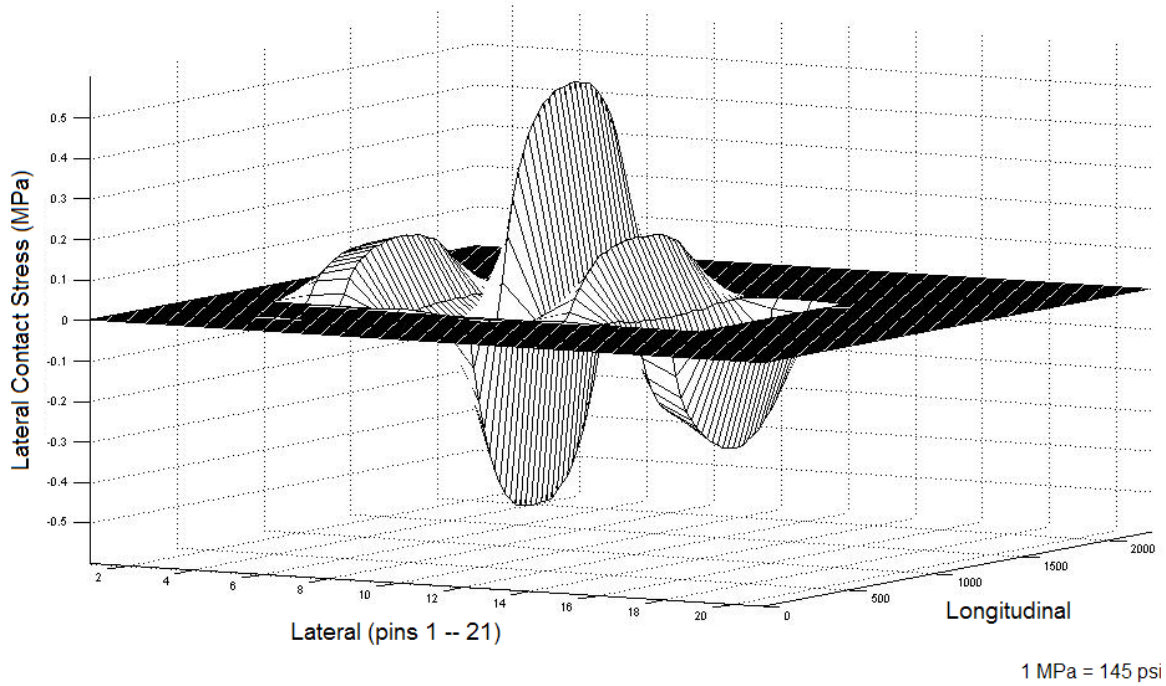

Figure B38. Measured Lateral Contact Stress Distribution for 11R24.5 Radial Tested at a Tire Load of 6200 lb and an Inflation Pressure of 100 psi.

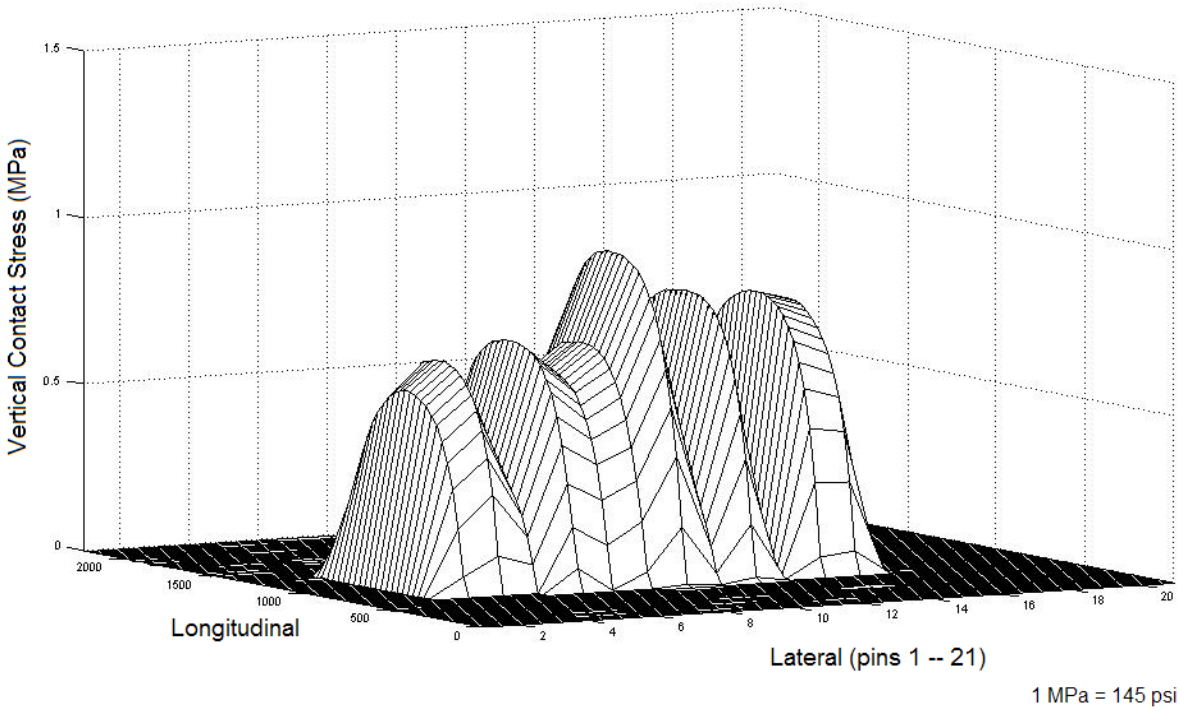

Figure B39. Measured Vertical Contact Stress Distribution for 11R24.5 Radial Tested at a Tire Load of 6200 lb and an Inflation Pressure of 100 psi.

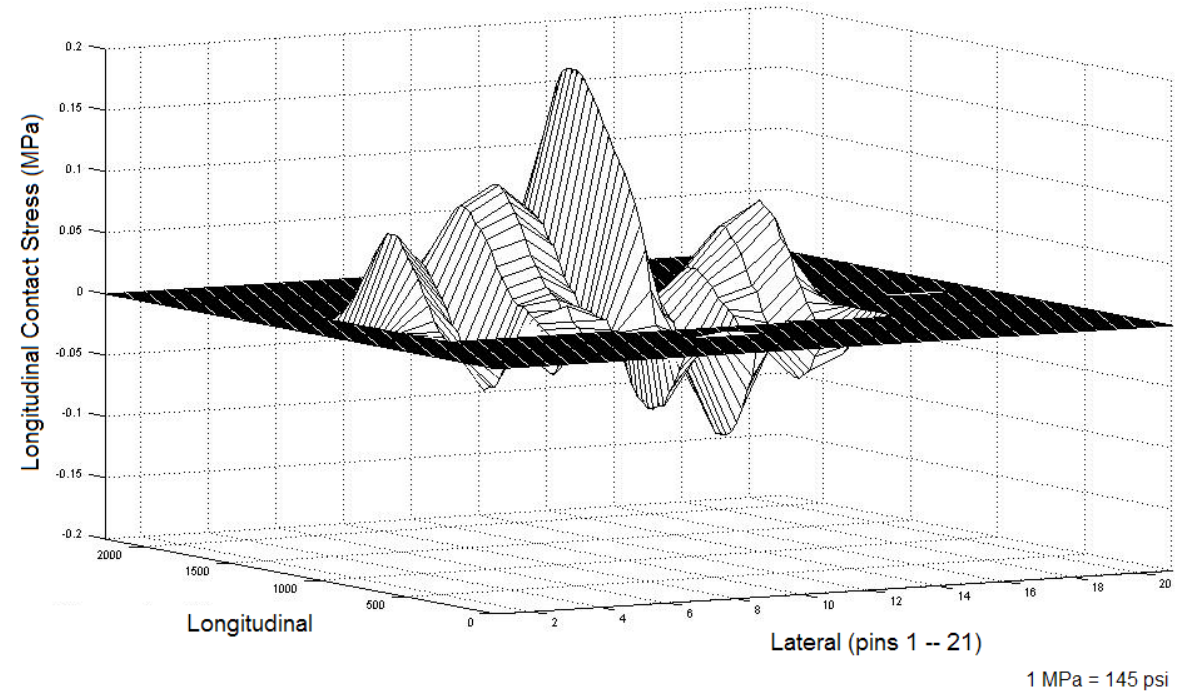

Figure B40. Measured Longitudinal Contact Stress Distribution for 11R24.5 Radial Tested at a Tire Load of 6200 lb and an Inflation Pressure of 115 psi.

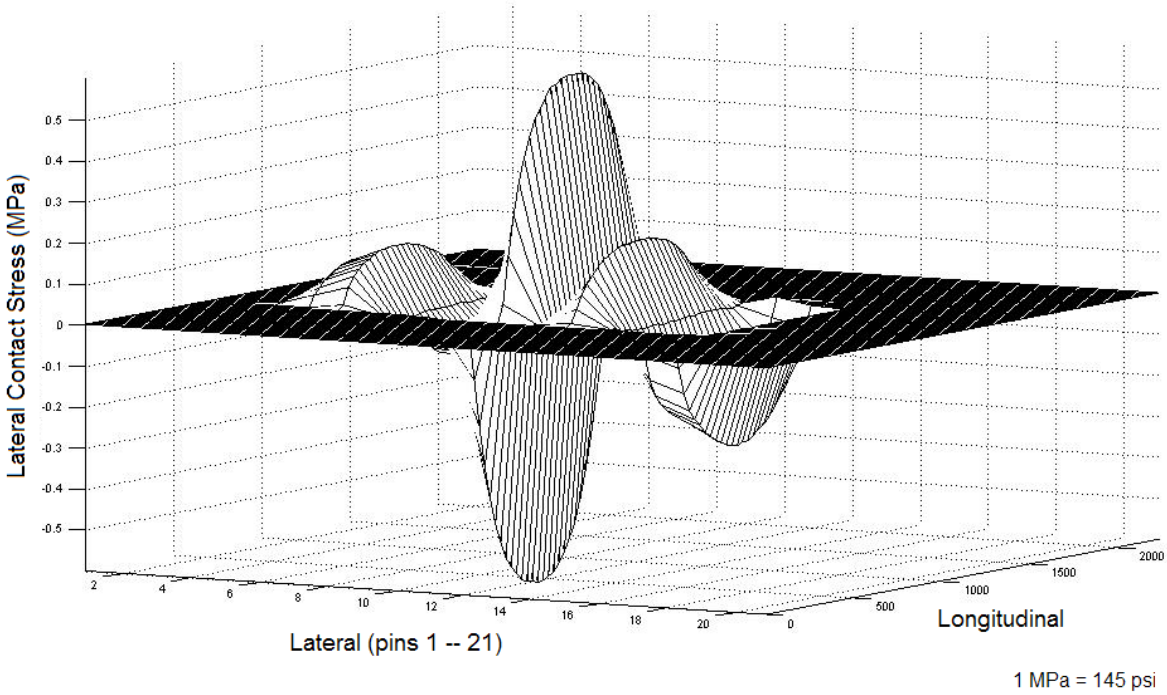

Figure B41. Measured Lateral Contact Stress Distribution for 11R24.5 Radial Tested at a Tire Load of 6200 lb and an Inflation Pressure of 115 psi.

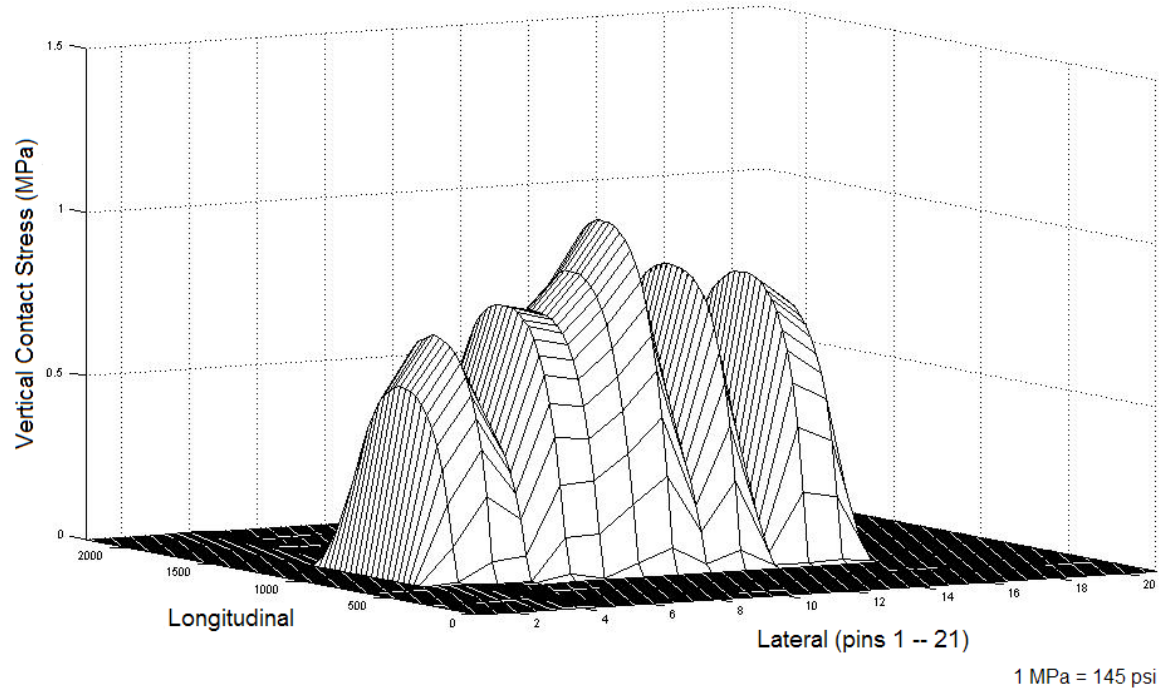

Figure B42. Measured Vertical Contact Stress Distribution for 11R24.5 Radial Tested at a Tire Load of 6200 lb and an Inflation Pressure of 115 psi.

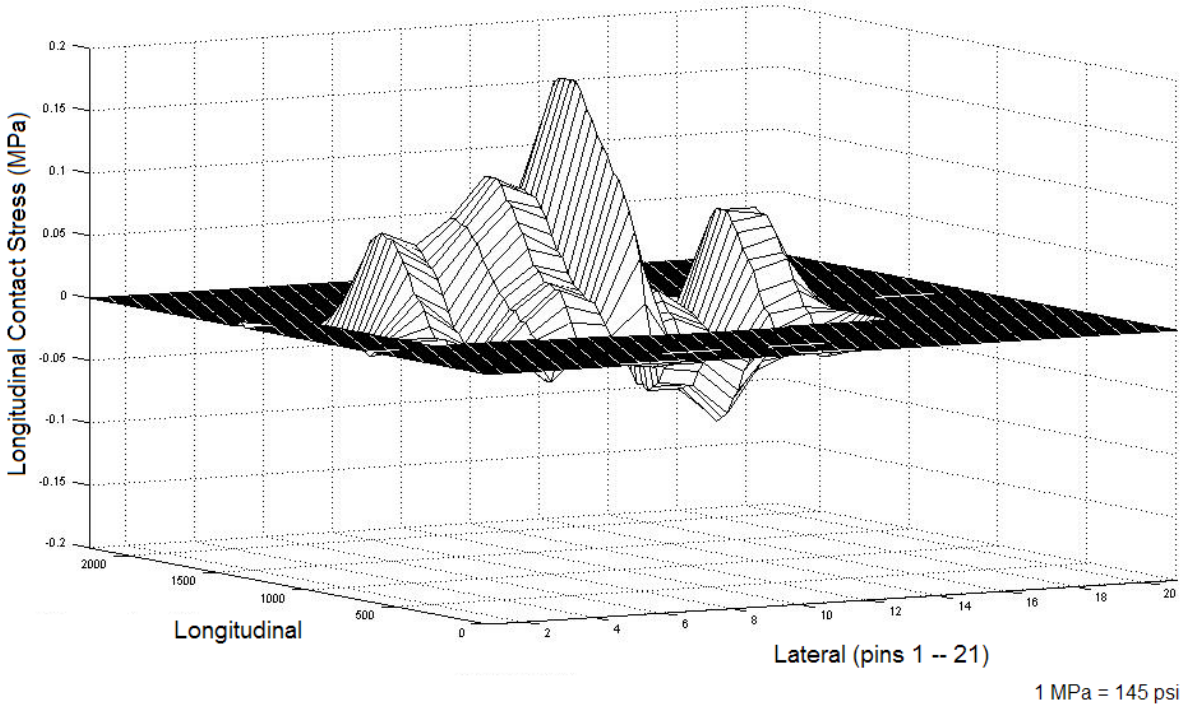

Figure B43. Measured Longitudinal Contact Stress Distribution for 11R24.5 Radial Tested at a Tire Load of 6200 lb and an Inflation Pressure of 130 psi.

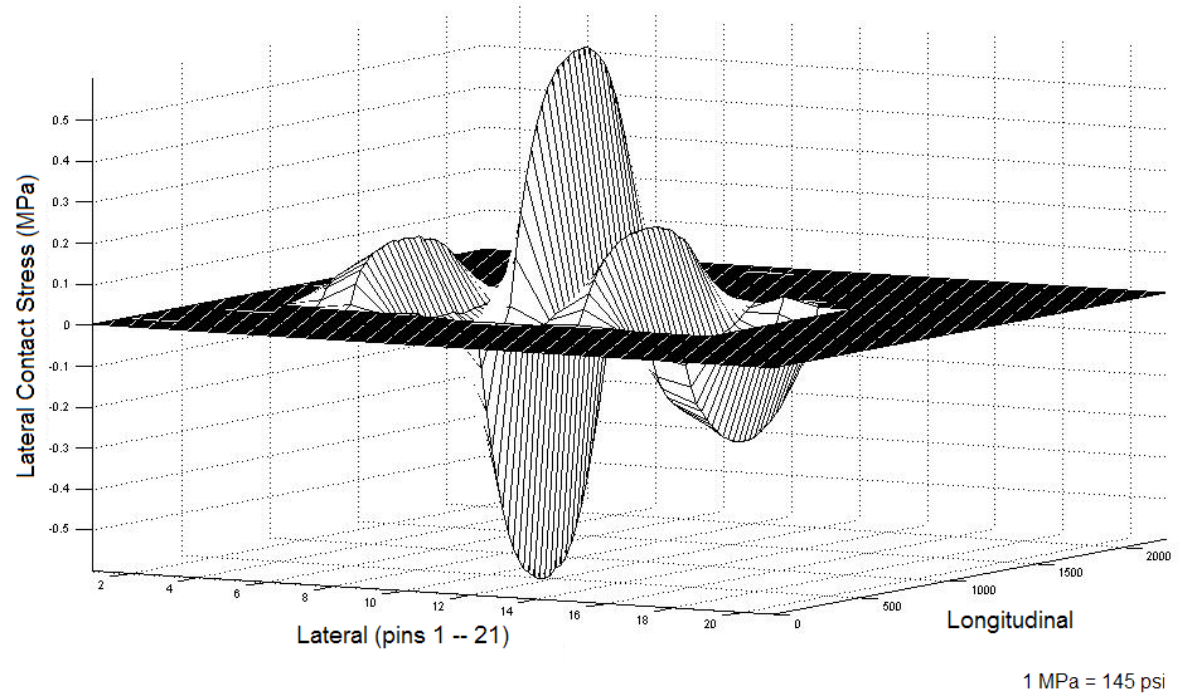

Figure B44. Measured Lateral Contact Stress Distribution for 11R24.5 Radial Tested at a Tire Load of 6200 lb and an Inflation Pressure of 130 psi.

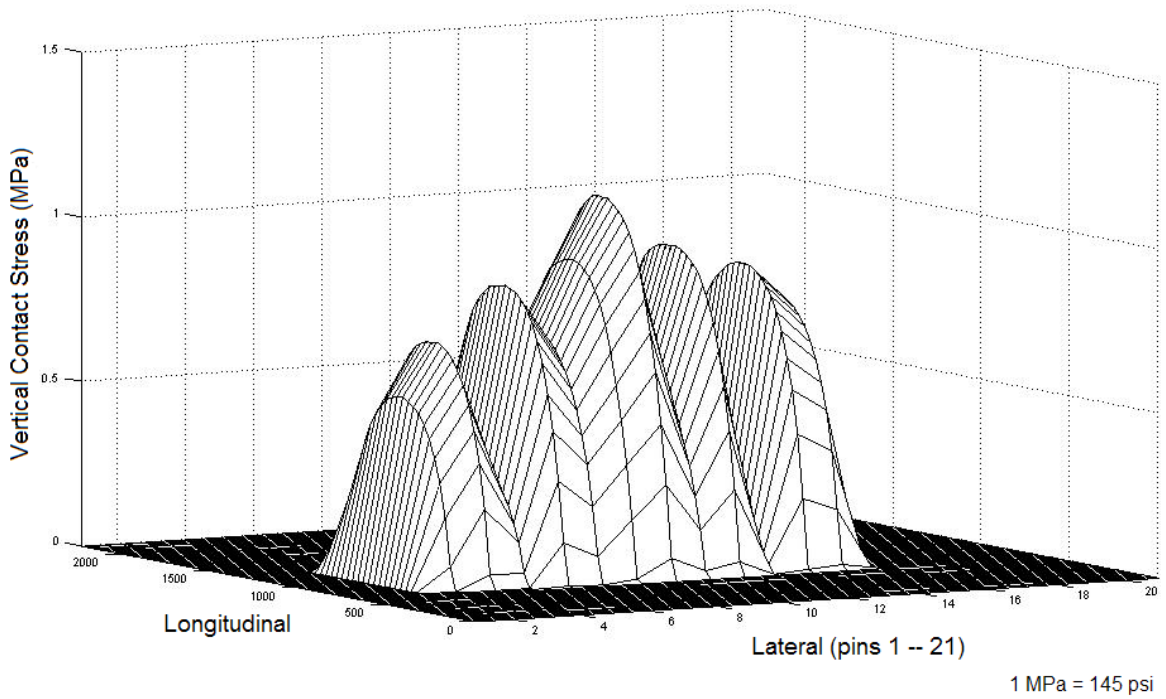

Figure B45. Measured Vertical Contact Stress Distribution for 11R24.5 Radial Tested at a Tire Load of 6200 lb and an Inflation Pressure of 130 psi.

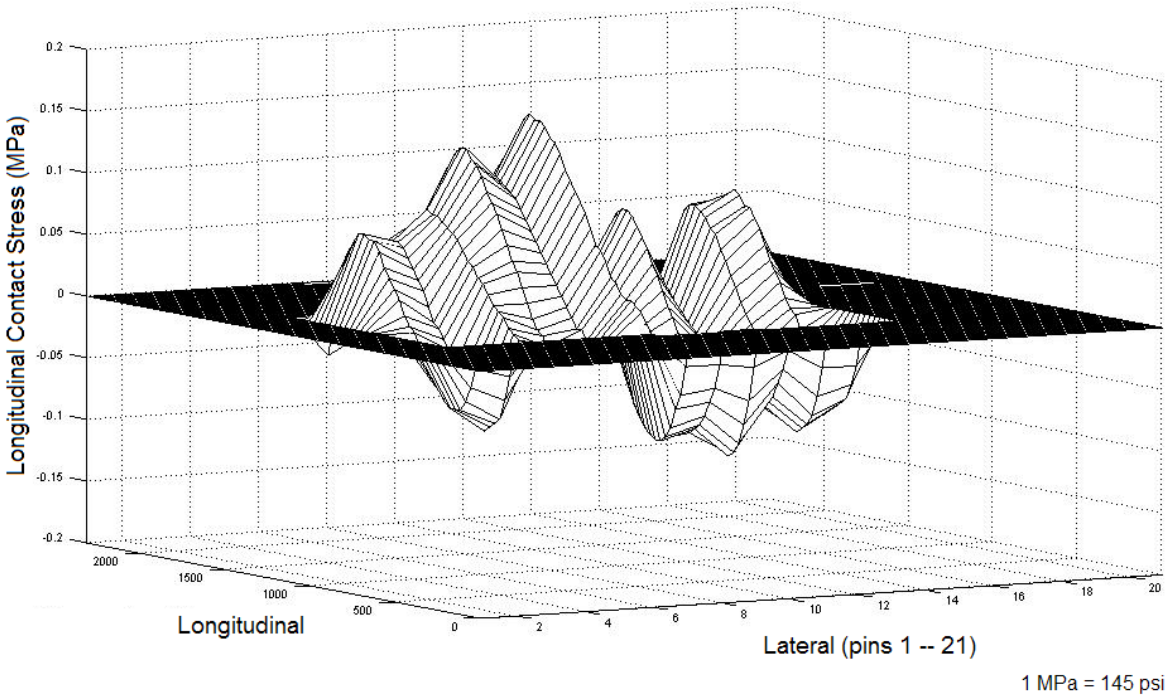

Figure B46. Measured Longitudinal Contact Stress Distribution for 11R24.5 Radial Tested at a Tire Load of 7000 lb and an Inflation Pressure of 70 psi.

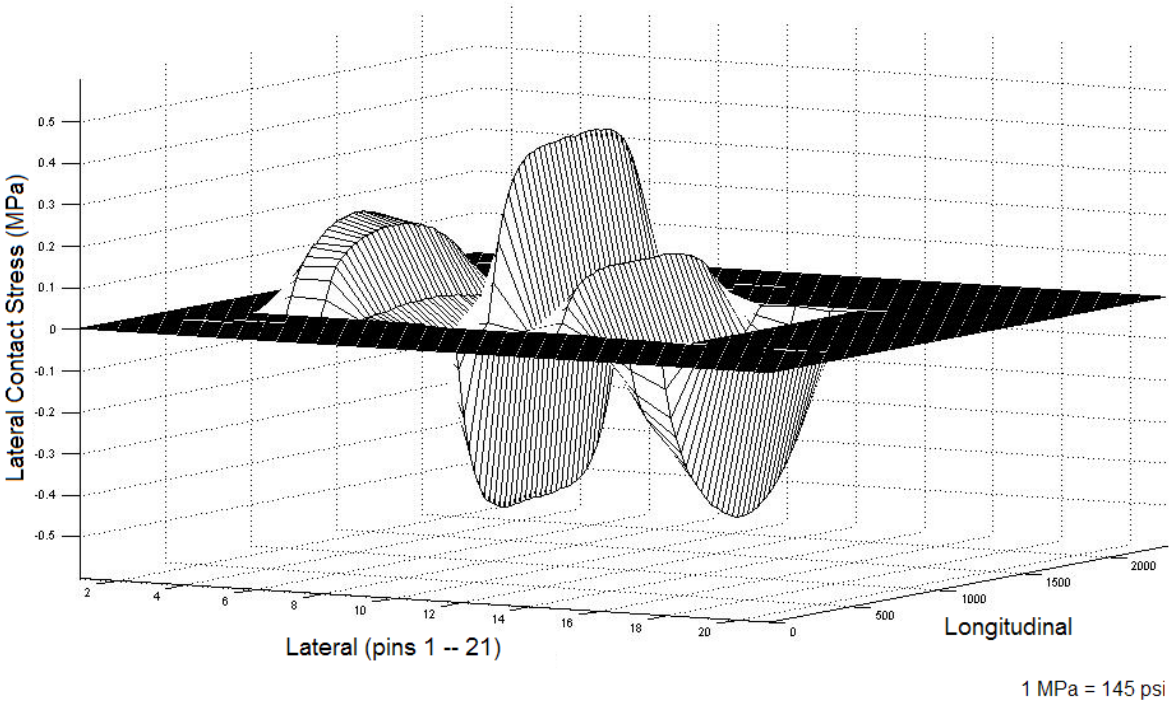

Figure B47. Measured Lateral Contact Stress Distribution for 11R24.5 Radial Tested at a Tire Load of 7000 lb and an Inflation Pressure of 70 psi.

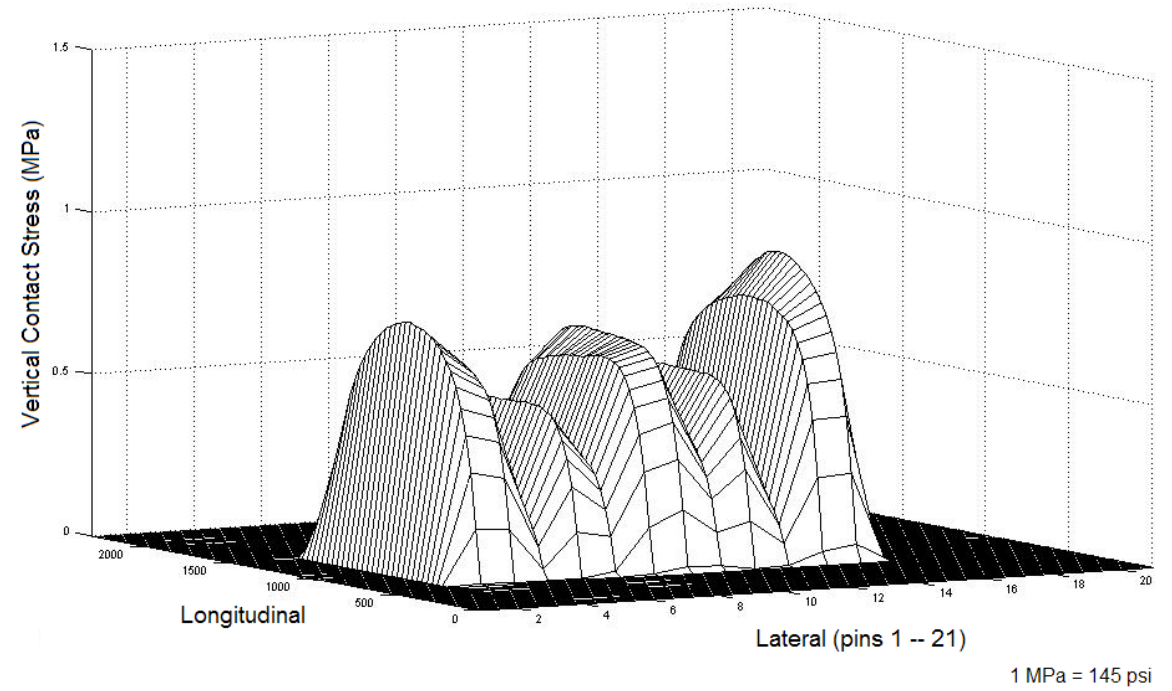

Figure B48. Measured Vertical Contact Stress Distribution for 11R24.5 Radial Tested at a Tire Load of 7000 lb and an Inflation Pressure of 70 psi.

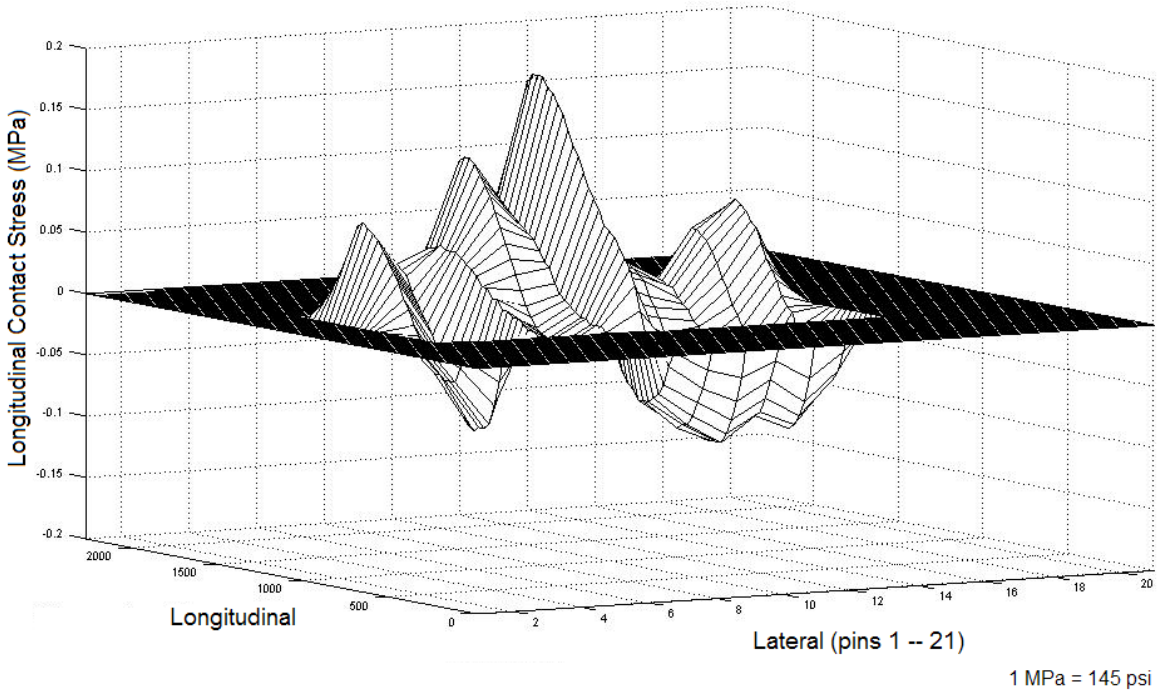

Figure B49. Measured Longitudinal Contact Stress Distribution for 11R24.5 Radial Tested at a Tire Load of 7000 lb and an Inflation Pressure of 85 psi.

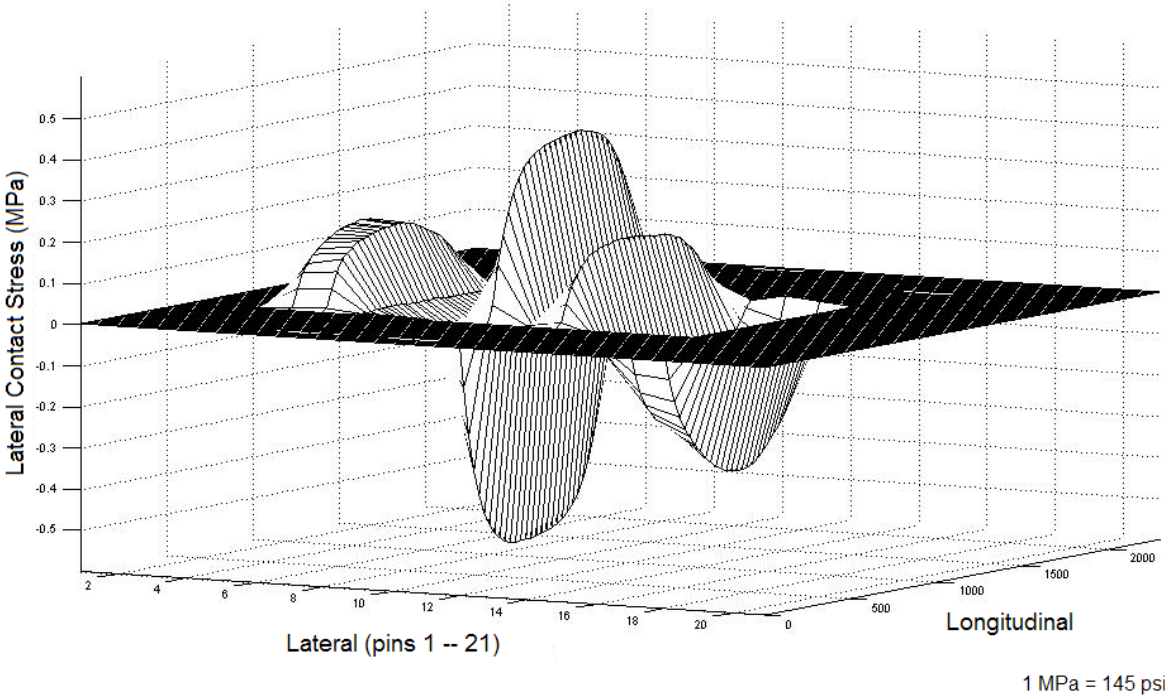

Figure B50. Measured Lateral Contact Stress Distribution for 11R24.5 Radial Tested at a Tire Load of 7000 lb and an Inflation Pressure of 85 psi.

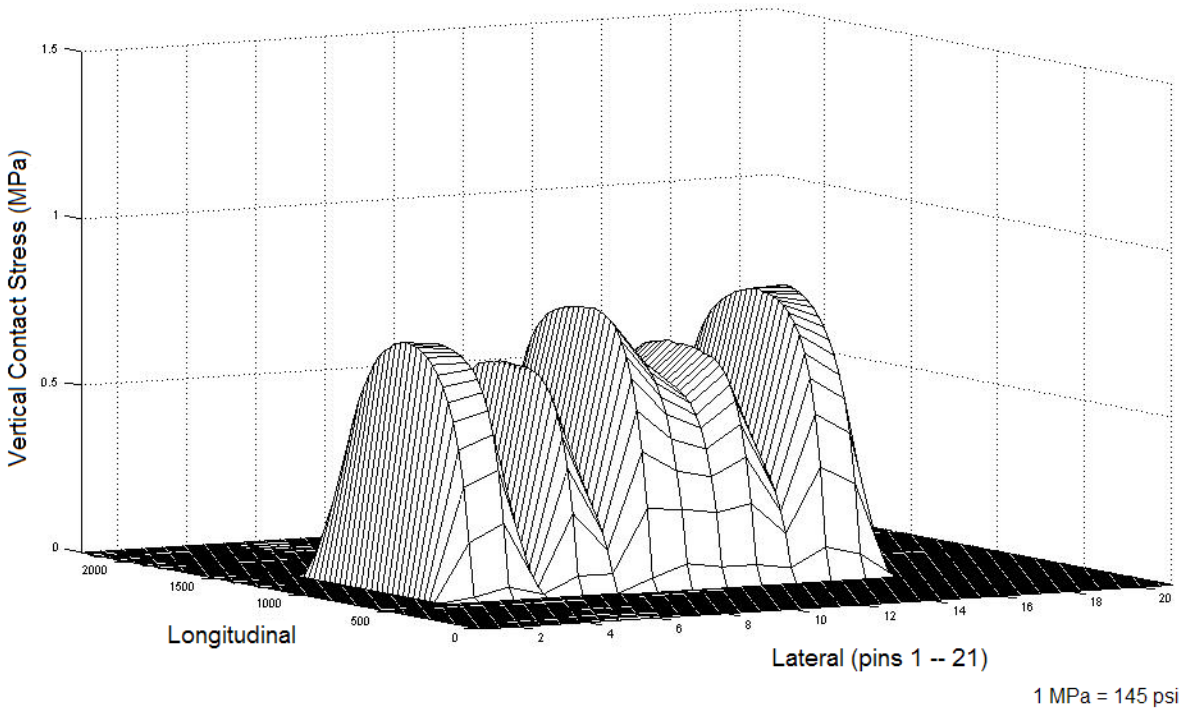

Figure B51. Measured Vertical Contact Stress Distribution for 11R24.5 Radial Tested at a Tire Load of 7000 lb and an Inflation Pressure of 85 psi.

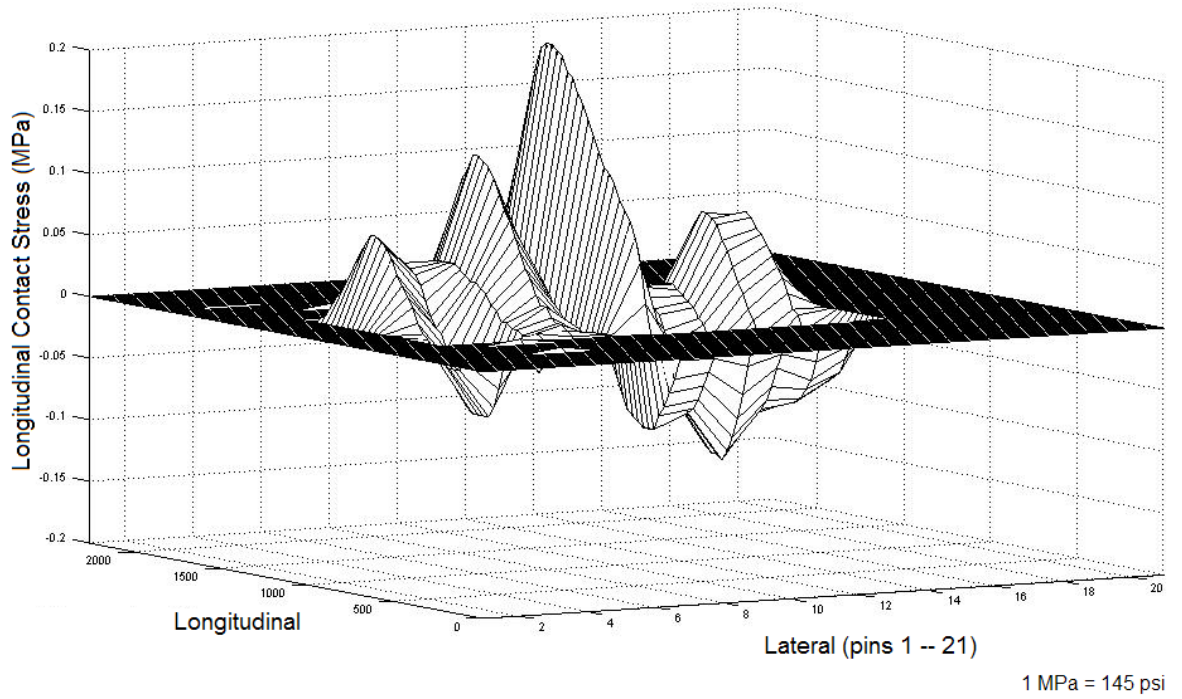

Figure B52. Measured Longitudinal Contact Stress Distribution for 11R24.5 Radial Tested at a Tire Load of 7000 lb and an Inflation Pressure of 100 psi.

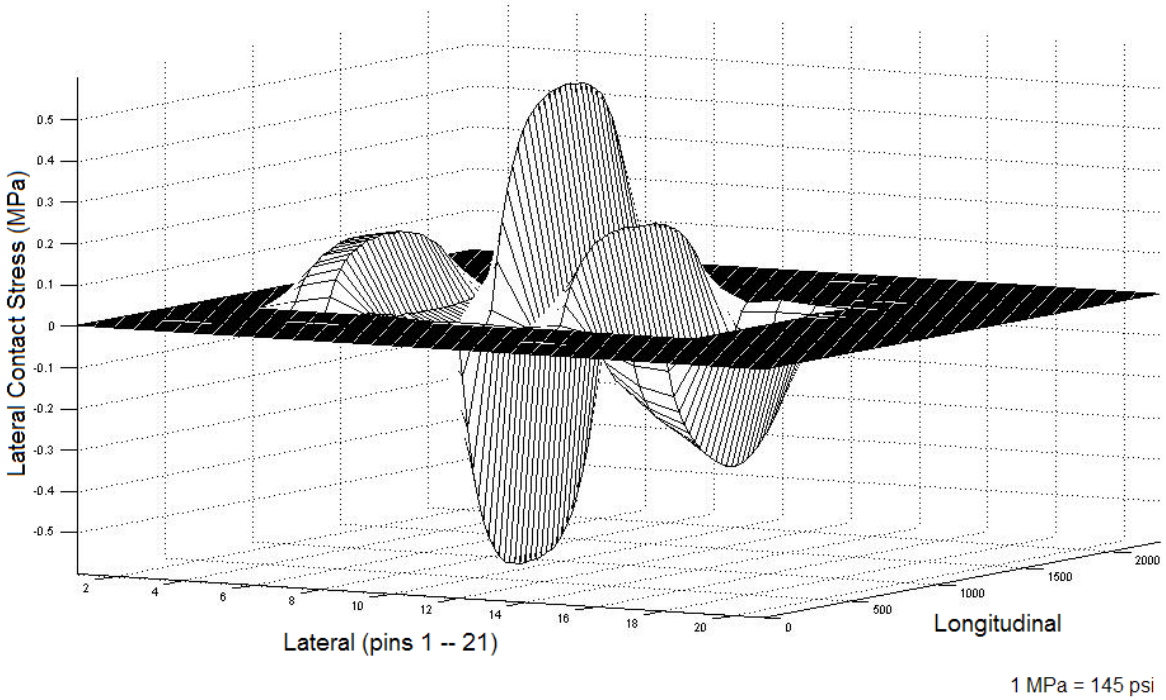

Figure B53. Measured Lateral Contact Stress Distribution for 11R24.5 Radial Tested at a Tire Load of 7000 lb and an Inflation Pressure of 100 psi.

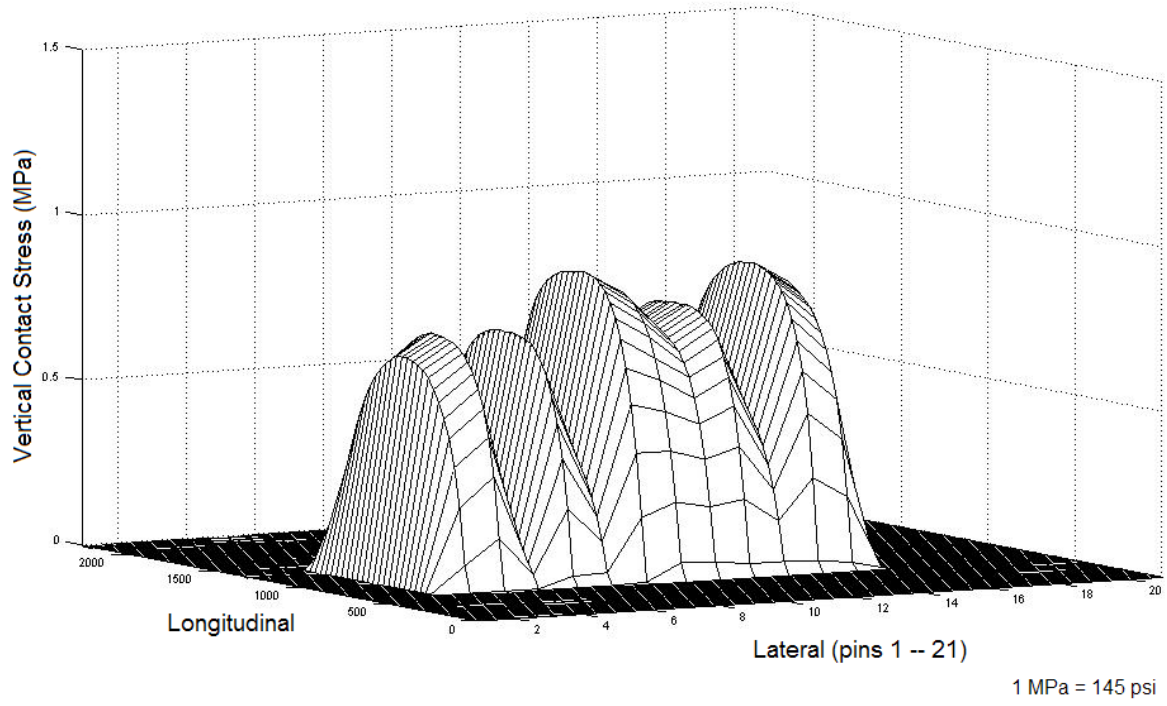

Figure B54. Measured Vertical Contact Stress Distribution for 11R24.5 Radial Tested at a Tire Load of 7000 lb and an Inflation Pressure of 100 psi.

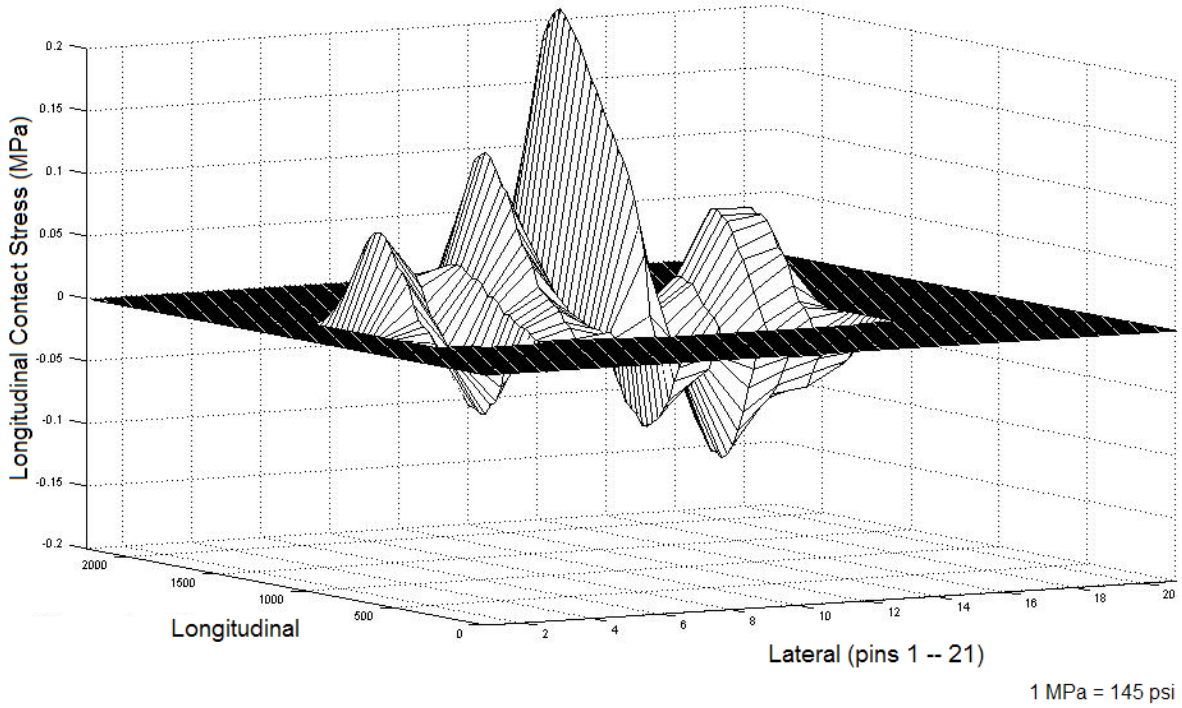

Figure B55. Measured Longitudinal Contact Stress Distribution for 11R24.5 Radial Tested at a Tire Load of 7000 lb and an Inflation Pressure of 115 psi.

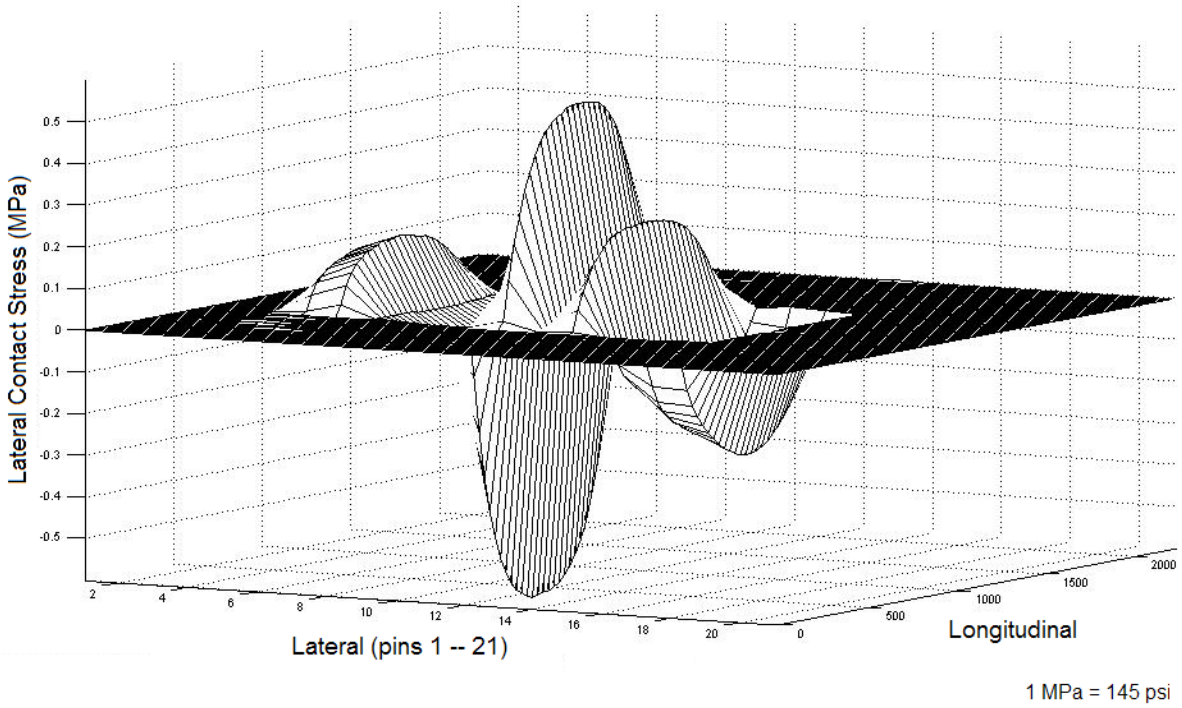

Figure B56. Measured Lateral Contact Stress Distribution for 11R24.5 Radial Tested at a Tire Load of 7000 lb and an Inflation Pressure of 115 psi.

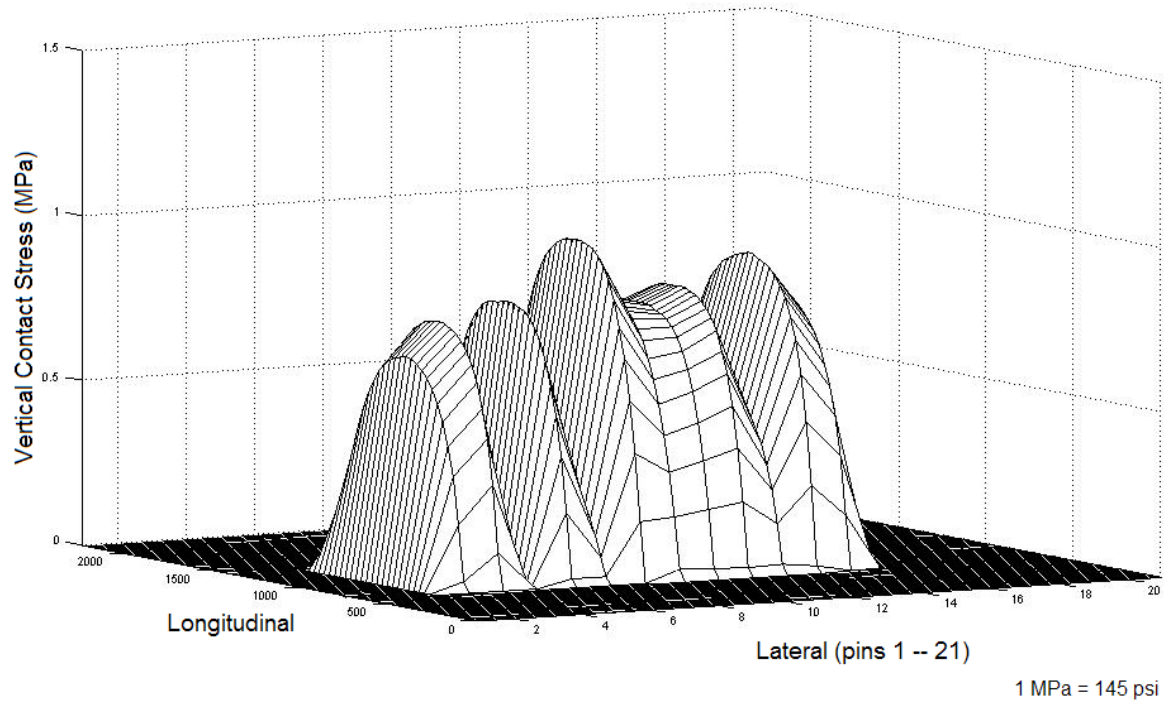

Figure B57. Measured Vertical Contact Stress Distribution for 11R24.5 Radial Tested at a Tire Load of 7000 lb and an Inflation Pressure of 115 psi.

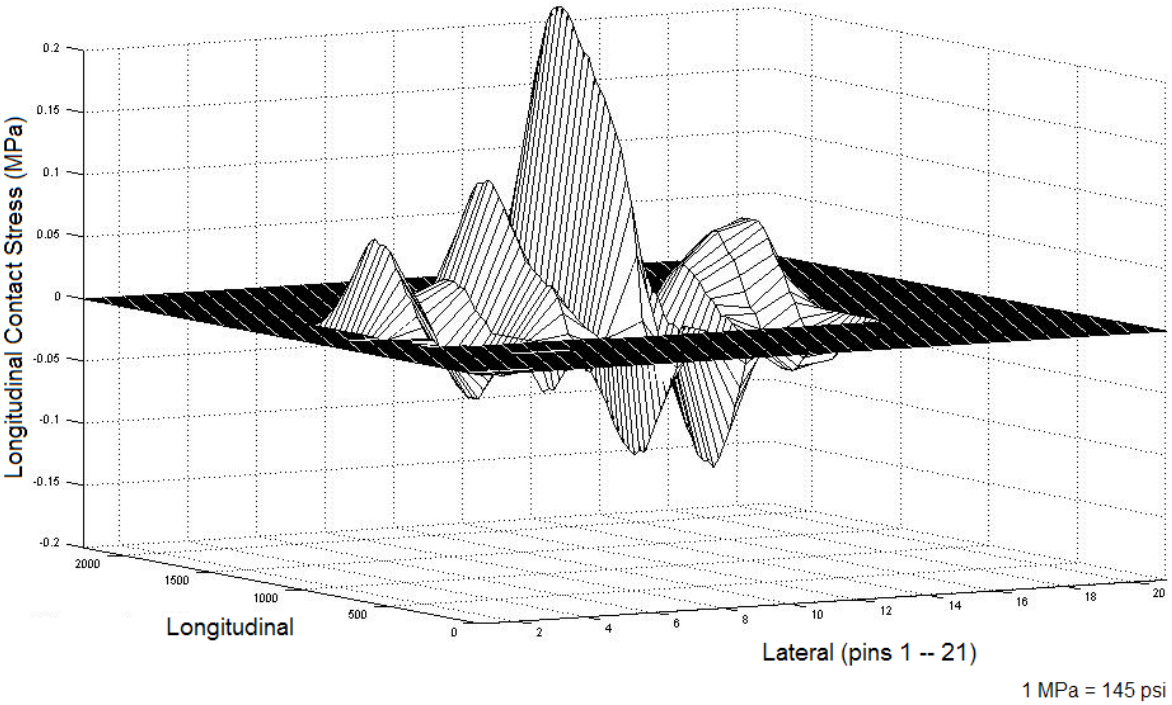

Figure B58. Measured Longitudinal Contact Stress Distribution for 11R24.5 Radial Tested at a Tire Load of 7000 lb and an Inflation Pressure of 130 psi.

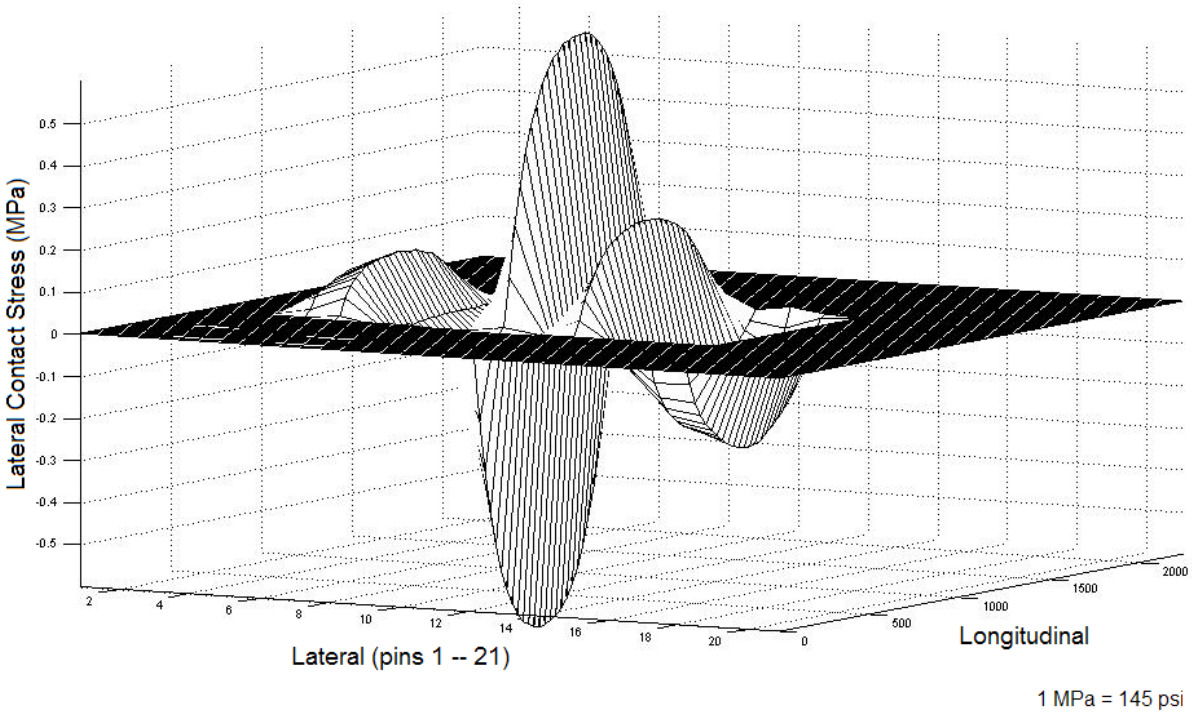

Figure B59. Measured Lateral Contact Stress Distribution for 11R24.5 Radial Tested at a Tire Load of 7000 lb and an Inflation Pressure of 130 psi.

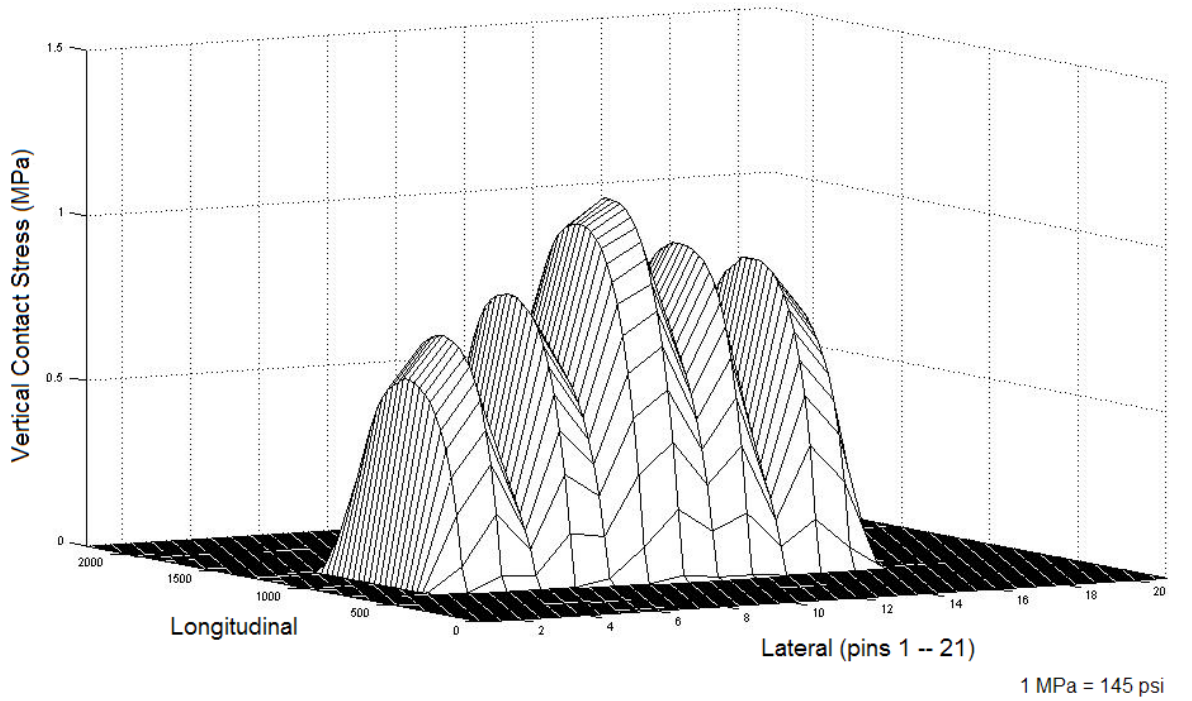

Figure B60. Measured Vertical Contact Stress Distribution for 11R24.5 Radial Tested at a Tire Load of 7000 lb and an Inflation Pressure of 130 psi.

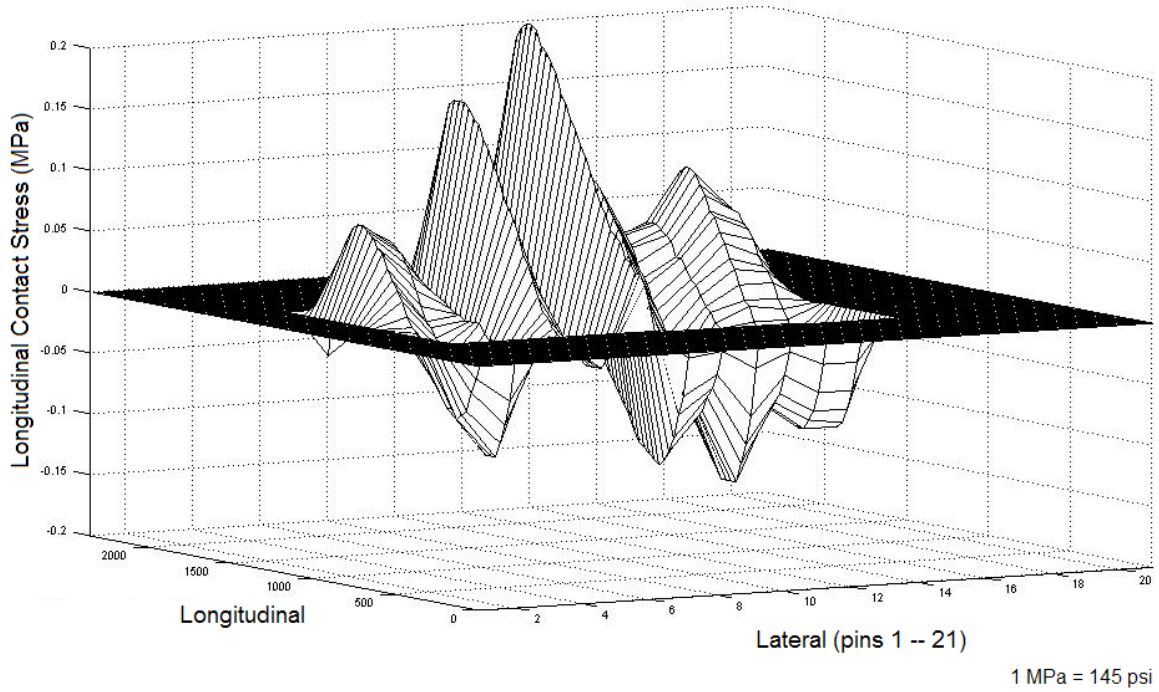

Figure B61. Measured Longitudinal Contact Stress Distribution for 11R24.5 Radial Tested at a Tire Load of 7800 lb and an Inflation Pressure of 70 psi.

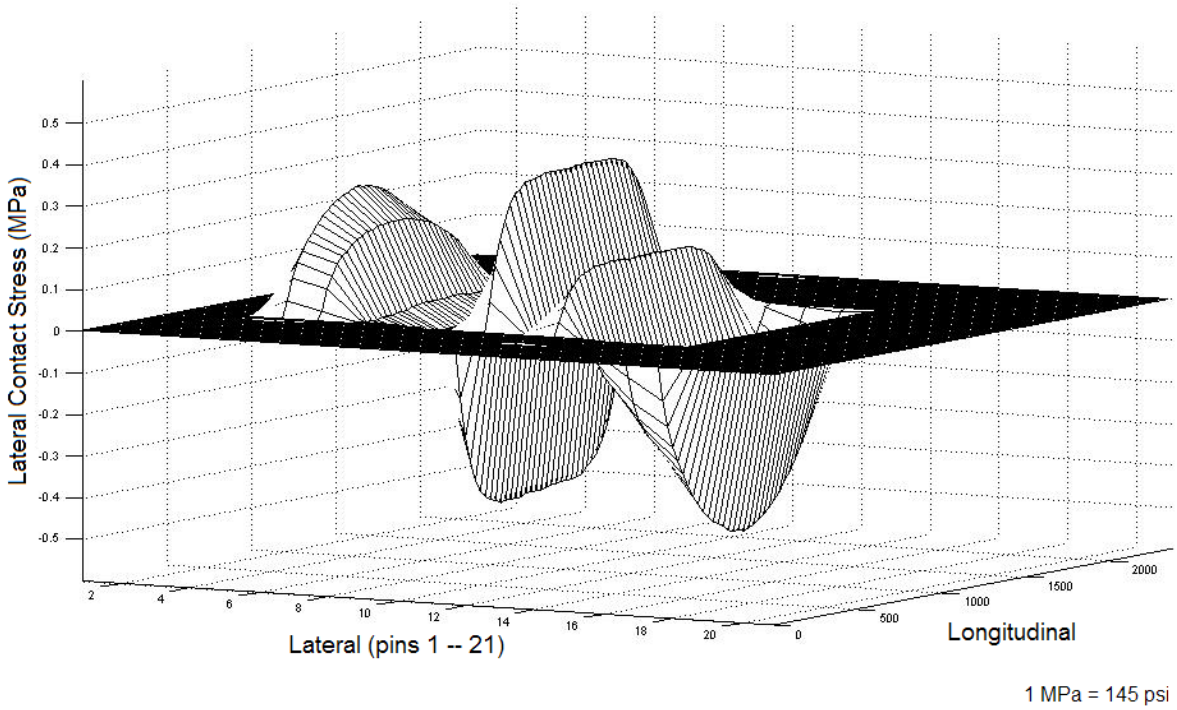

Figure B62. Measured Lateral Contact Stress Distribution for 11R24.5 Radial Tested at a Tire Load of 7800 lb and an Inflation Pressure of 70 psi.

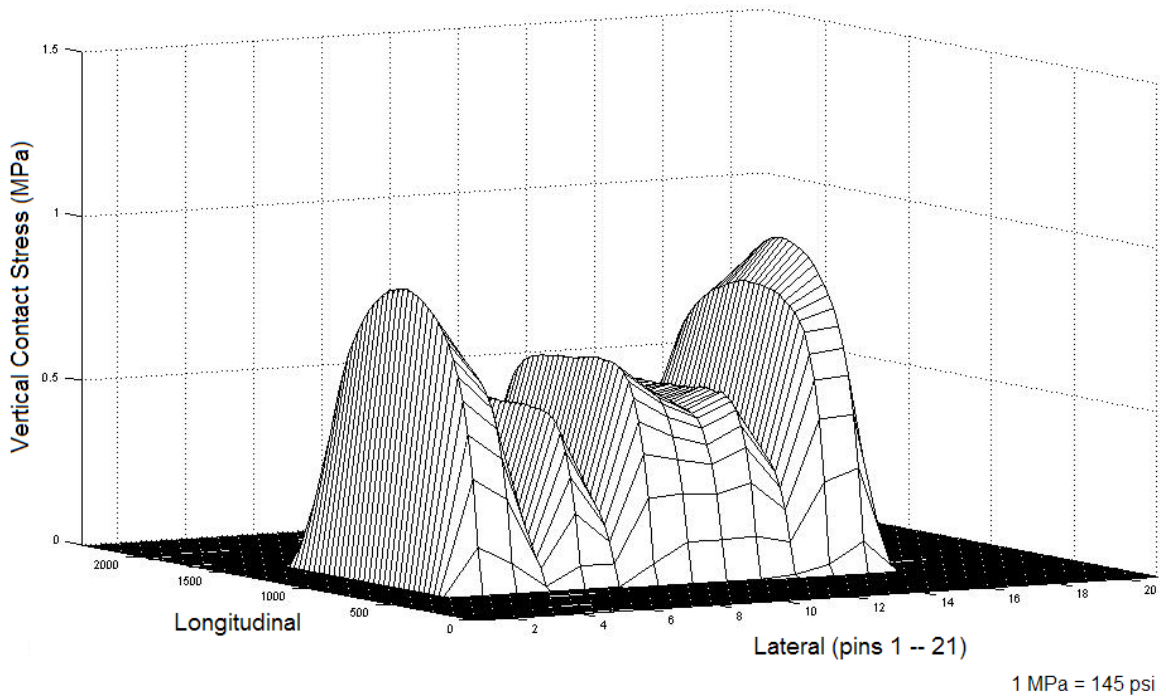

Figure B63. Measured Vertical Contact Stress Distribution for 11R24.5 Radial Tested at a Tire Load of 7800 lb and an Inflation Pressure of 70 psi.

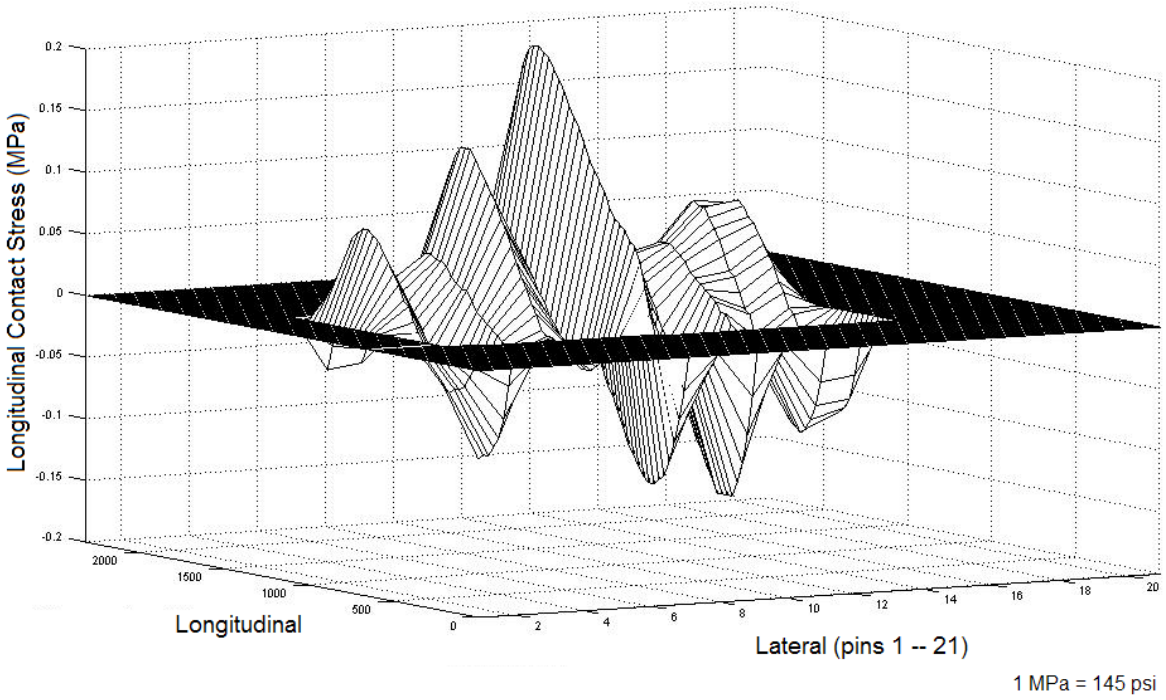

Figure B64. Measured Longitudinal Contact Stress Distribution for 11R24.5 Radial Tested at a Tire Load of 7800 lb and an Inflation Pressure of 85 psi.

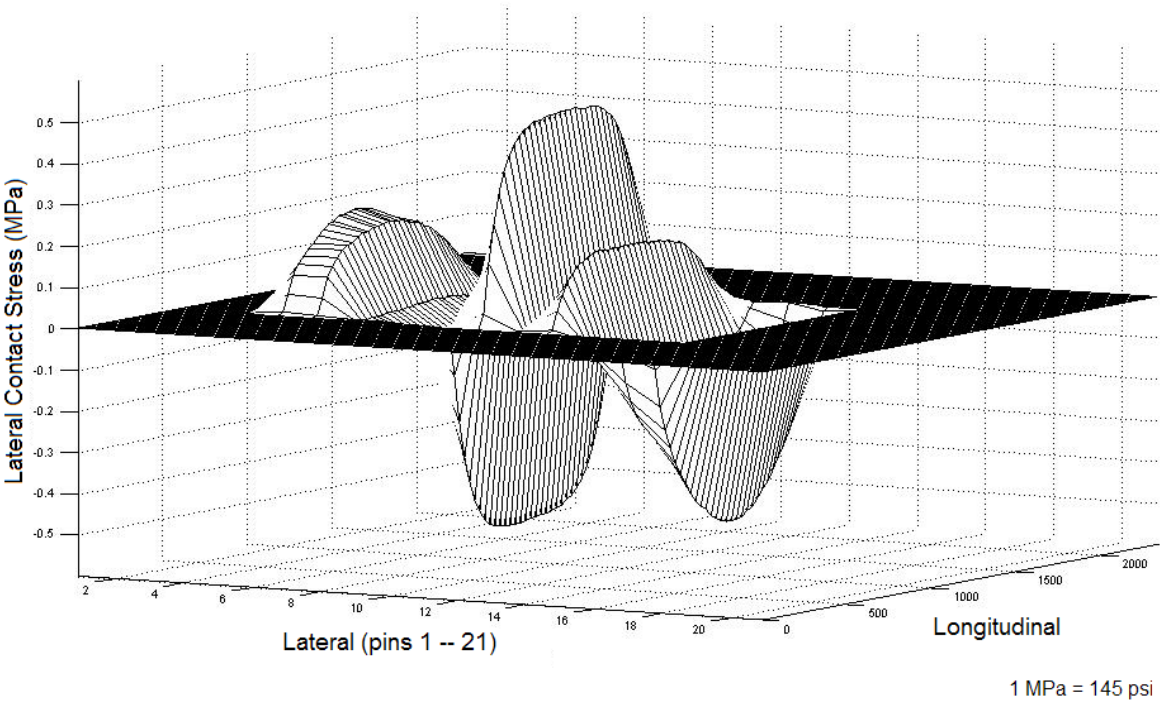

Figure B65. Measured Lateral Contact Stress Distribution for 11R24.5 Radial Tested at a Tire Load of 7800 lb and an Inflation Pressure of 85 psi.

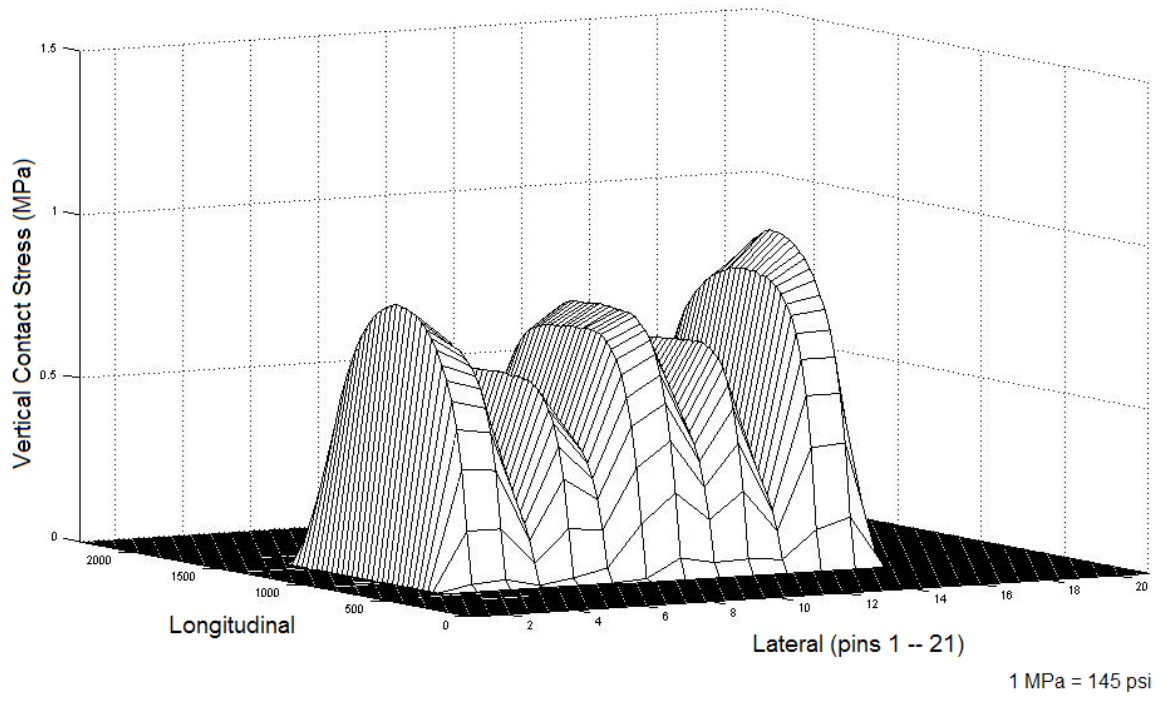

Figure B66. Measured Vertical Contact Stress Distribution for 11R24.5 Radial Tested at a Tire Load of 7800 lb and an Inflation Pressure of 85 psi.

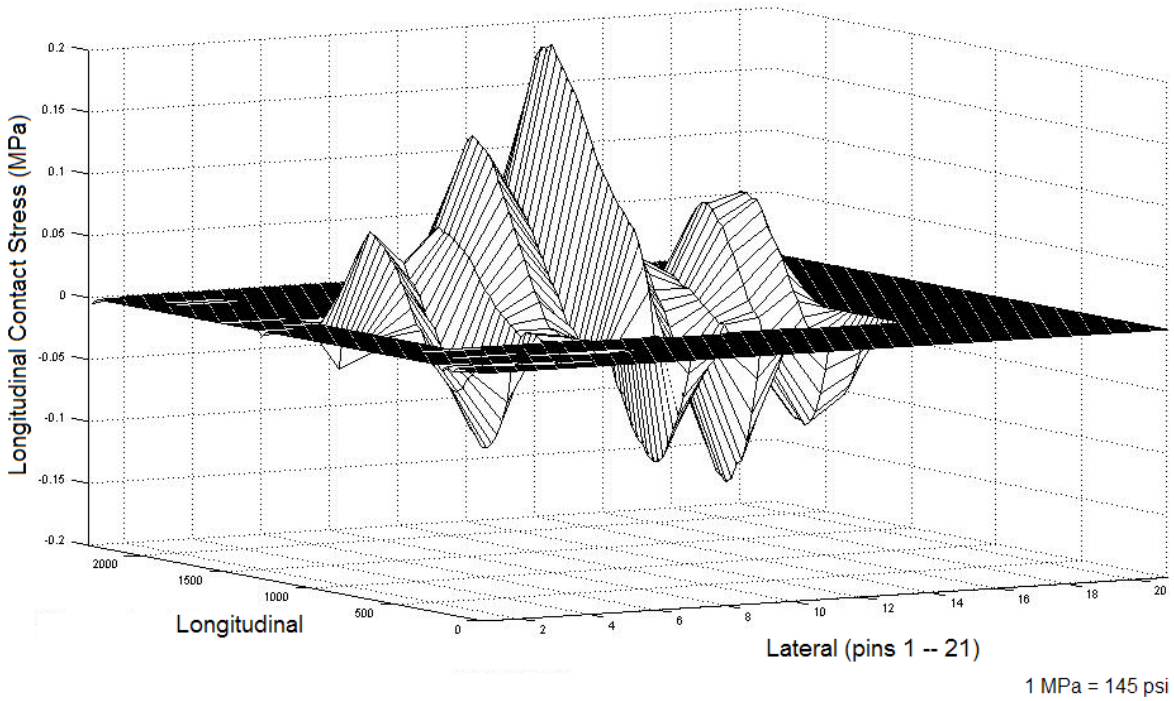

Figure B67. Measured Longitudinal Contact Stress Distribution for 11R24.5 Radial Tested at a Tire Load of 7800 lb and an Inflation Pressure of 100 psi.

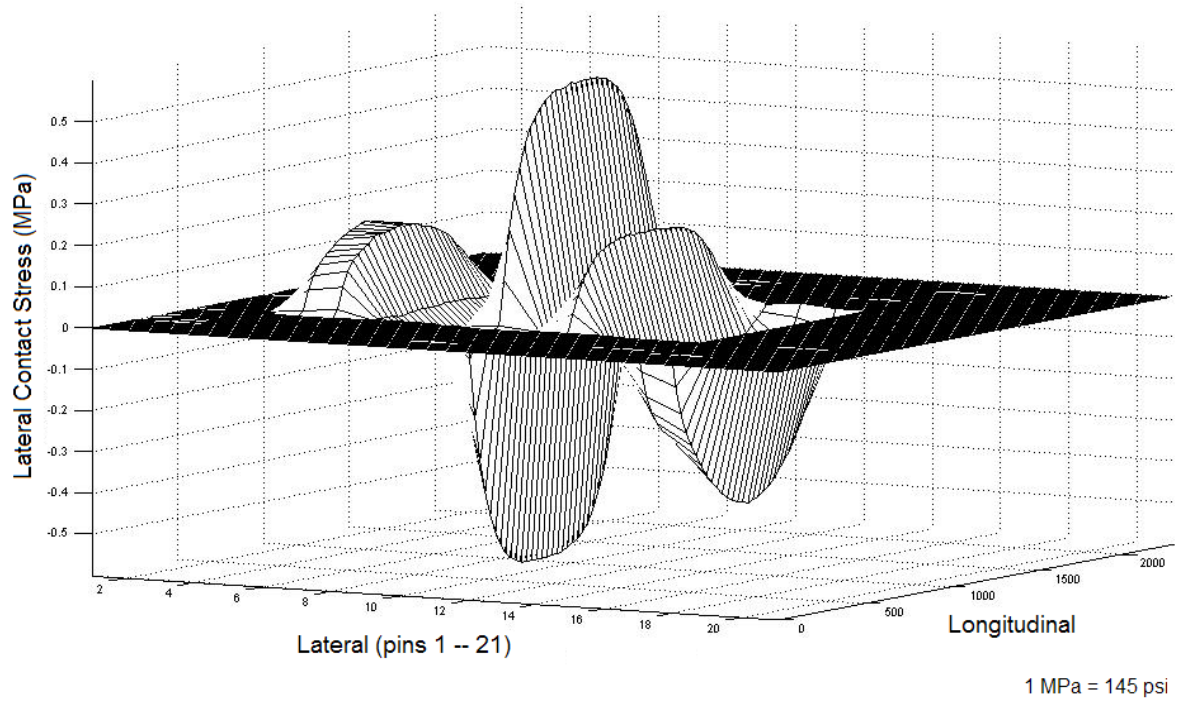

Figure B68. Measured Lateral Contact Stress Distribution for 11R24.5 Radial Tested at a Tire Load of 7800 lb and an Inflation Pressure of 100 psi.

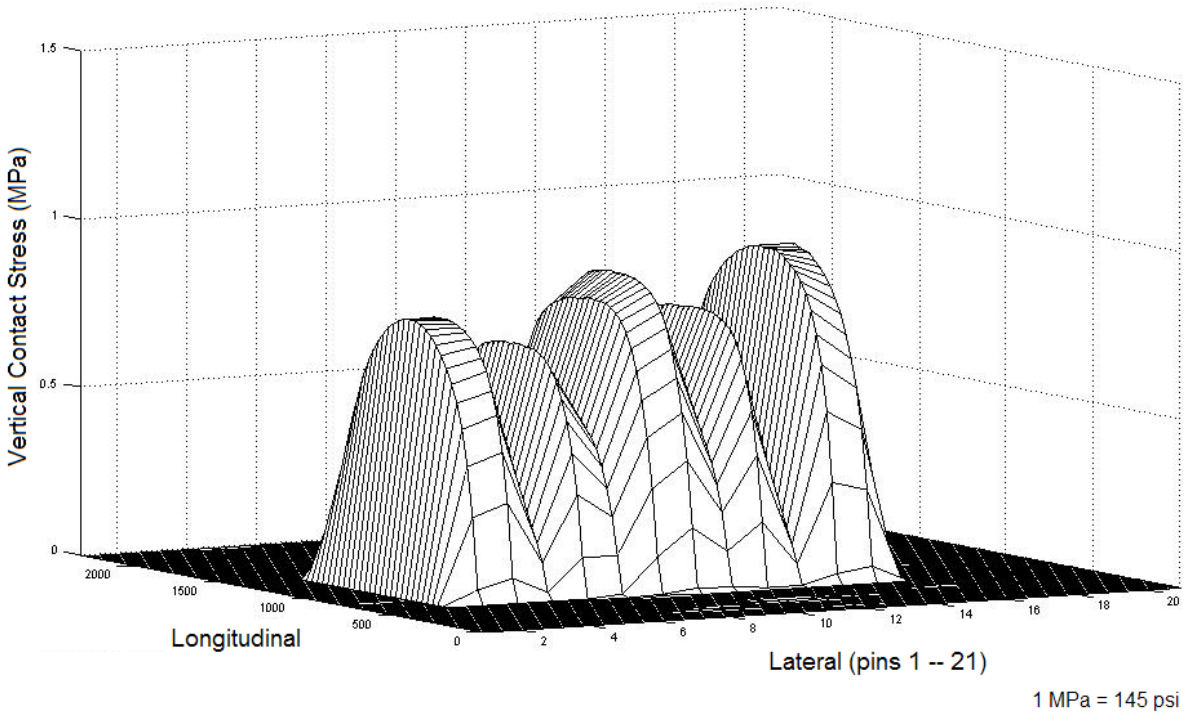

Figure B69. Measured Vertical Contact Stress Distribution for 11R24.5 Radial Tested at a Tire Load of 7800 lb and an Inflation Pressure of 100 psi.

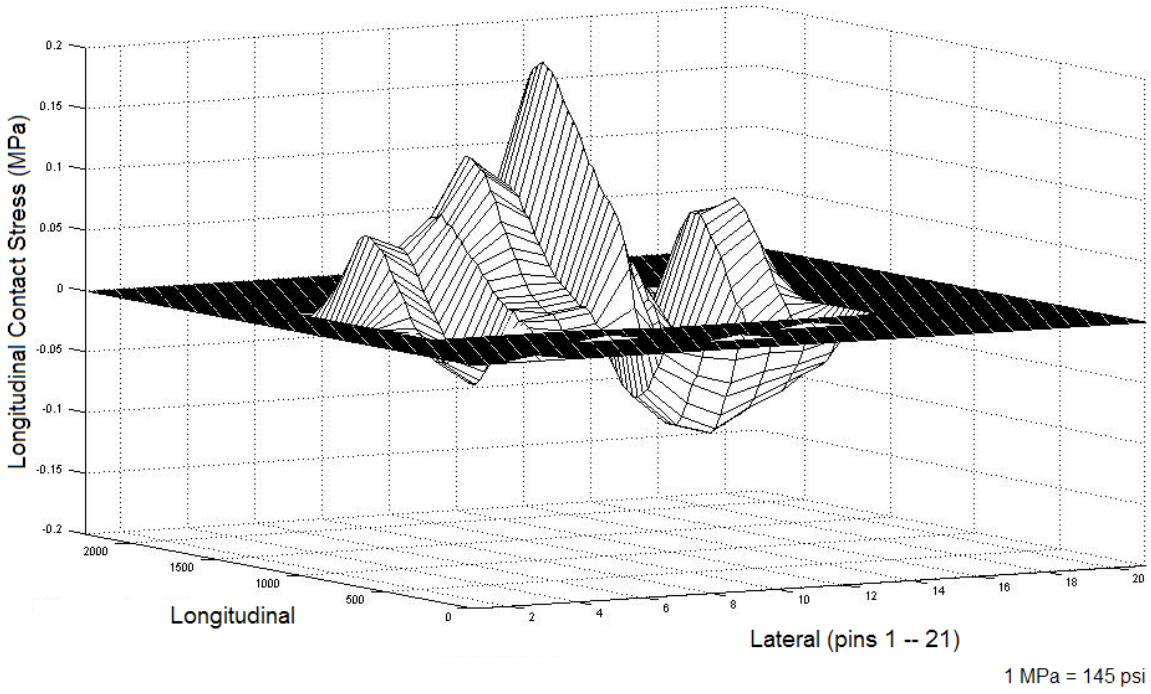

Figure B70. Measured Longitudinal Contact Stress Distribution for 11R24.5 Radial Tested at a Tire Load of 7800 lb and an Inflation Pressure of 115 psi.

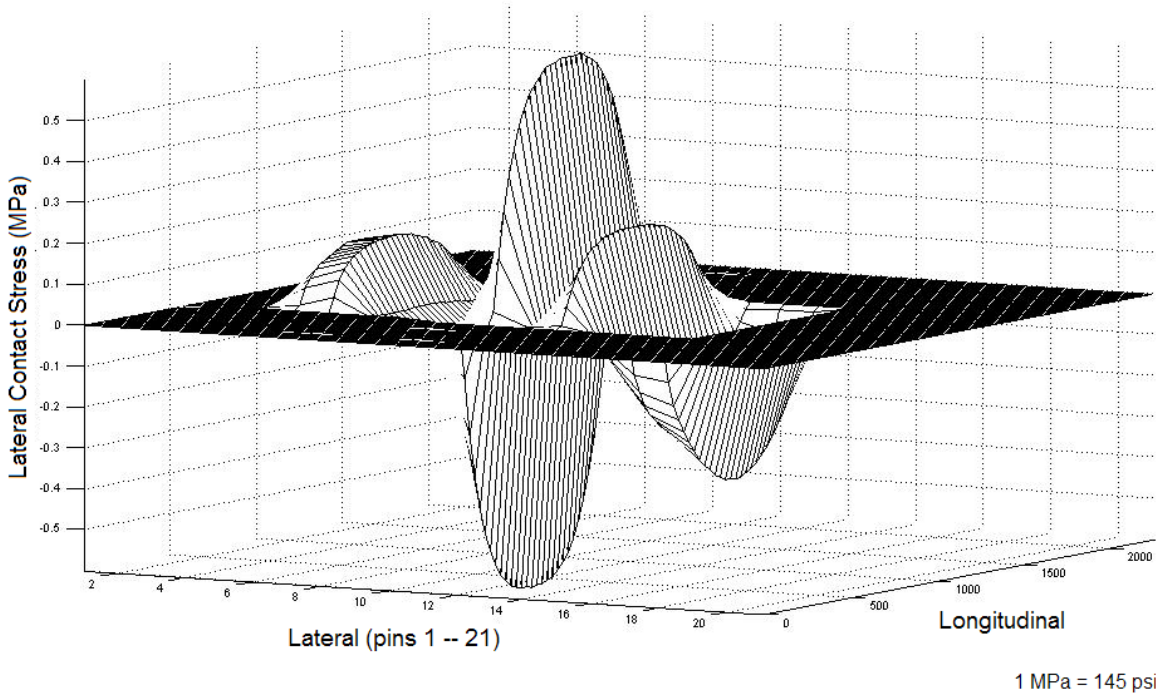

Figure B71. Measured Lateral Contact Stress Distribution for 11R24.5 Radial Tested at a Tire Load of 7800 lb and an Inflation Pressure of 115 psi.

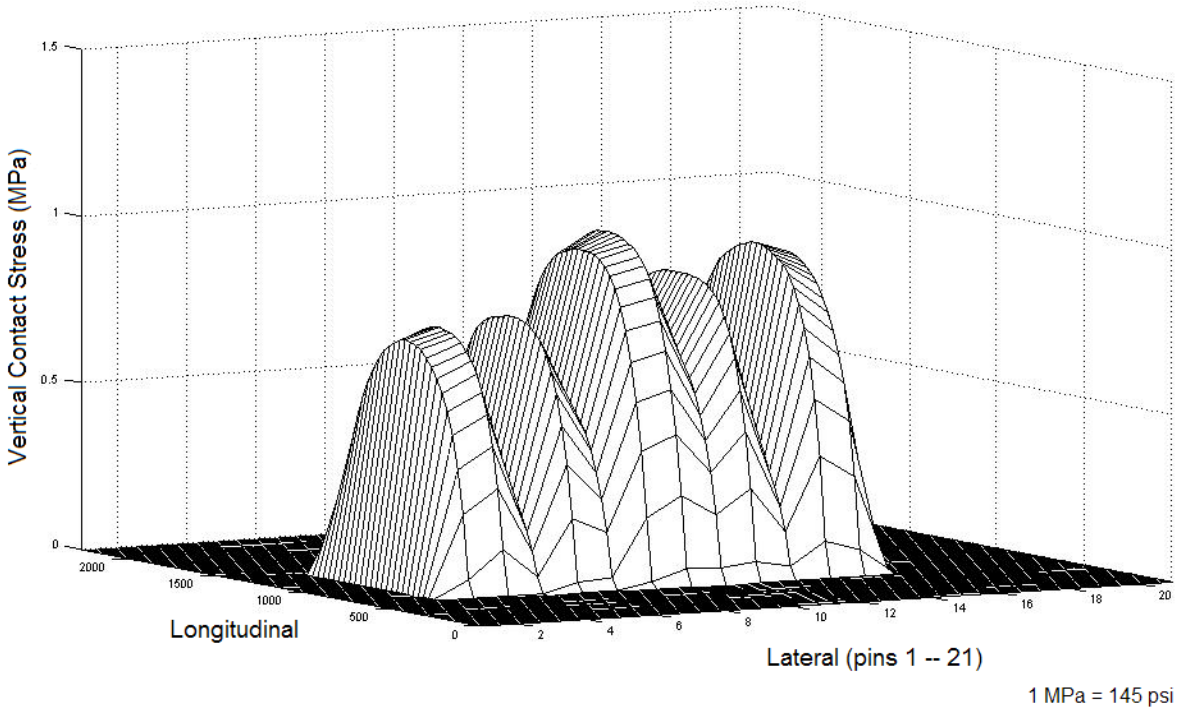

Figure B72. Measured Vertical Contact Stress Distribution for 11R24.5 Radial Tested at a Tire Load of 7800 lb and an Inflation Pressure of 115 psi.

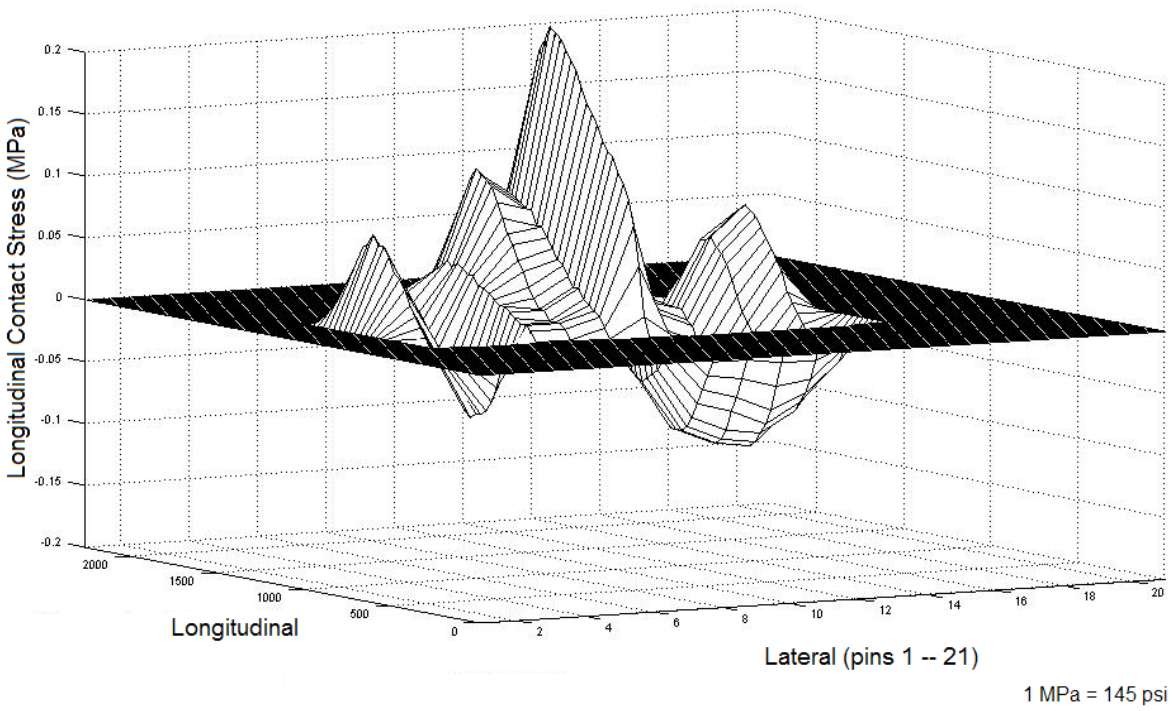

Figure B73. Measured Longitudinal Contact Stress Distribution for 11R24.5 Radial Tested at a Tire Load of 7800 lb and an Inflation Pressure of 130 psi.

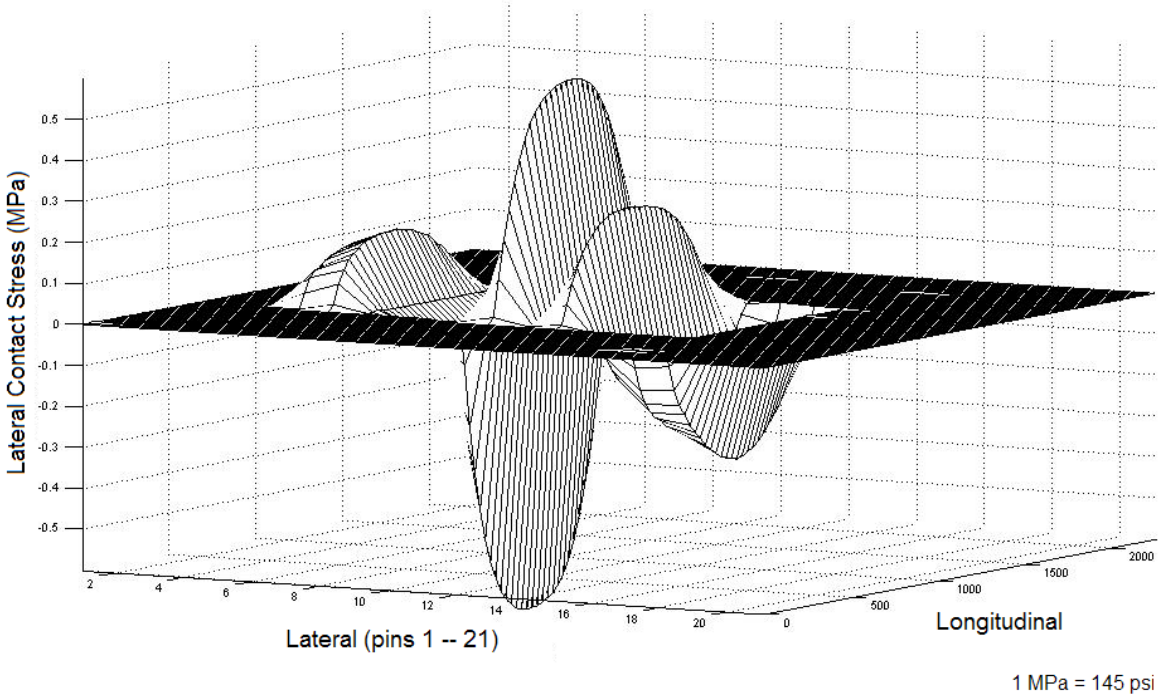

Figure B74. Measured Lateral Contact Stress Distribution for 11R24.5 Radial Tested at a Tire Load of 7800 lb and an Inflation Pressure of 130 psi.

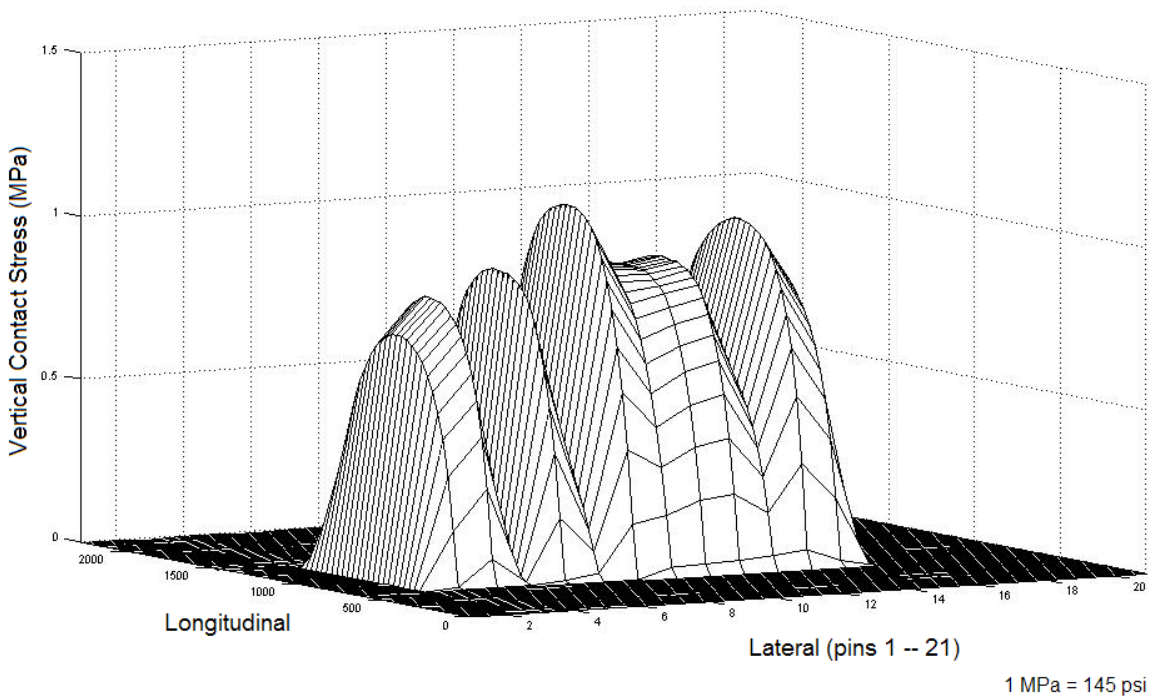

Figure B75. Measured Vertical Contact Stress Distribution for 11R24.5 Radial Tested at a Tire Load of 7800 lb and an Inflation Pressure of 130 psi.

APPENDIX C

CHARTS OF TIRE CONTACT STRESS DISTRIBUTIONS FROM TESTS CONDUCTED ON THE 215/75R17.5 RADIAL TIRE

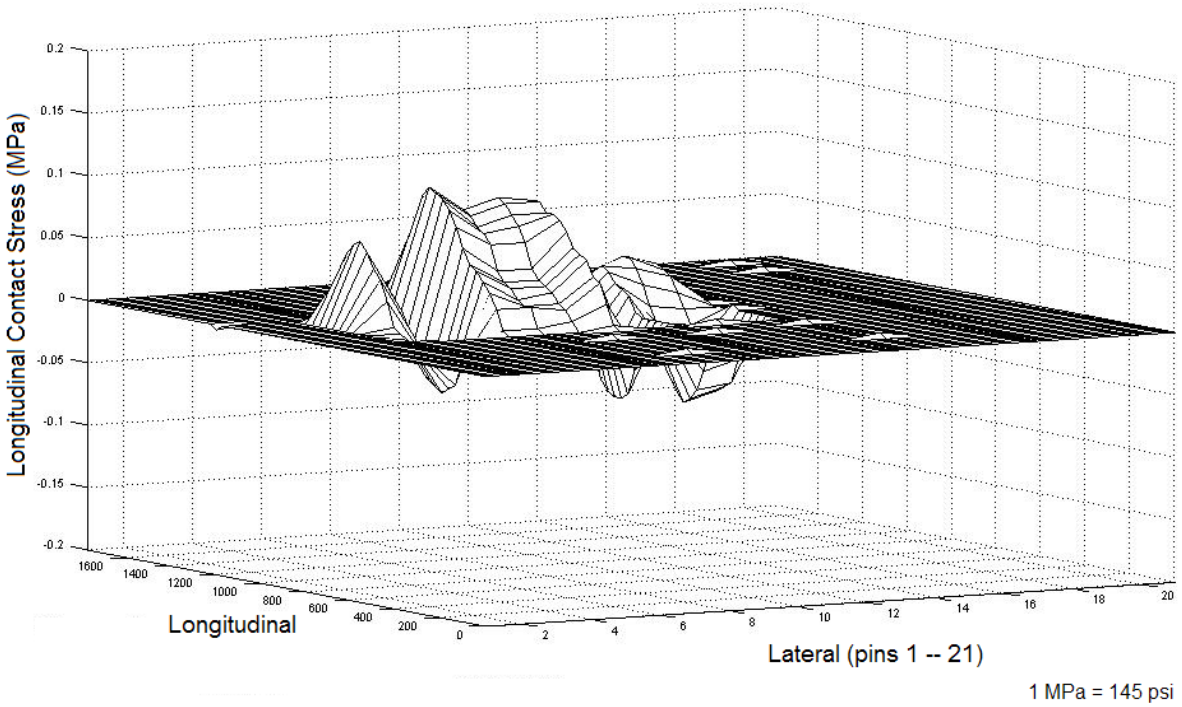

Figure C1. Measured Longitudinal Contact Stress Distribution for 215/75R17.5 Radial Tested at a Tire Load of 3000 lb and an Inflation Pressure of 85 psi.

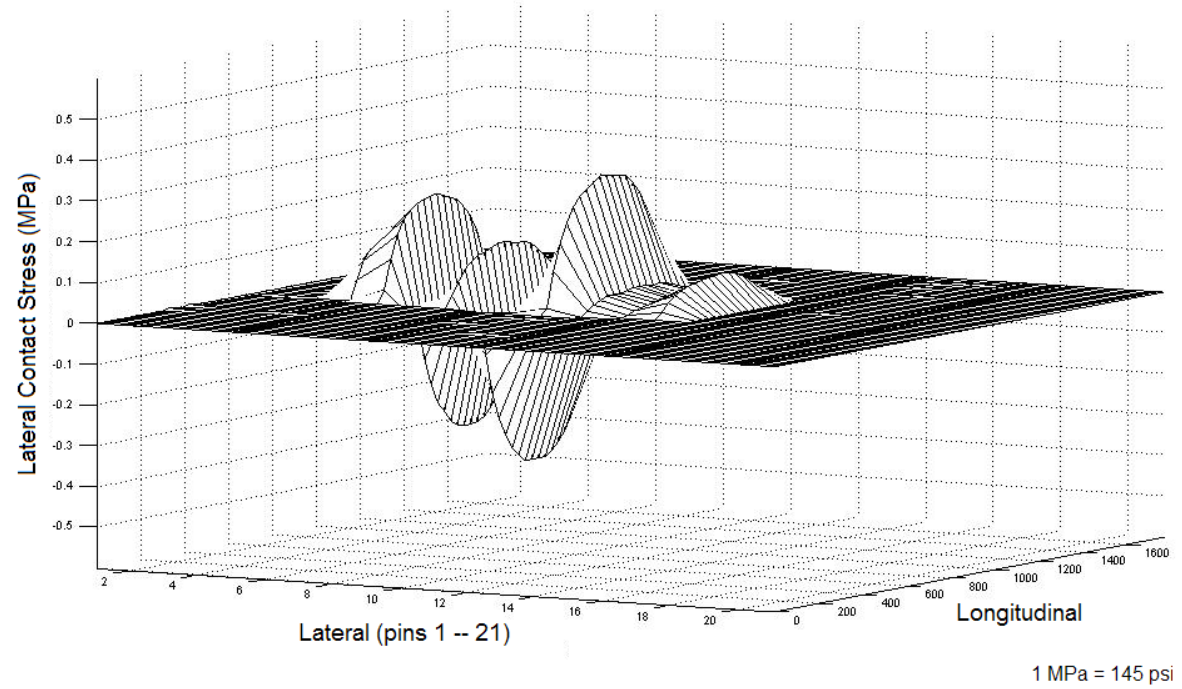

Figure C2. Measured Lateral Contact Stress Distribution for 215/75R17.5 Radial Tested at a Tire Load of 3000 lb and an Inflation Pressure of 85 psi.

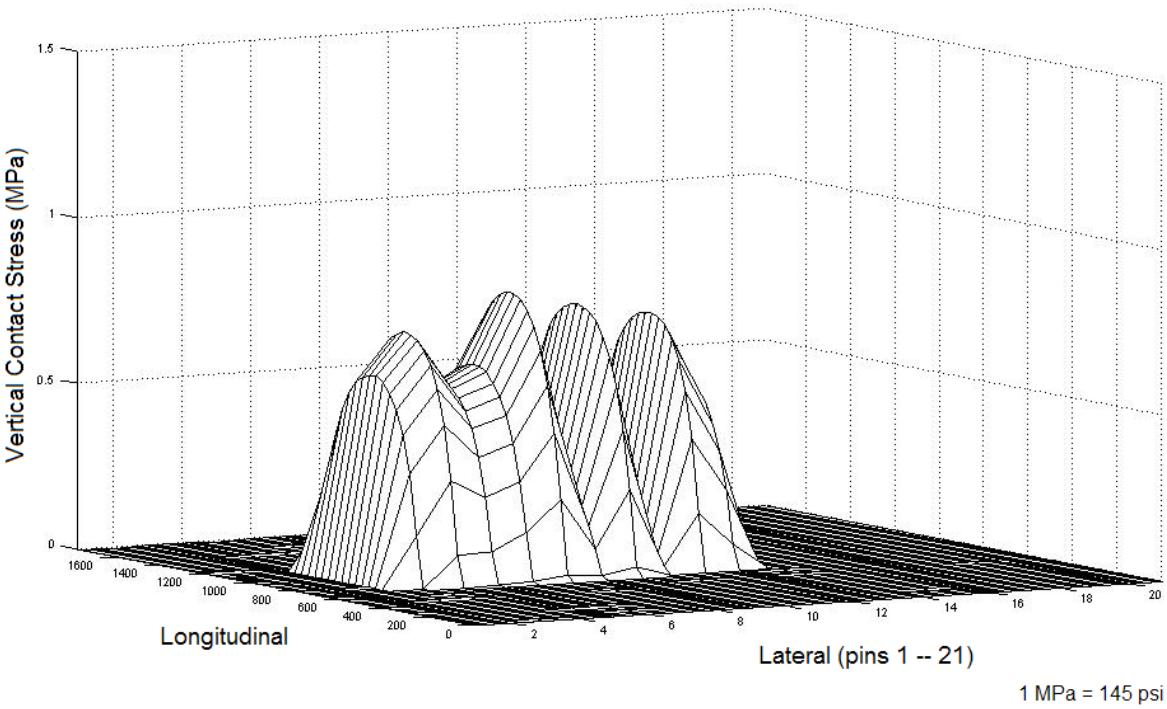

Figure C3. Measured Vertical Contact Stress Distribution for 215/75R17.5 Radial Tested at a Tire Load of 3000 lb and an Inflation Pressure of 85 psi.

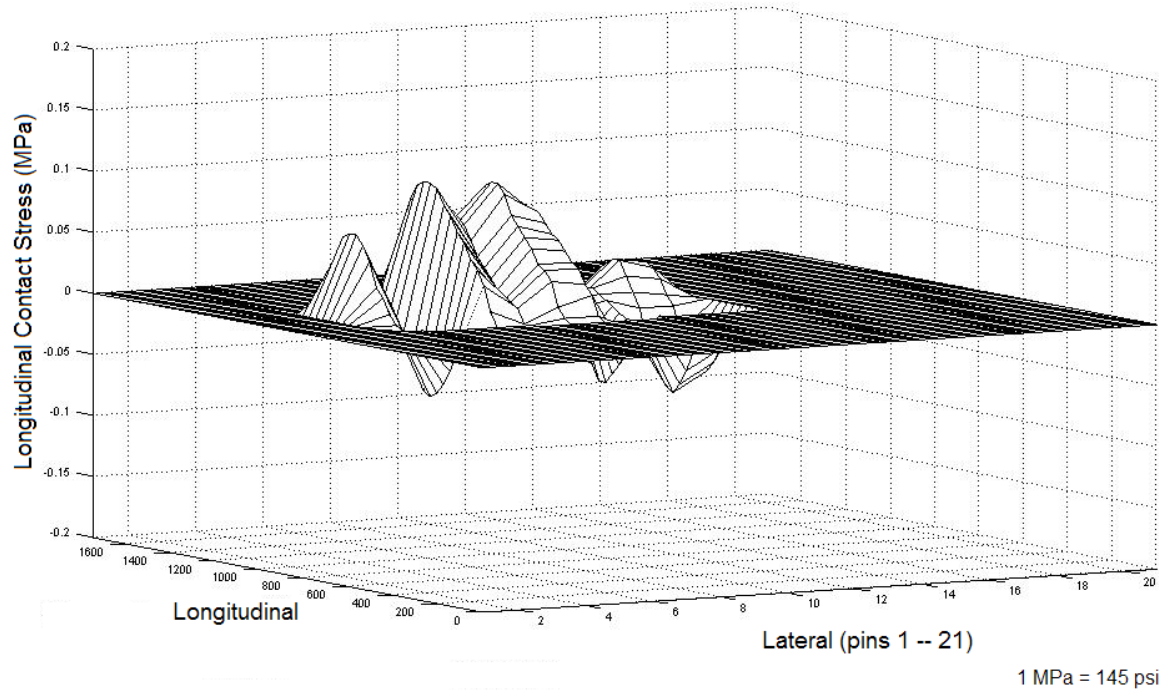

Figure C4. Measured Longitudinal Contact Stress Distribution for 215/75R17.5 Radial Tested at a Tire Load of 3000 lb and an Inflation Pressure of 100 psi.

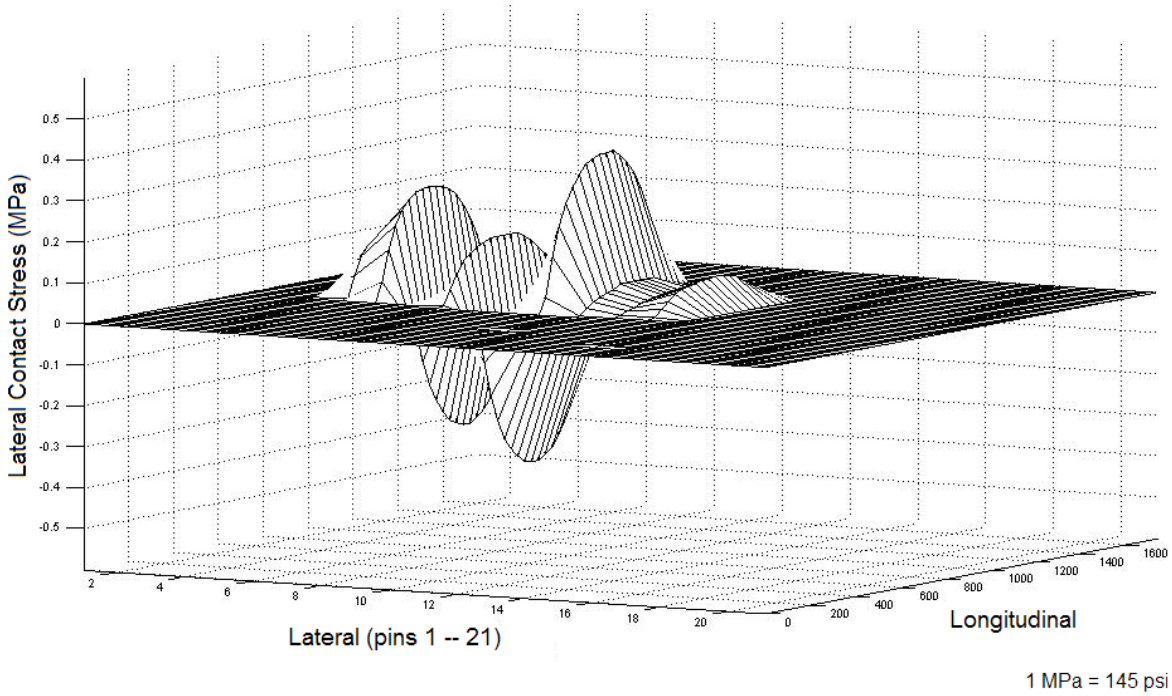

Figure C5. Measured Lateral Contact Stress Distribution for 215/75R17.5 Radial Tested at a Tire Load of 3000 lb and an Inflation Pressure of 100 psi.

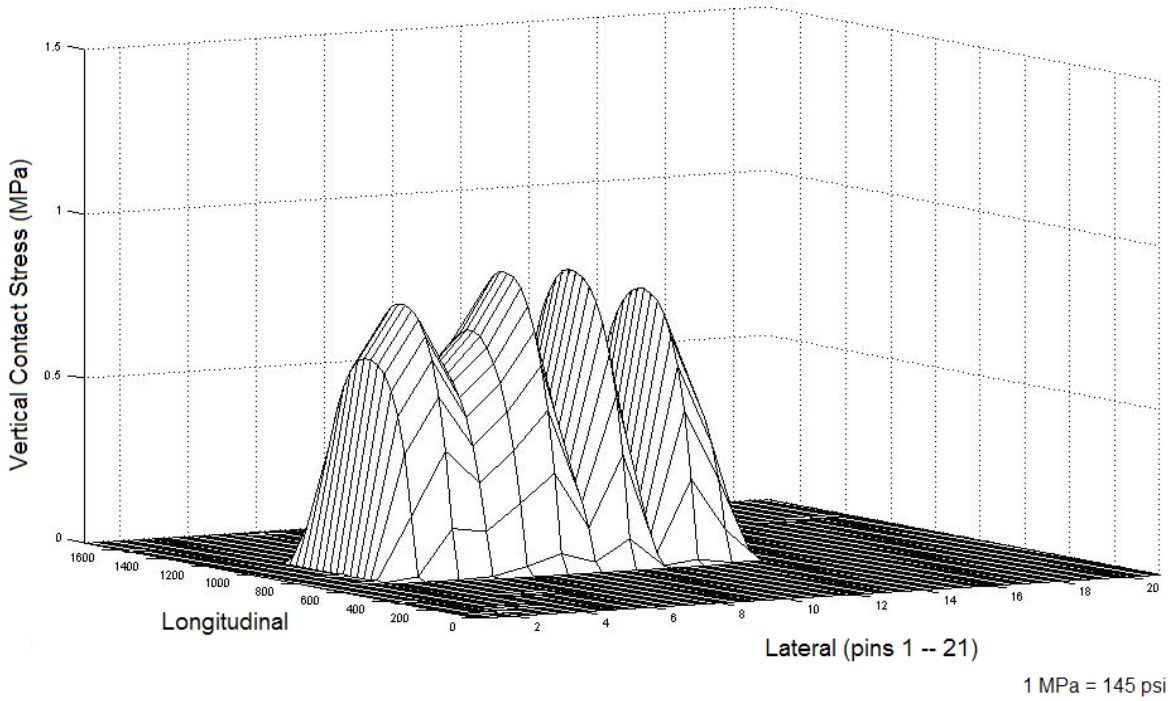

Figure C6. Measured Vertical Contact Stress Distribution for 215/75R17.5 Radial Tested at a Tire Load of 3000 lb and an Inflation Pressure of 100 psi.

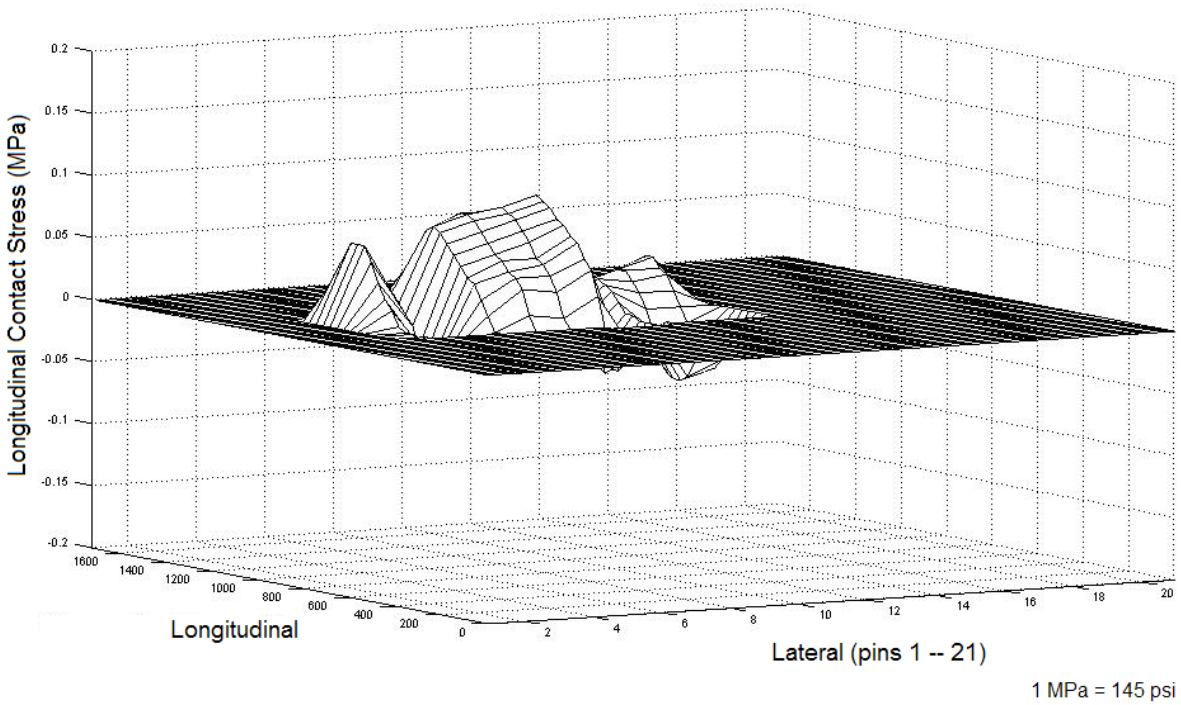

Figure C7. Measured Longitudinal Contact Stress Distribution for 215/75R17.5 Radial Tested at a Tire Load of 3000 lb and an Inflation Pressure of 115 psi.

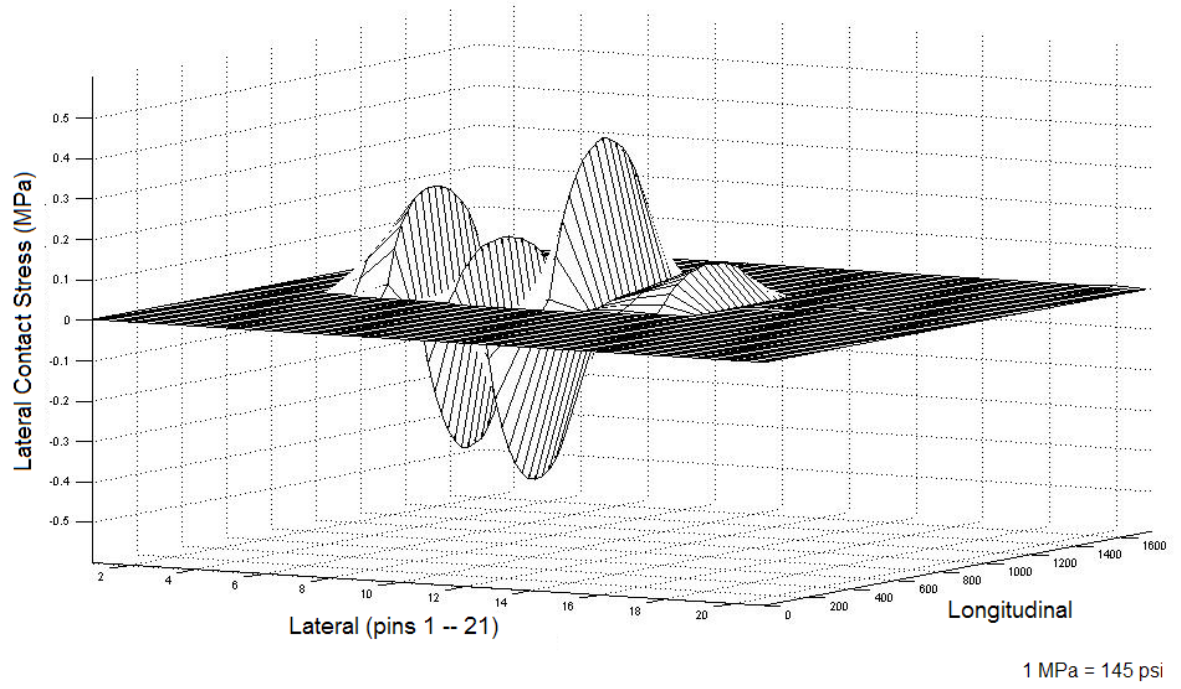

Figure C8. Measured Lateral Contact Stress Distribution for 215/75R17.5 Radial Tested at a Tire Load of 3000 lb and an Inflation Pressure of 115 psi.

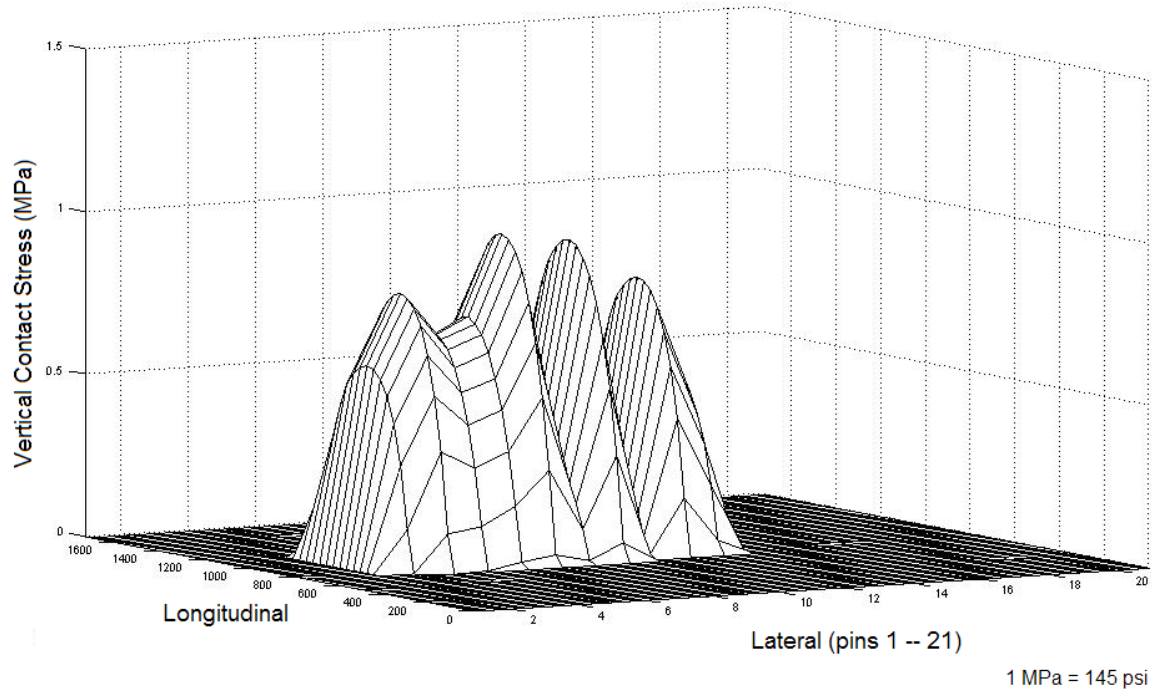

Figure C9. Measured Vertical Contact Stress Distribution for 215/75R17.5 Radial Tested at a Tire Load of 3000 lb and an Inflation Pressure of 115 psi.

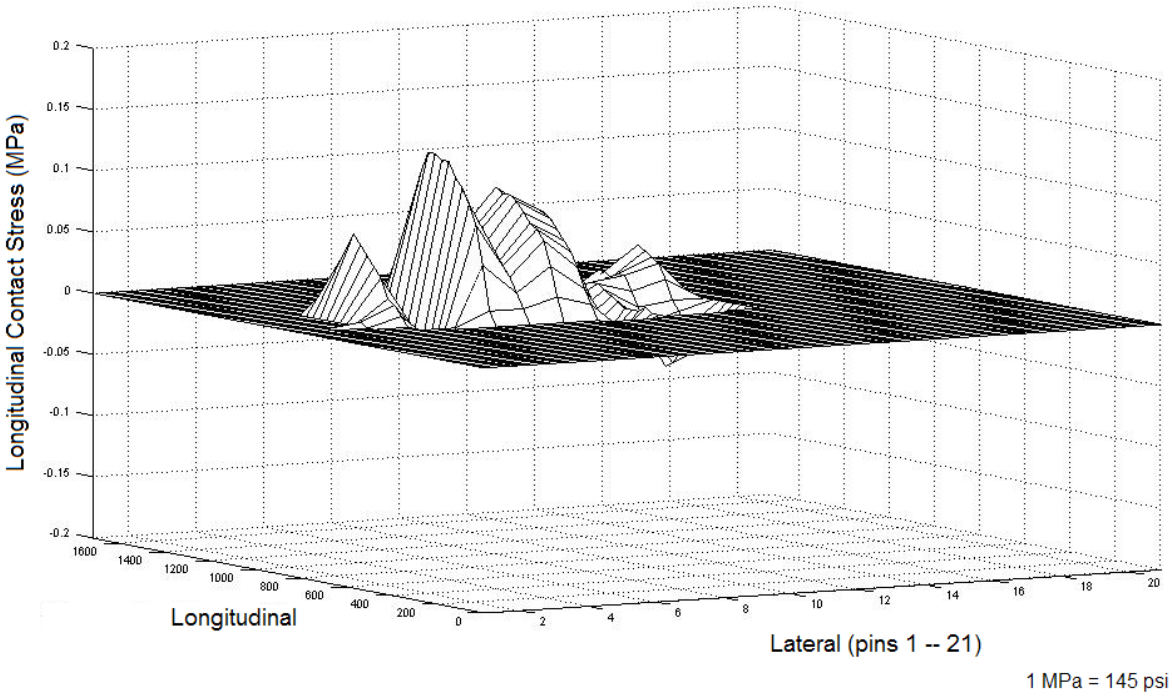

Figure C10. Measured Longitudinal Contact Stress Distribution for 215/75R17.5 Radial Tested at a Tire Load of 3000 lb and an Inflation Pressure of 130 psi.

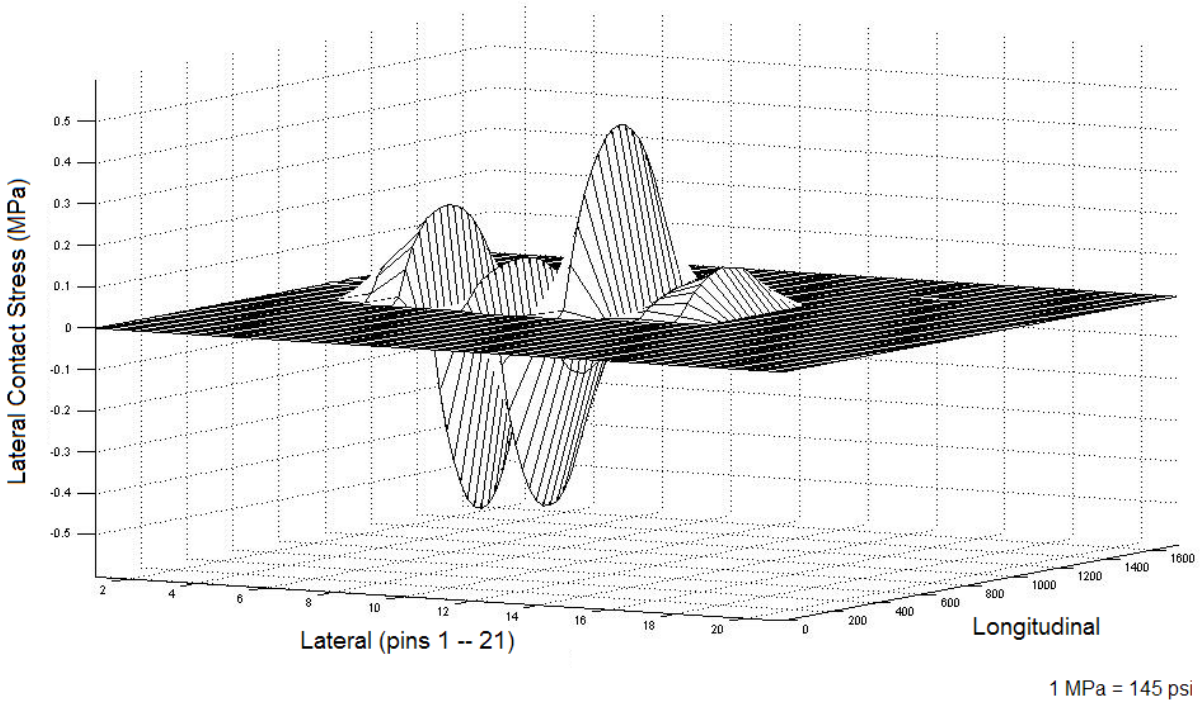

Figure C11. Measured Lateral Contact Stress Distribution for 215/75R17.5 Radial Tested at a Tire Load of 3000 lb and an Inflation Pressure of 130 psi.

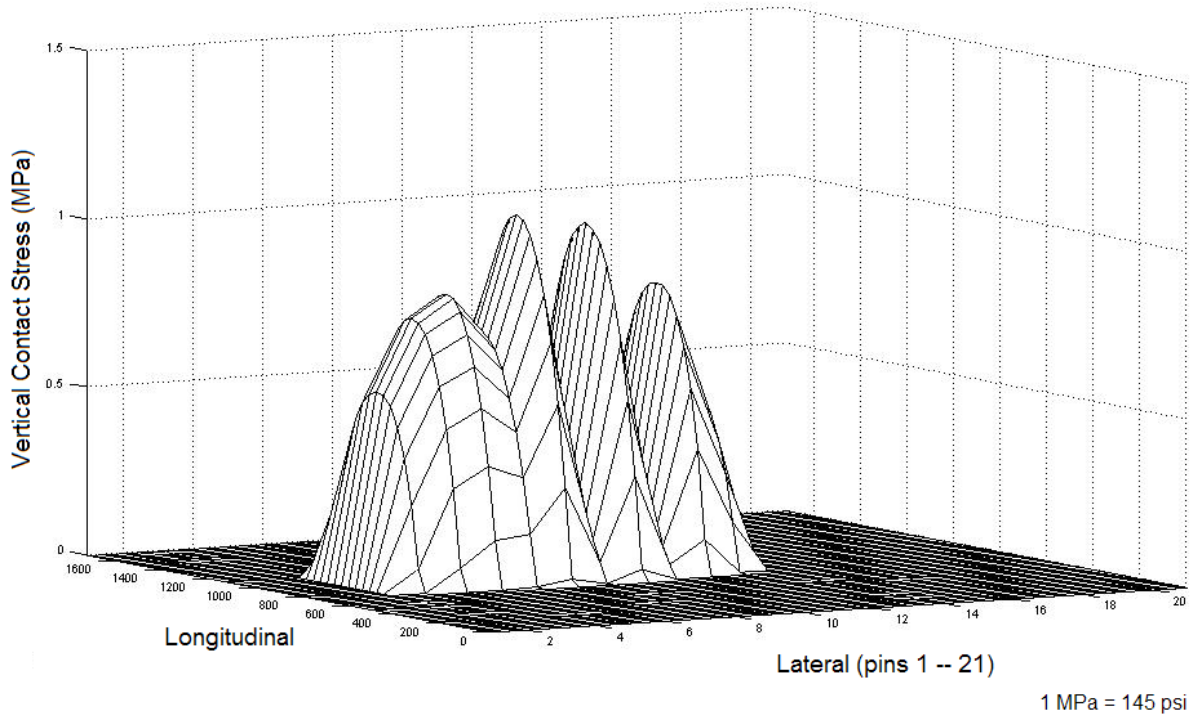

Figure C12. Measured Vertical Contact Stress Distribution for 215/75R17.5 Radial Tested at a Tire Load of 3000 lb and an Inflation Pressure of 130 psi.

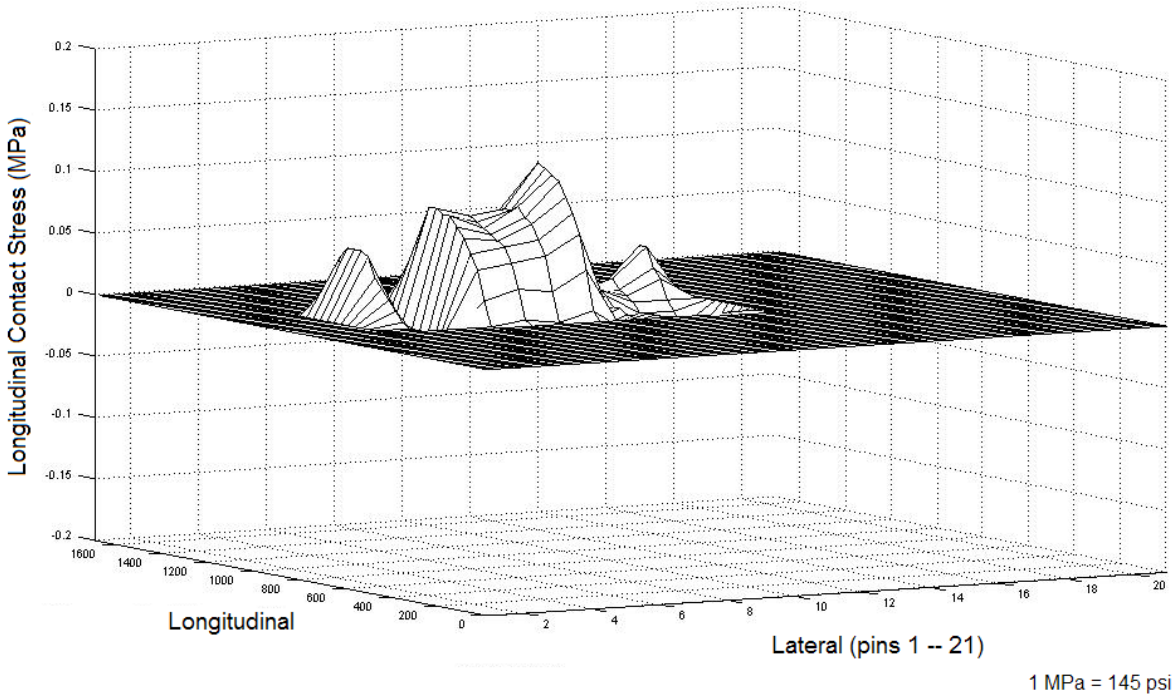

Figure C13. Measured Longitudinal Contact Stress Distribution for 215/75R17.5 Radial Tested at a Tire Load of 3000 lb and an Inflation Pressure of 145 psi.

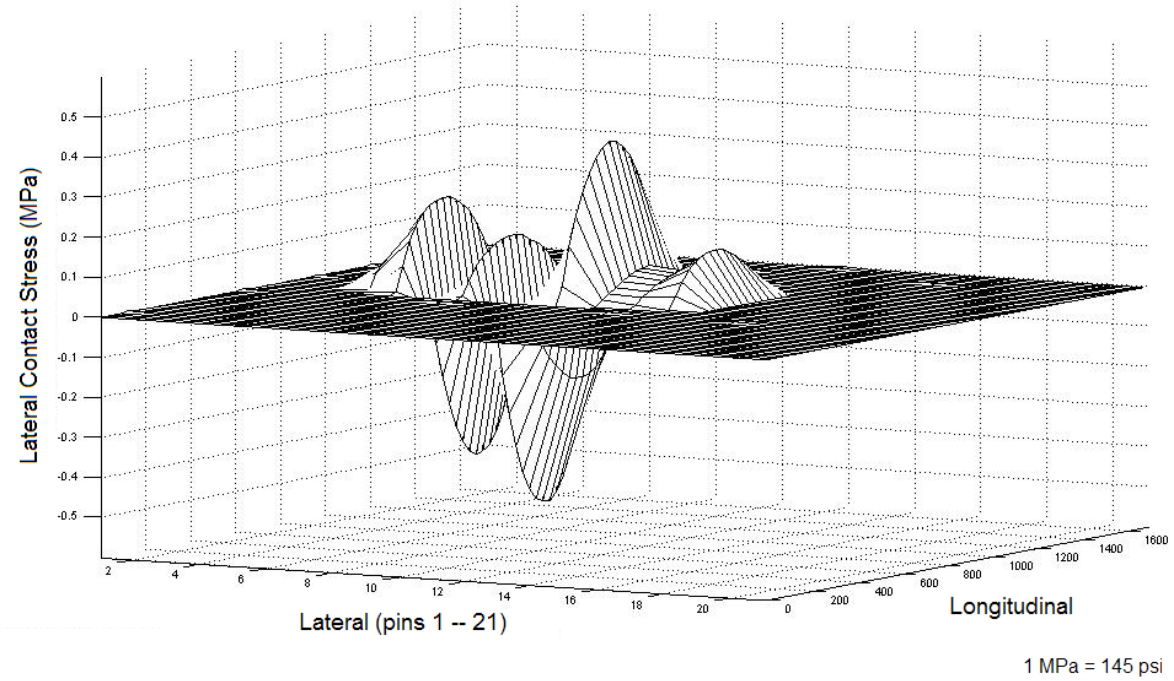

Figure C14. Measured Lateral Contact Stress Distribution for 215/75R17.5 Radial Tested at a Tire Load of 3000 lb and an Inflation Pressure of 145 psi.

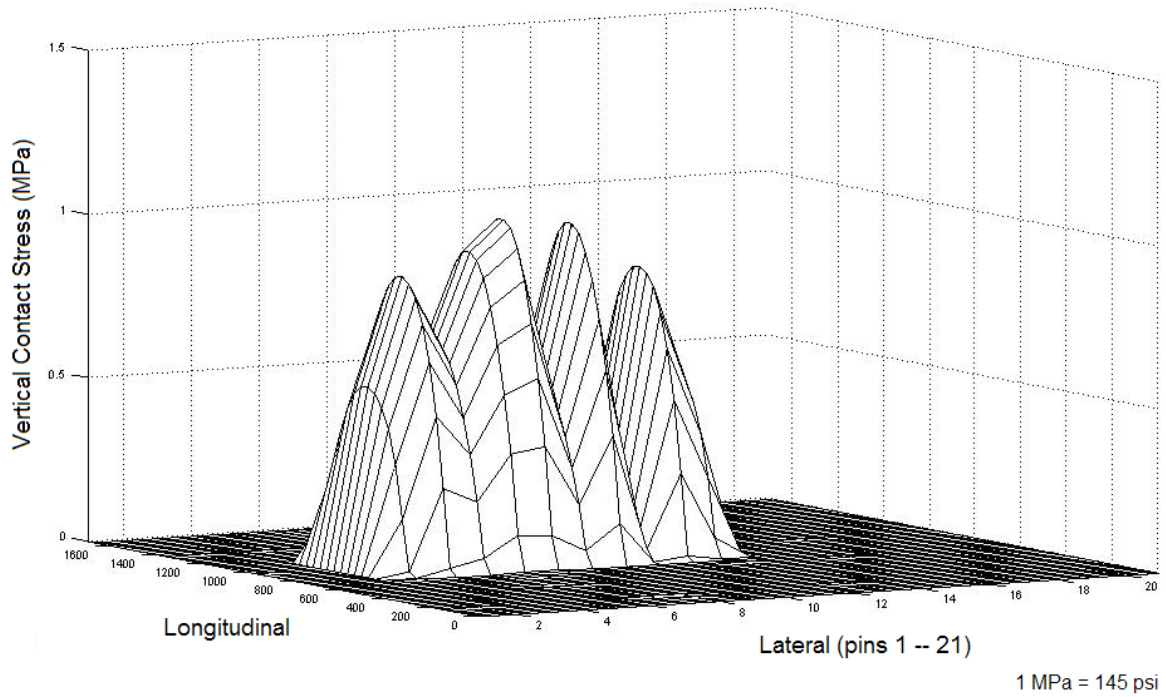

Figure C15. Measured Vertical Contact Stress Distribution for 215/75R17.5 Radial Tested at a Tire Load of 3000 lb and an Inflation Pressure of 145 psi.

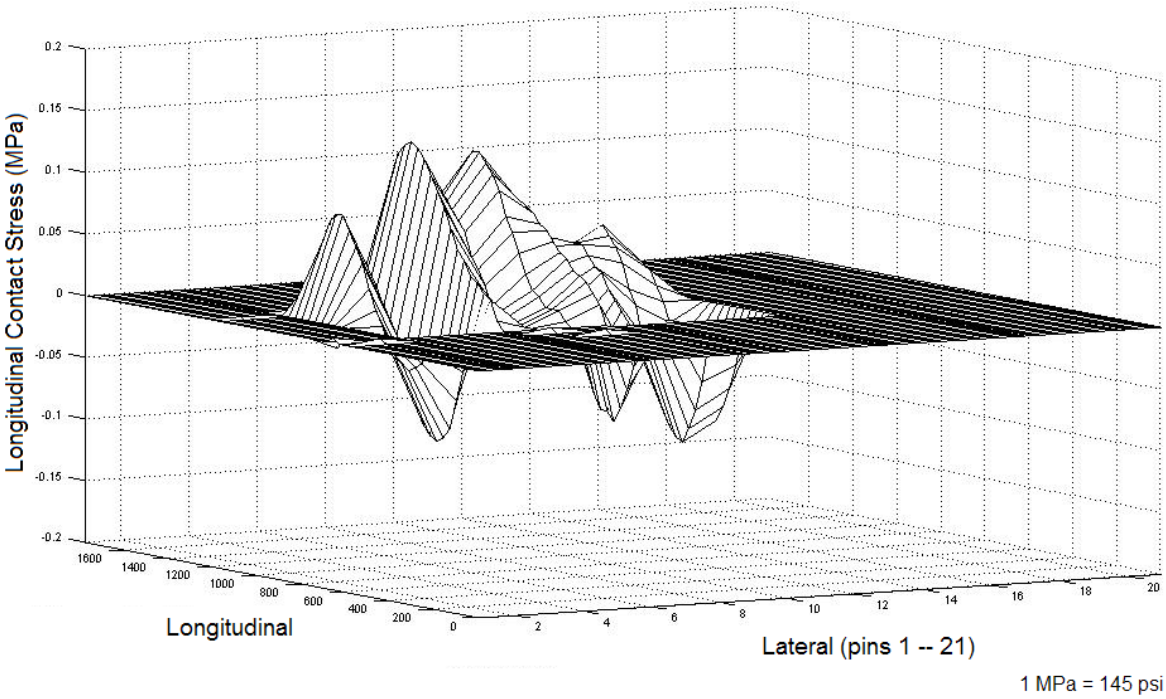

Figure C16. Measured Longitudinal Contact Stress Distribution for 215/75R17.5 Radial Tested at a Tire Load of 4000 lb and an Inflation Pressure of 85 psi.

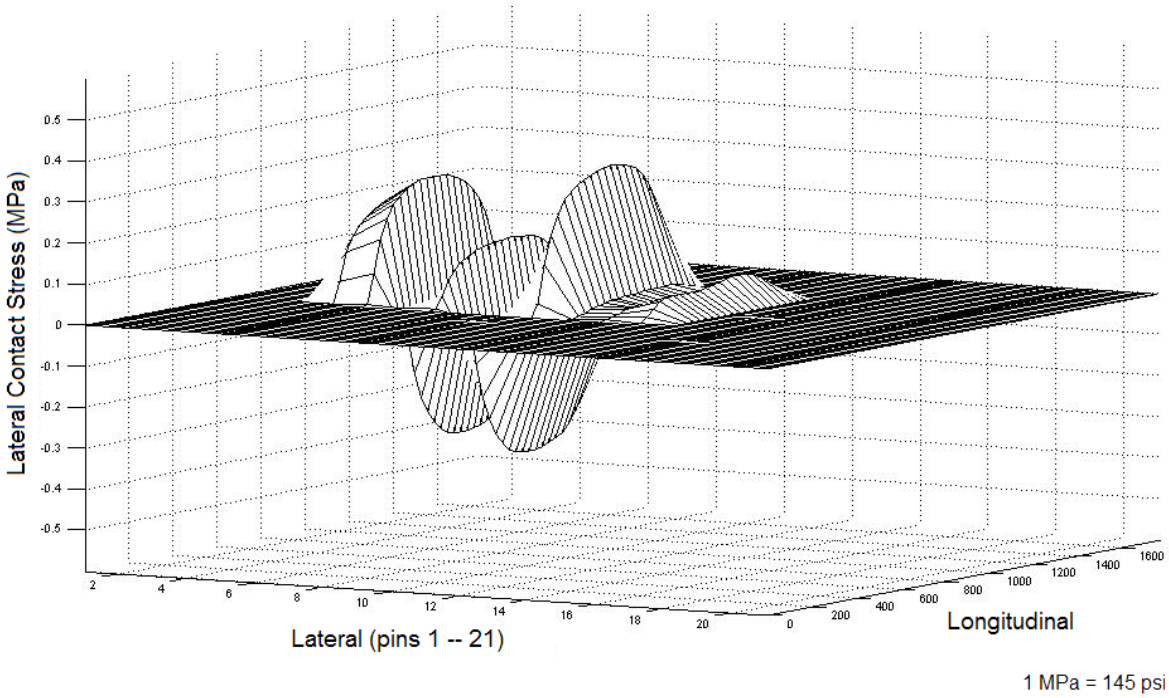

Figure C17. Measured Lateral Contact Stress Distribution for 215/75R17.5 Radial Tested at a Tire Load of 4000 lb and an Inflation Pressure of 85 psi.

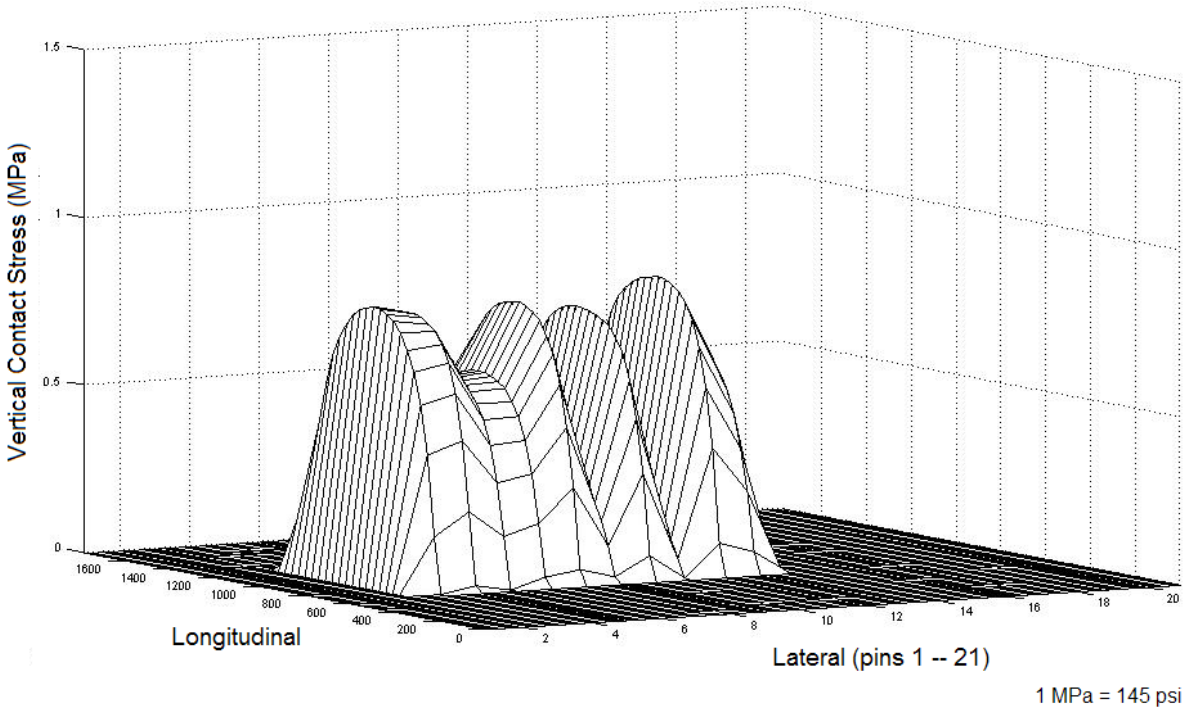

Figure C18. Measured Vertical Contact Stress Distribution for 215/75R17.5 Radial Tested at a Tire Load of 4000 lb and an Inflation Pressure of 85 psi.

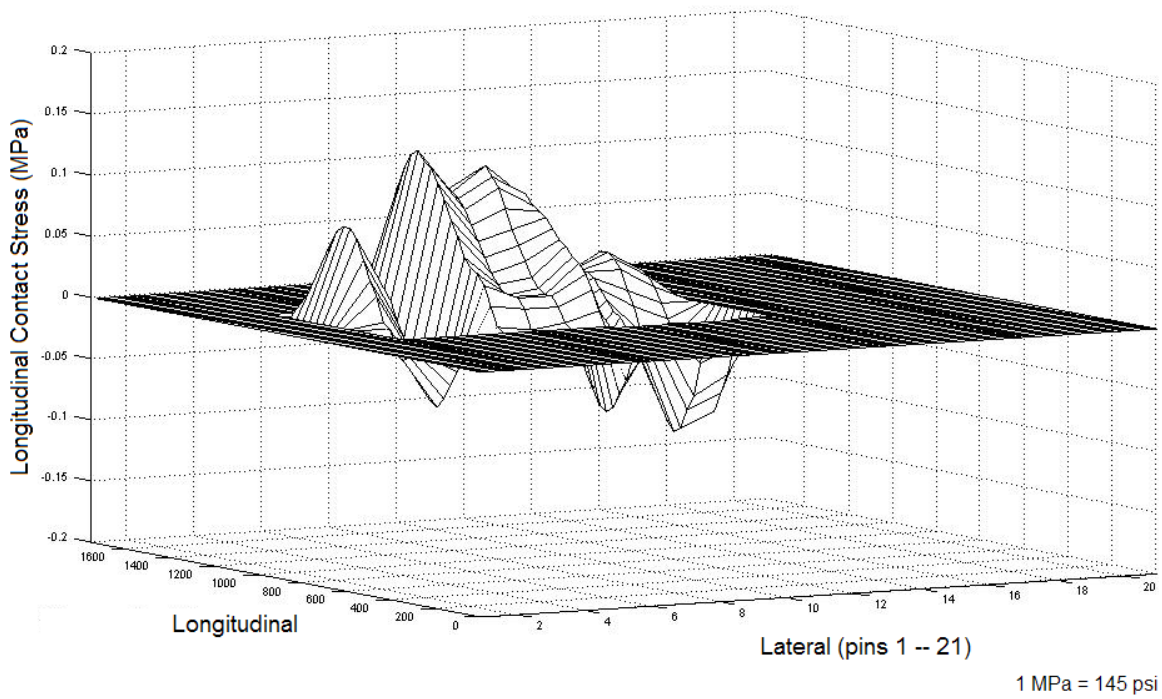

Figure C19. Measured Longitudinal Contact Stress Distribution for 215/75R17.5 Radial Tested at a Tire Load of 4000 lb and an Inflation Pressure of 100 psi.

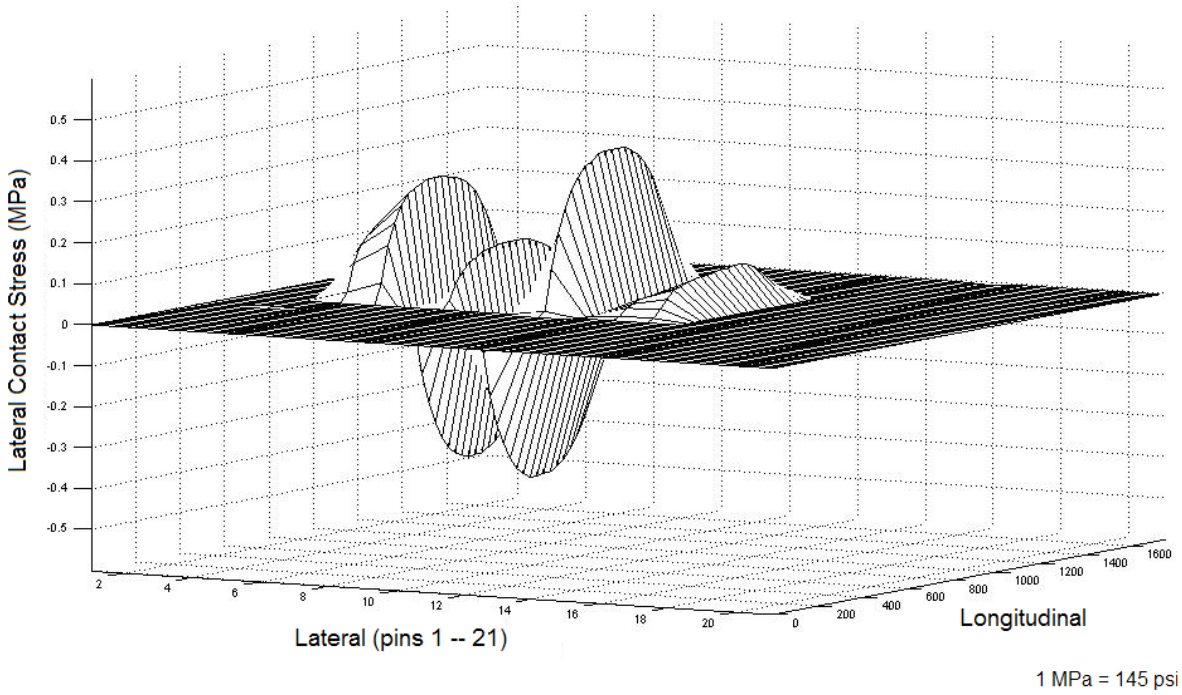

Figure C20. Measured Lateral Contact Stress Distribution for 215/75R17.5 Radial Tested at a Tire Load of 4000 lb and an Inflation Pressure of 100 psi.

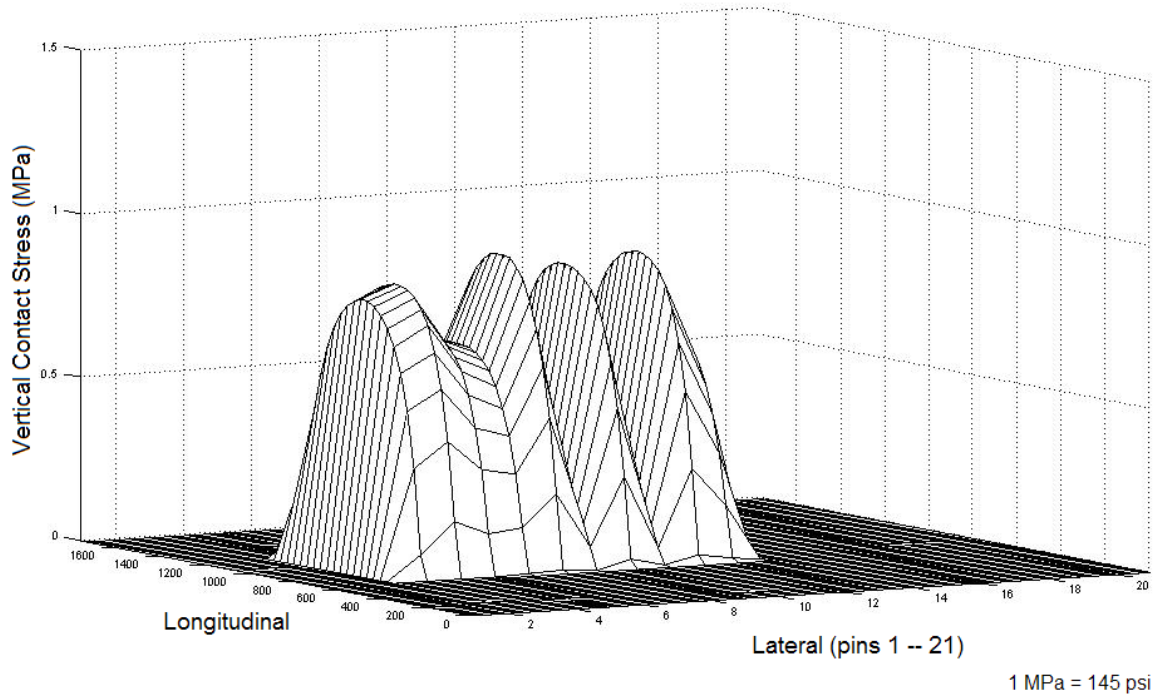

Figure C21. Measured Vertical Contact Stress Distribution for 215/75R17.5 Radial Tested at a Tire Load of 4000 lb and an Inflation Pressure of 100 psi.

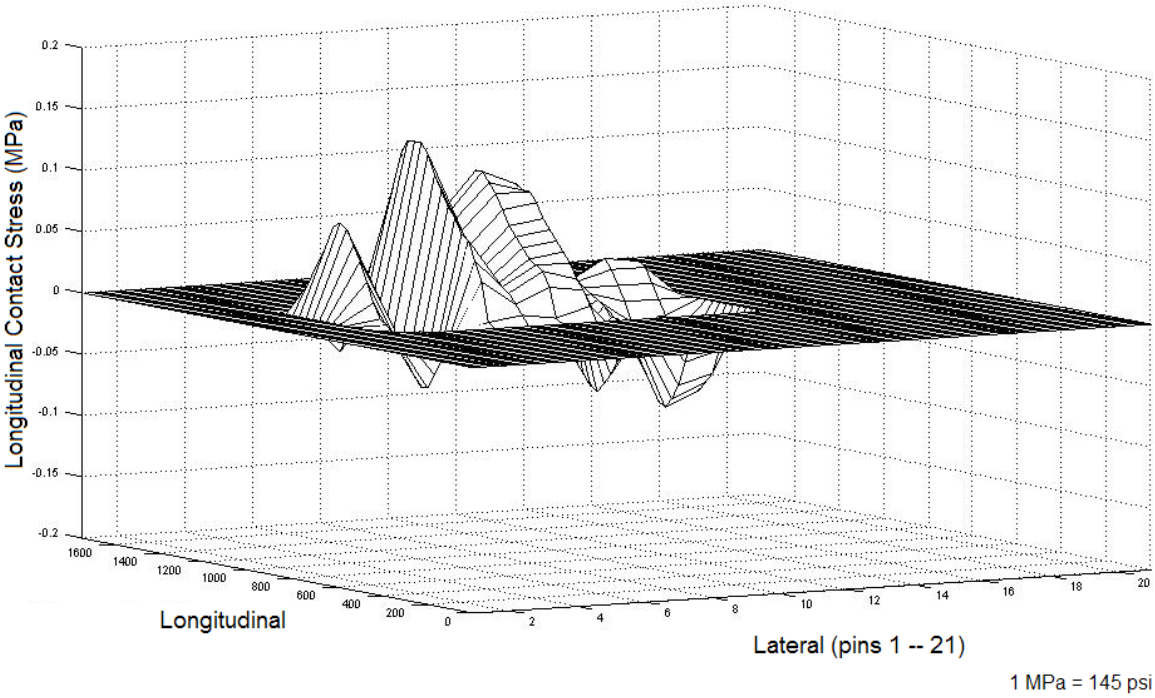

Figure C22. Measured Longitudinal Contact Stress Distribution for 215/75R17.5 Radial Tested at a Tire Load of 4000 lb and an Inflation Pressure of 115 psi.

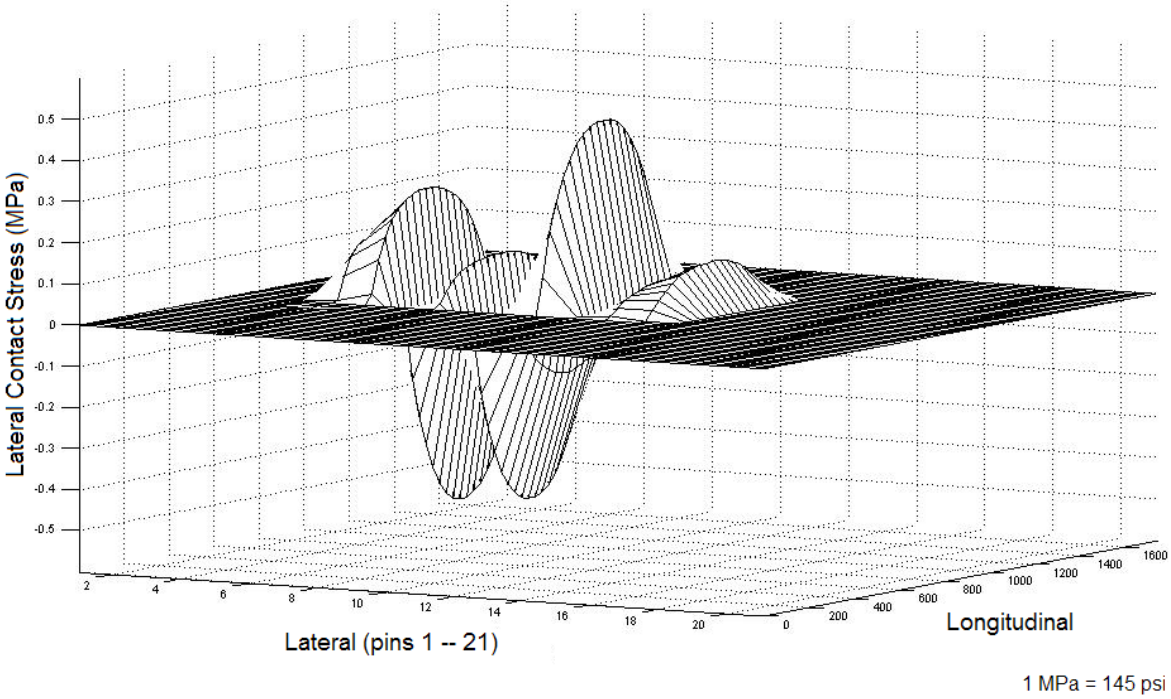

Figure C23. Measured Lateral Contact Stress Distribution for 215/75R17.5 Radial Tested at a Tire Load of 4000 lb and an Inflation Pressure of 115 psi.

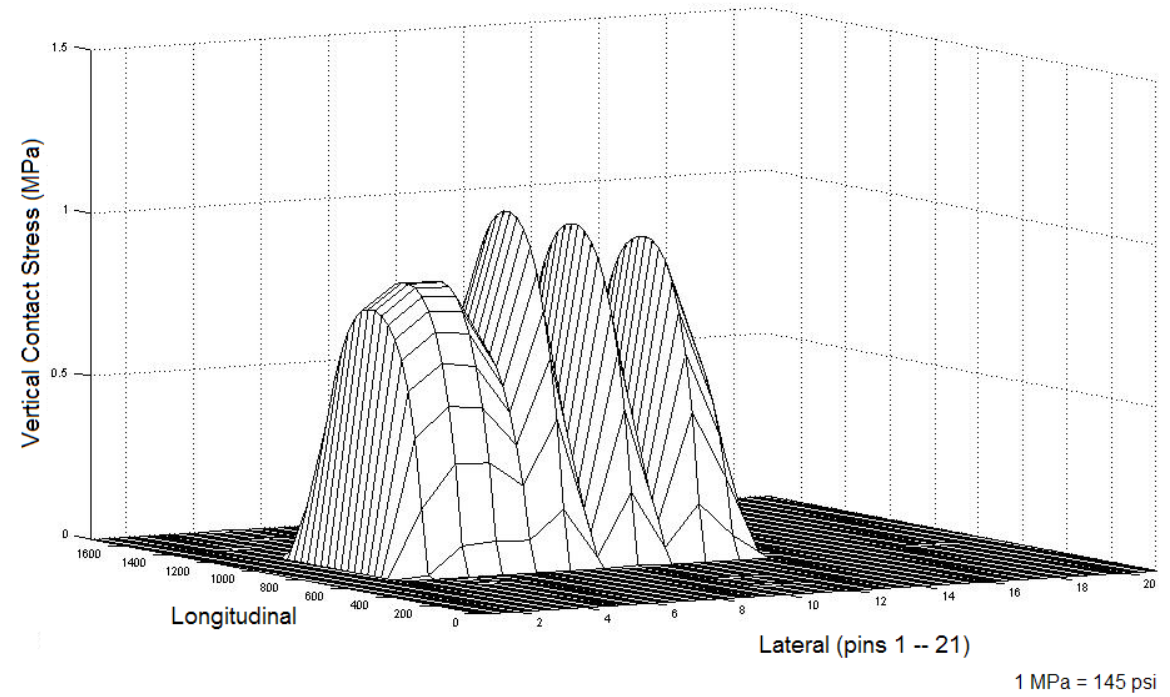

Figure C24. Measured Vertical Contact Stress Distribution for 215/75R17.5 Radial Tested at a Tire Load of 4000 lb and an Inflation Pressure of 115 psi.

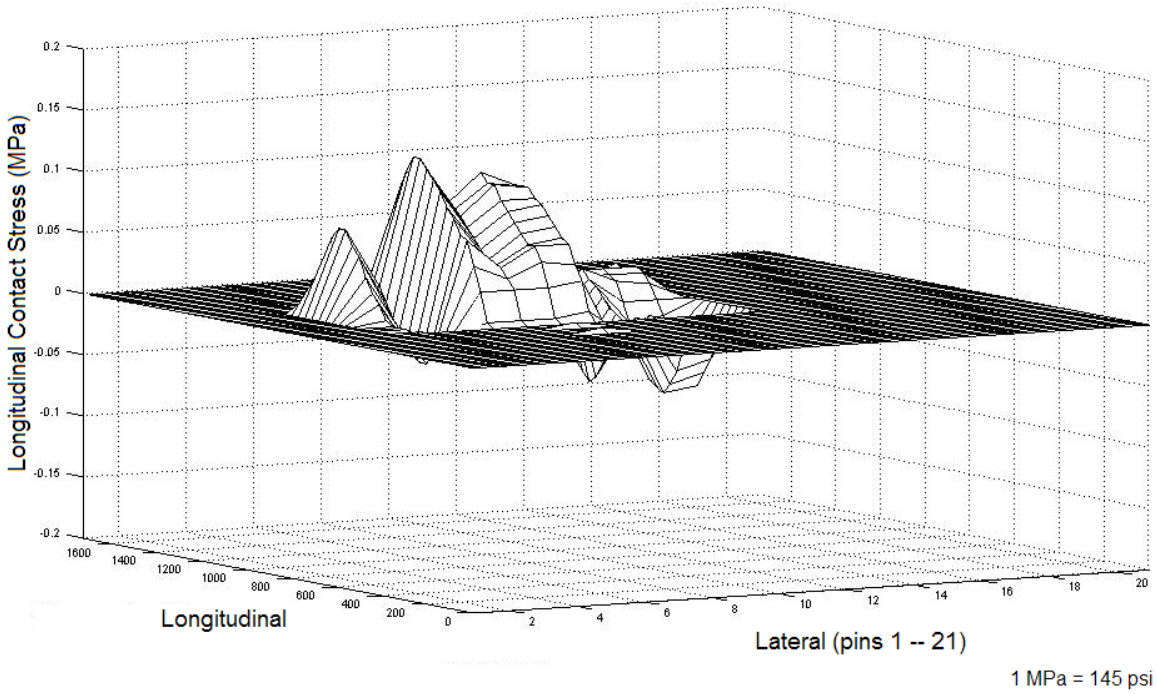

Figure C25. Measured Longitudinal Contact Stress Distribution for 215/75R17.5 Radial Tested at a Tire Load of 4000 lb and an Inflation Pressure of 130 psi.

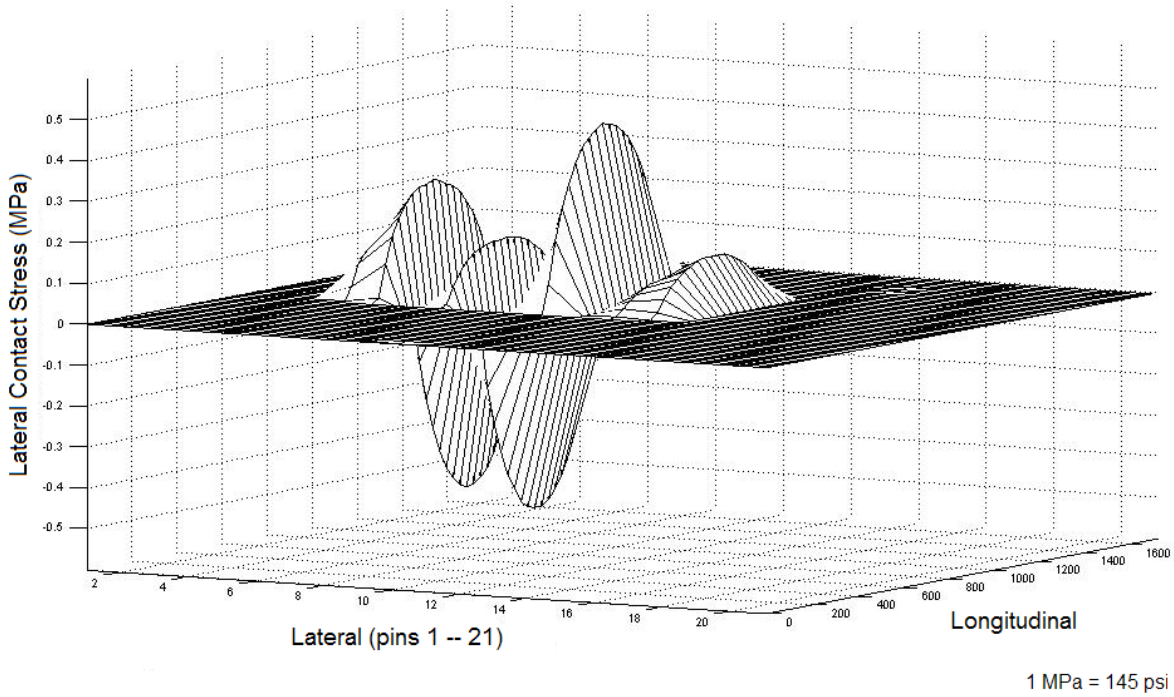

Figure C26. Measured Lateral Contact Stress Distribution for 215/75R17.5 Radial Tested at a Tire Load of 4000 lb and an Inflation Pressure of 130 psi.

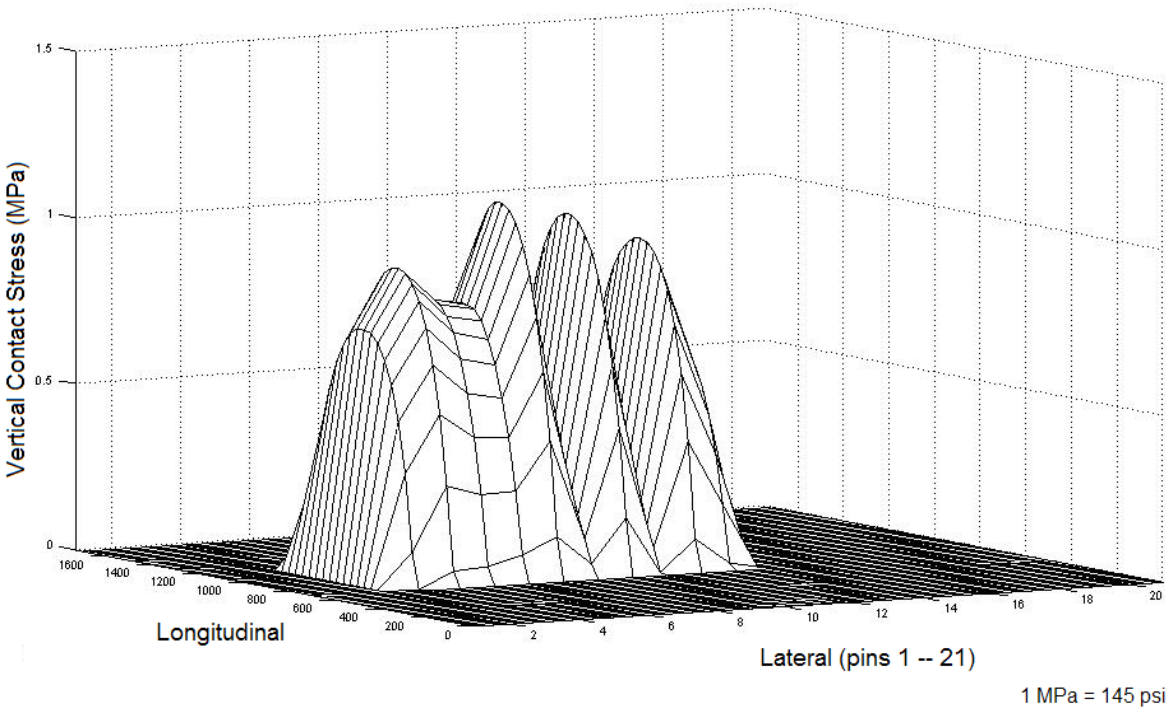

Figure C27. Measured Vertical Contact Stress Distribution for 215/75R17.5 Radial Tested at a Tire Load of 4000 lb and an Inflation Pressure of 130 psi.

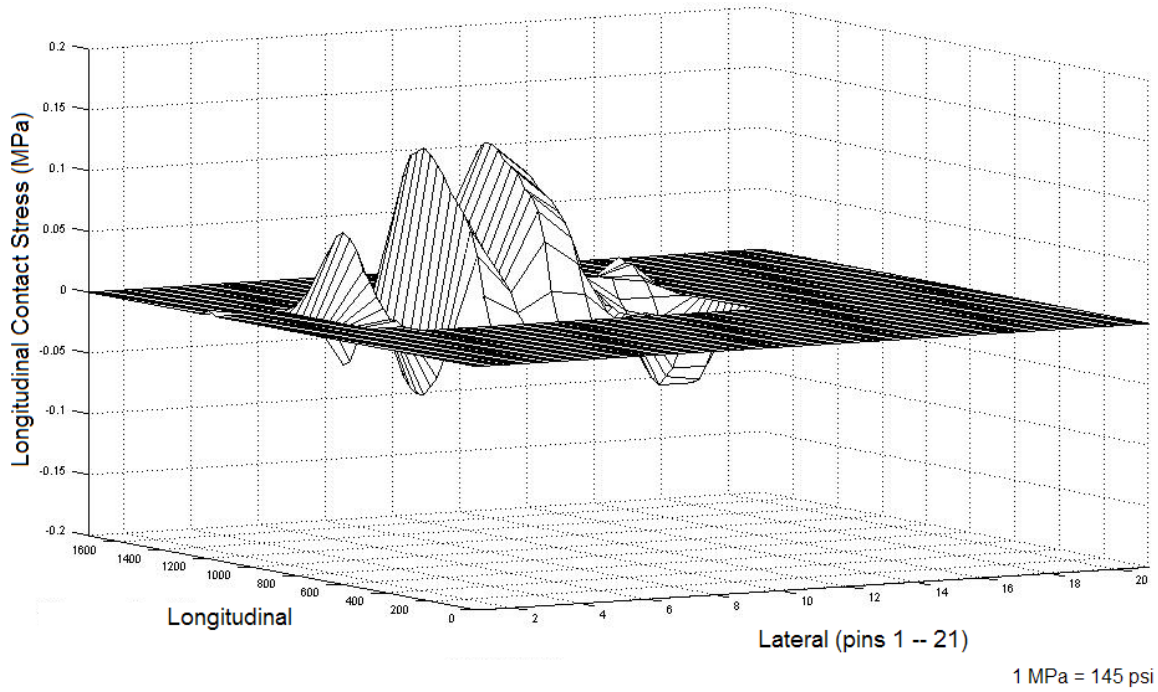

Figure C28. Measured Longitudinal Contact Stress Distribution for 215/75R17.5 Radial Tested at a Tire Load of 4000 lb and an Inflation Pressure of 145 psi.

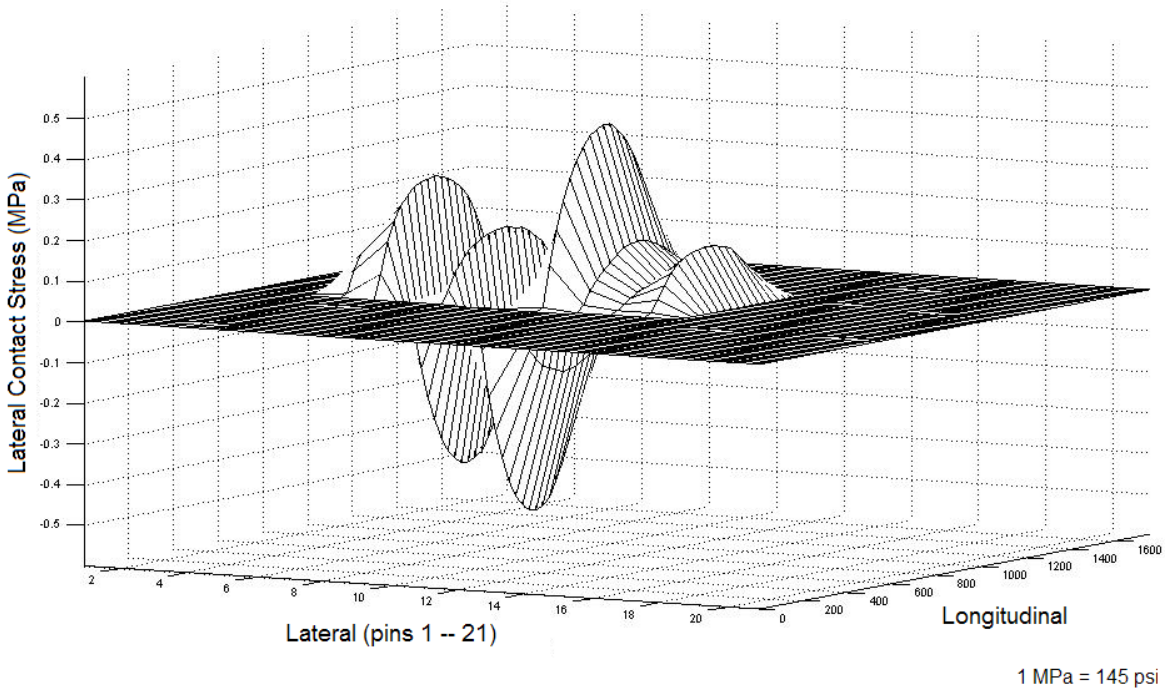

Figure C29. Measured Lateral Contact Stress Distribution for 215/75R17.5 Radial Tested at a Tire Load of 4000 lb and an Inflation Pressure of 145 psi.

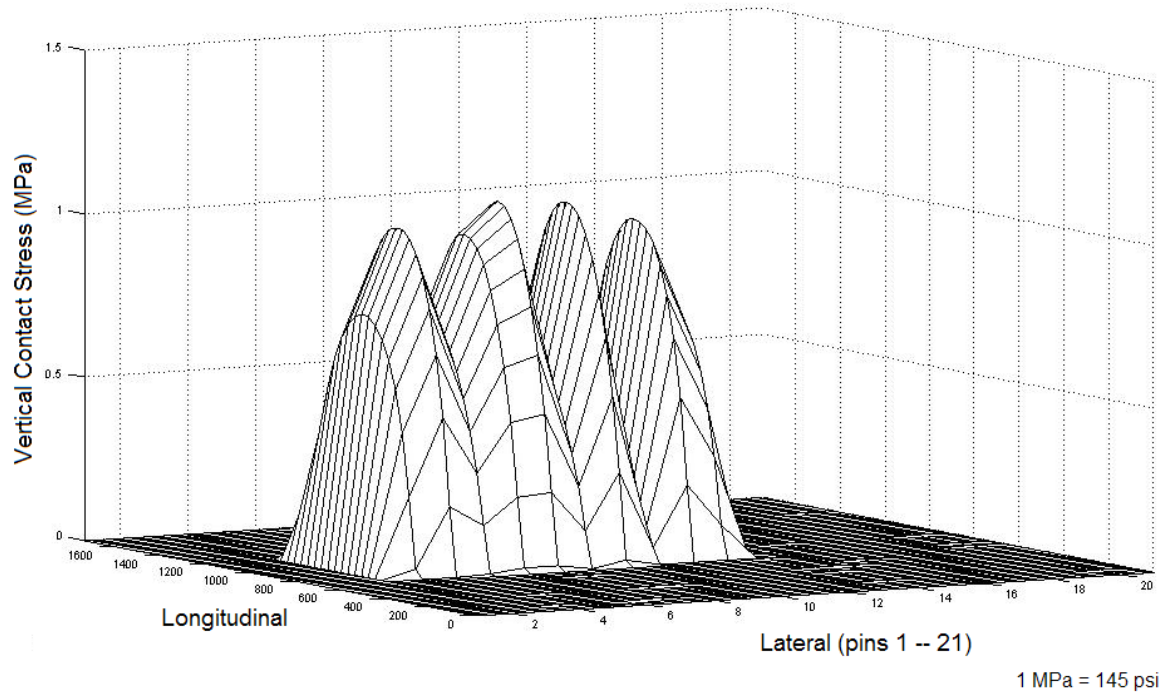

Figure C30. Measured Vertical Contact Stress Distribution for 215/75R17.5 Radial Tested at a Tire Load of 4000 lb and an Inflation Pressure of 145 psi.

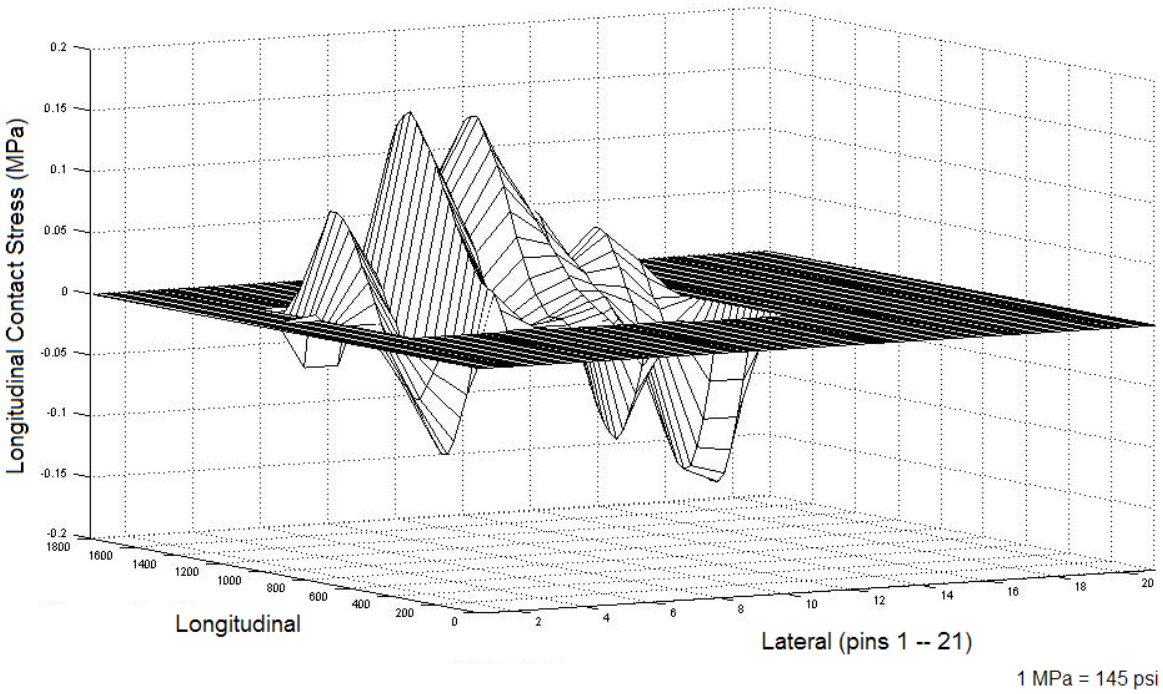

Figure C31. Measured Longitudinal Contact Stress Distribution for 215/75R17.5 Radial Tested at a Tire Load of 5000 lb and an Inflation Pressure of 85 psi.

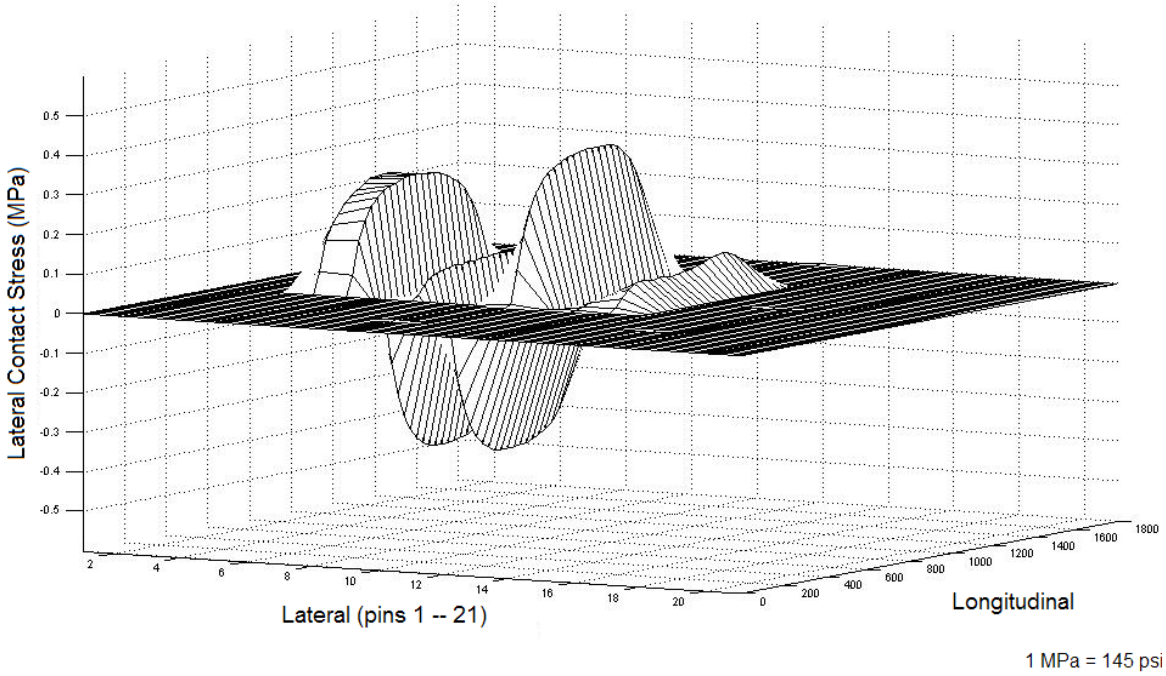

Figure C32. Measured Lateral Contact Stress Distribution for 215/75R17.5 Radial Tested at a Tire Load of 5000 lb and an Inflation Pressure of 85 psi.

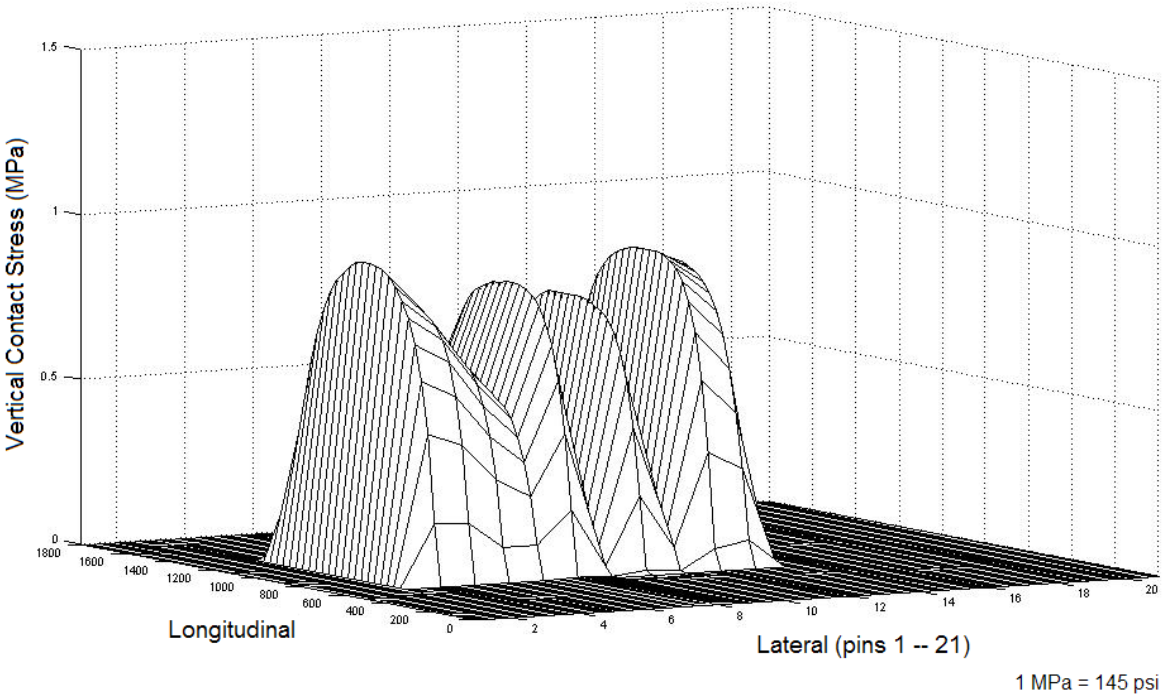

Figure C33. Measured Vertical Contact Stress Distribution for 215/75R17.5 Radial Tested at a Tire Load of 5000 lb and an Inflation Pressure of 85 psi.

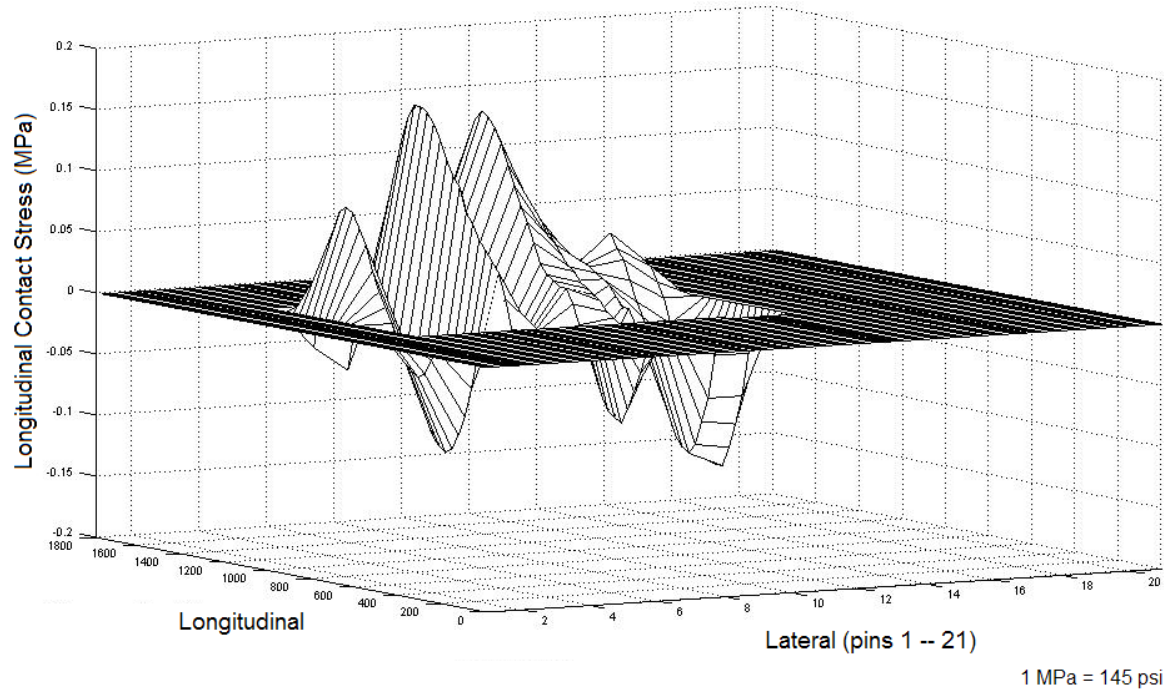

Figure C34. Measured Longitudinal Contact Stress Distribution for 215/75R17.5 Radial Tested at a Tire Load of 5000 lb and an Inflation Pressure of 100 psi.

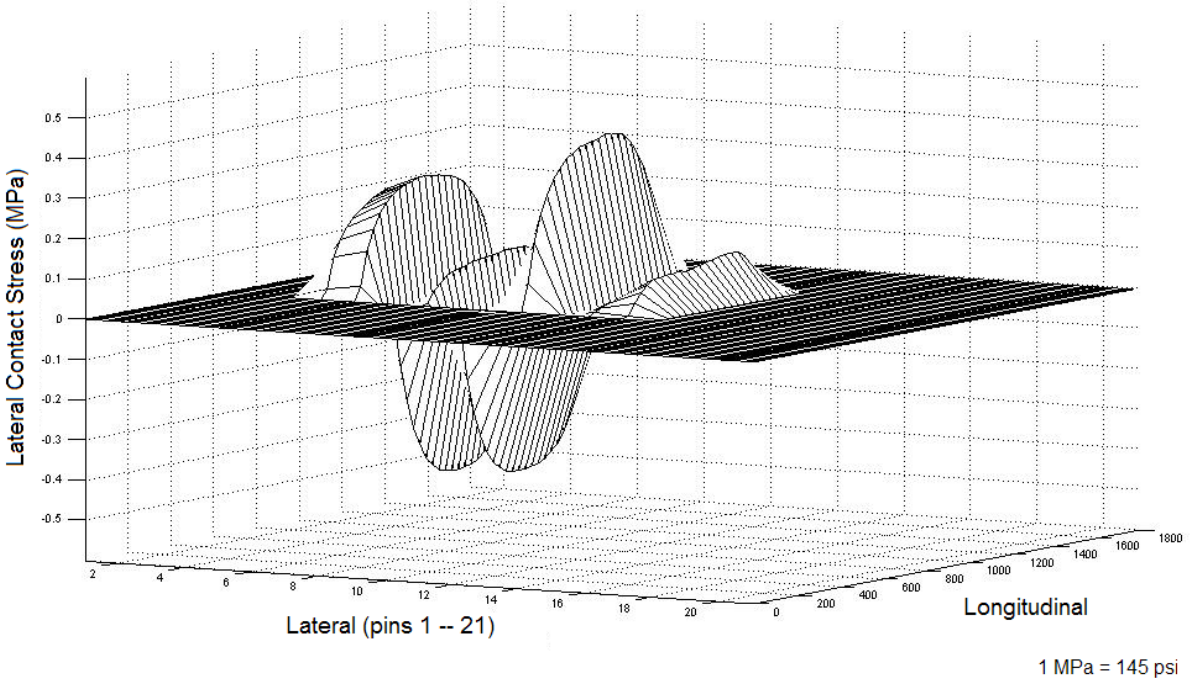

Figure C35. Measured Lateral Contact Stress Distribution for 215/75R17.5 Radial Tested at a Tire Load of 5000 lb and an Inflation Pressure of 100 psi.

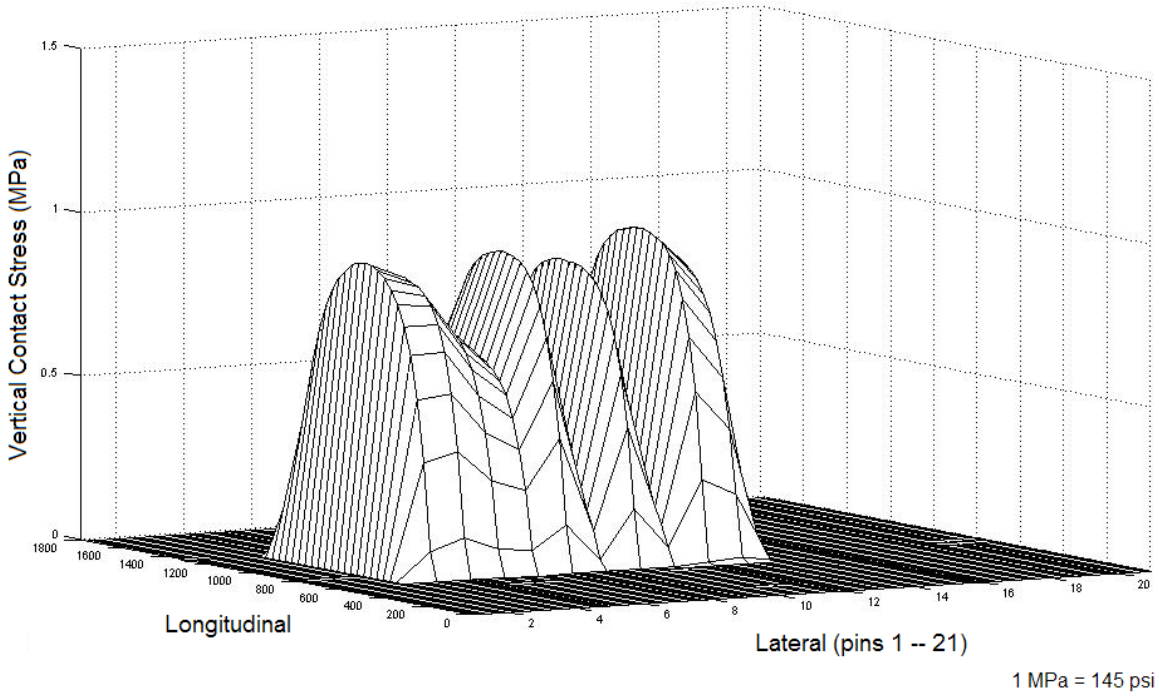

Figure C36. Measured Vertical Contact Stress Distribution for 215/75R17.5 Radial Tested at a Tire Load of 5000 lb and an Inflation Pressure of 100 psi.

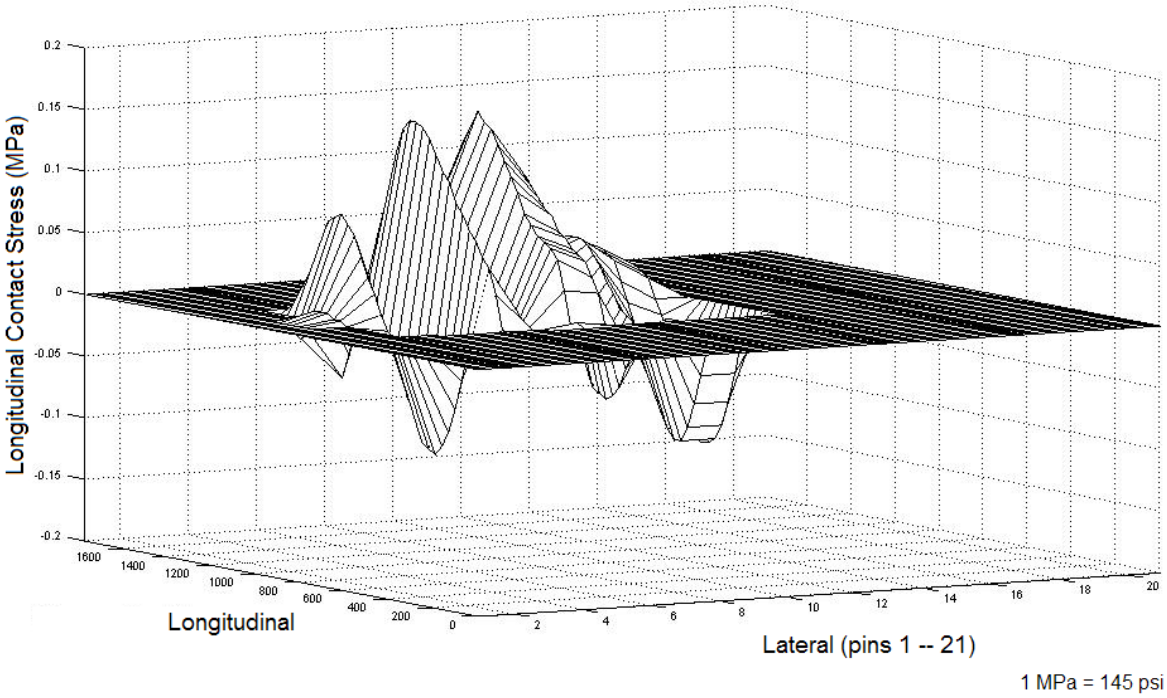

Figure C37. Measured Longitudinal Contact Stress Distribution for 215/75R17.5 Radial Tested at a Tire Load of 5000 lb and an Inflation Pressure of 115 psi.

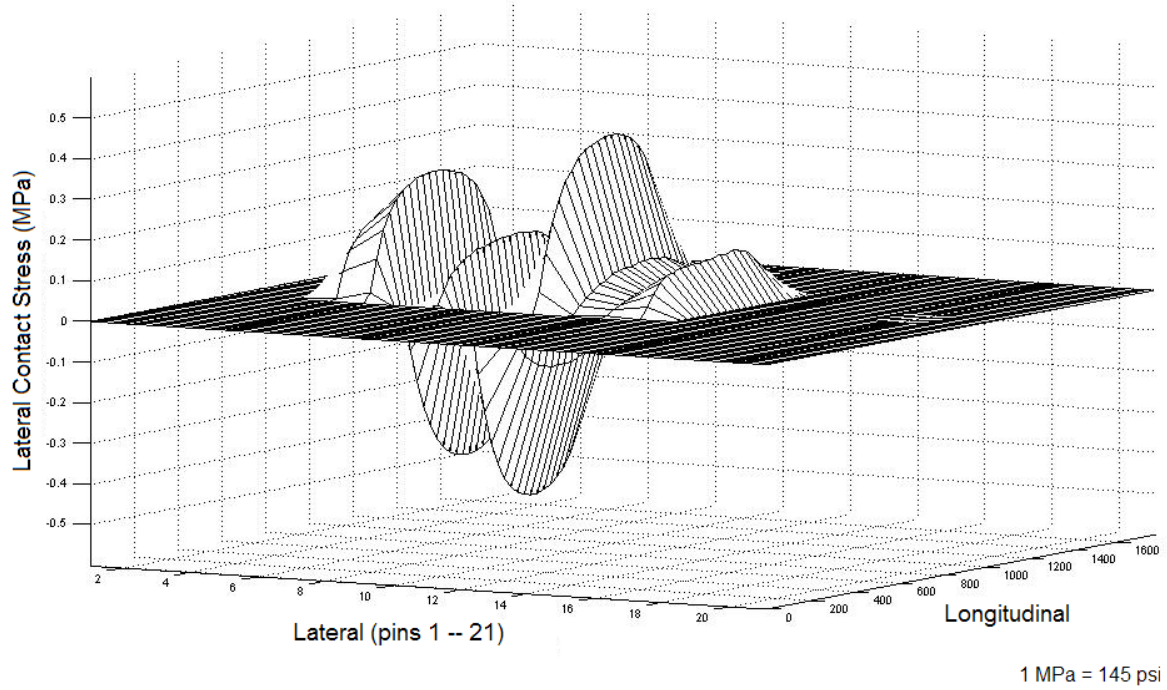

Figure C38. Measured Lateral Contact Stress Distribution for 215/75R17.5 Radial Tested at a Tire Load of 5000 lb and an Inflation Pressure of 115 psi.

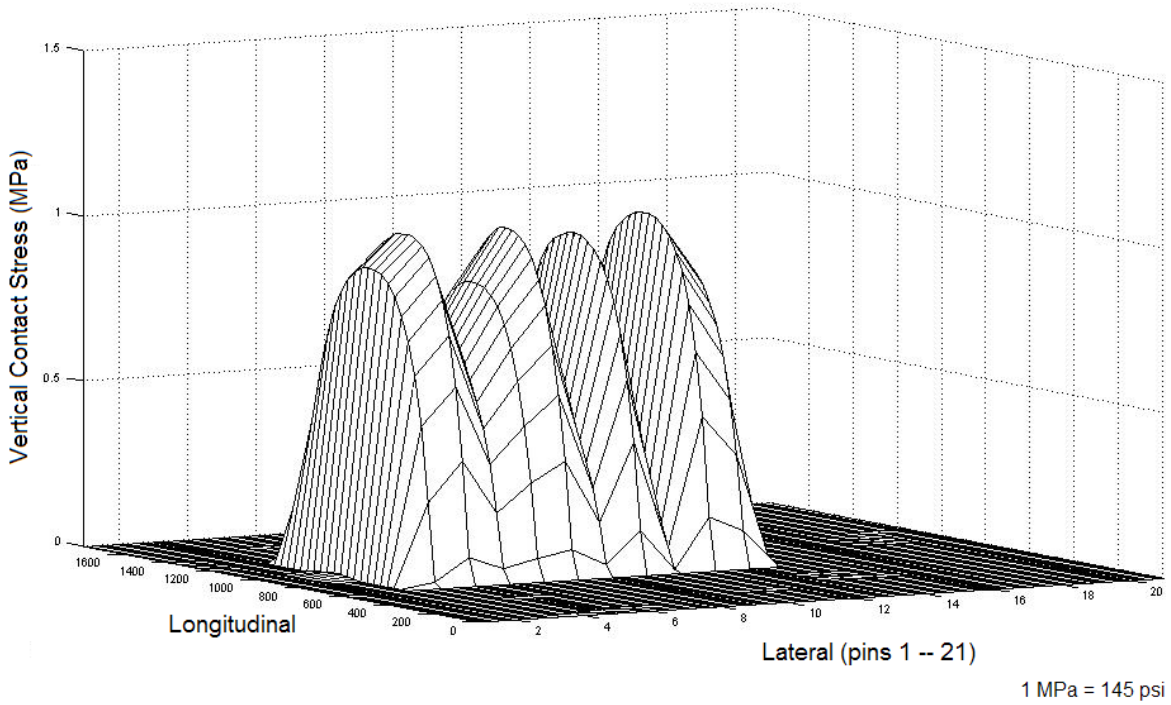

Figure C39. Measured Vertical Contact Stress Distribution for 215/75R17.5 Radial Tested at a Tire Load of 5000 lb and an Inflation Pressure of 115 psi.

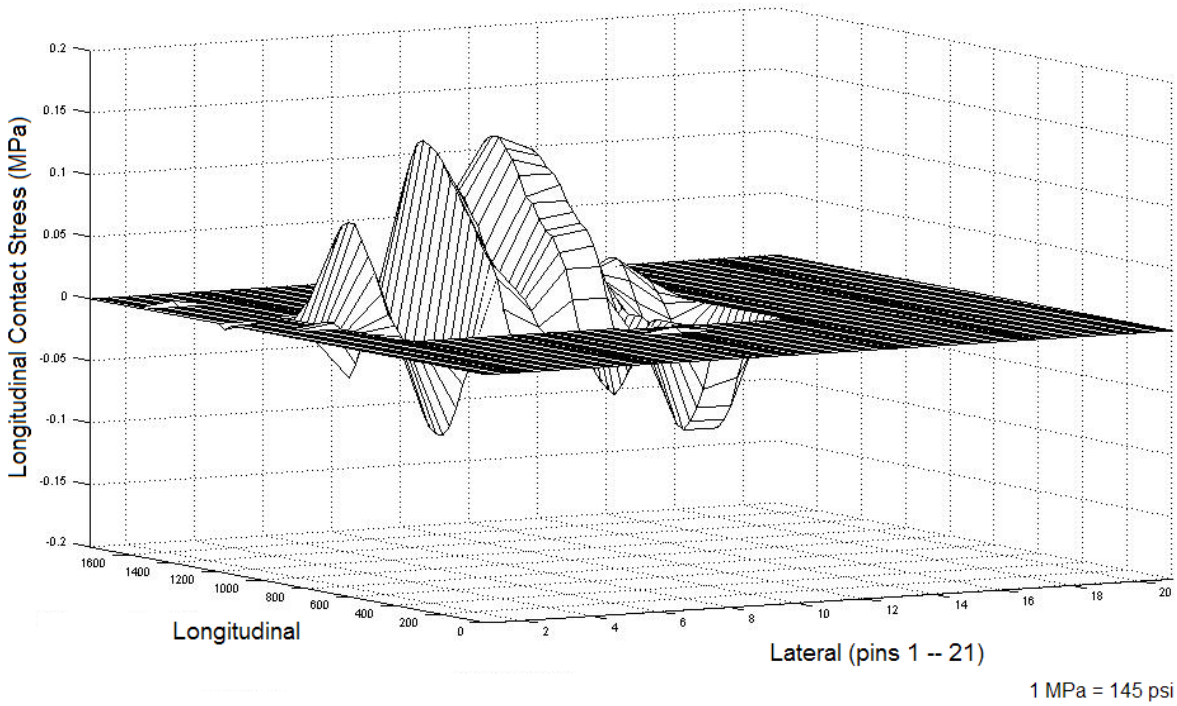

Figure C40. Measured Longitudinal Contact Stress Distribution for 215/75R17.5 Radial Tested at a Tire Load of 5000 lb and an Inflation Pressure of 130 psi.

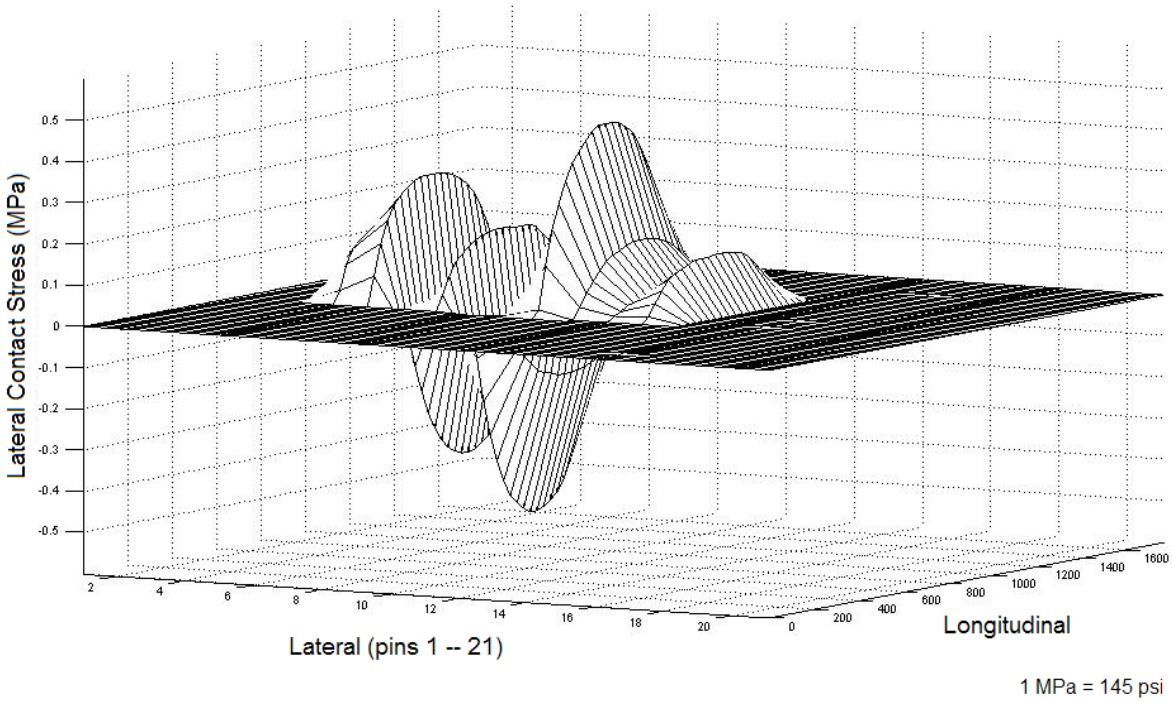

Figure C41. Measured Lateral Contact Stress Distribution for 215/75R17.5 Radial Tested at a Tire Load of 5000 lb and an Inflation Pressure of 130 psi.

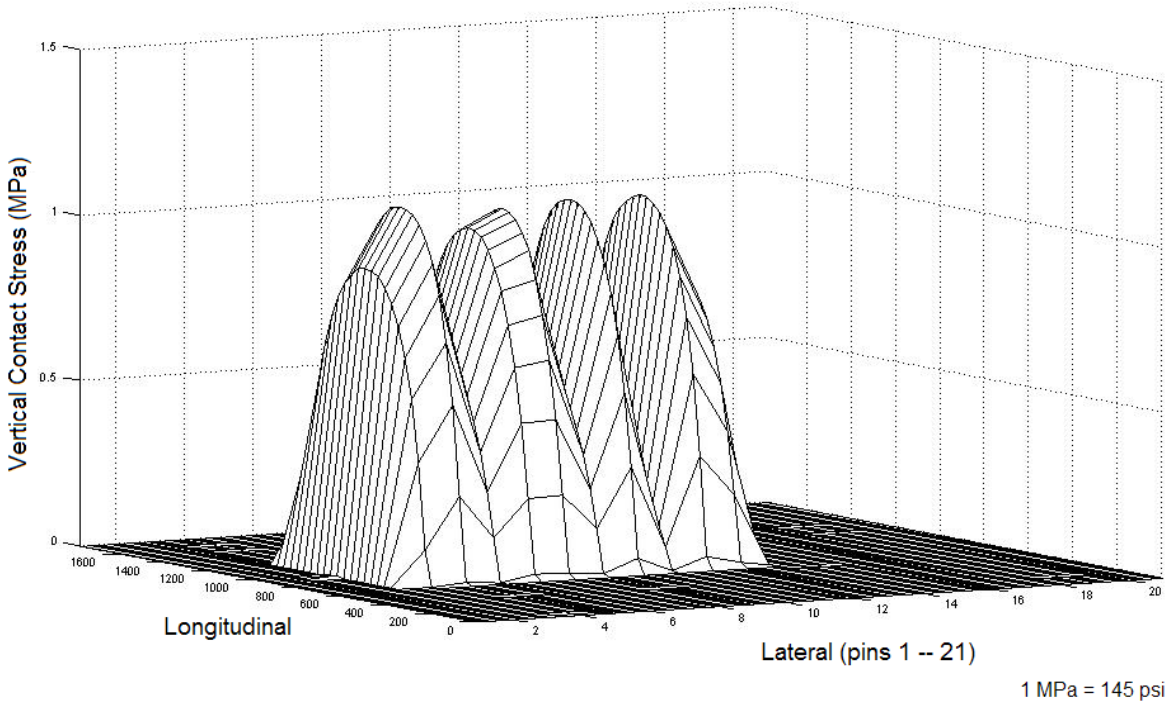

Figure C42. Measured Vertical Contact Stress Distribution for 215/75R17.5 Radial Tested at a Tire Load of 5000 lb and an Inflation Pressure of 130 psi.

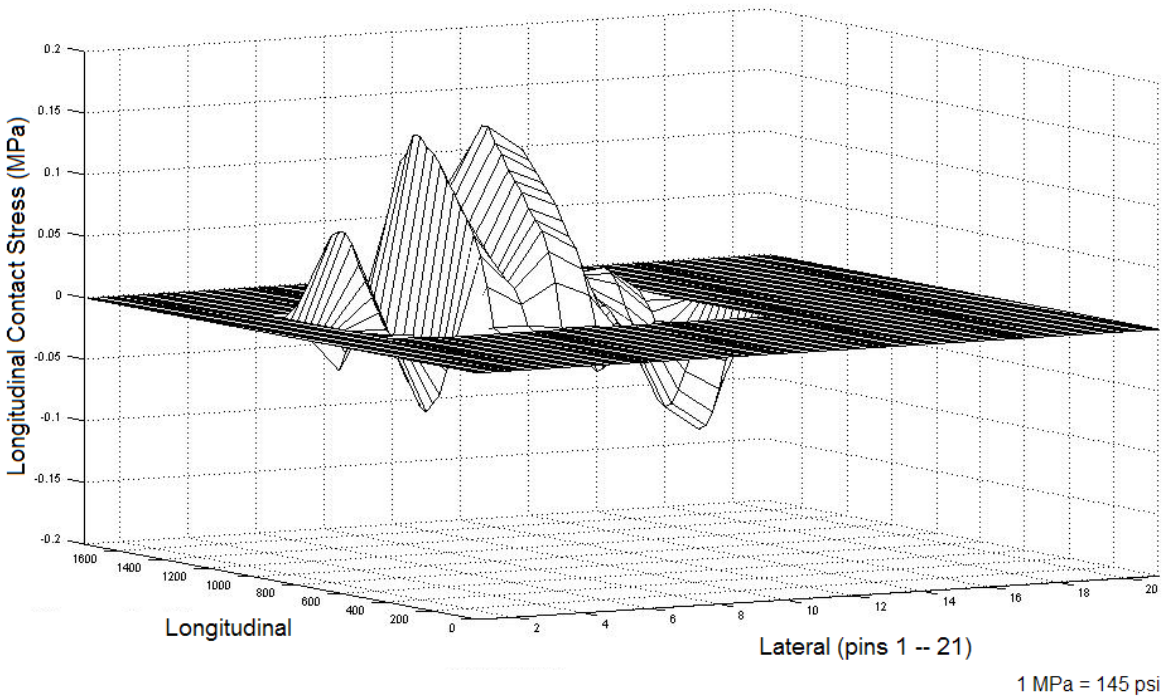

Figure C43. Measured Longitudinal Contact Stress Distribution for 215/75R17.5 Radial Tested at a Tire Load of 5000 lb and an Inflation Pressure of 145 psi.

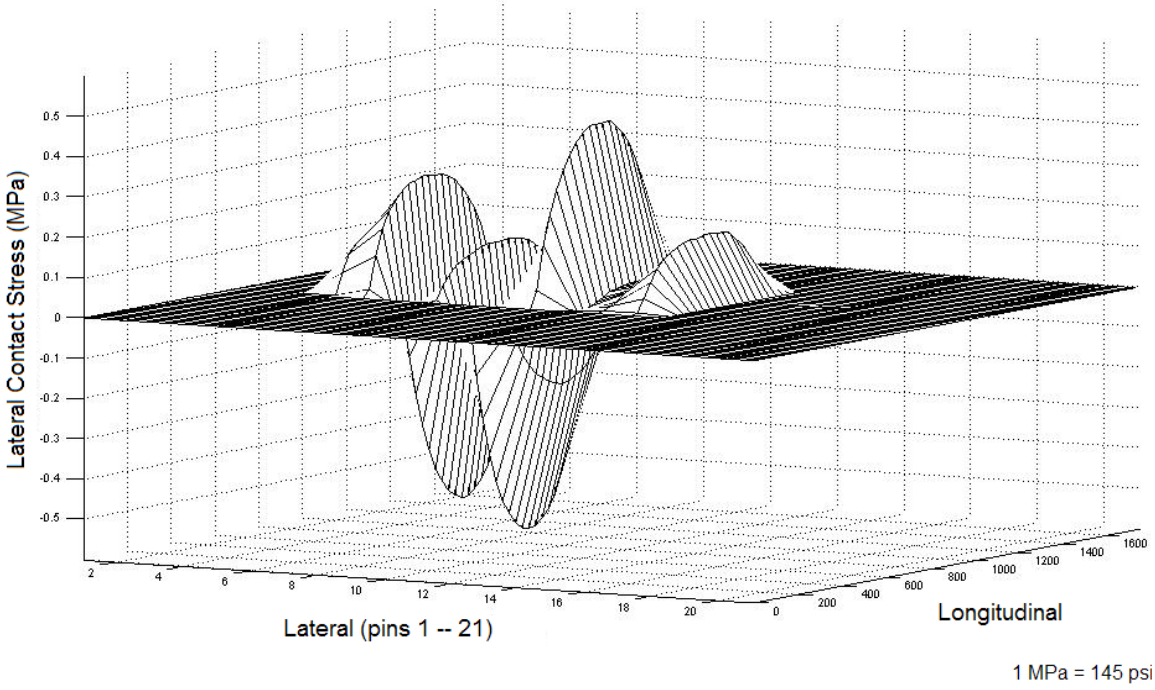

Figure C44. Measured Lateral Contact Stress Distribution for 215/75R17.5 Radial Tested at a Tire Load of 5000 lb and an Inflation Pressure of 145 psi.

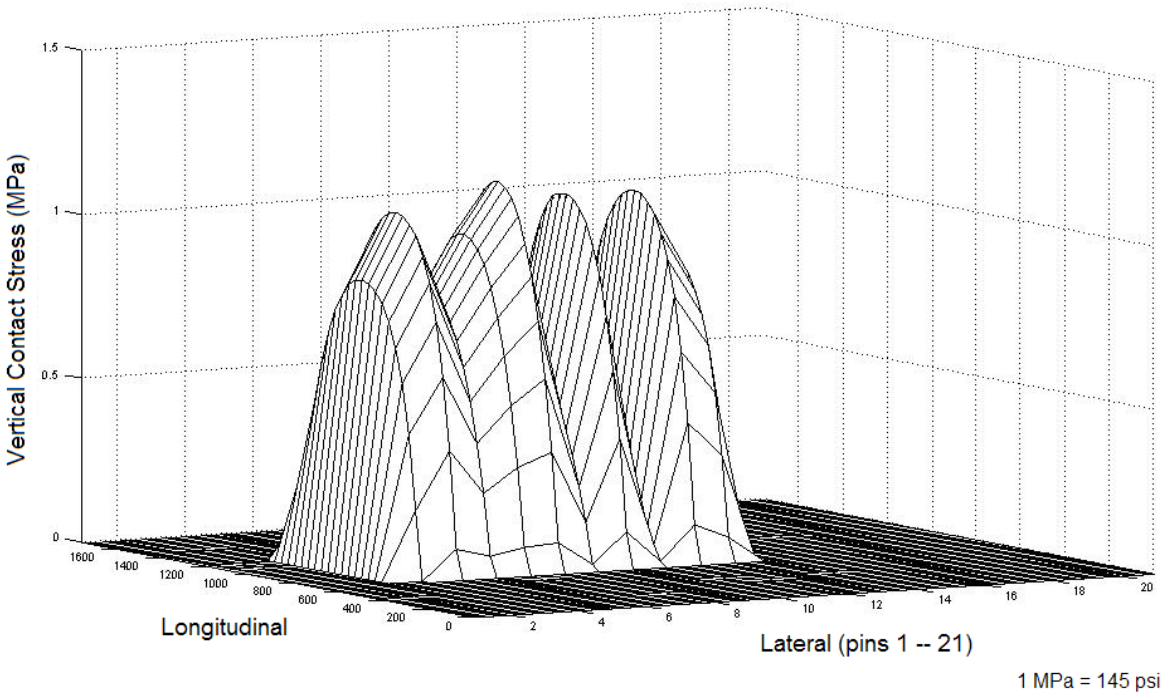

Figure C45. Measured Vertical Contact Stress Distribution for 215/75R17.5 Radial Tested at a Tire Load of 5000 lb and an Inflation Pressure of 145 psi.

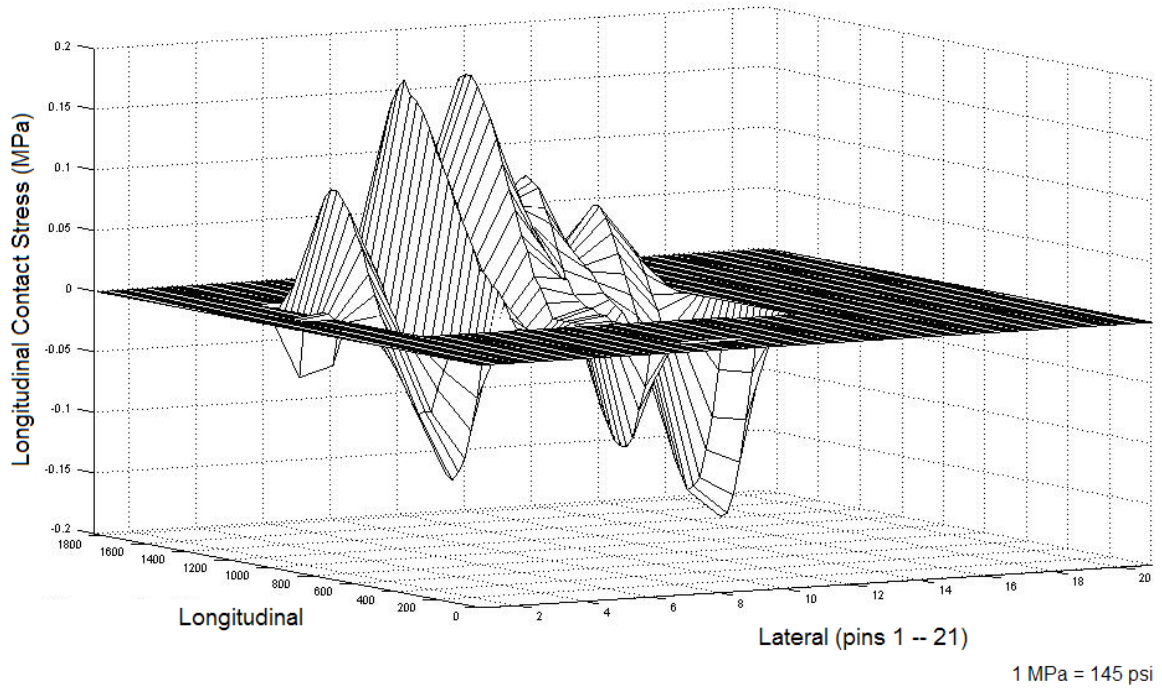

Figure C46. Measured Longitudinal Contact Stress Distribution for 215/75R17.5 Radial Tested at a Tire Load of 6000 lb and an Inflation Pressure of 85 psi.

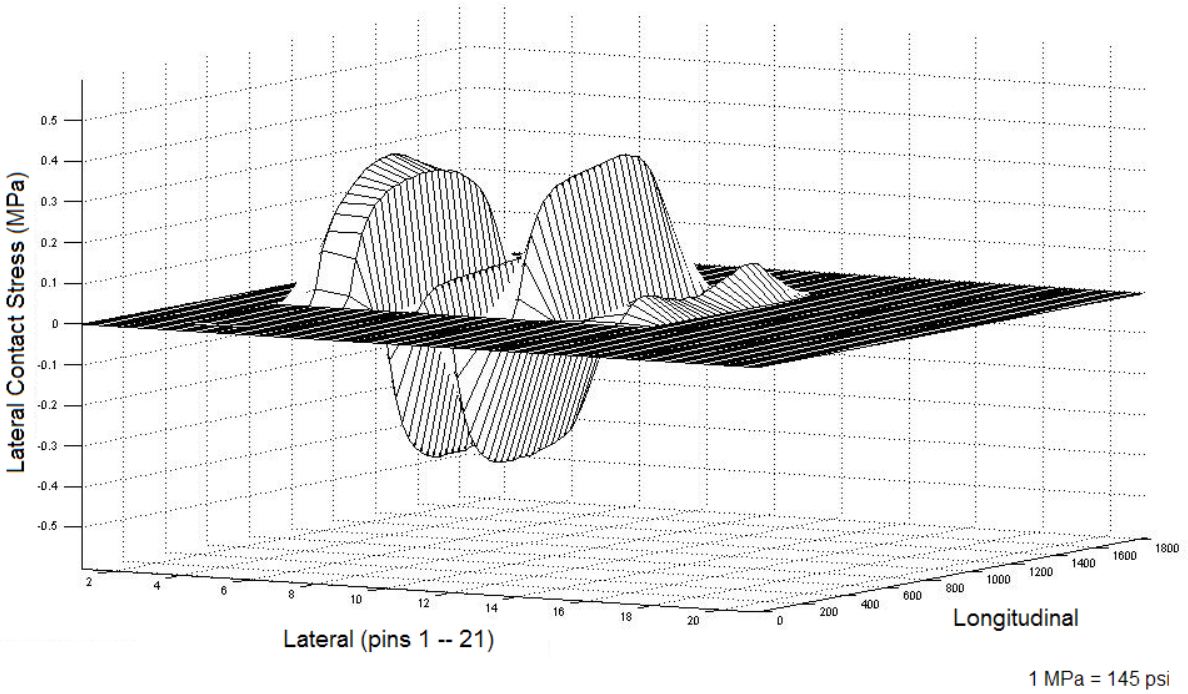

Figure C47. Measured Lateral Contact Stress Distribution for 215/75R17.5 Radial Tested at a Tire Load of 6000 lb and an Inflation Pressure of 85 psi.

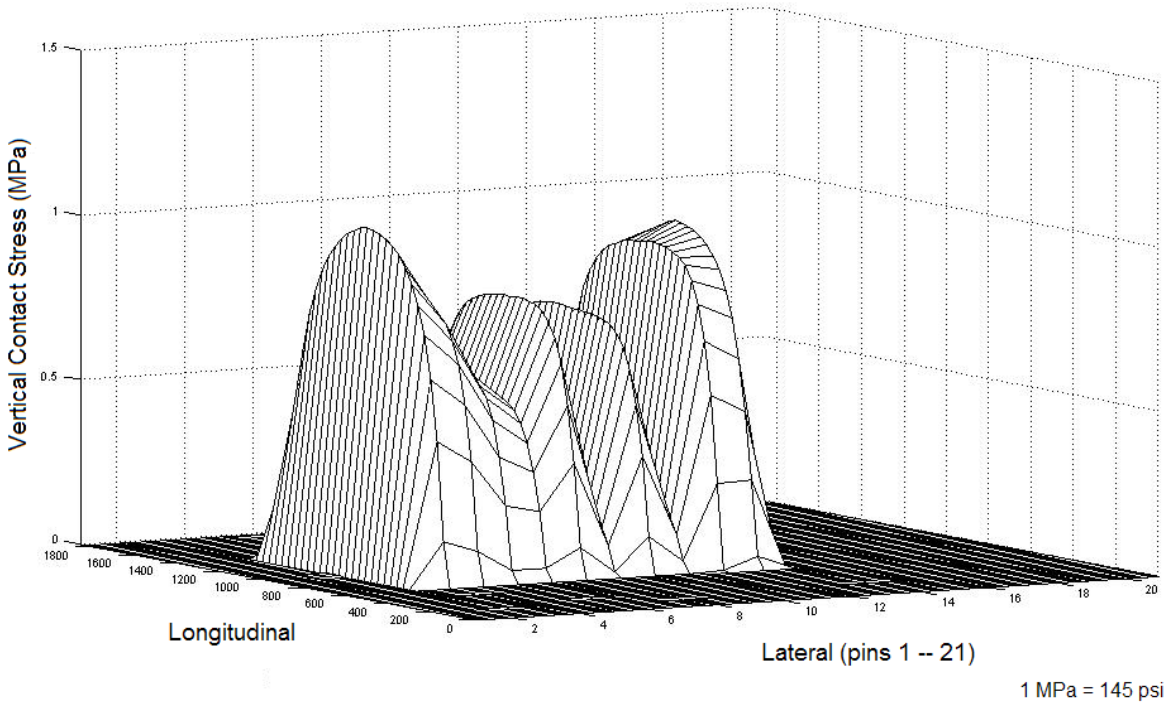

Figure C48. Measured Vertical Contact Stress Distribution for 215/75R17.5 Radial Tested at a Tire Load of 6000 lb and an Inflation Pressure of 85 psi.

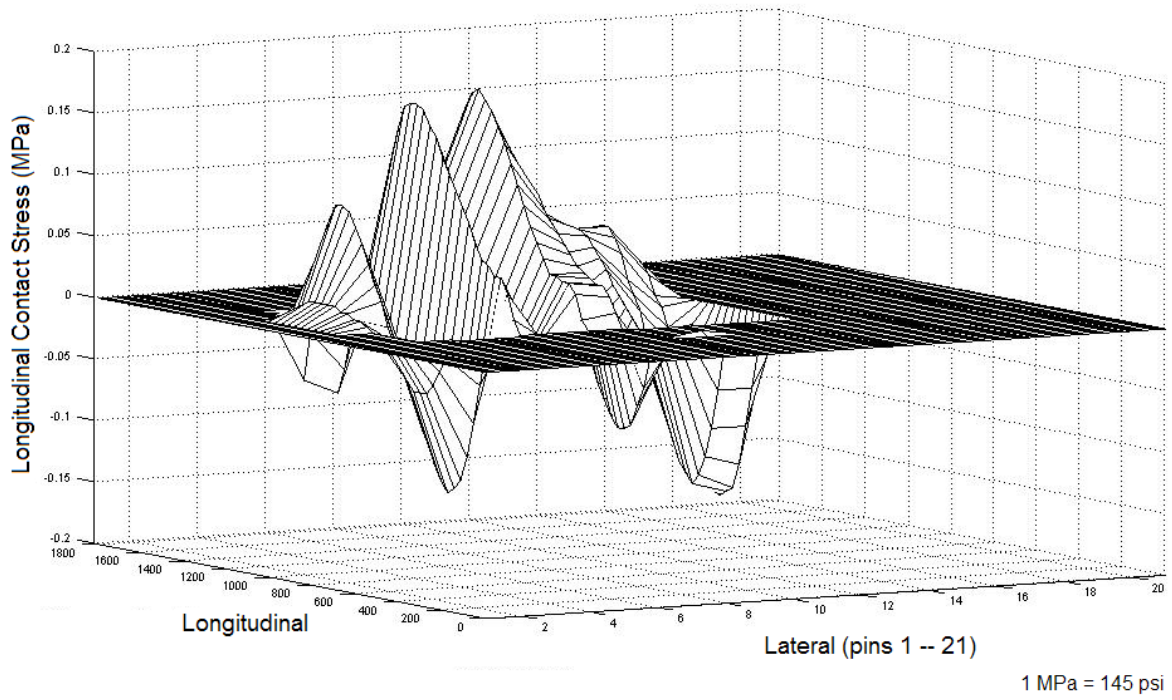

Figure C49. Measured Longitudinal Contact Stress Distribution for 215/75R17.5 Radial Tested at a Tire Load of 6000 lb and an Inflation Pressure of 100 psi.

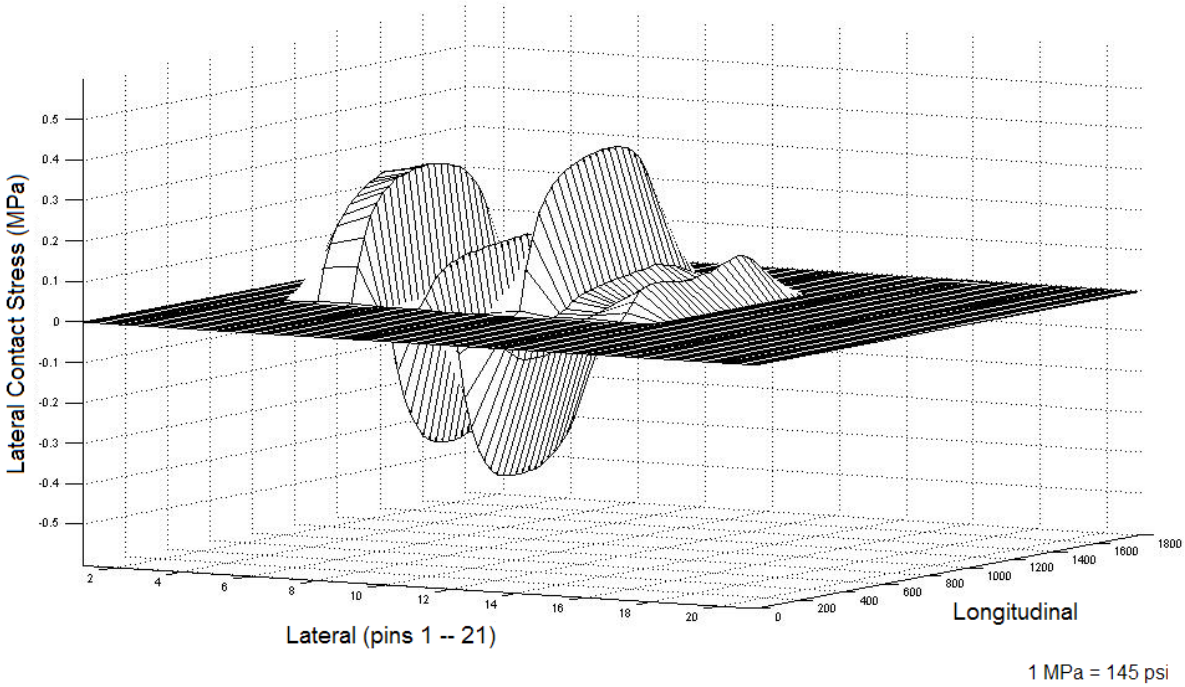

Figure C50. Measured Lateral Contact Stress Distribution for 215/75R17.5 Radial Tested at a Tire Load of 6000 lb and an Inflation Pressure of 100 psi.

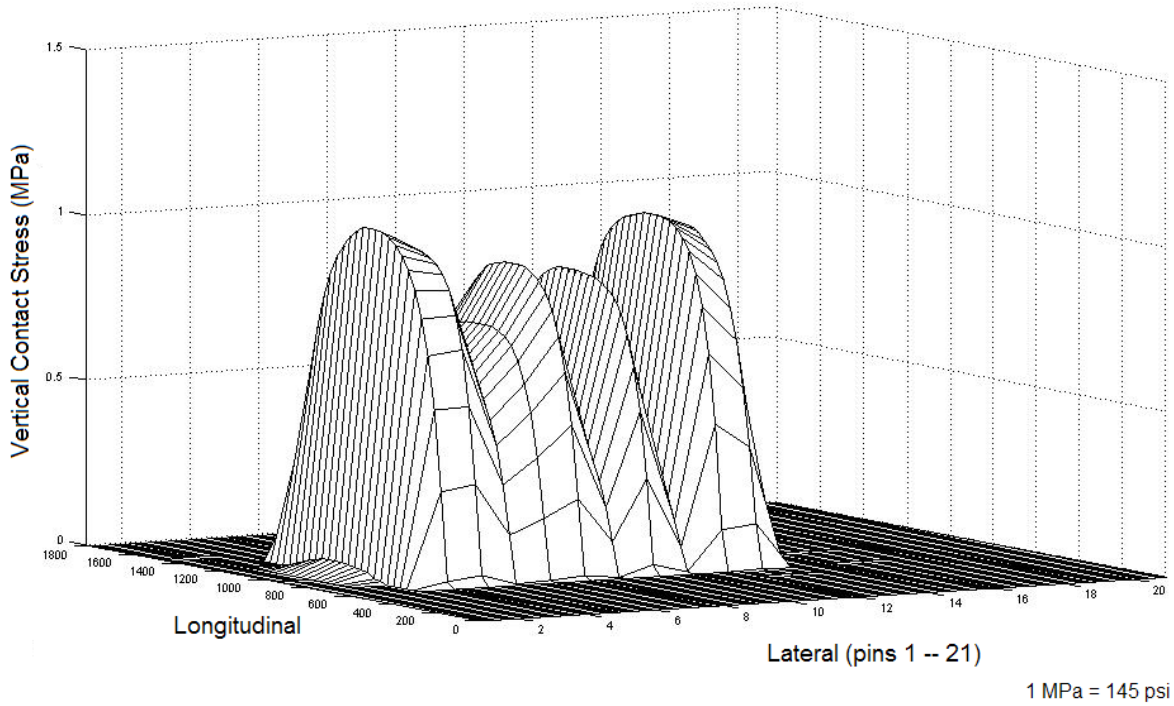

Figure C51. Measured Vertical Contact Stress Distribution for 215/75R17.5 Radial Tested at a Tire Load of 6000 lb and an Inflation Pressure of 100 psi.

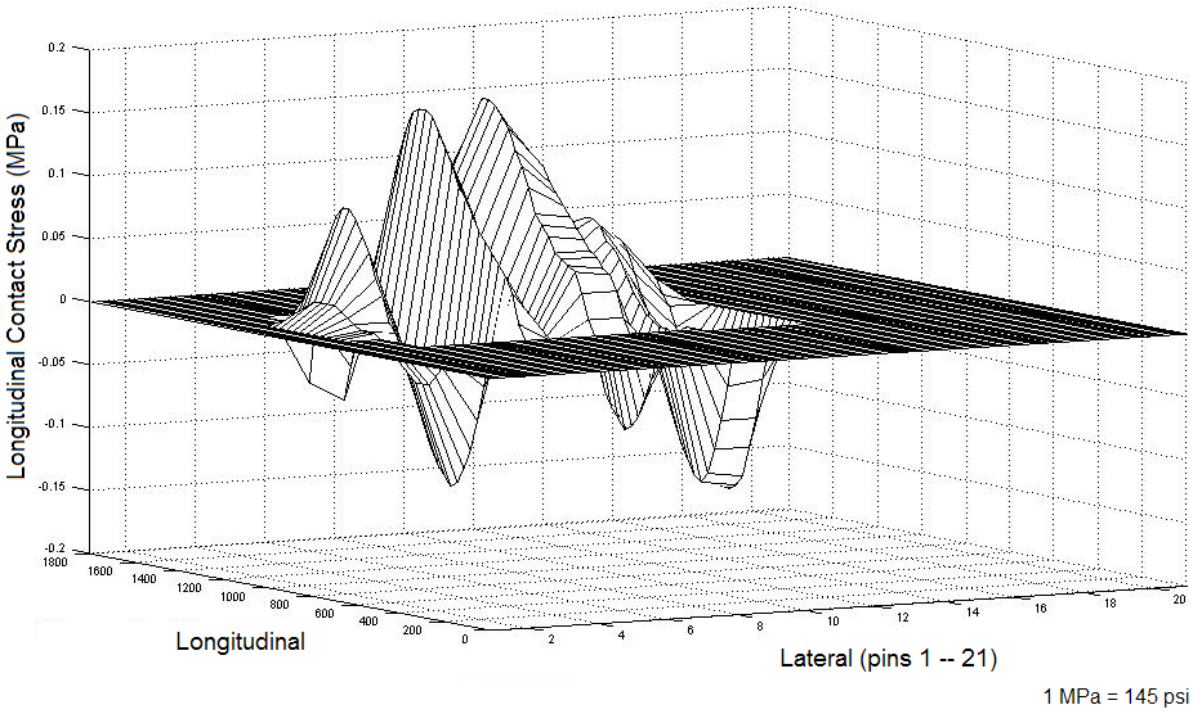

Figure C52. Measured Longitudinal Contact Stress Distribution for 215/75R17.5 Radial Tested at a Tire Load of 6000 lb and an Inflation Pressure of 115 psi.

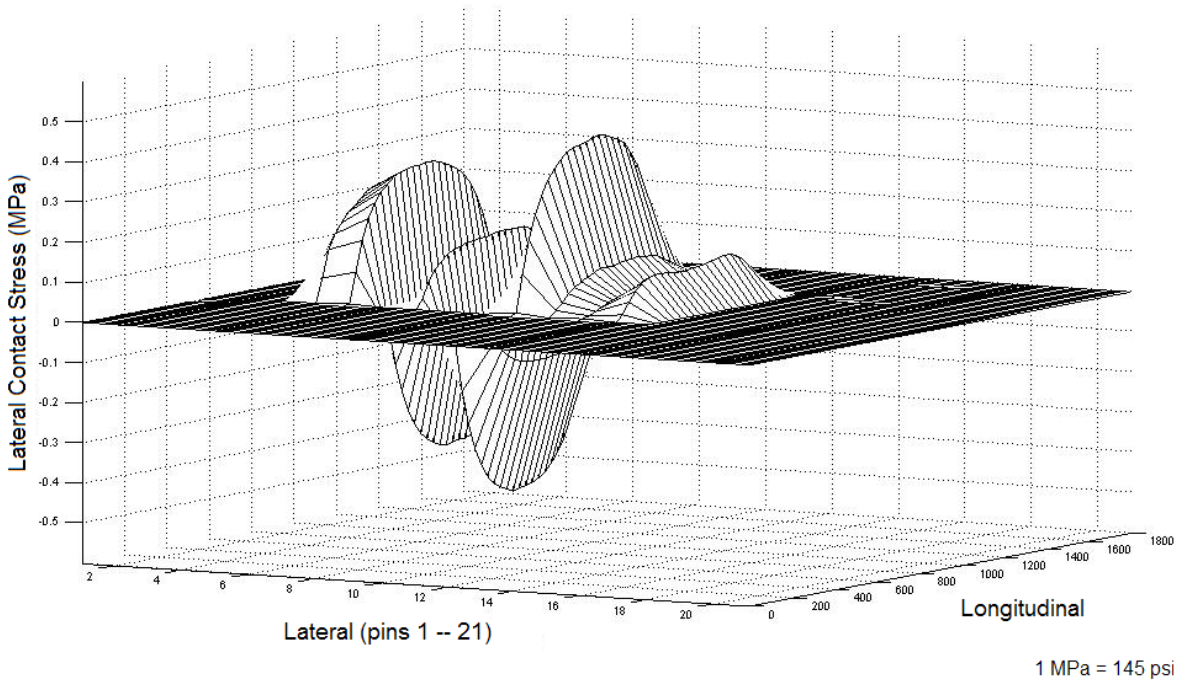

Figure C53. Measured Lateral Contact Stress Distribution for 215/75R17.5 Radial Tested at a Tire Load of 6000 lb and an Inflation Pressure of 115 psi.

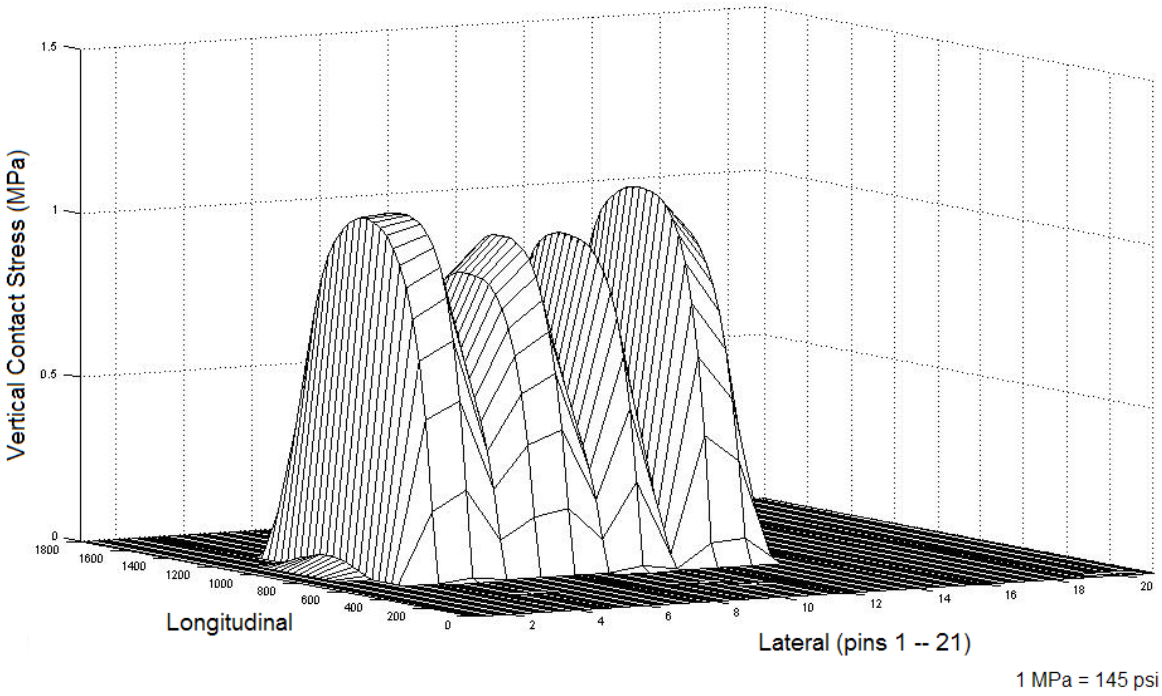

Figure C54. Measured Vertical Contact Stress Distribution for 215/75R17.5 Radial Tested at a Tire Load of 6000 lb and an Inflation Pressure of 115 psi.

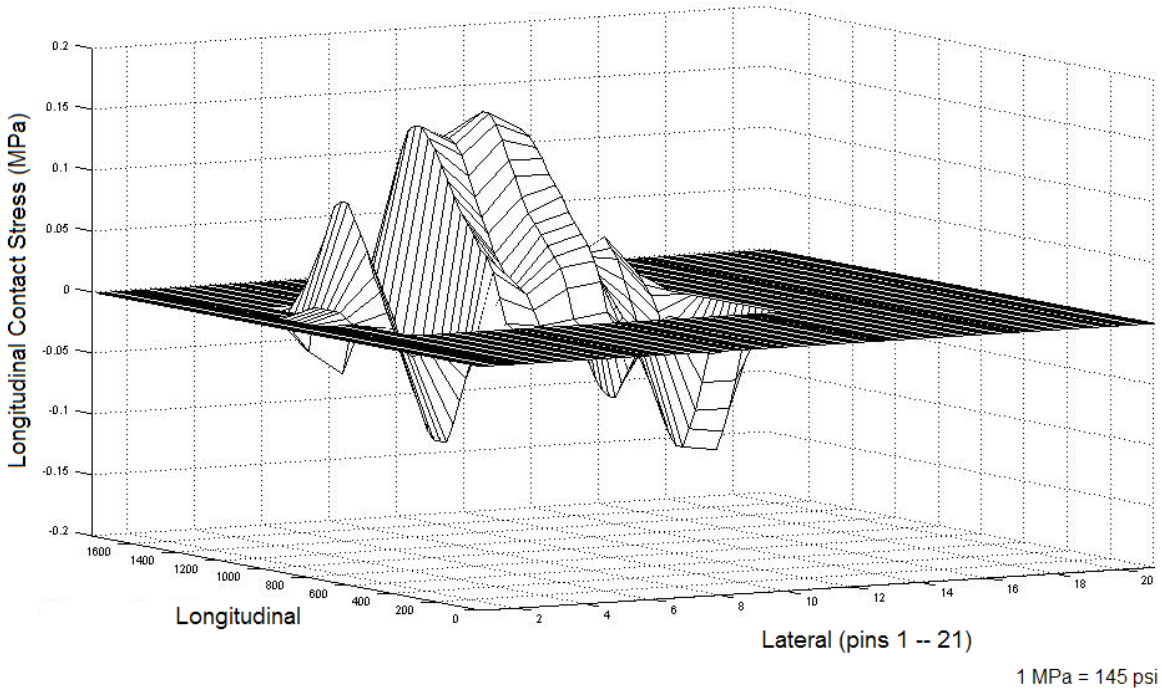

Figure C55. Measured Longitudinal Contact Stress Distribution for 215/75R17.5 Radial Tested at a Tire Load of 6000 lb and an Inflation Pressure of 130 psi.

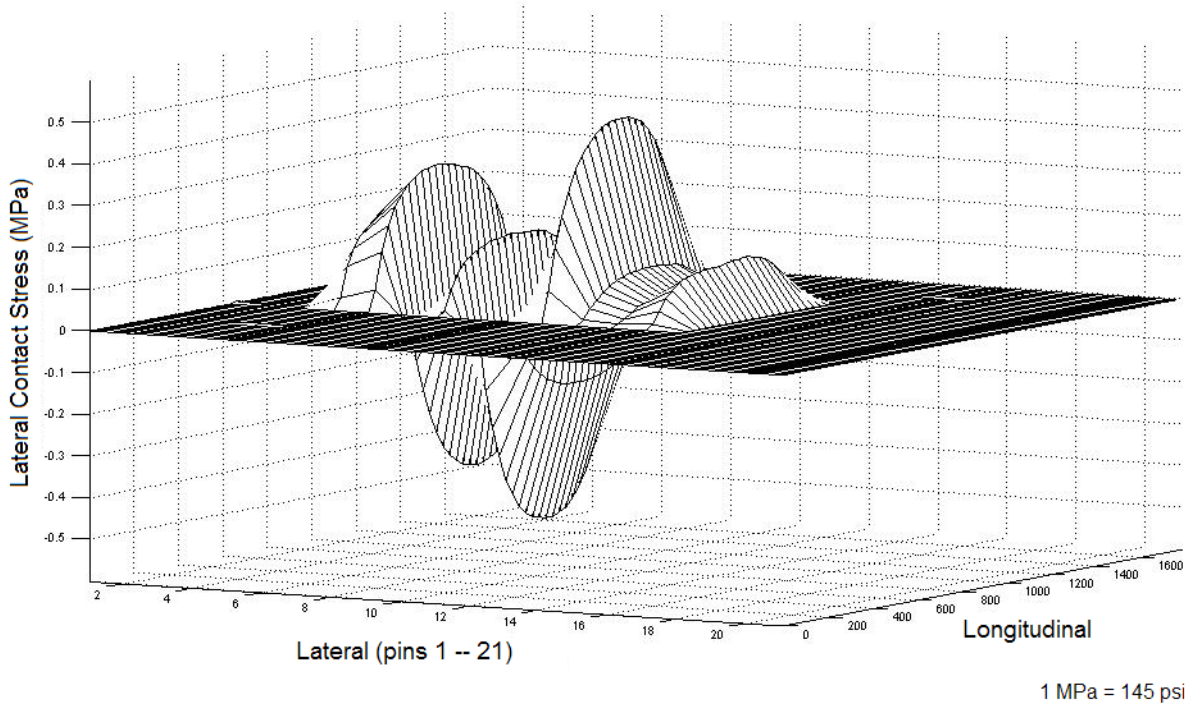

Figure C56. Measured Lateral Contact Stress Distribution for 215/75R17.5 Radial Tested at a Tire Load of 6000 lb and an Inflation Pressure of 130 psi.

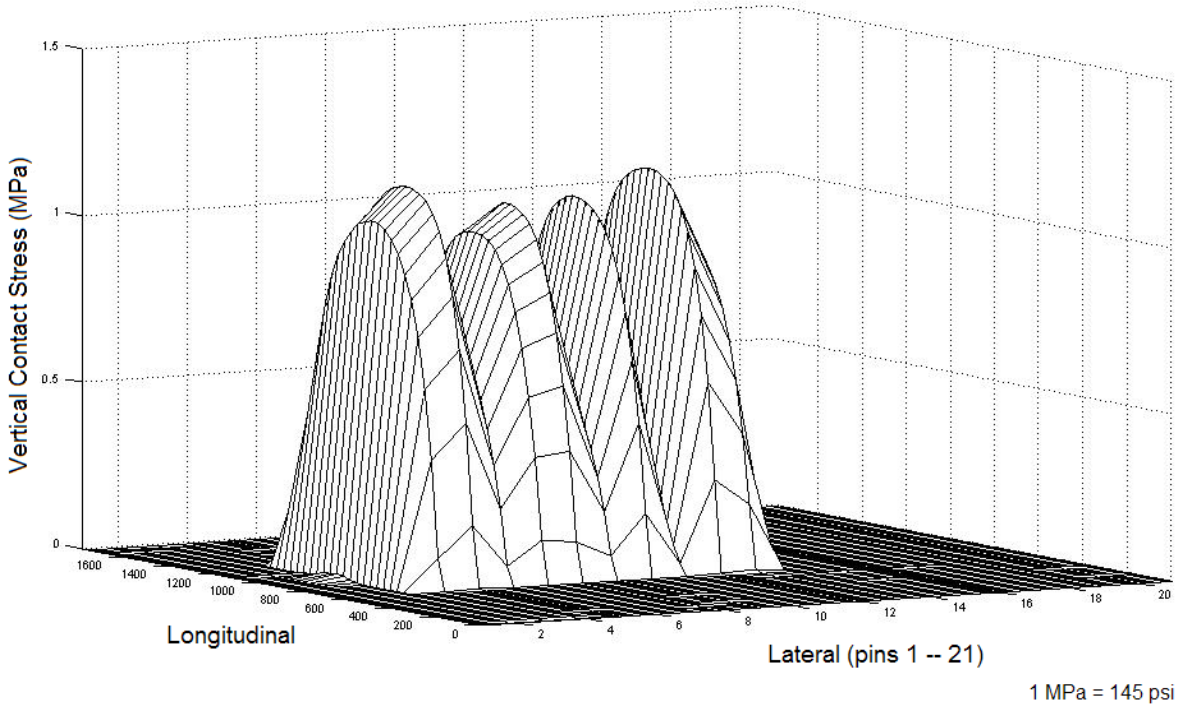

Figure C57. Measured Vertical Contact Stress Distribution for 215/75R17.5 Radial Tested at a Tire Load of 6000 lb and an Inflation Pressure of 130 psi.

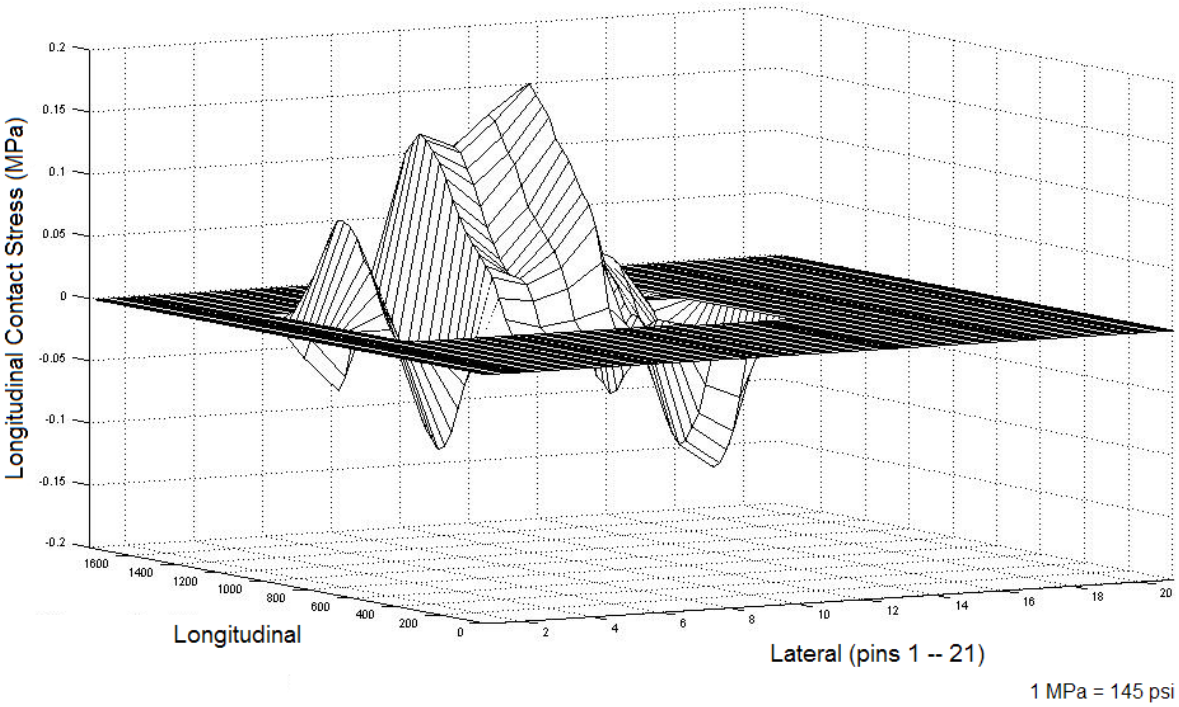

Figure C58. Measured Longitudinal Contact Stress Distribution for 215/75R17.5 Radial Tested at a Tire Load of 6000 lb and an Inflation Pressure of 145 psi.

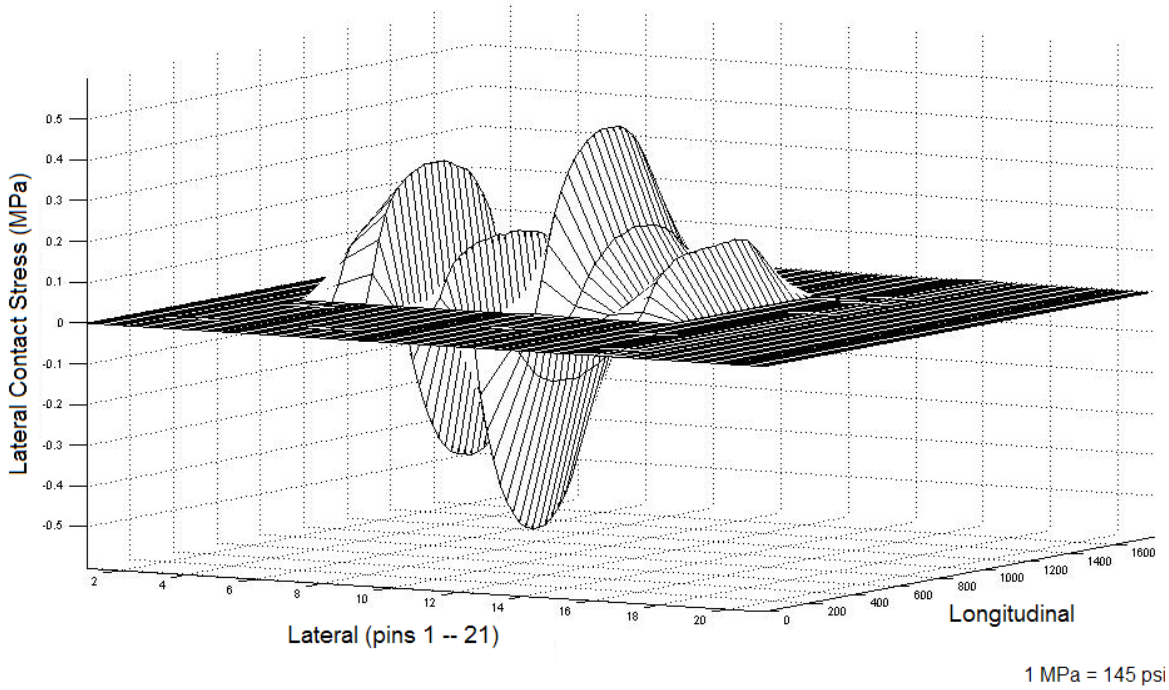

Figure C59. Measured Lateral Contact Stress Distribution for 215/75R17.5 Radial Tested at a Tire Load of 6000 lb and an Inflation Pressure of 145 psi.

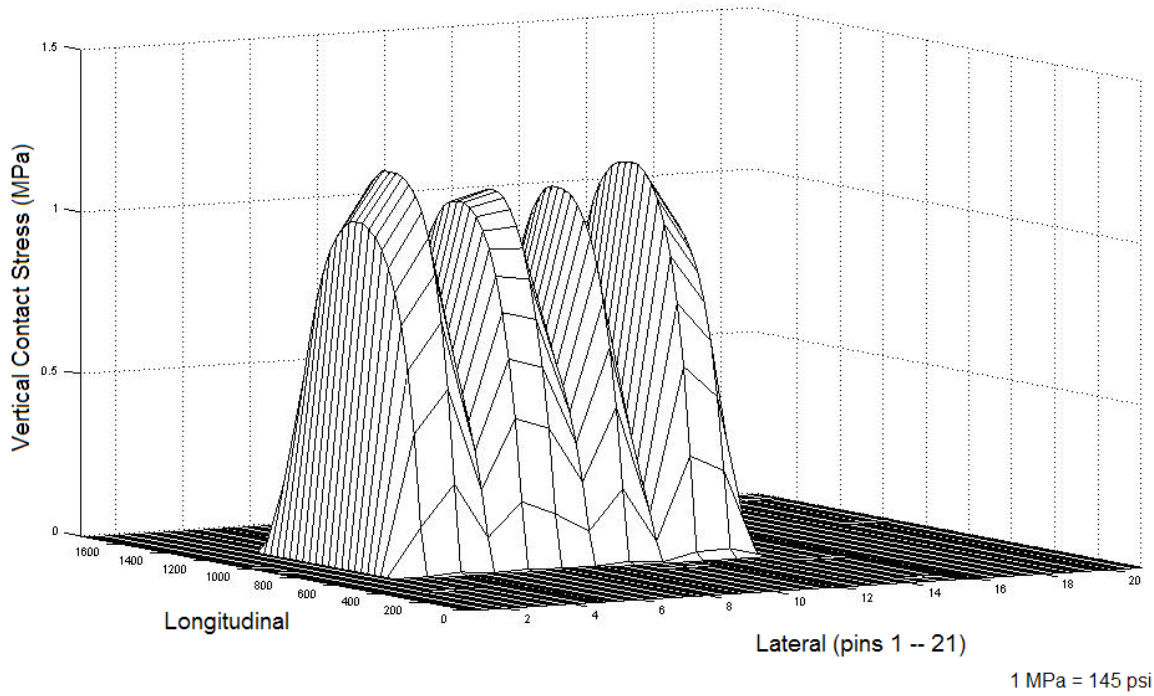

Figure C60. Measured Vertical Contact Stress Distribution for 215/75R17.5 Radial Tested at a Tire Load of 6000 lb and an Inflation Pressure of 145 psi.

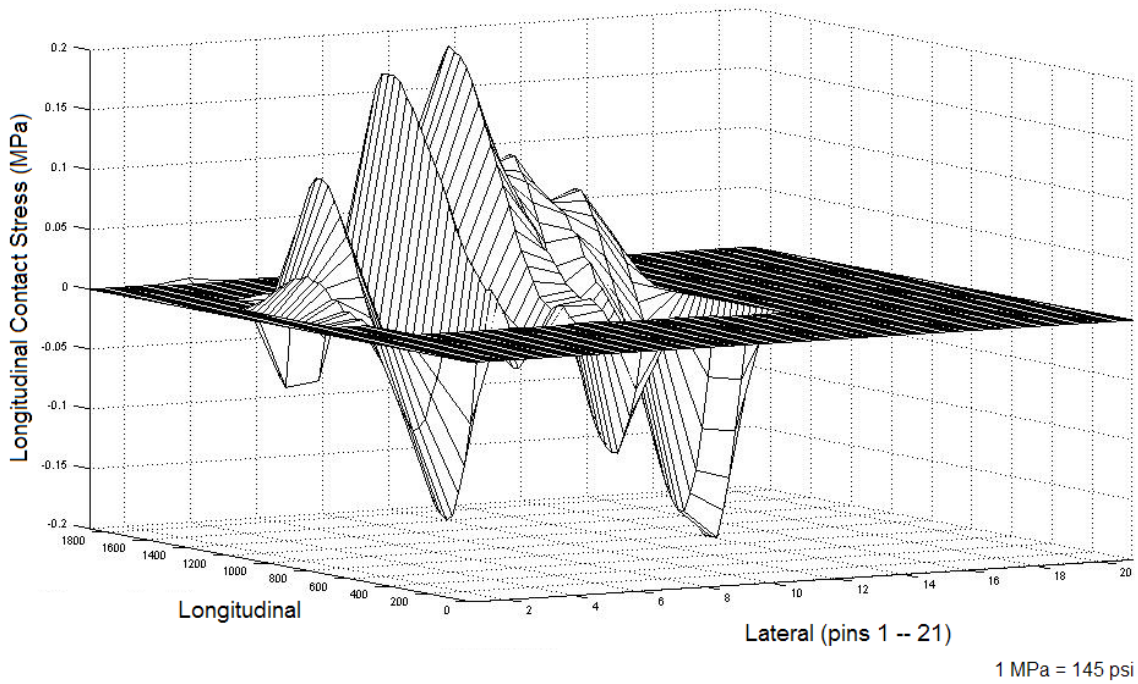

Figure C61. Measured Longitudinal Contact Stress Distribution for 215/75R17.5 Radial Tested at a Tire Load of 7000 lb and an Inflation Pressure of 85 psi.

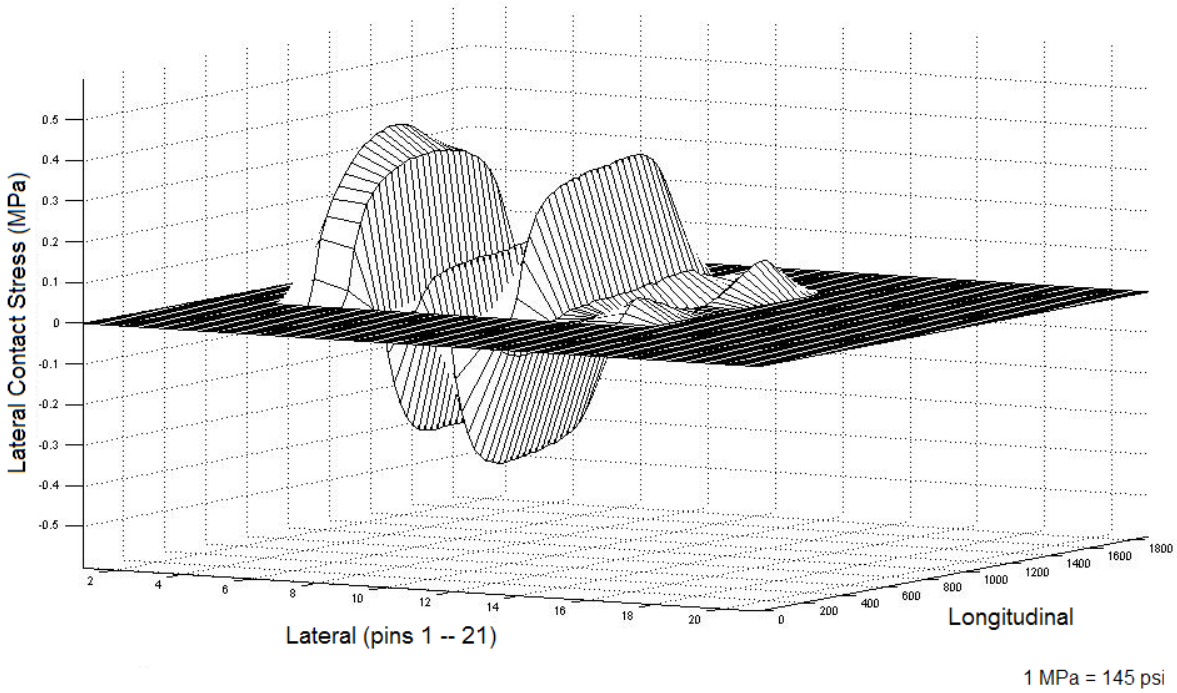

Figure C62. Measured Lateral Contact Stress Distribution for 215/75R17.5 Radial Tested at a Tire Load of 7000 lb and an Inflation Pressure of 85 psi.

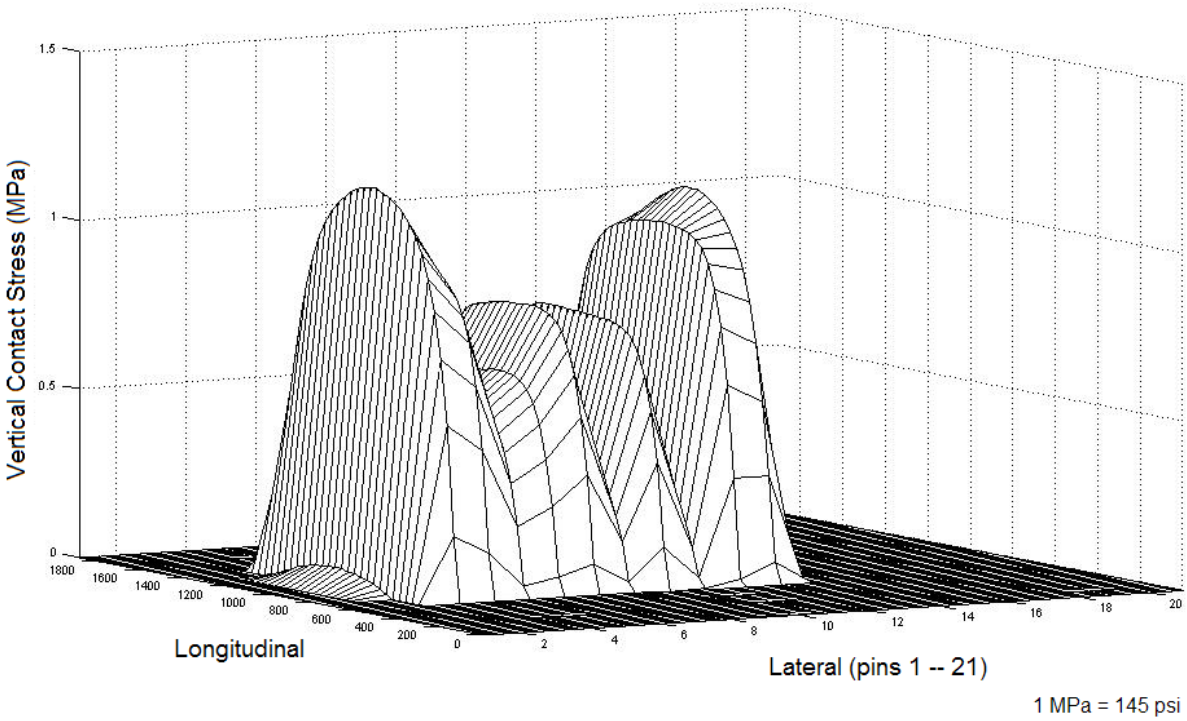

Figure C63. Measured Vertical Contact Stress Distribution for 215/75R17.5 Radial Tested at a Tire Load of 7000 lb and an Inflation Pressure of 85 psi.

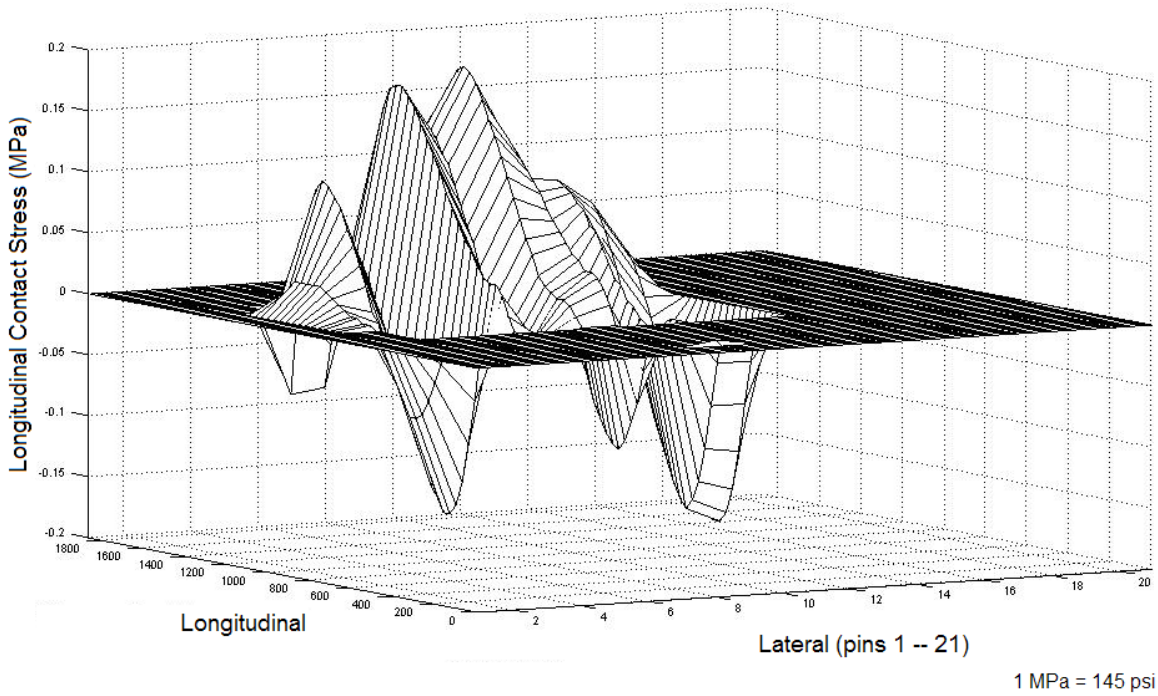

Figure C64. Measured Longitudinal Contact Stress Distribution for 215/75R17.5 Radial Tested at a Tire Load of 7000 lb and an Inflation Pressure of 100 psi.

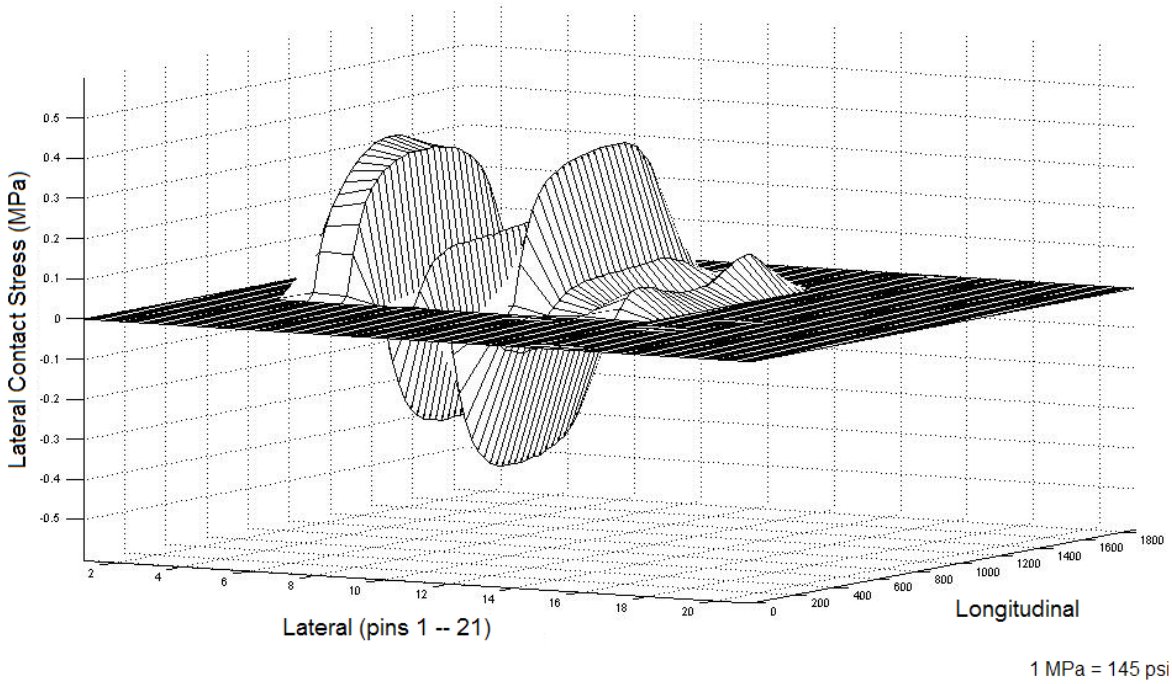

Figure C65. Measured Lateral Contact Stress Distribution for 215/75R17.5 Radial Tested at a Tire Load of 7000 lb and an Inflation Pressure of 100 psi.

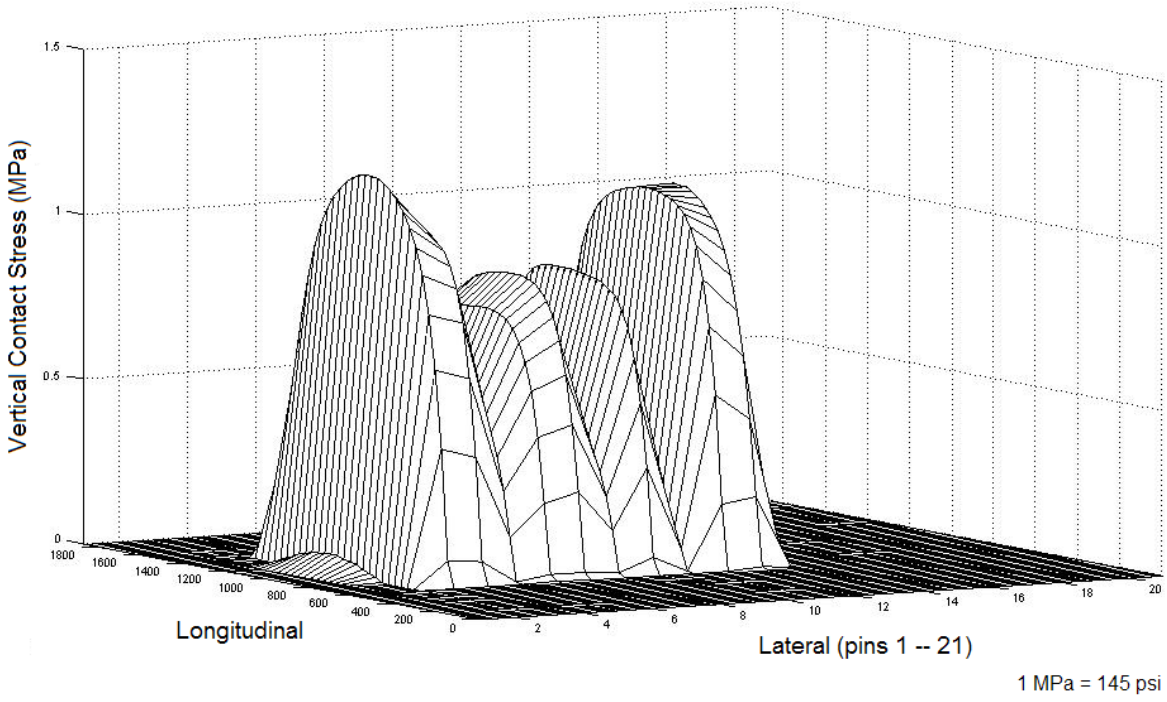

Figure C66. Measured Vertical Contact Stress Distribution for 215/75R17.5 Radial Tested at a Tire Load of 7000 lb and an Inflation Pressure of 100 psi.

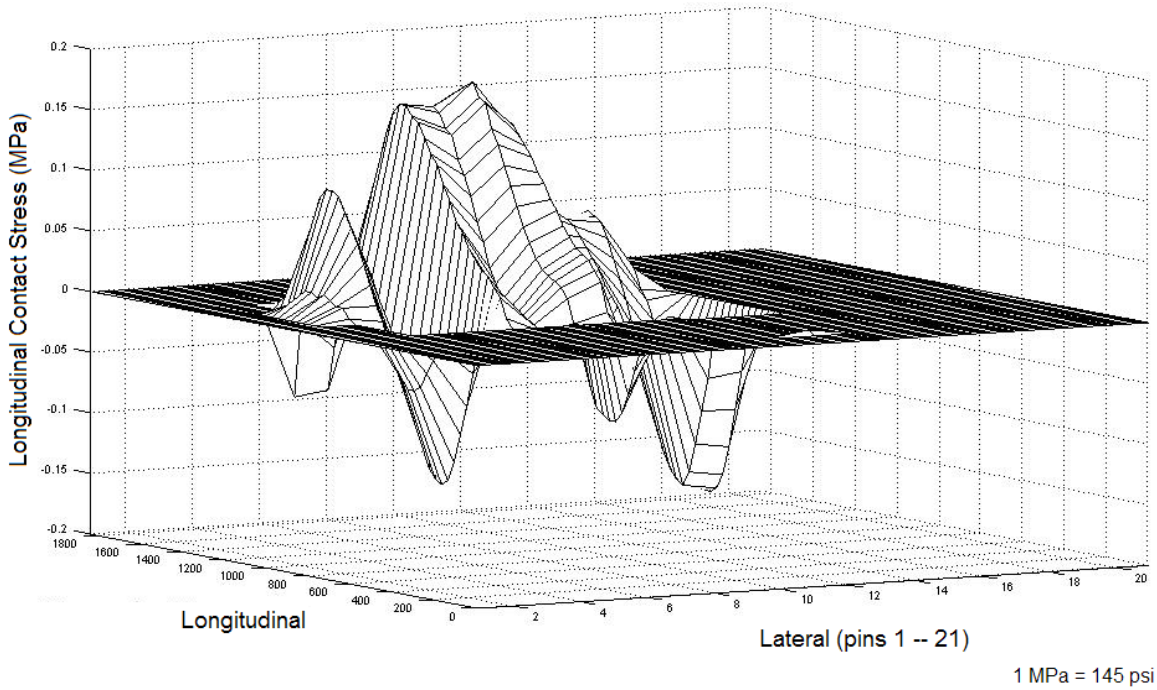

Figure C67. Measured Longitudinal Contact Stress Distribution for 215/75R17.5 Radial Tested at a Tire Load of 7000 lb and an Inflation Pressure of 115 psi.

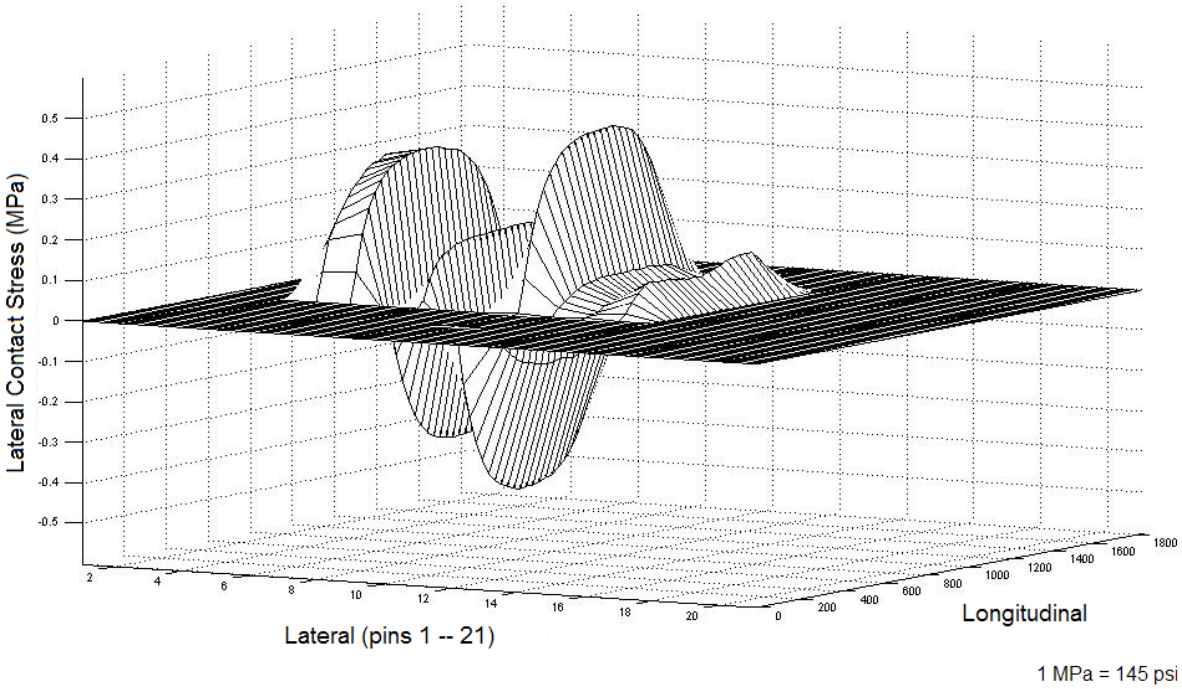

Figure C68. Measured Lateral Contact Stress Distribution for 215/75R17.5 Radial Tested at a Tire Load of 7000 lb and an Inflation Pressure of 115 psi.

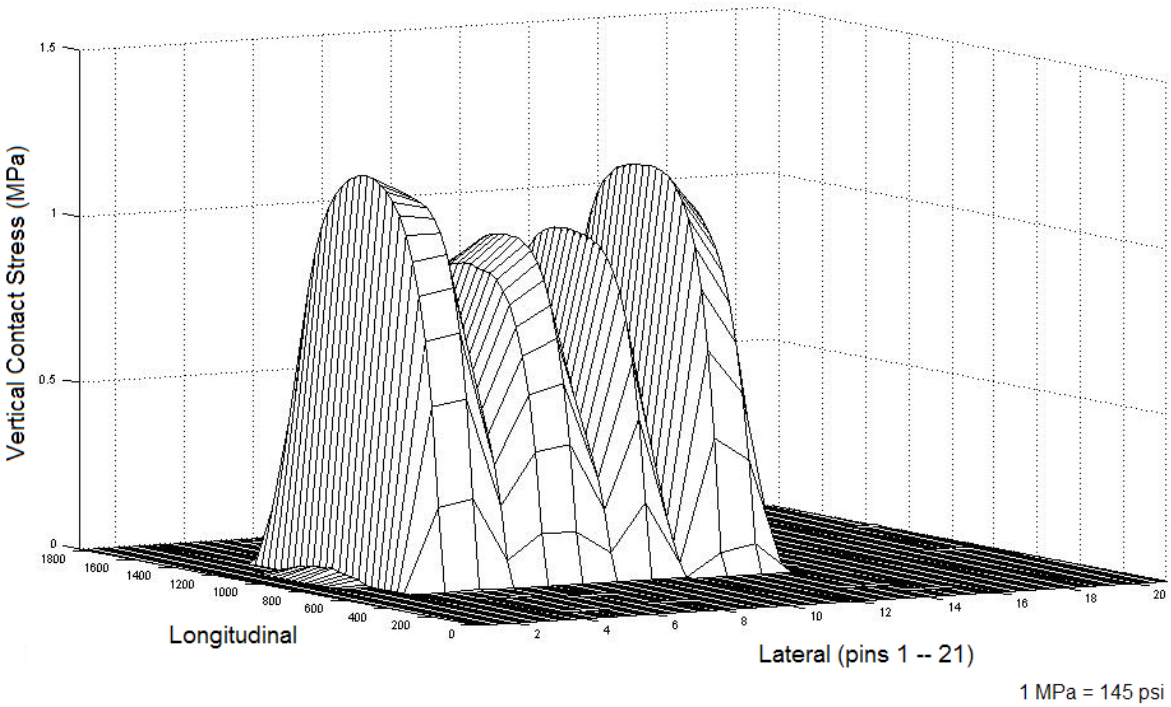

Figure C69. Measured Vertical Contact Stress Distribution for 215/75R17.5 Radial Tested at a Tire Load of 7000 lb and an Inflation Pressure of 115 psi.

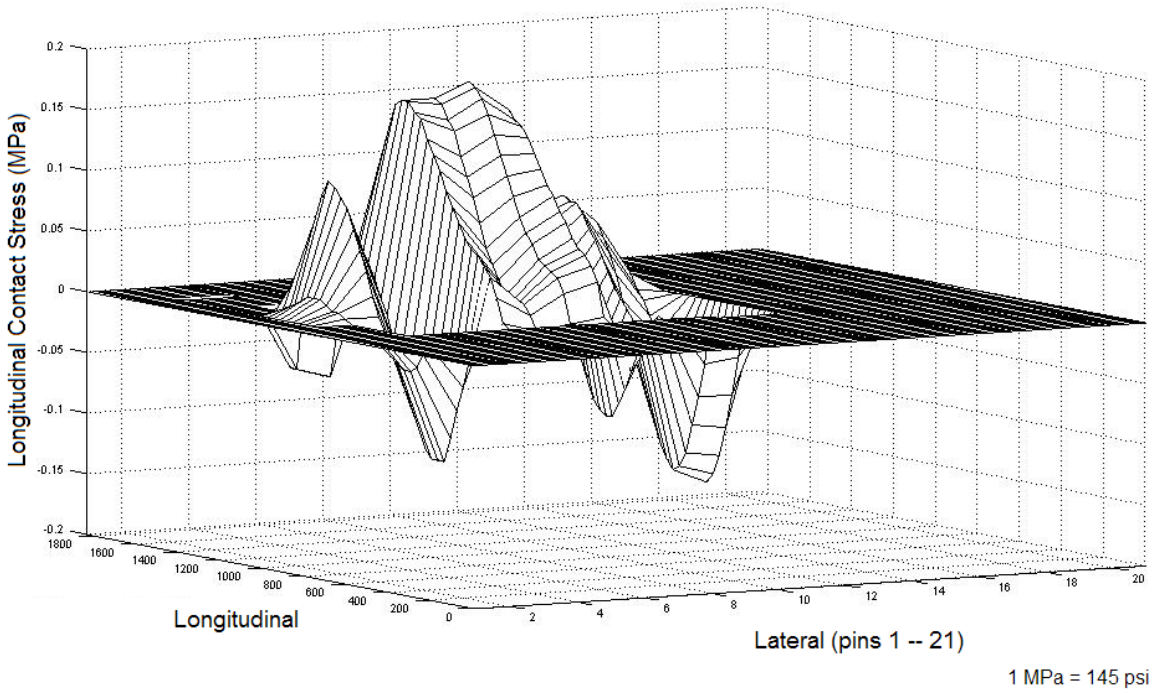

Figure C70. Measured Longitudinal Contact Stress Distribution for 215/75R17.5 Radial Tested at a Tire Load of 7000 lb and an Inflation Pressure of 130 psi.

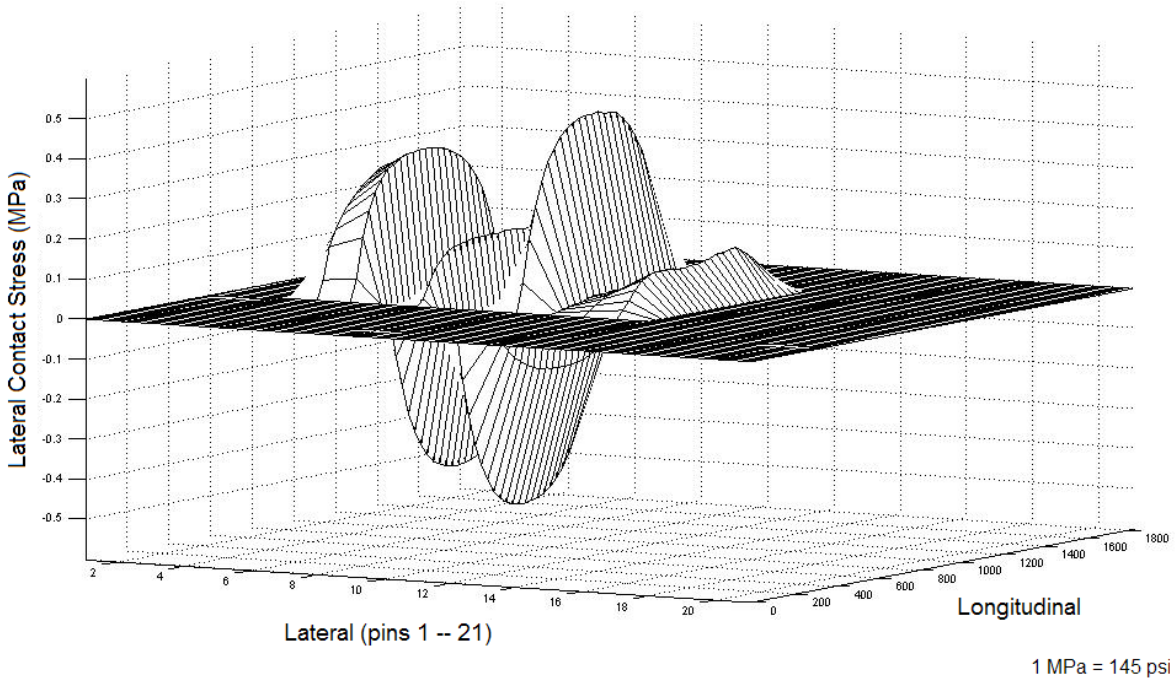

Figure C71. Measured Lateral Contact Stress Distribution for 215/75R17.5 Radial Tested at a Tire Load of 7000 lb and an Inflation Pressure of 130 psi.

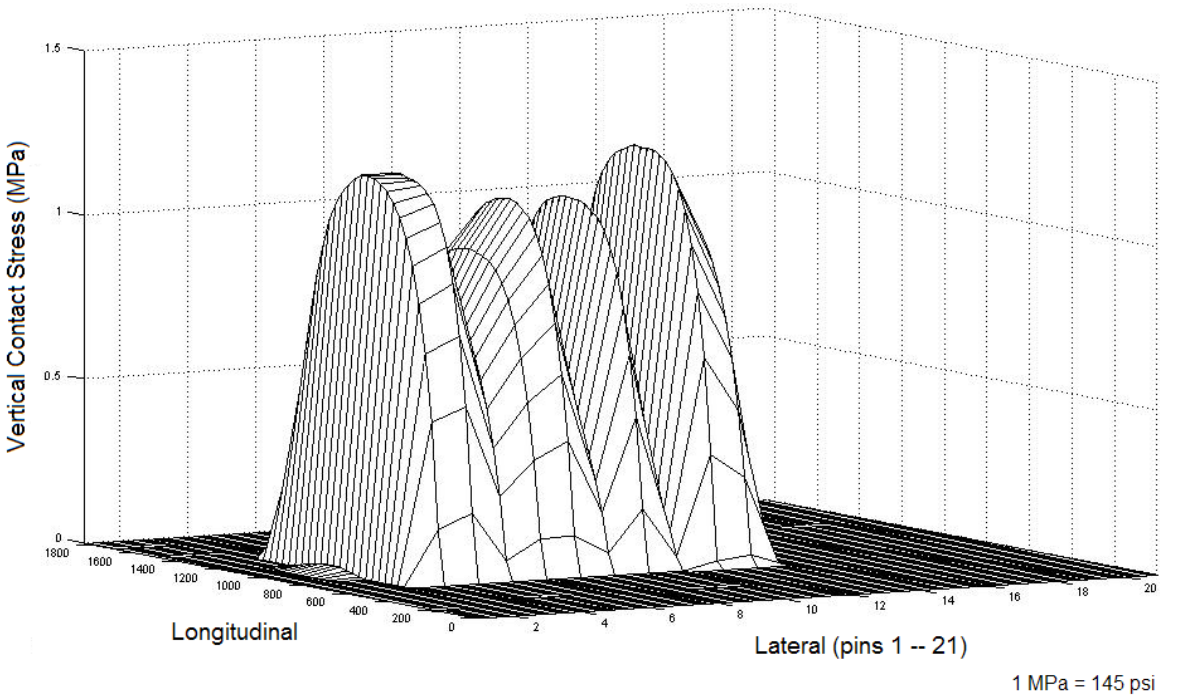

Figure C72. Measured Vertical Contact Stress Distribution for 215/75R17.5 Radial Tested at a Tire Load of 7000 lb and an Inflation Pressure of 130 psi.

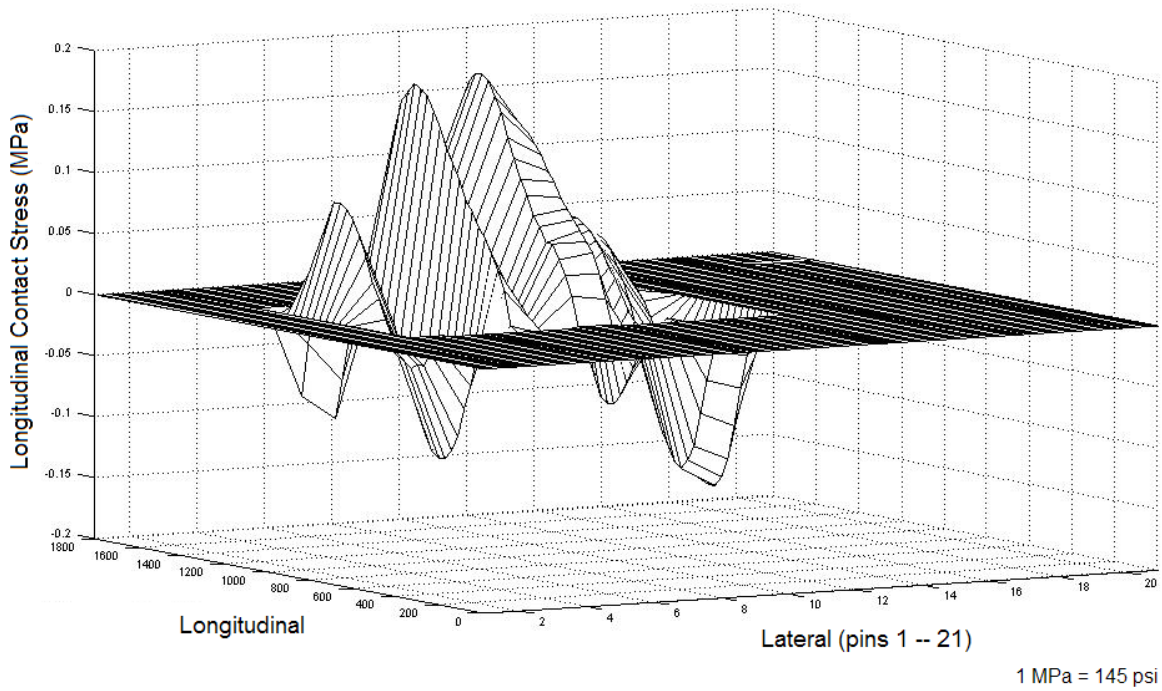

Figure C73. Measured Longitudinal Contact Stress Distribution for 215/75R17.5 Radial Tested at a Tire Load of 7000 lb and an Inflation Pressure of 145 psi.

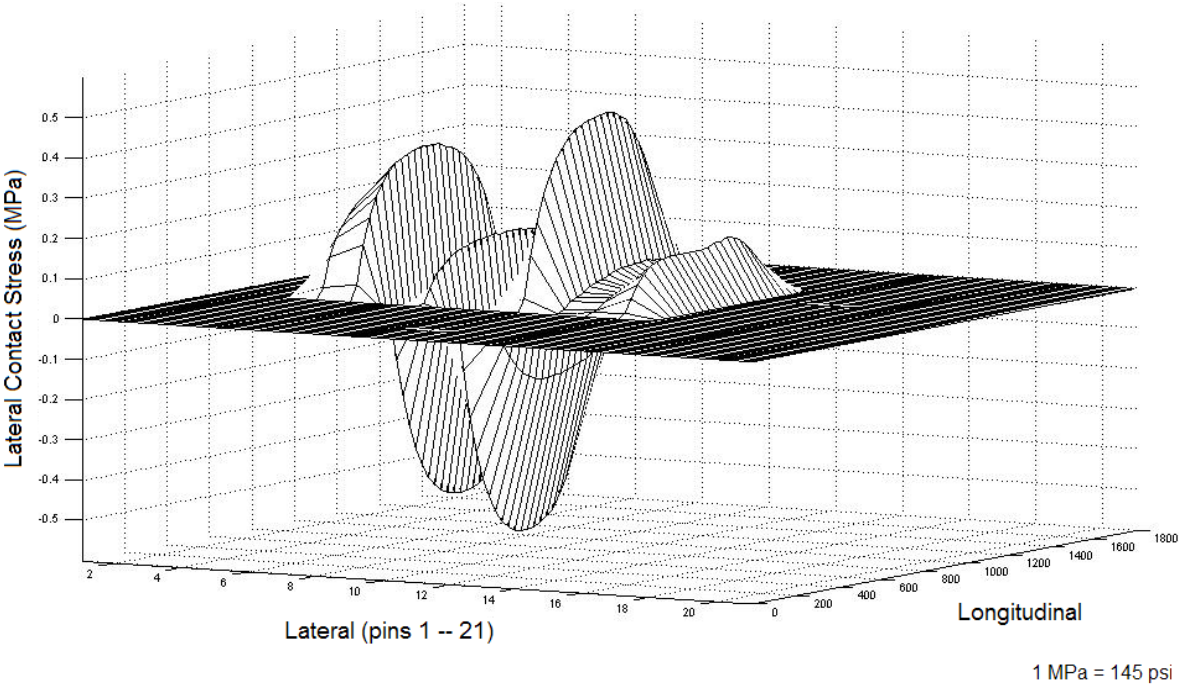

Figure C74. Measured Lateral Contact Stress Distribution for 215/75R17.5 Radial Tested at a Tire Load of 7000 lb and an Inflation Pressure of 145 psi.

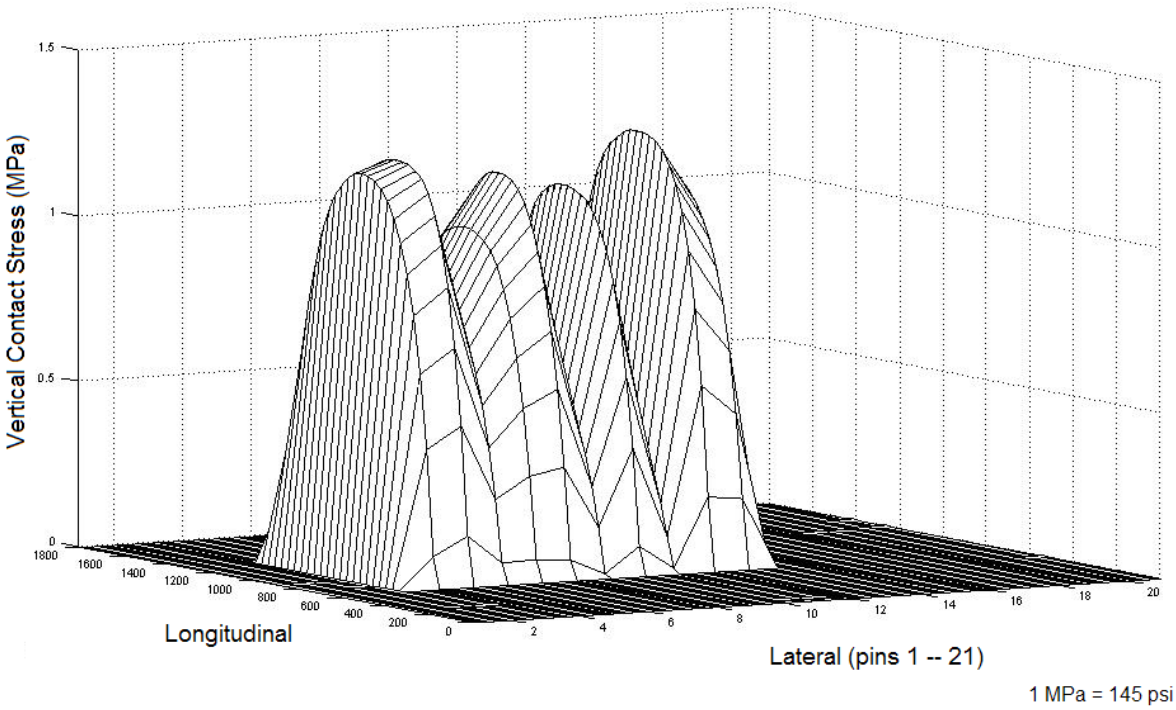

Figure C75. Measured Vertical Contact Stress Distribution for 215/75R17.5 Radial Tested at a Tire Load of 7000 lb and an Inflation Pressure of 145 psi.

APPENDIX D

TIRE IMPRINTS FROM TESTS CONDUCTED ON 11R24.5 AND 215/75R17.5 RADIAL TIRES

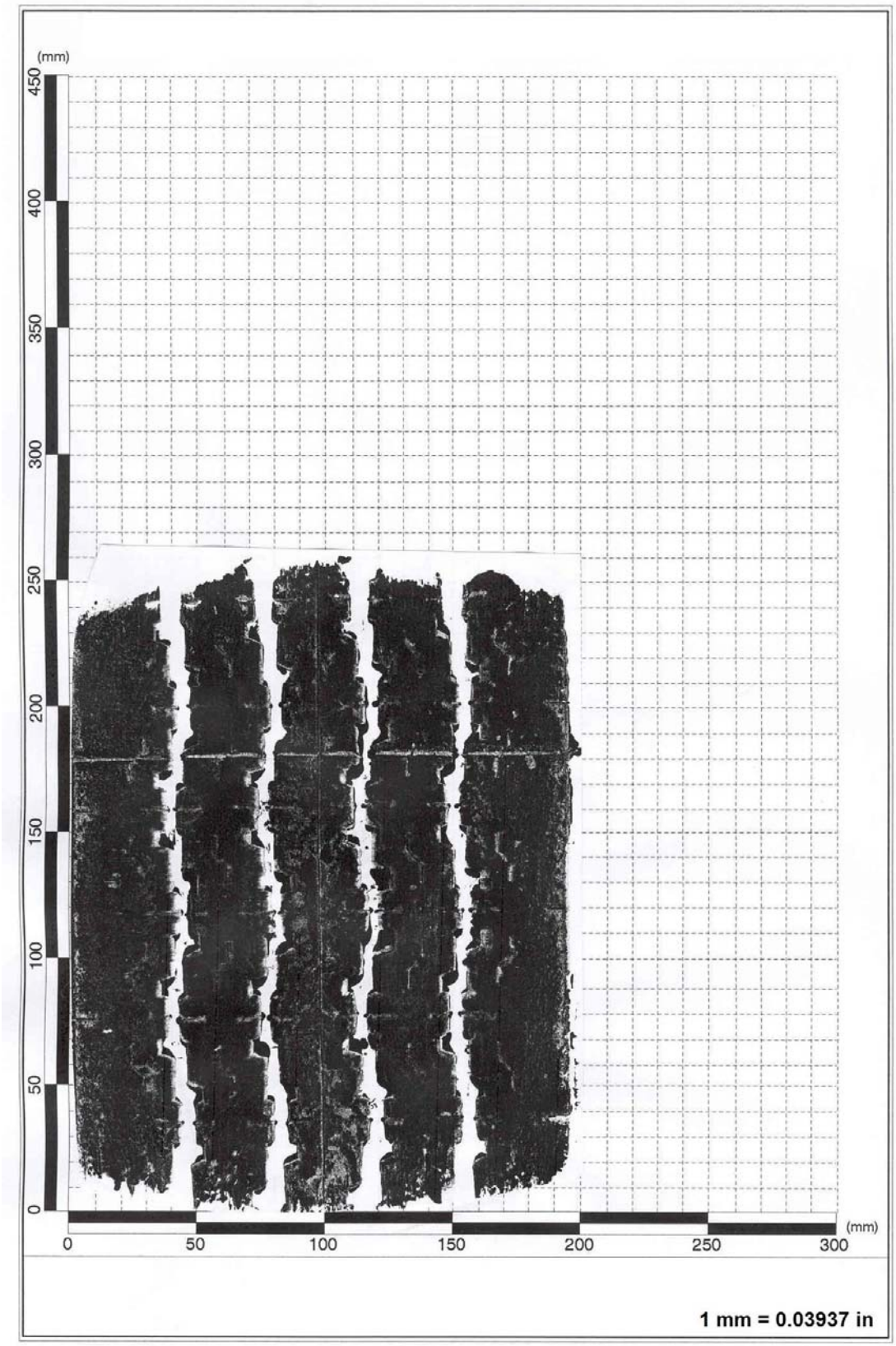

Figure D1. Tire Imprint for 11R24.5 Tire Taken at a Tire Load of 4600 lb and an Inflation Pressure of 70 psi.

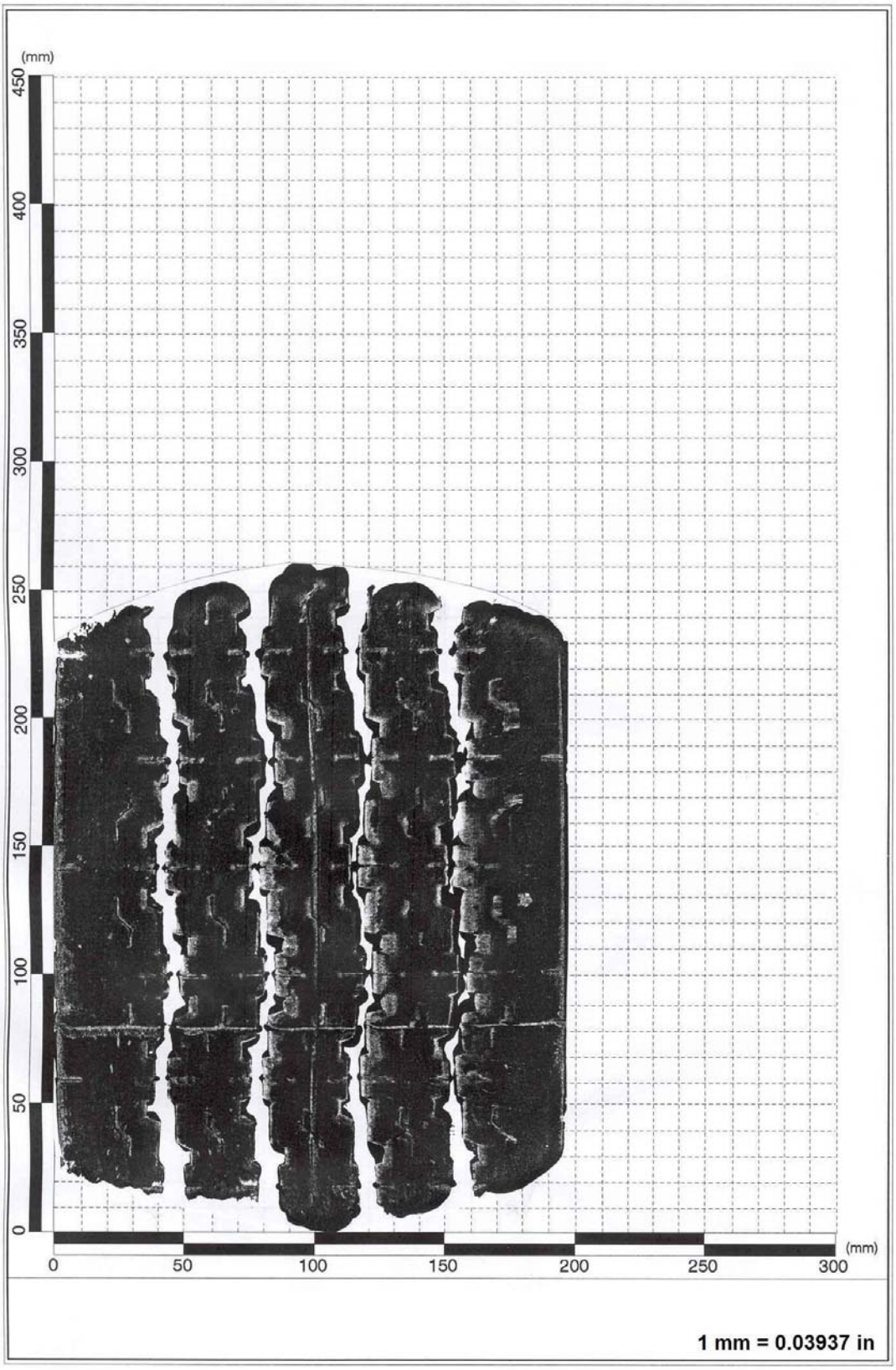

Figure D2. Tire Imprint for 11R24.5 Tire Taken at a Tire Load of 4600 lb and an Inflation Pressure of 85 psi.

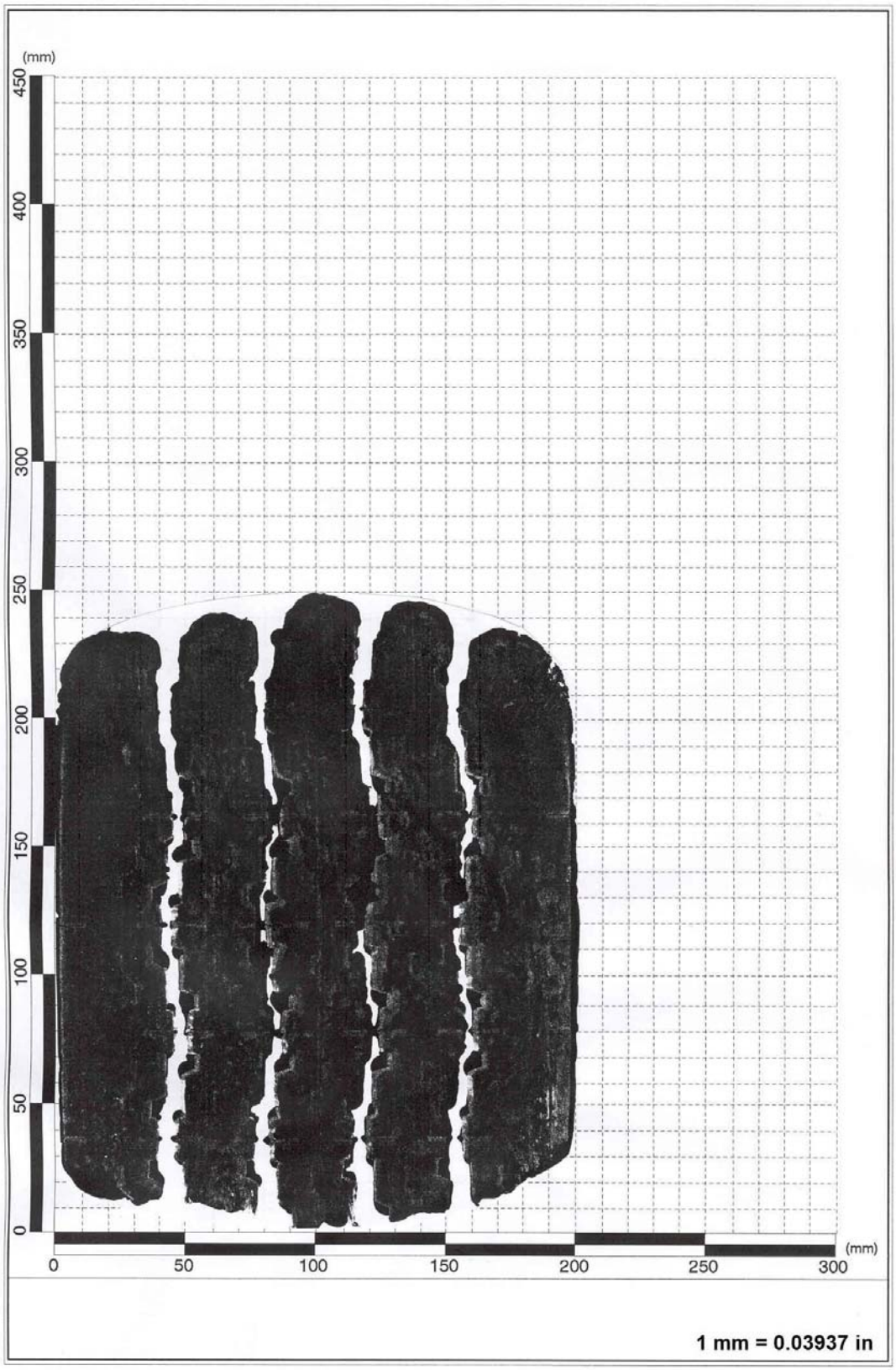

Figure D3. Tire Imprint for 11R24.5 Tire Taken at a Tire Load of 4600 lb and an Inflation Pressure of 100 psi.

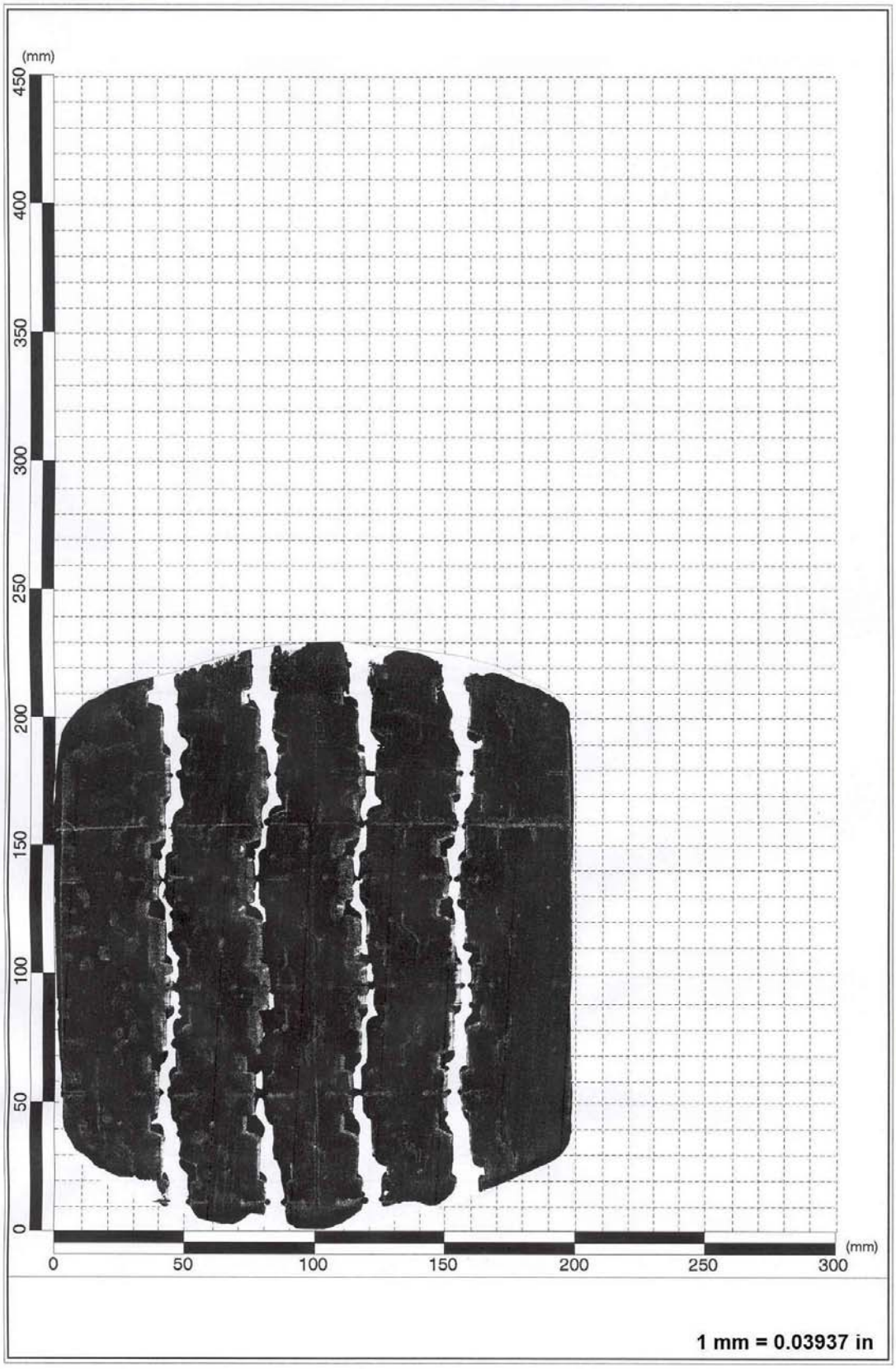

Figure D4. Tire Imprint for 11R24.5 Tire Taken at a Tire Load of 4600 lb and an Inflation Pressure of 115 psi.

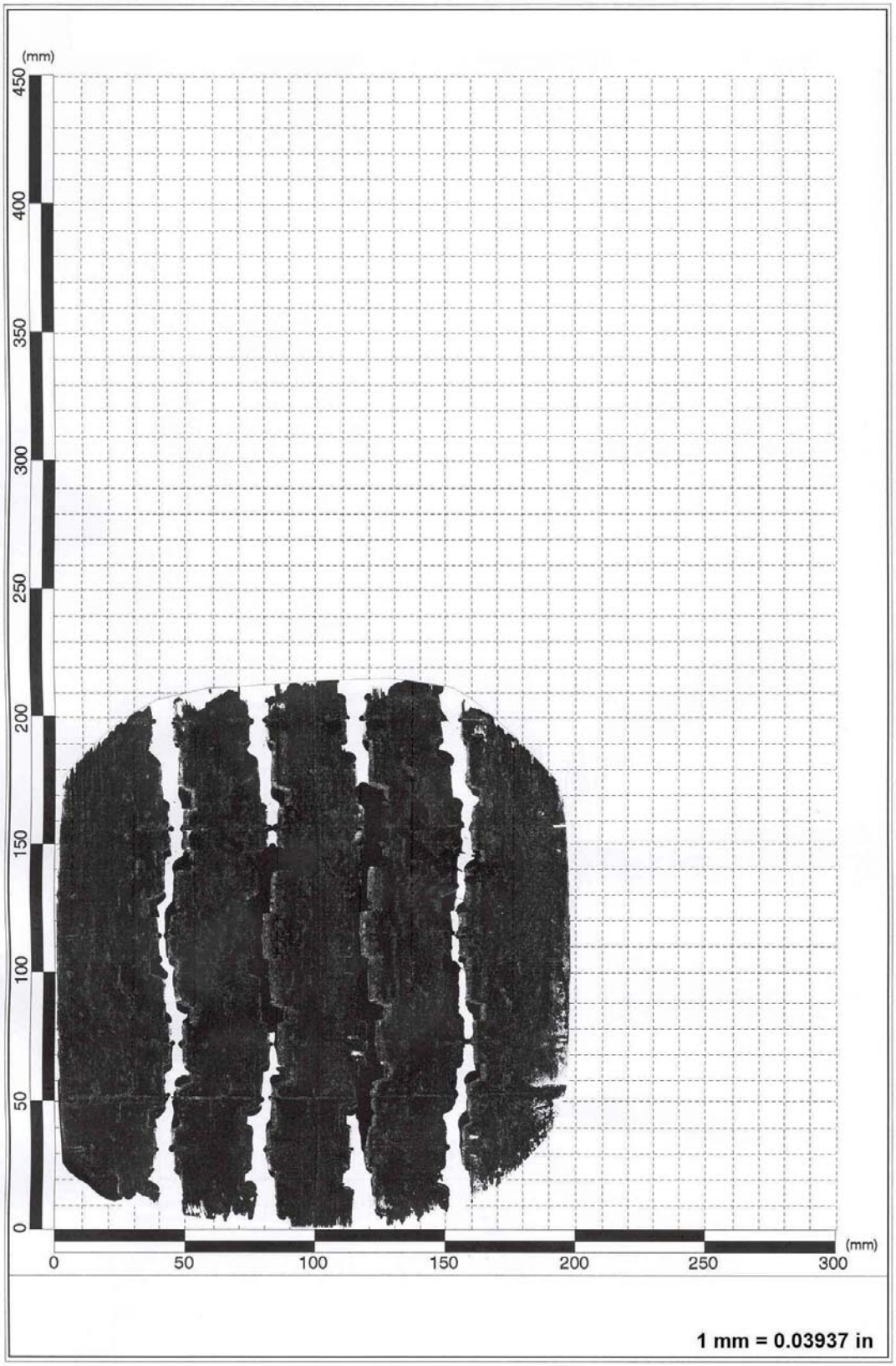

Figure D5. Tire Imprint for 11R24.5 Tire Taken at a Tire Load of 4600 lb and an Inflation Pressure of 130 psi.

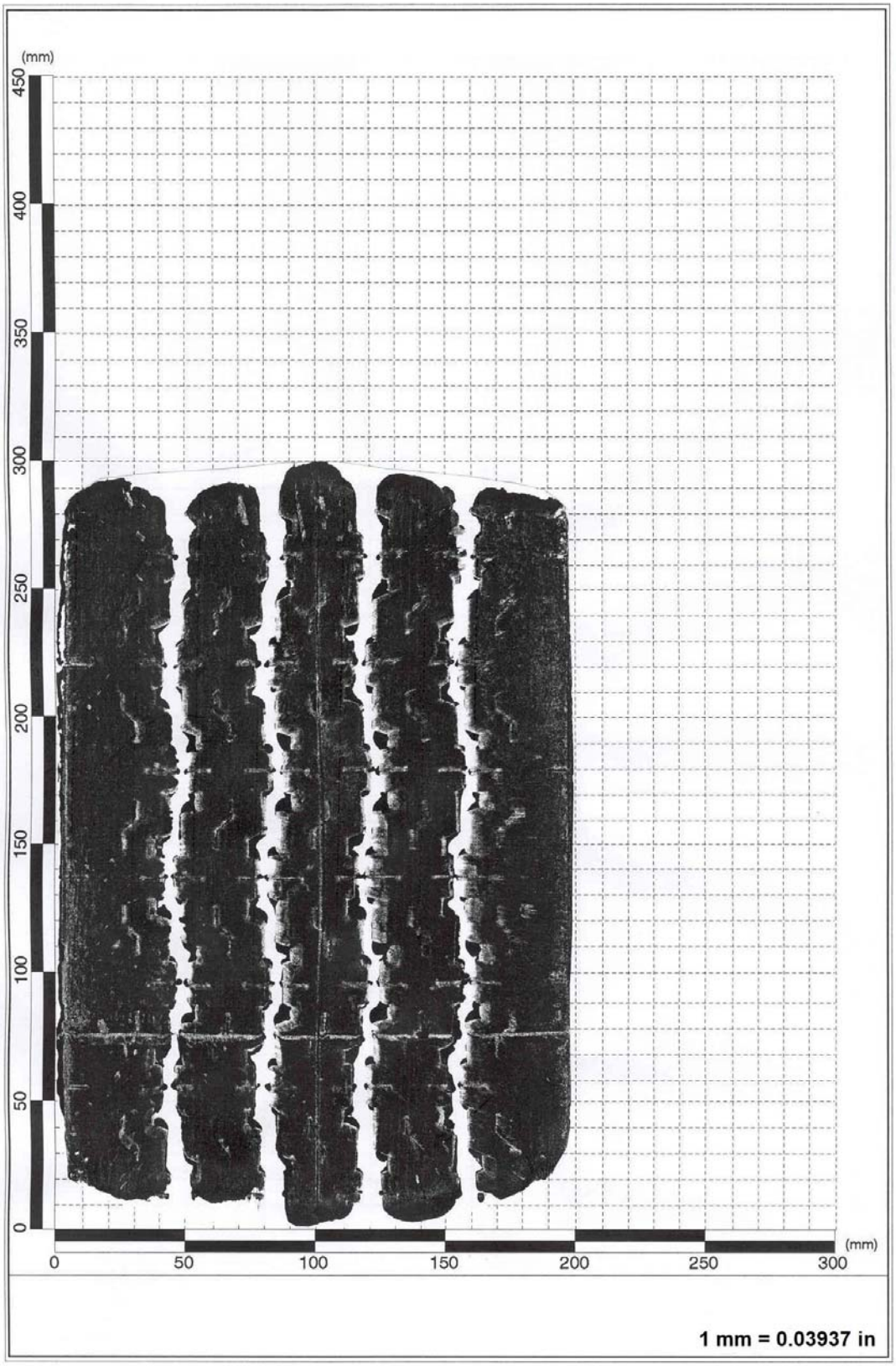

Figure D6. Tire Imprint for 11R24.5 Tire Taken at a Tire Load of 5400 lb and an Inflation Pressure of 70 psi.

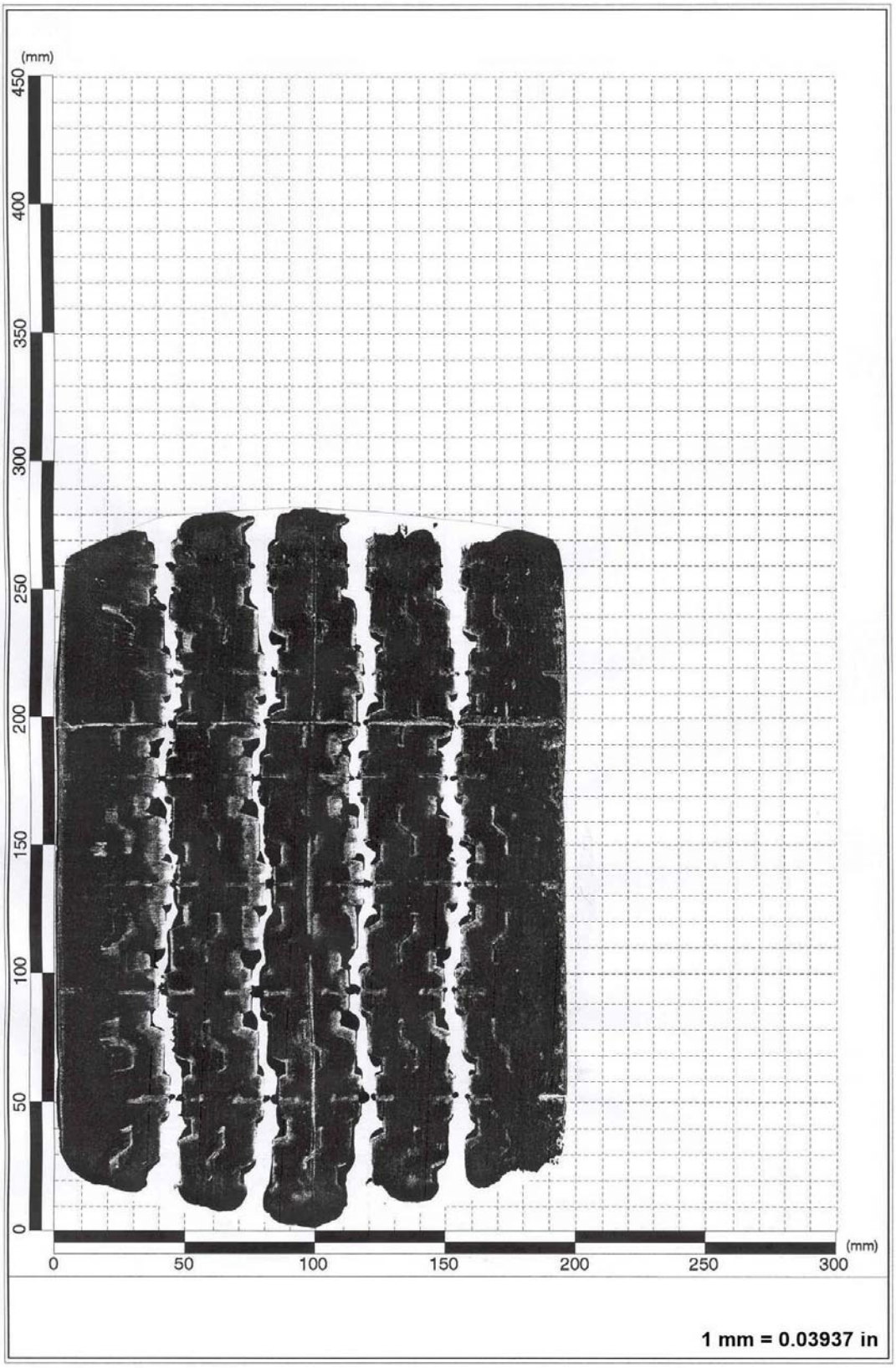

Figure D7. Tire Imprint for 11R24.5 Tire Taken at a Tire Load of 5400 lb and an Inflation Pressure of 85 psi.

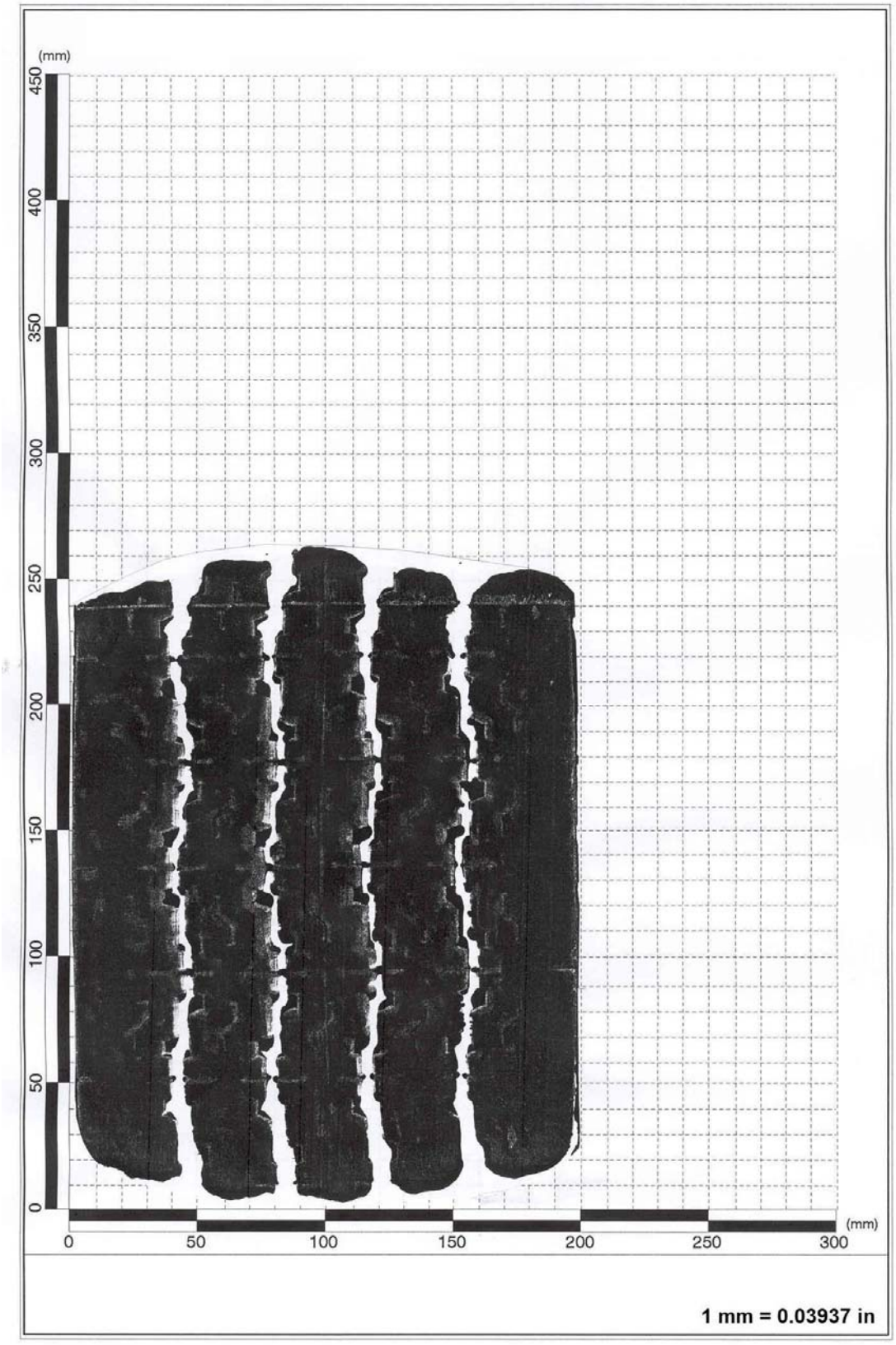

Figure D8. Tire Imprint for 11R24.5 Tire Taken at a Tire Load of 5400 lb and an Inflation Pressure of 100 psi.

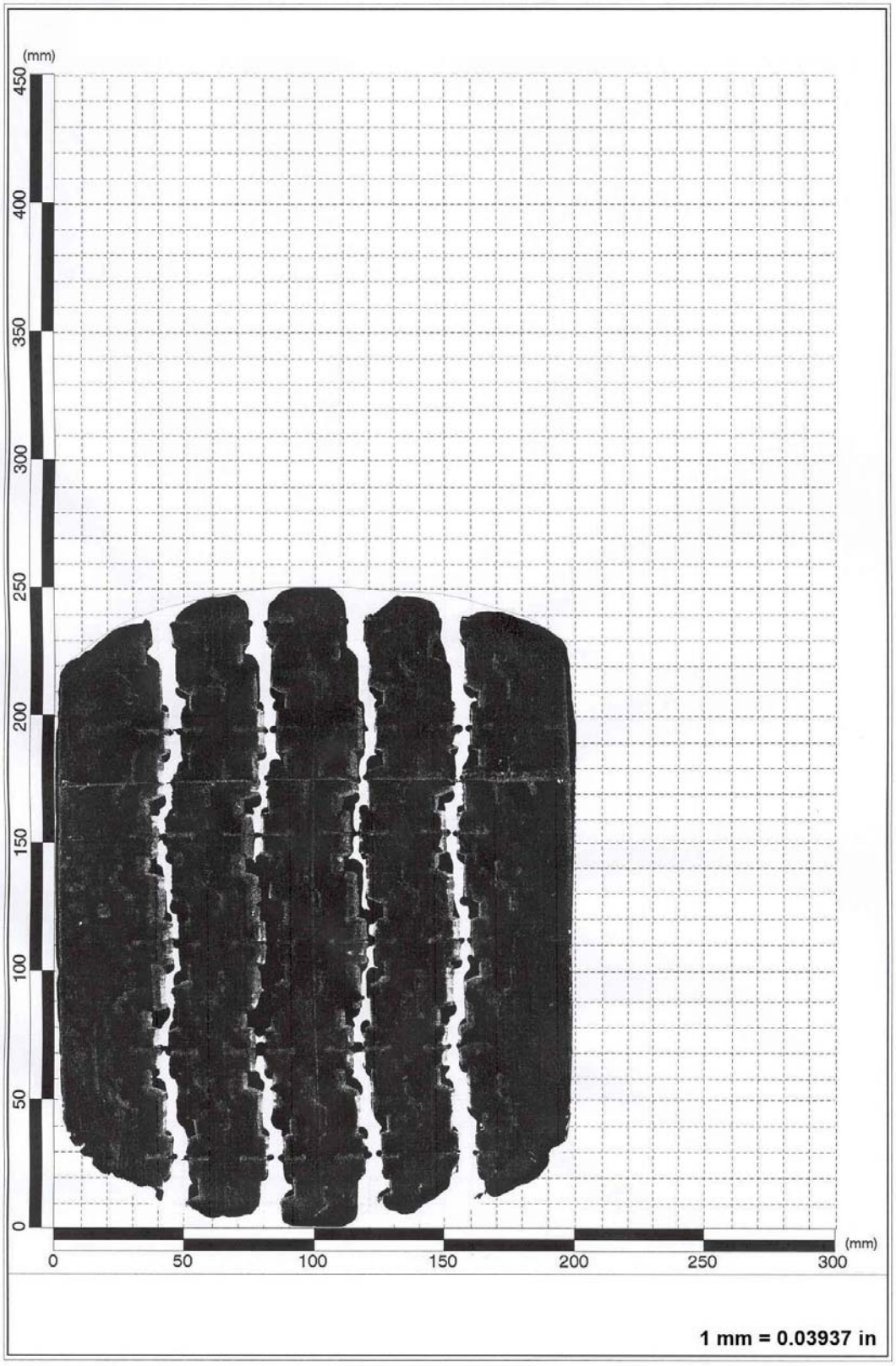

Figure D9. Tire Imprint for 11R24.5 Tire Taken at a Tire Load of 5400 lb and an Inflation Pressure of 115 psi.

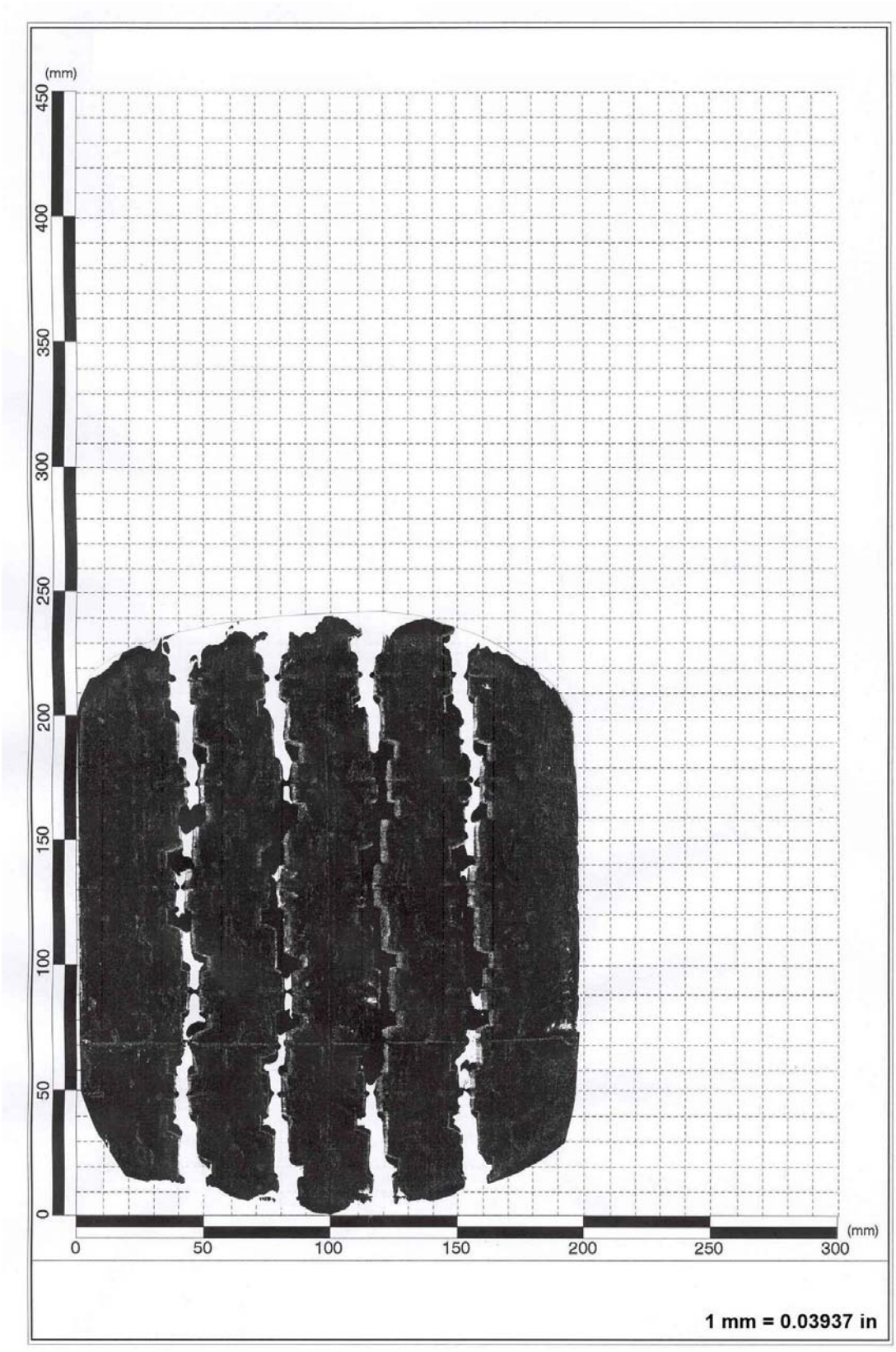

Figure D10. Tire Imprint for 11R24.5 Tire Taken at a Tire Load of 5400 lb and an Inflation Pressure of 130 psi.

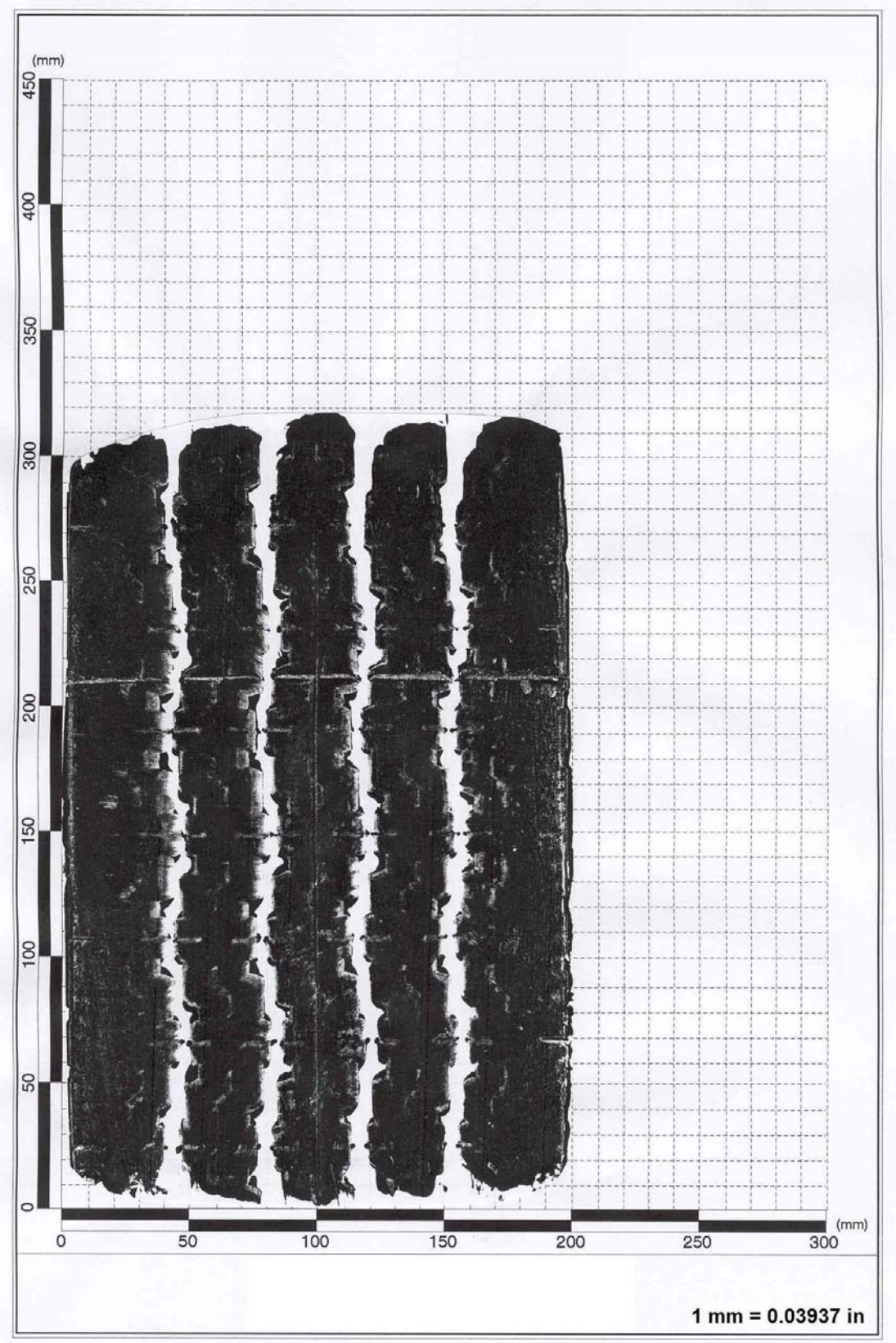

Figure D11. Tire Imprint for 11R24.5 Tire Taken at a Tire Load of 6200 lb and an Inflation Pressure of 70 psi.

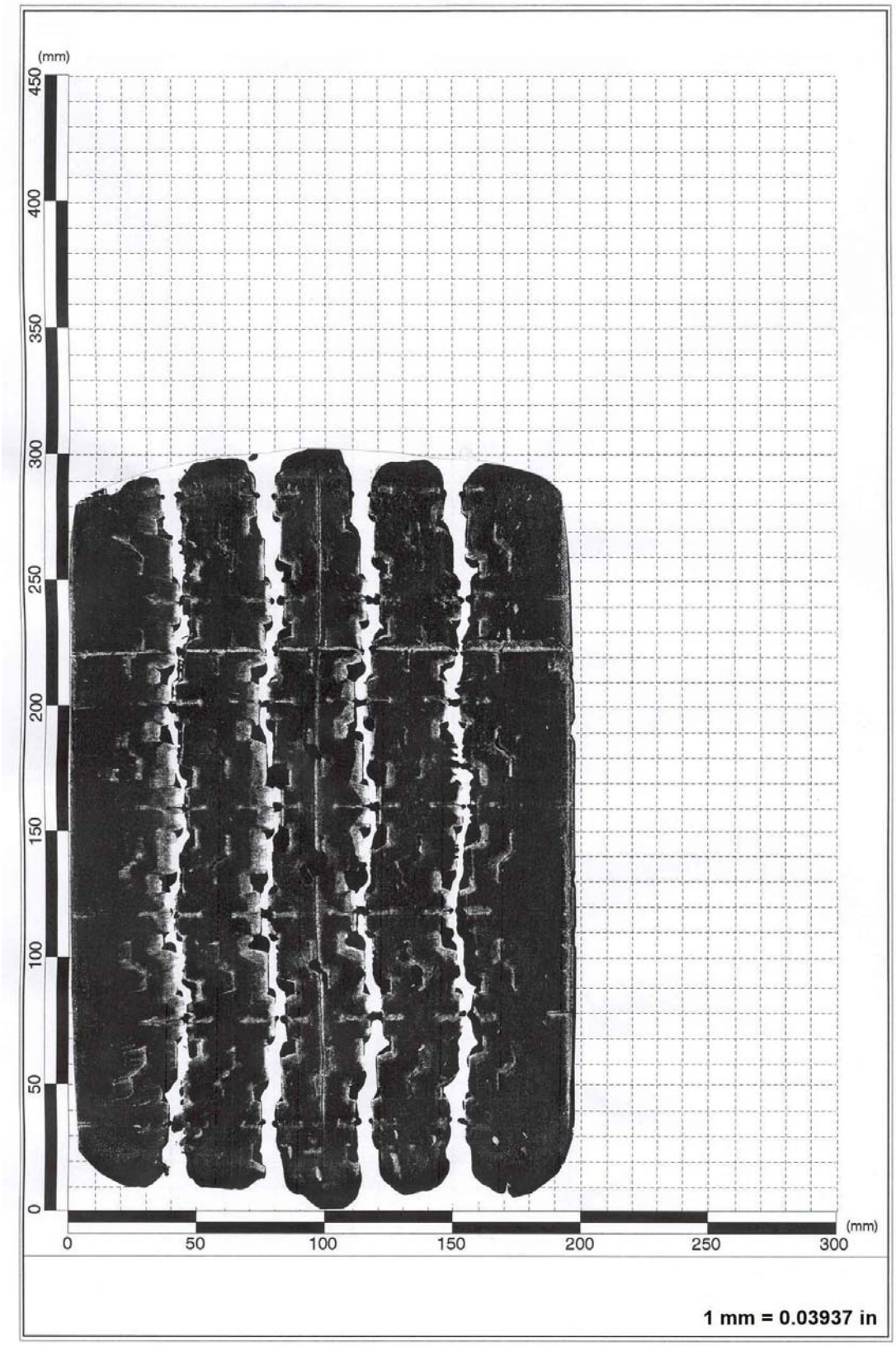

Figure D12. Tire Imprint for 11R24.5 Tire Taken at a Tire Load of 6200 lb and an Inflation Pressure of 85 psi.

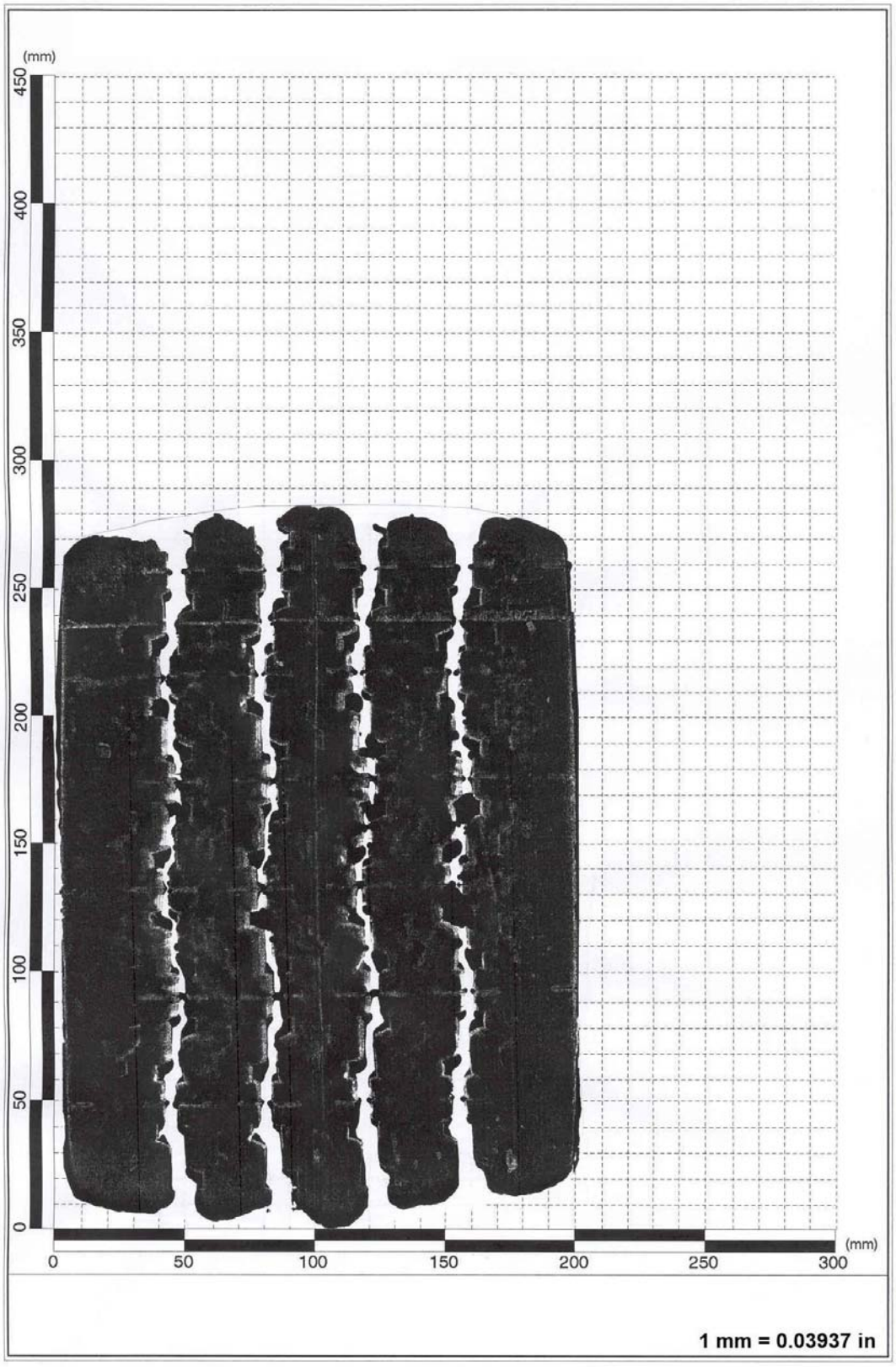

Figure D13. Tire Imprint for 11R24.5 Tire Taken at a Tire Load of 6200 lb and an Inflation Pressure of 100 psi.

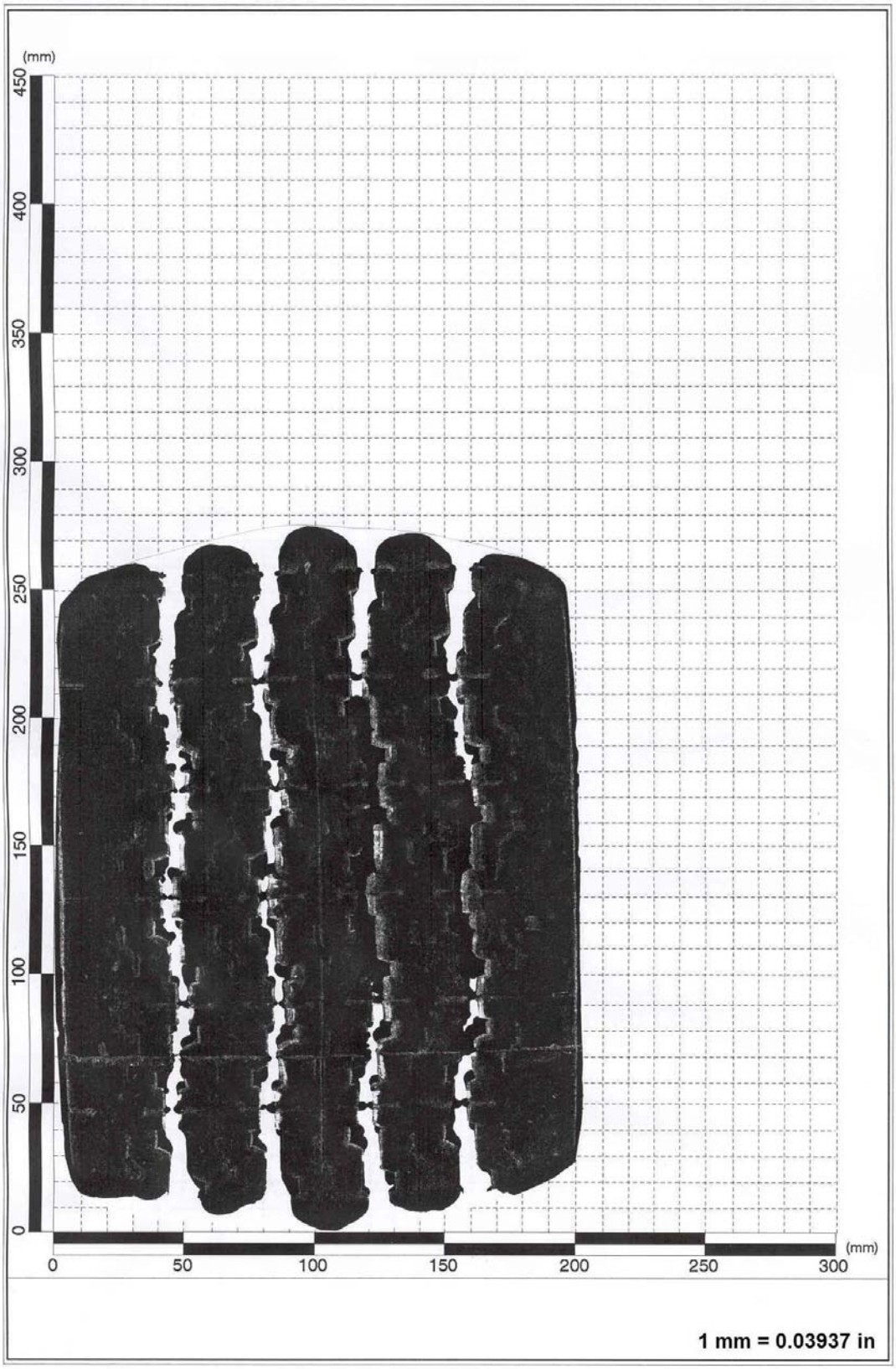

Figure D14. Tire Imprint for 11R24.5 Tire Taken at a Tire Load of 6200 lb and an Inflation Pressure of 115 psi.

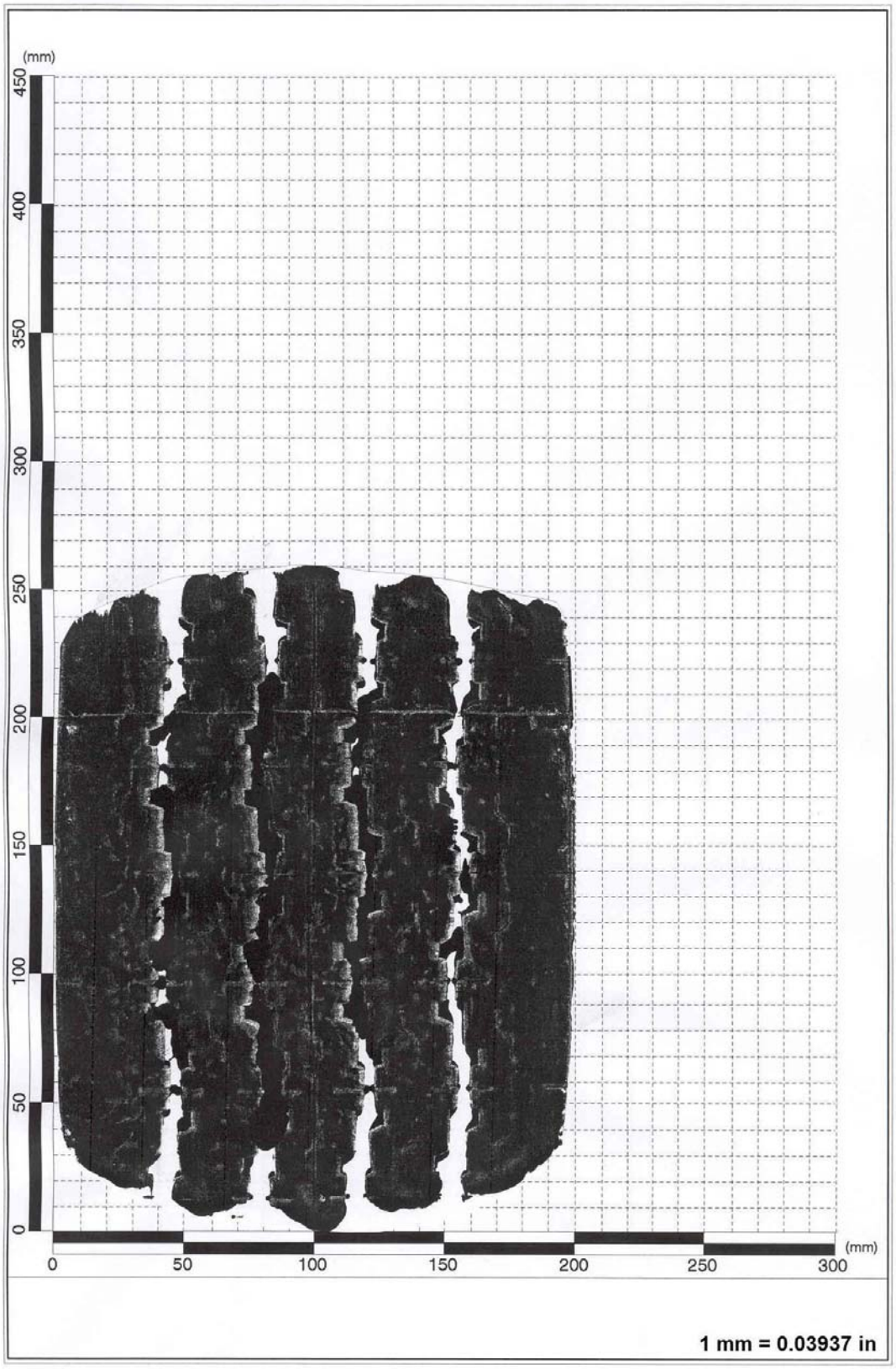

Figure D15. Tire Imprint for 11R24.5 Tire Taken at a Tire Load of 6200 lb and an Inflation Pressure of 130 psi.

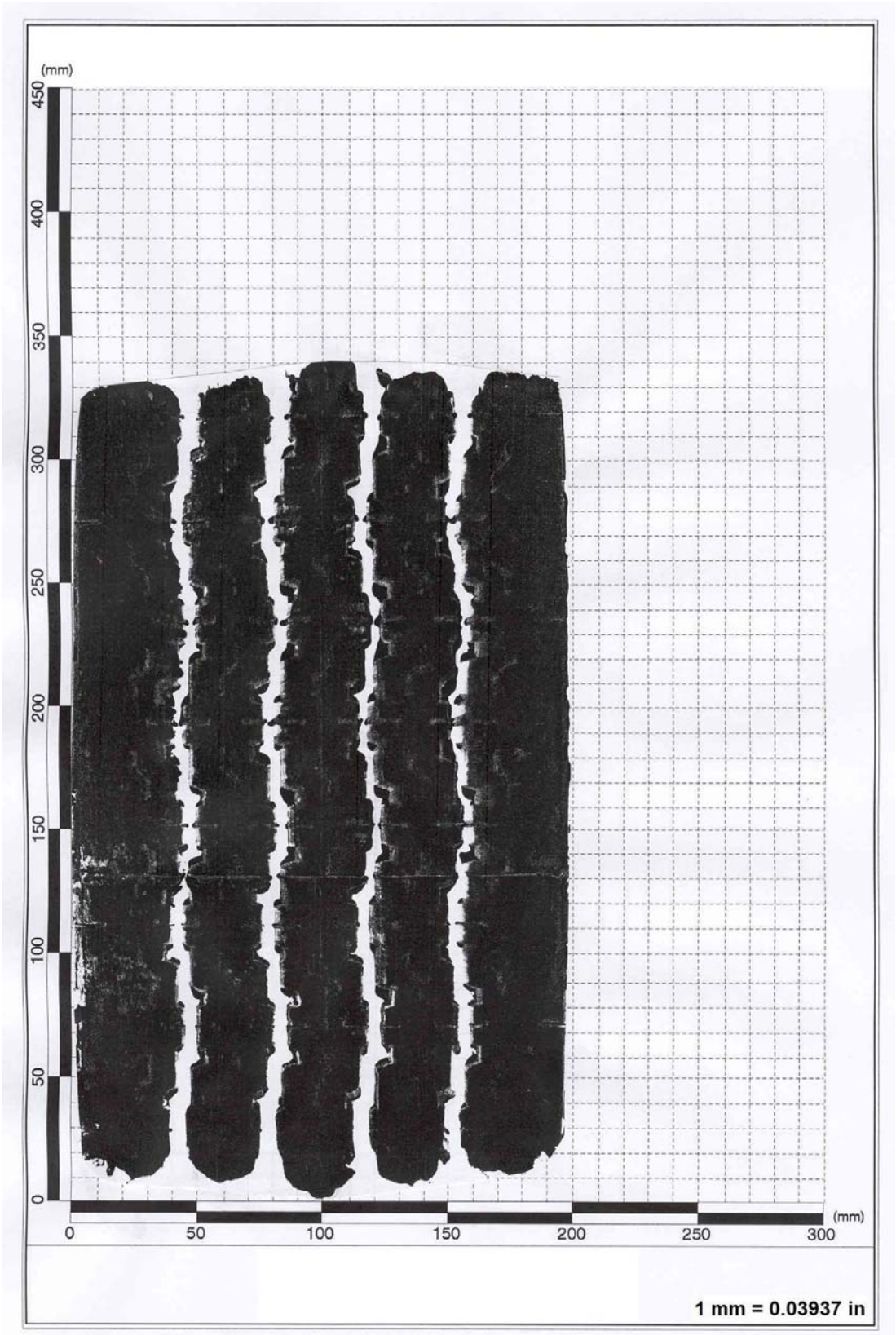

Figure D16. Tire Imprint for 11R24.5 Tire Taken at a Tire Load of 7000 lb and an Inflation Pressure of 70 psi.

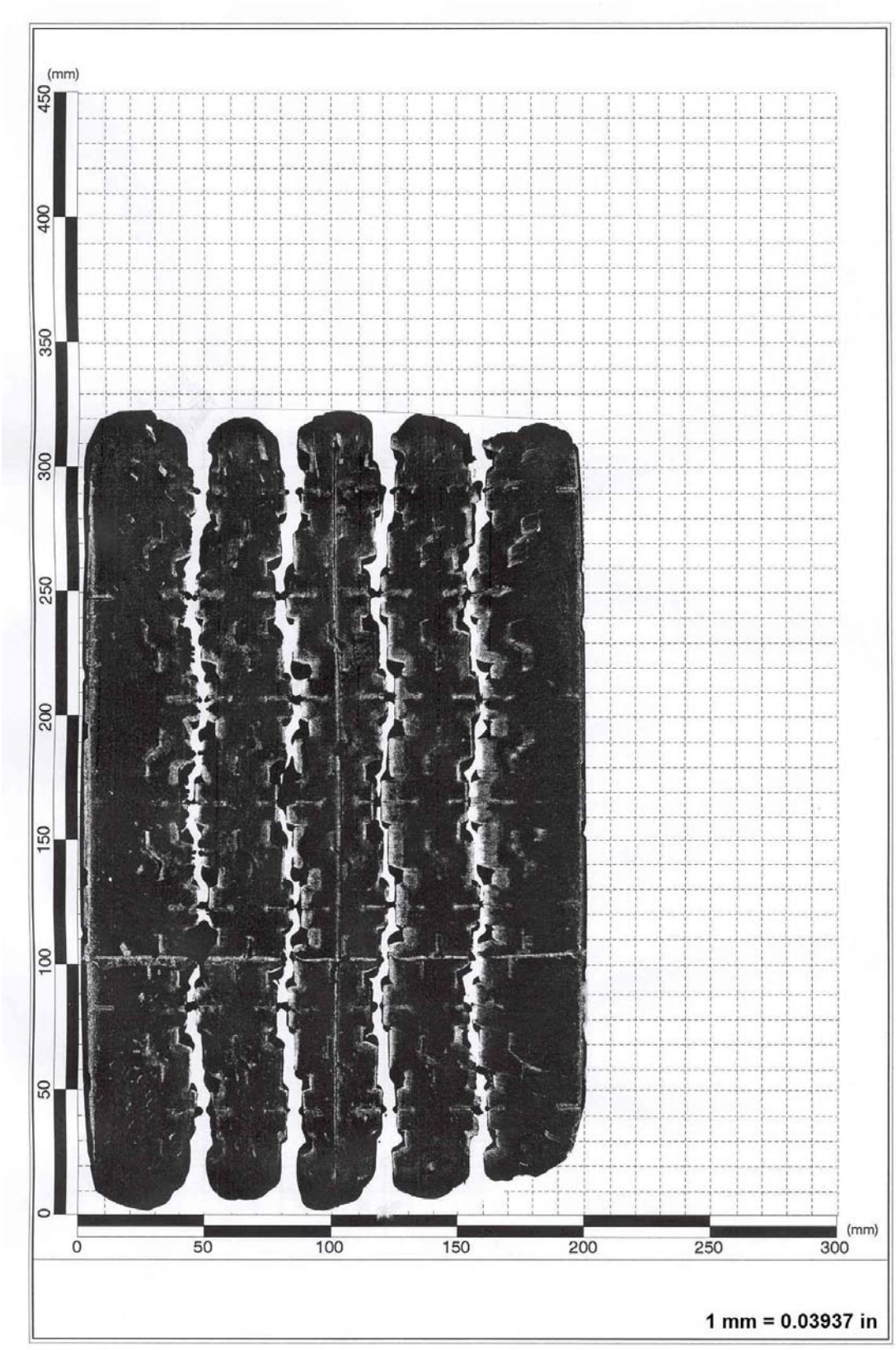

Figure D17. Tire Imprint for 11R24.5 Tire Taken at a Tire Load of 7000 lb and an Inflation Pressure of 85 psi.

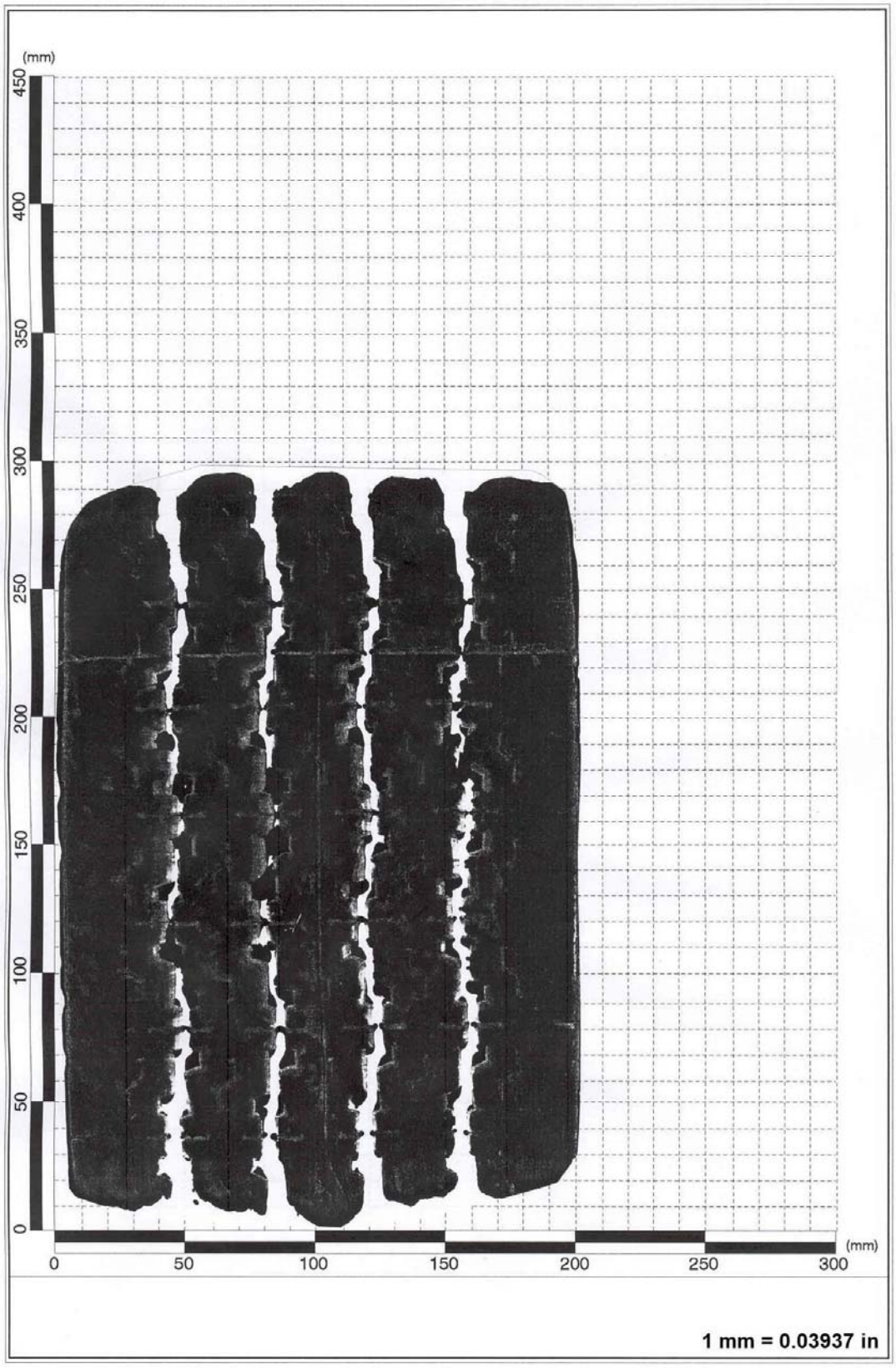

Figure D18. Tire Imprint for 11R24.5 Tire Taken at a Tire Load of 7000 lb and an Inflation Pressure of 100 psi.

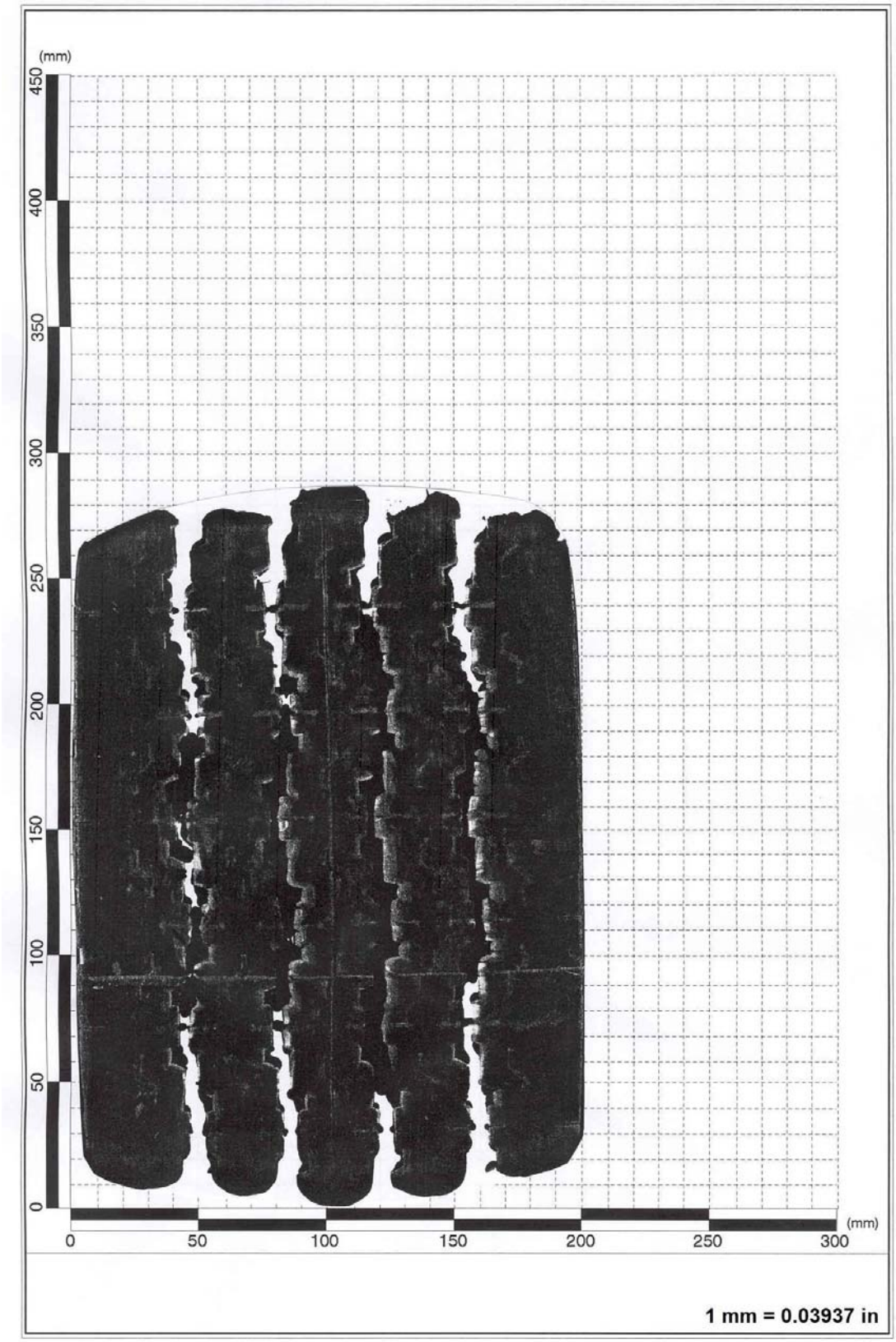

Figure D19. Tire Imprint for 11R24.5 Tire Taken at a Tire Load of 7000 lb and an Inflation Pressure of 115 psi.

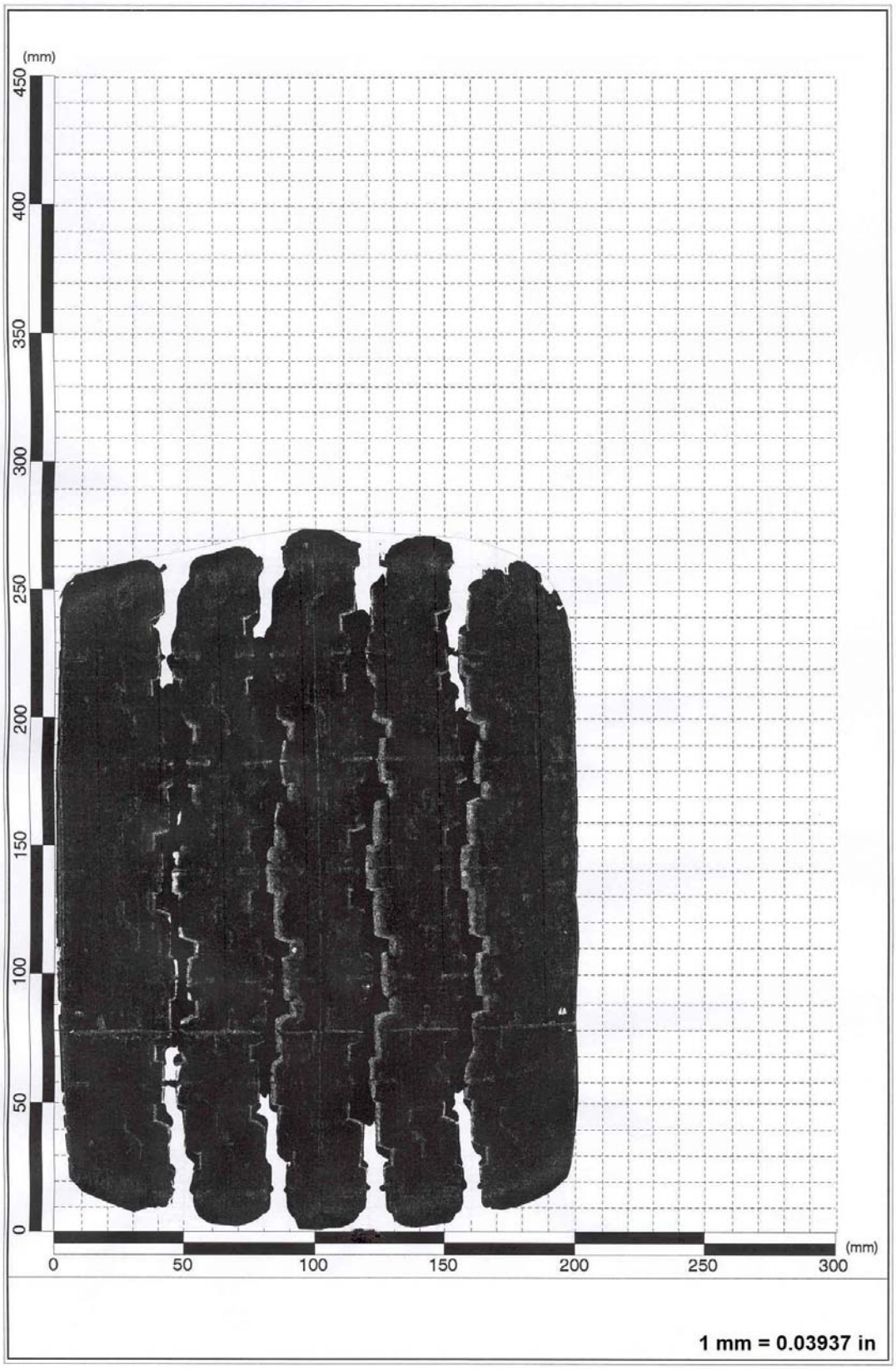

Figure D20. Tire Imprint for 11R24.5 Tire Taken at a Tire Load of 7000 lb and an Inflation Pressure of 130 psi.

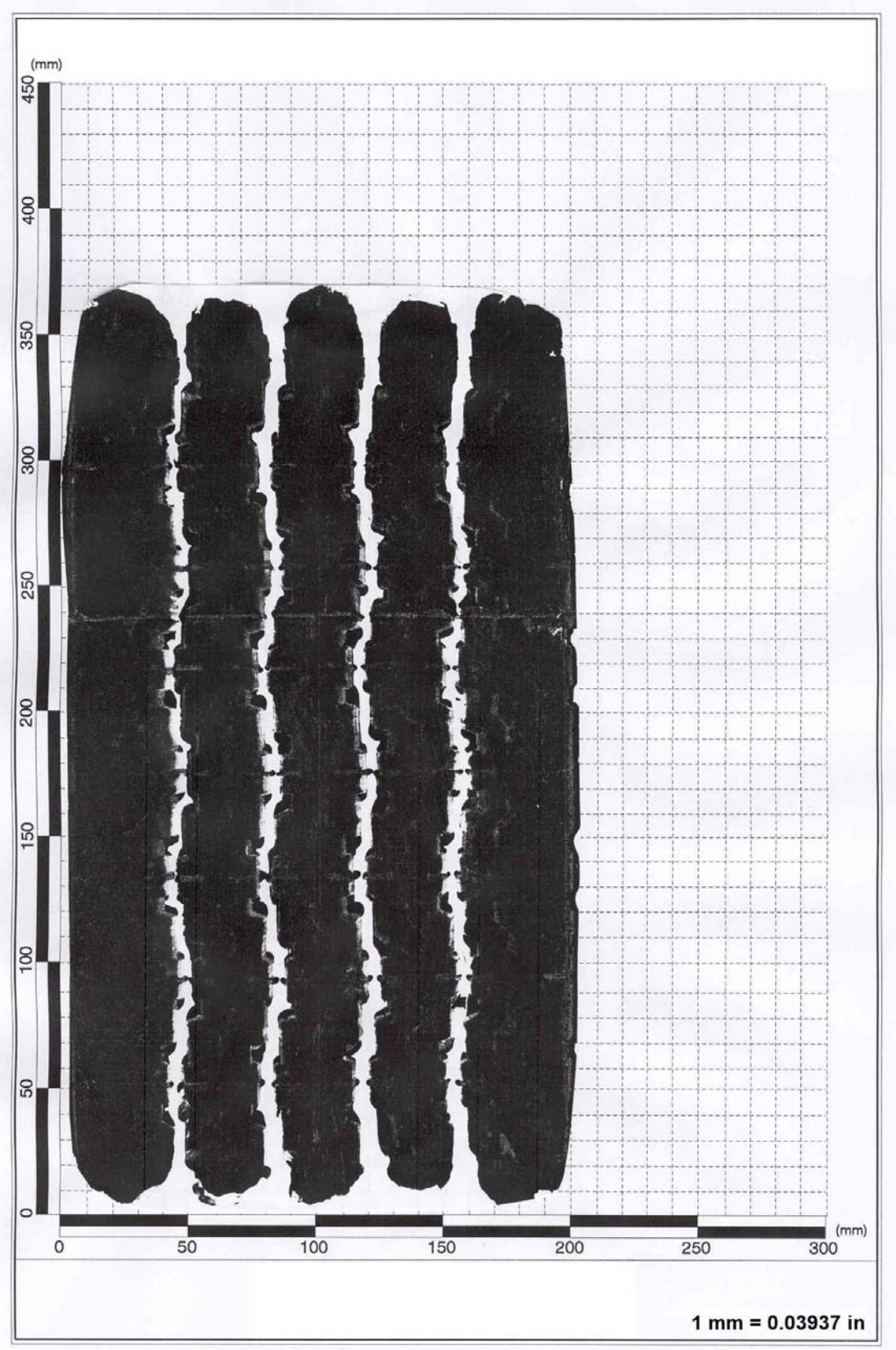

Figure D21. Tire Imprint for 11R24.5 Tire Taken at a Tire Load of 7800 lb and an Inflation Pressure of 70 psi.

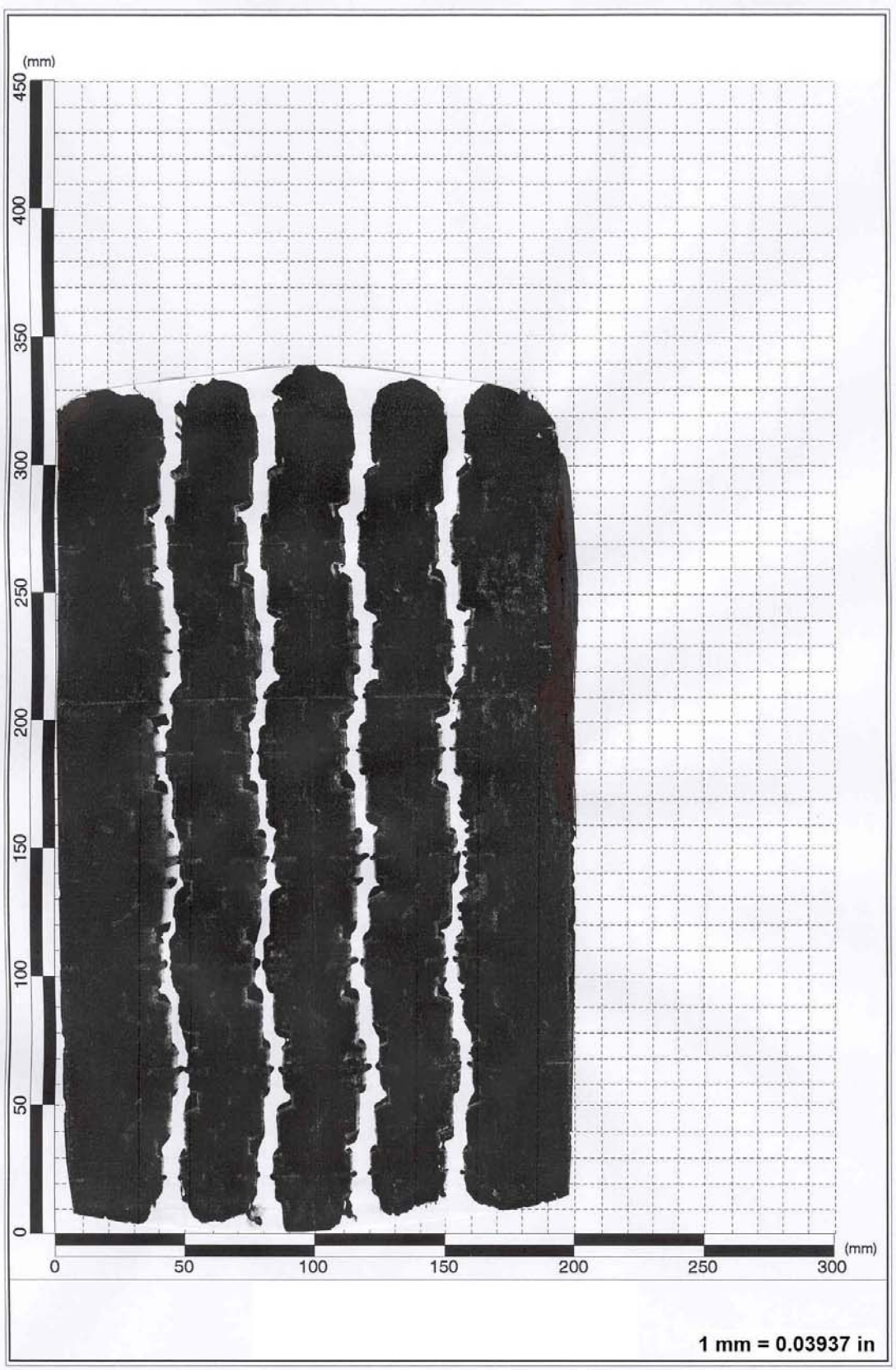

Figure D22. Tire Imprint for 11R24.5 Tire Taken at a Tire Load of 7800 lb and an Inflation Pressure of 85 psi.

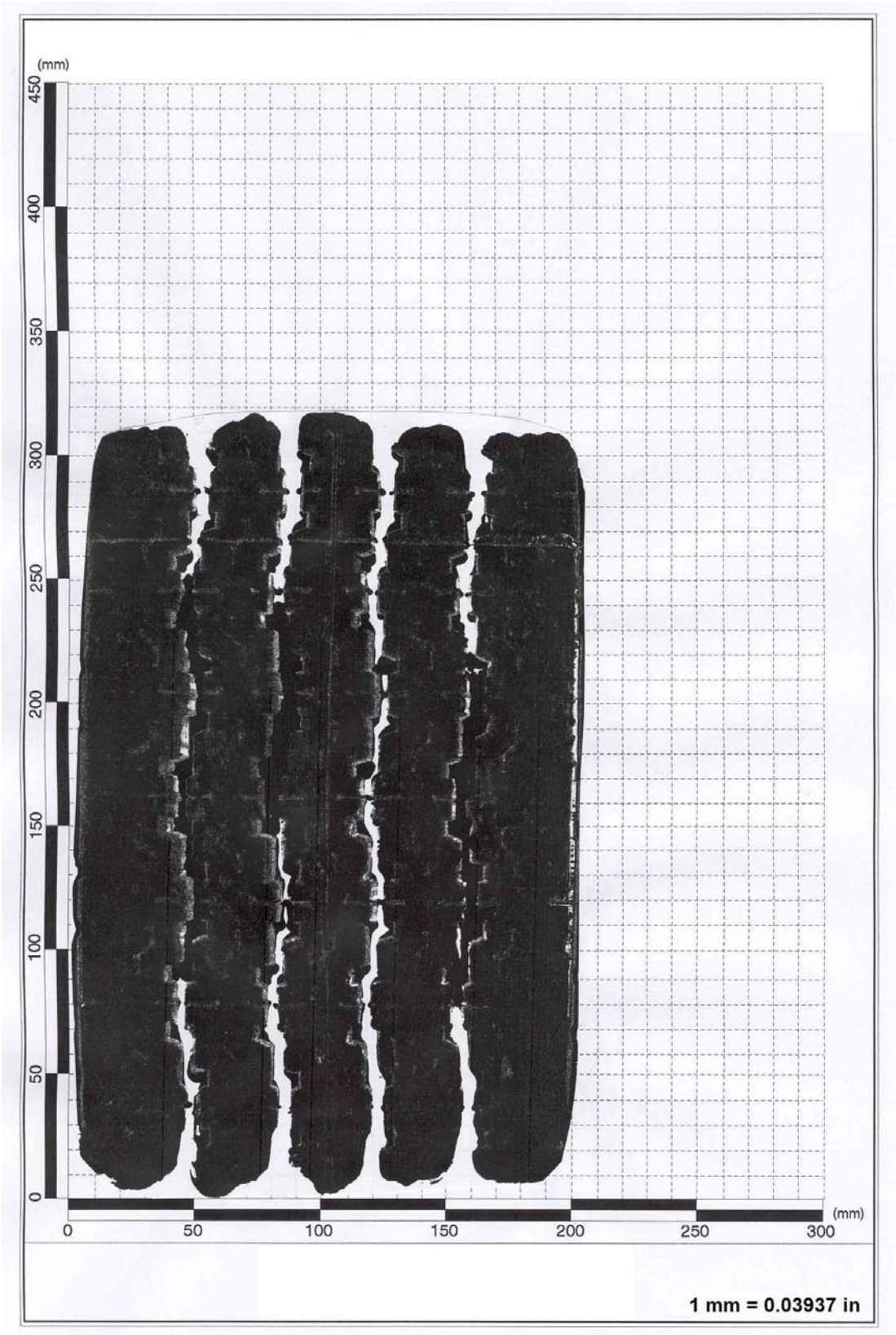

Figure D23. Tire Imprint for 11R24.5 Tire Taken at a Tire Load of 7800 lb and an Inflation Pressure of 100 psi.

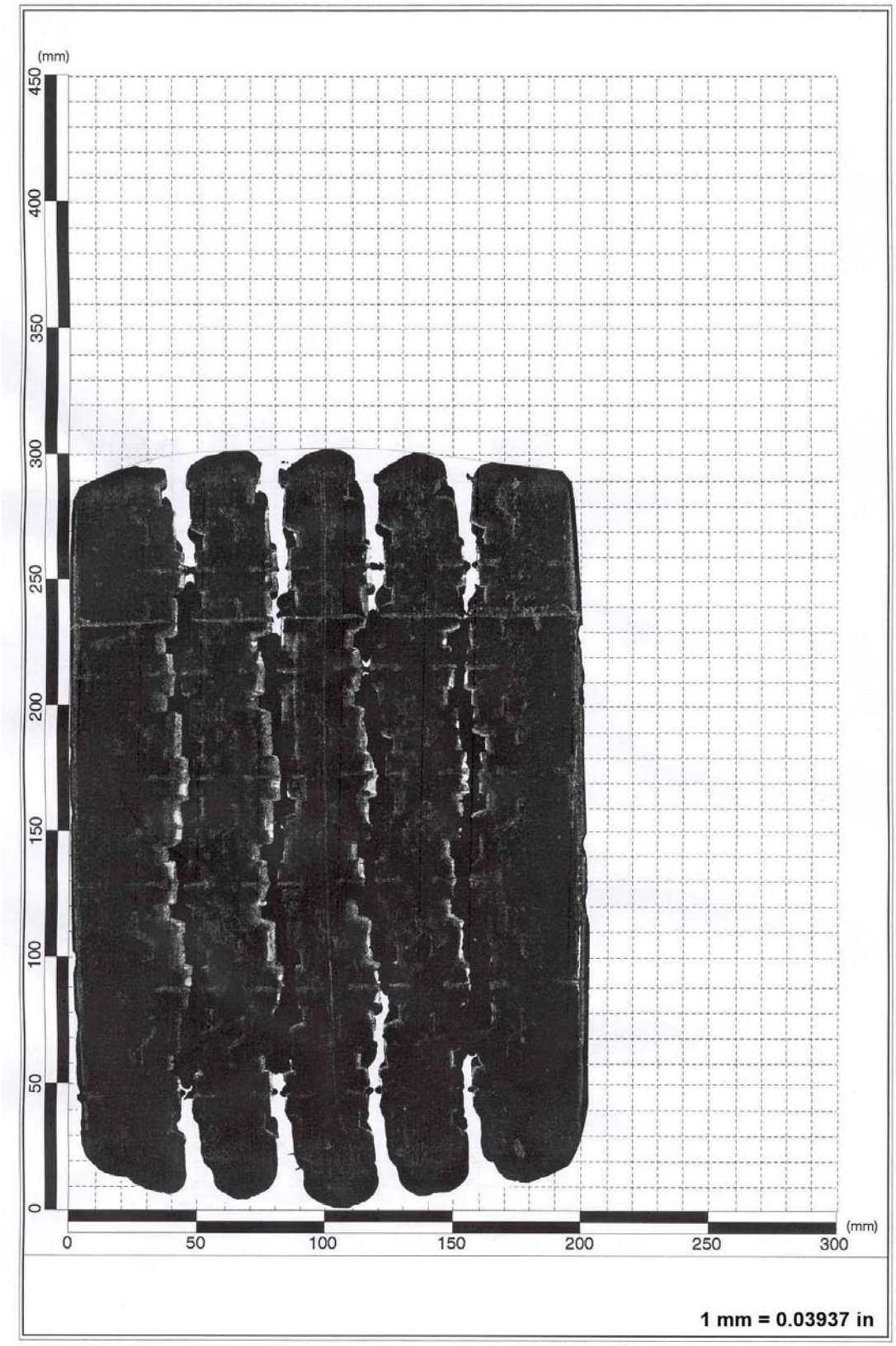

Figure D24. Tire Imprint for 11R24.5 Tire Taken at a Tire Load of 7800 lb and an Inflation Pressure of 115 psi.

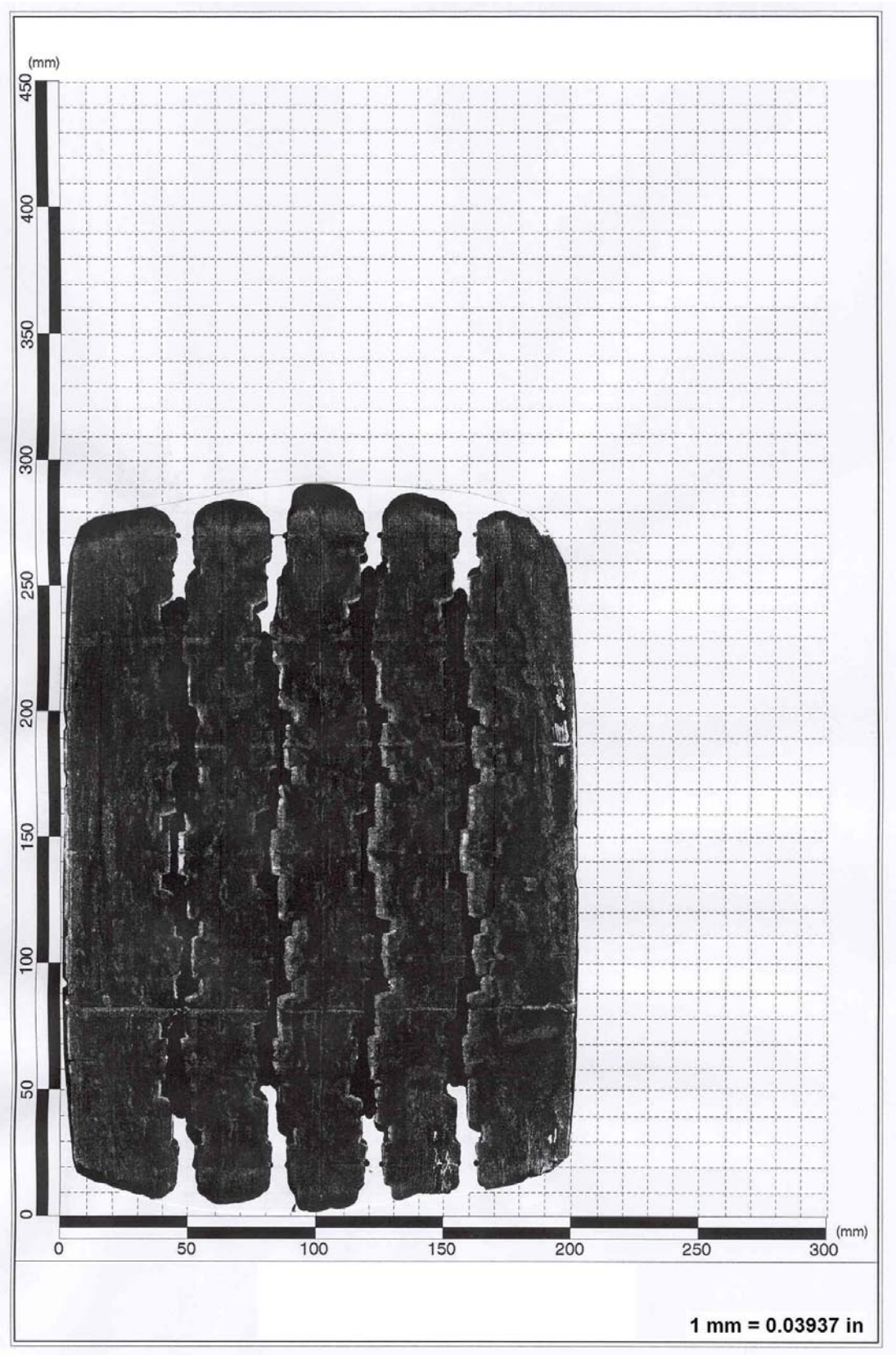

Figure D25. Tire Imprint for 11R24.5 Tire Taken at a Tire Load of 7800 lb and an Inflation Pressure of 130 psi.

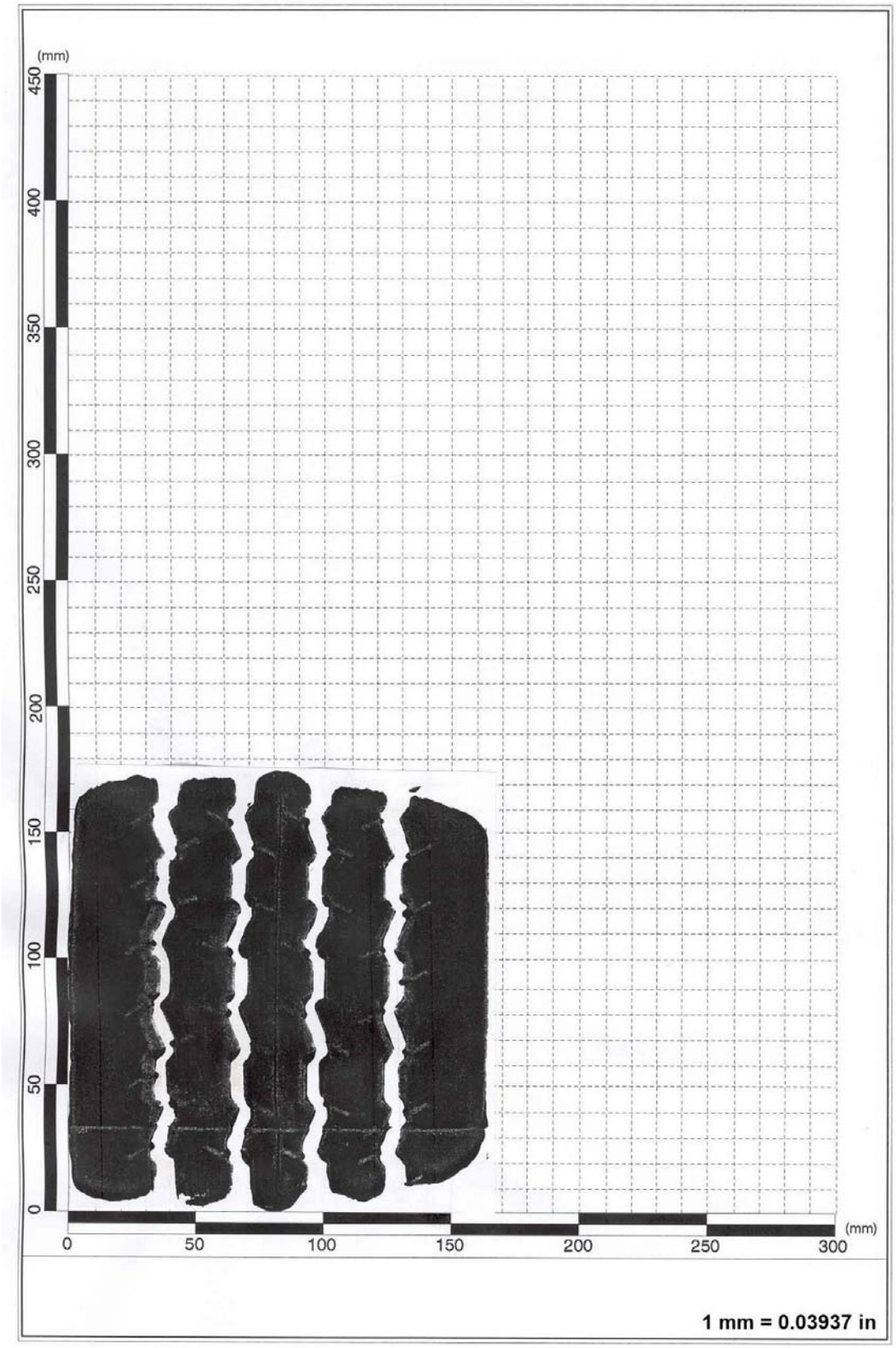

Figure D26. Tire Imprint for 215/75R17.5 Tire Taken at a Tire Load of 3000 lb and an Inflation Pressure of 85 psi.

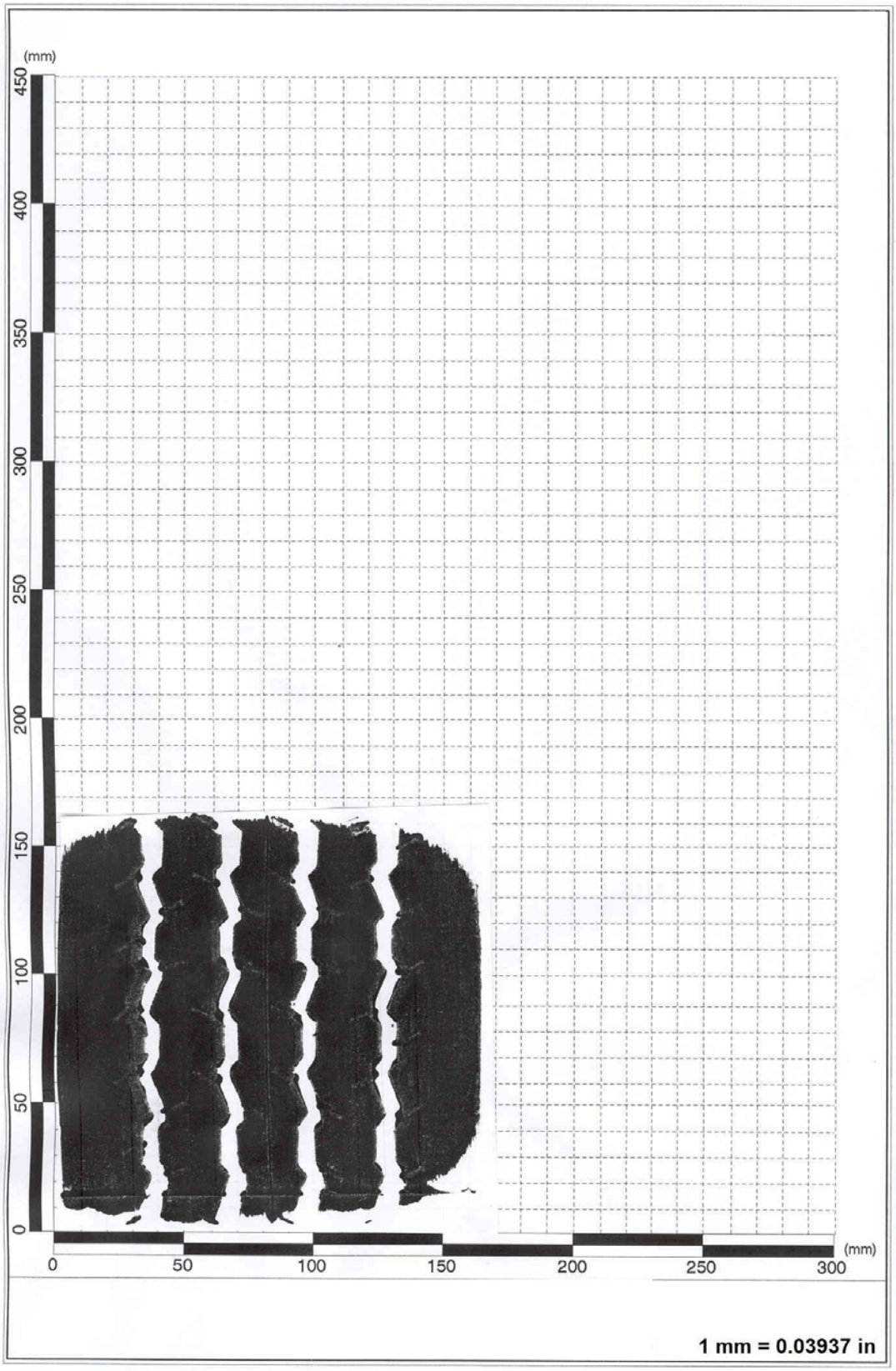

Figure D27. Tire Imprint for 215/75R17.5 Tire Taken at a Tire Load of 3000 lb and an Inflation Pressure of 100 psi.

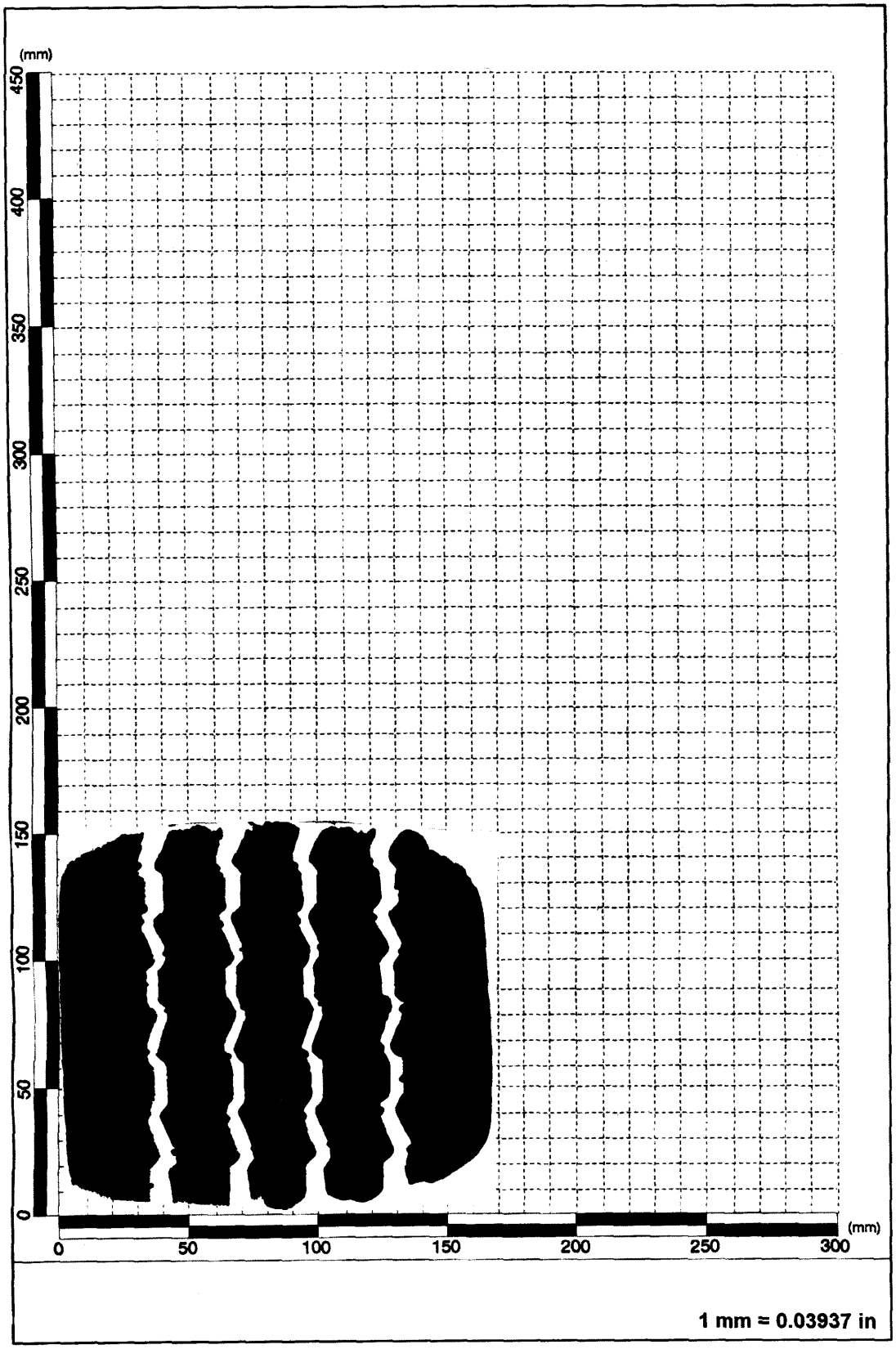

Figure D28. Tire Imprint for 215/75R17.5 Tire Taken at a Tire Load of 3000 lb and an Inflation Pressure of 115 psi.

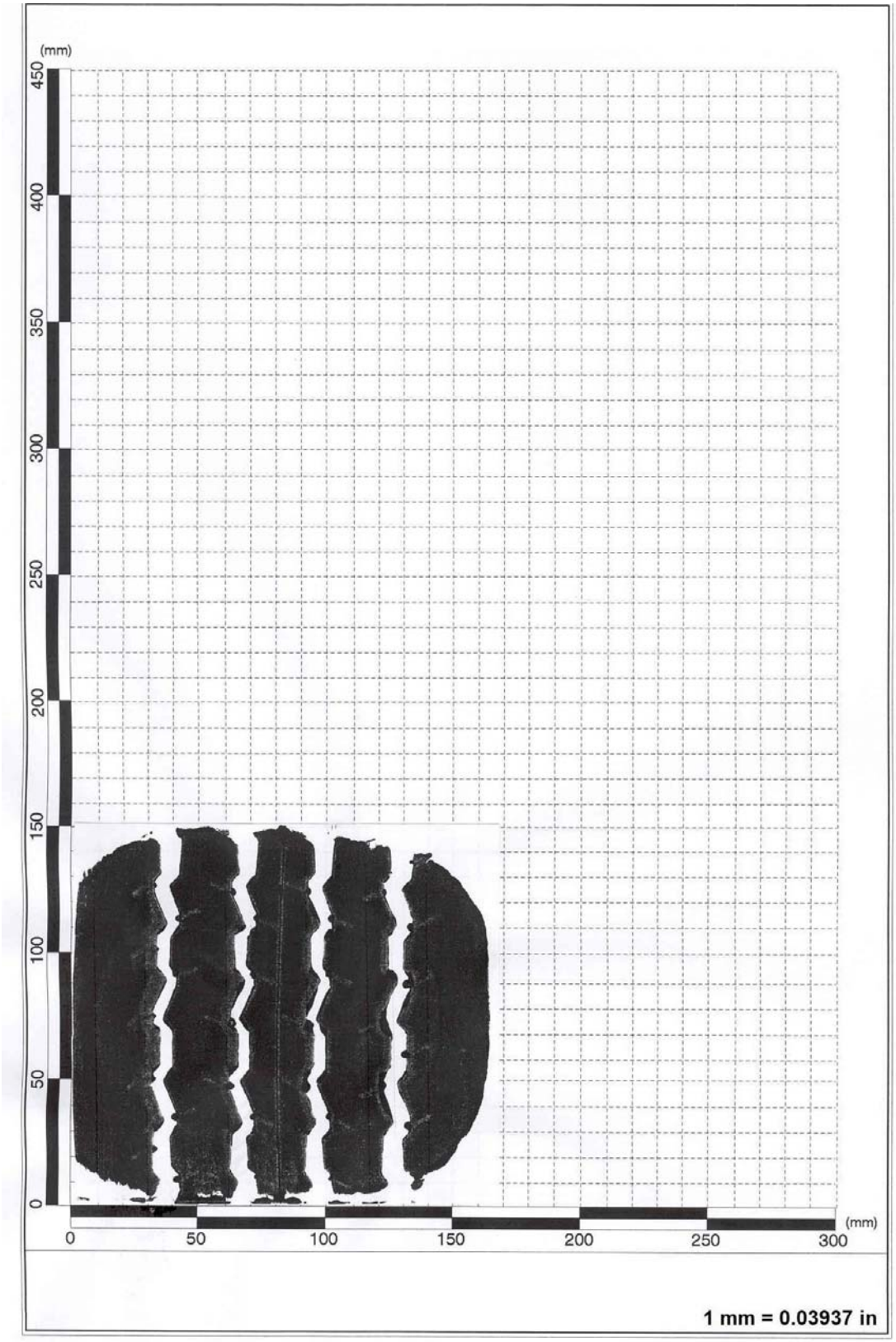

Figure D29. Tire Imprint for 215/75R17.5 Tire Taken at a Tire Load of 3000 lb and an Inflation Pressure of 130 psi.

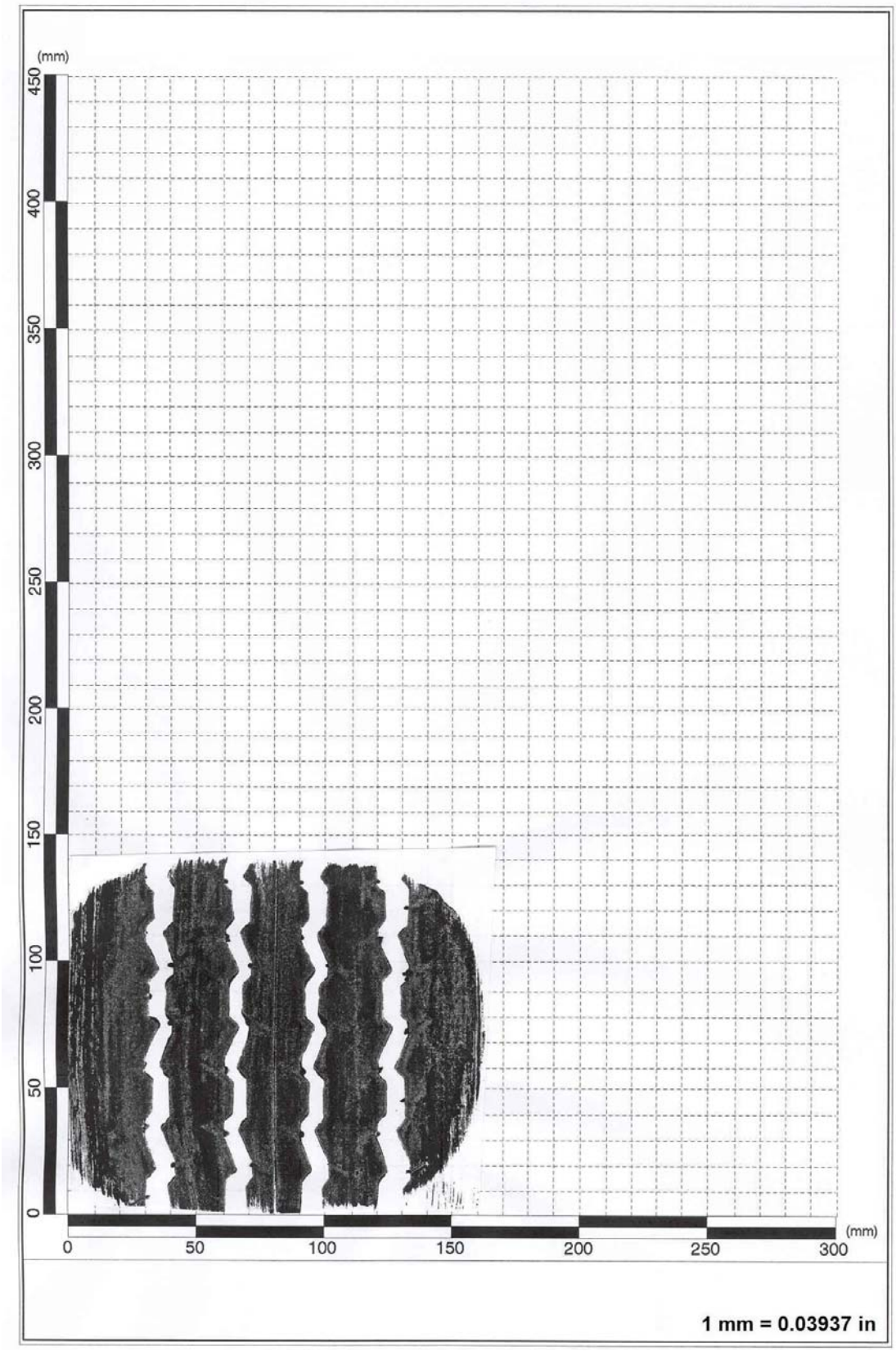

Figure D30. Tire Imprint for 215/75R17.5 Tire Taken at a Tire Load of 3000 lb and an Inflation Pressure of 145 psi.

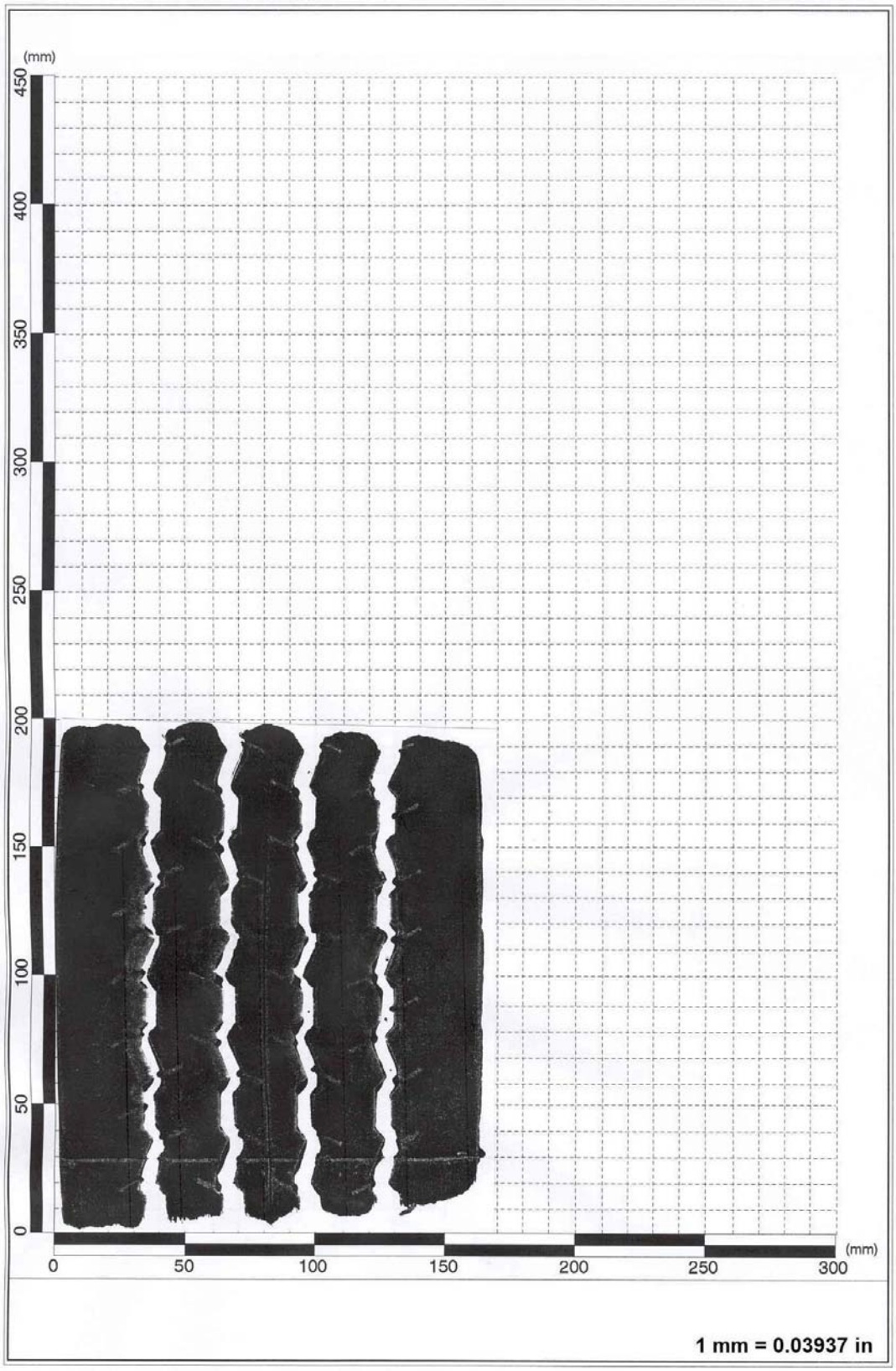

Figure D31. Tire Imprint for 215/75R17.5 Tire Taken at a Tire Load of 4000 lb and an Inflation Pressure of 85 psi.

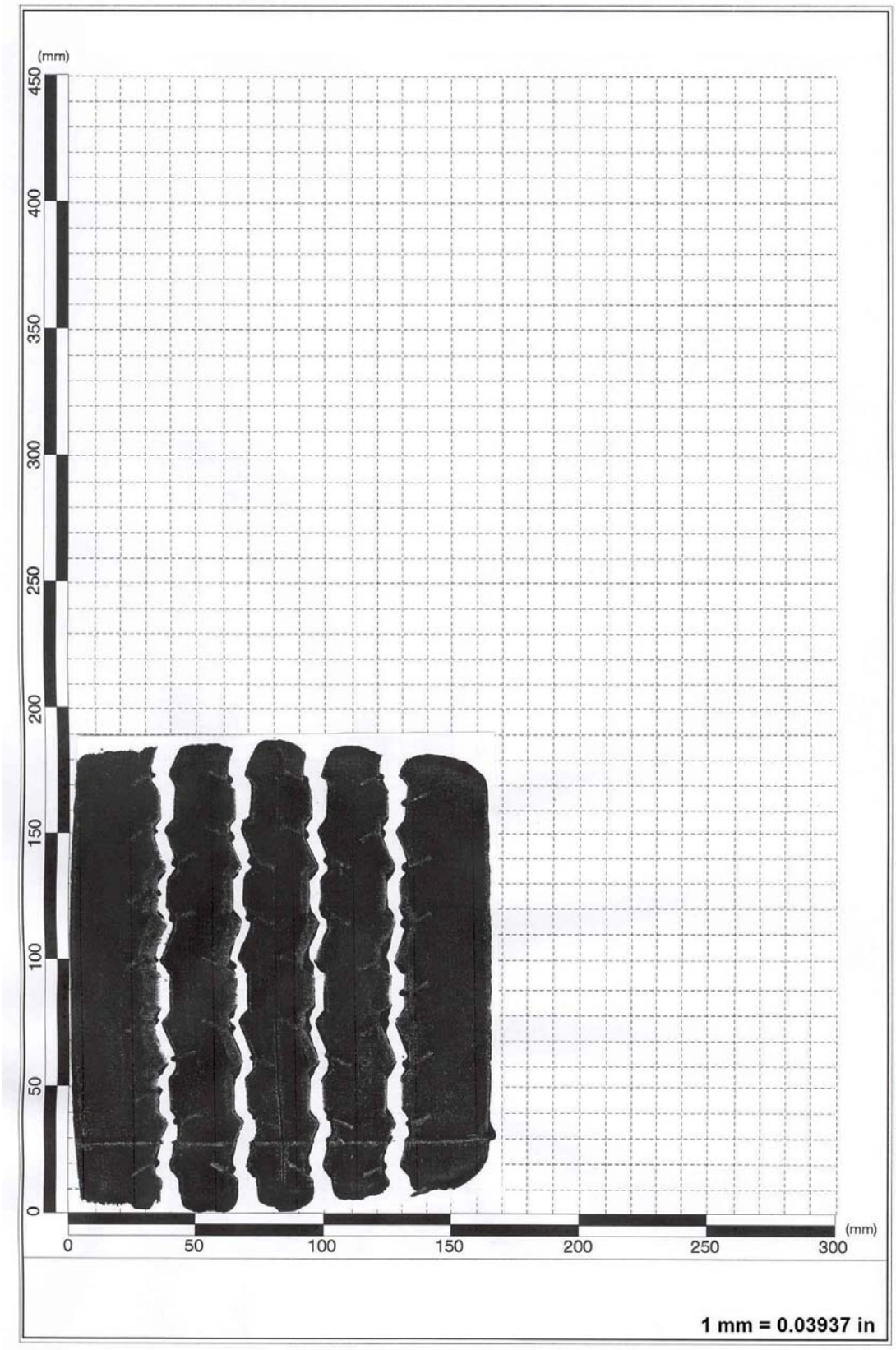

Figure D32. Tire Imprint for 215/75R17.5 Tire Taken at a Tire Load of 4000 lb and an Inflation Pressure of 100 psi.

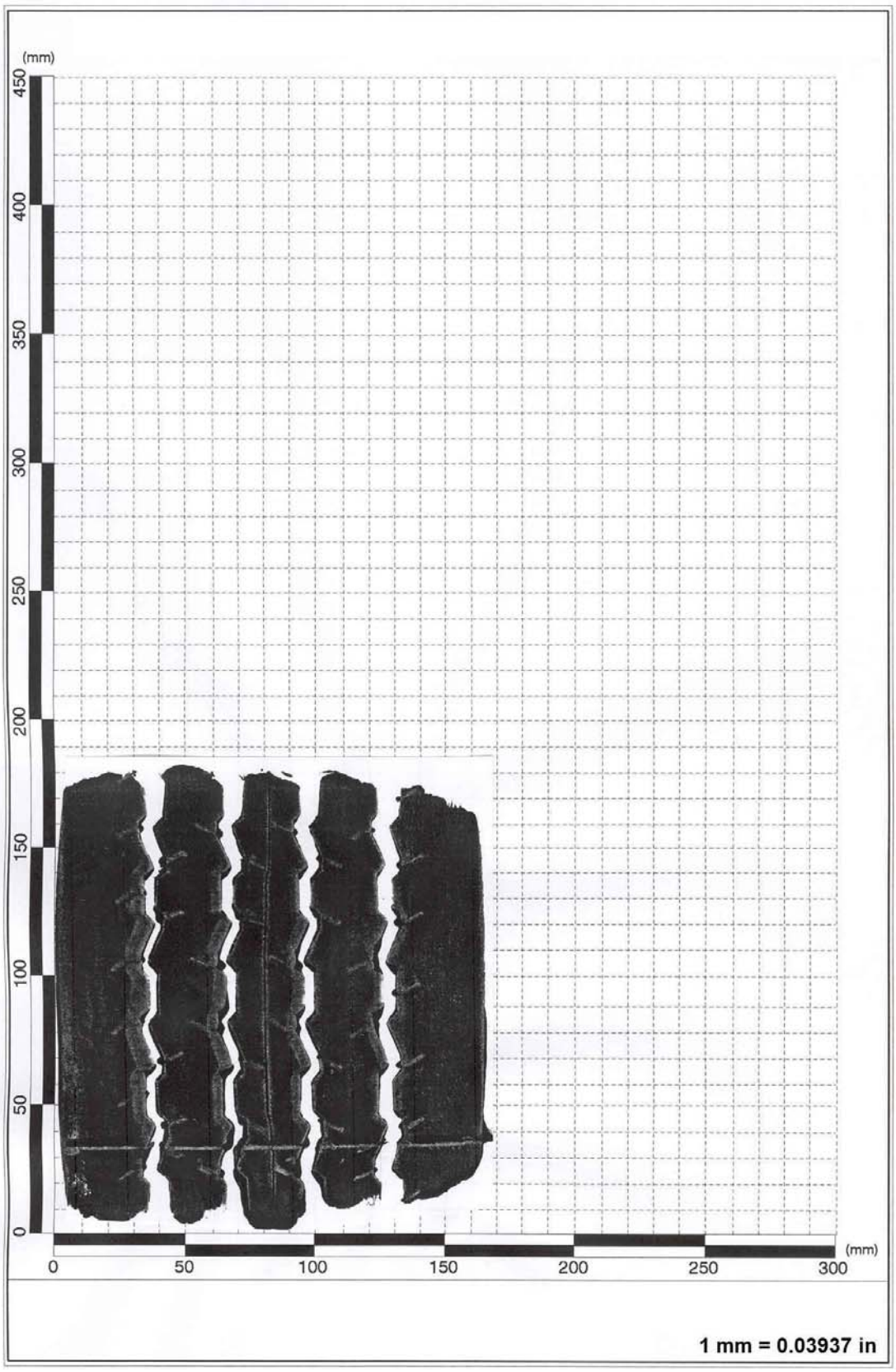

Figure D33. Tire Imprint for 215/75R17.5 Tire Taken at a Tire Load of 4000 lb and an Inflation Pressure of 115 psi.

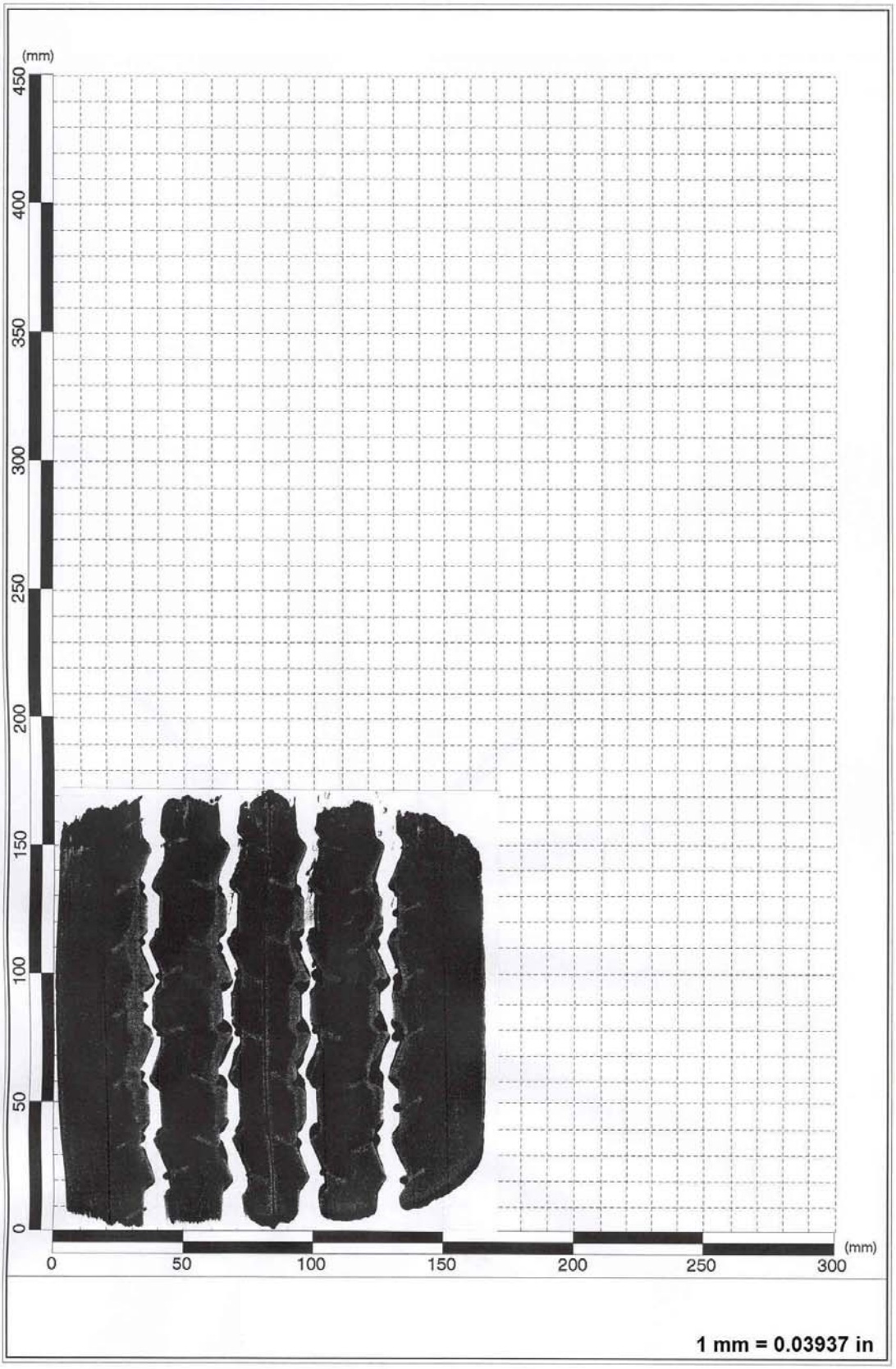

Figure D34. Tire Imprint for 215/75R17.5 Tire Taken at a Tire Load of 4000 lb and an Inflation Pressure of 130 psi.

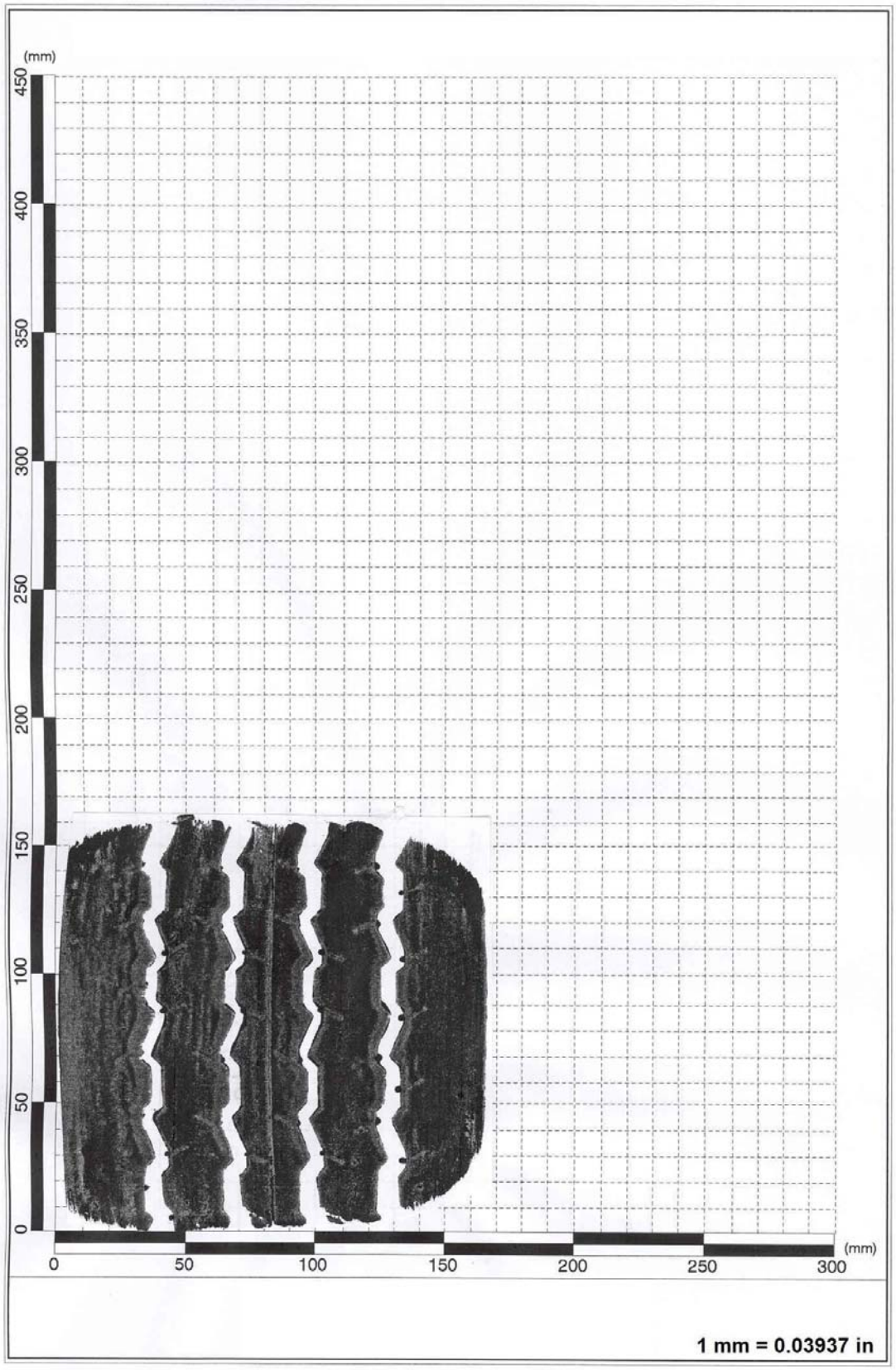

Figure D35. Tire Imprint for 215/75R17.5 Tire Taken at a Tire Load of 4000 lb and an Inflation Pressure of 145 psi.

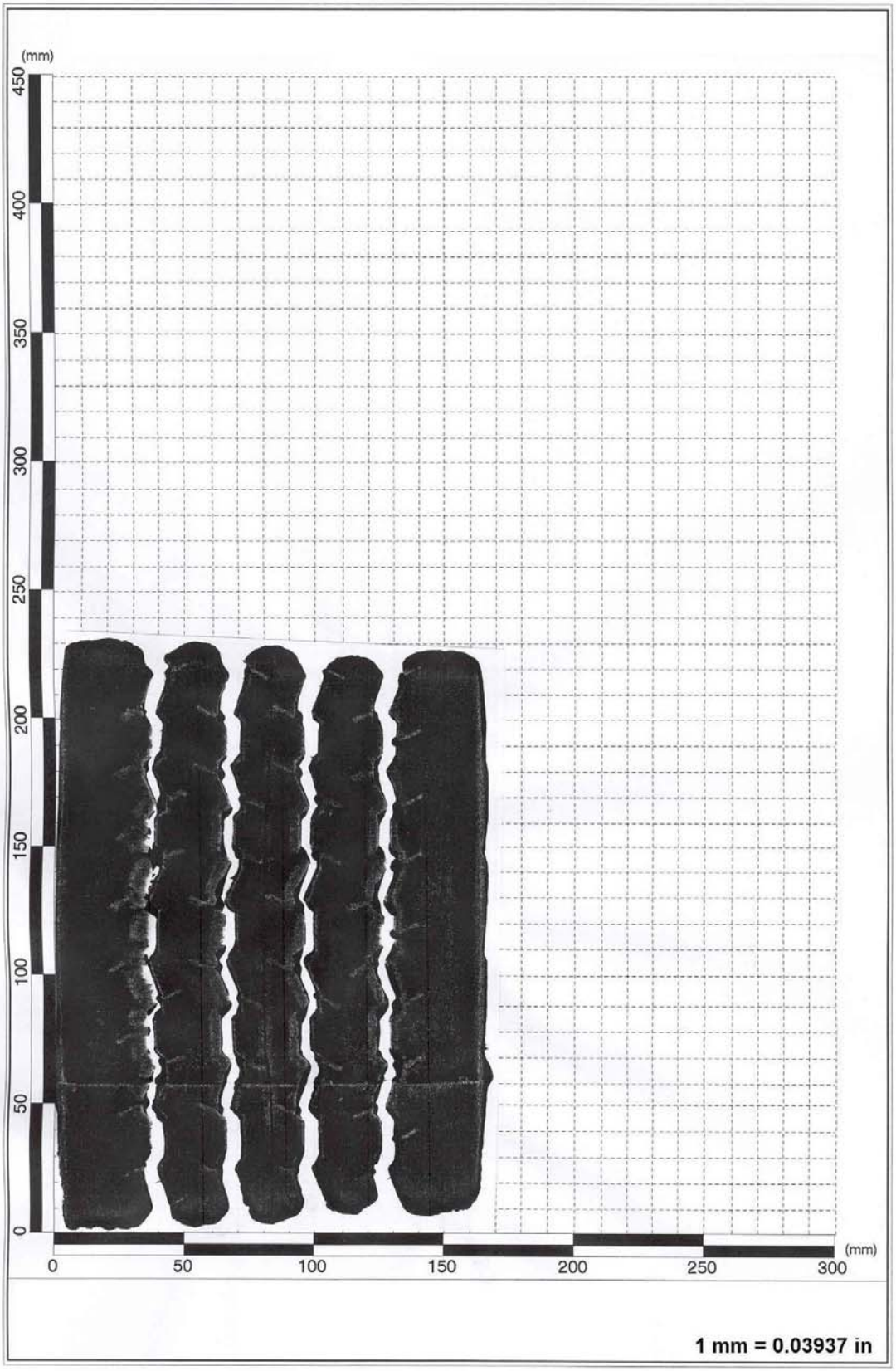

Figure D36. Tire Imprint for 215/75R17.5 Tire Taken at a Tire Load of 5000 lb and an Inflation Pressure of 85 psi.

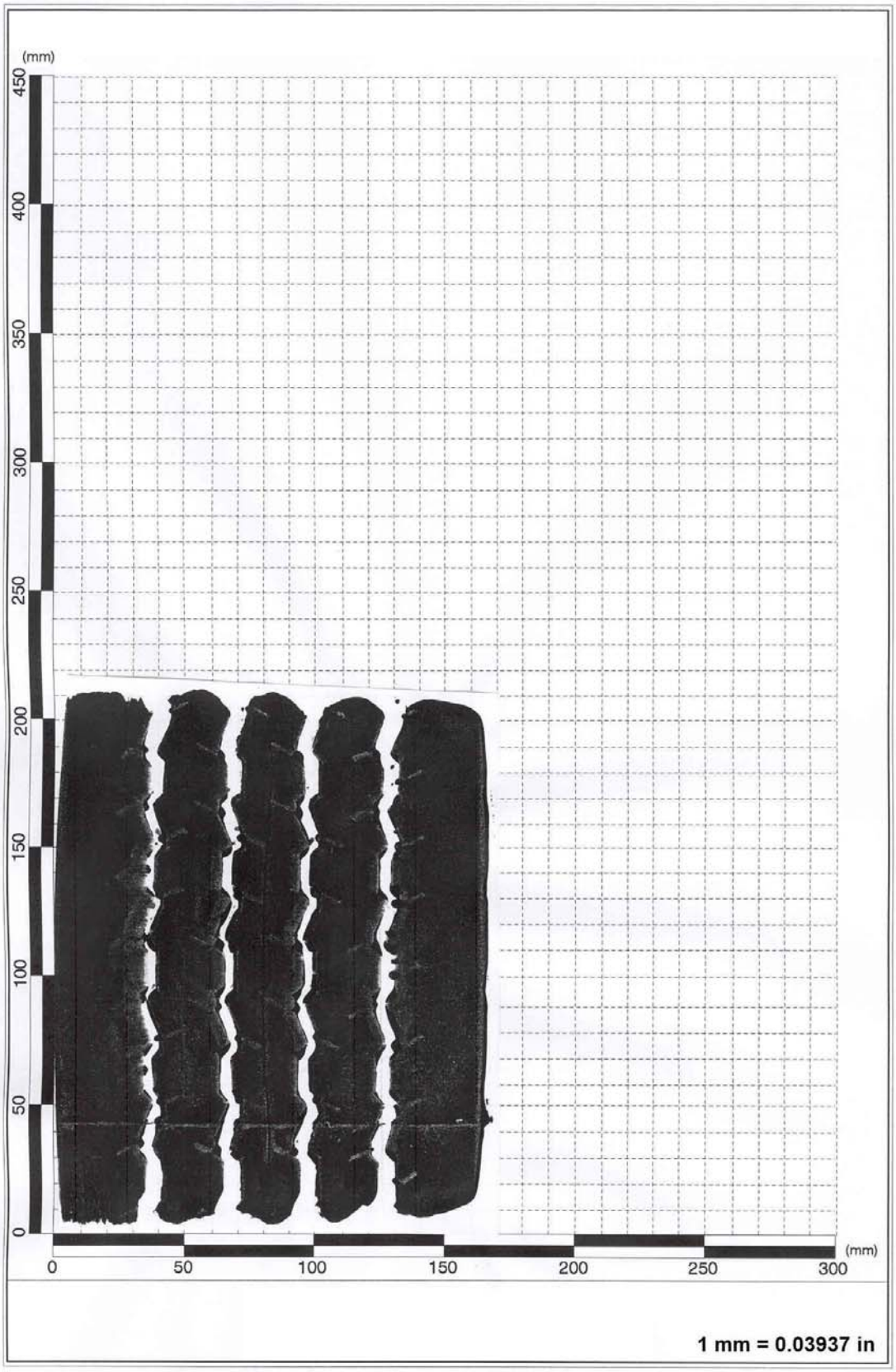

Figure D37. Tire Imprint for 215/75R17.5 Tire Taken at a Tire Load of 5000 lb and an Inflation Pressure of 100 psi.

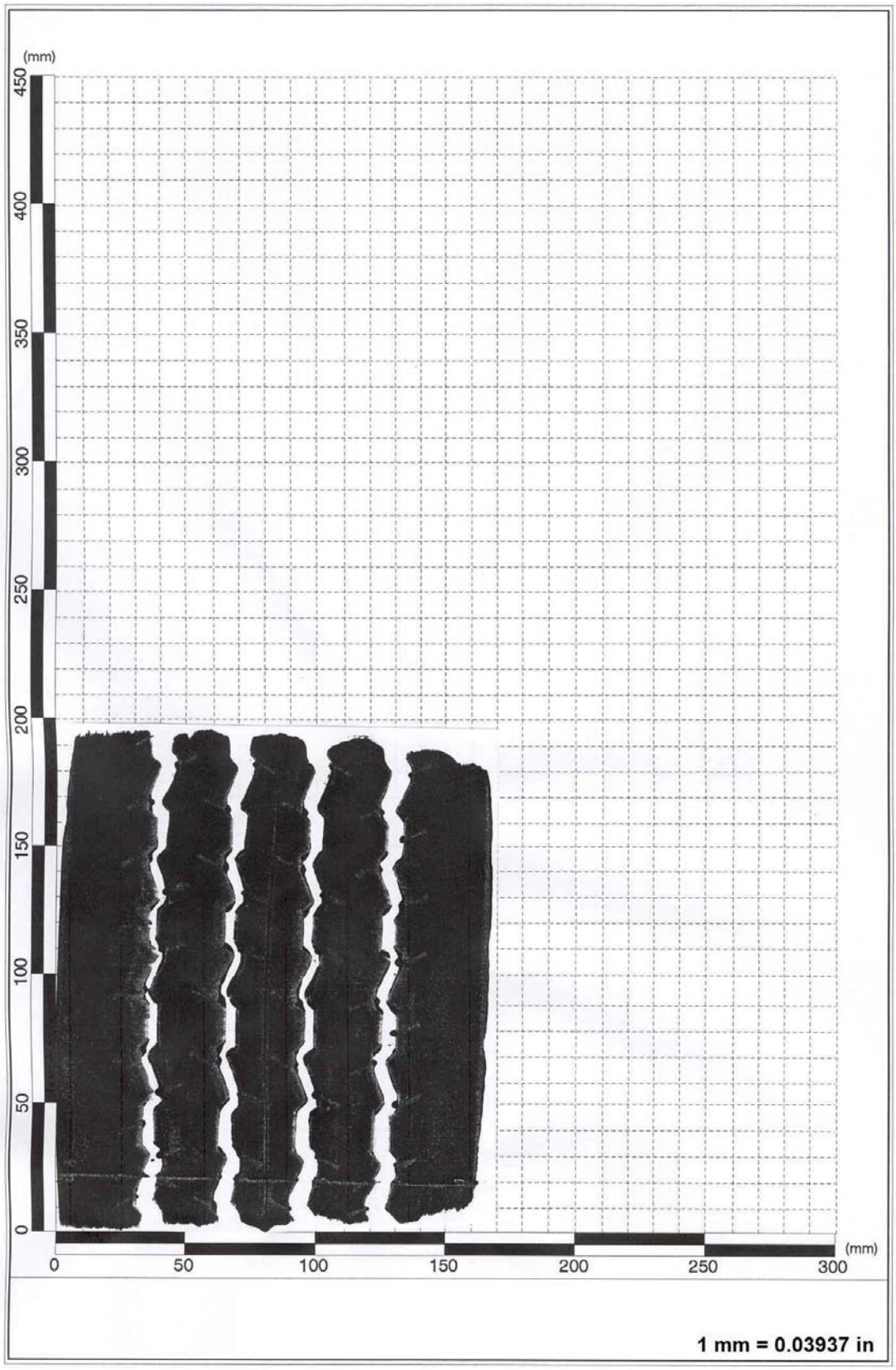

Figure D38. Tire Imprint for 215/75R17.5 Tire Taken at a Tire Load of 5000 lb and an Inflation Pressure of 115 psi.

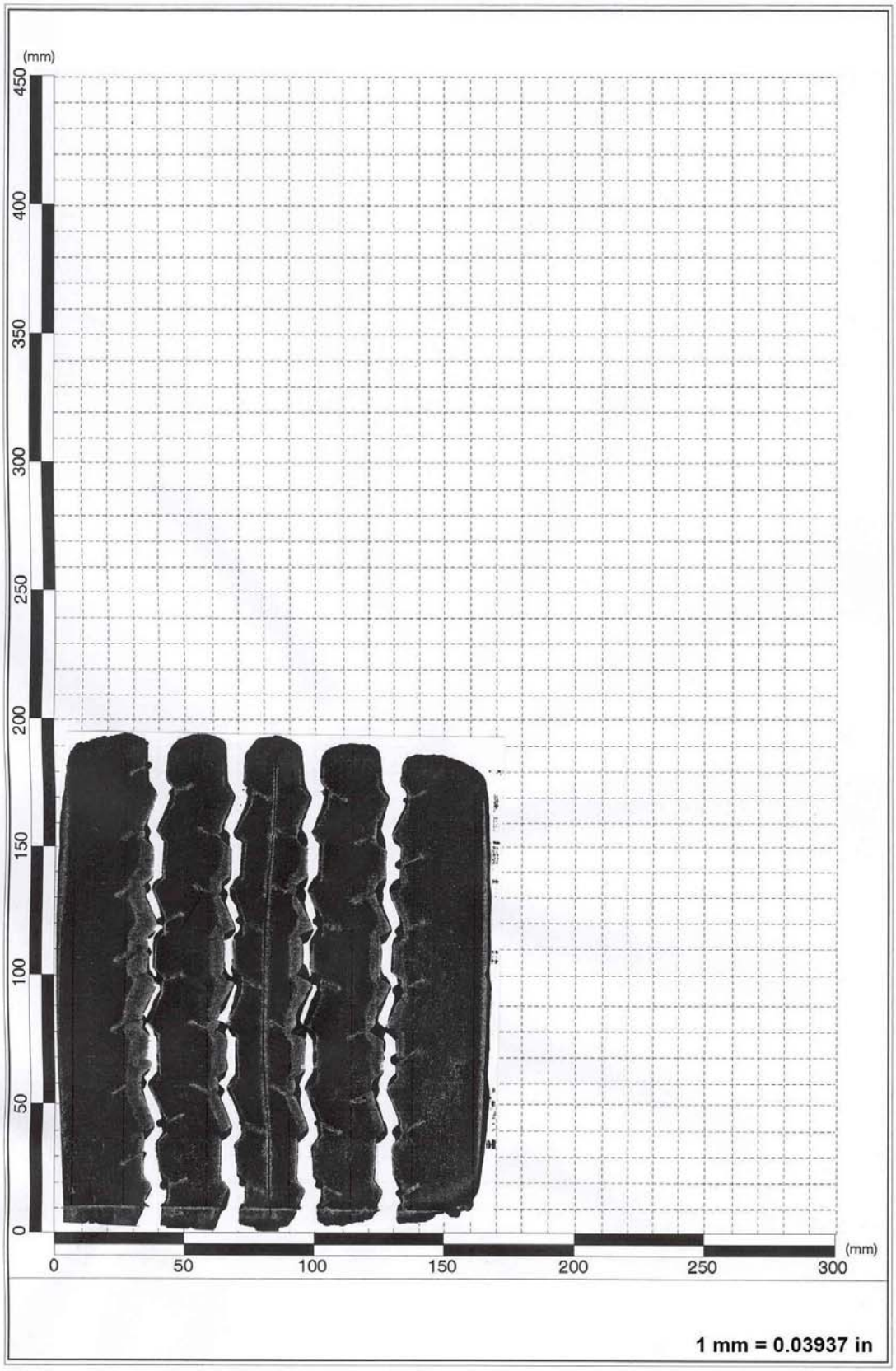

Figure D39. Tire Imprint for 215/75R17.5 Tire Taken at a Tire Load of 5000 lb and an Inflation Pressure of 130 psi.

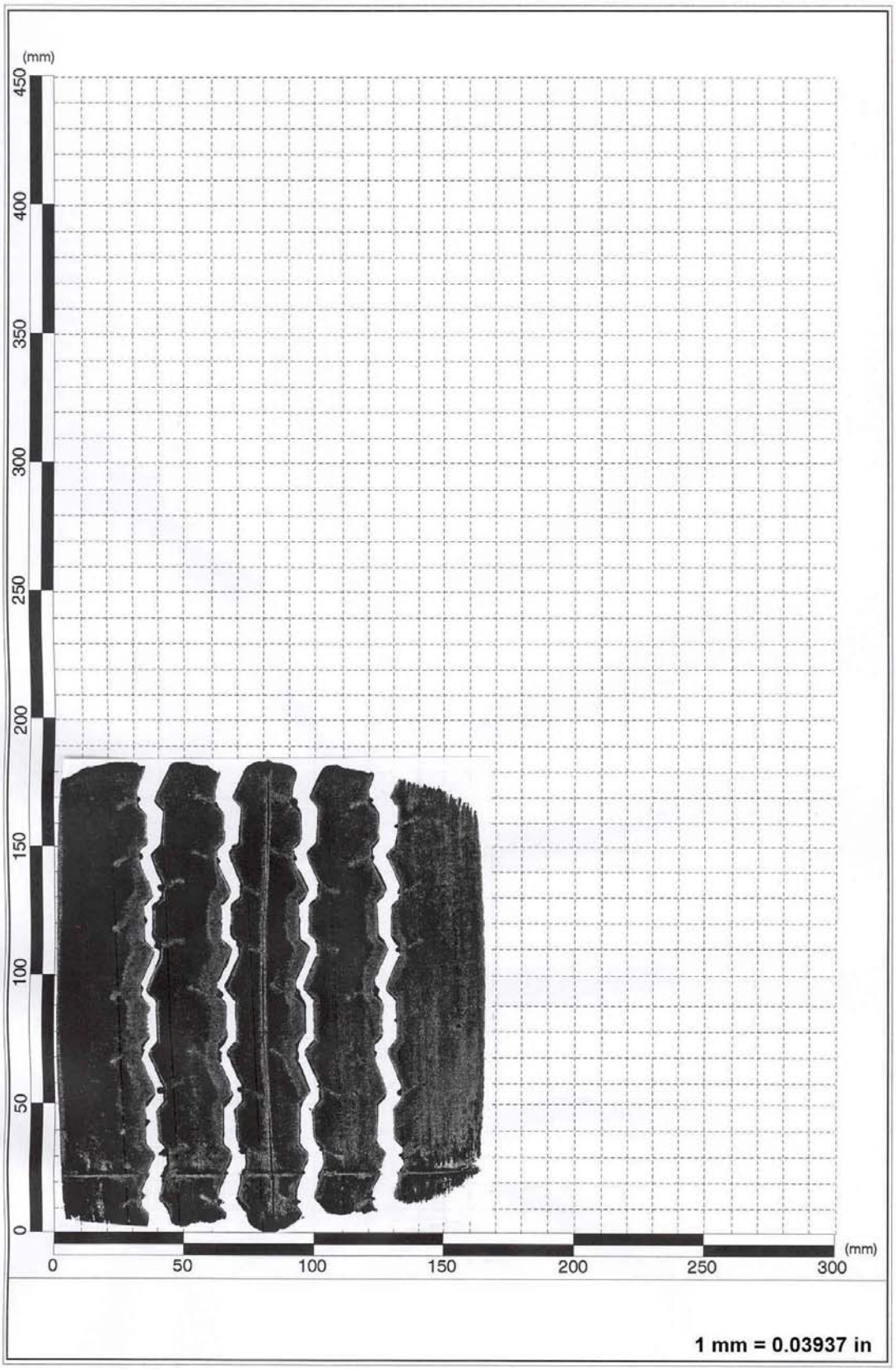

Figure D40. Tire Imprint for 215/75R17.5 Tire Taken at a Tire Load of 5000 lb and an Inflation Pressure of 145 psi.

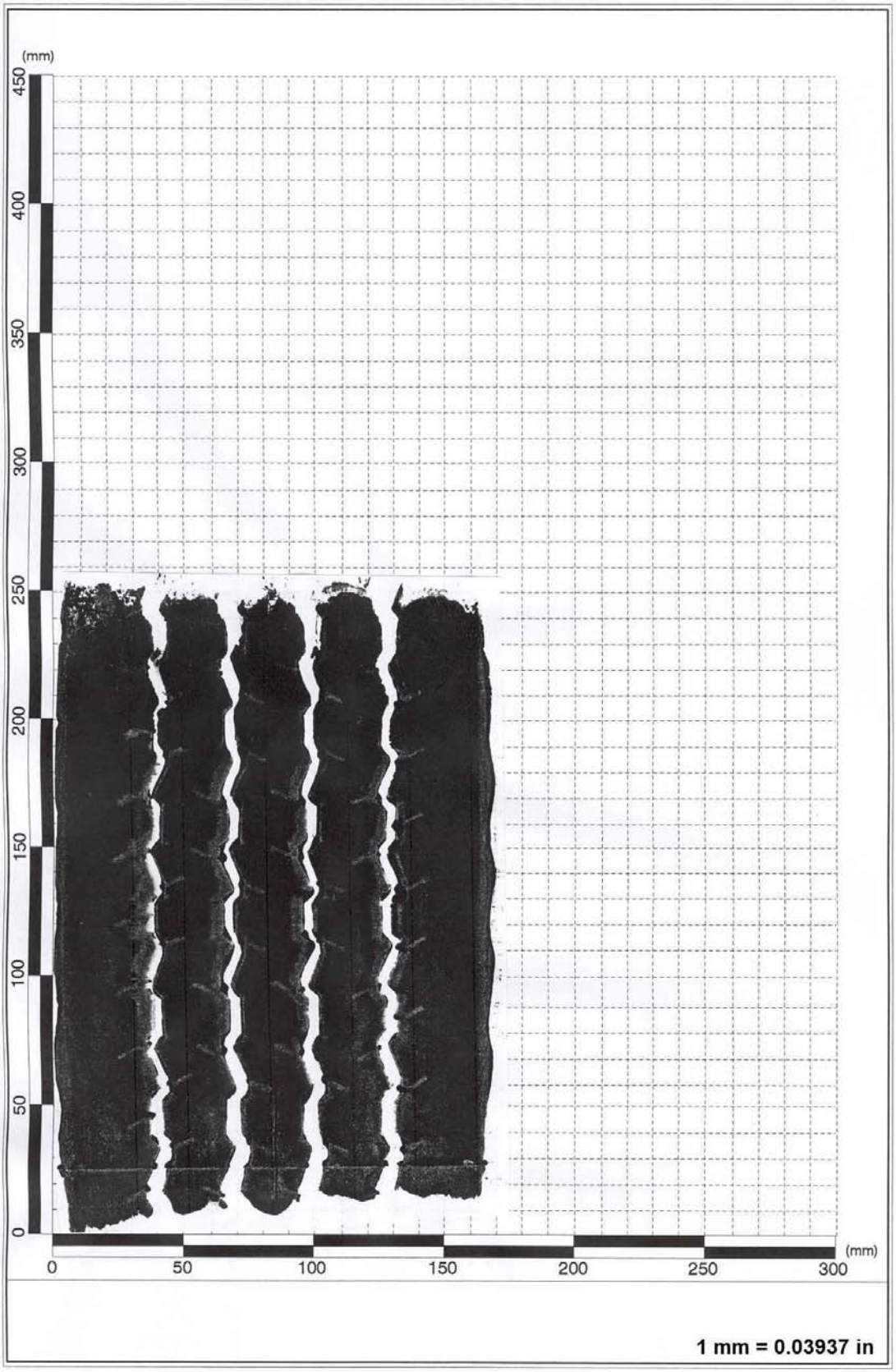

Figure D41. Tire Imprint for 215/75R17.5 Tire Taken at a Tire Load of 6000 lb and an Inflation Pressure of 85 psi.

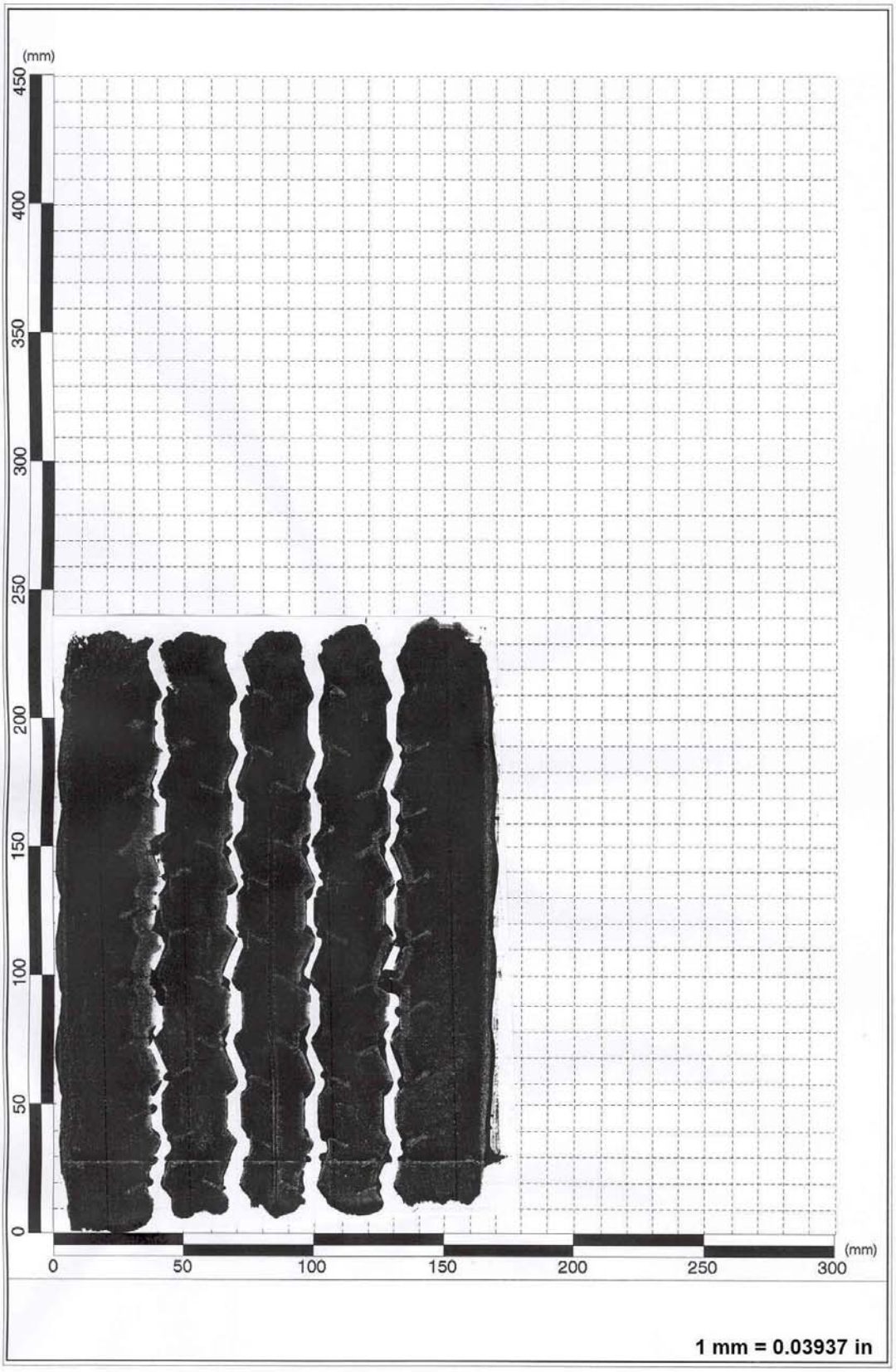

Figure D42. Tire Imprint for 215/75R17.5 Tire Taken at a Tire Load of 6000 lb and an Inflation Pressure of 100 psi.

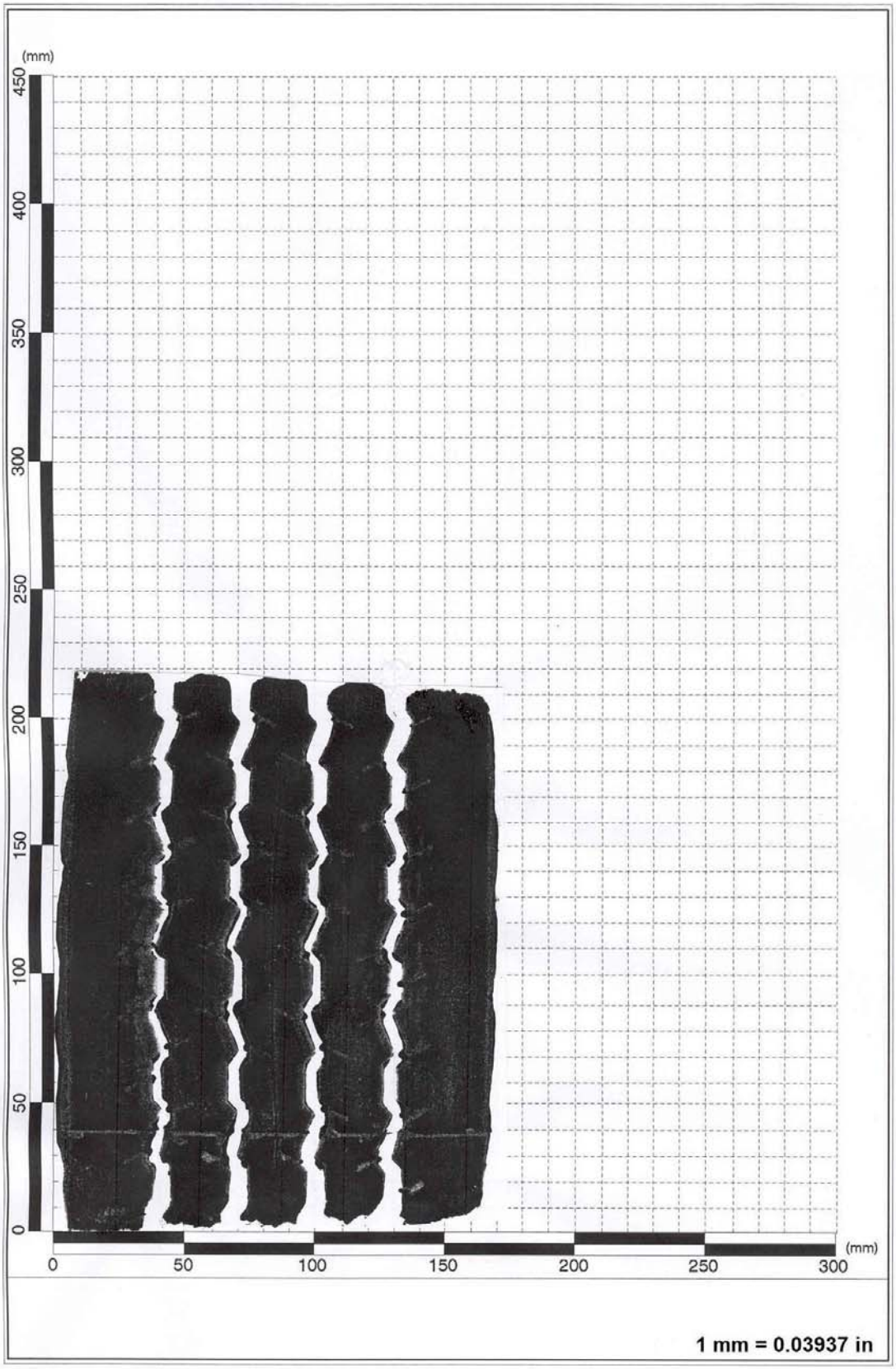

Figure D43. Tire Imprint for 215/75R17.5 Tire Taken at a Tire Load of 6000 lb and an Inflation Pressure of 115 psi.

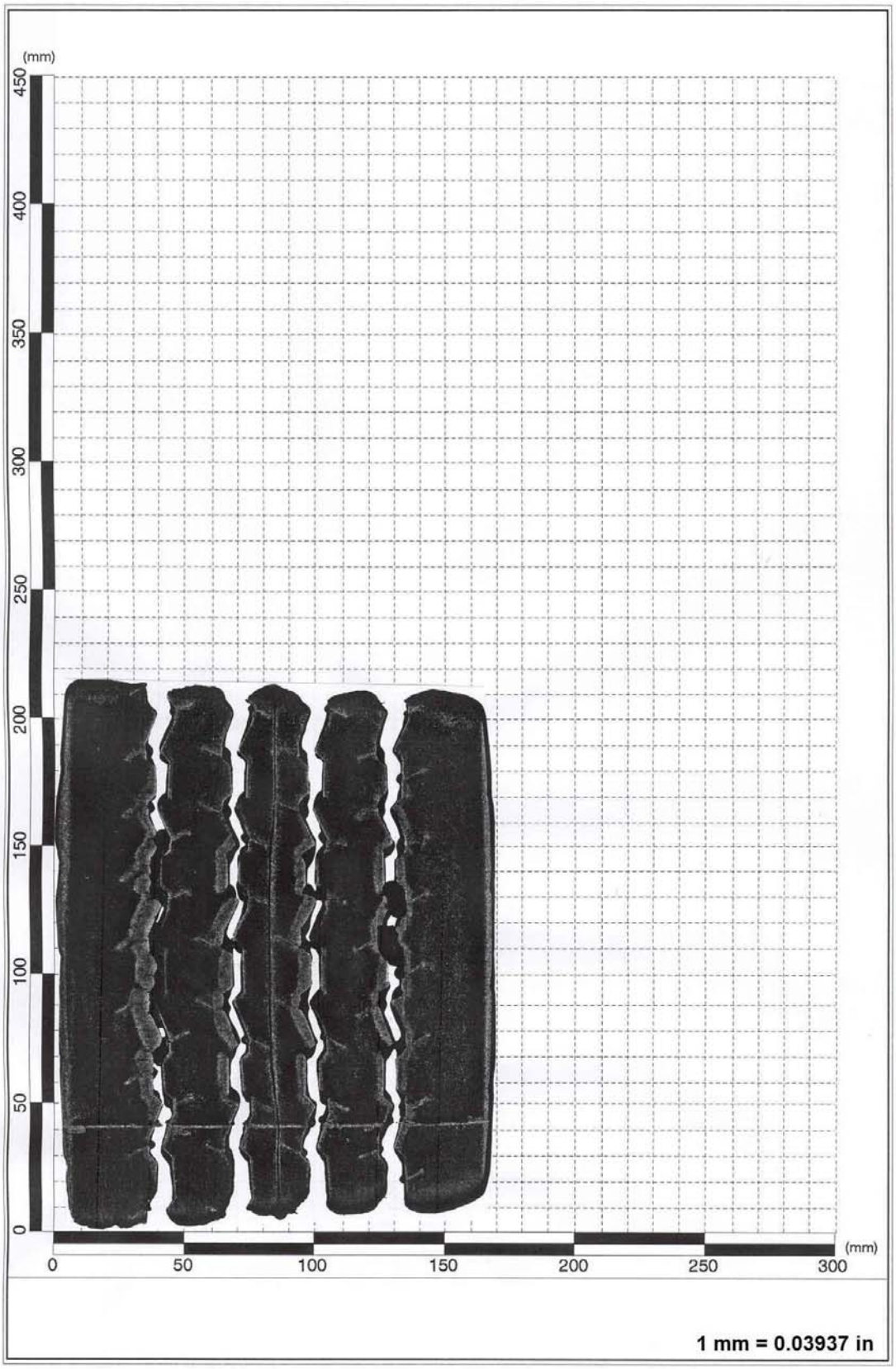

Figure D44. Tire Imprint for 215/75R17.5 Tire Taken at a Tire Load of 6000 lb and an Inflation Pressure of 130 psi.

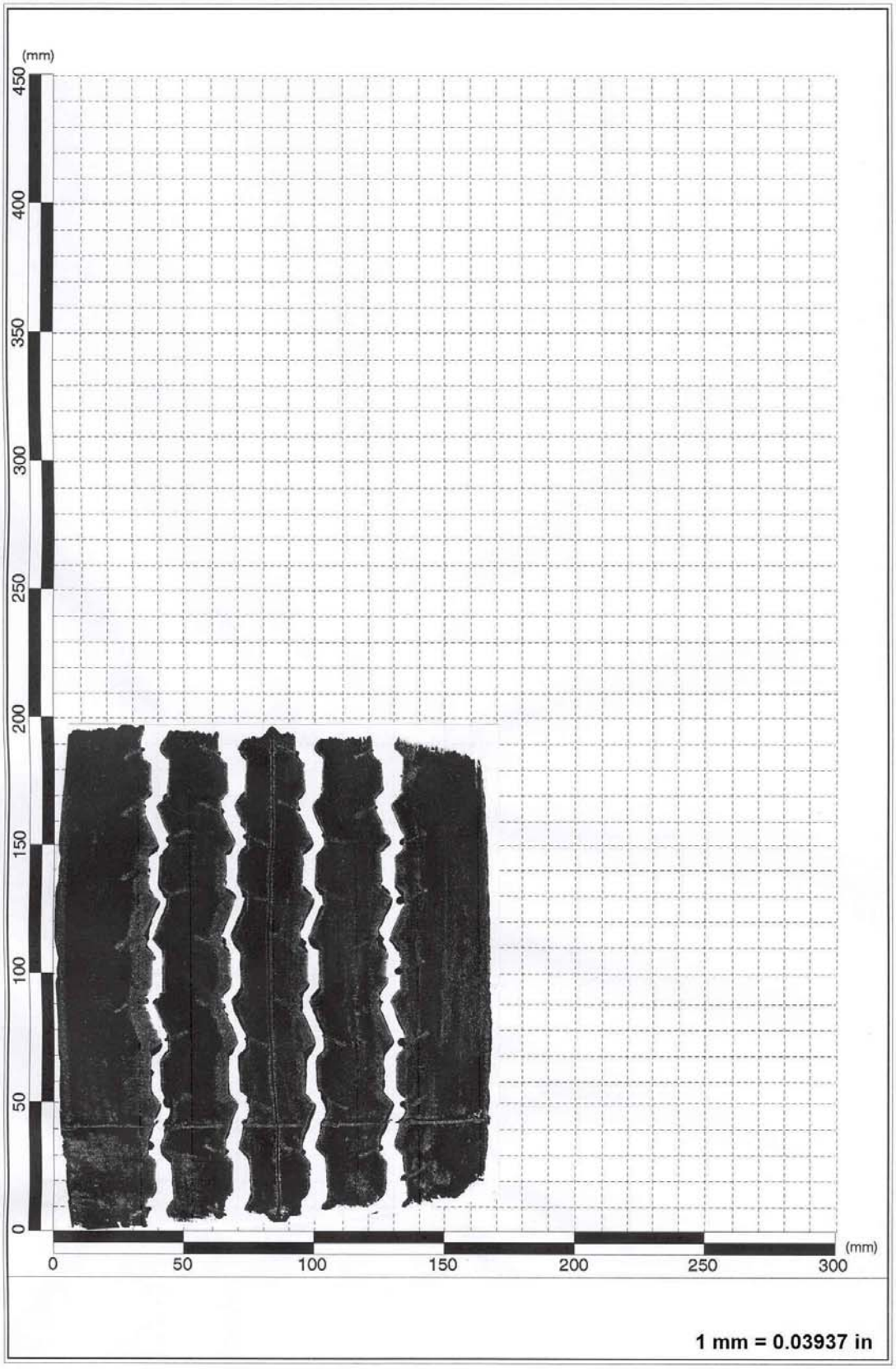

Figure D45. Tire Imprint for 215/75R17.5 Tire Taken at a Tire Load of 6000 lb and an Inflation Pressure of 145 psi.

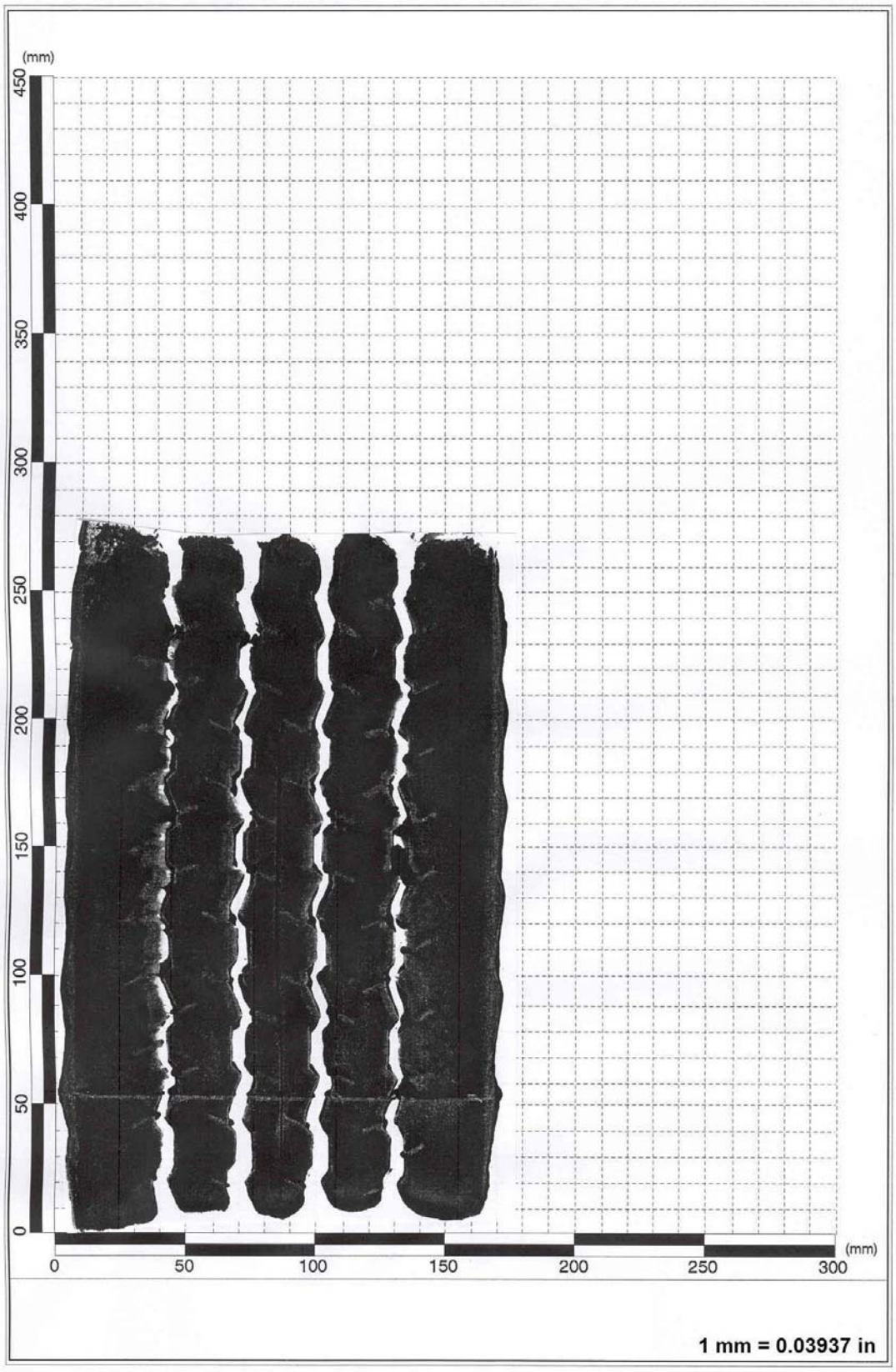

Figure D46. Tire Imprint for 215/75R17.5 Tire Taken at a Tire Load of 7000 lb and an Inflation Pressure of 85 psi.

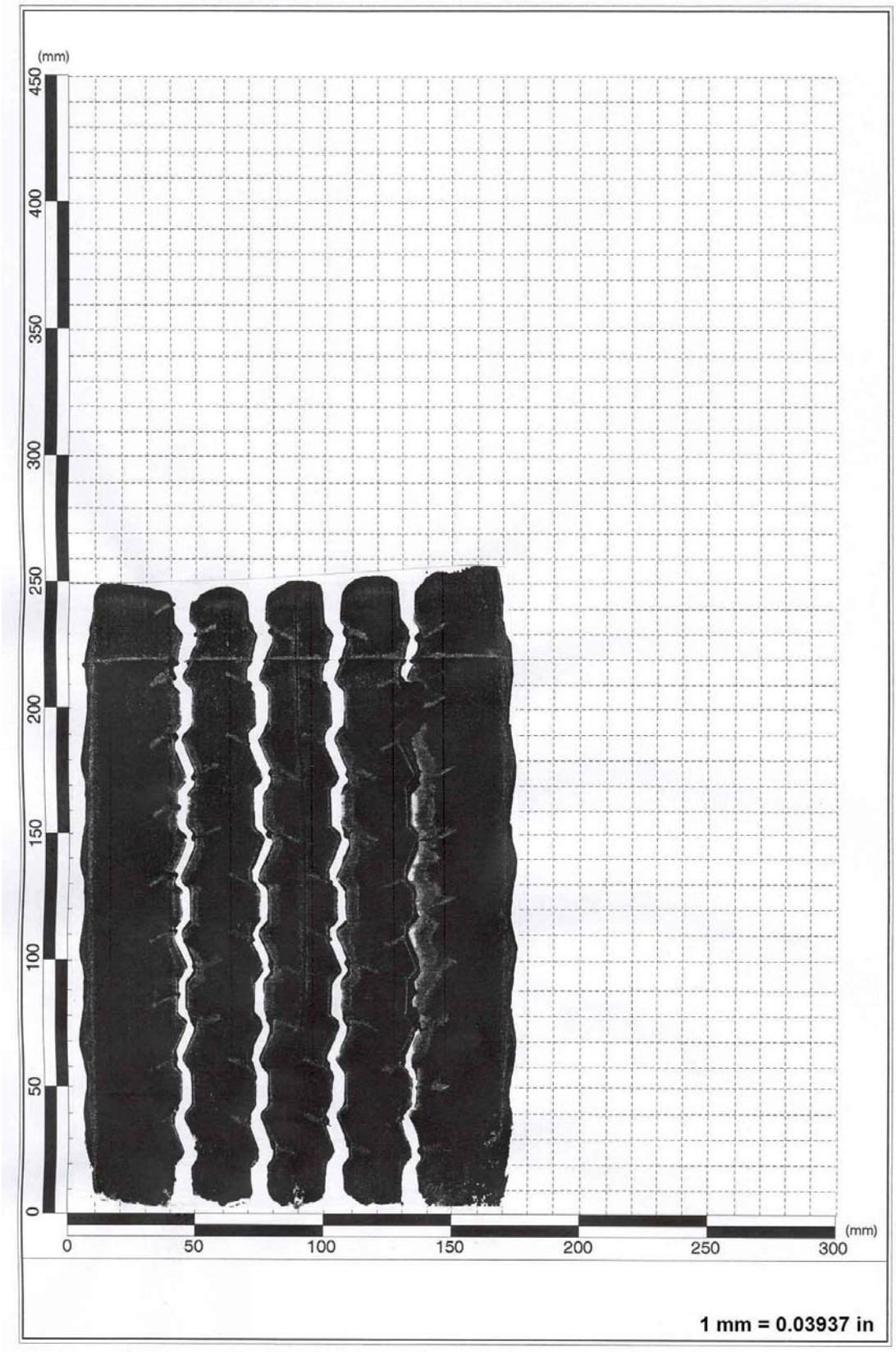

Figure D47. Tire Imprint for 215/75R17.5 Tire Taken at a Tire Load of 7000 lb and an Inflation Pressure of 100 psi.

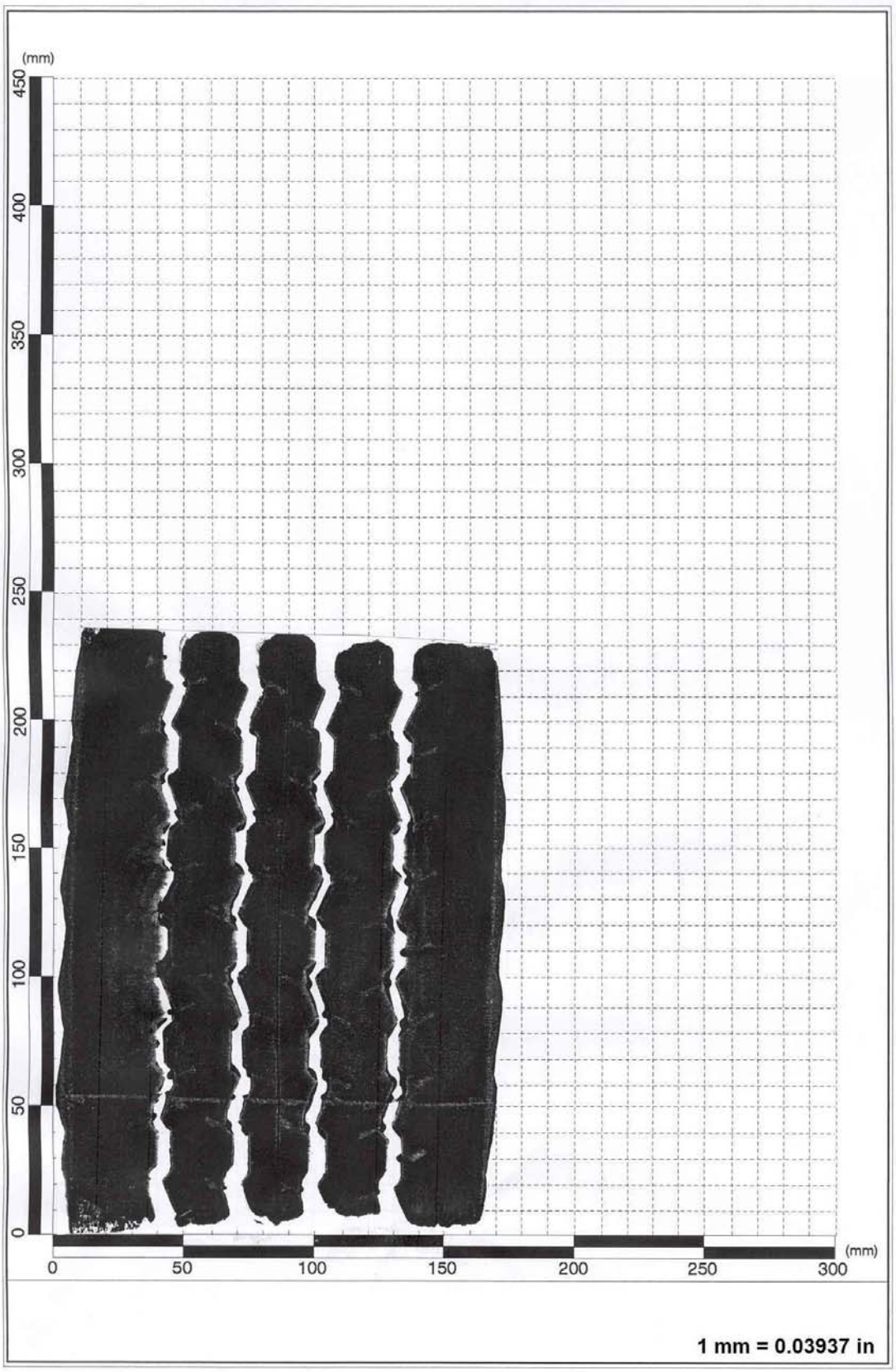

Figure D48. Tire Imprint for 215/75R17.5 Tire Taken at a Tire Load of 7000 lb and an Inflation Pressure of 115 psi.

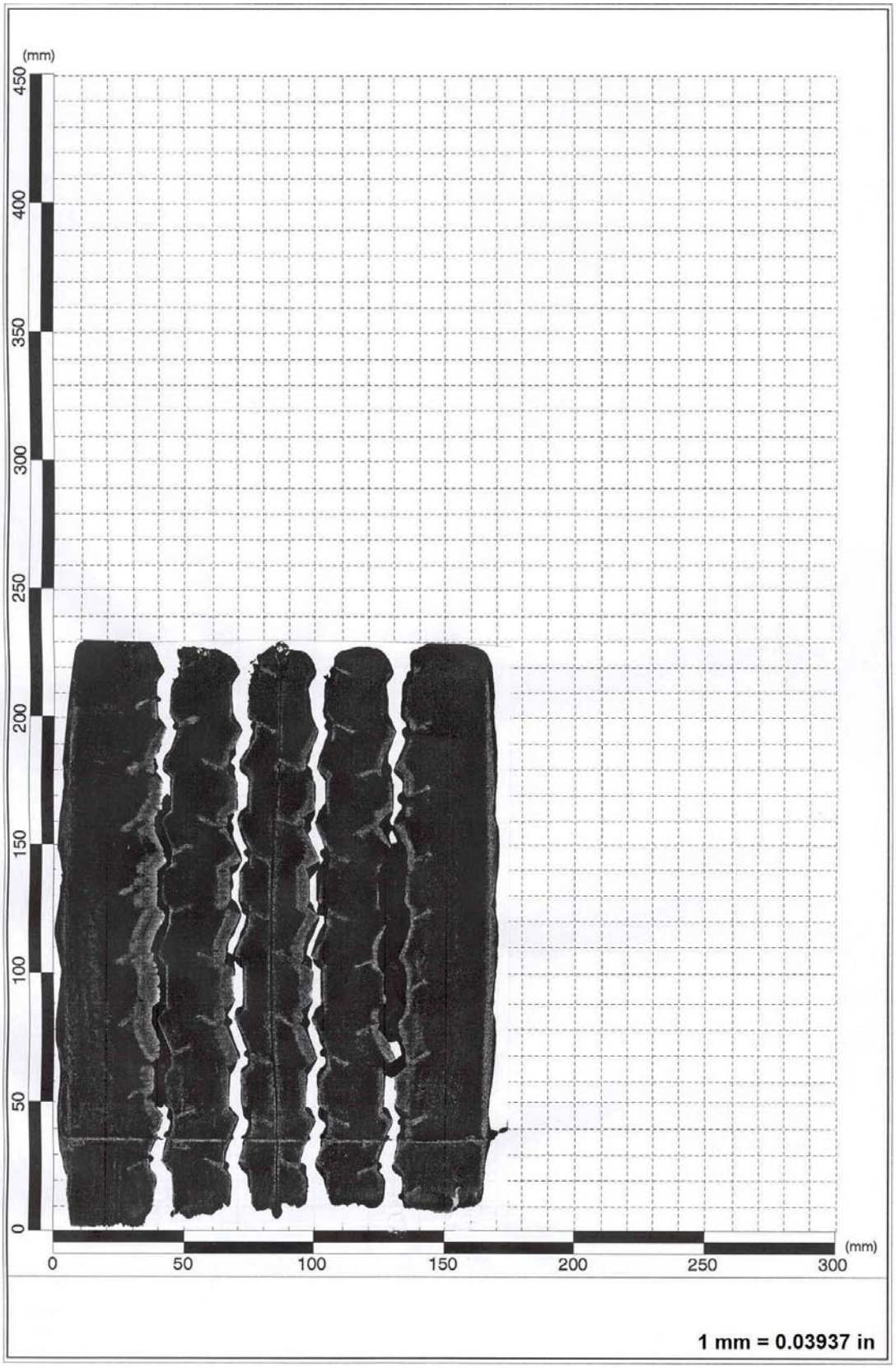

Figure D49. Tire Imprint for 215/75R17.5 Tire Taken at a Tire Load of 7000 lb and an Inflation Pressure of 130 psi.

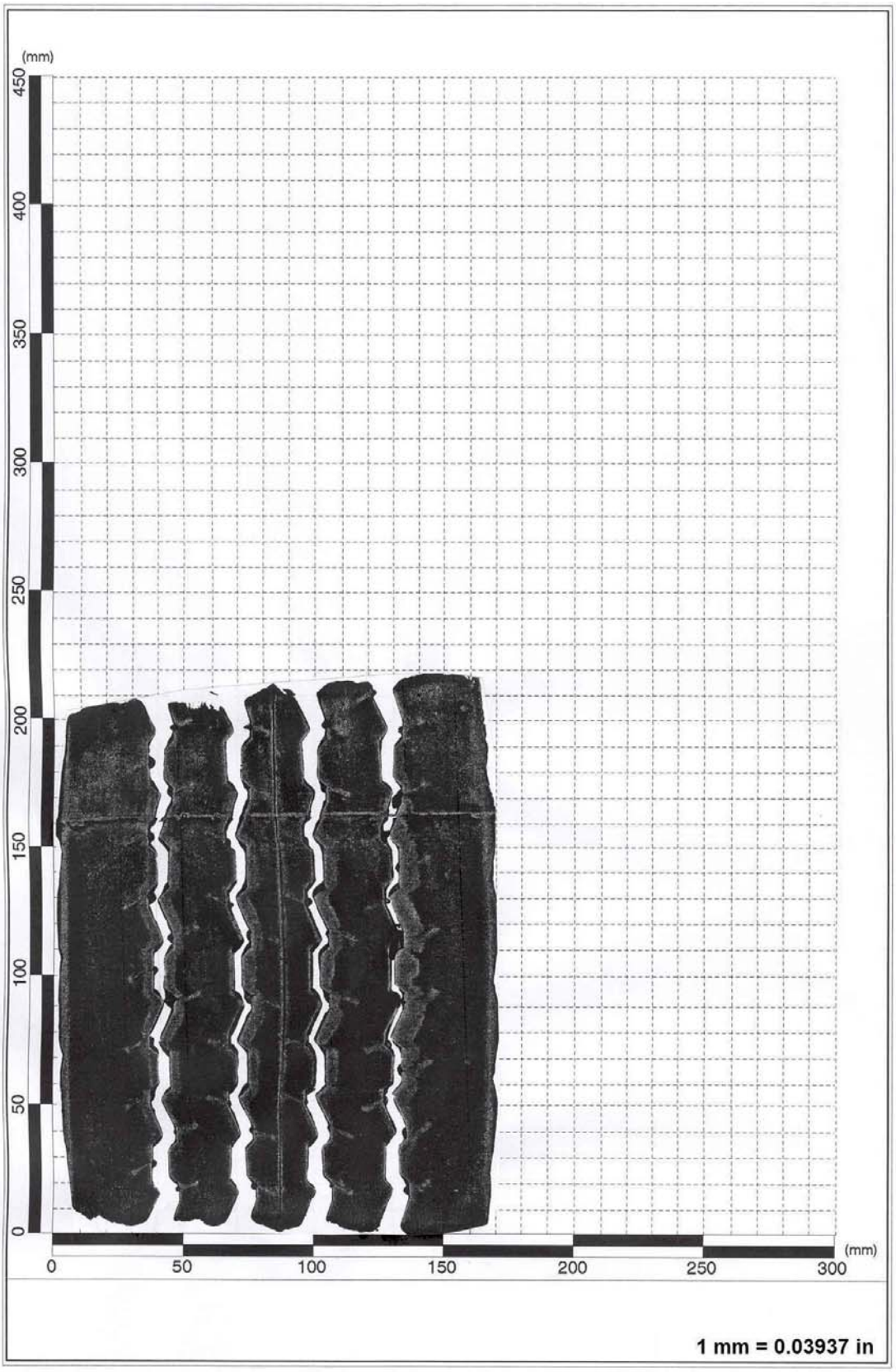

Figure D50. Tire Imprint for 215/75R17.5 Tire Taken at a Tire Load of 7000 lb and an Inflation Pressure of 145 psi.